UNIVERSITE DE LILLE 1

U.F.R. DES SCIENCES DE LA TERRE
59 655 Villeneuve d'Ascq Cédex

Mémoire présenté en vue de l'obtention de l'Habilitation à Diriger des Recherches

par

Olivier Averbuch

Maître de Conférences à l'Université de Lille 1

Laboratoire Géosystèmes, FRE 3298 du CNRS

CONTRIBUTION A L'ETUDE GEODYNAMIQUE DU SYSTEME OROGENIQUE VARISQUE :

RELATIONS DE LA CHAINE AVEC LE BASSIN DE PARIS, DYNAMIQUE DU FRONT DE CHAINE SEPTENTRIONAL DANS LE NORD DE LA FRANCE ET IMPACT DE LA SURRECTION SUR LE CLIMAT ET LES ENVIRONNEMENTS TERRESTRES

Soutenue le 30 novembre 2010,

Devant le jury composé de:

- Michel Faure (Université d'Orléans), rapporteur
- Jérôme Gaillardet (Institut de Physique du Globe de Paris), rapporteur
- François Roure (Institut Français du Pétrole, Rueil Malmaison), rapporteur
- Jean-Bernard Edel (EOST Strasbourg), examinateur
- Dominique Frizon de Lamotte (Université de Cergy Pontoise), examinateur
- Francis Meilliez (Université de Lille 1), examinateur
- Bruno Vendeville (Université de Lille 1), garant

Remerciements

Au terme de cette « HdR », qui m'a occupé un certain nombre années, mes pensées vont à toutes les personnes qui m'ont aidé, par leur travail ou leur soutien, dans sa réalisation. Elle sont très nombreuses et, à coup sûr, je vais en oublier certaines dans les lignes qui suivent. Aussi, j'espère qu'elles trouveront, dans tous les cas, dans l'accomplissement de ce travail, de nombreux motifs de satisfaction.

En premier lieu, mes pensées vont, bien sûr, vers Jean-Louis Mansy. Son soutien, tant sur le plan scientifique que sur le plan humain, depuis les premiers jours de mon arrivée à Lille, m'a permis de développer une grande partie des recherches présentées ici. Je pense qu'il aurait grandement apprécié voir cette synthèse arriver à son terme ; hélas, il est parti un peu trop tôt pour voir son achèvement. En tout cas, une chose est sûre, elle lui doit beaucoup.

Je tiens aussi à remercier chaleureusement Nicolas Tribovillard, avec qui j'ai mené l'aventure du projet « Eclipse ». Il est probable que, sans soutien, je ne me serai pas lancé dans ce projet qui nécessitait de rassembler une communauté scientifique pluri-disciplinaire venant d'horizons variés. Je pense qu'à deux, nous avons assez bien réussi à animer cette petite communauté et qu'au final, nous avons répondu aux objectifs fixés dans le cadre d'Eclipse. L'avenir dira si nous avons vu juste, mais, en tout cas, cette large collaboration restera pour moi un grand motif de satisfaction.

Il est évident que les recherches présentées ici doivent également beaucoup aux étudiants en thèse ou en Master qui ont bien voulu travaillé avec moi au cours de ces années. Je pense ici à Xavier Devleeschouwer, Frédéric Lacquement, Rafal Szaniawski, Laurent Riquier, Bruno Minguely, Vincent Lefebvre, Marie Patin, Mustapha Ouzgaït, Xuran Zuo, Laurent Folens, Amélie Leduc, et j'en oublie probablement. Merci à eux tous.

Les techniciens du laboratoire et le personnel administratif du SN5 ont également, à un moment ou un autre, d'une façon ou une autre, contribué à la réalisation de ces recherches. Je les remercie tous de leur participation à cette tache, souvent obscure, mais si importante dans le déroulement de nos recherches.

Je remercie Bruno Vendeville, d'avoir bien voulu me servir de garant pour cettte habilitation. Sa collaboration, ces dernières années, dans le domaine de la modélisation analogique m'a été précieuse pour avancer dans la compréhension des structures étudiées.

Un grand merci à Michel Faure, Jérôme Gaillardet et François Roure, qui ont bien voulu être les rapporteurs de ce mémoire d'habilitation ainsi qu'à Jean-Bernard Edel, Francis Meilliez et Dominique Frizon de Lamotte qui ont bien voulu en être examinateurs.
J'ai une pensée particulière pour ce dernier (Dominique), éternel optimiste, qui a suivi mon parcours de loin depuis la fin de ma thèse mais qui a grandement inspiré ma conception des domaines de front de chaîne. J'ai également une pensée pour Catherine Kissel qui m'a appris les rudiments du magnétisme des roches, me permettant ainsi de mettre à profit par la suite cette double compétence Tectonique-Magnétisme des roches.

Enfin, je remercie ma famille, ma femme Déborah, mes enfants Léo et Gabriel, ainsi que mes parents, pour m'avoir soutenu et supporté au cours de ces années. Je leur dédie ce travail qu'ils ne comprennent pas bien mais auxquels ils ont grandement contribué, rien qu'en me laissant de temps en temps « penser ».

Résumé

Le thème central de cette Habilitation à Diriger des Recherches concerne la géodynamique de la chaîne varisque (ou hercynienne). La lithosphère continentale d'Europe occidentale, et *a fortiori* de la France, a été structurée de façon primordiale lors de cet événement orogénique majeur au cours du Paléozoïque supérieur lors de la collision entre un bloc continental septentrional (la Laurussia, résultat de l'assemblage entre Avalonia, Baltica et Laurentia) et un ensemble continental méridional (le Gondwana), préalablement soudé au bloc continental armoricain. Cet assemblage continental, initiateur du méga-continent Pangéen à la fin du Paléozoïque, a imprimé la configuration thermo-mécanique de base de la lithosphère ouest-européenne, qui a, depuis lors, contrôlé l'histoire géologique de nos régions. Cet héritage orogénique est particulièrement explicite dans le Nord de la France qui localise le front de déformation septentrional de la chaîne varisque. A la lumière des études menées sur la marge nord du Bassin de Paris et sur son substratum, impliqué dans le système orogénique varisque septentrional, les travaux, présentés ici, se proposent d'apporter une nouvelle vision de la géodynamique de la chaîne, depuis sa surrection jusqu'à son affaissement à l'orée du Mésozoïque.

De façon plus précise, la géodynamique de la chaîne a été abordée suivant 3 axes de recherche principaux: (1) le premier concerne l'évolution tardive de la chaîne (classiquement appelée tardi-varisque) et son impact sur l'évolution des bassins de couverture dans le nord de la France ; ce volet a été abordé à deux échelles différentes avec d'une part, les relations à grande échelle entre la formation du Bassin de Paris et les processus orogéniques tardifs visant à faire disparaître la racine lithosphérique de la chaîne (le phénomène de délamination lithosphérique), et d'autre part, l'influence à une échelle régionale, des zones de chevauchements varisques sur la localisation des failles activées lors de la mise en place des dépôts de la fin du Paléozoïque et du Mésozoïque et de leur déformation lors de la phase de compression tertiaire péri-alpine (la phase dite « d'inversion » tertiaire) ; (2) le second concerne la dynamique du front de chaîne varisque septentrional dans le nord de la France, entre le Boulonnais à l'ouest et les Ardennes à l'est ; deux volets ont été plus particulièrement explicités : le style spécifique du front chevauchant par rapport aux modèles classiques des fronts de chaîne et la segmentation latérale et la courbure du front de la chaîne dans le nord de la France. Nous proposons, en particulier, un nouveau modèle de front de chaîne (le modèle de « zone triangulaire frontale profonde ») impliquant l'existence de rétrochevauchements profonds dans l'avant-pays brabançon. Du point de vue de la segmentation latérale du front de chaîne et de sa courbure à toute échelle, nous soulignons l'impact important exercé par l'héritage structural, en particulier associé à la configuration initiale de la marge rhénohercynienne antérieurement à sa déformation au sein du prisme orogénique varisque ; (3) le dernier axe, d'échelle plus globale, concerne l'impact de la phase précoce de surrection de la chaîne varisque sur l'évolution des environnements terrestres et du climat au Dévonien supérieur (période Frasnien-Famennien). Cet axe, un peu marginal par rapport aux deux autres qui ont un ancrage fort à l'université de Lille depuis assez longtemps, fait appel à une étude intégrée de la géodynamique couplée, interne et externe, au cours de la mise en place des premiers reliefs varisques et de ce fait, intègre des données assez larges concourrant à la compréhension du système Terre à grande échelle (reconstitutions paléogéographiques et paléotectoniques, géochimie, magnétisme environnemental, modélisation du cycle du carbone). Il est proposé que l'épisode de surrection du relief (phase transitoire d'environ 1-2 Ma) au cours du Frasnien supérieur ait induit une déstabilisation rapide du cycle du carbone à travers l'intensification de l'érosion continentale et de l'altération chimique associée conduisant à une chute drastique de la teneur en CO2 atmosphérique et au final à un refroidissement sévère et durable du climat à partir du Dévonien supérieur.

Sommaire

N.B. : Les noms en italique correspondent aux étudiants encadrés dans le cadre de cette habilitation à diriger des recherches.

1. Présentation et contexte des recherches intégrées à ce mémoire

Ce mémoire d'Habilitation à diriger des Recherches présente un recueil des principaux travaux effectués dans le cadre de mes activités de recherche, depuis mon intégration au laboratoire de Géosciences (actuellement défini sous le nom de Géosystèmes) de l'Université de Lille 1 en 1994. Cette synthèse de mes travaux scientifiques, postérieurs à mon doctorat, ne résulte pas d'une démarche de recherche linéaire, décidée à priori, mais s'est construite petit à petit, suite à des réajustements thématiques réguliers, intervenus au gré des restructurations de laboratoire et des opportunités de collaboration et de financement de projets. C'est ce cheminement que je présenterai dans ce paragraphe introductif afin que le lecteur prenne connaissance du contexte général des recherches présentées ici.

Le thème central de mes travaux concerne la géodynamique de la chaîne varisque (ou hercynienne). La lithosphère continentale d'Europe occidentale (et à fortiori de la France) a été structurée de façon primordiale lors de cet événement orogénique majeur au cours du Paléozoïque supérieur (globalement entre le Dévonien moyen-supérieur et le Carbonifère terminal) lors de la collision entre un bloc continental septentrional (la Laurussia, résultat de l'assemblage entre Avalonia, Baltica et Laurentia) et un bloc continental méridional (le Gondwana). Cet assemblage continental, initiateur du méga-continent Pangéen à la fin du Paléozoïque, a imprimé la configuration thermo-mécanique de base de la lithosphère ouest-européenne, qui a, depuis lors, contrôlé l'histoire géologique de nos régions.
Bien qu'abondamment étudiée depuis la fin du 19ème siècle, la géodynamique du système varisque ne fait pas encore pour l'heure de consensus parmi la communauté géologique internationale (e.g. Faure et al, 2005). Il n'est pas dans mon intention dans ce mémoire de discuter de façon exhaustive les différents modèles géodynamiques en vigueur ni d'avoir une vue détaillée du système varisque dans son ensemble tant les données le concernant sont nombreuses et diverses. Cependant, la majorité des données géologiques et des modèles étant issus des massifs varisques internes (Massif central, Massif armoricain, Vosges et leurs homologues d'Europe centrale), il ne rendent généralement pas compte de façon satisfaisante des contraintes géodynamiques issues des travaux dans les zones externes septentrionales de la chaîne. Un des objectifs généraux des travaux présentés ici sera de souligner un certain nombre de points majeurs, issus des recherches menées ces dernières années au front septentrional de la chaîne, permettant d'envisager l'évolution du système orogénique varisque sous un autre angle que ceux généralement présentés.

De façon plus précise, la géodynamique de la chaîne a été abordée suivant 3 axes de recherche principaux que je développerai, tour à tour, dans le corps de ce mémoire:
(1) le premier concerne l'évolution tardive de la chaîne (classiquement appelée tardi-varisque) et son impact sur l'évolution des bassins de couverture dans le nord de la France ; ce volet a été abordé à deux échelles différentes avec d'une part, les relations à grande échelle entre la formation du Bassin de Paris et les processus orogéniques tardifs visant à faire disparaître la racine lithosphérique de la chaîne (le phénomène de délamination lithosphérique), et d'autre part, l'influence à une échelle régionale, des zones de chevauchements varisques sur la localisation des failles activées lors de la mise en place des dépôts de la fin du Paléozoïque et du Mésozoïque et de leur déformation lors de la phase de compression tertiaire péri-alpine (la phase dite « d'inversion » tertiaire) ;
(2) le second concerne la dynamique du front de chaîne varisque septentrional dans le nord de la France, entre le Boulonnais à l'ouest et les Ardennes à l'est ; deux volets seront plus spécifiquement explicités : le caractère spécifique du chevauchement frontal varisque (dit classiquement « faille du Midi » en référence à sa localisation systématique au sud du bassin d'avant-chaîne houiller du Nord-Pas de Calais) par rapport au modèles classiques des fronts de chaîne et la segmentation et la courbure du front de la chaîne dans le nord de la France.
(3) le dernier axe, d'échelle plus globale, concerne l'impact de la phase précoce de surrection de la chaîne varisque sur l'évolution des environnements terrestres et du climat au Dévonien supérieur (période Frasnien-Famennien). Cet axe, un peu marginal, par rapport aux deux autres qui ont un ancrage fort à l'Université de Lille depuis assez longtemps, a été guidé par la mise en place du programmme pluri-disciplinaire Eclipse au cours des années 2000. Il fait appel à une étude intégrée de la géodynamique couplée, interne et externe, au cours de la mise en place des premiers reliefs varisques et de ce fait, intègre des données assez larges concourrant à la compréhension du système Terre à grande échelle (reconstitutions paléogéogéographiques et paléotectoniques, géochimie, magnétisme environnemental, modélisation du cycle du carbone).

A mon arrivée à Lille, mes travaux de thèse m'avaient conduit à une spécialisation autour de la déformation des fronts de chaîne de montagne à partir de l'analyse structurale et du magnétisme des roches (anisotropie de susceptibilité magnétique et paléomagnétisme). Ces premières études m'avaient également conduit à m'intéresser aux structures de chevauchement et plissement au front des Pyrénées orientales (Corbières), des Apennins centraux (Italie) et du Taurus occidental (Turquie)(Averbuch et al, 1992 ; 1993 ; 1995 ; Kissel et al, 1993 ; Frizon de Lamotte et al, 1995). Lors de mon intégration au sein du laboratoire de « Dynamique sédimentaire et structurale » de l'Université de Lille, mes travaux de recherche ont, tout naturellement, obliqué vers la géométrie et la cinématique des déformations contemporaines de la mise en place du front de chaîne varisque septentrional, travaux entrepris en collaboration avec Jean-Louis Mansy et son équipe. Cet axe de recherche, profondément ancré à l'Université de Lille depuis les travaux précurseurs de Gosselet et Barrois à la fin du 19 ème siècle, a connu des avancées significatives ces vingt dernières années sous l'impulsion successive de Jean-François Raoult, Francis Meilliez et Jean-Louis Mansy.

Au cours des dix dernières années, de nombreuses données nouvelles ont été acquises au sein de l'Atelier régional « Nord de la France » du laboratoire. Ces nouvelles données concernent aussi bien les aspects cartographiques, recueillies dans le cadre de la réactualisation des cartes géologiques de Marquise (Boulonnais), Givet et Fumay (Ardennes) que des aspects structuraux de détail menés de l'échelle de l'affleurement à l'échelle régionale.

Dans le secteur ardennais (localisation en Fig. 1 en annexe), ces derniers ont été acquis, en particulier, au cours de la thèse de Frédéric Lacquement (2001), thèse réalisée sous la direction de Jean-Louis Mansy et Francis Meilliez, et à laquelle j'ai pris part, en particulier, en ce qui concerne l'analyse en trois dimensions des déformations par chevauchement-plissement (Lacquement et al, 2005). Je noterai également dans ces avancées récentes sur la compréhension du secteur ardennais les travaux synthétiques sur la pétrofabrique et les caractéristiques tectono-métamorphiques des roches cambriennes du Massif de Rocroi, réalisés dans le cadre d'une collaboration avec Philippe Robion de l'Université de Cergy-Pontoise et Manuel Sintubin de l'Université de Leuven (Robion et al, 1999).

Dans le secteur boulonnais (localisation en Fig. 1 en annexe), les relevés de détail acquis dans les principales carrières en exploitation ont permis de préciser la géométrie et la cinématique des déformations plissées-faillées au mur du chevauchement frontal majeur (faille du Midi)(Averbuch al, 2001 ; 2004). Cette synthèse régionale se fonde en grande partie sur l'analyse géométrique et cinématique de détail d'une structure en duplex, d'échelle hectométrique, le « duplex de la carrière Basse-Normandie » à Rinxent (Averbuch et al, 1998). Cette structure géologique, hors norme, illustre les processus de déformation à la semelle des grands chevauchements, en particulier, en ce qui concerne l'évolution des séquences de chevauchement dans un système orogénique en cours de propagation.

Dans le cadre d'une collaboration avec F. Hanot du BRGM (projet Référentiel géologique), ces données d'affleurement ont été complétées par une base de données des profils de sismique-réflexion dans le Nord de la France (Fig. 2 en annexe), base de données intégrée par la suite au sein d'un logiciel d'analyse sismique 3D (le logiciel Kingdom suite, pour lequel j'ai contracté une licence académique auprès du concepteur américain Seismic MicroTechnologies). Plusieurs de ces profils ont fait l'objet d'études préliminaires, en particulier en Artois dans le cadre de travaux de DEA (D. Rolin (2000), M. Patin (2004)) ou en Avesnois dans le cadre de la thèse de F. Lacquement. La majeure partie des profils recueillis a été synthétisée, cependant, dans le cadre de la thèse de B. Minguely (2007) que j'ai co-dirigée avec Jean-Louis Mansy (puis dirigé seul après le décès de ce dernier en mai 2006). Cette approche de la géométrie profonde du front de chaîne a été couplée à une synthèse des données de forage et des données gravimétriques, disponibles sur la région Nord de la France. Ces travaux ont permis d'une part d'établir un modèle géométrique 3D de la couverture sédimentaire méso-cénozoïque à l'échelle du nord de la France (Fig. 3 en annexe) argumentant le contrôle des chevauchements varisques sur la localisation et la déformation des dépôts de couverture et d'autre part de proposer un nouveau modèle conceptuel rendant compte de la géométrie et cinématique très particulière du front de chaîne (le concept de zone triangulaire frontale)(Minguely, 2007 ; Minguely et al, 2010). Afin de mieux comprendre la cinematique et les principaux facteurs de contrôle de zones chevauchantes triangulaires frontales et de systèmes de réactivation en extension des chevauchements (inversion structurale négative), des travaux de modélisation analogique ont, par ailleurs, été entrepris, en collaboration avec Bruno Vendeville au laboratoire de modélisation analogique lillois (Minguely et al, 2008 ; Ouzgaït et al, 2010).

Ces données, focalisées sur le front chevauchant varisque en Artois, enfoui sous les dépôts crétacés et tertiaires, complètent une première synthèse des données géologiques (à l'affleurement) et géophysiques, qui avait été entreprise sur le bassin du Weald-Boulonnais (à l'interface entre France, Belgique et Grande-Bretagne) dans le cadre d'une collaboration mise en place par J-L. Mansy et regroupant outre moi-même, G. Manby de l'Université de Greenwich (GB), M. Everaerts de l'Institut Royal des Sciences de Belgique, F. Bergerat et J. Lamarche de l'Université Paris VI, B. Van Vliet-Lanoe de l'Université de Lille et S. Vandycke de la Faculté polytechnique de Mons (Belgique)(Mansy et al, 2003 ; Minguely et al, 2005).

Parallèlement, à ces études sur la dynamique du front chevauchant, une attention particulière a été portée à la compréhension en 3D du système. Au cours de ma thèse, j'avais accordé déjà une attention particulière à la caractérisation des terminaisons latérales des écailles chevauchantes et aux déformations spécifiques qui les caractérisent (Averbuch et al, 1993 ;

Frizon de Lamotte et al, 1995), par une démarche intégrant analyse des déformations et étude des rotations autour d'axes verticaux par le paléomagnétisme. La segmentation latérale du front septentrional de la chaîne varisque a été étudiée sur ce même modèle couplant les données structurales à des études paléomagnétiques à différentes échelles, depuis l'échelle régionale (couloir transpressif de la Meuse, Szaniawski et al, 2003 ; Lacquement et al, 2005) à l'échelle de la chaîne (la virgation du front de la Manche au Rhin, Marton et al, 2000). Ces données ont été acquises dans le cadre de deux projets en collaboration financés par le Ministère des Affaires Etrangères :

- un projet Balaton (France-Hongrie), établi avec l'Université de Budapest (L. Csontos) et l'Institut de Géophysique de Hongrie Eötvös Lorand (E. Marton) entre 1996 et 1998 (Etude pluridisciplinaire du champ de déformation au sein de complexes orogéniques arqués. Application aux massifs carpathiques internes de Hongrie et à l'arc varisque d'Europe occidentale (responsables J-L. Mansy, Université de Lille et L. Csontos, Université de Budapest)).
- un projet Polonium (France-Pologne) établi avec l'Institut de géophysique de Varsovie sur la période 2000-2004 (responsables J-L. Mansy, Université de Lille et M. Lewandowski, Institut de géophysique de l'Académie des Sciences de Varsovie). Ce projet a servi de support à la thèse en co-tutelle de Rafal Szaniawski (2004) sur l'étude paléomagnétique des séries dévono-carbonifères des Ardennes et de l'Artois, travaux que j'ai encadrés pour partie avec J-L. Mansy et M. Lewandowski.

Pour clore le volet concernant le système chevauchant varisque septentrional et ses relations avec le bassin de Paris, une étude à plus grande échelle s'est dessinée à partir de 2006 suite à une collaboration avec C. Piromallo de l'Institut de Géophysique de Rome. Cette dernière a, en effet, mis à ma disposition, son modèle de tomographie sismique du manteau établi avec son collègue A. Morelli (le modèle PM0.5)(Piromallo et Morelli, 2003). Les données de tomographie permettent, en effet, de donner une image assez surprenante au premier abord des racines mantéliques de la chaîne varisque sous le bassin de Paris. Ces données m'ont conduit à discuter de l'impact du caractère hétérogène du processus de délamination lithosphérique tardi-orogénique et de son rôle possible dans l'initiation du bassin de Paris (Averbuch et Piromallo, 2007a, b; en cours).

L'impact du soulèvement de la chaîne varisque sur les environnements terrestres et le climat constitue, chronologiquement, le dernier axe développé dans le cadre de mes travaux de recherche. En effet, au cours de la restructuration de l'unité de recherches lilloise pendant la période 2000-2001, il nous a été demandé collectivement de mettre en place des projets de recherche nouveaux répondant de plus près aux grandes questions scientifiques du moment. Dans ce cadre, j'ai amorcé une réorientation d'une partie de mes recherches en lancant un projet pluridisciplinaire visant à étudier l'impact d'une orogenèse sur les variations des environnements terrestres et du climat. Le projet en question découle de travaux préliminaires menés dans le cadre de la thèse de Xavier Devleeschouwer (1999), thèse en cotutelle entre l'Université de Lille (dir. : J-L. Mansy) et l'Université de Bruxelles (dir. : A. Préat), avec pour thématique l'analyse des faciès sédimentaires et des cortèges argileux lors de la crise du Frasnien-Famennien (Dévonien supérieur, ca 375 Ma BP). Dans le cadre de la thèse de Xavier Devleeschouwer, j'avais été associé à l'étude pour tester l'outil susceptibilité magnétique comme marqueur des variations des paléoenvironnements anciens. Nous avions alors montré que la susceptibilité magnétique pouvait être un excellent marqueur des variations du niveau marin et des apports détritiques résultants, même dans des séries carbonatées fortement diagénétiques. Au final, cette étude était, cependant, resté sur un constat mitigé quant aux causes des variations des environnements marins au Dévonien supérieur, le climat et la tectonique très active de cette période pouvant être invoqués comme facteur de contrôle prépondérant. C'est sur la base de ce constat préliminaire que m'est venu l'idée d'un couplage potentiel entre la surrection des premiers reliefs varisques et le climat au travers du cycle du carbone et de l'effet de serre associé au CO_2 atmosphérique. Ce projet, que j'ai mis en place et piloté, a été financé par le programme Eclipse du CNRS sur 3 ans (2001-2003). Il a été cloturé par un colloque spécialisé tenu à Lille en 2003 sous l'impulsion de Nicolas Tribovillard (le colloque Tectoclim) et a servi de support à deux thèses lilloises que j'ai co-encadrées : la thèse de Laurent Riquier (2005), concrétisée par 5 publications (Averbuch et al, 2005 ; Riquier et al, 2005, 2006, 2007, 2009), et la thèse de Vincent Lefebvre (2009) (Diester-Haas et al, 2009 ; Lefèbvre et al, 2010 ; Lefebvre et al, en cours).

Les principaux résultats, issus de ces différentes études, seront présentés en plus grand détail dans les chapitres suivants, chapitres basés sur des articles ciblés, déjà parus pour la plupart ou en cours de processus éditorial pour certains. La liste complète de mes publications est, par ailleurs, disponible en annexe.

2. La Chaîne varisque dans le Nord de la France : aperçu géodynamique et relations avec le Bassin de Paris.

2.A. Un nouveau modèle géodynamique pour l'affaissement de la chaîne varisque et l'initiation du bassin de Paris : la délamination lithosphérique hétérogène

Ce premier volet est explicité dans l'article 1, présenté dans les pages suivantes. Cet article pourrait former aussi bien l'introduction de ce travail sur la chaîne varisque dans la mesure où il met en place le contexte structural général que sa conclusion puisqu'il tente d'intègrer l'ensemble des résultats récents sur la chaîne au sein d'un modèle géodynamique explicitant, en particulier, ses relations avec le bassin de Paris.

Le thème central de cet article concerne le mécanisme de délamination lithosphérique, mécanisme par lequel une chaîne de montagne va perdre sa racine mantélique pour que la lithosphère retrouve sur le long-terme son état d'équilibre thermo-mécanique (e.g., Nelson, 1992; Kay and Kay, 1993). Ce processus, nécessaire au rétablissement des conditions permettant le mouvement des plaques lithosphériques continentales, reste encore assez méconnu dans le détail. Un des points, sur lequel la communauté des tectoniciens s'accordent, cependant, est que la délamination lithosphérique va induire une remontée localisée de l'asthénosphère sous la chaîne de montagne, remontée à l'origine d'un réchauffement, d'une surrection et extension de la lithosphère (Platt and England, 1993; de Boorder et al, 1998; Arnold et al, 2001; Gögus and Pysklywec, 2008) ainsi que d'un magmatisme intense contrôlé par la fusion du manteau asthénosphérique par décompression (Kay and Kay, 1993). Le refroidissement postérieur de la lithosphère est à l'origine, par ailleurs, d'une subsidence thermique long-terme de la chaîne conduisant, au final, au développement d'un bassin sédimentaire (« sag basin » selon Nelson, 1992) recouvrant les zones de suture de l'ancienne chaîne.

Ces phénomènes caractérisent assez bien l'évolution tardive de la chaîne varisque en France (ce qu'on appelle classiquement l'évolution « tardi-varisque ») et, ces dernières années, il a été suggéré que le magmatisme tardi-varisque (ainsi que toutes les manifestations hydrothermales associées) et la subsidence du bassin de Paris puissent résulter d'un événement de délamination lithosphérique de grande ampleur sous la chaîne varisque (Nelson, 1992 ; Prijac et al, 2000 ; Ziegler et al, 2004).

Dans la poursuite de ces premières études, qui se sont basées essentiellement sur la modélisation de la subsidence thermique dans le bassin de Paris, l'article 1 se propose d'appréhender la géométrie rélictuelle de la racine orogénique varisque sous le bassin de Paris à partir de l'analyse de la tomographie sismique du manteau dans le nord de la France. Ce type d'étude, habituellement mené sur les phénomènes géodynamiques actifs (car contrôlé en premier ordre par des anomalies mantéliques d'origine thermique), a été étendu aux zones de suture orogéniques anciennes ces dernières années avec, pour objectif, de mettre en évidence l'hétérogénéité de composition du manteau hérité de subductions passées (e.g., Zielhuis and Nolet, 1994 ; Poupinet et al, 1997 ; Poupinet et al, 2002 ; Judenherc et al, 2002; Sol et al, 2002; Poupinet et al, 2003).

Les données de tomographie sismique du manteau, présentées dans l'article 1, sont issues d'une collaboration avec Claudia Piromallo de l'Institut de Géophysique de Rome. Avec son collègue A. Morelli, elle a développé un modèle de vitesse sismique des ondes P dans le manteau dans les contrées européennes limitrophes de la Méditerranée (le modèle PM0.5) par inversion des données du Centre Séismologique International enregistrées sur la période 1964-1995 (Piromallo et Morelli, 2003). Ce modèle, qui a été beaucoup utilisé ces dernières années pour caractériser les processus géodynamiques autour de la Méditerrannée (Facenna et al, 2003; 2004, 2006; Vignaroli et al, 2008; Jolivet et al, 2009), donne également une image, de bonne résolution, des hétérogénéités de vitesse sismique dans le manteau sous le bassin de Paris.

Un point tout à fait intéressant, mis en avant par le modèle PM0.5 sous le bassin de Paris, est l'existence d'une anomalie positive de vitesse sismique dont l'ampleur (1,5 à 2% supérieure au modèle de vitesse de référence sp6 de Morelli et Dziewonski (1993)) avoisine celle que l'on peut observer sous la chaîne des Alpes. Le corps principal de cette anomalie, particulièrement visible entre 100 et 200 km de profondeur sous la partie occidentale du bassin, suit une direction approximativement NW-SE avec une bordure NE, quasi-linéaire, se moulant sur la zone de suture nord-varisque dans le Nord de la France i.e. la zone de chevauchement du Pays de Bray (e.g., Matte et Hirn, 1988). De façon plus significative encore, l'anomalie de vitesse sismique du manteau se corrèle spatialement, mais légèrement décalée vers le SW, avec la grande anomalie magnétique du Bassin de Paris. Bien que son origine reste encore débattue, l'anomalie magnétique du Bassin de Paris est classiquement interprétée comme le résultat de l'existence d'écailles intra-crustales de roches océaniques basiques intégrées à la zone de suture nord-varisque (e.g. Autran et al, 1994). A plus grande échelle, les isovaleurs d'anomalie de vistesse sismique du manteau suivent le tracé de la zone de suture nord-varisque, caractérisé par la grande virgation reliant la zone faillée NW-SE du Pays de Bray à la zone de suture rhéno-hercynienne ENE-WSW, exprimée en surface par la faille de Metz et son prolongement vers l'est, la faille du Hunsrück (failles limitant au nord le bassin stéphano-permien de Sarre-Lorraine).

En coupe, la forme de l'anomalie est difficile à caractériser, là où elle atteint son amplitude maximum, en raison de sa coalescence avec une anomalie superficielle centrée sur la zone de suture sud-varisque dans le Massif armoricain (Judenherc et al, 2002). Au niveau de son extrémité SE, les transects transverses à l'anomalie montrent, cependant, clairement un pendage très fort vers le sud évoquant un panneau plongeant jusqu'à environ 250 km sous la partie méridionale du bassin de Paris.

Les caractéristiques géométriques de l'anomalie de forte vitesse sismique sous le Bassin de Paris, telles que le modèle PM0.5 les fait apparaître, rend difficile une interprétation ent terme d'anomalie thermique du manteau associée à un phénomène géodynamique récent. En effet, les seuls phénomènes thermiques de grande ampleur ayant affecté la région récemment sont dus aux points chauds localisés sur l'Eifel (Goes et al, 1999 ; Ritter et al, 2001) et l'est du Massif Central (Granet et al, 1995 ; Babuska et al, 2002). Ces domes thermiques sont à l'origine d'anomalies localisées de faible vitesse des ondes P dans le manteau supérieur mais ils ne permettent pas de rendre compte de l'anomalie observée qui, elle, nécessite des températures plus faibles que dans un manteau standard. Par ailleurs, il est peu probable qu'un panneau lithosphérique varisque subduit, il y a plus de 300 Ma, puisse engendrer une anomalie thermique résiduelle aussi longue comme le montre les modélisations thermiques considérant un rééquilibrage post-subduction (e.g., Stein et Stein, 1996). Ainsi que le suggèrent de façon générale les études tomographiques à travers les zones de suture anciennes (Judenherc et al, 2002 ; Sol et al, 2002 ; Poupinet et al, 2003 ; Artemieva et al, 2006), l'anomalie observée serait le résultat d'une hétérogénéité de composition du manteau héritée d'un événement de subduction au niveau de la zone de suture septentrionale varisque (la suture de l'Océan Lizard-Rhénohercynien). Selon toute vraisemblance, elle correspondrait, donc, à un panneau résiduel de lithosphère océanique (éclogitique ?), subduit sous le bloc continental armoricain à la fin du Carbonifère, et qui aurait échappé à un quelconque processus de délamination lithosphérique tardi-varisque.

La préservation d'un tel panneau plongeant varisque à la base de la lithosphère (jusque 200-250 km de profondeur) sur plus de 300 Ma amène un certain nombre de questionnements, en particulier sur le caractère extrèmement hétérogène du passage lithosphère-asthénosphère sous les continents (voir Artemieva et Mooney, 2002 et Poupinet et al, 2003 pour une discussion plus approfondie). En ce qui concerne la géodynamique varisque, un point frappant est l'anti-corrélation spatiale entre la localisation de ce panneau plongeant résiduel (au niveau du secteur Pays de Bray) et la localisation des fossés syn-rift stéphano-permiens majeurs à la base du bassin de Paris (le fossé de Sarre-Lorraine réactivant la suture « rhénohercynienne » et le fossé de Manche centrale réactivant la suture « Lizard »). Une telle anti-corrélation suggère d'une part que la géométrie de la racine mantélique telle qu'enregistrée par la tomographie sismique serait héritée des phénomènes tardi-varisques et d'autre part que les fossés profonds contemporains de la phase d'extension initiatrice du bassin de Paris (e.g., Prijac et al, 2000) seraient associés à la délamination lithosphérique de la chaîne varisque au niveau des tronçons rhénohercyniens et lizard de la zone de suture nord-varisque. La remontée asthénosphérique associée au détachement localisé de la racine orogénique varisque pourrait être, ainsi, considérée comme le moteur du magmatisme et du rifting stéphano-permien, initiateur du bassin de Paris. Son caractère hétérogène pourrait, par ailleurs, expliquer le caractère diachrone de la subsidence dans le bassin de Paris et la migration de la subsidence thermique post-rift depuis les zones de rifting initial (l'est du bassin de Paris et le secteur Manche) vers le domaine « Pays de Bray » où les premiers dépôts ne sont enregistrés qu'à la fin du Trias (e.g. Mégnien, 1980 ; Guillocheau et al, 2000). De façon plus générale, la subduction de l'océan Lizard-Rhénohercynien sous le bloc armoricain, soudé au Gondwana dès le Dévonien supérieur au niveau de la suture Sud Armoricaine-Massif Central, et le détachement final de la lithosphère océanique enfouie apparaissent comme des éléments moteurs du magmatisme et de l'extension affectant les zones internes varisques au cours du Carbonifère et peuvent être considérées, dès lors, comme des mécanismes non négligeables dans les processus régissant l'effondrement de la chaîne varisque à la fin du Paléozoïque.

Article 1.

Averbuch O. and Piromallo C. (en cours, pour soumission à Earth and Planetary Science Letters). Is there a remnant Variscan subducted slab in the mantle beneath the Paris basin ? Implications for the geodynamical evolution of Northern France.

Is there a remnant Variscan subducted slab in the mantle beneath the Paris basin? Implications for the geodynamical evolution of Northern France

O. Averbuch[a] and C. Piromallo[b]

[a] Université Lille-Nord de France, Lab. Géosystèmes, FRE CNRS 3298, 59655 Villeneuve d'Ascq cédex, France, olivier.averbuch@univ-lille1.fr

[b] Instituto Nazionale di Geofisica et Vulcanologia, Via di Vigna Murata 605, 00143 Rome, Italy, claudia.piromallo@ingv.it

Corresponding author: O. Averbuch, Université de Lille 1, Lab. Géosystèmes, FRE CNRS 3298, Cité scientifique, 59655 Villeneuve d'Ascq cédex, France; e-mail: olivier.averbuch@univ-lille1.fr, tel: 0033 320 33 71 30, fax: 0033 320 43 49 10.

Abstract

In northern France, the Paris basin represents a Late Paleozoic-Mesozoic intracratonic basin that settled upon the collapsed Variscan collisional belt. The mantle roots of the Variscan orogenic system, below the Paris basin, have been investigated here using a European-scale P-wave velocity tomographic model. Strikingly, tomography points out the existence of a significant high velocity anomaly in the upper mantle below the western part of the basin. In map view, at ~150-200 km depth, the latter extends with a NW-SE trend along the buried Northern France trace of the Northern Variscan Suture Zone i.e. the Bray Fault segment of the Upper Carboniferous Lizard-Rhenohercynian (LRH) suture zone. Moreover, the main high-velocity anomaly is spatially correlated with the prominent Paris Basin Magnetic Anomaly, though slightly shifted to its SW extension. In cross-sections, it extends through the lithospheric mantle to apparent depths greater than 200 km below the southern margin of the Paris basin. As suggested in previous tomographic studies below ancient suture zones, these data argue for such anomaly being the remnant of a Variscan subducted slab that escaped the extensive late orogenic delamination process affecting the Variscan root zones by Late Carboniferous-Early Permian times. As a whole, these data question the long-term evolution of subducted lithosphere into the mantle and in the case of the Western European Variscan belt, suggest the subduction of the LRH oceanic slab below the previously thickened Variscan crust, and its final detachment from the orogenic root, to have played an important role in the collapse of the belt inducing a significant amount of thermal erosion and extension of the overriding lithosphere all over Upper Carboniferous times. The spatial evolution of subsidence in the Paris basin is suggested to result primarily from the heterogeneous delamination of the Variscan root zones along strike and from the resultant pattern of asthenospheric rise.

Key words- Variscan belt, Paris basin, mantle tomography, lithospheric delamination, post-orogenic collapse

1. Introduction

In recent years, the question of the long-term evolution of lithospheric roots of collisional mountain belts has gained a growing interest from the scientific community. One of the main points emphasized by these studies is that a thickened continental lithosphere commonly "delaminates" at a certain degree of the orogenic development, the subducted lithospheric mantle being detached from the overlying crust and subsequently buried in the deeper mantle (e.g., Bird, 1979; Sacks and Secor, 1990; Nelson, 1992; Kay and Kay, 1993; Gvirtzman, 2002). The detailed processes, by which such sub-crustal delamination can operate, are still poorly known but thermo-mechanical models argue for the possibility of the base of the lithospheric orogenic root to be removed either by diffuse convective processes (Houseman et al, 1981; Platt and England, 1993; Houseman and Molnar, 1997; Pysklywec et al, 2000) and/or by localized decoupling along the Moho and break-off of the down-going slab due to its negative buoyancy (Bird and Baumgartner, 1981; Nelson, 1992; Davies and von Blankenburg, 1995; Morency and Doin, 2004; Moore and Wiltschko, 2004). Regardless of the mechanisms involved, the removal of the orogenic root has been suggested to induce the rise of the asthenospheric mantle at some lithospheric level below the mountain belt resulting in significant heating, uplift and extension of the previously thickened crust (Platt and England, 1993; de Boorder et al, 1998; Arnold et al, 2001; Gögus and Pysklywec, 2008) as well as in intense magmatism produced by decompression-induced melting of the upwelling asthenopheric unit (e.g., Kay and Kay, 1993; Davies and von Blankenburg, 1995; Keskin, 2003; Macera et al, 2008). The net long-term effects of these coupled mechanisms would be (1) the recovery of the thicknesses and thermo-mechanical properties of the standard continental lithosphere and (2) the burial of the collisional suture zones below a sedimentary basin dominantly controlled by thermal subsidence (a "sag" basin, following the terminology of Nelson, 1992).

Recent studies of seismic tomography of the mantle below continents challenge, however, a view considering a complete removal of the mantle roots of ancient orogens. Poupinet et al (2003), reviewing data of mantle seismic tomography across different ancient stable intracontinental suture zones, showed that they still display sharp contrasts of seismic velocities that can extend into the mantle up to 200-250 km depth. This is, for example, the case across some Paleozoic suture zones such as the Teisseyre-Tornquist zone (the so-called Trans-European Suture Zone)(Zielhuis and Nolet, 1994), the central Urals (Poupinet et al, 1997) or the Chinese Tien-Shan (Poupinet et al, 2002). The persistence of such sharp velocity contrasts over several hundred million years suggests that they result from compositional heterogeneities of the mantle and therefore imply the preservation of, at least, part of the subducted lithosphere on a long-term below these suture zones.

To further tackle this problem, we present here some data of seismic tomography of the mantle across the Upper Paleozoic Variscan suture zones of Northern France, now buried below the sedimentary cover of the Permian-Mesozoic Paris basin. The latter, resting upon the collapsed Variscan orogenic belt, has been considered in recent times as a possible product of some large-scale lithospheric delamination process (Nelson, 1992; Prijac et al, 2000; Ziegler et al, 2004). Images of the P-wave tomography of the mantle below the Paris basin, extracted from the Euro-Mediterranean PM0.5 velocity model of Piromallo and Morelli (2003), will be used here to constrain the present geometry of the mantle below the suture zone, thereby questioning a possible incomplete removal of the orogenic root. Integration of these results into the tectonic, metamorphic and magmatic framework of both orogenic development and subsequent basin formation will lead us to propose a new view of the geodynamical evolution of the Variscan belt and of the overlying Paris basin in Northern France.

2. The Paris basin and its Variscan substratum: geological constraints

2.1. Geological overview of the Paris basin

As previously mentioned, the Paris basin is a wide intracratonic trough, lying on top of the Upper Paleozoic Variscan suture zones and trapping in its present-day centre up to 3 km of Permian to Miocene sedimentary deposits (Fig. 1). As exemplified by the map of Fig. 1, its geometry has, however, been strongly modified by Cenozoic deformations expressed both by local anticlines (i.e. the Bray and Boulonnais-Artois anticlines) due to the tectonic inversion of some basin-controlling normal faults (Mansy et al, 2003; Ziegler and Dèzes, 2007) and the large-scale uplift and erosion of the eastern border of the basin in response to the combined effects of lithospheric rifting and buckling in the foreland of the Alpine collisional belt (Cloething et al, 1999; Guillocheau et al, 2000; Ziegler and Dèzes, 2007; Bourgeois et al, 2007).

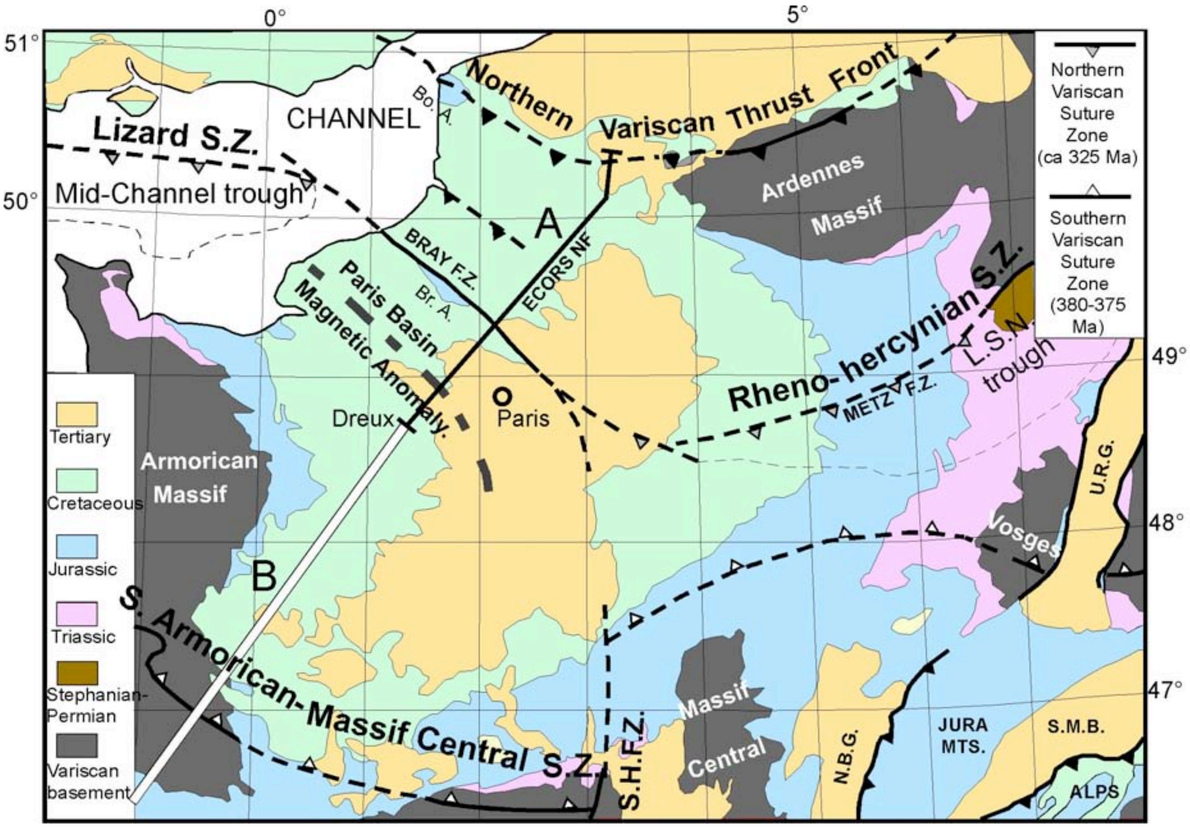

Fig. 1. Geological sketch map of the Paris basin and of the surrounding massifs (after Chantrainne et al, 1996) with location of the main buried tectonic features of the Variscan basement. A thick dashed line reports the main axis of the Paris Basin Magnetic Anomaly. Thin dashed lines report the general sub crop extensions of the Lorraine-Sarre-Nahe (L.S.N.) and Mid-Channel Late Carboniferous-Early Permian troughs. The lines A and B refer to the trace of the Northern France ECORS deep seismic reflexion profiles and to the general crustal-scale cross-section presented in Fig. 2; A: vertical survey; B: wide-angle survey (see original seismic data in Matte and Hirn, 1988). S.H.F.Z.: Sillon Houiller Fault zone; U.R.G.: Upper Rhine Graben; N.B.G.: Northern Bresse Graben; S.M.B.: Swiss Mollasic Basin; Br. A.: Bray anticline; Bo. A.: Boulonnais anticline.

Apart from this late uplift phase which controlled tertiary depositional systems, subsidence patterns within the Late Paleozoic-Mesozoic sequences suggest that the basin development was dominantly driven by a long-term thermal cooling of the lithosphere subsequent to an early phase of rifting during Stephanian-Lower Permian times (ca 300-280 Ma BP)(Prijac et al, 2000; Le Solleuz et al, 2004; Ziegler et al, 2004). Thick syn-rift continental deposits accumulated within two main intramontane half-grabens, closely juxtaposed to the Northern Variscan Suture zone (NVSZ) (Fig. 1): the Lorraine-Sarre-Nahe trough (L.S.N. in Fig. 1) along the Rhenohercynian segment of the NVSZ (Henk, 1993; Korsch and Schäfer, 1995; Oncken et al, 2000; Littke et al, 2000) and the Mid-Channel trough along the Lizard segment of the NVSZ (Bois et al, 1994; Ruffell et al, 1995). Deep seismic profiles across these main Late Paleozoic depositional centres provide evidence for high subsidence and extension rates (Lefort and Jaffal, 1994; Henk, 1993) allowing more than 4 km of Stephanian-Permian continental deposits to be trapped, for example, in the L.S.N. trough (Korsch and Schäfer, 1995; Littke et al, 2000). Such syn-rift troughs are, however, highly localized. Across the main part of the Paris basin, the Late Paleozoic syn-rift sequence is absent or developed very locally along narrow transtensional fault zones of the Variscan substratum thereby showing the persistence of a significant relief over much of the Paris basin area during that initial rifting stage. From Middle Permian times onward, post-rift thermal subsidence dominantly controlled the drawdown of the Variscan relief and the sedimentation propagated gradually onto the basin borders as shown by the progressive onlap of Triassic and Jurassic rocks onto the northern and southern margins of the basin (Fig. 1) (e.g. Mégnien, 1980; Guillocheau et al, 2000). During the initial rifting stage (classically referred to as the Late Variscan stage), an intense magmatic and hydrothermal activity affected both the incipient intramontane basins and the internal Variscan zones, situated mainly south of the NVSZ (i.e. Vosges, Black Forest, Alps, Armorican massif, Massif Central)(e.g., Bonin et al, 1993; Carron et al, 1994; Ploquin and Stussi, 1994; Schaltegger, 1997; von Seckendorff et al, 2004). As noted in the recent review of Prijac et al (2000), this extensive magmatic event, that relayed the synorogenic granitoid generation, is characterized by increased mantle melting and especially high thermal gradient in the lithosphere significant for the post-thickening extensional collapse of the Variscan belt and a possible associated lithospheric delamination.

2.2. Tectonic outline of the Variscan belt in Northern France

The main structural elements of the Variscan orogenic belt in Northern France are summarized on the geological map of fig. 1 and the general cross-section of fig. 2. As exemplified in these figures, it formed in Upper Paleozoic times as a wide double-verging orogenic wedge characterized by two major superimposed suture zones (e.g. Matte and Hirn, 1988; Autran et al, 1994; Matte, 2001; Franke, 2006):

(1) The Southern Variscan suture zone (SVSZ), generally referred to as the South Armorican-Massif Central suture zone, corresponds to the northward underthrusting of the Gondwana margin below the Armorica microplate (or Armorica Terrane Assemblage)(e.g., Matte, 2001; Franke, 2006). The SVSZ is relatively well exposed in the Armorican, Central

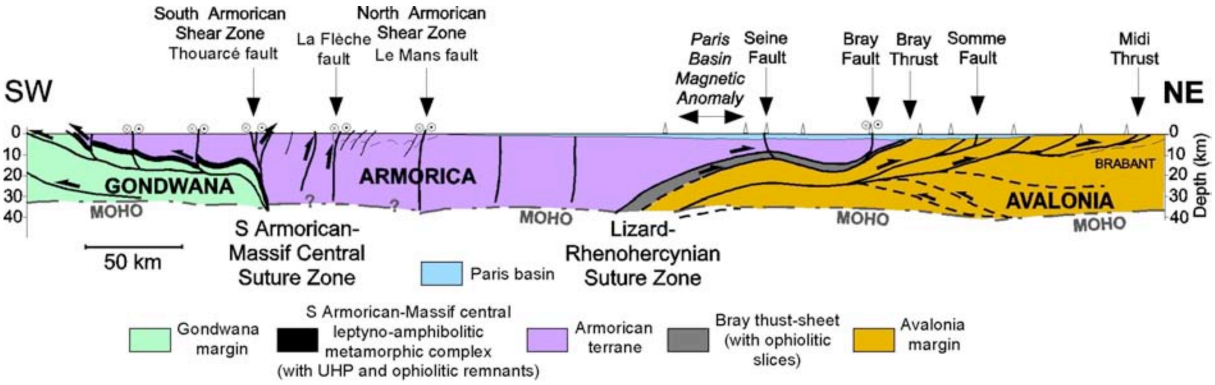

Fig. 2. Crustal-scale geological cross-section through the N France Variscan orogenic system and the overlying Paris basin based on the ECORS N France seismic data (see Matte and Hirn, 1988).

and Vosges massifs and involves a large stack of S-verging metamorphic nappes (Matte, 1986; Ledru et al, 1989). Although its precise structure still remains controversial, particularly regarding the number of pre-orogenic individual oceanic basins (Matte, 1998; Cartier et al, 2001; Ballèvre et al, 2009), it is characterized by widespread remnants of High Pressure (HP) and Ultra High Pressure (UHP) metamorphic units, buried at some lithospheric mantle depths (up to ca 100 km) during a continental subduction process, and subsequently exhumed and partly melted during the incipient collisional phase at about 380 Ma (Upper Devonian times)(Fig. 3)(Matte, 1998; Lardeaux et al, 2001; Faure et al, 2008; Ballèvre et al, 2009);

(2) The Northern Variscan suture zone (NVSZ), exemplified by the Lizard ophiolitic complex in Southern Britain (e.g., Cook et al, 2002) and the Northern Phyllite zone in the South-western Rhenish Massif in Germany (e.g., Anderle et al, 1995; Oncken et al, 1995), is completely buried in Northern France below the Permian-Mesozoic deposits of the Paris basin. Its general structure has however been imaged by deep seismic reflection profiles, i.e. the ECORS Northern France profile (Fig. 2)(Cazes et al, 1986; Matte and Hirn, 1988) and the SWAT profiles across the mid-Channel basin (Le Gall, 1990; Bois et al, 1994). Below the Paris basin, the suture zone is generally assumed to correspond to the N-verging Bray thrust, that extends, through a large structural bend, westward into the mid-Channel Lizard thrust and eastward into the Hunsrück-Northern Phyllite thrust zone of the Rhenohercynian domain (Fig. 1). Along the ECORS Northern France profile, it is characterized, south of the surface reactivated sub-vertical Bray fault, by prominent mid-crustal S-dipping reflectors that become less steep at shallow depth and join the base of the Paris basin sedimentary cover few kilometres north of the surface Bray fault (e.g. Cazes et al, 1986; Matte and Hirn, 1988). Such a crustal-scale ramp-flat attitude of the Bray thrust is accompanied by a general antiformal-stack geometry of the hangingwall thrust units (Fig. 2). Although still strongly debated (e.g.,

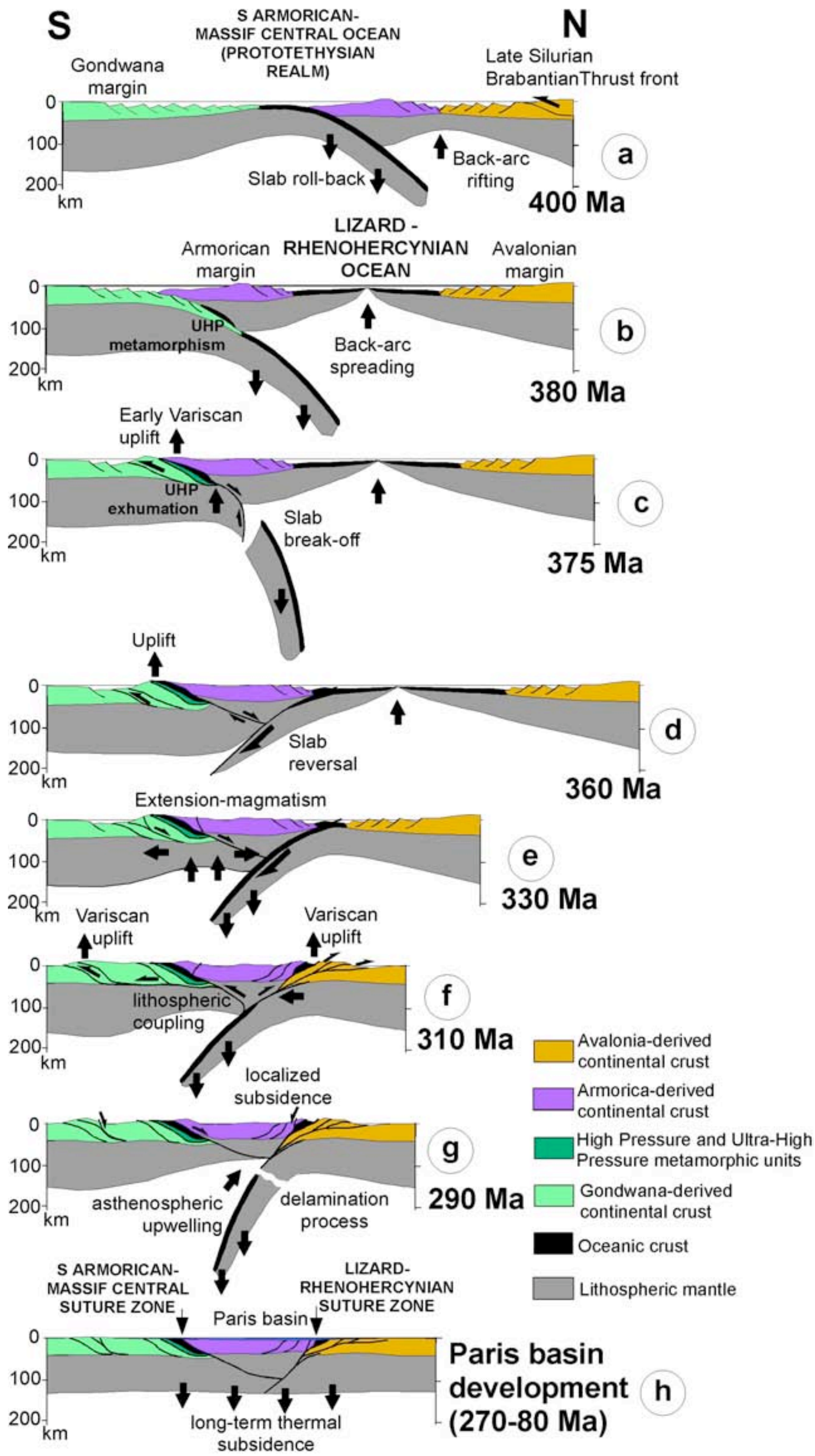

Fig. 3. Synthetic lithospheric-scale model of the geodynamical evolution of the Variscan orogenic system in France. a) Situation at 400 Ma BP: northward subduction of the S Armorican-Massif Central oceanic lithosphere below Armorica and back-arc rifting between Armorica and Avalonia. Note that the precursor Rheic ocean as defined by Cocks and Fortey (1982) has to be concealed before that time in the studied transect (see the recent synthesis on that topics in Shail and Leveridge, 2009); b) situation at 380 Ma BP: continental subduction of the Gondwana margin below Armorica (based on the continental subduction model of Matte, 1998) and oceanic spreading along the Lizard-Rhenohercynian back-arc realm; c) situation at 375 Ma BP: collision between Gondwana and Armorica (Early Variscan phase), exhumation of ultra-high pressure metamorphic rock

(S Armorican, Massif Central and Vosges massifs) and break-off of the S Armorican-Massif Central ocean slab (based on the model of Matte, 1998); d) situation at 360 Ma BP: Reversal of the subduction slab, initiation of the southward subduction of the Lizard-Rhenohercynian realm and final stage of thrusting propagation along the Gondwana margin; e) situation at 330 Ma BP: final stage of subduction of the Lizard-Rhenohercynian oceanic realm; note the related mantle upwelling below the upper plate and its possible impacts on the heating and weakening of the previously thickened Armorica-Gondwana continental assemblage (i.e. syn-orogenic magmatism, high-temperature metamorphism and extension); f) situation at 310 Ma BP: collision of the Armorica terrane assemblage and Avalonia (Variscan phase) inducing the inversion of Lizard-Rhenohercynian northern margin and the compressional (or locally transpressional) deformation of the Southern Variscan Suture Zone; note the high lithospheric coupling necessary for the propagation of shortening far into the upper plate (i.e. few hundred of kilometres south of the Northern Variscan Suture Zone, up to the present Pyrenees); g) situation at 290 Ma BP: delamination of the Variscan lithosphere and related asthenospheric upwelling culminating below the Northern Variscan Suture Zone; note the associated localized extension and subsidence controlling the development of Late Carboniferous-Early Permian troughs below the Paris basin (i.e. the Lorraine-Sarre-Nahe and Mid-Channel troughs); g) present situation after the thermal restoration of the lithosphere and the related long-term thermal subsidence driving primarily the Paris basin development.

Pham et al, 2000), classical interpretations consider this thrust stack to include lenses of basic and ultra-basic ophiolitic rocks that would create a large magnetic anomaly (the Paris Basin Magnetic Anomaly, PBMA) and an associated gravity anomaly when corrected for Mesozoic sedimentary deposits (Autran et al, 1986; Matte and Hirn, 1988; Autran et al, 1994). As shown in the map of Fig. 1, the first-order trace of the PBMA clearly follows the trend of the superficial Bray lineament as well as other main Variscan tectonic features thus suggesting its suture-related origin. Deep drilling (3,5 km) through the surface anomaly in the SE part of the PBMA (Sancerre-Couy borehole) could not however recover the rocks originating such significant magnetic anomaly (Guillen et al, 1990). Hence, the precise origin of the PBMA still remains unconstrained.

Although buried on a large part, a very striking feature of the NVSZ is the lack of exhumed HP metamorphic rocks. In the Northern Phyllite zone, for example, peak pressure conditions recorded at the suture zone do not exceed 6 kbars (Massonne, 1995) thus showing the limited amount of burial undergone by crustal units accreted at the northern Variscan thrust wedge. The latter units involve pieces of continental crust that belonged formerly to the southern margin of the Avalonia continent, separated from Armorica in Early Devonian times by opening of the Lizard-Rhenohercynian oceanic realm (Fig. 3)(Meilliez et al, 1991; Franke, 1995; 2000; Oncken et al, 2000; Littke et al, 2000; Shail and Leveridge, 2009). Subsequent southward underthrusting of the thinned Avalonian continental crust occurred during the final collisional process with the Armorica-Gondwana assemblage in Upper Carboniferous times (ca 325-305 Ma). During that collisional event, the former early Variscan structures situated within the Armorica-Gondwana upper plate were strongly deformed (e.g., Bitri et al, 2003), accommodating in particular, a significant component of dextral transpression expressed by some major crustal transcurrent shear zones (i.e. the South-Armorican and North-Armorican shear zones)(fig 2). On another hand, thrusting propagated southward into the Armorica-Gondwana assemblage as a retro-wedge some few hundred kilometres far from the NVSZ (i.e. up to the present Pyrenean belt) thereby indicating a strong mechanical coupling between the Avalonian and Armorican-Gondwanian lithospheres during the collisional process (Fig. 3). Such large deformation zone has been frequently compared to the Himalayan-Tibetan belt where active thrusting is transferred northward into Asia up to the Kun Lun-Qilian Shan ranges, about thousand kilometres north of the suture zone (e.g., Ménard and Molnar, 1988). Alike the Tibetan belt, some high Variscan plateaus have been suggested to occur through Late Carboniferous times within the internal zones of the belt (Ménard and Molnar, 1988; Becq-Giraudon and Van den Driessche, 1994). As convergence proceeded along the NVSZ, it is worth to note that the latter experienced pervasive extensional deformations, High Temperature metamorphism and magmatism as shown by a large set of studies in the Armorican, Central and Vosges massifs (e.g., Van den Driessche and Brun, 1989; Faure and Pons, 1991; Rey et al, 1992; Faure and Becq-Giraudon, 1993; Burg et al, 1994; Gardien et al, 1997; Cagnard et al, 2004). Thermal relaxation and the related gravitational collapse of the thickened Variscan crust have been generally considered as the main driving mechanisms for such syn- to late-orogenic extensional deformations (Ménard and Molnar, 1988; Malavieille et al, 1990; Costa and Rey, 1995; Le Pichon et al, 1997). The subduction of the Lizard-Rhenohercynian slab below the lithosphere of the Armorica-Gondwana Assemblage and its possible final removal at the end of Carboniferous times can be, however, regarded as competing mechanisms to explain increased heating and weakening of the previously thickened upper plate and the resultant extensional collapse of the Variscan internal zones (Fig. 3)(e.g. Henk et al, 2000, Prijac et al, 2000; Arnold et al, 2001).

3. Images of the mantle roots of the Variscan collisional belt below the Paris basin

In recent years, mantle seismic tomography has been increasingly used to image the geometry of ancient subducted slabs (e.g. Van der Voo et al, 1999; Bunge and Grand, 2000; Facenna et al, 2003). Long-lived compositional anomalies in the mantle resulting from past subduction

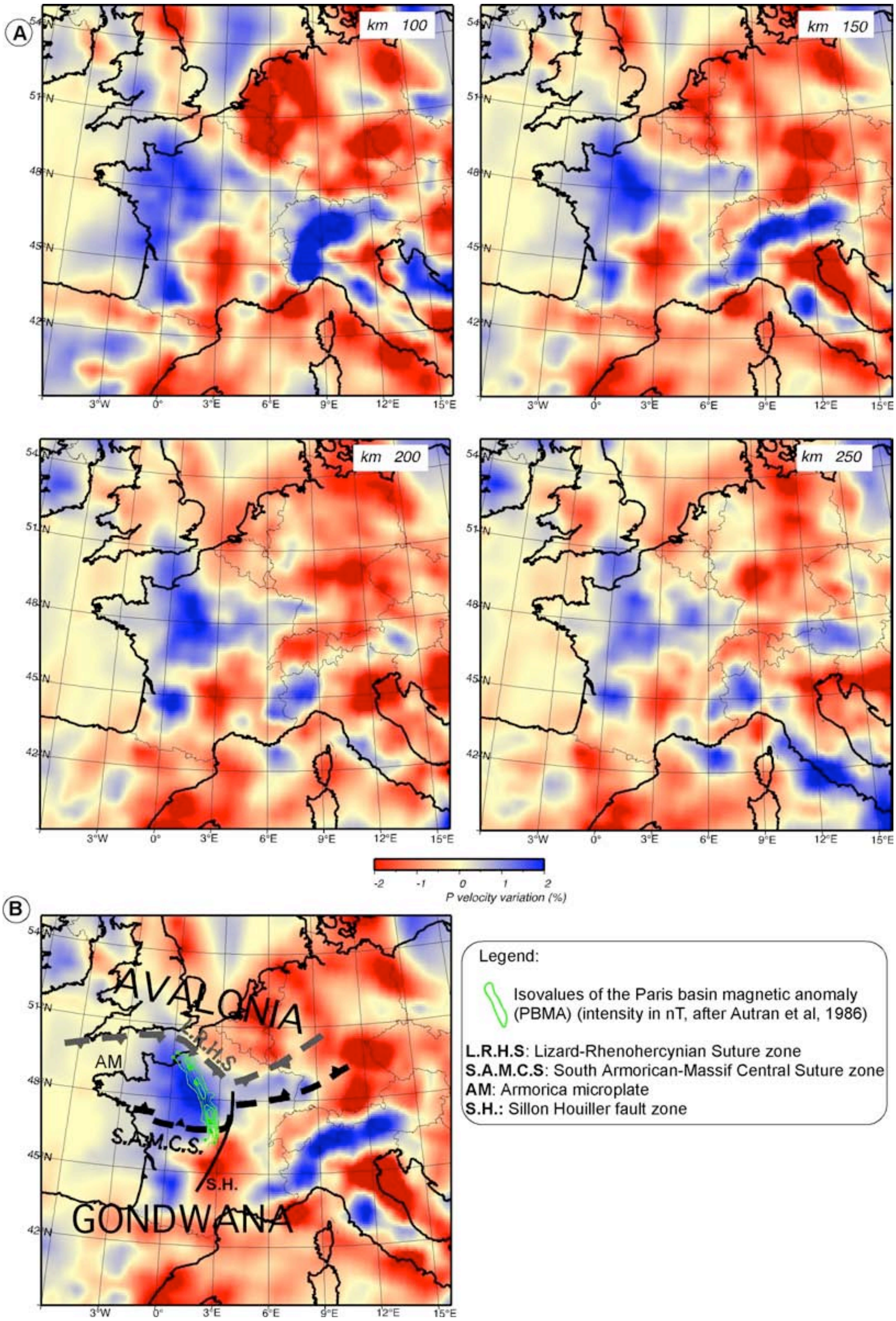

Fig. 4. A) 100, 150, 200 and 250 km depth horizontal slices of the European-scale PM0.5 mantle seismic tomography model centred on the Paris basin area. See Piromallo and Morelli (2003) for a description of the model at greater depths. P-velocity perturbation is displayed with respect to reference model *sp*6 (Morelli and Dziewonski, 1993); B) 150 km depth map of the PM0.5 model compared to the main structural features of the Paris basin substratum; note the general moulding of the high velocity mantle seismic anomaly on the buried Lizard-Rhenohercynian Suture Zone in Northern France and its spatial correlation with the Paris basin magnetic

anomaly (intensity isovalues after Autran et al, 1986); note also the eastward limitation of the main anomaly by the Sillon Houiller Fault Zone, a major transfer fault of the Variscan orogenic system.

events have been suggested to induce seismic velocity heterogeneities in the mantle that could persist over several hundred million years (Judenherc et al, 2002; Sol et al, 2002; Poupinet et al, 2003; Artemieva, 2009), i.e. much longer than if they were exclusively due to temperature variations. Therefore, in old suture zones, mantle seismic tomography can significantly help in defining remnants of ancient deeply buried slabs and thus in constraining geodynamical models for past orogenic systems. Following this approach, we present here images of the P-wave anomalies in of the mantle below the Paris basin extracted from the Euro-Mediterranean PM0.5 velocity model of Piromallo and Morelli (2003)(Fig. 4 and 5). This velocity model, obtained by inversion of the International Seismological Centre (1964-1995) P wave delay times, has been largely used to image recent geodynamical processes across the Alpine-Mediterranean belt (Facenna et al, 2003; 2004, 2006; Vignaroli et al, 2008; Jolivet et al, 2009). Alike such recent and active geodynamical zones across the Mediterranean area, the mantle anomalies below cratonic areas of most of continental Europe can be imaged by the model at a relatively short wavelength (see Piromallo and Morelli (2003) for a detailed description of the model resolution). A very striking feature, revealed by the PM0.5 tomographic model, is the existence of a significant positive seismic velocity anomaly in the upper mantle below the Paris basin (fig. 4). The latter is particularly well defined between 100 and 250 km depth (i.e. at the base of the lithosphere) and corresponds to P-wave seismic velocity exceeding 1.5-2% compared to the global reference velocity model sp6 of Morelli and Dziewonski (1993). Such amplitude of the anomaly is highly significant and comparable to that observed below the Alpine belt (fig. 4). Moreover, as shown by the ray density plot of the cross-sections of fig. 5c (see also the ray density map of Piromallo and Morelli (2003) for a more general view), the Paris basin and surrounding areas are well sampled by seismic rays and resolution of short-wavelength synthetic anomalies is fair (fig. 5d) showing that retrieved anomalies can be considered robust features of the upper mantle. In this respect, it is worth noting that the Paris basin seismic anomaly is also visible in the P-wave model developed by Bijwaard and Spakman (2000)(see the comparison between both models in Artemieva et al, 2006) thereby corroborating its robust character.

As shown in figure 4b, presenting a 150 km depth map slice of the tomographic model along with the main features of the Paris basin substratum, the contours of the anomaly strikingly fit the trace of the Northern Variscan Suture Zone i.e. the Lizard-Rhenohercynian Suture Zone.

In more detail, the maximum velocity anomaly (in dark blue in fig. 4) exhibits a NW-SE elongated shape with an overall linear NE border that parallels the northern border of the Armorica microplate (the Bray thrust zone). Though the amplitude of the positive P-wave velocity anomaly diminishes in intensity eastward (east of the 3°E meridian), its contours describe a significant curvature that follows the trace of the Rhenohercynian suture zone in Eastern France (the northern border of the L.S.N. trough, i.e. the so-called Metz fault in the Paris basin (fig. 1)). Towards the west, in Southern England, the anomaly is not well resolved due to the low density of seismic ray sampling in this area (Piromallo and Morelli, 2003). Considering the main NW-SE striking seismic velocity anomaly in the 100-200 km range, we observe a very significant spatial correlation with the Paris Basin Magnetic Anomaly (PBMA)(fig. 4b). The seismic anomaly clearly follows the general trend of the magnetic anomaly isovalues but is slightly shifted to the SW.

From these observations, it clearly appears that the high-velocity anomaly is somewhat mould on the Variscan tectonic framework below the Paris basin. Moreover, the spatial correlation of the PBMA with the seismic velocity anomaly at the base of the lithosphere suggests that the origin of both anomalies could be related to the superficial and deep expressions of a dense and magnetic subducted lithospheric unit, related to the Variscan geodynamics. In cross-section (fig. 5), the shape of the high velocity anomaly cannot be precisely determined along its main portion, mostly due to its coalescence upward with a surface high velocity anomaly located along the Southern Variscan Suture Zone in the Armorican massif (Judenherc et al, 2002)(see transect ab in Fig. 5). However, transverse sections cutting the anomaly across its SE tip give a more resolved image of the anomalous body. As exemplified by the section cd in Fig. 5, such transects suggest that the high velocity anomaly displays a very steep dip, rooting down to about 250 km depth below the Southern border of the Paris basin and joining at the surface the Northern Variscan suture zone i.e. the Lizard-Rhenohercynian suture zone. Along this section, the ray density distribution (fig. 5c) and the impulse recovery test results (fig. 5d) show that the seismic velocity pattern is fairly well resolved below the Paris basin. The downward extension of the anomaly is, however, difficult to define precisely due to smearing inherent in the heterogeneity of ray paths along the section. Despite such smearing effect around the high seismic velocity anomaly, the presented transverse sections argue for the existence of a sub vertical body pinned down to the base of the lithosphere and extending down to a depth greater than 200 km. The upward connection of the anomaly to the Northern Variscan suture zone and the spatial SW-ward shift of the main anomalous feature at 150 km depth with respect to the PBMA suggests that it could represent

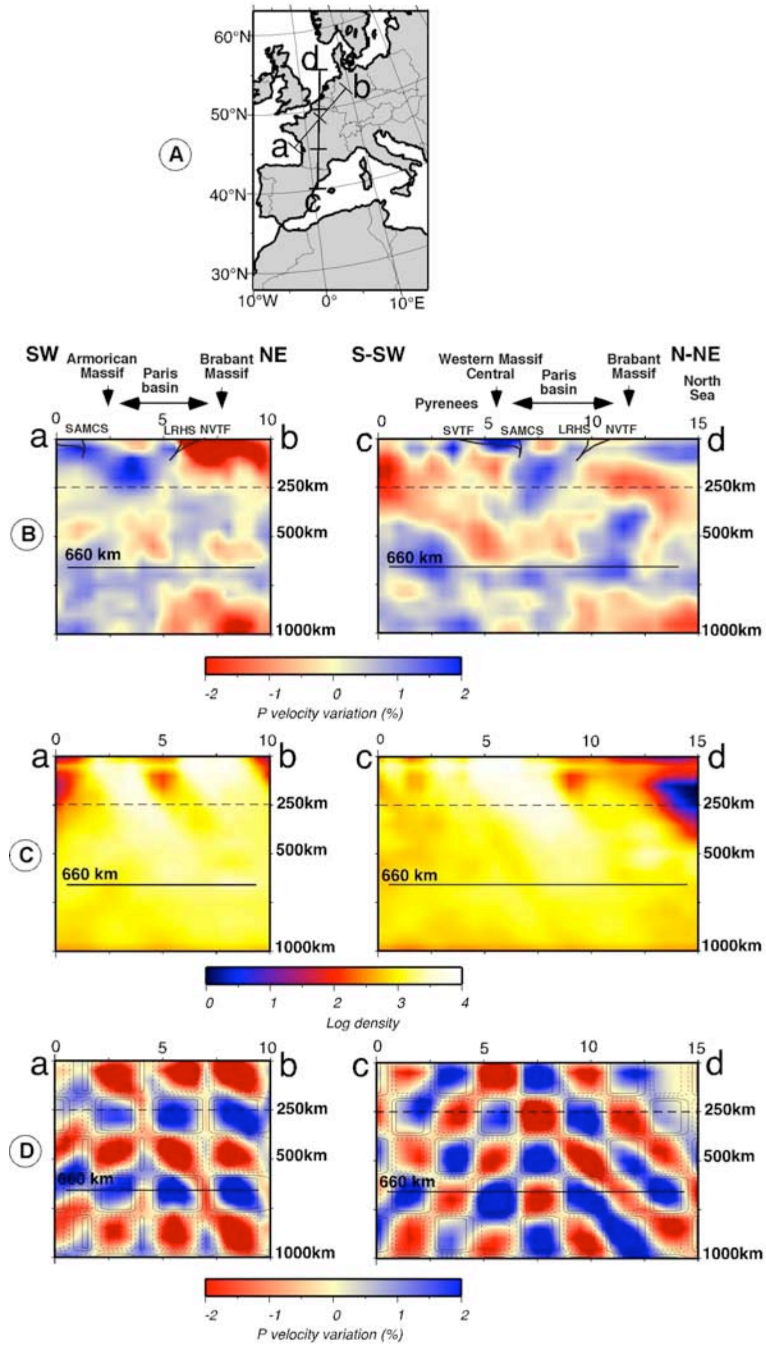

Fig. 5. A) Location of mantle seismic tomography transects of the PM0.5 model across the Paris basin high velocity anomaly. The length of the section ab is 10° along a great circle trending N050. The length of the section cd is 15° along a great circle trending N010. Ticks along the line segment indicate the distance from the southern extremity by 5° intervals. B) Mantle seismic velocity data along the sections compared to main structural features of the Variscan orogenic system and of the overlying Paris basin; NVTF: Northern Variscan Thrust Front; LRHS: Lizard-Rhenohercynian Suture Zone; SAMCS: South Armorican-Massif Central Suture Zone; SVTF: Southern Variscan Thrust Front. See text for description. C) Ray density distribution along the sections. Note the high ray density below the investigated area. D) Impulse recovery test results along the sections (contour levels of the input model at ±1% and ±3% are shown). See Piromallo and Morelli (2003) for a thorough description. P-velocity perturbation is displayed with respect to reference model *sp*6 (Morelli and Dziewonski, 1993).

a remnant of the south-dipping Lizard-Rhenohercynian subducted slab that escaped some Late orogenic removal process. Such possibility will be considered in the following thereby offering new perspectives in the understanding of the Late Variscan geodynamics in the Paris basin area.

4. Discussion and conclusion: a model of heterogeneous removal of the Variscan orogenic root below the Paris basin.

As previously mentioned, the high seismic velocity anomaly observed below the western part of the Paris basin, can be spatially correlated with the major Variscan tectonic features of the Paris basin substratum. The ca 300 Ma old subduction of the Lizard-Rhenohercynian slab along the Northern Variscan Suture zone is, however, unlikely to have induced a remnant thermal anomaly in the mantle for such a long time as shown by thermal modelling of slab/mantle interactions subsequent to subduction (e.g., Stein and Stein, 1996). Thermal perturbations induced by mantle plumes have been suggested to occur below the eastern Massif Central (Granet et al, 1995; Babuska et al, 2002) and the Eifel region in Germany (Goes et al, 1999; Ritter et al, 2001) thereby resulting in localized low-velocity seismic anomalies in the mantle (see fig. 4). Such recent thermal domes are, however, not possible to have exerted a significant influence on the observed positive velocity anomaly, which conversely requires lower temperatures than average in the mantle. Hence, no recent geodynamical process in the Paris basin area can be put forward to explain a possible thermal anomaly of the lithospheric mantle that could be responsible for the observed seismic velocity changes. These points all argue for the anomaly being the result of an heterogeneous composition of the mantle below the Paris basin inherited from the Variscan geodynamics.

Such a compositional heterogeneity of the mantle has been devoted increasing attention in recent years to account for observed seismic velocity anomalies below continents (Judenherc et al, 2002; Sol et al, 2002; Poupinet et al, 2003; Artemieva et al, 2006). The precise nature of the compositional contrasts originating such mantle seismic velocity anomalies remains, however, uncertain. Numerical seismic velocity simulations of varying continental mantle petrologic models suggest subducted eclogite layers (Sol et al, 2002) as well as iron-depleted upper mantle rocks (Deschamps et al, 2002; Artemieva, 2009) to be the main relevant contributors to such high seismic velocity anomalies in the mantle. As pointed out by Artemieva (2009), melt extraction during subduction process can produce a relative iron depletion of the surrounding mantle potentially resulting in a seismic velocity increase.

Hence, in the present state of knowledge, the depletion of orogenic roots and the occurrence of subducted eclogite layers into the upper mantle can be regarded as the most likely mechanisms to account for the observed high velocity anomalies associated with ancient suture zones.

In agreement with these recent studies, we interpret the Paris basin mantle anomaly as the result of a remnant slab of oceanic lithosphere (the Lizard-Rhenohercynian ocean) that was subducted during the Variscan orogenic process and preserved in a stable way for more than 300 Ma at the base of the continental lithosphere (down to about 250 km depth). A first implication of such interpretation concerns the necessary heterogeneity of the lithosphere-asthenosphere boundary below the Paris basin. As noted by Artemieva and Mooney (2002) and Poupinet et al (2003) reviewing mantle tomography data below continents, the lithosphere-asthenosphere boundary cannot be regarded as an homogeneous feature but rather as strongly heterogeneous with very large depth-variations over relatively short distances (the reworked continental keels of Artemieva and Mooney (2002)). The conditions for such orogenic roots to be preserved at the base of the continental lithosphere over several hundred millions years, were questioned by Artemieva and Mooney (2002) and Karato (2010), respectively on a geodynamical and rheological point of view. The main outcome of these studies is that the preservation of stable orogenic roots on several hundred million years timescale is possible in the case of low plate motion velocities (i.e. low basal drag) and large deep upper mantle rheological contrasts (possibly connected to the depleted nature of subducted slabs at the base of the lithosphere).

A second implication, inherent in the existence of a buried residual slab below the Paris basin, is the necessary incomplete removal of the Variscan root at the end of the orogenic process i.e. in Late Paleozoic times. Figure 6 depicts the geometry of the Lizard-Rhenohercynian slab inferred from mantle tomography. A very interesting point to be noticed on that 3-D geodynamical scheme is that the location of the inferred remnant slab is spatially anti-correlated with the occurrence at the surface of the deep Stephanian-Permian syn-rift troughs at the base of the Paris basin. As previously mentioned, the latter (i.e. the Lorraine-Sarre-Nahe (L.S.N.) trough and the Mid-Channel trough) are situated in the direct hangingwall of the Northern Variscan Suture Zone (N.V.S.Z.), reactivating at depth the main boundary thrust between Avalonia and the Armorica Terrane Assemblage (the Lizard thrust in the mid-Channel area and the Phyllite Zone boundary thrust in the Rhenohercynian area)(e.g., Henk, 1993; Bois et al, 1994; Ruffell et al, 1995; Oncken et al, 2000). Such significant change in the post-orogenic extension pattern along the N.V.S.Z. and its correlation with the present location of a residual slab suggest that the Variscan root was not homogeneously removed in Late Paleozoic times and that the present mantle geometry is primarily inherited from the Late Variscan delamination process. Hence, asthenospheric upwelling induced by detachment of the Northern Variscan slab along the Rhenohercynian and Lizard segments can be viewed as a major driver for the Stephanian-Permian magmatism and extension initiating the Paris basin subsidence. Such localized occurrence of asthenospheric upwelling and of the related thermal effects are consistent with the general subsidence pattern in the Paris basin that clearly displays a propagation with time from the early syn-rift depocenters (the L.S.N. and Mid-Channel troughs in Stephanian-Permian times) towards the Bray area where sediments deposited only by Latest Triassic times (e.g., Megnien, 1980; Guillocheau et al, 2000; Le Solleuz et al, 2004). The lateral conduction of the thermal anomaly from the zones of mantle upwelling to the adjacent lithosphere by Late Paleozoic-Early Mesozoic times would sustain some Variscan relief over the western part of the Paris basin up to the Late Triassic. The subsequent thermal subsidence that primarily drives the overall Paris basin development (Prijac et al, 2000; Le Solleuz et al, 2004) thereby would match such initial heat transfers from the zones where the Northern Variscan slab was detached to the zones where it was not (i.e. migrating towards the Bray area).

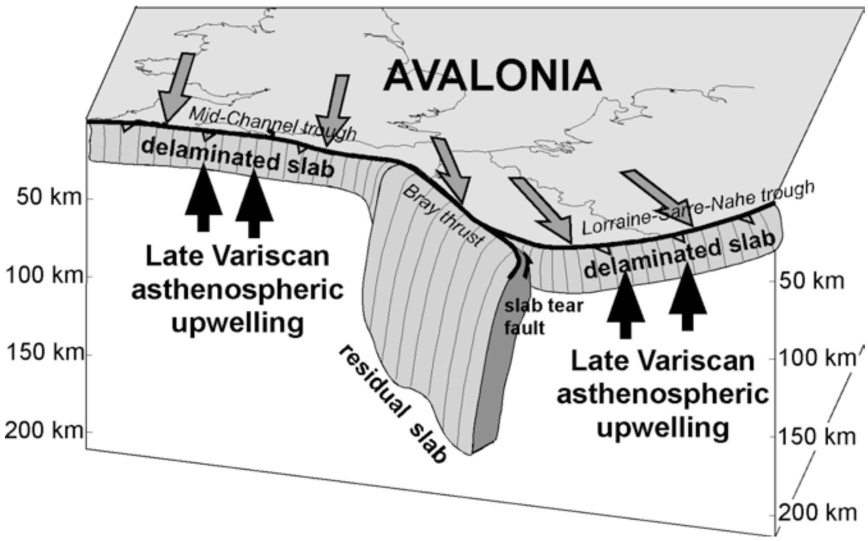

Fig. 6. 3D sketch diagram illustrating the geometry of the Variscan root zones below the Paris basin at the end of the orogenic process (i.e. Late Carboniferous-Early Permian times) as inferred from mantle seismic tomography data. Note the spatial correlation of delaminated lithospheric roots with the location of Stephanian-Early Permian syn-rift troughs at the bottom of the Paris basin (the Lorraine-Sarre-Nahe and Mid-Channel troughs). Note also the necessary occurrence of a slab tear fault limiting to the east the residual slab, spatially related to the Sillon Houiller transfer fault within the upper plate (see fig. 4B for location). The arrows along the Northern Variscan Suture Zone correspond to the convergence directions as deduced from structural data along the Northern Variscan thrust front.

At a larger scale, our data emphasize the role of the subduction of the Lizard-Rhenohercynian slab in the extension and collapse of the thickened Variscan lithosphere in Carboniferous times. As sketched in Fig. 6, the delamination of the Rhenohercynian orogenic root below the L.S.N. segment and its preservation along the Bray segment necessarily requires a segmentation of the subducted panel and the existence of a lateral slab tear fault in between these two decoupled slab parts (see Rosenbaum et al, 2008 for the description of the kinematics of such faults). The eastern limit of the buried residual slab (i.e. of the high velocity seismic anomaly) strikingly corresponds to a major Late Variscan transfer fault of lithospheric scale, the Sillon Houiller Fault Zone (S.H.F.Z.)(Burg et al, 1990)(see its location in Fig. 1 and in Fig. 4b). The latter represents actually a significant vertical boundary separating two different lithospheric blocks (the western and eastern Massif Central blocks) (Babuska et al, 2002) that suffered large differences of synorogenic extension by the end of the Carboniferous thereby resulting in about 70-100 km of apparent left-lateral offset between the two blocks (Burg et al, 1990). This tectonic line localizes some Stephanian-Permian coal-bearing pull-apart basins arguing for its main activity during Late Variscan times (e.g., Grolier and Letourneur, 1968; Bonijoly and Castaing, 1984) as the slab detachment occurred along the Rhenohercynian suture zone. Synorogenic granitic plutons emplaced along this line suggests however that it has been active as early as in Visean times (Thiery et al, 2009) when the subduction was still proceeding. As it limits, to the west, the eastern Massif Central block that suffered increased synorogenic extension compared to the western block (Burg et al, 1990), we can infer that the necessary retreat of the Rhenohercynian slab (east of the inferred slab-tear fault) before its detachment is likely to have exerted a significant control on the degree of extensional deformations of the Variscan internal zones in Carboniferous times. The Sillon Houiller Fault zone would thus represent a major transfer zone resulting from the upper plate accommodation of a slab tear fault limiting subducted slab segments suffering initially, variable amounts of retreat and finally, having been detached or not from the lithospheric orogenic root.

Ultimately, such inferences suggest some direct relationships between the dynamics of the Lizard-Rhenohercynian subducting slab segments during the incipient phase of the orogenic process and the possibility for the Variscan lithospheric orogenic roots to be delaminated at the final stage of the collisional process. As shown in Fig. 6, the orientation of the Bray segment is strongly oblique to the general N-S trending convergence between Avalonia and Armorica as revealed by shortening indicators along the Northern Variscan thrust system (e.g., Averbuch et al, 2004). In this area, this obliquity resulted in the partitioning of movement between NNE-verging thrusts and major dextral wrench faults such as the Bray fault in the hangingwall of the Bray thrust (Fig. 2)(Matte et al, 1986). As a consequence, the amplitude of shortening normal to the trench along the Bray segment is necessarily reduced compared to trench segments situated in more frontal position with respect to the convergence, such as the Rhenohercynian and Lizard segments. The length of the slab subducted along the trench should therefore have varied accordingly along these different segments thereby affecting the slab pull force, the lateral migration of both trench and slab and the resultant pattern of surrounding mantle flow (e.g. Becker et al, 1999; Funiciello et al, 2006; Jolivet et al, 2009). Hence, at the end of the collisional process, there were presumably some large variations in the slab pull force exerted on the subducted continental lithosphere along the different segments of the collision zone which can be considered as a first-order driving mechanism for the heterogeneous detachment of the subducted Variscan lithosphere (e.g., Davies and von Blankenburg, 1995). In this respect, the low negative buoyancy exerted by the restricted size of the slab subducted along the Bray segment could be considered as the main relevant parameter to explain its non-delamination at the end of the collisional process, by Late Carboniferous-Earliest Permian times.

Acknowledgements

The authors gratefully acknowledge C. Facenna, J. Ferrière and M. Seyler for their relevant scientific comments and constructive criticism on this study at different stages of its evolution. B. Minguely is thanked for his help in the geo-localization procedure of the PBMA.

References

Anderle, H.J., Franke W., Schwab, M., 1995. Northern Phyllite Zone-stratigraphy. In: Dallmeyer, R.D., Franke, W., Weber, K. (Eds.), Pre-Permian geology of Central and Eastern Europe. Springer-Verlag, Berlin, Heidelberg, pp. 99-107.

Arnold, J., Jacoby, W.R., Schmeling, H., Schott, B., , 2001. Continental collision and the dynamic and thermal evolution of the Variscan orogenic crustal root- numerical models. Journal of Geodynamics 31, 273-291.

Artemieva, I.M., Mooney, W.D., 2002. On the relations between cratonic lithosphere thickness, plate motions, and basal drag. Tectonophysics 358, 211-231.

Artemieva, I.M., Thybo, H., Kaban, M.K., 2006. Deep Europe today: geophysical synthesis of the upper mantle structure and lithospheric processes over 3.5 Ga. In: Gee, D.G., Stephenson, R.A. (Eds), European Lithosphere Dynamics. Geological Society, London, Memoirs 32, pp. 11-41.

Artemieva, I.M., 2009. The continental lithosphere: Reconciling thermal, seismic, and petrologic data. Lithos 109, 23-46. doi: 10/1016/j.lithos.2008.09.015.

Autran, A., Castaing, C., Debeglia, N., Guillen, A., Weber, C., 1986. Nouvelles contraintes géophysiques et géodynamiques sur l'interprétation de l'anomalie magnétique du bassin de Paris: hypothèse d'un rift paléozoïque refermé au Carbonifère. Bull. Soc. géol. France 8 (II), 125-141.

Autran, A., Lefort, J.P., Debeglia, N., Edel, J.B., Vigneresse, J.L., 1994. Gravity and magnetic expression of terranes in France and their correlation beneath overstep sequences. In: Keppie, J.D. (Ed.), Pre-Mesozoic geology in France and related areas. Springer-Verlag, Berlin, Heidelberg, pp. 49-72.

Averbuch, O., Mansy, J.-L., Lamarche, J., Lacquement, F., Hanot, F., 2004. Geometry and kinematics of the Boulonnais fold-and-thrust belt (N France): implications for the dynamics of the Northern Variscan thrust front. Geodinamica Acta 17/2, 163-178.

Babuska, V., Plomerova, J., Vecsey, L., Granet, M., Achauer, U., 2002. Seismic anistropy of the French Massif Central and predisposition of Cenozoic rifting and volcanism by Variscan suture hidden in the mantle lithosphere. Tectonics 21, 4,1029, doi: 10.1029/2001TC901035.

Ballèvre, M., Bosse, V., Ducassou, C., Pitra, P., 2009. Palaeozoic history of the Armorican massif: Models for the tectonic evolution of the suture zones. C.R. Geoscience 341, 174-201.

Becker, T.W., Faccenna, C., O'Connell, R.J., Giardini, D., 1999. The development of slabs in the upper mantle: insights from numerical and laboratory experiments. J. Geophys. Res. 104 (B7), 15207-15226.

Becq-Giraudon, J.F., Van den Driessche, J., 1994. Dépôts périglaciaires dans le Stéphano-Autunien du Massif Central: témoin de l'effondrement gravitaire d'un haut plateau hercynien. C. R. Acad. Sci. Paris 318 (II), 675-682.

Bijwaard, H., Spakman, W., 2000. Non-linear global P-wave tomography by iterated linearized inversion. Geophysical Journal International 141, 71-82.

Bird, P., 1979. Continental delamination and the Colorado Plateau. J. Geophys. Res. 84, 7561-7571.

Bird, P., Baumgartner, J., 1981. Steady propagation of delamination events. J. Geophys. Res. 86, 4891-4903.

Bitri, A., Ballèvre, M., Brun, J.-P., Chantraine, J., Gapais, D., Guennoc, P., Gumiaux, C., Truffert, C., 2003. Imagerie sismique de la zone de collision hercynienne dans le Sud-est du Massif armoricain (projet Armor 2/programme Géofrance 3D). C. R. Geoscience 335, 969-979.

Bois, C., Cazes, M., Choukroune, P., Gariel, O., Hirn, A., Le Gall, B., Lefort, J.P., Matte, P., Pinet, B., 1994. Seismic reflection images of the pre-Mesozoic crust in France and adjacent areas. In: Keppie, J.D. (Ed.), Pre-Mesozoic geology in France and related areas. Springer-Verlag, Berlin, Heidelberg, pp. 33-48.

Bonijoly, D., Castaing, C., 1984. Fracturation et genèse des bassins stéphaniens du Massif Central français en régime compressif. Ann. Soc. géol. Nord 103, 187-199.

Bonin, B., Brändlein, P., Bussy, F., Desmons, J., Eggenberger, U., Finger, F., Graf, K., Marro, C., Mercolli, I., Oberhänsli, R., Ploquin, A., von Quadt, A., von Raumer, J., Schaltegger, U., Steyrer, H.P., Vison, D., Vivier, G., 1993. Late Variscan magmatic evolution of the Alpine basement. In: von Raumer, J., Neubauer, F. (Eds.), The pre-Mesozoic geology in the Alps. Springer-Verlag, Berlin, Heidelberg, pp. 169-199.

Bourgeois, O., Ford, M., Diraison, M., Le Carlier de Veslud, C., Gerbault, M., Pik, R., Ruby, N., Bonnet, S., 2007. Separation of rifting and lithospheric folding signatures in the NW-Alpine foreland. Int. J. Earth Sci. 96, 1003-1031. doi: 10.1007/s00531-007-0202-2

Bunge, H.P., Grand, S.P., 2000. Mesozoic plate-motion history below the northeast Pacific Ocean from seismic images of the subducted Farallon slab. Nature 405 (6784), 337-340.

Burg, J.-P., Brun, J.-P.,Van den Driessche, J., 1990. Le Sillon Houiller du Massif Central français: Faille de transfert pendant l'amincissement crustal de la chaîne varisque? C. R. Acad. Sci. Paris 311, 147-152.

Burg, J.-P., Van den Driessche, J., Brun, J.-P., 1994. Syn- to post-thickening extension: mode and consequences. C. R. Acad. Sci. Paris 319, 1019-1032.

Cagnard, F., Gapais, D., Brun, J.-P., Gumiaux, C., Van den Driessche, J., 2004. Late pervasive crustal-scale extension in the South Armorican Hercynian belt (Vendée, France). Journal of Structural Geology 26, 435-449.

Carron, J.P., Le Guen de Kerneizon, M., Nachit, H., 1994. Variscan granites from Brittany. In: Keppie, J.D. (Ed.), Pre-Mesozoic geology in France and related areas. Springer-Verlag, Berlin, Heidelberg, pp. 231-239.

Cartier, C., Faure, M., Lardeux, H., 2001. The Hercynian Orogeny in the South Armorican Massif (Saint-Georges-sur-Loire Unit, Ligerian Domain, France): rifting and welding of continental stripes. Terra Nova 13, 143-149.

Cazes, M., Mascle, A., Torreilles, X., Bois, C., Damotte, X., Matte, P., Raoult, X., Pham, V.N., Hirn, A., Galdeano, X., 1986. Large Variscan overthrusts beneath the Paris basin. Nature 323 (6084), 144-147.

Chantrainne, J., Autran, A., Cavelier, C., 1996. Carte géologique de la France au 1/1 000 000. Bureau de Recherches Géologiques et Minières (Ed.), Orléans.

Cocks, L.R., Fortey, R.A., 1982. Faunal evidence for oceanic separations in the Paleozoic of Britain. J. Geol. Soc. London 139, 465-478.

Cook, C.A., Holdsworth, R.E., Styles, M.T., 2002. The emplacement of peridotites and associated oceanic rocks from the Lizard complex, southwest England. Geol. Mag. 139, 27-45.

Costa, S., Rey, P., 1995. Lower crustal rejuvenation and growth during post-thickening collapse: Insights from a crustal cross section through a Variscan metamorphic core complex. Geology 23 (10), 905-908.

Cotte, N., Pedersen, H.A., TOR Working Group, 2002. Sharp contrast in lithospheric structure across the Sorgenfrei-Tornquist Zone as inferred by Rayleygh wave analysis of TOR1 project data. Tectonophysics 360, 75-88.

Cloething, S.A.P.L., Burov, E., Poliakov, A., 1999. Lithosphere folding: Primay response to compression? (from Central Asia to Paris basin). Tectonics 18, 1064-1083.

Davies, J.H., von Blankenburg, F., 1995. Slab breakoff: A model of lithosphere detachment and its test in the magmatism and deformation of collisional orogens. Earth and Planetary Science Letters 129, 85-102.
De Boorder, H., Spakman, W., White, S.H., Wortel, M.J.R., 1998. Late Cenozoic mineralization, orogenic collapse and slab detachment in the European Alpine belt. Earth and Planetary Science Letters 164, 569-575.
Deschamps, F, Trampert, J., Snieder, R., 2002. Anomalies of temperature and iron in the uppermost mantle inferred from gravity data and tomographic models. Phys. Earth Planetary Interiors129, 245-264.
Facenna, C., Jolivet, L., Piromallo, C., Morelli, A., 2003. Subduction and the depth of convection in the Mediterranean mantle. J. Geophys. Res. 108 (B2), 2099, doi: 10.1029/2001JB001690.
Facenna, C., Piromallo, C., Crespo-Blanc, A., Jolivet, L., Rossetti, F., 2004. Lateral slab deformation and the origin of the western Mediterranean arcs. Tectonics 23, TC1012, doi:10.1029/2002TC001488.
Facenna, C., Bellier, O., Martinod, J., Piromallo, C., Regard, V., 2006. Slab detachment beneath eastern Anatolia: A possible cause for the formation of the North anatolian fault. Earth and Planetary Science Letters 242, 85-97.
Faure, M., Pons, J., 1991. Crustal thinning recorded by the shape of Namurian-Westphalian leucogranite in the Variscan belt of northwest Massif Central, France. Geology 19, 730-733.
Faure, M., Becq-Giraudon, J.-F., 1993. Sur la succession des épisodes extensifs au cours du désépaississement carbonifère du massif Central français. C. R. Acad. Sci. Paris 316 (II), 967-973.
Faure, M., Bé Mézème E., Cocherie, A., Rossi, P., Chemenda, A., Boutelier, D., 2008. Devonian geodynamic evolution of the Variscan belt, insights from the French Massif Central and Massif Armoricain. Tectonics 27, TC2005, doi: 10.1029/2007TC002115.
Franke, W., 1995. Rhenohercynian foldbelt: autochthon and non metamorphic nappe units-stratigraphy. In: Dallmeyer, R.D., Franke, W., Weber, K. (Eds.), Pre-Permian geology of Central and Eastern Europe. Springer-Verlag, Berlin, Heidelberg, pp. 33-49.
Franke, W., 2000. The mid-European segment of the Variscides: tectonstratigraphic units, terrane boundaries and plate tectonic evolution. In: Franke, W., Haak, V., Oncken, O., Tanner, D. (Eds.), Orogenic Processes: quantification and Modelling in the Variscan Belt. Geological Society, London, Special Publications 179, pp. 35-61.
Franke, W., 2006. The Variscan orogen in Central Europe: construction and collapse. In: Gee, D.G., Stephenson, R.A. (Eds.), European Lithosphere Dynamics Geological Society, London, Memoirs 32, pp. 333-343.
Funiciello, F., Moroni, M., Piromallo, C., Faccenna, C., Cenedese, A., Bui, H.A., 2006. Mapping mantle flow during retreat subduction: Laboratory models analyzed by feature tracking. J. Geophys. Res. 111, B03402, doi: 10.1029/2005JB003792.
Gardien, V., Lardeaux, J.-M., Ledru, P., Allemand, P., Guillot, S., 1997. Metamorphism during late orogenic extension: insights from the Franch Variscan belt. Bull. Soc. géol. France 168, 271-286.
Gögus, O.H., Pysklywec, R.N., 2008. Mantle lithosphere delamination driving plateau uplift and synconvergent extension in Eastern Anatolia. Geology 36 (9), 723-726. doi: 10.1130/G24982A.1
Goes, S., Sapkman, W., Bijwaard, H., 1999. A lower mantle source for Central European volcanism. Science 286, 1928-1931.
Granet, M., Wilson, M., Achauer, U., 1995. Imaging a mantle plume beneath the French Massif Central. Earth and Planetary Science Letters 136, 281-296.

Guillen, A., Bayer, R., Millon, R., Rousset, D., 1990. Evolution des hypothèses et modélisation pour l'interprétation de l'anomalie magnétique du bassin de Paris (région de Sancerre). Bull. Soc. géol. France 8 (VI), 739-748.

Guillocheau, F., Robin, C., Allemand, P., Bourquin, S., Brault, N., Dromart, G., Friedenberg, R., Garcia, J.P., Gaulier, J.M., Gaumet, F., Grosdoy, B., Hanot, F., Le Strat, P., Mettraux, M., Nalpas, T., Prijac, C., Rigollet, C., Serrano, O., Grandjean, G., 2000. Meso-Cenozoic geodynamic evolution of the Paris Basin: 3D stratigraphic constraints. Geodinamica Acta 2000, 189-246.

Grolier, J., Letourneur, J., 1968. Evolution tectonique du grand sillon houiller du Massif central français. XXIII int. Geol. Congr., vol. 1, 107-116.

Gvirtzman, Z., 2002. Partial detachment of a lithospheric root under the southeast Carpathians: Toward a better definition of the detachment concept. Geology 30 (1), 51-54.

Henk, A., 1993. Late orogenic basin evolution in the Variscan Internides: the Saar-Nahe Basin, southwest Germany. Tectonophysics 223, 273-290.

Henk, A., Von Blankenburg, F., Finger, F., Schaltegger, U., Zulauf, G., 2000. Syn-convergent high temperature metamorphism and magmatism in the Variscides: a discussion of potential heat sources. In: Franke, W., Haak, V., Oncken, O., Tanner, D. (Eds.), Orogenic Processes: quantification and Modelling in the Variscan Belt. Geological Society, London, Special Publications 179, pp. 387-399.

Houseman, G., Mc Kenzie, D.P., Molnar, P., 1981. Convective instability of a thickened boundary layer and its relevance for the thermal evoluion of continental convergent belts. J. Geophys. Res. 86, 6115-6132.

Houseman, G., Molnar, P., 1997. Mechanisms of lithospheric rejvenation associated with continental orogeny. In: Miller, J.A., Holdsworth, R.E., Buick, I.S., Hand, M., (Eds.), Continental Reactivation and Reworking. Geological Society, London, Special Publications 184, pp. 13-38.

Jolivet, L., Faccenna, C., Piromallo, C., 2009. From mantle to crust: Streching the Mediterranean. Earth and Planetary Science Letters 285, 198-209. doi: 10.1016/j.epsl.2009.06.017

Judenherc, S., Granet, M., Brun, J.P., Poupinet, G., Plomerova, J., Moquet, A., Achauer, U., 2002. Images of lithospheric heterogeneities in the Armorican segment of the Hercynian range in France. Tectonophysics 358, 121-134.

Karato, S., 2010. Rheology of the deep upper mantle and its implications for the preservation of the continental roots: A review. Tectonophysics 481, 82-98. doi: 10.1016/j.tecto.2009.04.011.

Kay, R.W., Kay, S.M., 1993. Delamination and delamination magmatism. Tectonophysics 219, 177-189.

Keskin, M., 2003. Magma generation by slab steepening and breakoff beneath a subduction-accretion complex: An alternative model for collision-related volcanism in Eastern Anatolia, Turkey, Geophys. Res. Lett., 30(24), 8046, doi:10.1029/2003GL018019.

Korsch, R.J., Schäfer, A., 1995. The Permo-Carboniferous Saar-Nahe Basin, south-west Germany and north-east France: basin formation and deformation in a strike-slip regime. Geol. Rundsch. 84, 293-318.

Lardeaux, J.M., Ledru, P., Daniel, I., Duchene, S., 2001. The Variscan French Massif Central-a new addition to the ultra-high pressure metamophic "club": exhumation processes and geodynamic consequences. Tectonophysics 332, 143-167.

Ledru, P., Lardeaux, J.-M., Santallier, D., Autran, A., Quenardel, J.-M., Floc'h, J.-P., Lerouge, G., Maillet, N., Marchand, J., Ploquin, A., 1989. Où sont les nappes dans le Massif central français. Bull. Soc. géol. France 8 (V), 605-618.

Lefort, J.-P., Jaffal, M., 1995. Anisotropie du fluage post-orogénique de la croûte inférieure litée dans la chaîne hercynienne (Manche). C. R. Acad. Sci. Paris 321 (II), 65-70.
Le Gall, B., 1990. Evidence of an imbricate crustal thrust belt in the Southern British Variscides: contributions of South-Western Approaches Traverse (SWAT) deep seismic reflection profiling recorded through the English Channel and the Celtic Sea. Tectonics 9 (2), 283-302.
Le Pichon, X., Henry, P., Goffé, B., 1997. Uplift of Tibet: from eclogites to granulites-implications for the Andean Plateau and the Variscan belt. Tectonophysics 273, 57-76.
Le Solleuz, A., Doin, M.-P., Robin, C., Guillocheau, F., 2004. From a mountain belt collapse to a sedimentary basin development: 2-D thermal model based on inversion of stratigraphic data in the Paris Basin. Tectonophysics 286, 1-27.
Littke, R., Büker, C., Hertle, M., Karg, H., Stroetman-Heinen, V., Oncken, O., 2000. Heat flow evolution, subsidence and erosion in the Rheno-hercynian orogenic wedge of central Europe.. In: Franke, W., Haak, V., Oncken, O., Tanner, D. (Eds.), Orogenic Processes: quantification and Modelling in the Variscan Belt. Geological Society, London, Special Publications 179, pp. 231-255.
Macera, P., Gasperini, D., Ranalli, G., Mahatsente, R., 2008. Slab detachment and mantle plume upwelling in subduction zones: an example from the Italian South-Eastern Alps. Journal of geodynamics 45, 32-48.
Malavieille, J., Guihot, P., Costa, S., Lardeaux, J.M., Gardien, V., 1990. Collapse of the thickened Variscan crust in the french Massif Central: Mont Pilat extensional shear zone and St Etienne late Carboniferous basin. Tectonophysics 177, 139-149.
Massonne, H.J., 1995. Northern Phyllite Zone- metamorphic evolution. In: Dallmeyer, R.D., Franke, W., Weber, K. (Eds.), Pre-Permian geology of Central and Eastern Europe. Springer-Verlag, Berlin, Heidelberg, pp. 132-137.
Matte, P., 1986. Tectonics and plate tectonics model for the Variscan belt in Western Europe. Tectonophysics 126, 329-374.
Matte, P., Respaut, J.-P., Maluski, H., Lancelot, J., Brunel, M., 1986. La faille NW-SE du Pays de Bray, un décrochement ductile dextre hercynien: déformation à 330 Ma d'un granite à 570 Ma dans le sondage Pays de Bray 201. Bull. Soc. géol. France 8 (II), 69-77.
Matte, P., Hirn, A., 1988. Seismic signature and tectonic cross section of the Variscan crust in Western France. Tectonics 7 (2), 141-155.
Matte, P., 1998. Continental subduction and exhumation of HP rocks in Paleozoic orogenic belts: Uralides and Variscides. GFF 120, 209-222.
Matte, P., 2001. The Variscan collage and orogeny (480-290 Ma) and the tectonic definition of the Armorica microplate: a review. Terra Nova 13, 122-128
Mansy, J.-L., Manby, G.M., Averbuch, O., Everaerts, M., Bergerat, F., Van Vliet-Lanoe, B., Lamarche, J., Vandycke, S., 2003. Dynamics and inversion of the Mesozoic basin of the Weald-Boulonnais area: role of basement reactivation. Tectonophysics 373, 161-179.
Mégnien, C., 1980. Tectogenèse du Bassin de Paris: étapes de l'évolution du bassin. Bull. Soc.géol. France XXII (4), 669-680.
Ménard, G., Molnar, P., 1988. Collapse of a Hercynian Plateau into a late Palaeozoic European Basin and Range province. Nature 334 (6179), 235-237.
Meilliez, F., André, L., Blieck, A., Fielitz, W., Goffette, O., Hance, L., Khatir, A., Mansy, J.L., Overlau, P., Verniers, J., 1991. Ardenne-Brabant. Sci. Géol. Bull. 44, 3-29.
Moore, V.M., Wiltschko, D.V., 2004. Syncollisional delamination and tectonic wedge development in convergent orogens. Tectonics, 23, TC2005, doi: 10.1029/2002TC001430.

Morelli, A., Dziewonski, A., 1993. Body wave traveltimes and a spherically symmetric P- and S-wave velocity model. Geophys. J. Int. 112, 178-194.
Morency, C., Doin, M.-P., 2004. Numerical simulations of the mantle lithosphere delamination. J. Geophys. Res. 109, B03410, doi: 10.1029/2003JB002414.
Nelson, K.D., 1992. Are crustal thickness variations in old mountain belts like the Appalachians a consequence of lithospheric delamination? Geology 20, 498-502.
Oncken, O., Franke H.J., Dittmar, U., Klügel, T., 1995. Northern Phyllite Zone- structure. In: Dallmeyer, R.D., Franke, W., Weber, K. (Eds.), Pre-Permian geology of Central and Eastern Europe. Springer-Verlag, Berlin, Heidelberg, pp. 108-117.
Oncken, O., Plesch, A., Weber, J., Ricken, W., Schrader, S., 2000. Passive margin detachment during arc-continent collision (Central European Variscides). In: Franke, W., Haak, V., Oncken, O., Tanner, D. (Eds.), Orogenic Processes: quantification and Modelling in the Variscan Belt. Geological Society, London, Special Publications 179, pp. 199-216.
Pham, V.N., Boyer, D., Le Mouel, J.L., 2000. Nouveaux arguments sur l'origine de l'anomalie magnétique du Bassin parisien (AMBP) d'après les propriétés électriques de la croûte. C.R. Acad. Sci. Paris 331, 443-449.
Piromallo, C., Morelli, A., 2003. P wave tomography of the mantle under the Alpine-Mediterranean area. J. Geophys. Res. 108 (B2), 2065, doi: 10.1029/2002JB001757.
Platt, J.P., England, P.C., 1993. Convective removal of lithosphere beneath mountain belts: thermal and mechanical consequences. American Journal of Science 293, 307-336.
Ploquin A, Stussi, 1994. Felsic plutonism and volcanism in the Massif Central. In: Keppie, J.D. (Ed.), Pre-Mesozoic geology in France and related areas. Springer-Verlag, Berlin, Heidelberg, pp. 363-378.
Poupinet, G., Thouvenot, F., Zolotov, E.E., Matte, P., Egorkin, A.V., Rackitov, V.A., 1997. Teleseismic tomography across the middle Urals: lithospheric trace of an ancient continental collision. Tectonophysics 276, 19-33.
Poupinet, G., Avouac, J.P., Jiang, M., Wei, S., Kissling, E., Herquel, G., Guilbert, J., Paul, A., Wittlinger, G., Su, H., Thomas, J.C., 2002. Intracontinental subduction and Paleozoic inheritance of the lithosphere suggested by a teleseismic experiment across the Chinese Tien Shan. Terra Nova 14, 18-24.
Poupinet, G., Arndt, N., Vacher, P., 2003. Seismic tomography beneath stable tectonic regions and the origin and composition of the continental lithosphere. Earth and Planetary Science Letters 212, 89-101.
Prijac, C., Doin, M.P., Gaulier, J.M., Guillocheau F.2000. Subsidence of the Paris basin and its bearing on the late Variscan lithosphere evolution: a comparison between Plate and Chablis models. Tectonophysics 323, 1-38.
Pysklyvec, R.N., Beaumont, C., Fullsack, P., 2000. Modeling the behavior of the continental mantle lithosphere during plate convergence. Geology 28 (7), 655-658.
Rey, P., Burg, J.-P., Caron, J.-M., 1992. Middle and Late Carboniferous extension in the Variscan Belt: Structural and petrological evidences from the Vosges Massif (Eastern France). Geodinamica Acta 5, 17-36.
Ritter, J.R.R., Jordan, M., Christensen, U.R., Achauer, U., 2001. A mantle plume below the Eifel volcanic fields, Germany. Earth and Planetary Science Letters 186, 7-14.
Rosenbaum, G., Gasparon, M., Lucente, F.P., Peccerillo, A., Miller, M.S., 2008. Kinematics of slab tear faults during subduction segmentation and implication for Italian magmatism. Tectonics 27, TC2008, doi: 10.1029/2007TC002143.
Ruffell, A., Coward, M.P., Harvey, M., 1995. Geometry and tectonic evolution of the Plymouth Bay Basin, English Channel. . In: Boldy, S.A.R. (Ed.), Permian and Triassic

Rifting in Northwest Europe. Geological Society, London, Special Publications 91, pp. 193-214.
Sacks, P.E., Secor, D.T., 1990. Delamination in collisional orogens. Geology 18, 999-1002.
Schaltegger, U., 1997. Magma pulses in Central Variscan Belt, episodic melt generation and emplacement during lithospheric thinning. Terra Nova 9, 242-245.
Shail, R.K., Leveridge, B.E., 2009. The Rhenohercynian passive margin of SW England: Development, inversion and extensional reactivation. C.R. Geoscience 341, 140-155.
Sol, S., Thomson, C.J., Kendall, J.M., White, D., VanDecar, J.C., Asudeh, I., 2002. Seismic tomographic images of the cratonic upper mantle beneath the Western Superior Province of the Canadian Shield- a remnant Archean slab? Phys. Earth Planetary Interiors 134, 53-69.
Stein, S., Stein, C.A., 1996. Thermomechanical evolution of oceanic lithosphere: implications for the subduction process and deep earthquakes. Geophys. Monogr. Am. Geophys. Union 96, 1-17.
Thiery, V., Rolin, P., Marquer, D., Cocherie, A., Fanning, M., Rossi, P., 2009. Visean sinistral wrench faulting along the Sillon Houiller in the French Massif Central: Late Variscan tectonic implications. Bull. Soc. géol. France 180 (6), 513-528.
Van den Driessche, J., Brun, J.-P., 1989. Un modèle cinématique de l'extension paléozoïque supérieure dans le sud du Massif Central. C. R. Acad. Sci. Paris 309 (II), 1607-1613.
Van der Voo, R., Spakman, W., Bijwaard, H., 1999. Mesozoic subducted slabs under Siberia. Nature 397 (6716), 246-249.
Vignaroli, G., Faccenna, C., Jolivet, L., Piromallo, C., Rossetti, F., 2008. Subduction polarity reversal at the junction between the Western Alps and the Northern Apennines, Italy. Tectonophysics 450, 34-50.
Von Seckendorff, V., Arz, C., Lorenz, V., 2004. Magmatism of the late Variscan intermontane Saar-Nahe Basin (Germany): a review. In: Wilson, M.., Neumann, E.R., Davies, G.R.., Timmerman, M.J., Heeremans, M., Larsen, B.T. (Eds.), Permo-Carboniferous Magmatism and rifting in Europe. Geological Society, London, Special Publications 223, pp. 361-391.
Zielhuis, A., Nolet, G., 1994. Deep seismic expression of an ancient plate boundary in Europe. Science 265, 79-81.
Ziegler, P.A., Dèzes, P., 2007. Cenozoic uplift of Variscan Massifs in the Alpine Foreland: Timing and controlling mechanisms. Global and Planetary Change 58, 237-269. doi: 10.1016/j.glopacha.2006.12.004
Ziegler, P.A., Schumacher, M.E., Dèzes, P., Van Wees, J.D., Cloethingh, S., 2004. Post-Variscan evolution of the lithosphere in the Rhine Graben area: constraints from subsidence modelling. In: Wilson, M.., Neumann, E.R., Davies, G.R.., Timmerman, M.J., Heeremans, M., Larsen, B.T. (Eds.), Permo-Carboniferous Magmatism and rifting in Europe. Geological Society, London, Special Publications 223, pp. 289-317.

2.B. Le contrôle de la pré-structuration varisque sur la localisation des aires de sédimentation post-orogéniques et sur leur déformation postérieure: l'exemple de la marge nord du bassin de Paris.

Comme on vient de le voir dans le paragraphe précédent sur un modèle à grande échelle des processus d'extension tardi-varisques (Stéphanien-Permien inférieur), initiateurs du bassin de Paris, la subsidence tectonique au cours de cet événement est localisée principalement au niveau de fossés profonds à l'aplomb de la zone de suture nord-varisque : le bassin de Sarre-Lorraine le long de la suture rhénohercynienne (plus de 4 km de sédiments continentaux stéphano-permiens piégés)(Korsch and Schäfer, 1995; Littke et al, 2000) et le bassin de Manche central le long de la suture du Lizard (socle accoustique à plus de 10 km de profondeur selon Ruffell et al, 1995). Pour autant, un certain nombre de petits bassins continentaux de cet âge, initialement intra-montagneux, se retrouvent à la base du bassin de Paris, en particulier le long de sa marge nord entre Pays de Bray et Boulonnais-Artois. C'est, en particulier, le cas le long de la faille de la Somme ainsi que l'ont montré les études associées au profil Ecors Nord de la France (Mascle et Cazes, 1988) mais également, le long du front de chevauchement nord varisque entre Artois et Boulonnais, ainsi que le montrent les articles 2 à 5 présentés ici. Cette sédimentation fluvio-lacustre stéphano-permienne éparse est difficilement caractérisable quantitativement d'une part parce qu'elle est généralement enfouie sous la couverture mésozoïque (jurassique à sa base dans le Boulonnais-Weald, crétacé moyen dans la majeure partie du nord de la France), d'autre part parce qu'elle a subi une intense érosion sub-aérienne avant même le dépôt de la couverture (cf. article 4). Par contre, nos études montrent clairement que cette sédimentation est controlée par des failles à fort pendage (généralement vers le sud) dont la localisation est, elle-même, contrôlée par les chevauchements varisques. Ce phénomène d'inversion tectonique négative du front de chaîne varisque est le point central des différents articles présentés dans ce paragraphe. Il est à noter que, pour la plupart, ces failles, avec une composante initialement normale, ont été réactivées en faille inverse au cours de l'épisode de compression tertiaire péri-alpin (phénomène d'inversion tectonique positive) et qu'on observe, donc une double réactivation de certains chevauchements variques en profondeur.

Dans le détail, les failles affectant la couverture sédimentaire post-varisque (stéphano-permienne comprise) sont disposées en relais complexe le long du front de chevauchement varisque Artois-Boulonnais montrant qu'elles se sont mises en place dans un système de déformation en transtension accommodant une composante coulissante sénestre et une

composante extensive sub-méridienne. Bien qu'on ait peu d'information directe sur la cinématique de la majeure partie de ces failles (en particulier, concernant l'âge précis de chacune d'elle), il semble qu'au sein de ce réseau, on ait une partition de la déformation entre des failles purement normales définissant des demi-grabens et des structures en « roll-over », par exemple, la faille d'Audincthun en Artois (cf. article 4) et des failles avec une composante décrochante plus significative, par exemple, la faille de Ferques, dans le massif paléozoïque du Boulonnais. La géométrie et la cinématique de cette dernière est explicitée dans l'article 2. Elle correspond au seul élément exhumé de ce réseau de failles, suite au soulèvement du Boulonnais lors de la phase d'inversion structurale tertiaire (cf. article 3) ; tous les autres éléments de ce réseau se trouvent enfouis sous la couverture transgressive du Crétacé moyen et leur caractérisation n'a été possible qu'à partir de critères géométriques issus des données de forage, des profils sismiques et des anomalies gravimétriques (cf. articles 3 et 4).
Comme le montrent les données explicitées dans l'article 2, la faille de Ferques présente une géométrie assez complexe, variant considérablement le long se son tracé cartographique, en particulier suite à l'existence de duplex décrochants (Woodcock et Fischer, 1986) s'anastosmosant latéralement. Les écailles à l'intérieur se disposent selon une structure globalement en fleur et sont séparées par des contacts subverticaux indiquant un mouvement à composante sénestre-normale ce qui tend à suggérer qu'elles se sont mises en place dans le cadre d'une déformation transtensive. La localisation de la faille (au niveau de la brisure entre rampe et palier inférieur associé au chevauchement basal du système d'écailles du Boulonnais) suggère qu'elle se raccorde à la base de la rampe du chevauchement frontal boulonnais. Il est à noter que deux autres failles normales (la faille du Griset et celle de Landrethun, l'équivalent latéral de la faille du Cap Gris Nez), situées au nord de la faille de Ferques, semblent également se raccorder à cette même rampe du chevauchement basal ; cependant, il est probable que ces dernières aient été activées (ou réactivées) lors de l'événement de rifting du Jurassique supérieur-Crétacé inférieur ainsi que le suggère la disposition des dépôts dans ce secteur (cf. article 3). L'absence de dépôts continentaux stéphano-permiens le long de ces failles ne permet pas d'accréditer un jeu tardi-varisque sur ces accidents au niveau du massif paléozoïque exhumé de Ferques. Cependant, au niveau de la faille du Cap Gris-Nez qui relaie vers l'ouest la faille de Landrethun, les forages montrent, sous les dépôts jurassiques, l'existence de niveaux non datés (généralement assimilés à du Trias, mais sans contrainte véritable) qui pourraient traduire cet événement initial de subsidence tectonique tardi-paléozoïque. En tout état de cause, cette faille du Cap Gris Nez constitue un élément majeur du dispositif extensif mis en place au cours du Jurassique

supérieur-Crétacé inférieur, lors de la phase de rifting majeur de l'Atlantique Nord et de la Mer du Nord (e.g., Ziegler, 1990 ; Ziegler and van Hoorm, 1990). Les données de forage (article 3) montrent qu'elle localise en surface une discontinuité majeure qui limite brutalement l'extension des dépôts jurassiques vers le nord. Cette faille normale initiale a été inversée au cours de la phase compressive tertiaire ainsi que le montrent la flexuration générale des séries (article 3) ainsi que les plis et chevauchements affleurant sur la plage du Cap Gris-Nez à l'aplomb de la faille (e.g., Averbuch, 2009). Comme dans le cas de la faille de Landrethun plus à l'est, l'existence de Silurien directement sous les dépôts mésozoïques, au toit de la faille suggère quelle s'est mise en place au niveau d'une culmination anticlinale varisque développée au toit d'un chevauchement (cf. fig. 4 de l'article 3) réactivant la rampe du chevauchement en profondeur.

L'exemple le plus significatif d'inversion tectonique négative tardi-paléozoïque avérée est à rechercher en Artois, dans le prolongement oriental des structures du Boulonnais (article 4). A cet endroit, des séries conglomératiques, peu épaisses, d'origine fluviatile, d'âge tardi-paléozoïque (Mériaux, 1961)(permien selon les datations récentes de D. Vachard non publiées) affleurent localement le long du tracé des failles superficielles affectant la couverture crétacé-tertiaire à l'aplomb du front de chevauchement varisque (dites ici, failles de l'Artois, e.g., Gosselet, 1908 ; Bouroz, 1956). C'est le cas, en particulier, de la faille de Pernes et de son relai vers le NW, la faille d'Audincthun. Sur cette zone, l'interpolation des données de forage couplée à l'interprétation de deux profils sismiques transverses aux structures permet de donner une image relativement détaillée de ces petits bassins permiens (probablement stéphaniens pour les premiers dépôts). Ces données montrent que la faille d'Audincthun à pendage sud assez fort en surface, limite vers le nord, un petit graben à remplissage permien dont la géométrie, en éventail, traduit le caractère syn-rift des dépôts. La structure en « roll-over » et le basculement progressif des dépôts permiens, discordants sur les structures varisques, montrent que le pendage de la faille d'Audincthun tend à diminuer en profondeur à la manière des failles listriques caractéristiques des domaines de marges passives. Cette diminution de pendage traduit, en fait, le branchement de la faille de surface sur le chevauchement frontal varisque à pendage d'environ 30° vers le sud. Cette géométrie caractérise la réactivation en extension en profondeur du chevauchement frontal varisque et la dissection de l'unité chevauchante en surface par une faille néoformée à fort pendage (géométrie classique de type « short-cut » ; e.g., Williams et al, 1989) illustrant le processus d'inversion tectonique négative d'un chevauchement. Bien que les failles de l'Artois ne présentent pas toutes d'enregistrement sédimentaire associé, leurs géométries semblent toutes se calquer sur ce dispositif impliquant leur branchement en profondeur sur les différents chevauchements impliqués dans le front de déformation varisque. Le décalage systématique en jeu inverse observé pour la couverture crétacée à l'aplomb de ces failles (décalage à l'origine du soulèvement des collines de l'Artois par rapport à la plaine des Flandres) indique, comme dans le Boulonnais, l'existence d'une réactivation du système en contexte compressif au cours du Tertiaire soulignant le caractère répété du phénomène d'inversion tectonique du front de chevauchement varisque en Artois.

Dans le Boulonnais, comme en Artois, la zone de chevauchement frontal varisque apparaît, donc, comme une discontinuité mécanique majeure dans la croûte ayant localisé la déformation depuis le Carbonifère supérieur. En cela, ce tronçon s'oppose clairement au segment Avesnois-Ardennes, d'orientation ENE-WSW, où le front chevauchant ne montre pas d'indice clair d'une telle réactivation répetée. Comme le montre les courbes d'isoprofondeur temps du chevauchement frontal principal (la faille du Midi) établi à partir de la synthèse des différents profils sismiques recoupant le front de déformation varisque (article 4 et 5), on observe une diminution nette de l'ampleur du pendage du chevauchement frontal à l'est d'une ligne reliant approximativement Lens et Arras ce qui pourrait avoir eu un impact majeur sur les possibilités de réactivation en faille normale de cette discontinuité majeure (e.g. Facenna et al, 1995).

Afin de mieux contraindre les géométries et cinématiques caractéristiques du processus d'inversion tectonique négative et tester l'influence de différents paramètres de base contrôlant son développement (par exemple, le pendage du décollement basal et le niveau de troncature par érosion des structures de chevauchement), des expériences de modélisation analogique ont été entreprises en collaboration avec B. Vendeville. Ces dernières ont été effectuées dans le cadre du Master 2 de M. Ouzgaït soutenu en juin 2010 et leur interprétation reste encore grandement préliminaire au moment où j'écris ces lignes. L'exploitation de ces expériences de modélisation analogique, qui dépasse le cadre de l'étude du front de chaîne varisque, constitue un des volets prioritaires de mes recherches futures (cf. le paragraphe Conclusions et perspectives). L'article 5, destiné à une présentation au congrès GEOMOD tenu fin septembre 2010 à Lisbonne, en présente les principes et les résultats de base.

La figure 4 de cet article illustre les caractéristiques géométriques et cinématiques du développement d'un bassin post-orogénique. En particulier, notre étude corrobore parfaitement le fait que que les rampes des chevauchements localisent en profondeur les failles normales controllant la sédimentation syn-rift. Des grabens fortement dissymétriques (dépocentre décalé préférentiellement vers l'avant-pays) se mettent en place au toit des culminations chevauchantes avec des failles normales majeures enracinées sur les pro-chevauchements (à vergence vers l'avant-pays) et des failles antithétiques secondaires sur les rétro-chevauchements (à vergence vers l'arrière-pays). Ainsi que l'ont suggéré Roure et al (1992) et D'Agostino et al (1998), ces dernières semblent « accommoder » l'ajustement du toit sur la surface de chevauchement basal. Pour l'ensemble de ces failles, on observe une réactivation partielle du chevauchement au niveau de la rampe (la rampe n'étant, d'ailleurs, pas toujours réactivée sur toute son extension) et la formation d'une nouvelle faille à pendage fort en surface recoupant l'anticlinal de rampe associé au chevauchement sous-jacent. Cette géométrie défini une allure grossièrement listrique aux failles normales, en particulier pour les failles majeures, synthétiques des rampes chevauchantes, associées à des structures de « roll-over » plus ou moins marquées. Dans les premières phases d'extension, le déplacement normal est grandement réparti sur les différents chevauchements majeurs (une seule structure chevauchante n'étant pas réactivée) et on n'observe pas de séquence spécifique de propagation des failles normales au sein du modèle. Toutefois, au cours de l'expérience, on assiste à une localisation de plus en plus grande de la déformation sur la structure de rétrochevauchement majeur située au niveau du butoir mobile lors de la phase de compression initiale, résultant au final en une structure de « roll-over » particulièrement accentuée. Il est probable qu'il s'agisse ici d'un artefact associé aux conditions expérimentales induisant le fluage progressif de la silicone sur la pente basale appliqué au modèle (2,5° ici).

Au final, ces données illustrent les relations souvent obscures qui existent entre les chevauchements de socle enfouis et les bassins sédimentaires qui les surplombent et, si besoin en était, tendent à souligner l'importance de la pré-structuration du bâti géologique varisque sur l'évolution d'une région comme le nord de la France.

Article 2.

Averbuch O., Mansy J-L. et Lamarche J., (2001). Déformations tardi-paléozoïques au front septentrional de la chaîne varisque : l'exemple des massifs paléozoïques du Boulonnais (N France). Ann. Soc. Géol. Nord, 9, 13-24.

EXTRAIT DES ANNALES DE LA SOCIÉTÉ GÉOLOGIQUE DU NORD
T. 9 (2ème série), p.13
LILLE

Ann. Soc. Géol. du Nord.
T. 9 (2ème série), p. 13-24, Novembre 2001.

DÉFORMATIONS TARDI-PALÉOZOÏQUES AU FRONT SEPTENTRIONAL DE LA CHAINE VARISQUE: L'EXEMPLE DES MASSIFS PALÉOZOIQUES DU BOULONNAIS (N FRANCE).

Late Paleozoic deformations at the northern front of the Variscan belt: example of the Paleozoic inliers of the Boulonnais region (N France).

Par Olivier AVERBUCH (*), Jean-Louis MANSY (*) et Juliette LAMARCHE (*)(**)

Résumé. — En Europe de l'ouest, l'épisode de déformation tardi-varisque d'âge stéphano-permien (ca 300-260 Ma) est à l'origine d'une intense fracturation du substratum paléozoïque sur laquelle se superposent de nombreux bassins à remplissage continentaux. Dans le domaine Artois-Boulonnais, situé au front septentrional de la chaîne varisque, les accidents tardi-varisques se manifestent par un réseau de failles sub-verticales orientées WNW-ESE, parallèlement aux grandes failles de la Somme et du Bray, et disposées en relai le long du front de chevauchement majeur " du Midi ". Le seul élément exhumé de ce faisceau de failles, la zone faillée de Ferques, présente en carte une géométrie en duplex sub-vertical d'échelle kilométrique qui se traduit en coupe par une structure en fleur impliquant un mouvement à la fois décrochant et transverse matérialisé par le soulèvement relatif du compartiment nord. La composante décrochante est à jeu sénestre ainsi que l'indiquent les données des populations de microfailles et de fabrique magnétique des roches déformées au cœur de la zone faillée. Ces données caractérisent un épisode décrochant associé à une extension NNW-SSE et une compression ENE-WSW. Il est proposé que ces déformations soient associées à un système globalement en transtension, résultat de l'accommodation cinématique d'une extension tardi-orogénique sub-méridienne par un domaine fortement pré-structuré lors de la phase varisque.

Abstract. — *Late Paleozoic deformations are widespread in Europe and have been widely shown to control the geometry of the Meso-Cenozoic basins. They are characterized by an important set of strike-slip fault zones along which localized Stephano-Permian basins developed. Two major geodynamic models have been proposed for this period: (1) the first one considers the European Variscan belt as a diffuse plate boundary between Laurussia and Gondwana submitted to a pervasive E-W oriented dextral shearing (2) the second one points out a N-S late orogenic extension of the overthickened thermally unstable Variscan lithosphere. These models have been discussed mainly using data from the internal parts of the Variscan belt. This study investigates the geometry and kinematics of the Late Paleozoic deformations observed along the Boulonnais-Artois segment (N France) of the northern Variscan front and examines how they can be included in the proposed kinematic models.*

Subsurface maps of the coal-bearing N Variscan foreland basin and gravimetric anomaly maps show that the Boulonnais-Artois Variscan thrust front is affected by a set of an échelon longitudinal Late Paleozoic fault zones that systematically induce the subsidence of their southern border. Towards the west, the Ferques Fault Zone (F.F.Z), an element of this this fault network is exhumed in the core of the Cenozoic inverted Boulonnais massif.

Geological mapping as well as cross-sections show that the Ferques fault zone is a complex structural element oriented about N100 that comprises numerous laterally anastomozing susbsidiary faults. The resulting kilometric scale strike-slip duplex structure show in cross-section a typical flower attitude involving both a strike-slip displacement and uplift of the northern border of the fault (the Ferques unit). Microfaults analysis within the fault zone as well as the anisotropy of magnetic susceptibility of the Upper Carboniferous coal-bearing layers involved in the deformed zone document a major left-lateral displacement. An associated normal component observed along numerous faults of the F.F.Z. characterizes a general transtensional event induced in a NNW-SSE extension and a ENE-WSW compression.

The observed Stephanian-Permian deformation pattern of the Boulonnais inliers does not fit with the common interpretation of this zone to be part of a diffuse plate boundary submitted to pervasive E-W trending dextral shearing. It is rather interpreted as the result of the kinematical accommodation of a general N-S extension by the strongly structured Variscan thrust front. This mechanism is likely to contribute to the thermal re-equilibration and thinning of the external part of the overthickened Variscan crust.

(*) Sédimentologie et Géodynamique, FRE 2255, Université de Lille 1, 59655 Villeneuve d'Ascq Cedex.
(**) Nouvelle adresse : GeoForschung Zentrum Potsdam, Telegrafenberg C427, 14473 Potsdam, Allemagne.

I. — INTRODUCTION.

La période tardi-varisque (d'âge stéphano-permien, ca 300-260 Ma) correspond à un épisode de déformation important en Europe. Ce dernier est, en effet, à l'origine d'une intense fracturation du substratum et a joué un rôle majeur dans la configuration des bassins méso-cénozoïques. Les déformations tardi-paléozoïques sont caractérisées sur l'ensemble de l'ancienne chaîne varisque par des grands décrochements (e.g. Arthaud et Matte, 1977; Ziegler, 1990) le long desquels se développent de nombreux bassins à remplissage continental (fig 1) (e.g. Bonijoly et Castaing, 1984; Soula, 1984; Vallé *et al.*, 1988; Ziegler, 1990; Mattauer et Matte, 1998). Il a été proposé que l'ensemble de ces structures soient apparues au sein d'une limite de plaque intra-continentale diffuse entre les domaines gondwaniens et laurussiens soumise à un régime cisaillant dextre (Arthaud et Matte, 1977; Ziegler, 1990; Bard, 1997). Ce modèle s'accorde cependant assez mal avec l'aspect multi-directionnel des fractures et des axes de bassins (fig 1) ainsi que certaines données de cinématique des déformations cassantes à cette période (e.g Bonijoly et Castaing, 1984; Soula, 1984).

Par ailleurs, au cours de ces dernières années, la mise en évidence dans les zones internes de la chaîne d'une extension sub-méridienne très importante, contemporaine des bassins et des décrochements a relancé le débat autour des structures tardi-paléozoïques (Ménard et Molnar, 1984; Faure et Becq-Giraudon, 1993; Malavieille, 1993; Gapais *et al.*, 1993; Burg *et al.*, 1994; Lefort et Jaffal, 1994). Ces dernières seraient le résultat de l'effondrement de la croûte varisque surépaissie associé à une phase de réajustement thermique de la lithosphère. Dans ce modèle, les bassins se forment principalement au toit de failles normales listriques réactivant les chevauchements varisques [e.g.Van den Driessche et Brun, 1989 ; Echtler et Malavieille, 1990 ; Malavieille *et al.*, 1990; Legrand *et al.*, 1991 ; Becq-Giraudon et Van den Driessche, 1994) ; les décrochements sont, quant à eux, interprétés comme des failles à caractère transtensif (Faure et Becq-Giraudon, 1993) ou comme des failles de transfert découplant des domaines ayant subi une extension différentielle (Burg *et al.*, 1990).

Les discussions autour des phénomènes tardi-paléozoïques se focalisent essentiellement sur des données issues des domaines internes de la chaîne varisque. L'objet de cet article est d'examiner la géométrie et la cinématique des déformations tardi-paléozoïques au front septentrional de la chaîne et de voir comment celles-ci peuvent s'intégrer aux modèles proposés pour l'évolution géodynamique de cette période. Bien que la superficie des affleurements paléozoïques soit assez limitée (quelques dizaines de kilomètres carré), le domaine Boulonnais-Artois constitue une cible de choix pour l'étude des déformations tardi-paléozoïques dans la mesure où il est possible d'appréhender les déformations à la fois dans le socle et dans la couverture Jurassico-Crétacé. En raison de la réactivation fréquente des structures tardi-varisques, il est en effet essentiel d'avoir accès à la fois au socle paléozoïque et à sa couverture pour différencier les mouvements initiaux des déformations méso-cénozoïques.

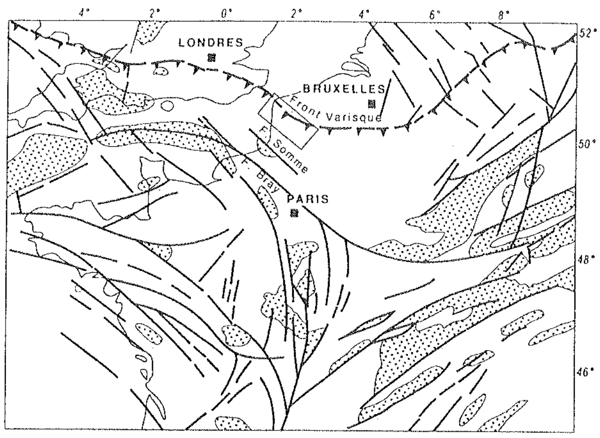

Fig. 1. — Schéma structural montrant la disposition des accidents et des bassins d'âge stéphano-permien (zones pointillées) dans la moitié nord de la France (modifiée de Ziegler, 1990).

Fig. 1. — Structural scheme showing the geometry of Late Variscan fault zones and associated Stephano-Permian basins (shaded area) within the northern part of France (modified from Ziegler, 1990).

II. — LE CONTEXTE STRUCTURAL.

Le trait structural majeur du front septentrional de la chaîne varisque dans le nord de la France est un chevauchement d'échelle crustale à vergence nord: le chevauchement du Midi (fig 2)(Raoult et Meilliez, 1987 ; Lacquement *et al.*, 1999). Il limite au sud le bassin d'avant-pays à remplissage houiller d'âge namuro-westphalien, plissé et écaillé lors de l'avancée des unités allochtones (e.g. Bouroz, 1950 ; Lacquement *et al.*, 1999). Cet ensemble, dont la structuration chevauchante s'est finalisée au Westphalien supérieur-Stéphanien inférieur, est affecté dans sa partie occidentale par un réseau d'accidents longitudinaux sub-verticaux (fig 2). Ceux-ci, orientés suivant une direction environ N110, sont parallèles aux grands accidents de socle de la Somme et du Bray dont le caractère profond et multiphasé a pu être mis en évidence lors du profil ECORS Nord de la France (Cazes *et al.*, 1985). Les données de subsurface, acquises lors de l'exploitation du bassin houiller, montrent qu'au cours d'un épisode de déformation tardi-paléozoïque, ces failles présentent systématiquement un compartiment méridional affaissé (Bouroz, 1948 ; Colbeaux, 1984). Ce dernier localise ponctuellement (par exemple au niveau de la faille de Pernes, fig 3) des dépôts conglomératiques d'épaisseur pluri-hectométrique d'âge probable carbonifère terminal, discordants sur les structures varisques (Mériaux, 1961 ; Becq-Giraudon, 1983). La cartographie sous-couverture du substratum paléozoïque dans le bassin houiller (Bouroz *et al.*, 1963) ainsi que des nouvelles données sur la distribution des anomalies gravimétriques et magnétiques (Everaerts et Mansy, 2001) permettent de montrer que ces accidents tardi-paléozoïques se disposent en échelon le long du front varisque en se relayant de façon complexe depuis l'Artois jusqu'au Boulonnais (fig 2). La géométrie du toit des séries paléozoïques (fig 3) montre, par ailleurs, que postérieurement aux événements tardi-varisques, un grand nombre de ces accidents sont

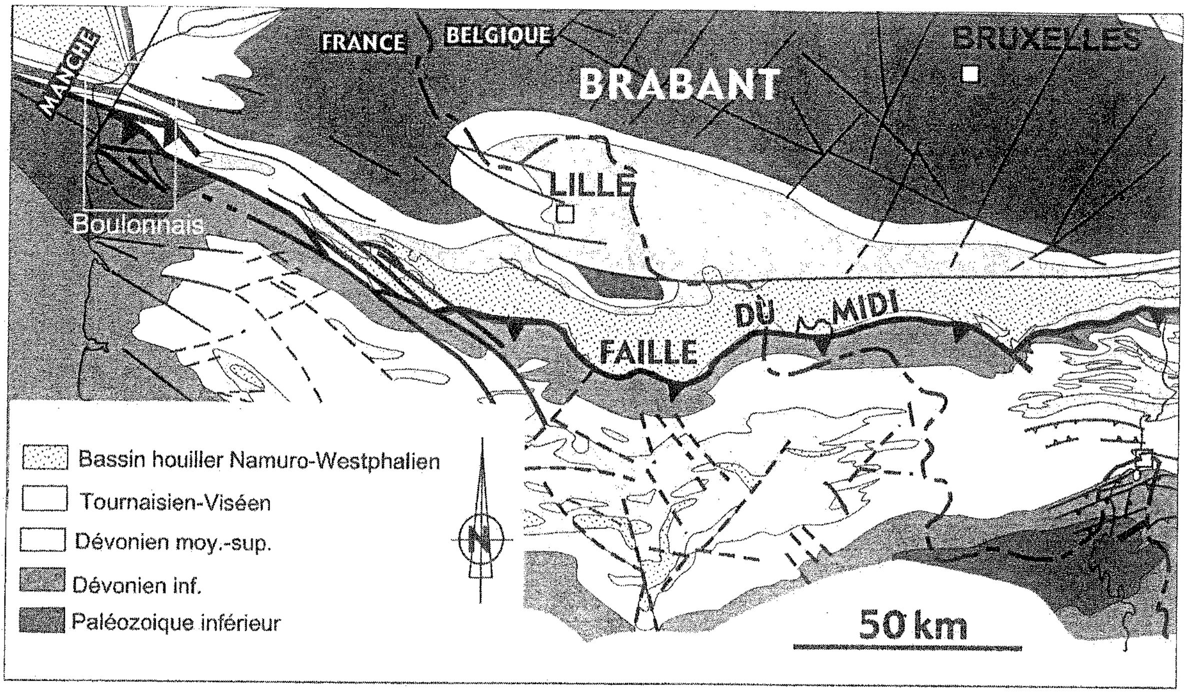

Fig. 2. — Ecorché infra-mésozoïque du nord de la France montrant la géométrie du front de chevauchement nord varisque et la localisation (rectangle blanc) de la zone d'étude.

Fig. 2 . Subsurface map of the Paleozoic units in northern France showing the geometry of the northern variscan thrust front and the location (white rectangle) of the study zone.

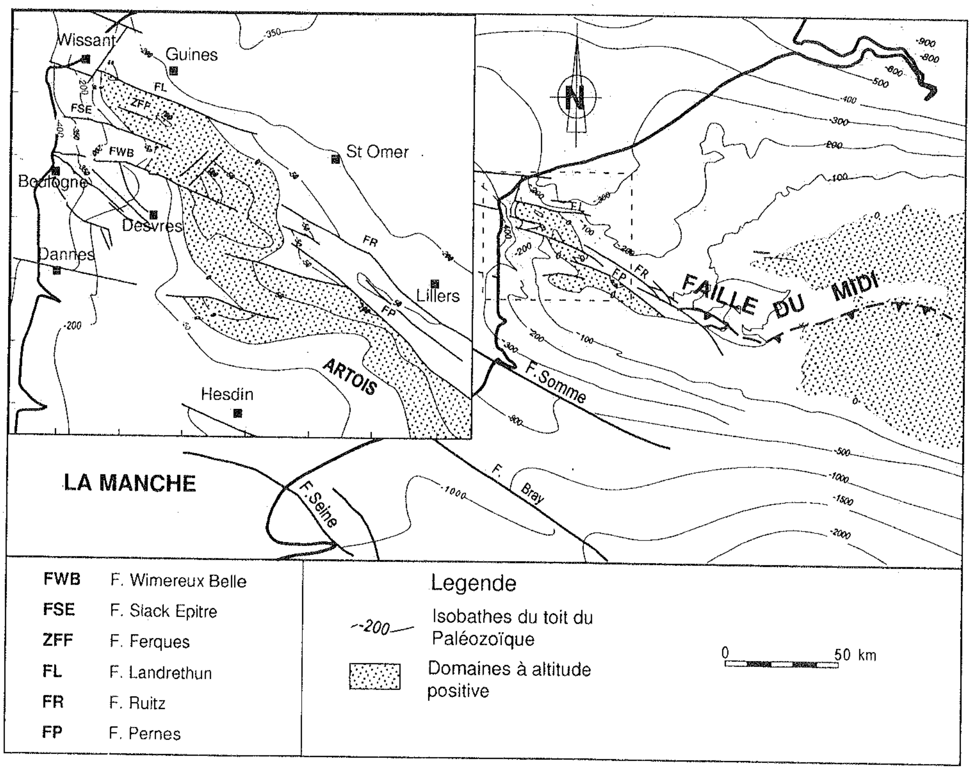

Fig. 3. — Carte en isobathe du toit des formations paléozoïques au niveau du front varisque du nord de la France et géométrie des accidents tardi-paléozoïques. En encart, géométrie détaillée au niveau du domaine Artois-Boulonnais.

Fig. 3. — Isobath map of the roof of the Paleozoic formations along the N France Variscan front and geometry of the Late Paleozoic faults. In the left upper part is shown the detailed geometry within the Artois-Boulonnais area.

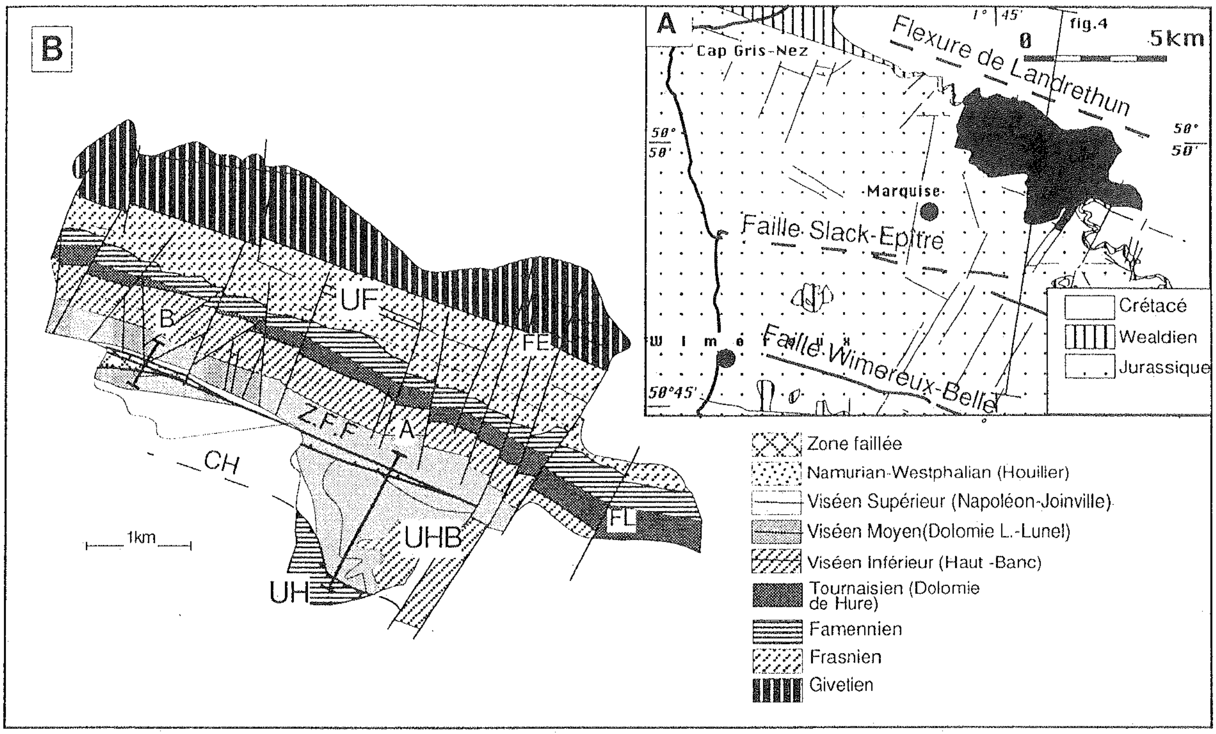

Fig. 4. — A. Carte géologique simplifiée du Nord du Boulonnais et localisation de la coupe générale de la fig.5. En noir, le Massif paléozoïque de Ferques. B. Carte géologique du massif paléozoïque de Ferques (d'après Mansy *et al.*, sous presse). UF : Unité de Ferques ; UHB : Unité du Haut-Banc ; UH : Unité d'Hydrequent; Z.F.F. : Zone faillée de Ferques; CH: chevauchement d'Hydrequent; FE: faille d'Elinghen; FL: faille de Locquinghen. Les sections A et B se réfèrent aux coupes de la fig. 6.

Fig.4. — A. Sketch geological map of the northern part of the Boulonnais area and location of the general cross-section of fig. 5. In black are reported the Ferques Paleozoic inliers. B. Geological map of the Ferques Paleozoic massif (after Mansy et al, in press). UF : Ferques unit ; UHB : Haut-Banc unit ; UH : Hydrequent unit; Z.F.F. : Ferques fault zone; CH: Hydrequent thrust; FE: Elinghen fault; FL: Locquinghen fault. The A et B sections refer to the cross-sections of fig. 6.

réactivés avec un jeu fini impliquant le réhaussement des compartiments méridionaux. Cet épisode d'inversion tectonique d'âge probable éocène supérieur, est à l'origine de la structuration générale en horst du Boulonnais; ce réhaussement tardif a permis l'exhumation du substratum paléozoïque au coeur duquel apparaît un élément quasiment non réactivé du système de failles longitudinales jalonnant le front varisque: la zone faillée de Ferques (Z.F.F.) (fig 3 et fig 4).

Dans le Boulonnais, les structures varisques ainsi que la zone faillée de Ferques sont scellées par une couverture sédimentaire d'âge Jurassique moyen (e.g. Lamarche *et al.*, 1996). Des failles transverses de direction subméridienne (fig 4) qui découpent localement la Z.F.F. et qui correspondent à des accidents conjugués d'ampleur plus modeste, sont, quant à elles, souvent karstifiées avec un remplissage de sables dont l'âge varie selon les endroits du Rhétien jusqu'à la base du Jurassique moyen (Mansy *et al.*, in press). Une étude paléomagnétique du remplissage de la Z.F.F. a permis, par ailleurs, de préciser le scénario des déformations en donnant un âge minimum Trias moyen aux mouvements les plus récents le long de cet accident (Lewandowski *et al.*, 1999). Le fonctionnement de la Z.F.F. peut donc être daté globalement entre le Stéphanien et le Trias moyen. Par analogie avec les structures jalonnant le front varisque, il est raisonnable de rattacher le système faillé de Ferques aux déformations tardi-varisques.

III. — GEOMETRIE DE LA ZONE FAILLEE DE FERQUES

Au sein des massifs paléozoïques du Boulonnais, la Z.F.F. sépare deux unités structurales superposées lors des mouvements varisques (fig 4 et fig 5): au nord, l'unité inférieure de Ferques (U.F.); au sud, affaissée par rapport à l'unité septentrionale d'environ 250 mètres (fig 5), l'unité chevauchante du Haut-Banc (U.H.B.). Ces unités sont elles-même chevauchées au sud par l'unité d'Hydrequent. Ces différentes unités imbriquées sont interprétées comme le substratum écaillé du chevauchement du Midi localisé classiquement quelques kilomètres au sud des massifs paléozoïques du Boulonnais (e.g. Everaerts et Mansy, 2001).

La Z.F.F. affleure sur quelques kilomètres dans le massif paléozoïque du Boulonnais selon une direction N100-110 mais elle n'est clairement visible que dans les grandes carrières exploitant les niveaux carbonatés viséens (fig. 4). De nombreuses confusions ont régné au sujet de cette faille, à la fois sur sa nature et sa localisation précise. Comme nous

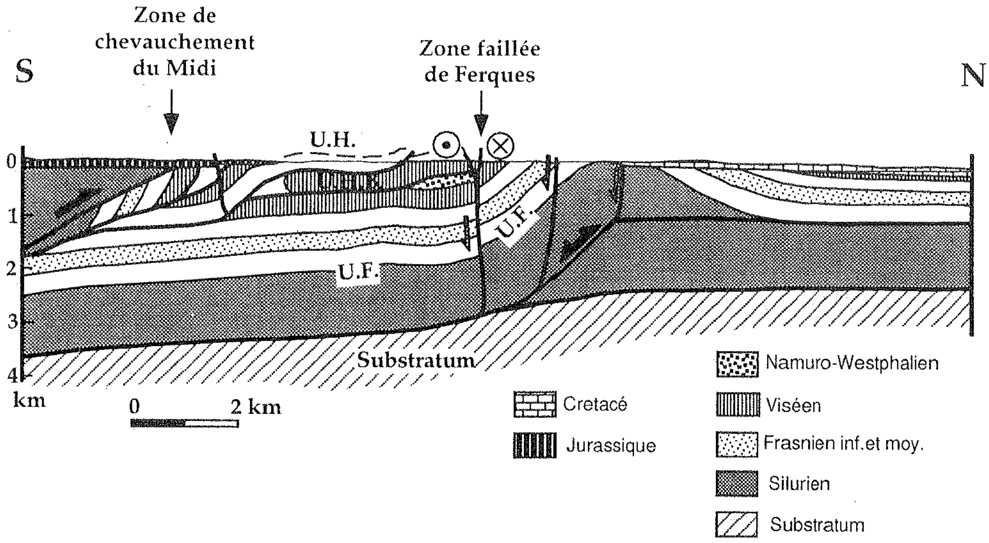

Fig. 5. — Coupe générale de la structure du front varisque dans le Boulonnais et relations avec les failles tardi-paléozoïques (modifiée de Averbuch et Mansy, 1998).

Fig. 5. — General cross-section of the Boulonnais thrust front and relationships with the Late Paleozoic faults (modified from Averbuch and Mansy, 1998).

le verrons, c'est en fait une zone faillée qui comprend plusieurs branches qui n'ont ni la même signification, ni le même aspect, entraînant des controverses importantes selon les auteurs et le lieu de description (Colbeaux et Leplat, 1982 ; Bouroz, 1985). A l'origine, la faille a été localisée et décrite à l'emplacement actuel des carrières du Boulonnais là où le houiller affleurait en surface. En se dirigeant vers l'Est, l'épaisseur du houiller jalonnant le contact faillé s'amenuise ce qui a été lié, par certains auteurs, à la disparition de la faille de Ferques. De nouvelles observations effectuées dans deux grandes carrières en exploitation permettent de mieux contraindre la géométrie de la zone faillée à la fois en ce qui concerne son tracé de surface et sa géométrie en coupe. Cette dernière est discutée à partir des deux coupes synthétiques de la figure 6.

1) **Géométrie du segment oriental** (fig 6A).

Sur la coupe orientale, on distingue du sud au nord, l'unité d'Hydrequent, constituée essentiellement de schistes et grès rouges d'âge famennien qui chevauchent l'U.H.B. carbonatée et viséenne en surface ; cette unité constitue le dôme du Haut Banc peu déformé sauf, sous le chevauchement d'Hydrequent où des duplex et de nombreux plis ont été décrits (Pruvost et Delépine, 1921 ; Cooper *et al.*, 1983 ; Averbuch et Mansy, 1998) ainsi qu'à proximité de la Z.F.F. En s'approchant de celle-ci, on distingue un petit synclinal hectométrique puis un anticlinal déversé vers le nord dont la partie supérieure est tronquée par la faille majeure à fort pendage vers le nord. Les lèvres de cette dernière sont écartées d'une dizaine de mètres et remplies de sédiments gréseux (F. Grès des Plaines) et charbonneux rapportés aux formations namuro-westphaliennes situées au toit de la série paléozoïque. Les épontes de cette zone faillée sont lissées et souvent gravées par des stries au pitch relativement faible traduisant une composante de déplacement décrochant selon la faille (voir la discussion sur la cinématique). Au nord de la faille principale, on reconnaît l'U.F. à pendage sud; celui-ci augmente en se rapprochant de la faille matérialisant un pli d'entrainement associé au réhaussement du compartiment nord. Sur le bord occidental de cette même carrière, le synclinal proche de la faille principale n'apparaît plus car la petite rampe qui l'a engendré disparaît très vite vers l'Ouest avec le pli à vergence Sud généré à son toit.

2) **Géométrie du segment occidental** (fig 6B).

On distingue au sud de la coupe l'Unité du Haut-Banc avec un pli pluridécametrique déversé vers le nord interprété comme un pli de propagation se bloquant sur une rampe à fort pendage (Mercier et Mansy, 1995). Durant ce processus, le pli subit un cisaillement important se marquant par un amincissement significatif du dressant. L'ensemble est tronqué par une faille à composante inverse à pendage nord (faille a en fig. 6B). Au nord de cette dernière, on observe deux cents mètres de roches viséennes et namuro-westphaliennes verticalisées et intensément déformées, constituées par de petits duplex métriques à décamétriques. Ces derniers sont séparés par des contacts très fortement pentés vers le sud et présentant de nombreux indices de coulissage (failles b et c en fig. 6B). Cet ensemble qui a été dénommé “ duplex des Moines ” en raison de sa limitation par des contacts faillés est à rattacher stratigraphiquement à l'unité tectonique de Ferques ainsi que l'attestent à la fois les faciès sédimentaires et les microfaunes (Prud'homme *et al.*, 1992). Il se termine par du houiller très déformé reposant en contact anormal sur les formations viséennes supérieures calcaires (Formation de Rety) en position sub-autochtone de l'unité de Ferques. En s'éloignant vers le Nord, on observe cette dernière dans sa totalité, avec un pendage qui diminue progressivement pour atteindre 40°.

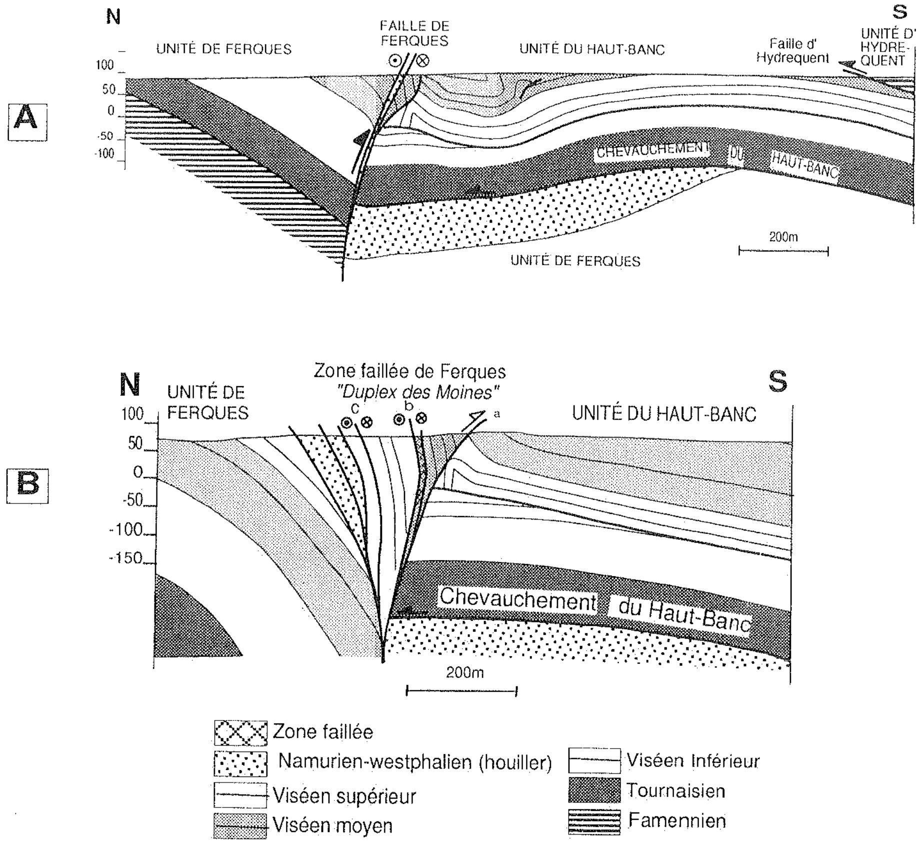

Fig. 6. — Géométrie en coupe de la zone faillée de Ferques. A. suivant une section orientale (carrières de la Vallée Heureuse, localisation en fig 4B); B. suivant une section occidentale (carrières des Moines, localisation en fig 4B).

Fig. 6. — Cross-section of the Ferques fault zone. A. eastern section (Vallée Heureuse quarry, location in fig. 4B); B. western section (Moines quarry, location in fig. 4B).

3) Synthèse sur la géométrie de la Z.F.F.

L'analyse de ces coupes N-S, distantes l'une de l'autre de quelques kilomètres amène un certain nombre d'enseignements sur la géométrie de cet accident. En premier lieu, elle montre que la Z.F.F. est un accident complexe impliquant localement (par exemple au niveau de la carrière des Moines) de nombreux contacts sub-verticaux. Ces derniers s'anastomosent latéralement puisque sur son segment oriental, elle n'est constituée que d'une zone faillée très réduite (quelques mètres). La Z.F.F. forme ainsi une structure en duplex décrochant (Woodcock et Fischer, 1986) d'échelle kilométrique (fig 4). Les mauvaises conditions d'affleurement ne permettent pas de préciser la géométrie exacte de branchement entre les différents contacts, en particulier sur l'extrémité occidentale de l'écaille. Comme le souligne Woodcock et Fischer (1986), ce type de structure est probablement le résultat d'une accommodation cinématique des conditions aux limites appliquées au système décrochant. Il s'agirait là d'une zone de relai le long du décrochement contrôlé par la géométrie initiale des unités varisques. En coupe, la géométrie en éventail divergent des contacts à l'intérieur de la zone faillée traduit l'allure caractéristique d'une structure en fleur (Harding, 1985 ; Naylor *et al.*, 1986) formée au cœur d'un dispositif décrochant contemporain du soulèvement relatif du compartiment nord de la faille. Sa géométrie en profondeur est peu contrainte. Néanmoins, son orientation là où elle présente la géométrie la plus simple (coupe orientale de la fig 6A), suggère un tracé en profondeur sub-vertical ou à pendage surélevé vers le Nord. Par ailleurs, la localisation de la zone faillée au niveau de la brisure des couches de l'unité de Ferques suggère qu'elle se raccorde à la base de la rampe chevauchante situé sous cette unité (fig 5) (Averbuch et Mansy, 1998) à la manière d'un rétro-chevauchement tardif (e.g. Frizon de Lamotte *et al.*, 1995) ou d'une faille normale consécutive à un phénomène d'inversion négative (e.g. Williams *et al.*, 1989). Il est à noter l'existence au nord de la faille de Ferques de deux failles à composante normale d'âge probable permo-triasique et à rejet vertical pluridécamétrique (les failles du Griset et de Landrethun) dont la géométrie laisse à penser qu'elle réutilise la rampe de base de l'édifice chevauchant.

IV. — CINEMATIQUE DES DEFORMATIONS AU SEIN DE LA ZONE FAILLEE DE FERQUES :

1) Analyse des microstructures cassantes.

L'étude des marqueurs de la déformation a été menée le long de la Z.F.F. au niveau des deux coupes proposées en fig 6. Les écailles calcaires impliquées dans la zone faillée des Moines (fig 6B) présentent un ensemble de microstructures cassantes très bien exprimées. En dehors des structures tangentielles à vergence NW héritées de la déformation varisque (Averbuch et Mansy, 1998), un ensemble de microfailles à jeu décrochant majeur peut être caractérisé (fig 7A) ; il s'agit pour la plupart de failles d'orientation subE-W à pendage relativement fort vers le sud présentant un déplacement oblique avec une composante sénestre majeure associée à une composante normale. Bien que la part relative de ces composantes de déplacement varie légèrement selon les failles, on note une faible tendance à la partition de la déformation au sein de la zone décrochante. Cette observation pourrait s'expliquer par l'absence d'un niveau de décollement important à la base de l'accident ainsi que le suggèrent les expériences de modélisation analogique (Richard et Cobbold, 1990). Associé à ces structures, on retrouve un ensemble de microfailles subverticales orientées entre N160 et N045 et présentant un jeu dextre avec localement une composante inverse. Cette famille de failles transverses dextres est également soulignée en carte par le décalage de la faille de Ferques et des couches d'orientation générale E-W (failles d'Elinghen (FE), de Locquinghen (FL) en fig. 4).

Le caractère non-coaxial des déformations observées dans la zone faillée des Moines ne permet pas d'appliquer les méthodes d'analyse tensorielle des contraintes. Par contre, on remarque que les failles mesurées s'organisent suivant des systèmes de Riedel (e.g. Tchalenko, 1970) (fig 7B) conférant à la zone faillée des Moines un jeu majeur décrochant sénestre induit dans un système en raccourcissement orienté environ N060 et en allongement suivant une direction environ N330.

Dans la carrière de la Vallée Heureuse (coupe de la fig 6A), l'analyse des microstructures autour de la zone faillée s'est avérée moins nette ; on note en particulier en plus de la fracturation décrite ci-dessus l'existence de failles E-W à jeu dextre inverse associées à des plans N-S à NE-SW à jeu sénestre (fig 7C). Ces déformations traduisent un raccourcissement orienté NNW-SSE parallèle à la direction de compression mise en évidence dans les formations jurassiques et crétacées sus-jacentes (Lamarche *et al.*, 1996). Ces dernières sont donc plutôt interprétées comme le résultat de réactivations localisées et mineures issues de l'épisode d'inversion tectonique post-Crétacé bien caractérisé dans la région (Bouroz, 1956 ; Lamarche *et al.*, 1997 ; Mansy *et al.*, in press).

2) Analyse de la fabrique magnétique.

Afin de contraindre le jeu majeur de la faille de Ferques dans la carrière de la Vallée Heureuse, la déformation finie des niveaux houillers entraînés le long de la faille a été analysée à partir de l'étude de l'Anisotropie de la Susceptibilité Magnétique (ASM). Cette méthode, largement utilisée maintenant en analyse structurale (e.g. Borradaile et Henry, 1997) traduit l'orientation préférentielle des minéraux magnétiques à l'intérieur de la roche. Dans les milieux déformés même faiblement, il a été montré que les axes principaux de l'ellipsoïde d'ASM permettaient de renseigner sur l'orientation des directions de raccourcissement et d'allongement de la déformation finie (Kligfield *et al.*, 1981 ; Averbuch *et al.*, 1993).

Dans les niveaux schisteux houillers étudiés, les faibles valeurs de susceptibilité magnétique (entre 100 et 200.10^{-6} SI) ainsi que la quantité importante en matériel argileux tend à faire penser que la fabrique magnétique mesurée est en grande partie le résultat de l'orientation préférentielle des phyllosilicates. Les niveaux échantillonnés, fortement déformés lors du jeu de la faille de Ferques, présente une anisotropie assez développée pour des roches sédimentaires avec un taux d'anisotropie moyen de 1.071. La fabrique montre une tendance globalement planaire ainsi que l'indique le diagramme de type Flinn linéation magnétique/foliation magnétique de la figure 8A. On peut remarquer cependant que le degré planaire de la fabrique augmente avec le taux d'anisotropie des échantillons rocheux (fig 8B). Cette évolution, indépendante de l'intensité de la susceptibilité magnétique et donc des variations de la minéralogie magnétique, peut être interprétée en terme de variation d'intensité de la déformation entre échantillons et traduit probablement le degré de pénétrativité d'une schistosité de pression-dissolution locale développée dans la zone faillée. Malgré ce caractère légèrement hétérogène de la déformation, l'orientation des axes principaux minimum, intermédiaires et maximum est remarquablement cohérente entre échantillons ainsi que l'attestent leur groupement visualisé sur le stéréodiagramme de la figure 8C. La foliation magnétique (plan perpendiculaire au groupement des axes miminum kmin) est parallèle au plan de schistosité de pression-dissolution observable très localement en bordure de la faille; la direction locale de raccourcissement, donnée par la direction moyenne de kmin, est d'environ N070. Dans le plan de foliation magnétique, la linéation magnétique (groupement des axes maximum) s'oriente selon la direction N143. Les axes minimum et maximum de susceptibilité magnétique déterminent donc un ellipsoïde d'ASM oblique sur la direction de faille et peuvent être ainsi utilisés pour déterminer son sens de déplacement ainsi qu'il a été montré par Borradaile *et al* (1989) dans le cas d'une faille décrochante du bouclier canadien. Il est à noter que l'orientation des axes minimum et maximum d'ASM correspondent à peu près aux directions de raccourcissement et d'allongement déduites de l'analyse des failles de la carrière des Moines. La fabrique magnétique provenant des niveaux houillers compris entre les lèvres de la Faille de Ferques dans la carrière de la Vallée Heureuse suggère un jeu majeur décrochant sénestre lié à un épisode en raccourcissement ENE-WSW et en extension NNW-SSE.

V. — DISCUSSION ET CONCLUSION.

L'analyse géometrique et cinématique des déformations dans les unités paléozoïques du Boulonnais ainsi que l'étude des relations entre socle varisque et couverture mésozoïque permettent de dégager un scénario d'évolution tectonique pour la période tardi-Paléozoïque au front septentrional de l'allochtone varisque.

La zone faillée de Ferques, qui constitue le seul élément exhumé du faisceau de failles de socle en échelon jalonnant le front varisque depuis l'Artois jusqu'au Boulonnais, présente une géométrie complexe impliquant de nombreux accidents d'orientation générale N100 s'anastomosant latéralement. La structure résultante en duplex décrochant d'échelle kilométrique présente en coupe une allure en fleur

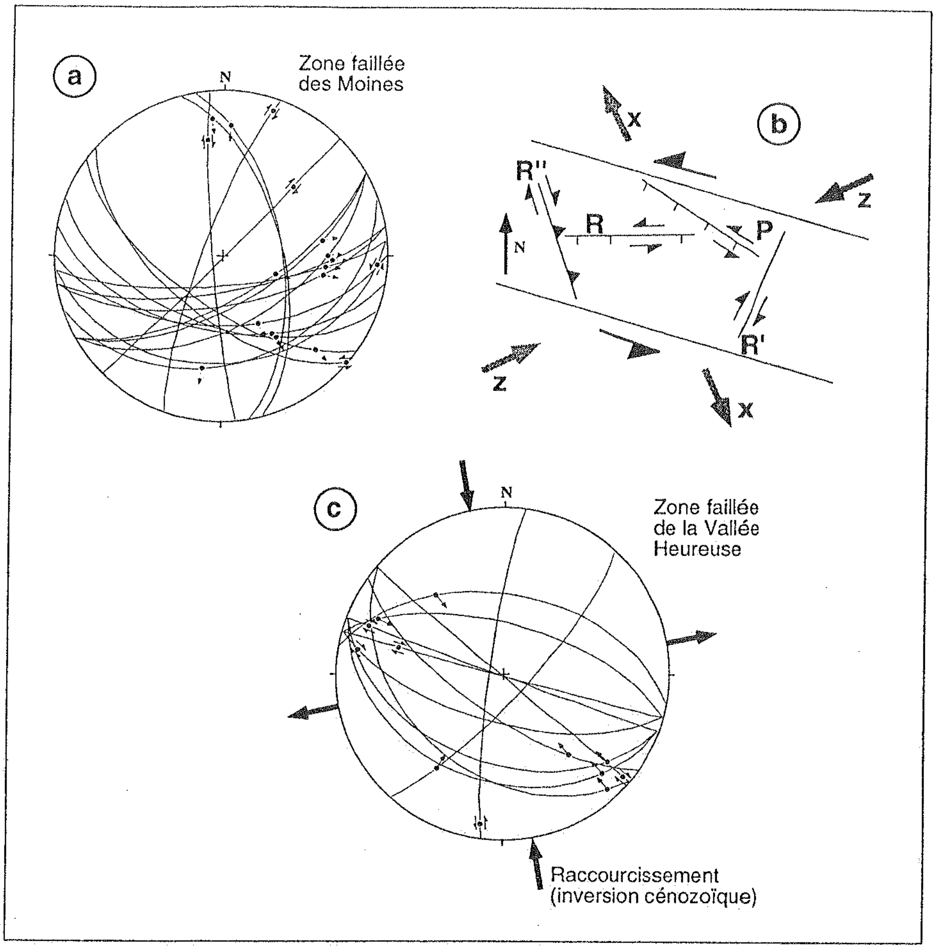

Fig. 7. — a. Projection stéréographique (hémisphère inférieur) des populations de microfailles mesurées dans le « duplex décrochant des Moines » (section occidentale de la zone faillée de Ferques); b. Interprétation dans un modèle de type Riedel; c. Projection stéréographique (hémisphère inférieur) des populations de microfailles associées au rejeu cénozoïque de la zone faillée (section orientale, Carrière de la Vallée Heureuse).

Fig 7. — a. Lower hemisphere stereodiagrams showing the kinematics of microfaults within the « Moines strike-slip duplex » (western section of the Ferques fault zone); b. Integration in a Riedel type model; c. Lower hemisphere stereodiagram showing the kinematics of the Cenozoic reactivation of some microfaults within the fault zone (eastern section, Vallée Heureuse quarry).

caractéristique d'un déplacement impliquant à la fois une composante décrochante et transverse. Les écailles verticalisées au coeur de la structure sont formées d'une série schisto-gréseuse houillère et carbonatée viséenne supérieure disloquée mais conservant une polarité telle que les niveaux les plus anciens se retrouvent sur le bord sud de la zone faillée. Ces écailles sont interprétées comme des lambeaux arrachés latéralement à l'unité de Ferques (compartiment nord de la zone faillée) et venus s'accréter progressivement au sein d'une zone de relai transtensif. La composante de déplacement normal observée sur les contacts fortement pentés vers le sud traduit le réhaussement concomitant du compartiment nord dont la partie sommitale était composée de Houiller. Ce dernier induit l'exhumation progressive de l'unité de Ferques ce qui se traduit par l'accrétion progressive de niveaux de plus en plus anciens au niveau de la bordure méridionale de la zone faillée.

Le déplacement horizontal total le long de la zone faillée est difficile à estimer précisément en carte. Cependant, compte tenu du pitch des stries observés sur les contacts à l'intérieur de la zone faillée (en moyenne entre 20° et 40°) et du rejet vertical constaté (environ 250 m), on peut estimer que le déplacement horizontal avoisine les 500m. Les mouvements coulissants majeurs sont à jeu sénestre ainsi que l'indiquent à la fois les données de la cinématique des microfailles et les données de fabrique magnétique des niveaux houillers déformés au sein de la zone faillée. Ces résultats sont à rapprocher des données cinématiques obtenues dans le Stéphano-Permien de Grande-Bretagne par Hibsch *et al* (1993) et Shail & Alexander (1997) et suggèrent l'existence d'un épisode décrochant associé à une extension NNW-SSE et une compression ENE-WSW. Dans le nord de la France, cet épisode de déformation a également été décrit en sub-surface dans le bassin houiller du Nord-Pas de Calais, en particulier en Artois au niveau des galeries de la fosse 24 d'Estevelles (Becq-Giraudon, 1983). Ces données s'intègrent bien, par ailleurs, au scénario d'évolution tectonique mis en évidence dans les bassins stéphano-permiens de Sarre-Lorraine où une phase d'extension N-S post-plis et antérieur au Permien moyen a pu être mise en évidence (Donsimoni, 1981). Dans les zones plus internes de l'orogène varisque, on

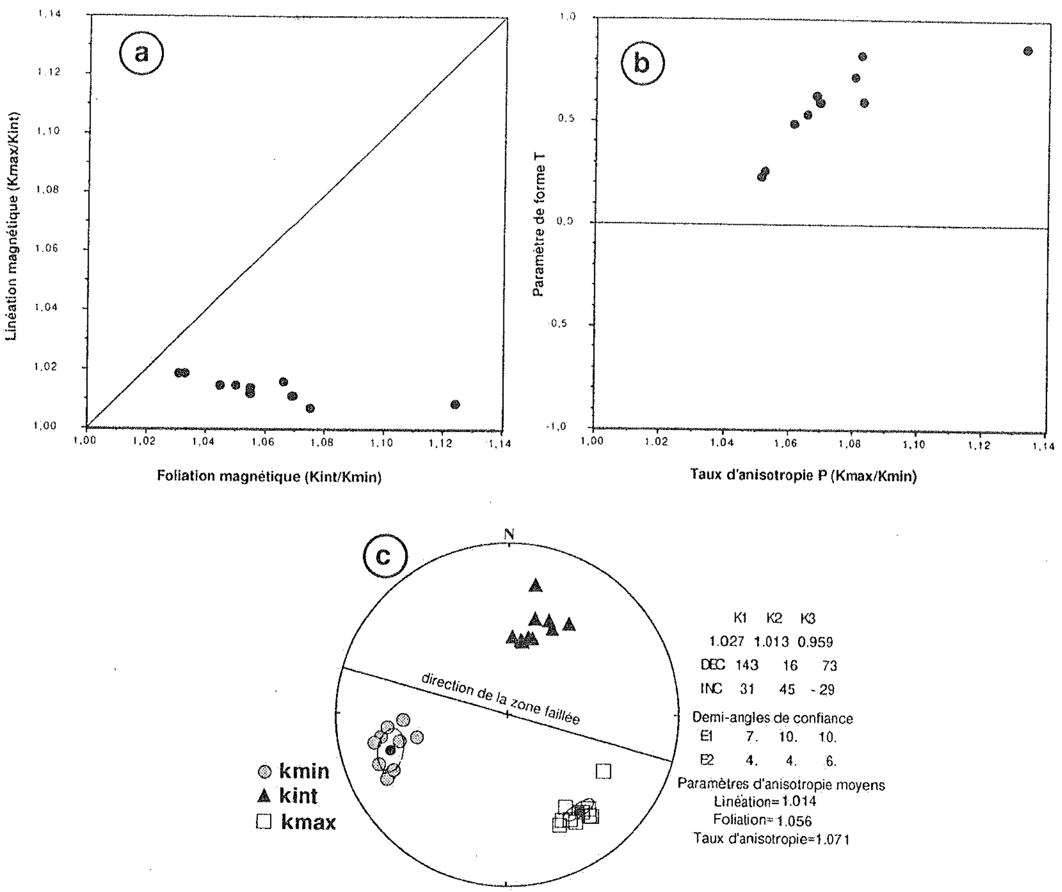

Fig. 8. — a. Diagramme de type " Flinn " reportant le paramètre de linéation magnétique (L=kmax/kint) en fonction de celui de foliation magnétique (F=kint/kmin). Les points situés au dessous de la droite L=F caractérisent une fabrique principalement planaire tandis que ceux situés au dessus montrent une fabrique principalement linéaire. b. Diagramme reportant le paramètre de forme T en fonction du taux d'anisotropie P (kmax/kmin). T= -1 correspond à une fabrique complétement linéaire, T=+1 à une fabrique complètement planaire. c. Stéréodiagramme (hémisphère inférieur, surfaces conservées) montrant l'orientation des axes principaux d'ASM mesurés dans les dépôts houillers coincés dans la zone faillée.

Fig. 8. — a. Flinn type diagram showing the magnetic lineation parameter L(kmax/kint) versus the magnetic foliation parameter F (kint/kmin). Points situated below the L=F line refer to dominantly planar fabrics; the ones situated above the L=F line refer to dominantly linear fabrics. b. Diagram reporting the T shape parameter versus the anisotropy degree P (kmax/kmin). T=-1 corresponds to completely linear fabrics, T=+1 to completely planar fabrics. c. Stereodiagram (lower hem., equal area) showing the orientation of the principal axes of AMS measured within the coal-bearing rocks deformed within the Ferques fault zone.

retrouve également cet événement tectonique ainsi que le montrent les données de cinématique des déformations tardi-paléozoïques dans le Massif Central (Bonijoly et Castaing, 1984 ; Vallé *et al.*, 1988), les Alpes occidentales (Handy *et al.*, 1999) ou le sud de la France (Soula, 1984 ; Genna et Debriette, 1994). L'ensemble de ces données illustrent ainsi la rotation systématique observée à cette époque pour la direction de compression depuis une orientation environ N-S varisque à une orientation E-W tardi-varisque (e.g. Ziegler, 1990).

Les données microstructurales ne permettent pas de mettre en évidence de jeu dextre d'âge stéphano-permien le long des failles subE-W jalonnant le front N-varisque ainsi qu'il est classiquement admis dans les reconstitutions tectoniques. Il est à noter, à cet égard, que le mouvement décrochant dextre défini sur la faille du Pays de Bray, parallèle à la Z.F.F., est daté à 330 Ma (Matte *et al.*, 1986) alors que le chevauchement du Midi ne s'est pas encore propagé sur le bassin houiller d'avant-chaîne (e.g. Lacquement, 2001). Il est probable que le jeu dextre de la faille du Pays de Bray matérialise un phénomène de partition de la déformation au sein d'un ensemble soumis à une convergence oblique. Ce processus, qui peut potentiellement s'étendre jusqu'au front chevauchant, relève de mécanismes syn-orogéniques d'âge Viséen à Stéphanien basal totalement différents de ceux associés aux déformations décrochantes tardi-paléozoïques mises en évidence.

Au sein du domaine nord varisque, l'ensemble des accidents orientés WNW-ESE jalonnant une région comprise entre le Pays de Bray et le front varisque Artois-Boulonnais peut être considéré à l'époque stéphano-permienne comme une zone de relai transtensif entre les bassins extensifs fortement subsidents de Manche occidentale et du sud de l'Angleterre (Chapman, 1989 ; Edwards *et al.*, 1997) et de Sarre-Lorraine (Donsimoni , 1981 ; Korsch and Schäfer, 1995) (fig 9) dont l'orientation est quasi-perpendiculaire à la

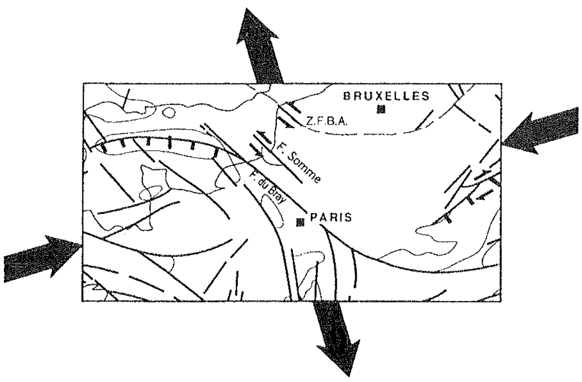

Fig. 9. — Schéma structural montrant la cinématique des déformations tardi-paléozoïques dans le nord de la France et leur intégration dans le motif géodynamique régional (fond structural modifié de Ziegler, 1990). Z.F.B.A. : Zone Faillée Boulonnais-Artois.

Fig. 9. — Structural map showing the kinematics of the Late Paleozoic deformations in the N of France and their integration in the regional geodynamic framework (structural map modified from Ziegler, 1990). Z.F.B.A. : Boulonnais-Artois Fault Zone.

direction d'extension NNW-SSE s'appliquant à cette époque. La cinématique de ce système s'intègre difficilement dans un modèle considérant le domaine varisque comme une limite de plaque diffuse soumise à un cisaillement dextre E-W. Ces déformations résultent plutôt de l'accommodation cinématique d'une extension oblique sub-méridienne par un domaine fortement pré-structuré au cours de l'orogénèse varisque ainsi que le montre le moulage des structures tardi-paléozoiques sur le front de chevauchement varisque. Ce mécanisme contribuerait au ré-équilibrage thermique et à l'amincissement de la partie la plus externe de la croûte varisque surépaissie et pourrait être à l'origine de l'individualisation du bassin de Paris dès le Stéphano-Autunien ainsi que le suggèrent les données de modélisation thermique du bassin (Prijac *et al.*, 2000). Sur la base d'expériences de modélisation thermo-mécanique de la lithosphère varisque (Henk, 1999), il a été par ailleurs suggéré que ce phénomène ne soit pas simplement le résultat d'un mécanisme d'extension tardi-orogénique *sensu stricto* tel qu'il est classiquement proposé mais implique également des contraintes extensives en bordure du système déformé. L'analyse de données cinématiques dans les domaines externes du système orogénique s'avère donc essentielle pour mieux comprendre la dynamique tardive de la chaîne varisque d'Europe occidentale.

Remerciements. — Les auteurs tiennent à remercier les carrières du Boulonnais et de la Vallée heureuse pour leur avoir permis l'accès aux affleurements. Merci également à G. Manby et M. Everaerts pour les discussions constructives qui ont permis de préciser certains aspects de cet article. M. Bocquet est remerciée pour son travail sur certaines figures de cet article.

BIBLIOGRAPHY

ARTHAUD F.et MATTE P.(1977). — Late Paleozoic strike-slip faulting in southern Europe and northern Africa: result of a right-lateral shear zone between the Appalachians and the Urals. *Geological Society of America Bulletin* 88, 1305-1320.

AVERBUCH O., FRIZON DE LAMOTTE D. et KISSEL C. (1992). — Magnetic fabric as a structural indicator of the deformation path within a fold-thrust structure: a test case from the Corbières (NE Pyrénées, France). *J. Struct. Geol.,* 14, 461-474.

AVERBUCH O. et MANSY J.L. (1998). — The "Basse-Normandie" duplex: evidence for an out-of-sequence thrusting overprint. *J. Struct. Geol.,* 20, 33-42.

BARD J.P. (1997). — Démembrement anté-mésozoïque de la chaîne varisque d'Europe occidentale et d'Afrique du Nord: rôle essentiel des grands décrochements transpressifs dextres accompagnant la rotation-translation horaire de l'Afrique durant le Stéphanien. *C.R. Acad. Sci. Paris*, 324, 693-704.

BECQ-GIRAUDON J.F. (1983). — Synthèse structurale et paléogéographique du bassin houiller du Nord et du Pas-de-Calais. *Mem. BRGM*, 123, 68p.

BECQ-GIRAUDON J.F.et VAN DEN DRIESSCHE J. (1994). — Dépôts périglaciaires dans le Stéphano-Autunien du Massif Central: témoin de l'effondrement gravitaire d'un haut plateau hercynien. *C.R. Acad. Sci. Paris*, 318, 675-682.

BONIJOLY D. et CASTAING C. (1984). — Fracturation et génèse des bassins stéphaniens du Massif central français en régime compressif. Ann. Soc. géol. Nord CIII (1984) 187-189.

BORRADAILE G.J., TELLA S. et MC ARTHUR J. (1989). — Magnetic fabric as a kinematic indicator of faults: a test case. *Annales Tectonicae*, 3, 3-11.

BORRADAILE G.J. et HENRY B. (1997). — Tectonic applications of magnetic susceptibility and its anisotropy. *Earth Science Reviews*, 42, 49-93.

BOUROZ A. (1948). — La structure du bassin houiller du Pas-de-Calais à l'ouest du méridien de Lens. *Annales Société géologique Nord*, 68, 93-105.

BOUROZ A. (1950). — Sur quelques aspects du mécanisme de la déformation tectonique dans le bassin houiller du Nord de la France. *Annales Société géologique Nord,* 70, 2-55.

BOUROZ A. (1956). — Contribution à l'étude des failles épicrétacées de l'Artois. *Annales Société géologique Nord*, 76, 51-62.

BOUROZ A. (1985) Coulissement dans le Paléozoïque du Boulonnais : la Faille de Ferques. *Annales Société géologique Nord*, 105, 37-41.

BOUROZ A. et COLL. (1963). — Carte des zones stratigraphiques à la côte -300 au 1/50000.*Houillères du Bassin du Nord et du Pas de Calais ed.*

BURG J.P., BRUN J.P. et VAN DEN DRIESSCHE J. (1990). — Le sillon houiller du Massif Central français: faille de transfert pendant l'amincissement crustal de la chaîne varisque? *C.R. Acad. Sci. Paris*, 311, 147-152.

BURG J.P., VAN DEN DRIESSCHE J. et BRUN J.P. (1994). — Syn- to post-thickening extension: mode and consequences. *C.R. Acad. Sci. Paris*, 319, 1019-1032.

CAZES M., BOIS C., TOREILLES G., DAMOTTE B., GALDEANO A., HIRN A., MASCLE A., MATTE P., PHAM V.N. et RAOULT J-F. (1985). — Structure de la croûte hercynienne du Nord de la France: premiers résultats du profil ECORS. *Bull. Soc. géol. France*, 8, 925-941.

CHAPMAN T.J. (1989). — The Permian to Cretaceous structural evolution of the Western Approaches Basin (Melville sub-basin), UK From Cooper M.A. & Williams G.D.(eds), Inversion Tectonics, *Geological Society Special Publication,* 44, 177-200.

COLBEAUX J-P. (1984). — L'évolution structurale du sud de la Belgique et du nord de la France: sa relation avec la dérive des continents- quelques hypothèses. *Bull. Soc. belge de Géol.,* 93,71-78.

COLBEAUX J.P. et LEPLAT J. (1982). — Apports de l'exploitation du charbon et des matériaux de construction à la connaissance de la structure du massif primaire du Boulonnais. *Ann. Soc. géol. Nord*, 102, 103-110.

COOPER M.A., GARTON M.R.et HOSSACK J.R. (1983). — The origin of the Basse Normandie duplex, Boulonnais. *J. Struct. Geol.,* 5, 139-152.

ECHTLER H.et MALAVIEILLE J. (1990). — Extensional tectonics, basement uplift and Stephano-Permian collapse basin in a Late Variscan metamorphic core complex (Montagne Noire, southern Massif Central). *Tectonophysics*, 177, 125-138.

EDWARDS R.A., WARRINGTON G., SCRIVENER R.C., JONES N.S., HASLAM, H.W et AULT L. AL (1997). — The Exeter Group, south Devon, England : a contribution to the early post-Variscan stratigraphy of northwest Europe. *Geol. Mag.,* 134, 177-197.

EVERAERTS M. et MANSY J-L. (2001). — Le filtrage des anomalies gravimétriques: une clé pour la compréhension des structures tectoniques du Boulonnais et de L'Artois (France). *Bull. Soc.géol. France*, 172, 267-274.

FAURE M. et BECQ-GIRAUDON J.F. (1993). — Sur la succession des épisodes extensifs au cours du désépaississement carbonifère du Massif Central français. *C.R. Acad. Sci. Paris*, 316, 967-973.

FRIZON DE LAMOTTE D., GUEZOU J.C. et AVERBUCH O. (1995). — Distinguishing lateral folds in thrust systems ; examples from Corbières (SW France) and Betic Cordilleras (SE Spain). *J. Struct. Geol.,*17, 223-245.

GAPAIS D., LAGARDE J.L., LE CORRE C., AUDREN C., JEGOUZO P., CASAS SAINZ A. et VAN DEN DRIESSCHE J. (1993). — La zone de cisaillement de Quiberon: témoin d'extension de la chaîne varisque en Bretagne méridionale au Carbonifère. *C.R. Acad. Sci. Paris,* 316, 1123-1129.

GENNA A. et DEBRIETTE P.J. (1994). — Structures en fleur dans le bassin houiller d'Alès. Implications structurales. *C.R. Acad. Sci. Paris*, 318, 977-984.

HANDY M.R., FRANZ L., HELLER F., JANOTT B. et ZURBRIGGEN R. (1999). — Multistage accretion and exhumation of the continental crust (Ivrea section, Italy and Switzerland). *Tectonics*, 18, 1154-1177.

HARDING T.P. (1985). — Seismic characteristics and identification of negative flower structures, positive flower structures and positive structural inversion. *Am. Ass. Petrol. Geol. Bull.,* 69, 582-600.

HENK A. (1999). — Did the Variscides collapse or were they torn apart ? : a quantitative evaluation of the driving forces for postconvergent extension in central Europe. *Tectonics*, 18, 774-792

HIBSCH C., CUSHING E.M., CABRERA J., MERCIER J., PRASIL P. et JARRIGE J.J. (1993). — Evolution des paléo-contraintes en Grande-Bretagne du Permien au Cénozoïque : approche géodynamique de l'évolution des bassins méridionaux du royaume uni. *Bull. C.R.E.D.P.*, 17, 304-330.

KLIGFIELD R., OWENS W.H. et LOWRIE W. (1981). — Magnetic susceptibility, anisotropy, strain and progressive deformation in Permian sediments from the Maritime Alps (France). *Earth and Planetary Science Letters*, 55, 181-189.

KORSCH R.J. et SCHÄFER A. (1995). — The Permo-Carboniferous Saar-Nahe Basin, south-west Germany and north-east France: basin formation and deformation in a strike-slip regime. *Geol. Rundsch.,* 84, 293-318.

LACQUEMENT F. (2001). — L'Ardenne varisque. Déformation progressive d'un prisme sédimentaire pré-structuré, de l'affleurement au modèle de chaîne. *Société géologique du Nord*, publication 29, 285p.

LACQUEMENT F., MANSY J-L., HANOT F. et MEILLIEZ F. (1999). — Retraitement et interprétation d'un profil sismique pétrolier méridien au travers du massif paléozoïque ardennais (Nord de la France). *C.R. Acad. Sci. Paris* , 329, 471-477.

LAMARCHE J., BERGERAT F. et MANSY J.L. (1996). — Tectonique plicative et cassante dans le Jurassique du Boulonnais: une histoire méso-cénozoïque polyphasée. *Annales Soc. géol. Nord*, 4, 171-179.

LAMARCHE J., BERGERAT F. et MANSY J.L. (1997). — Déformation cassantes et plicatives dans le Jurassique du Boulonnais, influence lithostructurale et héritage paléozoïque. *C.R.Acad. Sci., Paris,* 326, 57-63.

LEFORT J.P. et JAFFAL M. (1991). — Les témoins de l'extension post-hercynienne dans la croute inférieure litée de la Manche Occidentale et de la Mer celtique. *Bull.Centres Rech. Explor.-Prod. Elf Aquitaine* , 18, 421-436.

LEGRAND X., SOULA J.C. et ROLANDO J.P. (1991). — Effet d'une inversion tectonique négative dans le sud du Massif Central français: la structure " roll-over " du bassin permien de Saint-Affrique. *C.R. Acad. Sci. Paris* , 312, 1021-1026.

LEWANDOWSKI M., LAMARCHE J., MANSY J.L., AVERBUCH O. et SZANIAWSKI R. (1999). — Palaeomagnetic dating of brittle tectonics structures : case studies on Ferques Fault (Boulonnais, France) and two faults from the Holy Cross Mountains (Poland). *C. R. Acad. Sci.*, Paris, 329, 495-502.

MALAVIEILLE J. (1993). — Late orogenic extension in mountain belt: insights from the Basin and Range and the Late Paleozoic variscan belt. *Tectonics,* 12, 1115-1130.

MALAVIEILLE J., GUIHOT P., COSTA S., LARDEAUX J.M. et GARDIEN V. (1990). — Collapse of a thickened Variscan crust in the French Massif central: Mont-Pilat extensional shear zone and Saint-Etienne Upper carboniferous basin. *Tectonophysics*, 177, 139-149.

MANSY J.L., AMEDRO F., AUFFRET J.P., GUENNOC P., LAMARCHE J., LEFEVRE D., ROBASZYNSKI F., SOMME J. et VIDIER J.P. (sous presse). — Carte géologique de Marquise (50000ème). *2ème édition. B.R.G.M., Orléans.*

MANSY J.L., MANBY G.M., AVERBUCH O., EVERAERTS M., BERGERAT F., VAN VLIET-LANOE B. et LAMARCHE J. (sous presse). — Inversion of the Mesozoic basin of the Weald-Boulonnais area : role of basement reactivation. *Tectonophysics.*

MATTAUER M. et MATTE P. (1998). — Le bassin stéphanien de St-Etienne ne résulte pas d'une extension tardihercynienne généralisée: c'est un bassin pull-apart en relation avec un décrochement dextre.*Geodinamica Acta* , 11, 23-32.

MATTE P., RESPAUT J.P., MALUSKI H., LANCELOT J. et BRUNEL M. (1986). — La faille NW-SE du Pays de Bray, un décrochement ductile dextre hercynien: déformation à 330 Ma d'un granite à 570 Ma dans le sondage Pays de Bray 201. *Bull. Soc. géol. France*, 8, 69-77.

MÉNARD G. et MOLNAR P. (1988). — Collapse of a Hercynian Tibetan Plateau into a Late Paleozoic European Basin and Range province, *Nature*, 334, 235-237.

MERCIER E. et MANSY J.L. (1995). — Le blocage du transport sur le plat des plis de propagation : une cause possible des chevauchements hors séquence. *Geodinamica Acta*, 8, 199-210.

MERIAUX E. (1961). — Observations sur les conglomérats et marbres rouges de l'Artois. *Ann. Soc. Géol. Nord*, 81, 65-71.

NAYLOR M.A., MANDL G. et SIJPESTEIJN C.H.K. (1986). — Fault geometries in basement-induced wrench faulting under different intial stress states. *Journal of Structural Geology*, 8, 725-735.

PRIJAC C., DOIN M.P., GAULIER J.M. et GUILLOCHEAU F. (2000). — Subsidence of the Paris basin and its bearing on the Late Variscan lithosphere evolution : a comparison between Plate and Chablis models. *Tectonophysics*, 323, 1-38.

PRUD'HOMME A., VACHARD D. et MANSY J.L. (1992). — Séries carbonatées viséennes du Boulonnais (France). Mise en évidence d'un diachronisme et ses conséquences structurales. *C. R. Acad. Sci.*, 315, 363-369.

PRUVOST P. et DELEPINE G. (1921). — Observations sur la Faille d'Hydrequent et sur les couches de base du Carbonifère dans le Bas Boulonnais. *Bull. Soc. géol. Fr.*, (4) XXI, 189-206

RAOULT J-F et MEILLIEZ F. (1987). — The Variscan Front and the Midi fault between the Channel and the Meuse river. *J. Struct. Geol.*, 9, 473-479.

RICHARD P. et COBBOLD P. (1990). — Experimental insights into partitioning of fault motions in continental convergent wrench zones. *Annales Tectonicae*, 4, 35-44.

SHAIL R.K. et ALEXANDER A.C. (1997). — Late Carboniferous to Triassic reactivation of Variscan basement in the western English Channel : evidence from onshore exposures in south Cornwall. *J. Geol. Soc. London*, 154, 163-168.

SOULA J.C. (1984). — Genèse de bassins sédimentaires en régime de cisaillement transcurrent: modèles expérimentaux et exemples géologiques. *Bull. Soc. belge Géol.* 93, 83-104.

TCHALENKO J.S. (1970). — Similarities between shear zones of different magnitudes. *Geological Society of America Bulletin*, 81, 1625-1640.

VALLE B., COUREL L. et GELARD J.P. (1988). — Les marqueurs de la tectonique synsédimentaire et syndiagénétique dans le bassin stéphanien à régime cisaillant de Blanzy-Montceau (Massif Central, France). *Bull. Soc. géol. France*, 8, 529-540.

VAN DEN DRIESSCHE J. et BRUN J.P. (1989). — Un modèle cinématique de l'extension paléozoïque supérieure dans le sud du Massif Central. *C.R. Acad. Sci. Paris*, 309, 1607-1613.

WILLIAMS G.D., POWELL C.M. et COOPER M.A. (1989). — Geometry and kinematics of inversion tectonics. in: Cooper M.A. & Williams G.D.(Eds), Inversion Tectonics, *Geological Society Special Publication*, 44, pp. 3-15.

WOODCOCK N.H. et FISCHER M. (1986). — Strike-slip duplexes. *Journal of Structural Geology*, 8, 725-735.

ZIEGLER P.A. (1990). — Geological Atlas of Western and Central Europe. *Shell Internationale Petroleum Maatschappij B.V.*, 239p.

Article 3.

Mansy J.L., Manby G., Averbuch O., Everaerts M., Bergerat F., Van Vliet-Lanoe B., Lamarche J., Vandycke S. (2003)- Dynamics and inversion of the Mesozoic basin of the Weald-Boulonnais area: role of basement reactivation. Tectonophysics, 373, 161-179.

Available online at www.sciencedirect.com
SCIENCE DIRECT®
Tectonophysics 373 (2003) 161–179
TECTONOPHYSICS
www.elsevier.com/locate/tecto

Dynamics and inversion of the Mesozoic Basin of the Weald–Boulonnais area: role of basement reactivation

J.-L. Mansy[a,*], G.M. Manby[b], O. Averbuch[a], M. Everaerts[c], F. Bergerat[d], B. Van Vliet-Lanoe[a], J. Lamarche[a,d,1], S. Vandycke[e]

[a] *Laboratoire de Sédimentologie et Géodynamique, FRE 2255 CNRS, Université des Sciences et Technologies de Lille, 59655 Villeneuve d'Ascq Cedex, France*
[b] *Earth and Environmental Sciences, University of Greenwich, Chatham Maritime, Kent ME4 4TB, England, UK*
[c] *Belgian Royal Observatory, Av. Circulaire 3, B-1180 Brussels, Belgium*
[d] *Laboratoire de Tectonique, UMR7072 CNRS, Boîte 129, Université Paris VI, 4 Place Jussieu, 75252 Paris Cedex 05, France*
[e] *Laboratoire de Géologie Fondamentale et Appliquée, Faculté Polytechnique de Mons, 9, rue de Houdain, B-7000 Mons, Belgium*

Received 26 October 2001; accepted 12 December 2002

Abstract

The geometry and dynamics of the Mesozoic basins of the Weald–Boulonnais area have been controlled by the distribution of preexisting Variscan structures. The emergent Variscan frontal thrust faults are predominantly E–W oriented in southern England while in northern France they have a largely NW–SE orientation.

Extension related to Tethyan and Atlantic opening has reactivated these faults and generated new faults that, together, have conditioned the resultant Mesozoic basin geometries. Jurassic to Cretaceous N–S extension gave the Weald–Boulonnais basin an asymmetric geometry with the greatest subsidence located along its NW margin. Late Cretaceous–Palaeogene N–S oriented Alpine (s.l.) compression inverted the basin and produced an E–W symmetrical anticline associated with many subsidiary anticlines or monoclines and reverse faults. In the Boulonnais extensional and contractional faults that controlled sedimentation and inversion of the Mesozoic basin are examined in the light of new field and reprocessed gravity data to establish possible controls exerted by preexisting Variscan structures.

Keywords: Dynamics; Inversion; Mesozoic basin; Weald-Boulonnais

1. Introduction

The Mesozoic basin of the Weald–Boulonnais lies on the northern margin of the Variscan orogen and its formation and subsequent inversion have often been linked to the reactivation of the older basement structures (Figs. 1 and 2, inset). This basin forms part of a series of interconnected basins that are a part of the larger Wessex basin of southern England (Hamblin et al., 1992).

Recent commercial exploration in the English sector of the Channel has contributed much to the understanding of the Mesozoic evolution of the western part of the Wessex and Channel basins (e.g.,

* Corresponding author.
E-mail address: mansy@univ-lille1.fr (J.-L. Mansy).
[1] Present adress: Organische Geochemie und Kohlenwasserstoff-Systeme, GeoForschungsZentrum Potsdam, Telegrafenberg C, 14473 Potsdam, Germany.

0040-1951/$ - see front matter © 2003 Elsevier B.V. All rights reserved.
doi:10.1016/S0040-1951(03)00289-0

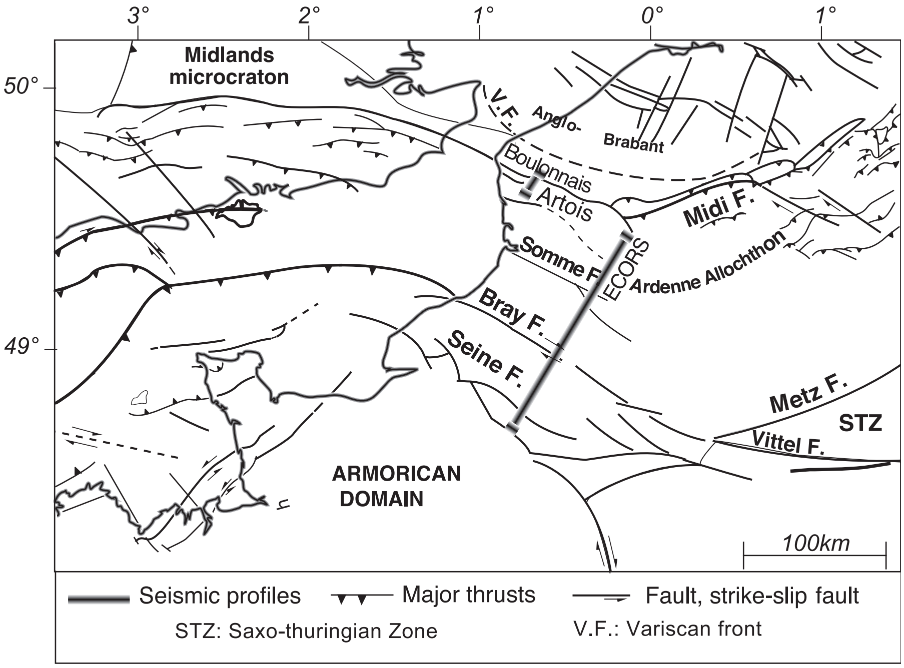

Fig. 1. Simplified map showing the main Variscan crustal blocks of northern France–southern England.

Underhill, 1998). Nevertheless, direct evidence for basement control on the location of Mesozoic basin faults is lacking and the connections between the basins of northern France and southern England remain unclear.

The Boulonnais represents the only locality in the study area where the Variscan basement is exposed and where the relationships between preexisting structures and basin forming faults and filling can be explored.

In this contribution new field and reprocessed gravity and seismic data from the Boulonnais area are presented to investigate the extent to which preexisting basement structures have influenced the formation of this Mesozoic basin and its subsequent inversion. The new filtered horizontal and vertical gradient gravity maps are used in an attempt to locate major structures within the sub-crop. To understand the extent to which the basement has controlled the evolution of the Mesozoic Basin of the Weald–Boulonnais area, some consideration must first be given to the nature of the Variscan orogen.

2. The Variscan Orogen

The northern margin of the Boulonnais Basin and its extension across the Channel into the SE England follows the trace of the Midi Fault (North France), that is, in the sub-crop, a major emergent Variscan thrust zone separating the Ardennes Allochthon in the hanging wall from the para-autochthonous Anglo-Brabant Massif in its footwall (Fig. 1).

The WNW–ESE Anglo-Brabant Massif (or Domain) consists of a basement of Cambrian to Silurian silici-clastic sediments that were metamorphosed to greenschist facies and deformed by the Acadian orogeny in Early Devonian time (Mansy et al., 1999). Devonian to Early Carboniferous post-orogenic (Caledonian) extension of the southern and eastern margins of the Anglo-Brabant Massif led to the development of the Rhenohercynian basin that was inverted during the Gondwana–Laurussia collision and creation of Pangea. The Anglo-Brabant Massif effectively formed the northern foreland of the Variscan orogen to the south.

The Ardennes Allochthon, in the hanging wall of the Midi Fault zone, has a very different pre-Variscan

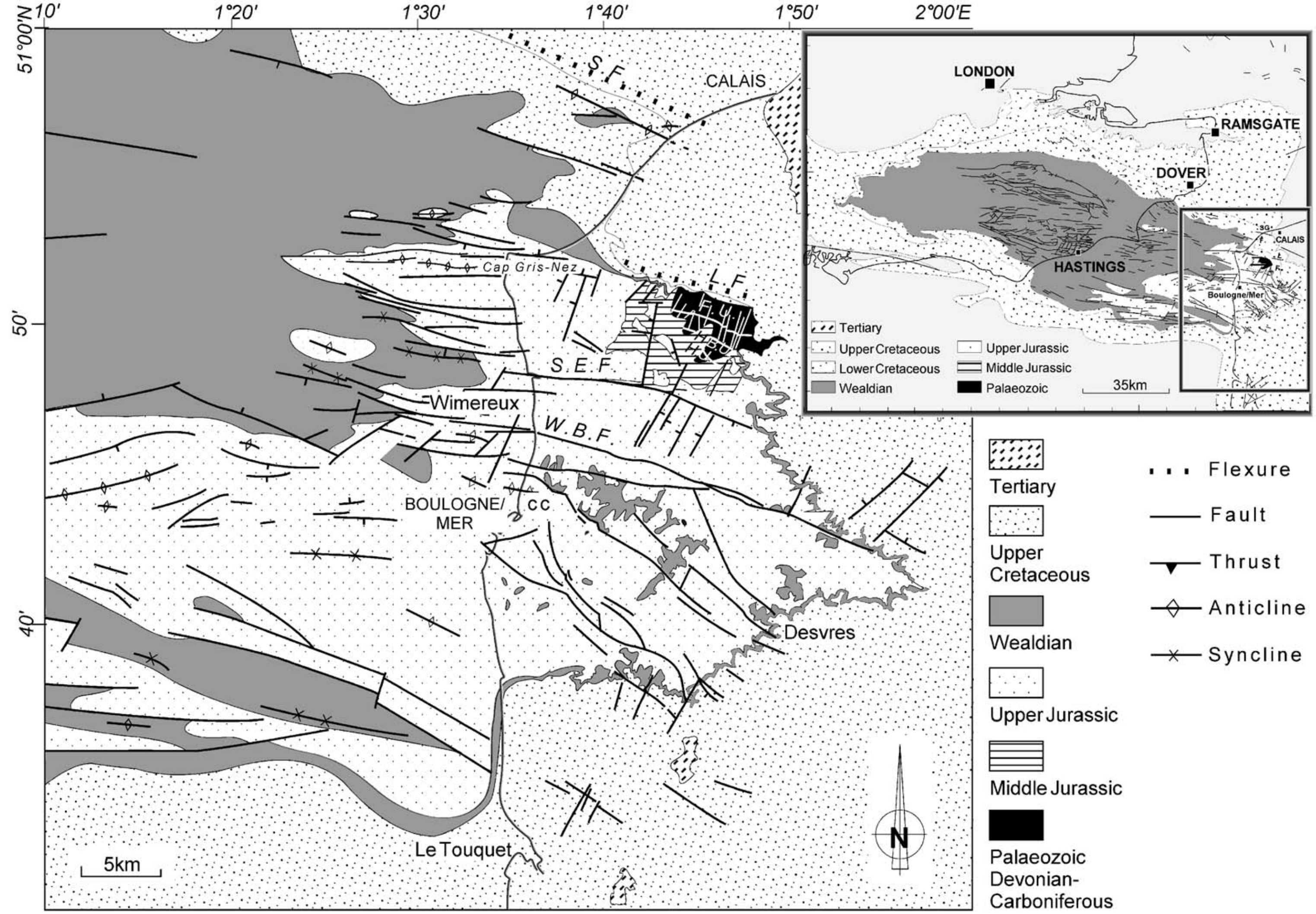

Fig. 2. The Mesozoic to Tertiary geology of northern France to show the extent of the Mesozoic basin of the Boulonnais area. Inset shows extent of the Weald–Boulonnais Basin. SF = Sangatte "Fault", LF = Landrethun "Fault", SEF = Slack-Epître Fault, CC = Cap de la Crèche, WBF = Wimereux-Belle Fault.

architecture and Upper Ordovician to Silurian sequences are uncommon. The Lower Palaeozoic rocks within the allochthon are exposed in inliers to the east but differences in lithologies, thickness and biozones make it difficult to correlate them with similar aged sequences on the Para-autochthon. The different patterns of sedimentation and orogenesis in the basement blocks of the Anglo-Brabant and Ardennes units suggest that they occupied more distant geotectonic settings than from Givetian time onward.

Although younger sediments hide large parts of the Variscan Orogen and its foreland recent seismic, gravity and magnetic surveys supported by drill core and field data in north France and Belgium have provided new information about its structure.

2.1. Anglo-Brabant Massif

Aeromagnetic and gravity data supported by drill core data have shown that the para-autochthonous Anglo-Brabant Massif consists of a complex fold pattern (De Vos et al., 1993; Chacksfield et al, 1993; Sintubin, 1997; Mansy et al., 1999). These trends are followed by the fault systems that controlled sedimentation patterns in Early Devonian to Late Carboniferous time along the Rhenohercynian Margin. The structure of the western part of the Massif is dominated by an anticlinal–synclinal fold pair that is cut on the southern border by a Late Acadian WNW strike-slip fault zone (De Vos et al., 1993; Everaerts et al., 1996; De Vos, 1997). The curved cleavage and fold trends are moulded around the granitic core of the Massif that is defined by an elongate NNW–SSE Bouguer gravity low (Sintubin, 1997; Mansy et al., 1999). These granitoids, with their equivalents running offshore from eastern England (Donato and Megson, 1990), may have been responsible for the persistent emergent character of the Anglo-Brabant Massif from Devonian into Late Carboniferous time.

2.2. Ardennes Allochthon

The ECORS 1, deep seismic profile of North France images the southern border of the Anglo-Brabant Massif in the footwall of the Variscan deformation front as a southward thinning wedge that tapers down to a strong reflector at the base of the crust (Cazes et al., 1985). The Variscan deformation ‘front’ is also imaged as a single major detachment zone that dips gently down to the base of the crust beneath the Paris Basin (Cazes et al., 1985). At the surface this detachment emerges as the Midi Fault array of thrust faults (Fig. 1) rather than a single structure (Meilliez and Mansy, 1990; Meilliez et al., 1991, 1994; Mansy and Meilliez, 1993; Lacquement et al., 1999). Deep seismic reflection data from southern England similarly indicate the presence of two shallow SSE dipping thrusts that have been identified as the lateral equivalent of the Midi Fault to the north and the Wardour Thrust to the south (Chadwick et al., 1983).

The Variscan deformation penetrated a large part of the coal basin of North France–Belgium and consequently the Midi Fault array should not be taken to represent the Variscan Front. The Midi Fault does, however, separate the northward vergent thrust sheets of the Rhenohercynian Zone from the Subvariscan Foreland (e.g. Meilliez and Mansy, 1990; Meilliez et al., 1991).

2.3. The Variscan of the Boulonnais and SE England

The Palaeozoic rocks that crop-out in the Boulonnais area consist of unmetamorphosed Devonian to Carboniferous sedimentary rocks that lie unconformably on Silurian shales (Fig. 3 and inset). The Lower Palaeozoic rocks do not crop out in the Weald area but are known from boreholes to be of Wenlock to Upper Llandovery age. Representatives of Lower Devonian to ORS facies rocks and Lower Carboniferous limestones are also known to underlie part of the Kent coalfield (Shephard-Thorn et al., 1972).

2.3.1. Structure

The domal Palaeozoic inlier of the Boulonnais area is traversed by the Ferques fault as well as the Variscan Haut Banc and Hydrequent thrust faults that divide the rocks into three litho-tectonic sub-units (Fig. 3 inset, and Fig. 4 cross section). The sequence of Palaeozoic sub-units was folded and thrust faulted in Late Visean to Westphalian time (Marton et al., 2000) The Ferques Unit, the lowest in the stack, includes a south-dipping sequence of Mid to Upper Devonian sandstones, limestones and shales, through Lower Carboniferous platform carbonates to Westphalian coal bearing strata that unconformably over-

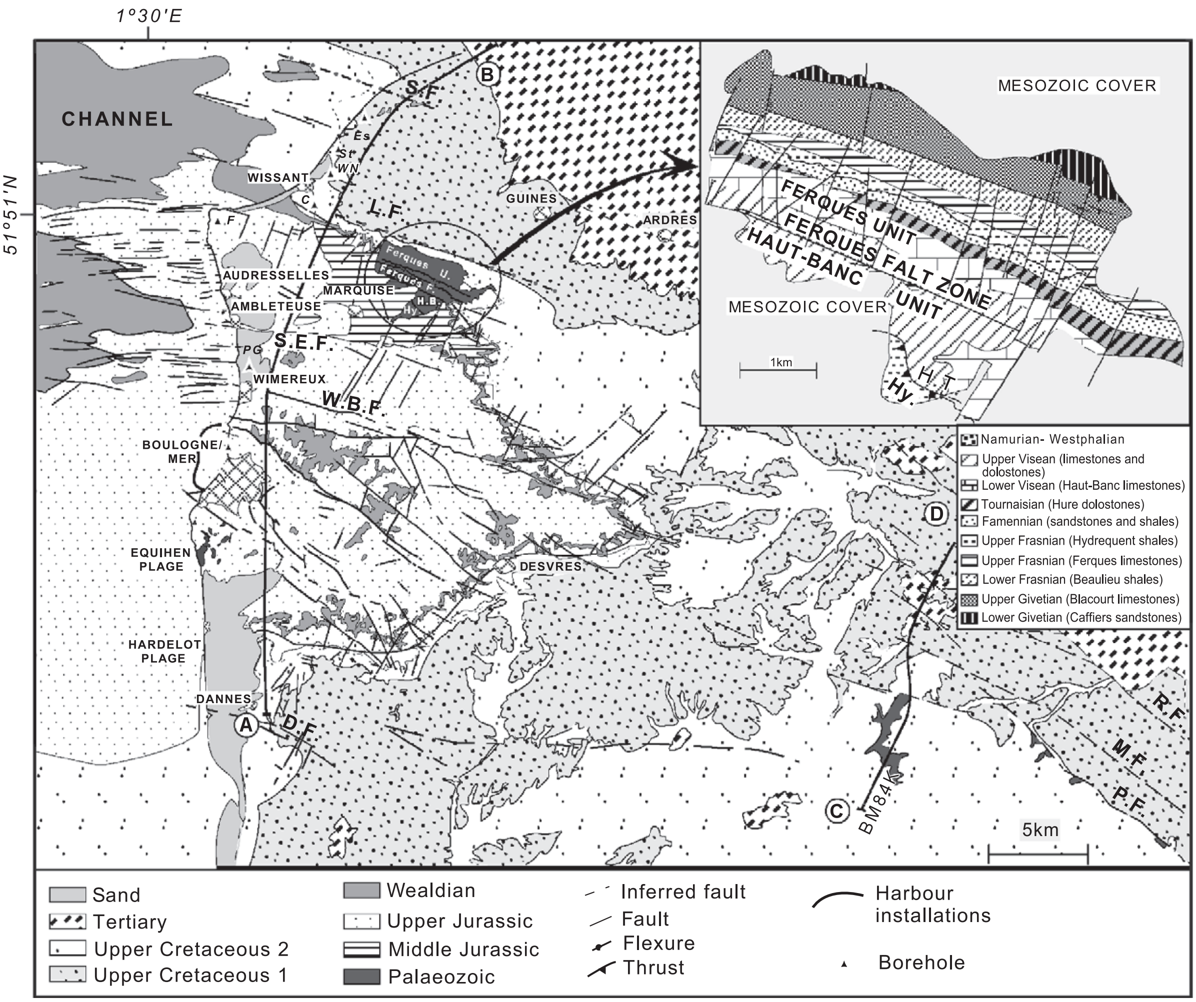

Fig. 3. Detailed geological map of the Boulonnais area showing location of the Palaeozoic inlier and the distribution of the main faults. AB, section line for Fig. 4. CD location of seismic section used to construct Fig. 7b–d. SF = Sangatte "Fault", RF = Ruitz Fault, PF = Pernes Fault, MF = Marqueffles Fault, WBF = Wimereux–Belle Fault, LF = Landrethun "Fault", HT = Hydrequent Thrust, SEF = Slack–Epître Fault.

lie the Silurian shales. The Haut Banc Unit to the south of the Ferques Fault (Fig. 3) and below the Hydrequent thrust contains mainly the Visean carbonates. Borehole data have shown, however, that these carbonates are thrust onto Namurian–Westphalian coal-bearing strata that form the roof to the Ferques Unit (Pruvost and Delepine, 1921). The so-called Basse–Normandie duplex (Cooper et al., 1983) lies in the footwall of the overthrust Hydrequent Unit, which is known from borehole data to consist largely of Upper Frasnian shales. The structure of the Palaeozoic inlier has long been considered to be autochthonous (e.g. Colbeaux and Leplat, 1985) and that the Variscan Frontal thrust corresponds to the Midi Fault, which in the Boulonnais is located a few kilometres south of the Palaeozoic Massif (Pasquet et al., 1983). The thrust faulted Palaeozoic rocks of the Boulonnais indeed represent the deformed footwall of the Midi Fault. A recent reconstruction of the sequence of thrust faulting exemplified by the Palaeozoic rocks of the Basse–Normandie duplex is summarised in Averbuch and Mansy (1998). In outline, the Palaeozoic rocks of the inlier were initially folded on top of buried thrust zone and then dissected by

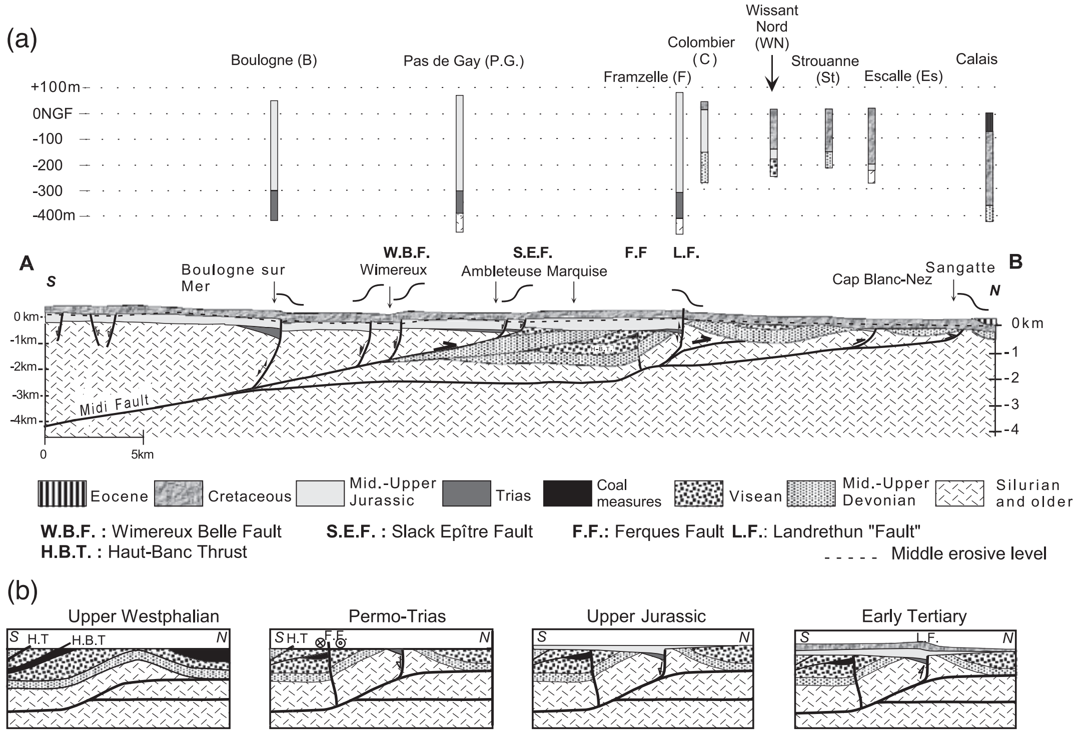

Fig. 4. (a) Geological cross section of the Boulonnais showing the relation of the inverted extensional faults to deeper Variscan thrust faults. Location of section is shown in Fig. 3, line A–B. (b) Reconstruction of extensional and inversion stages in the evolution of the Boulonnais part of the Weald–Boulonnais Basin.

thrust faults that developed in a break-back succession with the Haut Banc forming first, followed by the Hydrequent thrust with the Midi Fault partially overriding the stack from south to north (Averbuch and Mansy, 1998). The Silurian shales that are exposed in the core of the Landrethun flexure on the northern flank of the Palaeozoic block are the most likely host for the floor thrust to this sequence of thrust faults (Fig. 3, inset). Microstructural studies of the vertical Ferques Fault zone that crosscuts the whole thrust stack suggest that the fault was subject to a Late Variscan or Triassic sinistral displacement (Averbuch and Mansy, 1998; Mansy et al., in press).

Little is known of the Variscan deformation beneath the extension of this basin in SE England (Weald) and the location of the Midi Fault equivalent in Kent is not known with precision. Shephard-Thorn et al. (1972) suggested from Bouguer anomaly and aeromagnetic data that the Landrethun "Fault" (Fig. 3) approximated to the Variscan Frontal thrust fault (Everaerts and Mansy, 2001). These authors also identified a similar gravity anomaly in the Dover Strait that links with the western edge of the Kent coal basin in the Folkestone area. The offset of the two linear anomalies is attributed to a mid-channel dextral wrench fault with displacement of approximately 10 km (Shephard-Thorn et al., 1972). It is important to note, however, that in the Boulonnais area the coal-bearing rocks between Boulogne and Calais are caught up in the Variscan thrust faulting described above. How far the southwestern margin of the coal basin in Kent has been affected by the Variscan deformation is uncertain but it is thought to be fault-bounded (Shephard-Thorn et al., 1972).

3. The Weald–Boulonnais Mesozoic basin

The Weald–Boulonnais Basin, through much of Jurassic to Cretaceous time, was bordered by the

Anglo-Brabant Massif to the north and by the Hampshire–Dieppe High to the south (Fig. 5d). In southern England the northern border was effectively defined by the E–W array of London Platform Faults (see also Butler and Pullan, 1990) while the Wardour–Portsdown Fault array formed the southern border (PWF in Fig. 5d). In northern France, the Landrethun "Fault" to the north and the Boulogne Fault to the south represent the respective equivalent basin controlling faults (Fig. 5d). The general shape of the basin showing the major areas of post-Variscan subsidence can be gained from consideration of the depth to top of the Palaeozoic map for southern England and northern France (Fig. 6). It is evident from this map that the maximum subsidence (− 2500 m) was located in the western part of the basin with a gentle eastward shallowing toward the Boulonnais where the basement is exposed.

In the following sections, the utility of the newly reprocessed gravity data is explored to define limits of

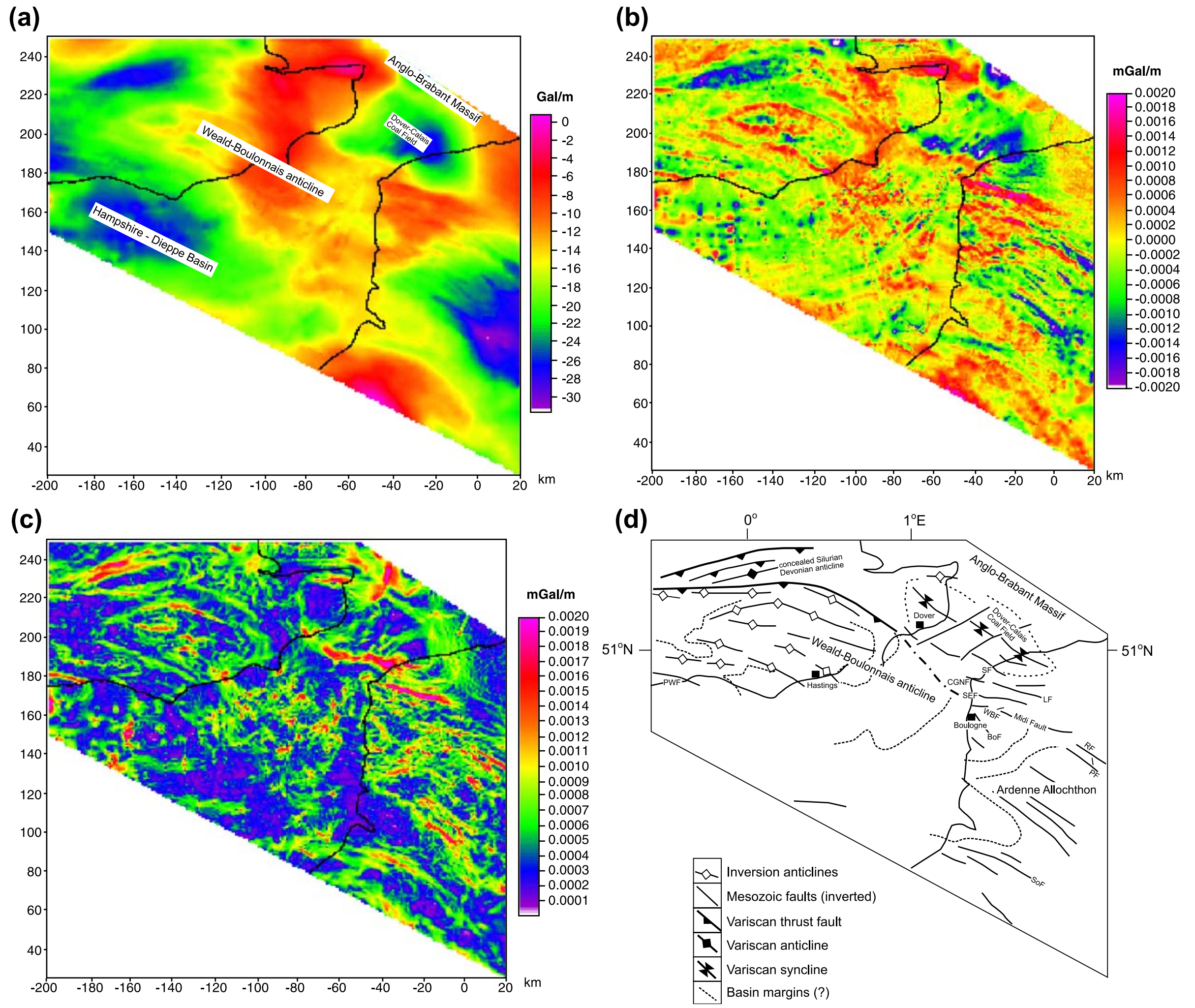

Fig. 5. (a) Unfiltered Bouguer anomaly map of the Weald–Boulonnais area. (b) Horizontal gradient of Bouguer anomaly. (c) Vertical gradient of Bouguer anomaly. (d) Line drawing of main features illustrated by gravity maps. Positions of known faults and folds in the Weald District are included to show close correspondence between field and gravity data. SF = Sangatte "Fault", CGNF = Cap Gris Nez Fault, SEF = Slack–Epitre Fault, RF = Ruitz Fault, PF = Pernes Fault, WBF = Wimereux–Belle Fault, LF = Landrethun "Fault", BoF = Boulogne Fault, SoF = Somme Fault.

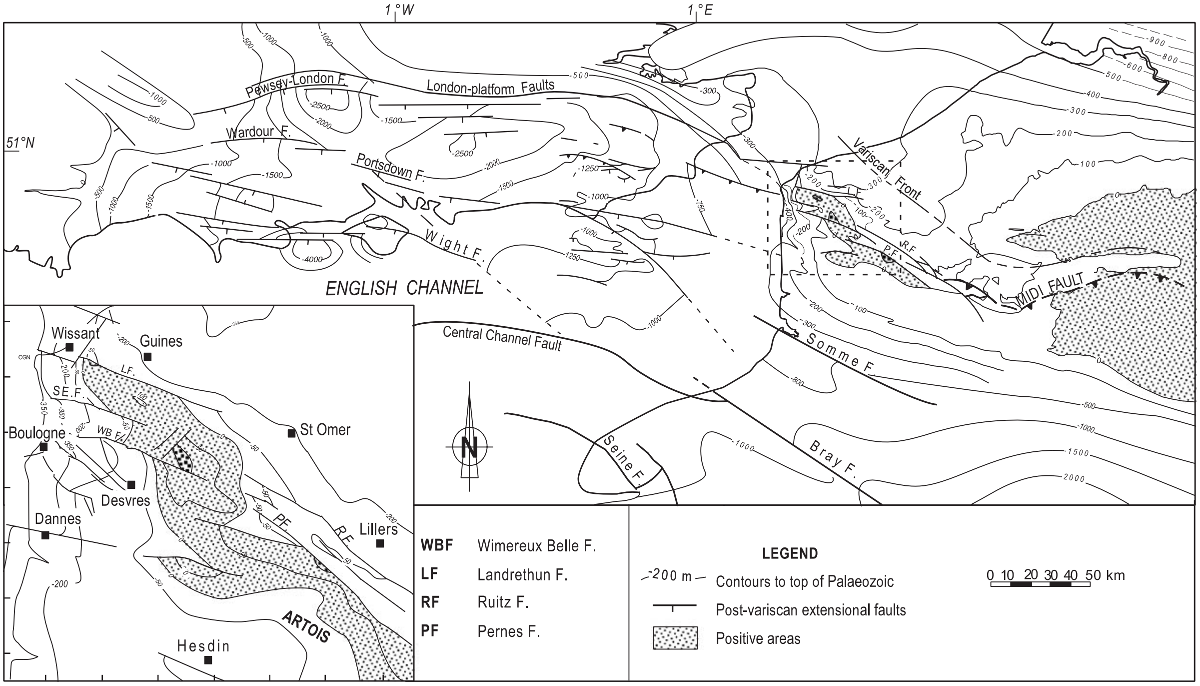

Fig. 6. Depth contours for the top of Palaeozoic in Weald–Boulonnais area. Compiled from various sources for northern France and from Smith (1985) for SE England.

the sedimentary basins in the study area and to locate some of the main structures that have influenced their geometry and inversion.

3.1. Potential field maps

3.1.1. Bouguer anomaly map: methods and general outline

A Bouguer anomaly map of the study area has been prepared using the gravity database of the Royal Observatory of Belgium, which contains more than 150,000 data points over Belgium and surrounding countries (Fig. 5a–b). The gravity coverage of the map varies from 1 to 5 stations per square kilometre and the onshore gravity values were computed using a density value of 2.10 g/cm^3 as a higher value creates artefacts due to the topography. The offshore values consist of the Free Air Anomaly. All gravity data are referenced to the gravity datum of Uccle, 1976 (IGSN71) and theoretical gravity was computed using the Geodetic Reference System formula (International Association of Geodesy, 1988). The onshore and offshore data sets were combined and their geodetic co-ordinates (latitude and longitude) converted to (x,y) co-ordinates in the Belgian Lambert projection. A griding procedure was performed using the Surfer kriging software with an interval of 1 km, a search radius of 30 km and a linear weighting coefficient to avoid aliasing in poorly covered areas.

3.1.2. The horizontal gradient of the Bouguer anomaly

Above a vertical contact between rocks with different mass densities the gravity field shows a slope with the high above the higher-density rocks and a low above the low-density rocks. The inflection of the slope from the convex to concave is normally located exactly above the contact. This inflection is used to locate abrupt lateral changes in density (Cordell and Grauch, 1982) and can be found by mapping the maximum of the horizontal gradient of the gravity field. The intensity of the local maximal values of this horizontal gradient is proportional to the steepness of the gradient. In the case of an inclined lithological contrast, the maximum is displaced down-dip from the contact outcrop.

In Fig. 5b the reddish colours represent local maxima signifying lateral lithological contrasts that often correspond to faults. From the contrast patterns on the horizontal gradient map a number of structural subdomains within the Weald to Boulonnais area can be distinguished and these are summarised in the line drawing; Fig. 5d. As the horizontal gradient enhances shallow features and because a large part of the area is characterised by shallow Mesozoic to Tertiary sedimentary rocks, a Bouguer density reduction of 2.1 was chosen for this map.

3.1.3. The vertical gravity gradient

On the Bouguer gravity map the overlapping of the gravity effects obscures a number of the details. In order to improve the resolution we have prepared a map of the vertical gradient (Fig. 5c) of the Bouguer gravity field by applying the vertical gradient operator in the frequency domain. The logic here is simply that the rate of change of the gravity field with elevation is much more sensitive to changes in rock densities occurring near the surface than the change occurring at depth. Lithological boundaries, therefore, should be revealed in the gravity gradient map with a greater precision than in the Bouguer gravity map itself. The improvement in the resolution is evident in Fig. 5c. (see also Everaerts and Mansy, 2001).

3.1.4. Results

The mathematical enhancement of the horizontal and vertical gradient gravity maps has made visible features that may reflect structures in the Mesozoic basins of the Weald to Boulonnais area and, to a lesser extent, the underlying Variscan orogen. The Bouguer anomaly maps (Fig. 5a–d) appear to illustrate well the known main features of the Mesozoic Basin. Interpretation of the gravity map was aided by combining processed gravity images with the geological maps for the study area. In Fig. 6a the narrow bright red to yellow lines on the horizontal gradient gravity map correspond to the greatest lithological contrasts and these coincide with the known faults or monoclinal fold structures.

On a gross scale the traces of steep faults that coincide with the tip line of the Midi Fault may be used to separate the Anglo-Brabant Massif to the north from the Ardennes Allochthon to the south (Fig. 5d). The trace of the Midi Fault equivalent appears to coincide with a series of discontinuous asymmetric inversion anticlines (e.g. Guilford–Dorking–Sevenoaks–Maidstone) with steep (faulted) north facing limbs. It is also seen to truncate the ENE–WSW trending Silurian–Devonian anticline in the footwall of the Variscan frontal thrust (Pharaoh et al., 1996; and Fig. 5d). Eastward toward the coast the fault trace turns from an E–W to a NW–SE trend as it crosses the Eastern Channel. Younger rocks obscure the course of the Midi Fault across the Channel but it must come ashore near Boulogne to meet the onshore array of out-of-sequence faults that accompany the Midi Fault in northwestern France. These faults are very clearly located by the gravity anomaly pattern but are not as continuous as indicated on the geological map. For example, the fault pattern in the Boulonnais area is oriented in a N110° direction while in the Artois area the faults are oriented N130° (Mansy et al., in press). Linkage between these two fault zones is not clear and their continuity, indicated on the geological map, is not confirmed. The locations of the Landrethun and Sangatte Faults on the geological map show a good correlation with those evident on the horizontal gradient gravity map (Fig. 5b and d). The discontinuous, stepped character of the fault pattern image on the gravity map is suggestive of a relay pattern with connecting transfer zones between the offset faults. Extensive drill core data from this area show that the Landrethun and Sangatte, Pernes and Ruitz faults (Fig. 5d) were active inversion structures during Late Cretaceous–Tertiary time.

The shape of the Kent (or Dover–Calais) coalfield can be seen to the north of the Midi Fault equivalent. The displacement of the coal basin outline and of the westward extension of the Sangatte fault coincides with narrow NE–SW anomalies interpreted here to indicate the presence of faults (Fig. 6d).

The southern margin of the Mesozoic basin of southern England and northern France is marked by the WNW–ESE trending Wardour–Portsdown Fault system (PWF, Fig. 5) and known inversion folds that coincide with a clear linear anomaly on the potential field maps.

Known fold and fault lines from the BGS Regional Guide to the Wealden District (Gallois, 1965) have been superimposed on the map and these coincide remarkably well with the observed anomalies on the gravity map. The close-spaced array of E–W oriented folds and faults in the vicinity of Tonbridge and Tunbridge Wells are particularly clear.

3.2. Basin development

The oldest post-Variscan rocks preserved in the Boulonnais Basin are of Triassic (?) age and these are known from boreholes in the Boulogne, Pas de Gay and Framzelle areas of northern France (Olry, 1904). Reconstructions of the geometry of this early fill suggest they thicken toward steep faults but it is not clear whether this reflects a syn-rift origin for these rocks. Recent studies of the reactivation histories of the Palaeozoic faults in the Boulonnais suggest that the Cap Gris Nez fault was active during Triassic sedimentation (Mansy et al., in press). Localised, fault-controlled, Triassic sediments (the Sherwood Sandstone and Mercia Mudstone Groups) are also reported from boreholes in the western part of the Weald (Smith, 1986).

In southern England the main area of subsidence in Early Jurassic time was located in the western part of the Weald Basin where a north and east shallowing mud-dominated shelf developed (Hawkes et al., 1998). Three divisions of the Lias are recognised with lower shales and limestones followed by sandy shales and limestones that are overlain by shales and mudstones (Gallois, 1965). Fault-controlled sedimentation in this part of the basin was limited to the northern London Platform Fault (LPF) and the Ashdown Fault (Fig. 5). Generally, however, an axial deepening of the basin with feather edging of strata onto the southern margin of the Anglo-Brabant Massif is evident (Gallois, 1965; Hamblin et al., 1992; Hawkes et al., 1998).

Except for a few metres of clays and marls found in shallow boreholes along the coast, Lower Jurassic strata are not preserved in the Boulonnais and this block was either emergent at this time or the sediment was eroded before the Mid-Jurassic. Liassic sediments are thought to continue, however, westward in the offshore areas on the northern border of the Hampshire–Dieppe High into eastern England. The top of the Lias in the Weald is marked by an angular unconformity, suggesting uplift and erosion of the basin at this time.

By Mid-Jurassic time, renewed subsidence affected much of northern France and southern England area and the preserved strata suggest that two main depocentres developed. The western depocenter in the Weald shows the continued control by the LPF and Ashdown faults on sediment accumulation (Ruffell, 1995). In northern France an eastern sub-basin was established in Bajocian time between the Anglo-Brabant Massif to the north and the northern margin of the Hampshire–Dieppe High to the south. Commercial seismic reflection profiles show that this sub-basin extends westward into the offshore area of the eastern Channel.

A N–S section from the Calais–Sangatte area to 5 km south of Boulogne crosses a number of E–W oriented faults. Borehole data indicate a general south-to-north thickening of the Mid-to Upper Jurassic strata toward the Landrethun Fault (Figs. 3 and 4). North of this fault the Jurassic thins rapidly to just north of Wissant where the Cretaceous rocks lie directly on the Variscan basement. Field and borehole data suggest that the Landrethun–Cap Gris Nez Fault actively controlled sedimentation during the Jurassic and that the fault soled onto a south-dipping Variscan thrust (Fig. 4).

In southern England Mid-Jurassic sedimentation was dominated by deposition of oolitic limestones on a subsiding carbonate platform. These facies thin eastward; although the Bathonian sediments in the Boulonnais area do include several metres of oolitic limestones they are thinner than similar aged facies toward the axis of the Weald Basin of southern England.

The Upper Jurassic sequences of northern France and southern England are cyclic in character but laterally persistent and suggest periodic subsidence followed by shallowing as uplifted source areas were eroded. The continued subsidence through Late Jurassic time led to a widening of the basin as the Hampshire–Dieppe high gradually became submerged. Although they probably remained connected, the Weald and Boulonnais areas constituted distinct depocentres with the fill thinning toward the eastern Channel as well as to the Anglo-Brabant Massif and the Hampshire–Dieppe High.

In Latest Jurassic to Early Cretaceous time, renewed rifting along the Atlantic margin reactivated earlier extension faults (e.g. the LPF faults) and an eastward migration of the main depocenter toward the Boulonnais occurred (cf Hawkes et al., 1998, Butler and Pullan, 1990). Wealden facies are only patchily preserved onshore in the Boulonnais area but they are extensively developed offshore where they lie unconformably over the Jurassic sequences (Figs. 2 and 3).

In Aptian time a change from the earlier active rifting to a broad thermal subsidence occurred that continued to affect sedimentation until Latest Cretaceous time. This transition is marked by the presence of an angular break-up unconformity as the thermal subsidence began (Ruffell, 1995; Hawkes et al., 1998). This subsidence caused the expansion of sedimentation over the adjacent emergent highs as the deposition of the chalk facies began. During this time the area from the Weald to the Boulonnais appears to have constituted a single depocenter although the thinning of sequences toward the east suggests the Boulonnais area was subsiding less rapidly than the western part of the basin.

In the N–S section across the Boulonnais area, E–W faults cutting the Jurassic sequences may have been reactivated during the early Cretaceous rifting but appear not to have affected Late Cretaceous sedimentation (Bergerat and Vandycke, 1994). All of these faults are interpreted to sole onto the Variscan Midi Fault out-of-sequence array (Fig. 4).

3.3. Late Cretaceous–Tertiary inversion

In Late Cretaceous to Palaeogene time the onset of the ca N–S oriented Alpine (s.l.) compression is widely considered as the cause of the inversion the Mesozoic basins of northern France and southern England and produced a 190-km long 50-km wide, roughly E–W, periclinal dome that stretched between the Hampshire downs and the Boulonnais. The main fold is symmetrical but a number of the subsidiary E–W periclines showing asymmetry, with steep northern limbs, are well known in the Wealden District. The fold geometries are influenced by competence variations of the rocks affected (Gallois, 1965). This compression also reversed many of the Liassic to Early Cretaceous extension faults across the basin. In the Wealden district, several of the earlier E–W extension faults were reversed and are associated with inversion anticlines (cf Gallois, BGS guide to the Wealden District, 1965). All the E–W faults appear to have been subject to a predominant dip-slip reverse displacement.

Asymmetric fold structures are also found accompanying some NW–SE-oriented reversed normal faults (e.g. Fig. 6, Butler and Pullan, 1990). The overall uplift produced by the Tertiary inversion in the eastern part of the Weald has been estimated to be as much as 1525 m that, interestingly, does not coincide with the area of maximum Upper Jurassic to Lower Cretaceous sediment accumulation (Butler and Pullan, 1990).

A similar pattern of minor folds has been shown to affect the Jurassic to Cretaceous sequences in the eastern Channel offshore from the Boulonnais (Fig. 3). A number of E–W to NNW–SSE folds are also present within the Jurassic rocks along the coastline and in some cases these correspond to inversion anticlines (e.g. Cap Gris Nez; cf Lamarche et al., 1996, 1997). The E–W oriented faults all show pure dip-slip displacement while the WNW–ESE faults, such as the Pernes and Ruitz faults (Fig. 3), record a dextral slip component as well.

The exploration for coal has provided much information on the Late to post-Cretaceous inversion in the Boulonnais area (Gosselet, 1908, 1910; Bouroz, 1956). Of the examples described by these earlier authors the section through the Ruitz to Marqueffles faults shows most clearly the relationship between the inverted structures and the Midi Fault (see Fig. 3 for location and Fig. 7 cross section and reconstruction). The Marqueffles Fault is of particular interest as it shows an approximate 450-m down-to-the-south normal displacement of the Midi Fault (Bouroz, 1956). The footwall block was more elevated in pre-Late Cretaceous time and the Midi fault was removed by erosion. The Marqueffles and Ruitz Faults accommodated the normal displacement of the hanging wall. Inversion has partially restored the extension on the Marqueffles Fault with about 100 m of top-to-the-north reverse slip (Bouroz, 1956). An unpublished industrial seismic line, currently being reprocessed, reveals a major south-dipping reflector (the Midi Fault) rising close to the surface near the Marqueffles Fault. Borehole information has shown that the latter fault shallows from near vertical at the surface to $\sim 56°$

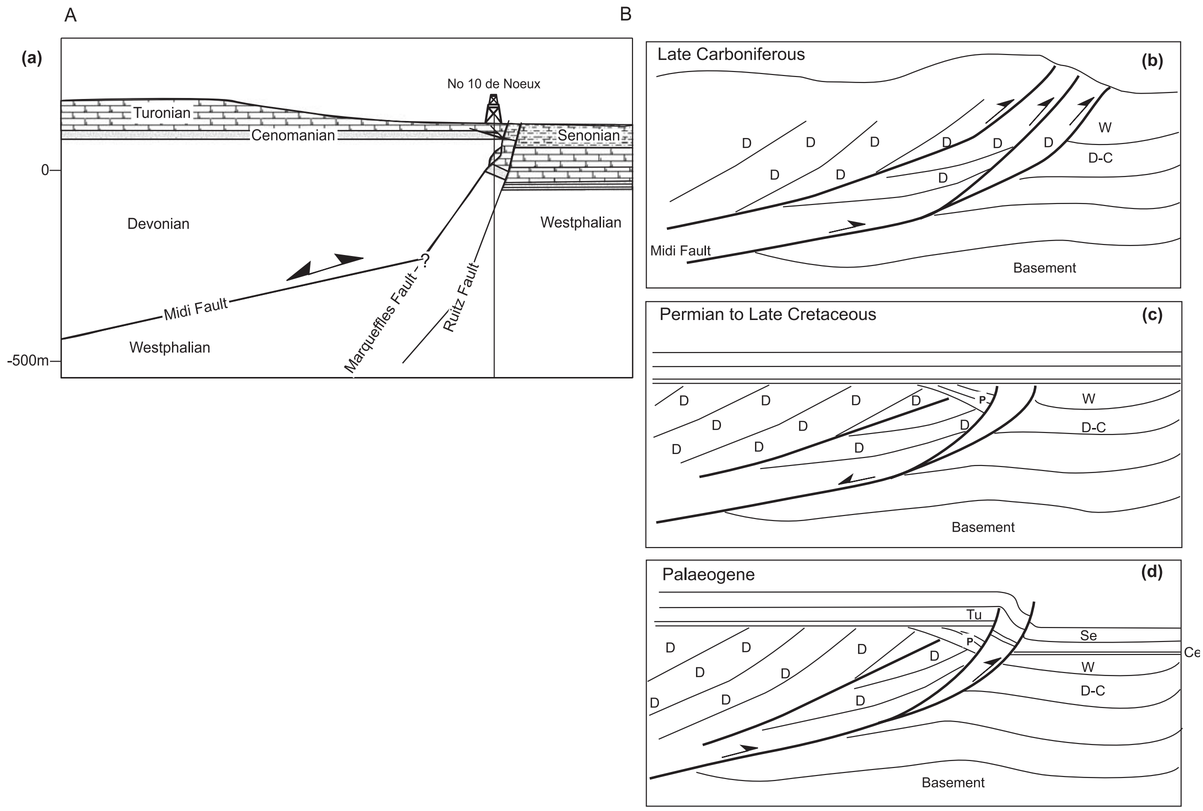

Fig. 7. Cross section through the Marqueffles Fault adapted from Bouroz (1956). (b–d) General reconstruction for the Artois area based on reprocessing of unpublished industrial seismic reflection profiles. In b–d abbreviations: D = Devonian, D-C = Devono-Carboniferous, W = Westphalian, P = Permian, C = Cenomanian, Tu = Turonian, Se = Senonian.

where it is intersected by the borehole at 100-m depth.

3.4. Kinematic data

A synthesis of the folds and fault plane microstructures gathered from the Jurassic and Cretaceous rocks in the Boulonnais–Kent area is given here to illustrate the orientations of the principal stress axes linked to the syn- and post-Jurassic deformation of this block. The reduced stress tensors have been calculated from the fault population bearing slickenside lineations using the method developed by Angelier (1990). The method gives the orientations of the maximum, intermediate and minimum principal stress axes, $\sigma 1$, $\sigma 2$ and $\sigma 3$. The calculated stress tensors are compared with the analyses of the fold data and the effects of lithological contrasts are also taken into account. Magnetic fabric data (see principles in e.g. Tarling and Hrouda, 1993 or Borradaile and Henry, 1997) were also used as strain indicators within local fold structures affecting Late Jurassic mudrocks in the Boulonnais (Boulogne–Cap de la Crèche section).

In general, exposure in the region is poor and data have been gathered from the limited coastal sections, road-cuttings and quarries. Within the same tectonic event the accommodation of the deformation is strongly dependent on the properties of the affected rocks. The competent Bajocian and Bathonian oolitic limestones like the Kimmeridgian and Tithonian sandstones provide better records of the brittle deformation than the incompetent Callovian and Oxfordian clays. The latter are, however, more commonly folded than the competent rocks. There are also notable differences in the responses of the various Cretaceous chalk facies to the brittle deformation events. The so-called

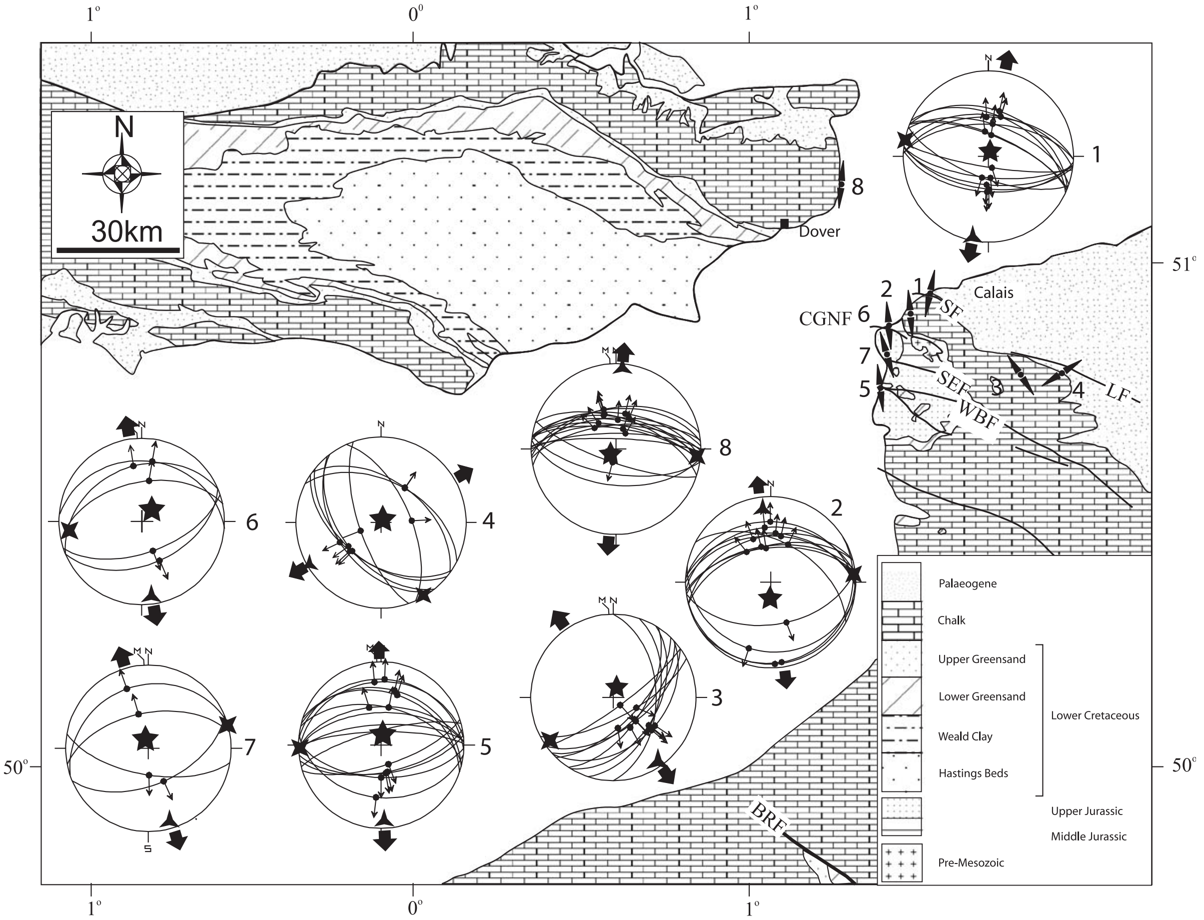

Fig. 8. The N–S extension in the Boulonnais–Kent–Sussex areas. Selected examples of fault patterns and computed axes of palaeo-stress tensors are shown. Stereo-plots are Schmidt's projection, lower hemisphere (N is geographic north, and M is magnetic north). Fault planes are shown as thin lines, slickenside lineations (striae) are small dots with single-centrifugal, single-centripetal or double thin arrows (normal, reverse or strike slip, respectively). Three-, four- and five-branched black stars are computed axes σ_3, σ_2, and σ_1, respectively. Large solid arrows are the corresponding directions of horizontal compression and extension. LF: Landrethun "Fault", CGNF: Cap Gris Nez Fault, SEF: Slack–Epître Fault, WBF: Wimereux–Belle Fault, BRF: Bray Fault, SF = Sangatte "Fault".

blue chalk, for example, is marly and weaker than the white chalk and does not record the deformation as well as the latter.

3.4.1. Jurassic–Cretaceous extension

Populations of E–W to ENE–WSW trending meso-scale normal faults developed in the competent Jurassic rocks near the Ferques (Fig. 8, site 3-FF), Cap Gris Nez (Fig. 8, site 6, CGNF), Slack–Epitre (Fig. 8, site 7, SEF) and Wimereux–Belle (Fig. 8, site 5, WBF) major faults have been analysed in terms of palaeo-stress reconstructions. The fault slip data reveal a N–S to NNW–SSE oriented extension. E–W and ESE–WNW faults in the Cretaceous provide evidence of a more divergent N–S to NNE–SSW extension. Meso-scale faults with this extension direction are found within the Gault Clay along the western extension of the Landrethun Fault on the Wissant beach (Fig. 8, site 2, LF), in the Cenomanian–Turonian chalk at Grand Blanc Nez just south of the Sangatte fault (Fig. 8, site 1, SF) and in the Santonian chalk in the Helfaut quarry south of the Landrethun Flexure (Fig. 8, site 4, LF). Some normal faults in the Cenomanian of Kent also record a NNE–SSW extension (Fig. 8, site 8). There is little evidence for the age of this extension but some syn-sedimentary structures are found in the Bathonian–Callovian and in the Kimmeridgian to Tithonian rocks (Colbeaux et al., 1993; Vidier et al., 1995; Proust et al., 1995). The south to north thickening of the Mid- to Upper Jurassic rocks toward the Landrethun–Cap Gris Nez Fault is probably due to syn-sedimentary growth faulting during the Jurassic and the stress tensor calculations confirm that the extension was N–S to NNE–SSW oriented. A second-order cluster of the maximum magnetic susceptibility axes around the N–S direction, within the bedding planes of the Kimmeridgian–Tithonian formations from the Boulogne cliffs (Fig. 9), support such an orientation for the Late Jurassic syn-depositional extension (see the case study of Mattei et al., 1997). This roughly N–S extensional period persisted at least until the Santonian.

The fault plane microstructures indicate that, in addition to this dominant N–S event, E–W, NE–SW and NW–SE oriented extensional events have affected the Cretaceous rocks of the Boulonnais and Weald areas. The relative chronologies of these events have been partly established from the crosscutting relations of faults or from fault planes bearing several generations of striae. Where such chronological criteria are found the earliest of these structures are consistent with N–S extension. Other fault plane striae may be the products of Cretaceous thermal subsidence (Bergerat and Vandycke, 1994; Vandycke and Bergerat, 2001) or a later Mio-Pliocene extension (Bevan and Hancock, 1986).

3.4.2. Late Cretaceous (?)–Tertiary compression

The Jurassic rocks in the Boulonnais contain a variety of compressional structures including folds, reverse faults and conjugate strike slip fault arrays while the Cretaceous rocks are only affected by rare strike-slip faults. The faulting within the Jurassic rocks is noticeably lithologically controlled with the strike-slip faults being most common in the competent rocks while the incompetent shales are more often cut by reverse faults. The effects of the dominantly N–S oriented (Fig. 10) compression are more intensely developed in the vicinity of the larger Landrethun (Fig. 10, site 1), Cap Gris Nez (Fig. 10, site 2), Wimereux (Fig. 10, site 4) and Slack–Epitre (Fig. 10, sites 5 and 6) faults. N–S compression is also recorded in the Cenomanian rocks at the Dannes Quarry (Fig. 10, site 7), at Petit Blanc Nez (Fig. 10, site 3) and in Kent.

Westward, analyses of fault plane microstructures in the Isle of Wight (Vandycke and Bergerat, 2001) and in the Middle to Upper Chalk along the Sussex

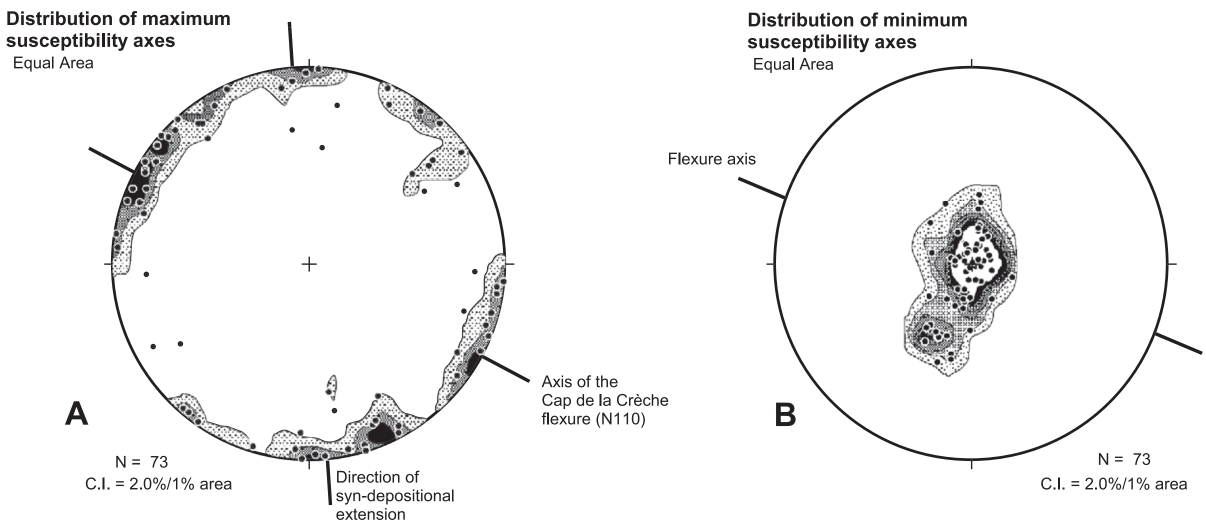

Fig. 9. Distribution (black dots) and contour density plots of principal axes of the anisotropy of magnetic susceptibility ellipsoid within Kimmeridgian–Tithonian samples from the Cap de la Crèche flexure. (A) Maximum axes in the bedding corrected frame; note a first-order cluster along the axis of the flexure and a second-order one along the NNW–SSE direction, suggested to be the syn-depositional direction of extension. (B) Minimum axes in the geographic frame, note the girdle pattern of distribution around the axis of the flexure.

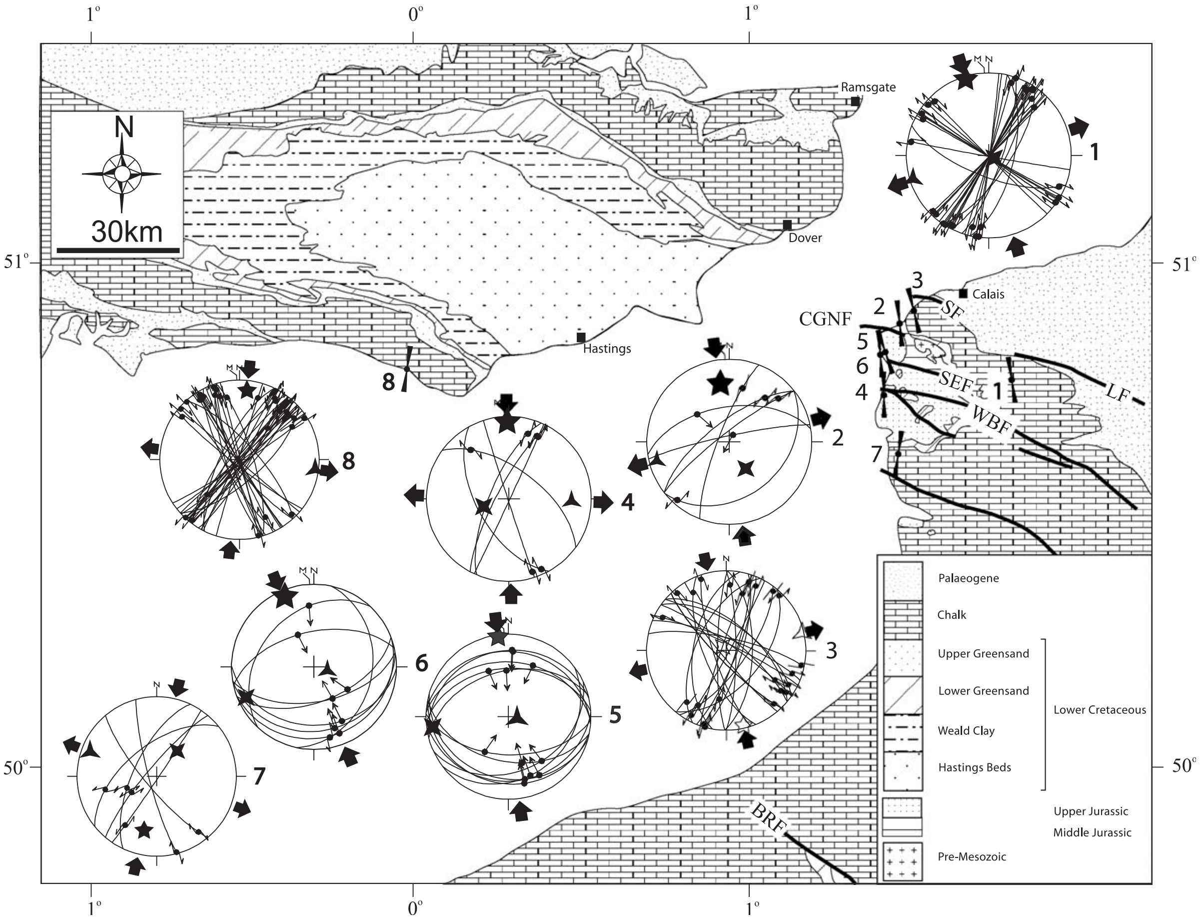

Fig. 10. The N–S compression in the Boulonnais–Kent–Sussex areas. Legend as for Fig. 8.

coast (Fig. 10, site 8; Vandycke et al., 1995) also indicate a consistent N–S compression associated with inversion. The best examples of folding related to the inversion is to be found in the vicinity of the Cap Gris Nez fault along the shoreline (Lamarche et al., 1997) and in the La Creche flexure, north of Boulogne. In the first case, the fold axes strike E–W as do small scale thrust faults and together these structures are consistent with N–S compression.

In the La Crèche fold, the girdle pattern, of the minimum axes of magnetic susceptibility (parallel to the bedding poles), as well as a major cluster of maximum axes along the flexure axis (Fig. 9) document a NNW–SSE shortening. These slight deviations of shortening are likely to be controlled by the orientation of inherited normal faults.

All these compressional structures are most likely related to the inversion but the precise age of this event and thus the faulting is not well constrained for the study area. If the inversion in the Weald to Boulonnais area was more or less synchronous with that in the Isle of Wight then a Mid to Late Eocene age seems likely (see Gale et al., 1999; Vandycke and Bergerat, 2001). The truncation of the Weald anticline by Thanetian littoral sands, preserved at elevations of around 200 m, suggests, however, that the inversion of this basin had begun by Late Palaeocene time (Curry, 1992). With the exception of a limited marine transgression in the London and the St Omer basins in late Eocene time (Lutetian and Bartonian), the remainder of the region appears to have been emergent at shoreface.

In Oligocene time the Weald remained emergent while the Hampshire basin continued to deepen with the accumulation of Rupelian lacustrine deposits (Pomerol, 1973). Rupelian marine microfauna are similar in Wight and in Belgium, indicating an early marine communication in the strait position at that time. The folding of the Rupelian deposits indicates continued compression.

In northern France the entire western section of the Variscan front was emergent at this time and this uplift appears to have been facilitated by movements on the many NW–SE faults south of the Boulonnais–Artois and on an E–W fault line close to the Monts de Flandre to the north.

Little is known about Miocene tectonic events in the northern France–southern England region but changing sea levels in Langhian–Serravalian and then in Tortonian time caused the incision of the Eastern Channel and Weald anticline (Larsonneur, 1971; Van Vliet-Lanoë et al., 1998, 2002). In latest Miocene time the fault-bound blocks of northern France were tilted to the south probably reflecting a weak inversion.

This tilting allowed a shift of the palaeo-valley system to the south side of the Channel (Van Vliet-Lanoë et al., 1998) that led, in early Pliocene time, to the opening of the Dover Straits (Dingwall, 1975; Margerel, 1989). A combined lowering of the global sea level and renewed uplift of the Variscan block caused the Dover Straits to close in late Pliocene to early Holocene (1–0.7 Ma) time (Zagwijn, 1989).

The only marine sediments preserved in the study area from this time are restricted to the inner Boulonnais, the St Omer basin, the lower Somme valley (Van Vliet-Lanoë et al., 2000a,b) and probably the Solent.

Several minor subsidence and uplift events are recorded in the changing drainage patterns and periodic tilting of the palaeo-relief surfaces through to the present day. The reopening of the Dover Straits can be explained by river capture accelerated by uplift along the Dover–Calais axis (Van Vliet-Lanoë et al., 1998, 2002).

All of these Neogene movements appear to have been focussed along the main Mesozoic basin controlling faults that are still active as seismic records for northern France to Belgium indicate. The active subsidence and uplift are interpreted to be in response to the combined Atlantic ridge push and Alpine (s.l.) collision.

4. Summary and conclusions

In a wider regional context it is apparent that the trends of those Mesozoic basins that overlie the Variscan orogen in western Europe follow closely the major structural trends in basement. The orientations of the major crustal block boundaries assembled during the Variscan orogeny have, in turn, strongly influenced the trajectories of the thrust faults (Mansy et al., 1999).

The deep seismic profile of southern England (Chadwick et al., 1983) revealed the presence of two major SSE dipping reflectors that are interpreted to be Variscan thrust faults. The tips of these thrusts were found to link to important Mesozoic basinal faults that, eastwards, correspond to the Pewsey–London Platform faults in the north and the Wardour–Portsdown Fault system in the south. These faults effectively define the northern and southern borders of the Mesozoic Weald sub-basin. The seismic profiles from northern France (Figs. 4 and 7) show that the Midi Fault is associated with an array of out-of-sequence thrusts that resembles the deep structure of southern England although in northern France the Midi Fault is the highest in the stack. Thus the spacing of the Variscan thrust faults has also, apparently, governed the spacing of the main Mesozoic faults although it is clear that many more smaller, parallel faults were generated by the N–S to NW–SE Tethyan and Atlantic rifting events. These subsidiary faults in most cases constitute syn-rift structures formed during Trias or Jurassic–Cretaceous time and the generation of these as subsidiary synthetic or antithetic faults are readily explained by reference to analogue models (e.g. Horsfield, 1977; McClay, 1989; Vendeville et al., 1987).

In southern England–northern France, Mesozoic sedimentation was concentrated into a number of sub-basins that were strongly controlled by fault activity. The main basin controlling faults were active at different times and at different rates through Triassic to Late Cretaceous time (Hamblin et al., 1992). It is notable that the faults with the greatest amount of throw are E–W oriented, orthogonal to the N–S extension direction (e.g. Fig. 8). The NW–SE oriented faults show less extensional throw and in northern France have had a lesser impact on sediment distribution patterns.

Except for the eastern part of the Weald Basin in Kent (e.g. Maidstone, Hastings), where the main faults trend NW–SE, the Late Cretaceous–Tertiary N–S Alpine compression in the southern England was orthogonal to the main basin controlling faults. On the coastal section of northern France the main faults are again approximately E–W oriented but in the Artois area they turn to a WNW–ESE orientation (e.g. the Pernes and Ruitz faults). As with the extension the compression, in the Boulonnais to Artois area, gave rise to a pure reverse slip on the E–W reactivated faults while those with NW–SE to WNW–ESE orientations were subject to a dextral reverse slip. The sense of slip on similarly oriented reactivated faults in Kent has not been recognised but a dextral reverse slip may be expected on NW–SE faults in the eastern part of the Weald. It is widely recognised that the complete reversal of steep normal faults by orthogonal compression is rarely accomplished. Commonly such faults are truncated by footwall shortcuts and such structures are invoked to explain some of the inversion structures along the Purbeck–Wight disturbance (e.g. Underhill and Paterson, 1998). In the Boulonnais, however, shortcut faults are not observed along the inverted E–W or the ~ NW–SE faults. Recently reprocessed (by the authors) industrial seismic lines from the area show that most of the reversed extensional faults sole in a listric manner on to reactivated Variscan low angle S to SW dipping thrust faults. This would suggest that the shallower listric faults are more easily reactivated than planar faults with larger initial extensional throws like those found in the Weald. Faults oblique to the principal compression direction are also more readily reactivated.

Irrespective of the orientation of the reactivated fault, it is common to find that fold axes follow the trends of the faults. En echelon fold patterns are not found in the inverted Mesozoic Basin of the Weald to Boulonnais area and the parallelism of the folds with the faults suggests that the faults have effectively conditioned the deformation pattern. The field data are not sufficient to determine whether this conditioning implies a partitioning of the deformation into an orthogonal compression to give the folds and a strike-slip component along the faults.

A reconstruction of the cover–basement relations in the Boulonnais area is presented in Fig. 4a together with an evolutionary model (Fig. 4b) to show how Variscan thrust faults have influenced Mesozoic basin formation and inversion. The model is based on field, borehole and seismic data from the area and projected into the line of the section. The Variscan thrust faults have been located from the borehole and seismic data although the projection of some of the lesser faults (e.g. the Wimereux–Belle Fault) down to the Midi Fault is conjectural. In the model the initial folding of the lower thrust sheet is attributed to a fault bend mechanism before the emplacement of the out-of-sequence higher thrusts. The Landrethun flexure–Cap Gris Nez fault line may have originated by the extensional relaxation of the lower thrust rising from the top of the ramp in Permo–Trias time (Fig. 4b). This would account for the thin wedge of Triassic rocks in hanging wall of the fault. The Ferques Fault was active at this time and records some sinistral strike-slip. The south-to-north thickening of the Mid–Upper Jurassic toward the Landrethun Fault and eventual overlap onto the footwall block is taken to indicate the growth activity. The Jurassic rocks seal the Ferques Fault and this structure was not inverted during the Alpine compression in contrast to the Landrethun–Cap Gris Nez faults.

The Mesozoic Basin of the Weald to Boulonnais area is one of the few examples where basement control on Mesozoic basin evolution in southern England–northern France can be studied in the field. The results of recent fieldwork presented here, for the North France region, combined with available borehole, gravity and released seismic profiles, have made it possible to demonstrate links between the reactivation of Variscan thrust faults and the location of controlling faults in this segment of the Weald–Boulonnais basin.

References

Angelier, J., 1990. Inversion of field data in fault tectonics to obtain the regional stress—III. A new rapid direct inversion method by analytical means. Geophys. J. Int. 103, 363–376.

Averbuch, O., Mansy, J.L., 1998. The "Basse–Normandie" duplex: evidence for an out-of-sequence thrusting overprint. J. Struct. Geol. 20, 33–42.

Bergerat, F., Vandycke, S., 1994. Palaeostress analysis and geodynamical implications of Cretaceous–Tertiary faulting in Kent and the Boulonnais. J. Geol. Soc. (Lond.) 151, 439–448.

Bevan, T.G., Hancock, P.L., 1986. A Late Cenozoic regional fracture system in southern England and northern France. J. Geol. Soc. (Lond.) 143, 355–362.

Borradaile, G.J., Henry, B., 1997. Tectonic applications of magnetic susceptibility and its anisotropy. Earth Sci. Rev. 42, 49–93.

Bouroz, A., 1956. Contribution à l'étude des Failles épicrétacées de l'Artois. Ann. Soc. Géol. Nord 76, 51–62.

Butler, M., Pullan, C.P., 1990. Tertiary structures and hydrocarbon entrapment in the Weald Basin of southern England. In: Hardman, R.F.P., Brookes (Eds.), Tectonic Events Responsible for Britains Oil and Gas Reserves. Special Publication-Geological Society of London, vol. 55, pp. 371–391.

Cazes, M., Torreilles, G., Bois, C., Damotte, B., Galdeano, A., Hirn, A., Mascle, A., Matte, P., Van Ngoc, P., Raoult, J.-F., 1985. Structure de la croûte hercynienne du Nord de la France: premiers résultats du profil ECORS. Bull. Soc. Géol. Fr. I (6), 925–941.

Chacksfield, B., Devos, W., D'hodges, L., Dusar, M., Lee, M., Poitevin, C., Roy Les, C., Verniers, J., 1993. A new look at the Belgian aeromagnetic and gravity data through image-based display and integrated modelling techniques. Geol. Mag. 13 (5), 583–591 (Cambridge).

Chadwick, R.A., Kenolty, N., Whittaker, 1983. Crustal Structure beneath southern England from deep seismic reflection profiles. J. Geol. Soc. (Lond.) 140, 893–911.

Colbeaux, J.P., Leplat, J., 1985. Le Massif Paleozoique du Bas-Boulonnais, Region Marquise. In: Géologie du Boulonnais, J.P. Colbeaux, coord., Science et Nature 3, Espace Naturel Régional 176.

Colbeaux, J.P., Amedro, F., Bergerat, F., Bracq, P., Crampon, N., Delay, F., Dupuis, C., Lamouroux, C., Robaszynski, F., Somme, J., Vandycke, S., Vidier, J.P., 1993. Un enregistreur des épisodes tectoniques dans le bassin de Paris: le Boulonnais. Bull. Soc. Géol. Fr. t. 164 (1), 93–102.

Cooper, M.A., Garton, M.R., Hossack, J.R., 1983. The origin of the Basse–Normandie duplex, Boulonnais, France. J. Struct. Geol. 5, 139–152.

Cordell, L., Grauch, V.J.S., 1982. Mapping Basement magnetic Zones from aeromagnetic data in the San Juan Basin, New Mexico. The utility of regional gravity and Magnetic anomaly maps. SEG, 181–197.

Curry, D., 1992. Tertiary. In: Duff, P.M.D., Smith, A.J. (Eds.), Geology of England and Wales. The Geological Society of London, pp. 389–411. Chap. 13.

De Vos, W., 1997. Influence of the granitic batholith of Flanders on Acadian and later deformation (Brabant Massif, Belgium). Aardk. Meded. 8, 49–52.

De Vos, W., Chackfield, B., D'hooge, L., Dusar, M., Lee, M., Poitevin, C., Royles, C., Verniers, J., 1993. Images based display and integrated modeling techniques. Geol. Mag. 130 (5), 583–591.

Dingwall, R.G., 1975. Sub-bottom infill channels in an area of the eastern English Channel. Philos. Trans. R. Soc. Lond. A279, 233–241.

Donato, J.A., Megson, J.B., 1990. A buried granite batholith beneath the East Midlands Shelf of the Southern North Sea Basin. J. Geol. Soc. (Lond.) 140, 133–140.

Everaerts, M., Mansy, J.L., 2001. Le filtrage des anomalies gravimétriques: une clé pour la compréhension des structures tectoniques du Boulonnais et de l'Artois (France). Bull. Soc. Géol. Fr. 172, 267–274.

Everaerts, M., Potevin, C., Devos, W., Sterpin, M., 1996. Integrated geophysical/geological modeling of the Western Brabant. Massif and structural implication. Bull. Soc. Belge Geol. 105 (1–2), 41–59.

Gale, A.S., Jeffery, P.A., Hugget, J.M., Connoly, 1999. Eocene inversion history of the Sandown Pericline, Isle of Wight, southern England. J. Geol. Soc. (Lond.) 156, 327–339.

Gallois, R.W., 1965. The Wealden District, British Regional Geology. British Geological Survey, HMSO, London.

Gosselet, J., 1908. Note sur quelques parties communes aux terrains crétacique et houiller de l'Artois. Ann. Soc. Géol. Nord t. 37, 80–109.

Gosselet, J., 1910. Les assises crétaciques et tertiaires dans les fosses et sondages du Nord de la France. Etudes des gîtes minéraux de la France. Fasc. 3. Paris.

Hamblin, R.J.O., Crosby, A., Balson, P.S., Jones, S.M., Chadwick, R.A., Penn, I.E., Arthur, M.J., 1992. The Geology of the English Channel. British Geological Survey, London. HMSO.

Hawkes, P.W., Fraser, A.J., Einchcomb, C.C.G., 1998. The tectonostratigraphic development and exploration history of the Weald and Wessex Basins, Southern England, UK. In: Underhill, J.R. (Ed.), Development, Evolution and Petroleum Geology of the Wessex Basin. Special Publication-Geological Society of London, vol. 133, pp. 39–66.

Horsfield, W.T., 1977. An experimental approach to basement controlled faulting. Geol. Mijnb. 56, 363–370.

International Association of Geodesy, 1988. In: Tcherning, C.C. (Ed.), The Geodesist's Handbook 1988, No. 3, Vol. 62. Bureau Central de l'association International de géodésie 140, rue de Grenelle 75700 Paris.

Lacquement, F., Mansy, J.L., Hanot, F., Meilliez, F., 1999. Retraitement et interprétation d'un profil sismique pétrolier meridien au travers du Massif paléozoique ardennais Nord de la France. C. R. Séances Acad. Sci., Paris 329, 471–477.

Lamarche, J., Bergerat, F., Mansy, J.L., 1996. Tectoniques plicatives et cassantes dans le Jurassique du Boulonnais: une histoire méso-cenozoïque polyphasée. Ann. Soc. Geol. Nord IV (2er serie), 171–179.

Lamarche, J., Bergerat, F., Mansy, J.L., 1997. Déformations cassantes et plicatives dans le Jurassique du Boulonnais (France), influence lithostructurale et héritage paléozoïque. C. R. Séances Acad. Sci., Paris 326, 57–63.

Larsonneur, C., 1971. Données sur l'évolution paléogéographique post-hercynienne de la Manche. Mem. BRGM, «Colloque sur la Géologie de la Manche» 79, 202–214.

Mansy, J.-L., Meilliez, F., 1993. Eléments d'analyse structurale à partir d'exemples pris en Ardenne-Avesnois. Affleurements visités lors de l'excursion de la SGN en Octobre 1991. Ann. Soc. Géol. Nord t. 2 (2ème série), 45–60.

Mansy, J.L., Everaerts, M., De Vos, W., 1999. Structural analysis of the Acadian and Variscan fold belts in Belgium and northern France from geophysical and geological evidence. Tectonophysics 309, 99–116.

Mansy, J.L., Amedro, F., Auffret, J.P., Guennoc, P., Lamarche, J., Lefevre, D., Robaszinski, F., Somme, J., Vidier, J.P., in press.

Carte géologique de Marquise (50 000ème). 2ème édition. B.R.G.M., Orléans.
Margerel, J.-P., 1989. Biostratigraphie des dépôts Néogènes de l'Ouest de la France: Constitution de biozones de foraminifères benthiques. Géol. Fr. (1–2), 235–250.
Marton, E., Mansy, J.-L., Averbuch, O., Csontos, L., 2000. The Variscan Belt of Northern France–Southern Belgium: geodynamic implications of new palaeomagnetic data. Tectonophysics 324, 57–80.
Mattei, M., Sagnotti, L., Facenna, C., Funiciello, R., 1997. Magnetic fabric of weakly deformed clay-rich sediments in Italian peninsula: relationship with compressional and extensional tectonics. Tectonophysics 271, 107–122.
McClay, K.M., 1989. Physical models of structural styles during extension. In: Tankard, A.J., Balkwill, H.R. (Eds.), Extensional Tectonics and the Stratigraphy of the North Atlantic Margins. Mem.-Am. Assoc. Pet. Geol., vol. 46, pp. 111–130.
Meilliez, F., Mansy, J.L., 1990. Déformation pelliculaire différenciée dans une série lithologique hétérogène: le Dévono-Carbonifère de l'Ardenne. Bull. Soc. Géol. Fr. 8, 177–188.
Meilliez, F., Andre, L., Blieck, A., Fielitz, W., Goffette, O., Hance, L., Khatir, A., Mansy, J.L., Overlau, P., Verniers, J., 1991. Ardenne-Brabant. Sci. Géol., Bull. 44, 3–29.
Meilliez, F., Fielitz, W., Laduron, D., Mansy, J.L., Manby, G.M., 1994. The deep structure of the Ardennes variscan thrust belt from structure and Ecors Seismic data: discussion. J. Struct. Geol. 16 (3), 431–432.
Olry, A., 1904. Topographie souterraine du Bassin houiller du Boulonnais ou Bassin d'Hardinghen. Et. Gîtes Min. France, VI. 240 pp.
Pasquet, J.F., Leplat, J., Becq-Giraudon, J.F., 1983. Premiers résultats du sondage de Réty-Rinxent (Massif paléozoïque de Ferques). Mem. BRGM 123, 171–178.
Pharaoh, T.C., Barron, A.J.M., Sumbler, M.G., Ivimey-Cook, 1996. Concealed rocks and basement structure. In: Sumbler, M.G. (compiler), London and the Thames Valley, 4th ed., British Geological Survey, London. HMSO.
Pomerol, L., 1973. Stratigraphie et paléogéographie: ère Cénozoïque (Tertiaire et Quaternaire). Masson. 269 pp.
Proust, J.N., Deconninck, J.F., Geyssant, J.R., Herbin, J.P., Vidier, J.P., 1995. A sequence analytical approach to the Late Kimmeridgian/Lower Tithonian storm dominated ramp deposits of the Boulonnais (Northern France). A landward time-equivalent to offshore source rocks. Geol. Rundsch. 84, 255–271.
Pruvost, P., Delepine, G., 1921. Observations sur la faille d'Hydrequent et sur les couches de base du Carbonifère dans le Bas-Boulonnais. Bull. Soc. Géol. Fr. 4 (XXI), 189–206.
Ruffell, A.H., 1995. Seismic stratigraphic analysis of non-marine Lower Cretaceous strata in the Wessex and North Celtic Sea Basins. Cretac. Res. 16, 603–637.
Shephard-Thorn, E.R., Lake, R.D., Atitullah, E.A., 1972. Basement control of structures in the Mesozoic rocks in the Strait of Dover region, and its reflexion in certain features of the present land and submarine topography. Philos. Trans. R. Soc. Lond. 272, 99–113.
Sintubin, M., 1997. Cleavage–fold relationships in the lower Palaeozoic Brabant Massif (Belgium). Belgian symposium on structural geology and tectonics. Aardkd. Meded. 8, 61–164.
Smith, M.J.P., 1985. Contours on the top of the pre-Permian surface of the United Kingdom, Map 2 1:1 000 000. BGS.
Smith, I.F., 1986. Mesozoic Basins. In: Downing, R.A., Gray, D.A. (Eds.), Geothermal Energy—The Potential in the United Kingdom. H.M.S.O., London.
Tarling, D.H., Hrouda, F., 1993. The Magnetic Anisotropy of Rocks. Chapman & Hall. 217 pp.
Underhill, J.R. (Ed.), 1998. Development, Evolution and Petroleum Geology of the Wessex Basin. Geol. Soc. Spec. Publ., 133.
Underhill, J.R., Paterson, S., 1998. Genesis of tectonic inversion structures: seismic evidence for the development of key structures along the Purbeck-Isle of Wight Disturbance. J. Geol. Soc. (Lond.) 155, 975–992.
Vandycke, S., Bergerat, F., 2001. Brittle tectonic structures and palaeostress analysis in the Isle of Wight, Wessex basin, southern UK. J. Struct. Geol. 23, 393–406.
Vandycke, S., Bergerat, F., Gaviglio, P., 1995. Paleostresses and grain-scale microstructures in faulted chalk. Communication Tectonic Studies Group Meeting, Cardiff Dec. 1995. 1 pp. 1 fig.
Van Vliet-Lanoë, B., Mansy, J.L., Margerel, J.P., Vidier, J.P., Lamarche, J., Everaerts, M., 1998. Le Pas de Calais un détroit cénozoïque à ouverture multiple. C. R. Séances Acad. Sci., Paris II a (326), 729–736.
Van Vliet-Lanoë, B., Laurent, M., Balescu, S., Bahain, J.L., Falguères, C., Field, M., Keen, D., Hallegouët, B., 2000a. Raised beach anomalies, Western Channel. Regional and global stratigraphic implications. J. Geodyn. 29, 15–41.
Van Vliet-Lanoë, B., Laurent, M., Everaerts, M., Mansy, J.L., Manby, G., 2000b. Evolution Neogene et Quaternaire de la Somme, une flexuration tectonique active. C. R. Séances Acad. Sci., Paris IIa (329), 151–158.
Van Vliet-Lanoë, B., Van Denberghe, N., Laignel, B., Laurent, M., Lauriat-Rage, A., Louwye, S., Mansy, J.L., Meilliez, F., Mercier, D., Hallégouët, B., Lacquement, F., Michel, Y., Moguedet, G., 2002. Paleogeographic evolution of Northwestern Europe during the Upper Cenozoïc. Geodiversitas 24 (3), 511–541.
Vendeville, B., Cobbold, P., Brun, J.P., Choukroune, P., 1987. Physical models of extensional tectonics at various scales. In: Coward, M.P., Dewey, J.F., Hancock, P.L. (Eds.), Continental Extensional Tectonics. Geol. Soc. London, Spec. Pub., vol. 28, pp. 99–107.
Vidier, J.P., Garcia, J.P., Thierry, J., Fauconnier, D., 1995. Le Dogger du Boulonnais (Nord du Bassin de Paris): nouveaux decoupages chronologique et séquentiel des formations carbonatées jurassiques en bordure du massif Londres-Brabant. C. R. Séances Acad. Sci., Paris 320, 219–226.
Zagwijn, 1989. The Netherlands during the Tertiary the Quaternary: a case history of coastal lowland evolution. Geol. Mijnb. 68, 107–120.

Article 4.

Minguely B., Averbuch O., *Patin M.,* Rolin D., Hanot F. and Bergerat F. (2010). Inversion tectonics at the northern margin of the Paris basin (Northern France) : new evidence from seismic profiles and boreholes interpolation in the Artois area. Bulletin de la Société Géologique de France, vol. 5.

Bull. Soc. géol. Fr., 2010, t. 181, n° 5, pp. 341-346

Inversion tectonics at the northern margin of the Paris basin (northern France): new evidence from seismic profiles and boreholes interpolation in the Artois area

BRUNO MINGUELY[1], OLIVIER AVERBUCH[1], MARIE PATIN[1], DAVID ROLIN[1], FRANCK HANOT[2, 4] and FRANCOISE BERGERAT[3]

Dedicated to Jean-Louis MANSY (deceased in May 2006), who initiated the present study

Key-words. – Variscan thrust front, Structural inheritance, Tectonic inversion, Paris basin, Northern France geodynamics

Abstract. – A synthesis of existing borehole data and seismic profiles has been conducted in the Artois area (northern France), along the northern border of the Paris basin, in order to explore the possible control exerted at depth by the Upper Carboniferous Variscan thrust front on the distribution of Late Paleozoic-Mesozoic depositional centers and their subsequent uplift in Tertiary times. Such control was demonstrated recently in the Weald-Boulonnais basin (Eastern Channel area) that forms the western prolongation of the area under study but was so far poorly constrained in the Artois area. Presented data provide evidence for the topography of the Artois hills and the altitude of sedimentary layers to be controlled by the activity of a network of relaying WNW-ESE striking faults inducing the systematic uplift of the southern fault blocks. Those steeply S-dipping faults branch downward onto the ramp of the Variscan thrusts forming listric faults that locally limit to the north buried half-graben structures, filled with fan-shaped fluviatile Stephanian-Permian deposits. Such clear syn-rift geometry shows that the ramp of the main Variscan frontal thrust (the Midi thrust) has been reactivated as a normal fault in Stephanian-Permian times thus forming a very demonstrative example of a negative inversion process. The reverse offset of the transgressive Middle Cretaceous-Lower Eocene layers covering unconformably the Paleozoic substratum argue for a Tertiary (Middle Eocene-Late Oligocene?) contractional reactivation of the fault network thereby documenting a repeated inversion process along the Artois Variscan thrust front. The Variscan frontal thrust zone is thus shown here to represent a prominent crustal-scale mechanical discontinuity that localized deformation in the Artois-Boulonnais area since Upper Paleozoic times.

Inversion tectonique en bordure septentrionale du bassin de Paris (nord de la France) : nouvelles contraintes à partir de profils sismiques et de l'interpolation de forages en Artois

Mots-clés. – Front de chevauchement varisque, Héritage structural, Inversion tectonique, Bassin de Paris, Géodynamique du Nord de la France

Résumé. – Une étude synthétique des données de forage et des profils sismiques existant a été entreprise dans la région de l'Artois (Nord de la France) afin de caractériser le contrôle potentiel exercé, en profondeur, par le front chevauchant varisque du Carbonifère supérieur sur la distribution des aires de sédimentation au cours du Paléozoïque terminal et du Mésozoïque et leur soulèvement plus tardif au cours du Tertiaire. Un tel contrôle a pu être démontré récemment dans le bassin du Weald-Boulonnais (Manche orientale) qui forme le prolongement occidental de la zone d'étude mais reste, pour l'heure, encore assez méconnu dans la région de l'Artois. Les données présentées montrent que la topographie des collines de l'Artois ainsi que l'altitude des niveaux sédimentaires de couverture sont contrôlées par l'activité d'un réseau de failles en relais, orientées suivant une direction WNW-ESE, induisant systématiquement le soulèvement du bloc sud. Ces failles, à fort pendage vers le Sud, se raccordent en profondeur aux rampes des chevauchements varisques. Les failles listriques résultantes localisent ponctuellement des petits bassins, enfouis, structurés en demi-graben dont le remplissage fluviatile d'âge stéphano-permien présente une géométrie caractéristique en éventail.

Cette configuration, caractéristique des dépôts syn-rift, montre que la rampe du chevauchement frontal varisque (le chevauchement du Midi) a été réactivée en faille normale au cours du Stéphano-Permien, illustrant de façon très démonstrative le phénomène d'inversion tectonique négative. Le décalage inverse observé systématiquement pour les niveaux transgressifs de couverture (Crétacé moyen-Eocène inférieur) reposant en discordance sur le substratum paléozoïque indique l'existence d'une réactivation tertiaire en contexte compressif (Eocène moyen-Oligocène terminal ?) montrant le caractère répété du phénomène d'inversion tectonique au niveau du front chevauchant varisque de l'Artois. La zone de chevauchement frontal varisque apparaît ainsi comme une discontinuité mécanique majeure d'échelle crustale ayant localisé la déformation dans le domaine Artois-Boulonnais depuis le Carbonifère supérieur.

1. Université de Lille 1, Géosystèmes, UMR CNRS 8157, 59655 Villeneuve d'Ascq cedex, France. Corresponding author: olivier.averbuch@univ-lille1.fr
2. Bureau de Recherches Géologiques et Minières, 3 avenue C. Guillemin, BP 6009, 45060 Orléans cedex 2, France.
3. Institut des Sciences de la Terre de Paris, UMR CNRS 7193, Université Pierre et Marie Curie, 4 place Jussieu, 75252 Paris cedex 05, France
4. Present adress: CDP Consulting, rue de la Grande Maison, 45380 La Chapelle St Mesmin
Manuscrit déposé le 5 février 2009; accepté après révision le 31 octobre 2009.

INTRODUCTION

The Paris basin is an intracratonic basin that developed above the collapsed Late Carboniferous Variscan orogenic belt [e.g. Roure *et al*., 1996]. Its geometry and subsidence through Late Paleozoic to Late Mesozoic times is thus strongly controlled by the initial thermomechanical configuration of the thickened Variscan lithosphere [Prijac *et al*., 2000; Guillocheau *et al*., 2000; Le Solleuz *et al*., 2004]. Whatever the large-scale processes driving the initiation of rifting in Stephanian-Lower Permian times (pure orogenic collapse, lithospheric mantle delamination) [Prijac *et al.,* 2000; Ziegler *et al.,* 2004], the reactivation of thrusts as normal faults (classically referred to as a negative tectonic inversion process) has been extensively observed throughout the basin substratum leading to the general moulding of extensional features upon the Variscan framework [Chadwick, 1986; Mascle and Cazes, 1988; Blundell, 1990; Legrand *et al*., 1991; Henk, 1993; Roure *et al*., 1996; Averbuch *et al*., 2004; Roure, 2008; Shail and Leveridge, 2009].

In northern France, along the northern border of the basin, the exposure of Paleozoic inliers in the core of Cenozoic anticlines in the Boulonnais-Weald area allowed considering the relationships between the Variscan substratum and its sedimentary cover and suggested the step-wise reactivation of the buried northern Variscan thrust front to control the distribution of depositional centers and their subsequent uplift in Tertiary times [Mansy *et al*., 2003a]. Such control exerted by the substratum geometry was so far poorly constrained along the northern border of the basin because basin-controlling structures are largely buried below the transgressive Upper Cretaceous chalk deposits (fig. 1). To advance in the characterization of the basement-cover relationships above the northern France Variscan thrust front, we performed the synthesis of existing deep boreholes data, collected in the project "Référentiel géologique" of the BRGM, and combined these data to the analysis of unpublished industrial seismic profiles. We focused our attention to the eastward prolongation of the Boulonnais-Weald axis in the Artois area, zone marked by a specific topographic signature (the Artois hills) delimiting to the south the Cenozoic deposits of the "Plaine des Flandres".

GEOLOGICAL SETTING

From a geological point of view, the Artois area in northern France corresponds to the eastern prolongation of a major geological structure crossing the English Channel, the Weald – Boulonnais Anticline [Hamblin *et al*., 1992; Mansy *et al*., 2003a]. The latter structure, particularly well expressed on geological maps due to the erosion of Upper Cretaceous chalk and the resultant exhumation of Jurassic rocks and of their Paleozoic substratum (fig.1), was uplifted in different steps mainly spanning Middle Eocene to late Oligocene times [Van Vliet-Lanoe *et al*., 1998]. Such far-field accommodation of the Africa-Europe convergence, described throughout the Central-Eastern Channel area [Simpson *et al*., 1989; Chadwick, 1993; Underhill and Paterson, 1998; Beeley and Norton, 1998] and the southern North Sea [Badley *et al*., 1989] has been shown to relate to the widespread reactivation of basin-controlling normal faults, themselves often controlled by the configuration of Variscan thrust faults [e.g. Shephard-Torn *et al*., 1972; Blundell, 1990; Chadwick and Evans, 1995; Beeley and Norton, 1998]. The northern border of the Weald-Boulonnais anticline particularly exemplifies such a tectonic scenario. It represents, indeed, a major paleogeographic feature of the Paris-London basin as it localizes the northward extension of Middle-Upper Jurassic and Lower Cretaceous deposits onto the Paleozoic Brabant massif. Recent tectonic studies suggested the Tertiary uplift in the Boulonnais area to be the direct result of the structural inversion of normal faults (classically referred to as a positive tectonic inversion process), that basically controlled the sedimentation of syn-rift Upper Jurassic-Lower Cretaceous deposits coeval with the N-Atlantic opening [Lamarche *et al*., 1997; Mansy *et al*., 2003a]. The characterization of the structural geometries both in the Jurassic-Cretaceous cover and the Paleozoic substratum furthermore argued for these normal faults to be rooted on some South-dipping thrusts, developed at the front of the buried northern Variscan thrust wedge [Mansy *et al*., 2003a; Averbuch *et al*., 2004].

In the Artois area, the Jurassic sequence is lacking due to the existence of a set of about N030 and N110 faults relaying in a complex way in the eastern part of the Boulonnais area (fig. 1). This fault system induced the general down-throw and subsidence of the western fault blocks, thereby restricting the preservation of Middle and Upper Jurassic rocks to the Boulonnais area [e.g., Mégnien, 1980]. Footwall uplift and large-scale thermal doming at the Jurassic-Cretaceous boundary [Ziegler, 1990; Mc Mahon and Turner, 1998] induced either a non-deposition of this sequence or its complete erosion before Aptian times. The progressive flooding of this topography occurred from Middle Aptian times onward within a general transgressive framework characteristic for a post-rift drowning of the basin margins. In the Artois region, the post-rift Upper Cretaceous sequence and its Tertiary cover thus directly lies, unconformably, on the Paleozoic basement, deformed during the Variscan orogeny (fig. 2) [e.g., Delattre, 1969].

More precisely, a significant set of boreholes shows that the Artois region localizes at depth the northern Variscan thrust front [e.g., CFP (M) *et al*., 1965]. Scarce Paleozoic outcrops, visible in the deepest parts of valleys and in a few quarries, document the existence of Lower Devonian rocks in the southern part of the area under study (fig. 1 and 2a). Along the northern France Variscan thrust system, the Lower Devonian shales and sandstones are only observed south of the main Variscan frontal thrust i.e. the Midi thrust zone or Midi fault in the regional terminology [e.g., Raoult, 1986]. Along this major thrust, the Namurian-Westphalian coal-bearing foreland basin overlying a reduced Middle Devonian-Carboniferous sequence is underthrusted below the allochthonous Variscan unit floored by the rheologically weak, thick Lower Devonian silicilastic sequence [Raoult and Meilliez, 1987; Le Gall, 1994; Lacquement *et al*., 1999]. Such a typical geometry has been interpreted recently to result from the inversion of the northern border fault of the Rheno-Hercynian basin that controlled the extension of the syn-rift Lower Devonian sequence [Oncken *et al*., 2000; Lacquement *et al*., 2005]. In the Artois area, these Lower Devonian rocks, characteristic for the allochthonous

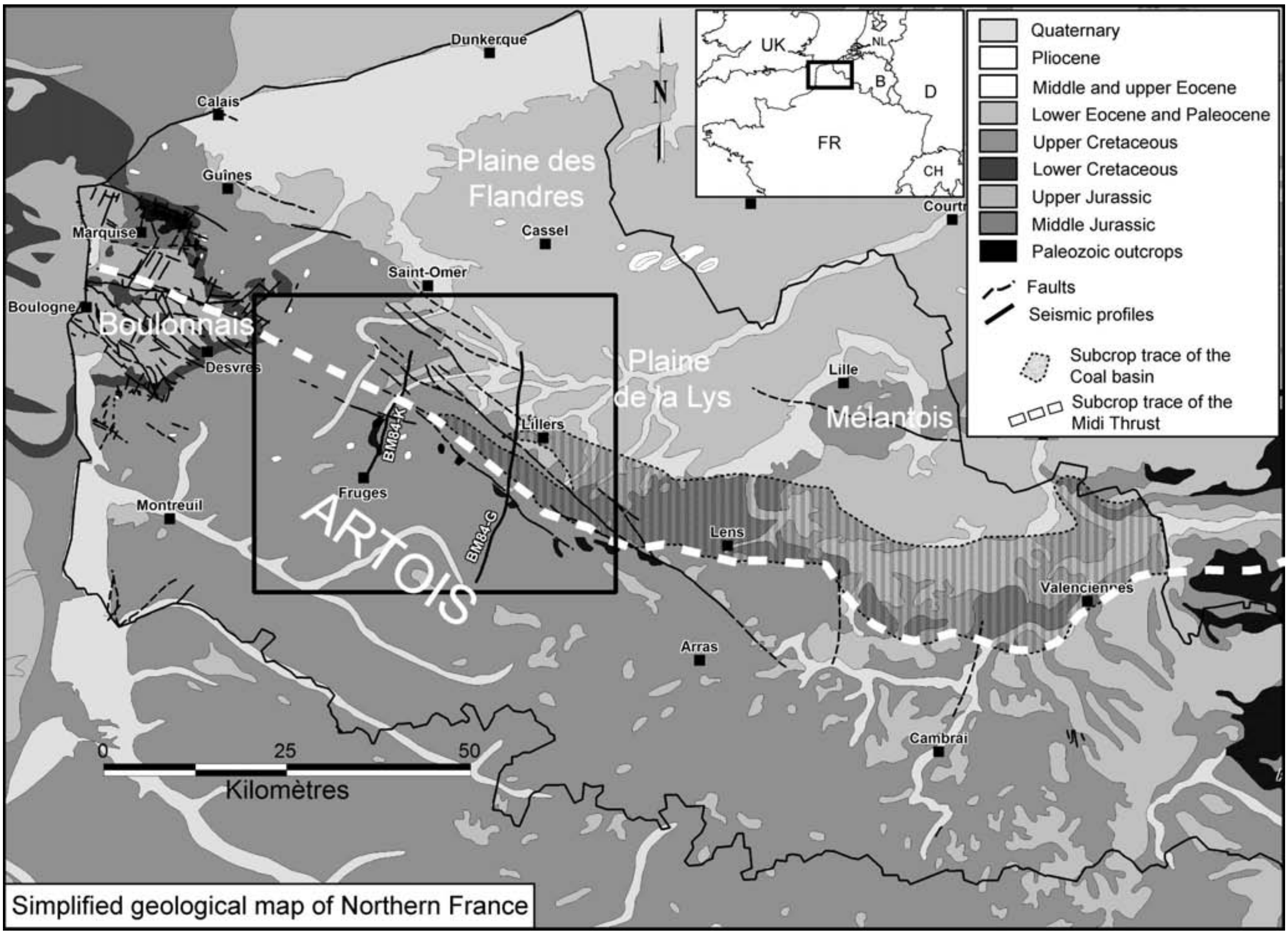

FIG. 1. – Simplified geological map of northern France reporting the extension at depth of the Nord-Pas-de-Calais coal basin (shaded area) and the general trace of the main northern Variscan frontal thrust i.e. the Midi thrust (dotted line). The rectangle locates the study area. The lines BM84K and BM84G correspond to the trace of the seismic sections under study.

FIG. 1. – *Carte géologique du Nord de la France montrant l'extension en profondeur du bassin houiller du Nord-Pas-de-Calais (surface grisée) et le tracé général du chevauchement frontal principal nord varisque i.e. le chevauchement du Midi (ligne pointillée). Le rectangle indique la localisation de la zone d'étude. Les lignes BM84K et BM84G correspondent au tracé des sections sismiques étudiées.*

Variscan units, end towards the north against a network of *en-échelon* steeply S-dipping faults with a N110-N130 orientation, the so-called "Artois faults" [Gosselet, 1908; Briquet, 1924; Bouroz, 1948, 1956]. The latter cut across the Upper Cretaceous and Paleocene sedimentary cover arguing for a Tertiary activation of this fault network (i.e. Middle Eocene-Late Oligocene?). Such a recent age for the "Artois faults" activation is corroborated by the Digital Elevation Model of the region, clearly showing a control of the topography by the fault network (fig. 2b).

On the other hand, some of these faults (the Audincthun Fault, AF and the Pernes Fault, PF in fig. 2a) exhibit in their direct hangingwall (southern part) some very localized outcrops of enigmatic red conglomeratic continental deposits, lying unconformably on top of Lower Devonian rocks and considered traditionally as latest Carboniferous to Permian in age [Mériaux, 1961]. The recent discovery of reworked *microcodium* allowed defining a Middle Permian age for the upper part of the conglomeratic sequence thus corroborating a possible Stephanian-Middle Permian age for the entire sequence [Mansy *et al.*, 2003b]. The localization of these deposits in the direct hangingwall of the faults suggests a possible fault-controlled subsidence during that particular time, coeval with the initial rifting stage of the Paris basin. The precise geometry and dynamics of such possible fault-controlled basins are, however, still to be constrained.

Northeast of the "Artois fault" network, the Paleozoic rocks are buried below the Upper Cretaceous-Tertiary cover (fig. 2a). The geometry at depth is, however, relatively well known in the SE part of the Artois area, due to coal mining exploration at the western tip of the "Nord-Pas de Calais" coal basin (see its subcrop extension in fig. 1). As previously mentioned, the latter includes Namurian-Westphalian molassic deposits that accumulated in the Variscan foreland basin and were subsequently deformed in the direct footwall of the main frontal thrust, the Midi thrust zone. Borehole-based sections through the southern border of the SE Artois coal basin gave a first insight into the geometry of the thrust front at depth corroborating the existence of a significant post-orogenic extensional event, responsible for the collapse of the southern fault blocks of the "Artois fault" system [Bouroz, 1948, 1956]. On the other hand, the reversal of the finite displacement of the Cretaceous strata on these faults led Bouroz [1956] to infer a post-Cretaceous

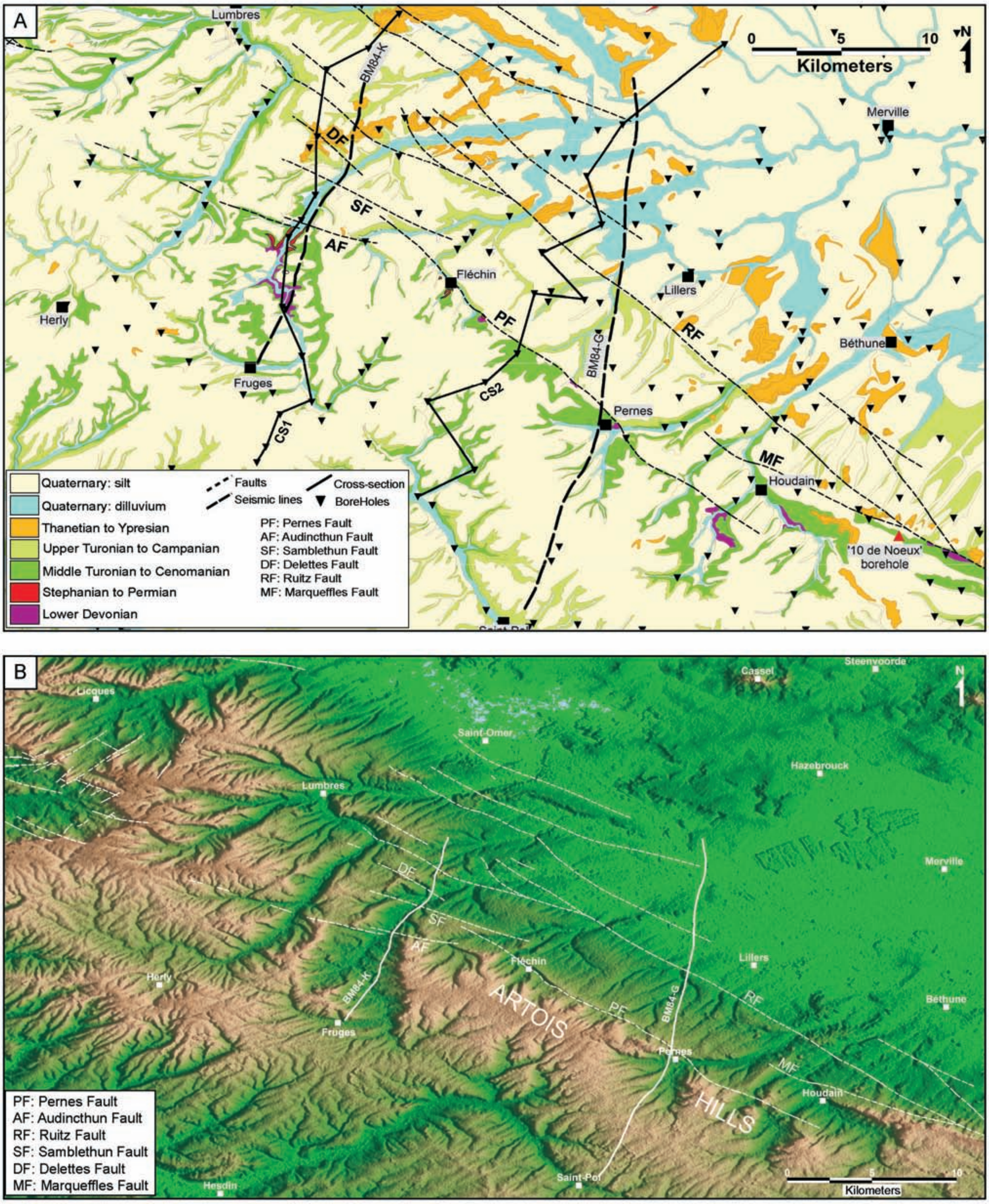

FIG. 2. – A. Geological map of the studied area (modified from the numerical geological map of northern France of the BRGM by Lacquement *et al.* [2004]) reporting the location of available boreholes and seismic lines. Borehole-based superficial cross sections CS1 and CS2 are also reported. B. Digital elevation model of the Artois region; the faults extracted from the geological map database are reported for a comparison.

FIG. 2. – A. *Carte géologique du secteur d'étude (modifiée de la carte géologique harmonisée du Nord-Pas-de-Calais du BRGM de Lacquement* et al. *[2004]) montrant la localisation des forages et des lignes sismiques utilisés. Les coupes superficielles CS1 et CS2, basées sur l'interpolation des forages, sont également reportées.* B. *Modèle numérique de terrain du secteur d'étude ; les failles, extraites de la base de données géoréférencée associée à la carte géologique, sont reportées pour comparaison.*

compressional event that induced the inversion of the fault movement in the cover (the "epi-cretaceous" faults of Bouroz [1956]). The relationships of the superficial faults with the deeper thrusts have, so far, not been clearly defined.

Geological data, presented above, thus show that the present geometry of the "Artois fault" system is the result of at least three superimposed tectonic events: (1) a Variscan (Late Westphalian, ca 305 Ma) thrusting event basically controlling, at depth, the structure of the Paleozoic substratum, (2) a Late Paleozoic (Stephanian–Permian?) extensional event inducing the development of small intramontane basins and (3) a Tertiary compressive event responsible for uplift along the Artois hills. In the following, we will characterize more precisely the geometry of the deformations of both the substratum and the cover, accommodating these successive tectonic events.

INTERPOLATION OF BOREHOLE DATA

Isobaths maps

Isobaths maps have been made using boreholes interpretation from the BRGM boreholes database of the RGF ("Référentiel Géologique de France") program. This database updates some previous syntheses done by Gosselet [1922], Caulier [1974] and a consortium of petroleum companies [CFP (M) *et al.*, 1965]. Obviously, this large database (a total of 2071 boreholes distributed in northern France) includes strongly heterogeneous data collected as well for local, industrial or academic purposes and therefore required to be thoroughly checked and formatted according to a uniform stratigraphic chart [Minguely, 2007]. Specifically, the stratigraphic succession in a large number of boreholes was only defined in term of lithological sequences and was not based on precise paleontological dating. Therefore, only a first-order stratigraphic definition was possible at the total set scale by interpolation with precisely dated neighbouring boreholes. The stratigraphic chart includes 9 well-defined horizons spanning from the top of the Paleozoic substratum (including localized Stephanian-Permian deposits) to the top of Ypresian (basal Eocene) levels (see Delattre [1969] for a precise stratigraphic description). In the Artois area, which was submitted to Tertiary uplift, erosion strongly affected Late Cretaceous chalk and Paleocene-Eocene horizons. To compute isobath maps, we therefore focused our attention on two specific horizons that can be precisely defined within the borehole dataset and that were not deeply truncated by erosion. The first one is the top of Cenomanian deposits (fig. 3a) and, the second one, the top of the Paleozoic substratum (fig. 3b). Isobaths maps were constructed using fault discontinuities based on outcrop data (see the geological map of fig. 2).

As a whole, both horizons display the same geometry suggesting very little deformation of the substratum during the deposition of the post-rift Albian-Cenomanian sequence. Isobath curves define a general NW-SE elongated culmination with a maximum vertical offset of about 300 m between the main uplifted areas (Pernes-Flechin-Herly) and the zones of depression in the St Omer-Hazebrouck Tertiary basin. As clearly shown on both maps, the geometry of the culmination is strongly asymmetric and discontinuous due to the existence of the Artois fault network, localizing a significant step in the depths of the horizons. The zone of maximum uplift extends along the southeastern wall of the Pernes-Audincthun fault system (PF and AF in fig. 3), relayed southward by the Marqueffles fault (MF in fig. 3). To the south of the culmination, both horizons display a gentle dip towards the SE (block A in fig. 3). North of the Pernes fault zone, however, a first significant downward step of about 100 m is observed in the depths of both the top Paleozoic and top Cenomanian surfaces (block B in fig. 3). A second one of about the same amplitude is observed north of the Ruitz fault thereby inducing the accommodation of about 200 m of total vertical offset of both horizons along the Artois fault network. North of the fault system, the altitude of both horizons diminishes gently northward up to the St Omer-Hazebrouck depression (block C in fig. 3) where the top of Paleozoic substratum goes down to –240 m.

In more detail, the geometry of isobath maps provides evidence for a strong segmentation of the culmination due to the partitioning of displacement into different faults relaying from SE to NW. This point is particularly obvious considering the zone of maximum altitude of horizons, with 3 segmented zones along the main culmination: a first one from the south of Vimy to Houdain along the southern border of the Marqueffles fault, a second one from Pernes to Flechin along the Pernes fault and a third one in the Herly area south of the Audincthun fault. This geometry defines intermediate panels in the zones of relay between those faults such as the one situated between the Pernes and Marqueffles-Ruitz faults (block B). Such a complex pattern of relay between the different faults forming the Artois fault network has been recognized for long and is likely to have implied some strike-slip components at some stage of their development [Colbeaux, 1974; Averbuch *et al.*, 2001]. Due to the possible control by inherited substratum structures, it is, however, difficult to precisely determine the importance and age of such lateral movements.

To conclude with the configuration in map of both these reference horizons, it is worth noting that isobath curves provide a geometry that can be strongly correlated with the topography, imaged by the Digital Elevation Model of figure 2b, thereby corroborating the control of the Artois fault system on the topography, the altitudes of sedimentary layers and the general distribution of Paleozoic outcrops in the Artois region.

Superficial cross-sections

In order to have a better view of the phenomenon described before, two cross-sections have been done by interpolation of selected boreholes along a general NE-SW strike (normal to the axis of the culmination) (fig. 4). The first cross-section (CS1 in fig. 4) has been constructed along the seismic profile BM 84K that we will discuss in the following section (see fig. 2 for location). The second one is situated more to the east crossing the core of the Artois hills and close to the seismic line BM84G (CS2 in fig. 4). To better visualize the vertical movements (of maximum few hundred meters), the vertical scale has been largely expanded with regards to the horizontal one (sections of about 30 km). These sections have been correlated to a well-known borehole, the n°10 of Noeux-les-Mines (fig. 5), situated east of the CS1 and CS2 sections, that provides a direct insight into

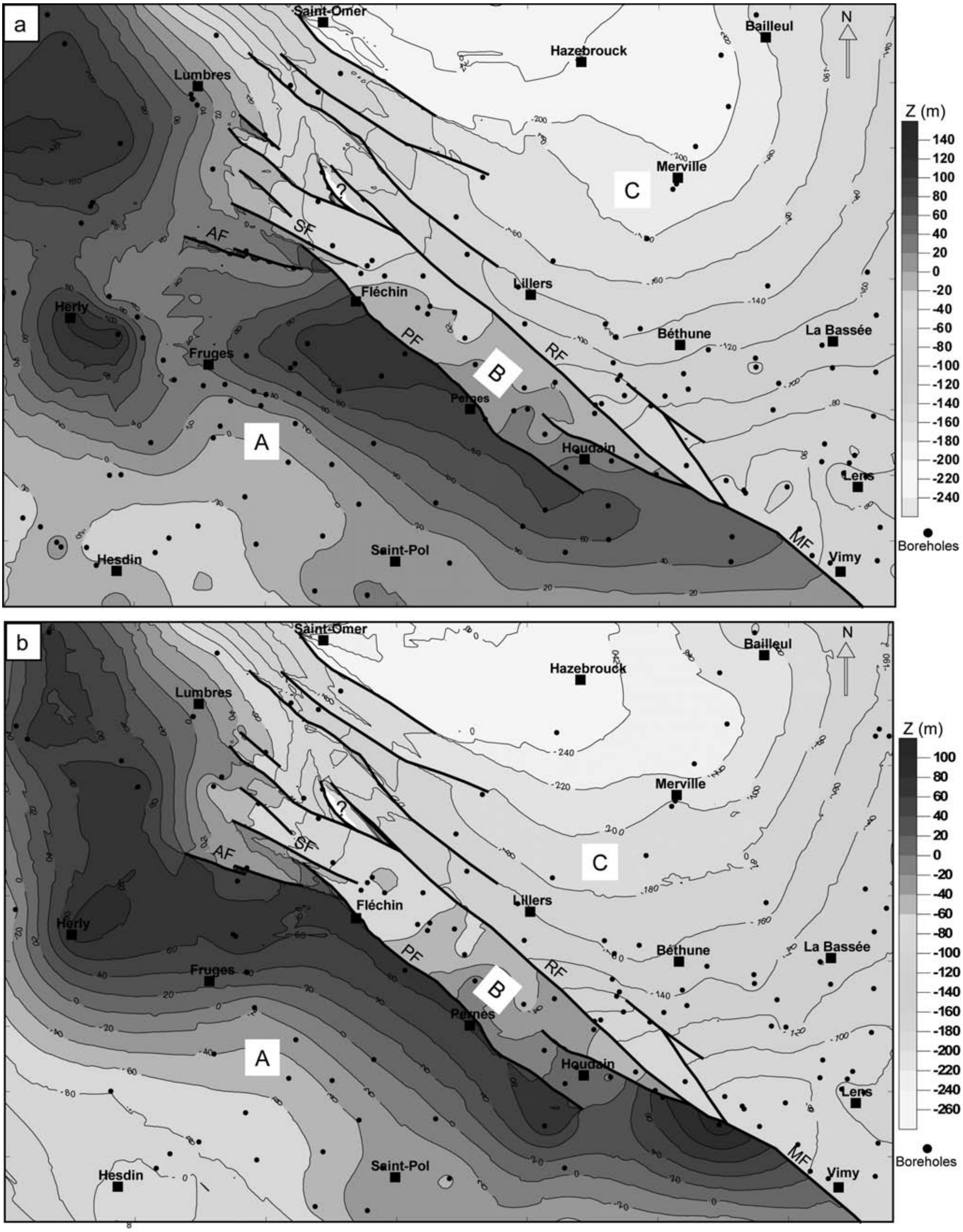

FIG. 3. – a. Isobath map of the top of Cenomanian layers (marly chalk) b. Isobath map of the top of the Paleozoic substratum (Stephanian-Permian included). Black dots represent the boreholes used for interpolation. PF: Pernes Fault, RF: Ruitz Fault, MF: Marqueffles fault, AF: Audincthun Fault, SF: Samblethun Fault. Units A, B and C refer to the different fault blocks discussed in the text.

FIG. 3. – a. *Carte des isobathes du toit des niveaux cénomaniens (craie marneuse).* b. *Carte des isobathes du toit du substratum paléozoïque (incluant les niveaux stéphano-permiens). Les points noirs représentent les forages utilisés pour l'interpolation.* PF : *faille de Pernes,* RF : *faille de Ruitz,* MF : *faille de Marqueffles,* AF : *faille d'Audincthun,* SF : *faille de Samblethu. Les domaines A, B et C se réfèrent aux différents blocs décrits dans le texte.*

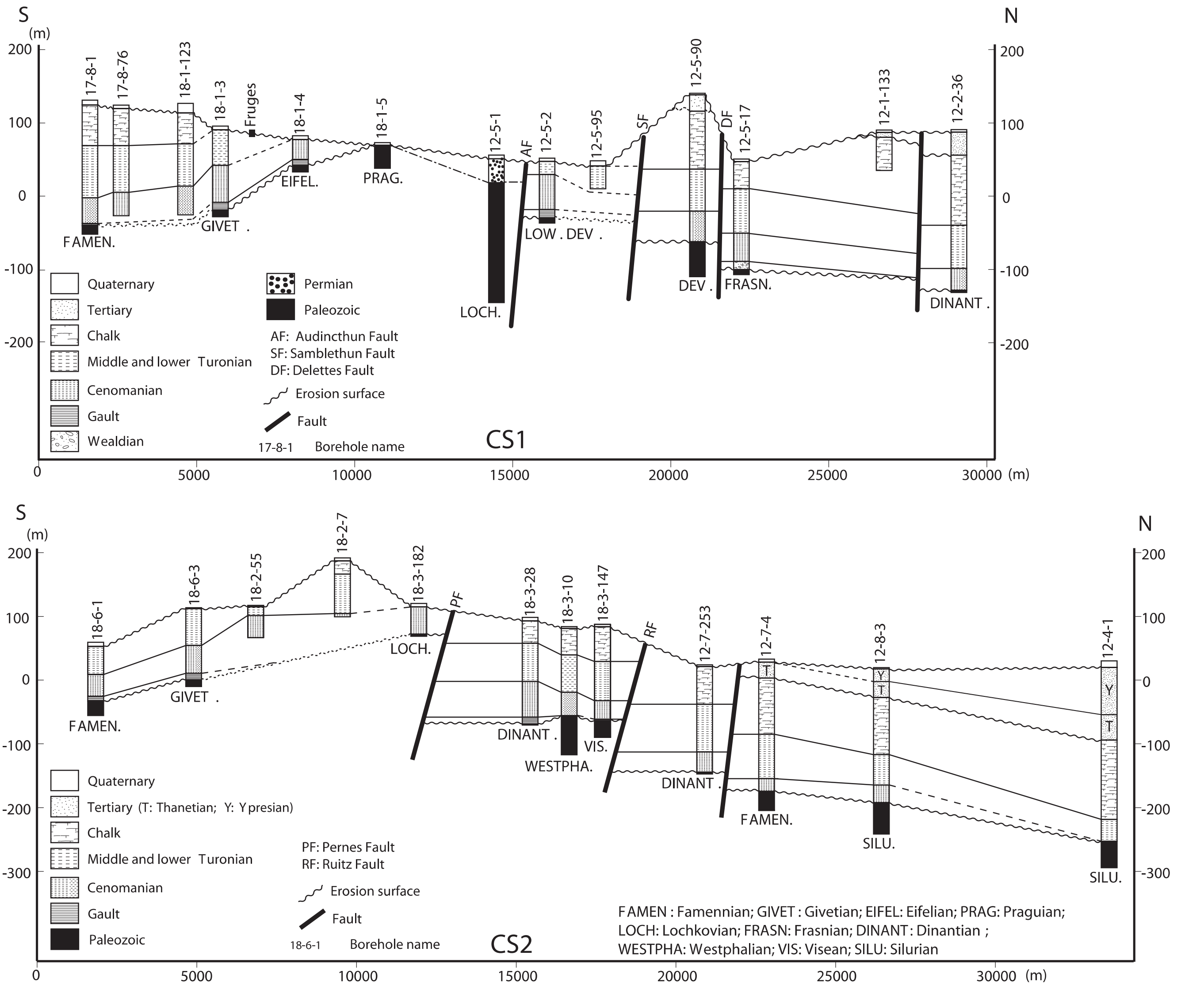

FIG. 4. – Superficial schematic sections across the Artois hills based on boreholes interpolation. The location of profiles is reported in figure 2A.
FIG. 4. – *Coupes superficielles sché*matiques à travers les collines de l'Artois établies par interpolation des forages. La localisation des coupes est reportée en figure 2A.

the geometry of the Marqueffles fault, a component of the Artois fault network [Bouroz, 1956].

The culmination of the Paleozoic substratum and the fault-related step geometry of sedimentary layers, discussed above, are clearly visible along the sections with globally uplifted southern blocks, offset vertically up to 140 m along individual faults. As shown by the reference n°10 borehole of figure 5, the Paleozoic rocks (Lower Devonian sandstones in the borehole 10) and the Cenomanian-Turonian cover south of the fault are displaced upward by about 100 m over the footwall block, arguing for a reverse post-Middle Turonian movement along the south-dipping Marqueffles fault. One important point to notice is that the Cenomanian-Turonian cover of the footwall block does not lie upon Lower Devonian rocks but upon the Upper Carboniferous (Namurian-Westphalian) coal-bearing molasse from the foreland basin. On another hand, a restricted **horst ?????** of such coal-bearing shales and sandstones is trapped within the fault zone in between Lower Devonian and Middle Turonian rocks (fig. 5). As previously discussed, the contact between the Lower Devonian siliciclastics and the Upper Carboniferous molasse is always considered in the region to represent the emergence of the main Variscan frontal thrust (the Midi thrust). Borehole 10 thus clearly argues for the superficial Marqueffles fault to be localized along the main Variscan frontal thrust, reactivating it directly at depth and cross-cutting the Cretaceous cover at the surface [Bouroz, 1956; Mansy *et al.*, 2003a]. No previous extensional reactivation can be, however, clearly demonstrated here along the Marqueffles fault.

Such typical geometry is also observed along the CS1 and CS2 profiles, west of the Marqueffles fault, with Lower Devonian rocks of the hangingwall of the Midi thrust always situated at the top of the fault-bounded culmination and the Carboniferous rocks of the footwall along its northern forelimb. In more detail, it is interesting to note the gradual decay of the age of Paleozoic rocks towards the south of the culmination (from Lochkovian to Famennian)

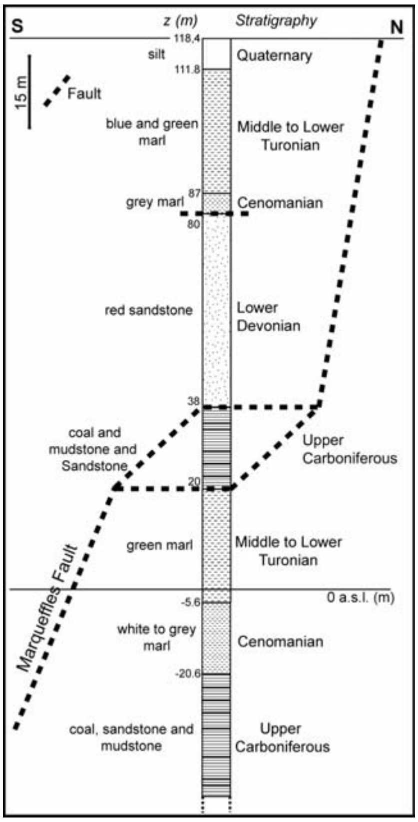

FIG. 5. – Schematic description of the "n°10 de Noeux" borehole through the Marqueffles fault (modified from Bouroz [1956]).
FIG. 5. – *Description schématique du puit n°10 de Noeux à travers la faille de Marqueffles (modifié de Bouroz [1956]).*

showing the general south-dipping monoclinal attitude of the Devonian layers in the direct hangingwall of the Midi thrust. Such monoclinal geometry at the hangingwall of the Midi thrust is significant for a ramp-type geometry of the main Variscan frontal thrust in the Artois area and exemplifies the significant denudation of the thrust structure before the deposition of the Cretaceous cover. Taking into account this particular geometry, we can deduce that the allochthon of the Midi thrust extends up to the Pernes fault in the CS2 profile and approximately to the Samblethun fault in the CS1 profile. In the latter, the contact is not well defined due to the lack at depth of the characteristic coal-bearing rocks in the direct footwall of the Midi thrust in response to the south-eastern plunge of foreland fold-thrust structures along the Artois thrust front [CFP (M) *et al.*, 1965]. The CS1 profile thus exposes the Midi thrust ramp truncating footwall layers in more basal position i.e. Dinantian (fig. 4). On the other hand, some overturned thrust sheets of Devonian-Carboniferous rocks can be observed frequently at the base of the Midi thrust thus explaining the presence of Upper Devonian and Dinantian rocks in boreholes in the vicinity of the main frontal thrust. In the footwall of this major thrust system, Paleozoic layers below the Cretaceous cover exhibit a general older age towards the north indicating also a south-dipping monoclinal attitude of the Variscan foreland, leading to the emergence of the Silurian rocks of the Caledonian Brabant massif at the northern tip of the section CS2. Finally, the last significant point to notice on the sections is the presence of Stephanian-Permian fluviatile deposits in the direct hangingwall of the Audincthun fault. As previously mentioned, this depositional pattern argues for a possible extensional movement of some of the segments of the Artois fault network in Late Variscan times. This point will be further discussed in the next section devoted to the characterization of structural geometries at depth.

GEOMETRY AT DEPTH ALONG THE ARTOIS FAULT NETWORK : INSIGHT FROM SEISMIC PROFILES

In 1984-1985, an industrial seismic survey has been performed in the Artois area in order to image the Variscan thrust front and the geometry of the underthrusted coal-bearing foreland basin. Two of these profiles have been particularly studied here to characterize the geometry at depth of the Artois fault network and its relationships with the main Variscan frontal thrust zone: the profile BM84K (18.3 km long) (fig. 6A), located along the CS1 profile and the profile BM84G (32.2 km long) (fig. 6B) in the vicinity of the CS2 section. The profile 84K has been the subject of a specific reprocessing at the Compagnie Générale de Géophysique providing a renewed image of the main reflectors at depth [Rolin, 2000].

Figure 6 provides for each profile a line drawing of prominent reflectors (up to 3 s TWT i.e. about 7 km following classical velocity laws) as well as a geological interpretation based on both surface data and the projection onto the section of closest borehole data. For both profiles, the base of the Cretaceous cover can be relatively well defined, documenting low amplitude undulations and vertical offsets localized in the vicinity of the Artois faults. Below the mid-Cretaceous unconformity, the geometry of the reflectors within the Paleozoic substratum documents a clear asymmetry of Variscan structures characteristic for a general south-dipping attitude of both thrusts and bedding. As usually observed on seismic profiles (for example along the ECORS transect [Cazes and Toreilles, 1988]), the main Variscan frontal thrust (Midi thrust) is characterized by a set of well-defined S-dipping reflectors extending to about 2.5 s TWT at the southern end of the profiles. In both profiles, the hangingwall of this major thrust is not strongly reflective, but it displays however a localized energetic reflector almost parallel to the underlying thrust. The Marest deep borehole, situated just south of the thrust front in the vicinity of the profile BM84G, documented the existence of a thin package of Latest Silurian shales at the base of the allochthonous unit [Stievenard, 1949]. We thus postulated that the prominent reflector in the hangingwall of the Midi thrust may sign at depth the transition between the Lower Devonian sandstone-dominated sequence and this latest Silurian shaly unit. In the present state of knowledge, such an interpretation is, however, impossible to check elsewhere along the Artois thrust front as such Late Silurian rocks have not been recognized in outcrop. Below the main frontal thrust, the para-autochthonous cover of the Brabant massif is also notably deformed due to the existence of several secondary thrusts thickening the Middle Devonian-Carboniferous rocks. Those thrusts branch at depth onto a main décollement zone situated approximately at the interface between the cover and the Lower Paleozoic substratum. Such geometry is very close to that observed in the Boulonnais area where this para-autochthonous thrust system is partially exhumed [Averbuch *et al.*, 2004]. Some deeper foreland-dipping reflectors can be observed in the

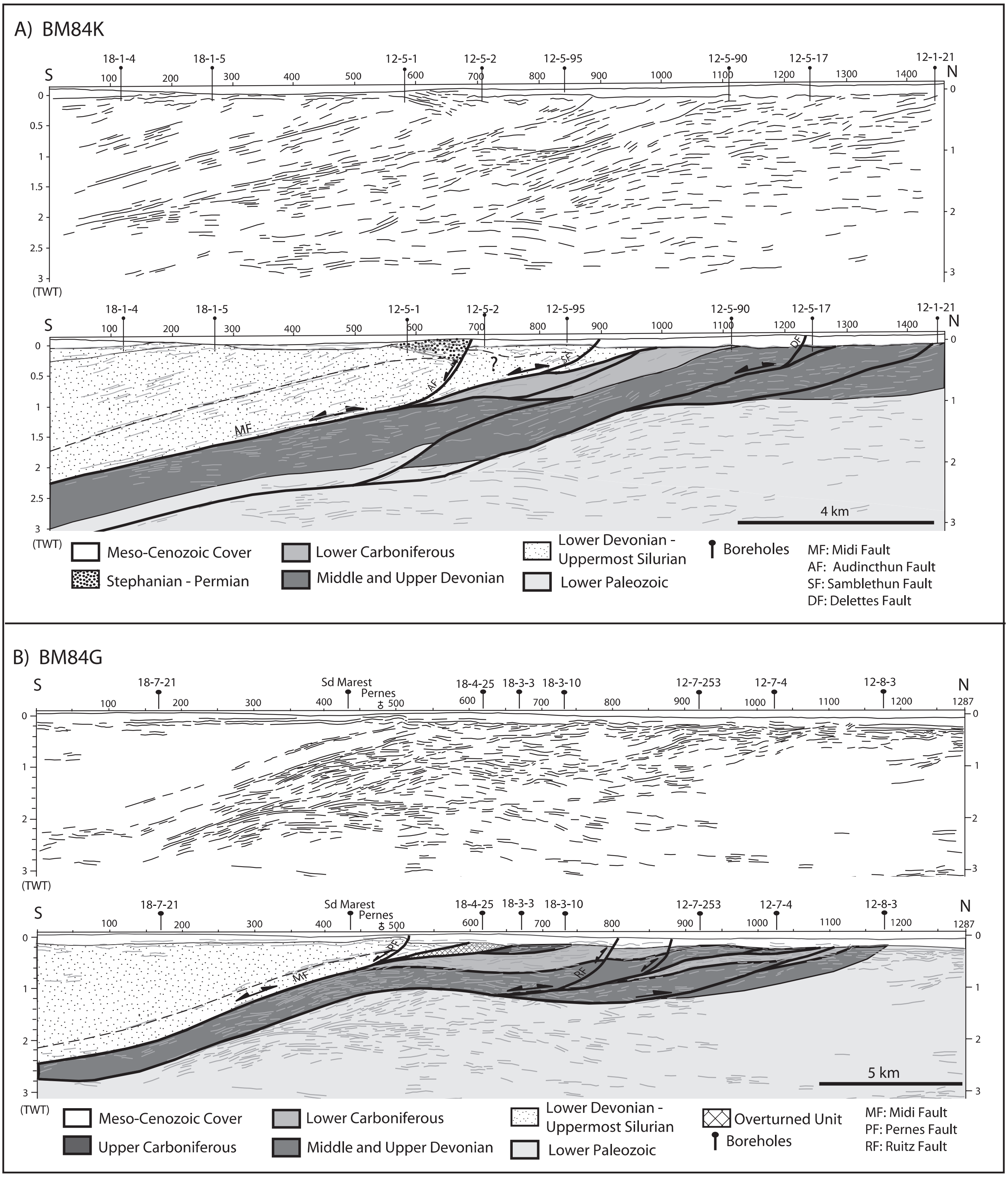

FIG. 6. – Line drawings showing the geometry of prominent reflectors and geological interpretations of the BM84K (A) and BM84G seismic profiles (B) (see the location of profiles on fig. 1 and 2a). Vertical scale in seconds TWT.

FIG. 6. – *Pointé des réflecteurs et interprétations géologiques des profils sismiques BM84K (*A*) et BM84G (*B*) (localisation des profils en fig. 1 et 2a). L'échelle verticale est en secondes temps-double.*

Lower Paleozoic basement, especially on the profile BM84G, whose length allows a better resolution at depth than on the profile 84K. Such kinds of deep N-dipping reflectors have been frequently observed in the footwall of the main Variscan frontal thrust, for example along the N France ECORS and S Britain SWAT profiles [e.g. Bois *et al.*, 1994] but their interpretation is still a matter of debate and won't be discussed here in more detail as it does not interfere directly with our main purpose [see Minguely *et al.*, 2008 for a discussion].

The main point that we want to emphasize here is the geometrical relationship between the Artois fault network and the Variscan thrusts at depth. This geometry is especially well exemplified along the Audincthun fault (the westward relay of the Pernes fault) on profile BM84K (fig. 6 and 7). As previously mentioned, the latter fault limits to the North a very narrow post-orogenic basin filled with Stephanian-Permian conglomeratic deposits. On the profile BM84K, these deposits are easily distinguishable as they correspond to prominent N-dipping reflectors lying on the top of the S-dipping reflectors of the Variscan thrust wedge. A very striking point is that the Stephanian-Permian N-dipping layers display a very clear fan geometry characteristic for the syn-rift infill of a progressively tilted half-graben, developed above a listric normal fault (fig. 7) [e.g. Dula, 1991; Legrand *et al.*, 1991; Vendeville, 1991; Roure *et al.*, 1992; Henk, 1993]. Such geometry implies that the Audincthun fault, which exhibits a steep southern dip at the surface, necessarily has to curve downwards to get a more gentle southern dip. This curvature of the Audincthun fault at depth is corroborated on the seismic section by the apparent continuity (at the resolution scale of the seismic data) of the reflectors associated with the Midi thrust zone (fig. 6 and 7), thereby suggesting that the surface fault does not cut across the deeper thrust ramp but rather branches on it as classically observed during a negative tectonic inversion process [Chadwick, 1986; Powell and Williams, 1989; Williams *et al.*, 1989; Gorini *et al.*, 1991; Roure *et al.*, 1994; Averbuch *et al.*, 1995; Tavarnelli, 1999]. The structural pattern, observed on the profile BM84K, clearly argues for the reactivation at depth of the ramp of the Midi thrust as an extensional detachment and the formation of a shortcut steeply dipping normal fault, more superficially (the Audincthun fault). Such extensional reactivation of the Midi thrust ramp in Stephanian-Permian times induced some significant amount of subsidence thereby inducing the formation of very narrow intramontane troughs trapping coarse-grained fluviatile sediments. The apparent thickness of this sequence, along the section BM84K, is about few hundred meters but it is worth noting that it is strongly eroded on top and covered up unconformably by the mid-Cretaceous sedimentary layers. This basal unconformity of the Cretaceous cover cannot be defined just south of the Audincthun fault as it has been almost totally removed by erosion but north of it, it can be defined at about 0.15 s TWT (about –50 m after borehole data) showing the finite reverse displacement of the base of the Cretaceous cover along the Audincthun fault. Such characteristic reversal of displacement argues for a tectonic inversion of the Audincthun half-graben and the necessary reactivation at depth of the Midi thrust in a compressional setting. North of the Audincthun fault, the Samblethun and Delettes faults also display some slight vertical displacement of the base cover unconformity (fig. 6A), thus corroborating the inferences from the interpolation of the borehole dataset that showed a distribution of the Cenozoic shortening on the different individual faults involved in the Artois fault network. It is worth noting that both these surface faults are situated very close to the emergence of two thrusts at the base of the cover (the Midi thrust for the Samblethun fault and a subsidiary foreland thrust for the Delettes fault) and that the resolution of the seismic data does not allow imaging the precise geometrical relationships between these surface faults and the underlying thrusts. The Samblethun fault is, however, clearly associated to curved reflectors at depth (fig. 6a), suggesting its listric character. As documented by the attitude of the Audincthun fault, we thus postulated in the interpreted sections that the Samblethun and Delettes faults were branched on the underlying thrust ramps shortcutting the superficial tips of the thrust surfaces; however, a direct link between the thrusts and the listric surface faults could be an acceptable alternative solution for the observed geometries. On the profile BM84G (fig. 6B), the Pernes fault, which corresponds to the SE relay of the Audincthun fault, does not display the specific roll-over geometry exposed along the Audincthun half-graben due to the lack of Stephanian-Permian deposits directly along the BM84G section. These conglomeratic deposits are, however, well known in outcrop in the direct hangingwall of the Pernes fault, at its NW tip, in the Flechin area (fig. 2A). On the seismic section, the Pernes fault displays some noticeable vertical offset and flexure of the base cover unconformity indicative of the finite upward movement of the S block. On the other hand, as observed in BM84K profile, the reflectors, matching the Midi thrust, situated directly below the surface fault present an overall continuity suggesting the listric character of the Pernes fault and its downward rooting onto the underlying thrust. Despite the absence of Stephanian-Permian deposits on the profile BM84G, the geometrical features observed for the Pernes fault are thus very similar to those of the Audincthun fault and the repeated inversions, observed for the Audincthun fault, are very likely to have affected also the Pernes fault.

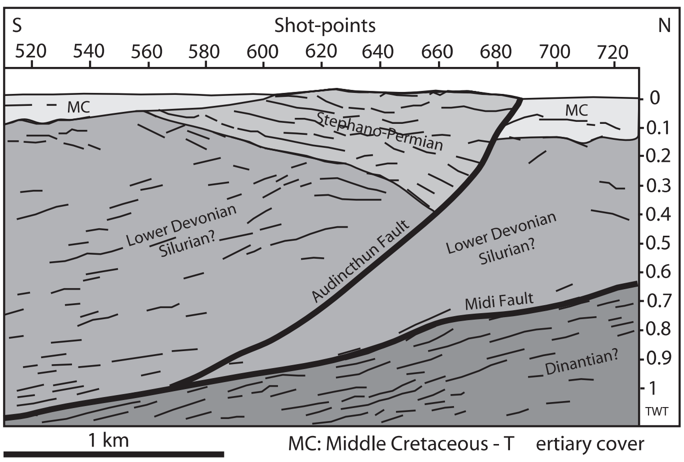

FIG. 7. – Detailed view of the line drawing of the seismic profile BM84K illustrating the relationships between the Stephanian-Permian deposits, the Audincthun fault and the main Variscan frontal thrust.

FIG. 7. – *Vue de détail du pointé de réflecteurs du profil sismique BM84K montrant les relations entre les dépôts stéphano-permiens, la faille d'Audincthun et le chevauchement frontal principal varisque.*

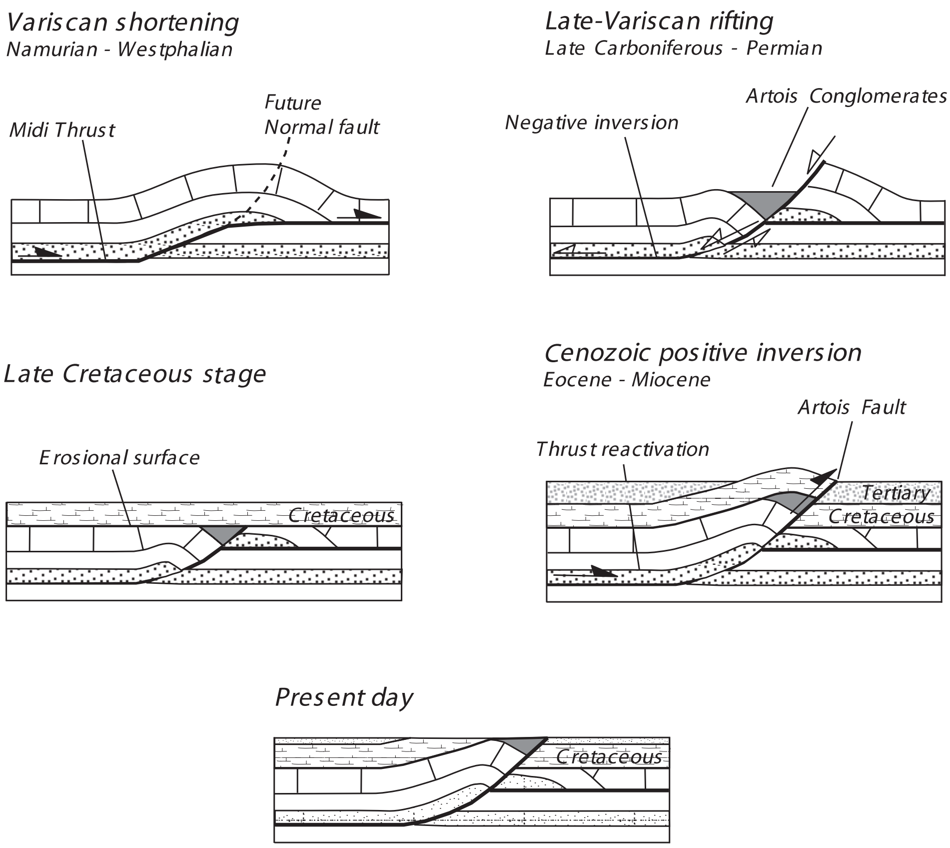

FIG. 8. – Schematic model for the kinematics of tectonic inversion in the Artois region (a) Namurian - Westphalian (thrust tectonics); (b) Late Carboniferous - Permian (negative tectonic inversion); (c) Upper Cretaceous (marine transgression); (d) Cenozoic (positive tectonic inversion); (e) Present state; (drawings based on a figure of Tavarnelli [1999]).

*FIG. 8. – Modèle cinématique schématique de l'inversion tectonique en Artois : (*a*) Namurien - Westphalien (tectonique chevauchante varisque) ; (*b*) Carbonifère terminal - Permien (inversion tectonique négative) ; (*c*) Crétacé supérieur (transgression marine) ; (*d*) Cénozoïque (inversion positive) ; (*e*) Actuel ; (schémas inspirés d'une figure de Tavarnelli [1999]).*

In this respect, the heterogeneous preservation of the Late Paleozoic rocks along the fault would be mostly due to the degree of truncation of the Paleozoic layers that occurred by sub-aerial erosion before Mid-Cretaceous times rather than significant differences in the kinematics of the Artois faults along strike.

CONCLUSION : TOWARDS A KINEMATICAL MODEL OF TECTONIC INVERSION ALONG THE VARISCAN THRUST FRONT IN NORTHERN FRANCE

The integration of surface and sub-surface geological data in the Artois area, at the northern margin of the Paris basin, document a repeated tectonic inversion process, basically governed by the existence of the buried northern Variscan frontal thrust zone at depth (fig. 8). In more detail, borehole and seismic data argue for the buried ramps of Variscan thrusts to have controlled subsequent Stephanian-Permian extensional deformation by localizing normal movement, thereby inducing the reactivation of deeper parts of thrust as detachments. The development in superficial areas of faults with a shortcut geometry (due to the flat attitude of thrusts), linked downward to the thrust ramps, are suggested to induce the individualization of listric normal faults along which stepwise subsidence and block tilting localized the accumulation of fan-shaped fluviatile sequences. It is, however, worth noting that such very narrow intramontane basins seem to be restricted to the Audincthun and Pernes faults that branch directly on the main Variscan frontal thrust (the Midi fault). Along other faults from the Artois fault network, which branch on foreland secondary thrusts, the reactivation was probably less pronounced thereby not inducing enough subsidence to trap continental sedimentation. The intense erosion of this Late Paleozoic configuration until the mid-Cretaceous prevents, however, any precise view of the restricted Stephanian-Permian depositional pattern. Such first negative inversion event, coeval with the initial rifting stage in the Paris basin, is also recorded locally in the Boulonnais area (although nor firmly dated) with, in particular, some left-lateral transtensional movements along the Ferques fault zone [Averbuch *et al.*, 2001] and localized deposition in the hanging-wall of the deep fault controlling the northern border of the basin in the "Cap Gris-Nez" area [Mansy *et al.*, 2003a]. By contrast, the significant Late Jurassic-Early Cretaceous rifting event, well defined in the Boulonnais area, has not been recorded in the Artois region that was, alike the major part of northern France, submitted to widespread uplift, denudation and karstification in that particular time [Wyns *et al.*, 2003]. In post-Albian times, the post-rift transgression progressed northwards along the northern border of the Paris basin, flooding progressively the Lower Cretaceous relief [Minguely, 2007]. Widespread chalk deposition occurred by Upper Cretaceous times until the base of the Tertiary. This was probably the time for incipient uplift of the Artois area as documented by the paleogeography of Paleocene and Lower Eocene deposits that was moulded on early topographic highs centered on the Artois fault system [Dupuis, 1979]. The main event of positive inversion of the Artois fault network occurred, however, later as suggested locally by the map trace of faults that truncates the Paleocene-Eocene layers. As proposed for the Boulonnais, further west [Van-Vliet-Lanoe *et al.*, 1998], a Middle Eocene-Late Oligocene age is likely for the main phase of positive inversion along the Artois fault network.

Basically, the presented data illustrate the role of structural inheritance in the control of sedimentation and topography along the northern border of the Paris basin. The Variscan frontal thrust zone is really the main tectonic discontinuity at depth in northern France governing the overall tectonic pattern since Late Paleozoic times. Along the northern Variscan deformation front, this thrust zone strongly localized shortening by the end of the Variscan orogeny (i.e. Late Westphalian times) accommodating more than 20 km of displacement towards the NNE in the Boulonnais-Artois area. At a larger scale, the interpolation of interpreted seismic sections along the thrust front from the Avesnois area to the Artois allows providing a general insight into the 3D geometry of the main Variscan frontal thrust [Minguely, 2007]. As presented in the map of figure 9, curves of time-depth isovalues of the prominent reflectors marking this thrust zone, clearly show that the dip of the main Variscan frontal thrust diminishes stepwise eastward with different lateral discontinuities striking about NNE-SSW. For example, a prominent lateral discontinuity can be defined joining roughly Lens and Arras. A very striking feature is that the Artois fault network disappears east of this line illustrating the absence of significant tectonic inversion of the Variscan frontal thrust zone along the Avesnois-Ardennes segment. Whatever the precise orientation of extension during the Stephanian-Permian rifting event, such correlation suggests a direct control of the dip of the Variscan frontal thrust on the enhancement of extensional reactivation as classically shown both by deformation mechanics concepts and analogue modelling [e.g. Facenna *et al.*, 1995; Turner and Williams, 2004]. The origin of such steeper dip of the main frontal thrust in the Boulonnais-Artois still requires to be explained. Some large-scale oblique convergence active along the Artois-Boulonnais-SE England Variscan segment [Rippon *et al.*, 1997; Averbuch *et al.*, 2004] as well as some possible foreland basement culmination due to the reactivation of Caledonian thrusts [Minguely *et al.*, 2008] could be possible driving factors for such increased dip of the thrust front. New constraints on the structure at depth and analogue modelling studies are thus still needed to provide further insight into the main

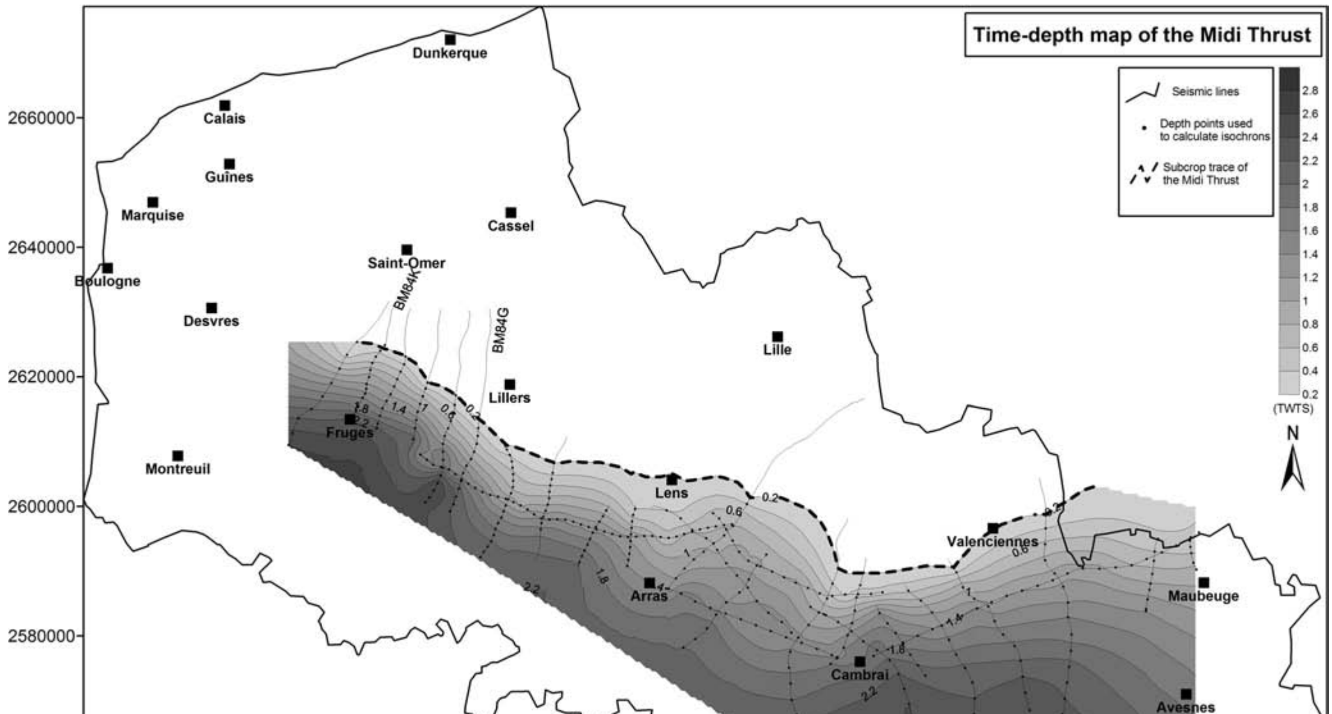

FIG. 9. – Time-depth map of the main Variscan frontal thrust (Midi fault) based on the interpretation of seismic profiles distributed along the northern France Variscan deformation front (after Minguely [2007]).

FIG. 9. – *Carte temps-profondeur du chevauchement frontal principal varisque (faille du Midi) établi à partir de l'interprétation de profils sismiques répartis le long du front de déformation varisque du Nord de la France (d'après Minguely [2007]).*

parameters that controlled the repeated tectonic inversion of the Variscan thrust front in the Artois area.

Acknowledgements. – This paper is dedicated to Jean-Louis Mansy who initiated the study presented here and shaped a noticeable part of the ideas included in the text. It forms a synthesis of different works carried out, in collaboration with the BRGM, during the PhD thesis of B. Minguely (2007) and the Master 2 studies of M. Patin (2004) and D. Rolin (2000). It benefited from numerous discussions at different stages of the evolution of the study with L. Csontos, M. Everaerts, J. Lamarche, F. Lacquement, G. Manby, D. Vachard and B. Van-Vliet-Lanoe. The reviewers, F. Roure and M. Sintubin and the associate editor N. Bellahsen are greatly thanked for their valuable comments that helped improving the preliminary version of this article.
Rédacteur associé Nicolas Bellahsem

References

AVERBUCH O., MATTEI M., KISSEL C., FRIZON DE LAMOTTE D. & SPERANZA F. (1995). – Cinématique des deformations au sein d'un système chevauchant aveugle: l'exemple de la "Montagna dei Fiori" (front des Apennins centraux, Italie). – *Bull. Soc. géol. Fr.*, **166**, 451-461.

AVERBUCH O., MANSY J.-L. & LAMARCHE J. (2001). – Déformations tardi-paléozoïques au front septentrional de la chaîne Varisque: l'exemple des massifs paléozoïques du Boulonnais (N France). – *Ann. Soc. Géol. Nord*, **9**, 13-24.

AVERBUCH O., MANSY J.-L., LAMARCHE J., LACQUEME NT F. & HANOT F. (2004). – Geometry and kinematics of the Boulonnais fold-and-thrust belt (N France): implications for the dynamics of the northern Variscan thrust front. – *Geodin. Acta*, **17, 2**, 163-178.

BADLEY M.E., PRICE J.D. & BACKSHALL L.C. (1989). – Inversion, reactivated faults and related structures: seismic examples from the southern North Sea. *In*: M.A.COOPER & G.D. WILLIAMS, Eds, Inversion tectonics. – *Geol. Soc. London Spec. Pub.*, **44**, 201-219.

BEELEY H.S. & NORTON M.G. (1998). – The structural development of the Central English Channel High constraints from section restoration. *In*: J.R. UNDERHILL, Ed., Development, evolution and petroleum geology of the Wessex basin. – *Geol. Soc. London Spec. Pub.*, **133**, 283-298.

BLUNDELL D.J. (1990). – Relationships between deep crustal structure and sedimentary basins around Britain. *In*: B. PINET & C. BOIS, Eds, The potential of deep seismics profiling for hydrocarbon exploration. – Technip, Paris, 317-333.

BOIS C., CAZES M., CHOUKROUNE P., GARIEL O., HIRN A., LE GALL B., LEFORT J-P., MATTE P. & PINET B. (1994). – Seismic reflection images of the pre-Mesozoic crust in France and adjacent areas. *In*: J.D. KEPPIE, Ed., Pre-Mesozoic geology in France and related areas. – Springer Verlag Berlin Heidelberg, 3-48.

BOUROZ A. (1948). – La structure du bassin houiller du Pas-de-Calais à l'ouest du méridien de Lens. – *Ann. Soc. Géol. Nord*, **LXVIII**, 93-105.

BOUROZ A. (1956). – Contribution à l'étude des failles épicrétacées de l'Artois. – *Ann. Soc. Géol. Nord*, **????**, 51-62.

BRIQUET A. (1924). – Carte tectonique de l'Artois et des régions voisines. – Congrès Géologique International XIIIème session, Liège.

CAZES M. & TORREILLES G. (1988). – Etude de la croûte terrestre par sismique profonde. Profil Nord de la France. – Technip, Paris, 260 p.

C.F.P. (M) C., R.A.P. & S.N.P.A (1965). – Contribution à la connaissance des bassins paléozoïques du Nord de la France. – *Ann. Soc. Géol. Nord*, **LXXXV**, 273-283.

CAULIER P. (1974). – Etude des faciès de la craie et de leurs caractéristiques hydrauliques dans la région du Nord. – Thèse de l'Université des Sciences et technologies de Lille, 157 p.

CHADWICK R.A. (1986). – Extension tectonic in the Wessex basin, southern England. – *J. Geol. Soc. London,* **143**, 465-488.

CHADWICK R.A. (1993). – Aspects of basin inversion in southern Britain. – J. *Geol. Soc. London*, **150**, 311-322.

CHADWICK R.A. & EVANS D.J. (1995). – The timing and direction of Permo-Triassic extension in southern Britain. *In*: S.A.R. BOLDY, Ed., Permian and Triassic rifting in Northwest Europe. – *Geol. Soc. London Spec. Pub.*, **91**, 161-192.

COLBEAUX J.-P. (1974). – Mise en évidence d'une zone de cisaillement nord-Artois. – *C. R. Acad. Sci.,* Paris, **278**, 1159-1161.

DELATTRE C. (1969). – Les grands traits géologiques de l'Artois. – *Ann. Soc. Géol. Nord*, **LXXXIX**, 79-90.

DULA W.F. (1991). – Geometric models of listric normal faults and rollover folds. – *Bull. Am. Assoc. Petrol. Geol.*, **75**, 1609-1625.

DUPUIS C. (1979). – Esquisse paléogéographique du nord et du nord-ouest du bassin de Paris au Paléocène et à l'Eocène inférieur. Incidences structurales. – *C. R. Acad. Sci.,* Paris, **288**, 21, 1587-1590.

FACENNA C., NALPAS T., BRUN J-P. & DAVY P. (1995). – The influence of pre-existing thrust faults on normal fault geometry in nature and experiments. – *J. Struct. Geol.*, **17**, 1139-1149.

GORINI C., VIALLARD P. & DERAMOND J. (1991). – Modèle d'inversion structurale négative : la tectonique extensive post-nappe du fossé de Narbonne-Sigean (Corbières, Sud de la France). – *C. R. Acad. Sci.,* Paris, **312**, 1013-1019.

GOSSELET J. (1908). – Note sur quelques failles communes aux terrains crétaciques et houiller de l'Artois. – *Ann. Soc. Géol. Nord*, **37**, 80-109.

GOSSELET J. (1922). – Les assises crétaciques et tertiaires dans les fosses et les sondages du Nord de la France : Etude topographique du soubassement paléozoïque. – Etudes des Gîtes Minéraux de la France, Imprimerie Nationale Paris, 121p.

GUILLOCHEAU F., ROBIN C. *et al.* (2000). – Meso-Cenozoic geodynamic evolution of the Paris basin: 3D stratigraphic constraints. – *Geodin. Acta*, **13**, 189-246.

HAMBLIN R.J.O., CROSBY A., BALSON P.S., JONES S.M., CHADWICK R.A., PENN I.E. & ARTHUR M.J. (1992). – United Kingdom offshore regional report: the geology of the English Channel. – HMSO for the British Geological Survey, London, 108 p.

HAYWARD A.B. & GRAHAM R.H. (1989). – Some geometrical characteristics of inversion. *In*: M.A.COOPER & G.D. WILLIAMS, Eds, Inversion tectonics. – *Geol. Soc. London Spec. Pub.*, **44**, 17-39.

HENK A. (1993). – p 6 ????????????????????????????????

HENK A. (2003). – Late orogenic basin evolution in the Variscan Internides: the Saar-Nahe Basin, southwest Germany. – *Tectonophysics*, **223**, 273-290.

LACQUEMENT F., MANSY J.-L., HANOT F. & MEILLIEZ F. (1999). – Retraitement et interprétation d'un profil sismique pétrolier méridien au travers du Massif paléozoïque ardennais (Nord de la France). – *C. R. Acad. Sci.,* Paris, **329**, 471-477.

LACQUEMENT F., BARCHI P. & QUESNEL F. (2004). – Carte géologique harmonisée de la région Nord-Pas de Calais. – BRGM/RP53484-FR, 188 p.

LACQUEMENT F., AVERBUCH O., MANSY J.-L., SZANIAWSKI R. & LEWANDOWSKI M. (2005). – Transpresional deformations at lateral boundaries of propagating thrust-sheets: the example of the Meuse Valley Recess within the Ardennes Variscan fold-and-thrust belt (N France-S Belgium). – *J. Struct. Geol.,* **27**, 1788-1802.

LAMARCHE J., BERGERAT F. & MANSY J-L. (1997). – Déformations cassantes et plicatives dans le Jurassique du Boulonnais, influence lithostructurale et héritage paléozoïque. – *C. R. Acad. Sci.,* Paris, **326**, 57-63.

LE GALL B. (1994). – Deformation of the Nord-Pas de Calais carboniferous coalfield (France) in the Variscan frontal tectonic pattern. *In*: A. MASCLE, Ed., Hydrocarbon and petroleum geology of France. – Springer-Verlag, 245-268.

LEGRAND X., SOULA J-C. & ROLANDO J-P. (1991). – Effet d'une inversion tectonique négative dans le sud du Massif Central français : la structure «roll-over» du bassin permien de Saint-Affrique. – *C. R. Acad. Sci.,* Paris, **312**, 1021-1026.

LE SOLLEUZ A., DOIN M-P., ROBIN C. & GUILLOCHEAU F. (2004). – From a mountain belt collapse to a sedimentary basin development: 2D thermal model based on inversion of stratigraphic data in the Paris basin. – *Tectonophysics,* **386**, 1-27.

MASCLE A. & CAZES M. (1988). – La couverture sédimentaire du bassin parisien. *In*: M. CAZES & G. TORREILLES, Eds, Etude de la croûte terrestre par sismique profonde. Profil Nord de la France. – Technip, Paris, 157-169.

MC MAHON N.A. & TURNER J. (1998). – The documentation of a latest Jurassic-earliest Cretaceous uplift throughout southern England and adjacent offshore areas. *In*: J.R. UNDERHILL, Ed., Development, evolution and petroleum geology of the Wessex basin. – *Geol. Soc. London Spec. Pub.*, **133**, 215-240.

MANSY J.-L., MANBY G.M., AVERBUCH O., EVERAERTS M., BERGERAT F., VAN VLIET-LANOE B., LAMARCHE J. & VANDYCKE S. (2003a). – Dynamics and inversion of the Mesozoic Basin of the Weald-Boulonnais area: role of basement reactivation. – *Tectonophysics*, **373**, 161-179.

MANSY J.-L., CSONTOS L., ROLIN D., HANOT F., BERGERAT F. & VACHARD D. (2003b). – Variscan structures and their reactivation in Artois, northern France. – *Geophys. Res. Abstr.*, **5**, 01985.

MEGNIEN C. (1980). – Tectogenèse du bassin de Paris : étapes de l'évolution du bassin. – *Bull. Soc. géol. Fr.*, **XXII**, 669-680.

MÉRIAUX E. (1961). – Observations sur les conglomérats et marbres rouges de l'Artois. – *Ann. Soc. Géol. Nord*, **LXXXI**, 65-71.

MINGUELY B. (2007). – Caractérisation géométrique 3-D de la couverture sédimentaire méso-cénozoïque et du substratum varisque dans le Nord de la France : apports des données de sondages et des données géophysiques. – Thèse de l'Université des Sciences et Technologies de Lille, Lille, 230 p.

MINGUELY B., FOLENS L., AVERBUCH O. & VENDEVILLE B.C. (2008). – Formation of deep-seated triangle zones by interaction between two orogenic thrust fronts having opposite vergence: structural evidence from the Caledonian-Variscan system in northern France and preliminary analogue modelling. – *Boll. Geofis.*, **49(2)**, 242-246.

ONCKEN O., PLESCH A., WEBER J., RI CKEN W. & SCHRADER S. (2000). – Passive margin detachment during arc-continent collision (Central European Variscides). *In*: W. FRANKE, V. HAAK, O. ONCKEN & D. TANNER, Eds, Orogenic processes: quantification and modelling in the Variscan belt. – *Geol. Soc. London Spec. Pub.*, **179**, 199-216.

PATIN (2004) remerciements??????????????????

POWELL C.M. & WILLIAMS G.D. (1989). – The Lewis Thrust/Rocky Mountain trench faults system in Northwest Montana, USA: an example of negative inversion tectonics? *In*: M.A.COOPER & G.D. WILLIAMS, Eds, Inversion tectonics. – *Geol. Soc. London Spec. Pub.*, **44**, 223-234.

PRIJAC C., DOIN M-P., GAULIER J-M., & GUILLOCHEAU F. (2000). – Subsidence of the Paris basin and its bearing on the Late Variscan lithosphere evolution: a comparison between the Plate and Chablis models. – *Tectonophysics*, **323**, 1-38.

RAOULT J-F. (1986). – Le front varisque du Nord de la France d'après les profils sismiques, la géologie de surface et les sondages. – *Rev. Géol. Dyn. Géog. Phys.*, **27**, 247-268.

RAOULT J-F. & MEILLIEZ F. (1987). – The Variscan front and the Midi fault between the Channel and the Meuse River. – *J. Struct. Geol.*, **9**, 473-479.

RIPPON J.H., GAYER R.A. & MILIORIZOS M. (1997). – Variscan structures in the Kent coalfield, southeast England, and their regional significance. – *Geol. Mag.*, **134**, 885-867.

ROURE F. (2008). – Foreland and hinterland basins: what controls their evolution? – *Swiss J. Geosci.*, **101**, 5-29.

ROURE F., BRUN J-P., COLLETTA B. & VAN DEN DRIESSCHE J. (1992). – Geometry and kinematics of extensional structures in the Alpine foreland basin of southeastern France. – *J. Struct. Geol.*, **14**, 503-519.

ROURE F., BRUN J-P., COLLETTA B. & VIALLY R. (1994). – Multiphase extensional structures, fault reactivation and petroleum plays in the Alpine foreland basin of southeastern France. *In*: A. MASCLE, Ed., Hydrocarbon and petroleum geology of France. – Springer-Verlag, Heidelberg, 45-268.

ROURE F., CHOUKROUNE P. & POLINO R. (1996). – Deep seismic reflection data and new insights on the bulk geometry of mountain ranges. – *C. R. Acad. Sci.,* Paris, **322**, 345-359.

ROLIN D. (2000). – Héritage et inversions tectoniques en Artois. – Mémoire de D.E.A., Université de Lille 1-Université de Paris XI-Orsay, **XX?????????** p.

SHAIL R.K. & LEVERIDGE B.E. (2009). – The Rhenohercynian passive margin of SW England: development, inversion and extensional reactivation. – *C.R. Geoscience*, **341**, 140-155.

SHEPHARD-THORN E.R., LAKE R.D. & ATITULLAH E.A. (1972). – Basement control of structures in the Mesozoic rocks in the Strait of Dover region, and its reflexion in certain features of the present land and submarine topography. – *Phil. Trans. R. Soc. London*, **272**, 99-113.

STIÈVENARD M. (1949). – Précisions sur la Grande Faille du Midi d'Ourton à Douai. – *Ann. Soc. Géol. Nord,* **LXIX**, 315-351.

SIMPSON I., GRAVESTOCK M., HAM D., LEACH H. & THOMPSON S.D. (1989). – Notes and cross-sections illustrating inversion tectonics in the Wessex basin. *In*: M.A.COOPER & G.D. WILLIAMS, Eds, Inversion tectonics. – *Geol. Soc. London Spec. Pub.*, **44**, 123-129.

TAVARNELLI E. (1999). – Normal faults in thrust sheets: pre-orogenic extension, post-orogenic extension or both? – *J. Struct. Geol.*, **21**, 1011-1018.

TURNER J.P. & WILLIAMS G.A. (2004). – Sedimentary basin inversion and intra-plate shortening. – *Earth-Science Rev.*, **65**, 277-304.

UNDERHILL J.R. & PATERSON S. (1998). – Genesis of tectonic inversion structures: seismic evidence for the development of key structures along the Purbeck-Isle of Wight Disturbance. – *J. Geol. Soc. London*, **155**, 975-992.

VAN VLIET-LANOE B., MANSY J.-L., MARGEREL J.-P., VIDIER J.-P., LAMARCHE J. & EVERAERTS M. (1998). – Le Pas de Calais, un détroit cénozoïque à ouvertures multiples. – *C. R. Acad. Sci.,* Paris, **326**, 729-736.

VENDEVILLE B. (1991). – Mechanisms generating normal fault curvature: a review illustrated by physical models. In: A.M. ROBERTS, G. YIELDING & B. FREEMAN, Eds, The Geometry Of Normal Faults. – *Geol. Soc. London Spec. Pub.*, **56**, 241-249.

WILLIAMS G.D., POWELL C.M. & COOPER M.A. (1989). – Geometry and kinematics of inversion tectonics. *In*: M.A. COOPER & G.D. WILLIAMS, Eds, Inversion tectonics. – *Geol. Soc. London Spec. Pub.*, **44**, 3-15.

WYNS R., QUESNEL F., SIMON-COINÇON R., GUILLOCHEAU F. & LACQUEMENT F. (2003). – Major weathering in France related to lithospheric deformation. – *Géol. Fr.,* **1**, 79-87.

ZIEGLER P.A. (1990). – Evolution of the North Atlantic-an overview. *In*: B. TANKARD & H.R. BALKWILL, Eds, Extensional tectonics and stratigraphy of the North Atlantic margins. – *Am. Ass. Petrol. Geol. Mem.*, **46**, 111-129.

ZIEGLER P.A., SCHUMACHER M.E., DÈZES P., VAN WEES J-D. & CLOETHING S. (2004). – Post-variscan evolution of the lithosphere in the Rhine Graben area: constraints from subsidence modelling. *In*: M. WILSON, E-R. NEUMANN, G.R. DAVIES, M.J. TIMMERMAN, M. HEEREMANS, B.T. LARSEN, Eds, Permo-Carboniferous magmatism and rifting in Europe. – *Geol. Soc. London Spec. Pub.*, **223**, 289-317.

Article 5.

Ouzgaït M., Averbuch O., Vendeville B.C. *Zuo X*. and *Minguely B*., 2010. The negative tectonic inversion of thrust faults : insights from seismic sections along the Northern France Variscan thrust front and analogue modelling experiments. Geomod 2010, Lisbon.

THE NEGATIVE TECTONIC INVERSION OF THRUST FAULTS: INSIGHTS FROM SEISMIC SECTIONS ALONG THE NORTHERN FRANCE VARISCAN THRUST FRONT AND ANALOGUE MODELLING EXPERIMENTS

M. Ouzgaït [*], O. Averbuch [*], B. C. Vendeville[*], X. Zuo [*] and B. Minguely [*]

[*] *Université Lille-Nord de France, Laboratoire Géosystèmes, FRE CNRS 3298, 59 655 Villeneuve d'Ascq cédex (France)*

Introduction

The extensional reactivation of buried thrusts has often been suggested as a major deformational mechanism in post-orogenic sedimentary basins (e.g., Roure, 2008). Its recognition is generally based on combined structural features including the collapse of the backlimb of thrust-related fold structures, the development of post-orogenic syn-rift deposits upon the crest of anticlines and the general parallelism of extensional and compressional structures in map view. The direct relationships between normal faults and the underlying thrust faults are however rarely exposed due to the general burial of these structures below a sedimentary cover controlled by the tectonic subsidence. Seismic profiles across post-orogenic basins generally does not allow neither to provide, at depth, a precise image of such relationships due to the overall structural complexity. Based on geomechanical criterion (e.g., Ivins et al, 1990; Faccenna et al, 1995) and the rare direct observations in collapsed fold-thust belts (D'Agostino et al, 1998), the amplitude of the dip of the initial thrust faults has been suggested as a major controlling parameter for a possible extensional reactivation. As the thrust surfaces flattens or steepens across the crustal layers depending on their relative weakness (the classical staircase geometries of thrusts), only part of the thrust surfaces is mechanically relevant for a reactivation in superficial domains. The footwall ramps, that exhibit the strongest dips along the thrust fault, have thus largely been considered to localize some post-compressional normal displacement. Such partial reactivation of the thust (reactivation of the ramp and the basal décollement) and the dissection of the forelimb of the thrust-related anticline by a newly formed steep fault generate an overall listric normal fault that can localize subsidence of the crest of the anticline, tilting of the hangingwall block and deposition of fan shaped syn-rift layers. Such a mechanism, that accounts for both geometric and mechanical constraints of thrusts reactivation has been generally considered as the typical model for the negative tectonic inversion process (Fig. 1)(Williams et al, 1989 ; Tavarnelli, 1999).

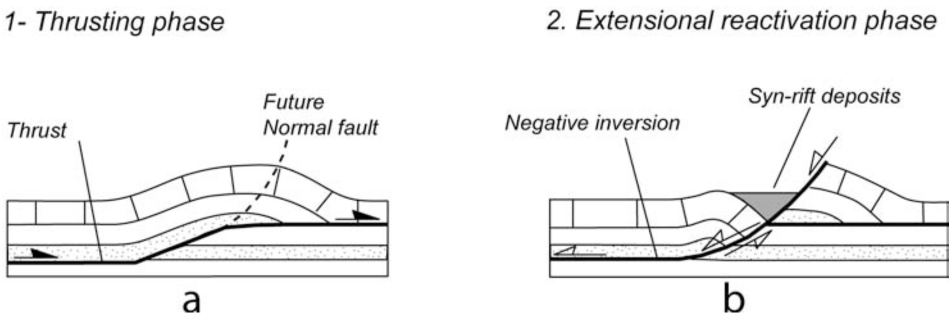

Figure 1. Sketch diagram showing the basic geometric characters of extensionally reactivated thrust structures and of the related syn-rift sedimentation (modified from Tavarnelli, 1999).

To provide further insight into this mechanism, we present here a new example of the extensional reactivation of a thrust structure based on seismic profiles imaging the buried N France Variscan thrust front. This structural approach is complemented by analogue modelling experiments that allows constraining the geometries and kinematics of the negative tectonic inversion process and discussing the possible parameters that control the reactivation of basement thrusts during a subsequent extension.

The negative tectonic inversion of the Variscan thrust front: structural evidence

The Variscan (ca. 300 Ma) thrust front in Northern France extends, below the thin Mesozoic sedimentary cover of the Paris Basin, from the English Channel to the west (Calais-Boulogne area in Fig. 2), to the Ardennes massif to the east (Valenciennes-Maubeuge area in Fig. 2). Outcrops located at both extremities (Boulonnais and Ardennes Paleozoic massifs), as well as seismic profiles and numerous boreholes show that the frontal thrust system is characterized by a major crustal-scale thrust zone, dipping gently Southward (the main frontal Variscan thrust), whose emergence corresponds to a large out-of-sequence thrust, knwown as the Midi thrust (e.g., Averbuch et al., 2004). Analysis of recent seismic data suggests that the total amount of slip along this thrust zone could be as much as 70 km in the Western Ardennes area (Lacquement et al., 1999), thereby strongly dissecting the Southern border of the coal-bearing molassic foreland basin of Namurian-Westphalian age. This foreland basin (up to 3-4 km thick) formed at the top of a reduced Devonian-Carboniferous sedimentary sequence resting unconformably on a Lower Paleozoic basement, which crops out a few tens of km North of the Variscan thrust front, in the Belgian Brabant Massif.

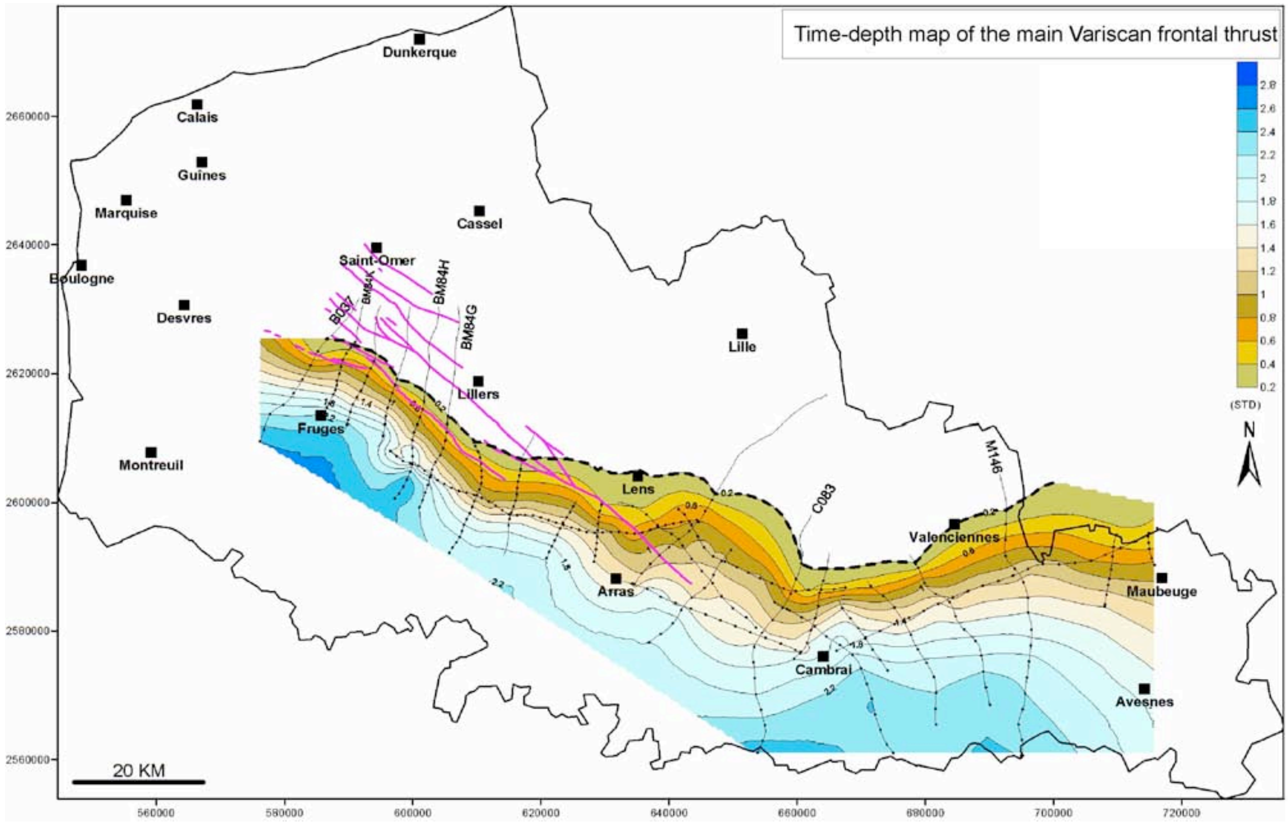

Figure 2. Subcrop trace (dashed thick line: Midi thrust) and time-depth isochrons of the main Variscan frontal thrust in Northern France (modified from Minguely et al, 2010). Colours brown to blue refer to increasing time-depth values from 0 to 2.8 seconds (two-way time travel). The black sections report the trace of the analysed seismic profiles. Profile 84K presented in Fig. 3 is located between Fruges and St Omer in the Artois region. The pink lines report the trace of the surface faults mapped in the Paris basin sedimentary cover and supposed to be controlled by basement thrusts connected to the Variscan thrust front.

Such general structural pattern of the thrust front is however slightly complicated along its western part (the Boulonnais-Artois domain, between Boulogne and Arras in Fig. 2) as it is affected by a network of steep S-dipping faults cutting through both the post-orogenic cover and the Paleozoic layers of the substratum (Fig. 2). As shown by the interpreted seismic section of Fig. 3, some of the steep S-dipping faults limits to the North some very narrow post-orogenic intramontane basins filled up with Stephanian-Permian conglomeratic deposits. These post-orogenic levels are characterized by prominent N-dipping reflectors, lying on top of the S-dipping reflectors of the Variscan deformed layers and displaying a fan geometry characteristic for the infill of progressively tilted half-graben associated with a listric normal fault. The latter apparently branch at depth upon the main Variscan frontal thrust as suggested by the continuity of the reflectors associated with this major thrust zone. Along its footwall, the Paleozoic sequences (i.e. the base Carboniferous reflector in Fig. 3) are clearly truncated whereas they are parallel to the thrust along the hangingwall (the base Lower Devonian reflector in fig. 3) illustrating the ramp geometry of the deeply eroded frontal thrust zone below the Middle Cretaceous sedimentary cover of the Paris basin. These data clearly document the negative structural inversion of the Variscan thrust front and argue for the buried ramp of the Variscan frontal thrust to have controlled subsequent Stephanian-Permian extensional deformation by localizing normal displacement, thereby inducing the reactivation of deeper parts of the thrust as an extensional detachment. The development in superficial areas of steep faults, linked downward to the thrust ramp, is suggested to induce the individualization of listric normal faults along which stepwise subsidence and block tilting induced the deposition of fan-shaped continental sequences.

Moreover, as shown by the reverse finite displacement of the unconformable Cretaceous cover, these faults were subsequently positively inverted during the Alpine s.l. Tertiary compressional stage.

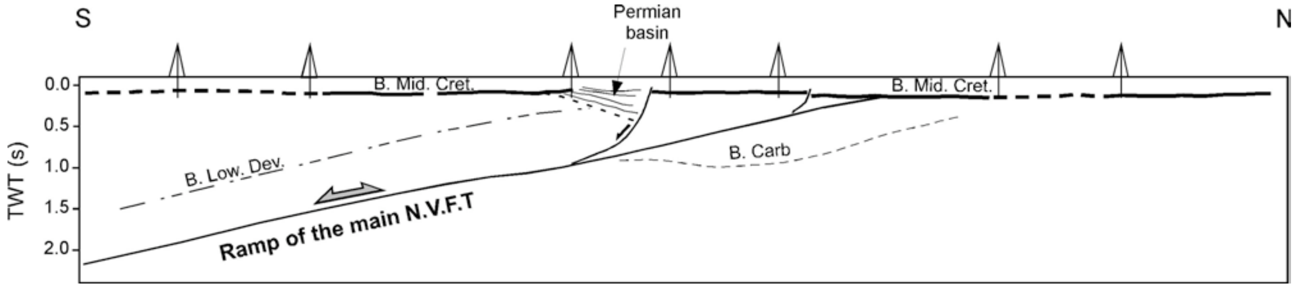

Figure 3. Interpreted seismic sections BM84K across the Variscan thrust front in the Artois area (onshore N France) constrained by borehole data and gravity modelling (modified from Minguely et al, 2010). N.V.F.T.: Northern Variscan frontal thrust; B. Mid. Cret.: Base of the mid-Cretaceous cover of the Paris basin; B. Carb.: Base of the Carboniferous rocks in the foreland of the N.V.F.T.; B. Low. Dev.: Prominent reflector at the hangingwall of the N.V.F.T. supposed to be the base of the siliciclastic Lower Devonian “red sandstone” sequence.

As exemplified in Fig. 2, the eastern part of the thrust front (the Ardennes domain), does not exhibit such post-Variscan steep faults resulting from the negative inversion of the thrust front. Time-depth map of the main Variscan frontal thrust zone based on the compilation of a large set of seismic profiles across the thrust front (Fig. 2) document a significantly lower dip of the thrust in the Ardennes domain compared to the Boulonnais-Artois area thereby suggesting a possible control of the thrust dip on the occurence of post-orogenic negative inversion.

Analogue modelling: preliminary results

We designed a set of analogue experiments in order to investigate the geometry and kinematics of the extensional reactivation of pre-existing thrusts and test some basic parameters controlling its possible development (i.e. the dip of the basal slope of the thrust wedge and the degree of truncation of thrust structures by erosion). We conducted these experiments at the tectonic modelling laboratory of the University of Lille 1. In the following, we will present only one experiment with a basal slope of 2.5° during the extensional phase and without any erosion of the first-phase compressional structures. The general set up was as follows. All models were constructed using a brittle, cohesionless, dry, porous 3 cm-thick sand unit overlying a basal silicone 1 cm-thick layer. All models, initially 111,5-cm long and 49 cm large, were built above a flat, horizontal, rigid base.The entire model was subjected to a first phase of shortening by moving progressively at a constant speed (0.5 cm/hour) the left-hand wall until a value of about 39% bulk shortening was reached (87 hours of shortening). An orogenic wedge formed against the moving wall, then propagated progressively rightward by formation of new forethrusts and by bulk thickening of the wedge itself. Four main foreland-directed thrust structures with associated minor backthrusts formed during that stage as well as major back-thusting and internal deformation along the left-hand moving wall (Figure 4). Shortening stopped, and a post-tectonic sand layer was deposited on the topographic relief of the fold-and-thrust structures to form an horizontal top surface. In the first experiment, the right border of the model was uplifted to simulate a basal slope of the thrust wedge of 2.5° and the model was then subjected to a phase of extension by moving backwards the mobile left-hand wall (speed: 1 cm/hour). As extension proceeded, the initially horizontal top surface of the model subsided locally along fault-bounded grabens that were incrementally filled-up with sand layers of different colours to simulate the progressive syn-rift deposits. The extensional stage was stopped until about 23.5% of extension was reached (16 hours of extension).
Results of this experiment are illustrated on the Fig. 4 showing on a representative section, cut near the center of the model, the final geometry of the rifted basin and the relationships of the basin-controlling normal faults with the underlying thrusts. The section was incrementally restaured at the different main steps of the basin development using 2D-Move (courtesy of Midland Valley Ltd) but this procedure won’t be discussed here.
This first experiment emphasizes the characteristic geometric and kinematic features of post-orogenic basin development, and especially, it argues for the ramps of fore- and backthrusts to localize at depth respectively the master normal faults controlling depocenters and some antithetic secondary faults possibly accommodating the adjustement of the hangingwall over the basal thrust surface (Roure et al, 1992; D’Agostino et al, 1998). In the first stages of extension, normal displacement is greatly partitioned into the different underlying thrusts and no sequence of normal fault propagation can be pointed out in the model. Against the mowing wall, however, initial major back-thrusting localizes a significant antithetic normal fault zone whose displacement incrases with time compared to the other master normal faults thereby inducing a late major roll-over structure. The increased flow with time of the silicone due to the basal slope (2.5°) is likely to have had a major role on this possible experimental artefact.

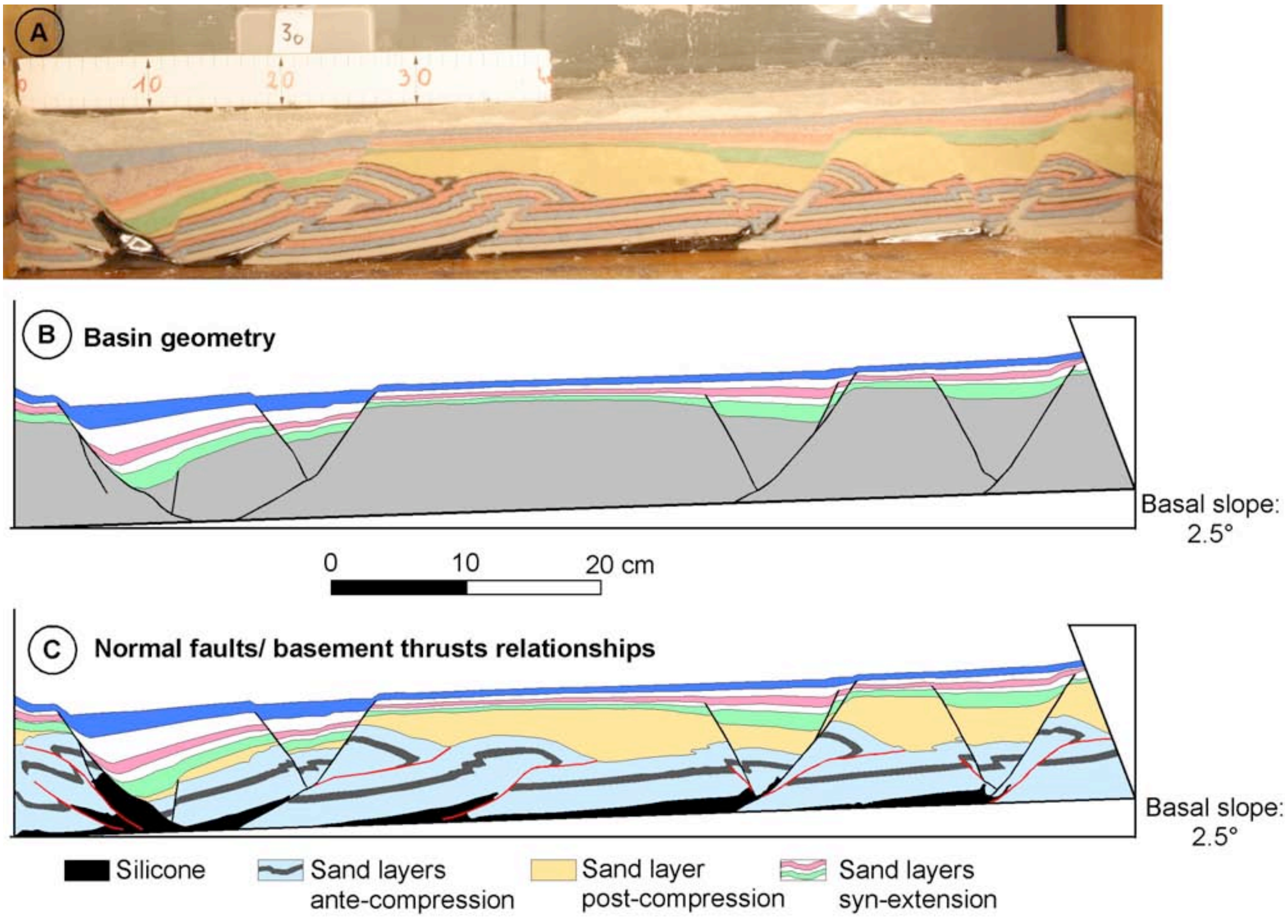

Figure 4. A: Photograph of a section cut near the model's centre (Experiment 1 with a basal slope of 2.5°). Scale in centimetres. B: Interpretation of the final geomety of the extensional stage (extension rate: 23.5%). C. Interpretation of the final geometry of the model illustrating the relationships between normal faults and thrusts inherited from the early compressional stage.

REFERENCES

- Averbuch O., Mansy J-L., Lamarche J., Lacquement F. and Hanot F.; 2004: *Geometry and kinematics of the Boulonnais fold-and-thrust belt (N France): implications for the dynamics of the Northern Variscan thrust front.* Geodinamica Acta, 17, 163-178.
- D'Agostino N., Chamot-Rooke N., Funiciello R., Jolivet L., Speranza F.; 1998: *The role of pre-existing thrust faults and topography on the styles of extension in the Gran Sasso range (Central Italy)*. Tectonophysics, 292, 229-254.
- Facenna C., Nalpas T., Brun J-P. and Davy P.; 1995: *The influence of pre-existing thrust faults on normal fault geometry in nature and experiments.* J. Struct.. Geol, 17, 1139-1149.
- Lacquement F., Mansy J-L., Hanot F. and Meilliez F.; 1999: *Retraitement et interpretation d'un profil sismique pétrolier méridien au travers du massif paléozoïque ardennais (N de la France).* C.R.Geosciences, 329, 471-477.
- Ivins E.R., Dixon T.H. and Golombek M.P.; 1990: *Extensional reactivation of abandoned thrust: a bound on shallowing in the brittle regime.* J. Struct. Geol., 12, 303-314.
- Minguely B., Averbuch O., Patin M., Rolin D., Hanot F. and Bergerat F.; 2010: *Inversion tectonics at the Northern margin of the Paris basin (Northern France): new evidence from seismic profiles and boreholes interpolation in the Artois area.* Bull. Soc. géol. France, 5.
- Roure F., Brun J-P., Coletta B. and Van den Driessche J.; 1992: Geometry and kinematics of extensional structures in the Alpine Foreland Basin of southeastern France. J. Struct. Geol., 14-5, 503-519.
- Roure F.; 2008: *Foreland and Hinterland basins: what controls their evolution?.* Swiss. J. Geosci., 101, S5-S29.
- Tavarnelli E.; 1999: *Normal faults in thrust sheets: pre-orogenic extension, post-orogenic extension, or both?* J. Struct. Geol., 21, 1011-1018.
- Williams G.D., Powell C.M. and Cooper M.A., 1989. *Geometry and kinematics of inversion tectonics*. In: Cooper M.A., Williams G.D. (Eds), Inversion Tectonics, Geol. Soc. London Spec. Pub., 44, pp. 3-15.

3. Géométrie et cinématique du front de chaîne varisque dans le Nord de la France.

Au sein de la chaîne varisque, qui présente un double déversement nord et sud, seul le front septentrional peut être suivi de façon quasi-continu, le front méridional ayant été totalement disloqué lors de l'ouverture des domaines océaniques en relation avec la Téthys, puis de leur fermeture ayant abouti au système orogénique pyrénéo-alpin *sensu lato*. L'étude du front de déformation varisque septentrional revêt donc un intérêt tout à fait particulier puisqu'il peut permettre de caractériser la dynamique tardive de la collision varisque (à la fin du Carbonifère) alors que les domaines internes, préalablement structurés dès le Dévonien supérieur, tendent à s'affaisser au coeur du système orogénique (e.g., Ménard and Molnar, 1988; Malavieille et al, 1990; Faure and Becq-Giraudon, 1993; Burg et al, 1994).

Le front de déformation nord de la chaîne résulte de l'inversion progressive de la marge sud du bloc continental Avalonia, bloc soudé aux continents Baltica et Laurentia lors des phases orogéniques calédoniennes (de l'Ordovicien supérieur et Silurien supérieur) pour former l'ensemble continental dit des « Vieux Grès Rouges » ou Laurussia (e.g., Ziegler, 1988). Ainsi qu'il a été démontré tout au long de son tracé, depuis le sud de l'Angleterre (Shail and Leveridge, 2009) jusqu'au nord de l'Allemagne (Franke, 1995; 2000; Oncken et al, 2000; Littke et al, 2000), en passant par le nord de la France et le sud de la Belgique (Meilliez et al, 1991), la marge passive sud-avalonienne s'est structurée au cours d'une phase de rifting majeure, datant du Dévonien inférieur (globalement entre Lochkovien et Eifelien), associée à l'ouverture d'un domaine océanique Lizard-Rhénohercynien de taille assez réduite entre Avalonia et le bloc Armorica-Saxothuringia. Contrairement à ce qui est très souvent admis dans les reconstitutions géodynamiques générales, il ne s'agit pas là d'un océan Rheic ouvert à l'Ordovicien, tel que défini par Cocks et Fortey sur la base des assemblages de faune (1982) mais d'un océan plus tardif, probablement de type marginal arrière-arc en relation avec la subduction vers le nord de l'océan sud armoricain-massif central, ouvert lui au cours de l'Ordovicien (e.g., Ballèvre et al, 2002)(voir Shail and Leveridge, 2009 pour une discussion récente de ce problème et l'article 1 pour la présentation de l'évolution géodynamique générale de la chaîne).

Au cours du Viséen terminal (aux alentours de 325 Ma BP), la collision entre le bloc continental des Vieux Grès Rouges et l'assemblage méridional Armorica-Gondwana soudé dès le Dévonien supérieur le long de la suture sud armoricaine (e.g., Matte, 2001; Franke, 2006 ; Faure et al, 2008 ; Ballèvre et al, 2009) induit la propagation vers le nord des chevauchements au sein de la marge avalonienne (ou rhénohercynienne si l'on se réfère au domaine océanique). La flexuration associée de la lithosphère continentale avalonienne sous la charge orogénique donne naissance au bassin d'avant-chaîne varisque septentrional, bassin qui jalonne le front chevauchant depuis le Pays de Galles jusqu'au nord de l 'Allemagne. Au cours du Namurien et du Westphalien (dénommés maintenant selon la nomenclature internationale Serpukhovien, Bashkirien et Moscovien), la molasse houillère va combler celui-ci conduisant localement à la mise en place de plus de 4 km de dépôts silicoclastiques synorogéniques au front de la chaîne dans le nord de la France et le sud de la Belgique (e.g., Han et al, 2000).

Sur ce tronçon franco-belge, bien qu'en partie masqué par la couverture sédimentaire du bassin de Paris, on peut suivre le front de déformation septentrional depuis les massifs paléozoïques du Boulonnais à l'ouest jusqu'au massif des Ardennes à l'est. Les articles 6 à 13 présentés dans ce chapitre, illustrent la géométrie et la cinématique du front de chaîne varisque septentrional entre Boulonnais et Ardennes. Plus précisément, l'accent sera mis sur deux résultats majeurs issus de ces études : (I) l'aspect atypique du front de chaîne, caractérisé par une localisation très importante de la déformation sur la zone de chevauchement frontal (dite faille du Midi en égard à sa situation limitant au sud le bassin houiller d'avant-chaîne) lors de la dissection tardive (hors-séquence) du front chevauchant ; un nouveau modèle sera proposé pour rendre compte de ce dispositif assez peu classique ; (II) la segmentation et la courbure du front de chaîne ; on insistera ici sur l'évolution latérale du front de chaîne entre le segment Boulonnais-Artois orienté WNW-ESE et le segment Avesnois-Ardennes, orienté ENE-WSW, évolution dont on dicutera, en particulier, l'origine : héritée de la structuration initiale du bassin rhénohercynien ou acquise tardivement par rotations autour d'axes verticaux associées à des gradients de déplacement au sein du front de chaîne.

3.A. Un front de chaîne atypique : localisation du déplacement sur le chevauchement frontal majeur (faille du Midi) et dissection hors-séquence du front de chaîne.

Le trait structural le plus caractéristique du front de chaîne varisque du nord de la France est l'existence d'un chevauchement frontal extrêmement marqué, localisant plusieurs dizaines de kilomètres de déplacement, et disséquant totalement le flanc sud du bassin d'avant-chaîne houiller. L'émergence de ce chevauchement frontal majeur au dessus des dépôts molassiques d'avant-chaîne correspond à la zone faillée du Midi, zone de faille particulièrement bien contrainte suite à l'exploitation du bassin houiller du Nord-Pas de Calais et de sa prolongation dans le sud de la Belgique (Mons-Namur-Liège).

Ce dispositif structural caractéristique est particulièrement explicite sur le segment oriental du front de chevauchement du nord de la France (à l'est de l'Artois), ainsi que l'ont montré l'interprétation des profils sismiques issus de la campagne ECORS Nord de la France dans la région de Cambrai (Raoult, 1986 ; Raoult et Meilliez, 1987 ; Le Gall, 1994) ou, plus récemment, du retraitement de profils industriels dans la région de Valenciennes (Lacquement et al, 1999 ; cf. fig. 2b de l'article 7). A cet endroit, le chevauchement basal de l'unité allochtone varisque est souligné par un réflecteur très net à faible pendage (de l'ordre de 10°), qui s'étend sur plus de 40 km du N au S, et induit un déplacement total de plus de 70 km vers le NNW de l'unité chevauchante sur l'avant-pays brabançon (dit « para-autochtone brabançon »). Ce dernier, surmonté des dépôts molassiques houillers d'avant-chaîne, s'enfonce très largement (plus de 20 km pour les dépôts houillers) sous l'unité allochtone ainsi que le montrent les forages profonds d'Epinoy et de Jeumont (e.g. Raoult, 1986) situés à proximité des profils étudiés. Cette unité sous-charriée présente un pendage globalement faible vers le sud qui tend, cependant, à s'accroître aux abords du massif du Brabant, faisant ainsi émerger le socle calédonien des unités sédimentaires dévono-carbonifères déposées sur la marge rhénohercynienne. Cette flexure, extrêmement localisée et située à l'aplomb de l'émergence du chevauchement frontal, n'avait pas, antérieurement aux travaux présentés ici, retenu l'attention. Nous verrons, par la suite, qu'elle trouve totalement sa place dans le nouveau modèle cinématique du front chevauchant varisque présenté dans les articles suivants. Il est à noter, enfin, pour conclure cet état des lieux sur le front chevauchant varisque du nord de la France, l'existence d'écailles renversées de grande ampleur au mur du chevauchement frontal varisque, écailles impliquant le substratum paléozoïque inférieur et sa couverture, y compris la molasse namuro-westphalienne. Ces écailles sont délimitées par des failles « en cuillère » à vergence nord, caractéristiques du style structural observable dans le bassin houiller (Bouroz, 1949 ; Raoult, 1986 ; Le Gall, 1994), assimilables à des cisaillements de type Riedel développés progressivement sous l'unité allochtone au cours de son déplacement sur le chevauchement frontal (la faille du Midi). Ce cisaillement de grande ampleur des écailles renversées illustre l'évolution tardive classique des structures frontales de chevauchement-plissement (Frizon de Lamotte et al, 1995) et, dans le cas de la chaîne varisque du Nord de la France, traduit le caractère « hors-séquence » du système chevauchant frontal qui dissèque séquentiellement la retombée avant d'un anticlinal de rampe majeur, initialement enfoui sous les dépôts namuriens-westphaliens d'avant-chaîne (Lacquement, 2001).

Ainsi que le montrent les articles 6, 7, 8 présentés ici (ainsi que les données encore non publiées de la thèse de Bruno Minguely, 2007), la géométrie du front de chaîne varisque sur le segment Boulonnais-Artois diffère sensiblement de l'image explicitée ci-dessus, en particulier, en raison de la réduction significative de l'épaisseur résiduelle des dépôts molassiques d'avant-chaîne sur ce tronçon. Comme l'ont montré Chalard (1960), Becq-Giraudon (1983) et Meilliez (1989), cette réduction de l'épaisseur des dépôts syn-orogéniques sur l'Artois est, pour partie, d'origine sédimentaire traduisant une subsidence réduite de l'avant-pays brabançon dans le domaine Artois-Boulonnais (décrit comme le haut-fond de St Omer par Becq-Giraudon (1983)) par rapport au domaine Bassin houiller Nord-Pas de Calais-Ardennes. Par ailleurs, comme le montre la disposition en carte (sous la couverture) des affleurements du substratum paléozoïque inférieur au sein de l'avant-pays brabançon (fig. 2a de l'article 7), le plongement général des structures vers le SE au sein de cet avant-pays implique que l'on recoupe le front de chevauchement en position plus basale, les parties les plus superficielles des structures chevauchantes ayant été plus profondément érodées sur le transect Artois-Boulonnais. Cette configuration générale traduit ainsi une surrection différentielle de l'avant-pays brabançon au sein du domaine Artois-Boulonnais par rapport au domaine Bassin houiller Nord-Pas de Calais-Ardennes, surrection enregistrée dès la mise en place de la sédimentation synorogénique et qui se poursuit au moins jusqu'à la propagation du front chevauchant dans sa position actuelle.

Pour autant, le caractère « hors-séquence » du front chevauchant et la dissection progressive des structures plissées-faillées reste une constante du dispositif structural frontal nord-varisque. Ce volet est explicité plus particulièrement dans les articles 6 et 7. De l'échelle hectométrique (les écailles de la carrière « Basse-Normandie » à Rinxent dans le Boulonnais, cf. article 6) à l'échelle pluri-kilométrique (le front chevauchant du Boulonnais, cf. article 7), on retrouve le même schéma caractéristique impliquant la migration initiale des chevauchements en rampes et paliers vers l'avant-pays, puis le blocage du transfert vers l'avant et le découpage séquentiel vers l'arrière des structures préalables (en particulier, le flanc avant des anticlinaux de rampe). Ce processus induit une dissection très importante des unités situées au mur du chevauchement frontal dont le pendage (d'environ 30-40 degrés vers le sud) est notablement supérieur à celui observé le long du transect Bassin houiller Nord-Pas de Calais-Ardennes (de l'ordre d'une dizaine de degrés). Sur une distance N-S d'environ 10 kilomètres, la restauration des unités plissées et faillées au mur du chevauchement frontal du Midi dans le Boulonnais fait apparaître un taux de raccourcissement très important (52%)(cf. fig. 10 de l'article 7) montrant le caractère localisé de la déformation sur cette zone de chevauchement frontal. La séquence de propagation des déformations et leur localisation sur la zone de chevauchement frontal implique que l'avant-pays brabançon ait agi comme une zone de butoir, empêchant le transfert du déplacement vers l'avant sur des niveaux de décollement superficiels. Dans l'article 7, nous proposions que cette butée frontale soit le résultat de l'activation en profondeur d'un rétrochevauchement de socle induisant le redressement de l'unité la plus frontale (l'unité de Ferques) et la localisation associée d'une flexure extrêmement marquée ainsi que le développement de plis secondaires rétrodéversés au sein des couches globalement monoclinales formant cette unité. Cette hypothèse était également appuyée par les données d'anomalies gravimétriques qui suggéraient l'existence d'une discontinuité profonde marquée à l'applomb de la culmination de socle (Silurien) située en bordure nord du système chevauchant (Everaerts et Mansy, 2001).

L'analyse des profils sismiques le long du front chevauchant varisque en Artois, effectuée dans le cadre de la thèse de B. Minguely (2007), est venue conforter grandement cette hypothèse. Ces données n'ont pas, pour l'heure, été publiées dans leur ensemble mais l'article 8, présenté au congrès GEOMOD de 2008, présente une version assez synthétique des résultats acquis sur le front chevauchant varisque de l'Artois. L'interpolation de 14 profils sismiques pétroliers (11 transverses au front, 3 longitudinaux) issus de la campagne Boulogne-Maubeuge acquise en 1984-1985 a permis de préciser la géométrie en profondeur du front chevauchant. Les profils les plus longs comme le BM84G (32 km) dont l'interprétation est proposée en fig. 2 de l'article 8, permettent, en particulier, d'imager des réflecteurs profonds au sein du socle paléozoïque inférieur (au delà de 2 secondes temps-double, soit à peu près 5-6 km de profondeur selon les lois de vitesse classique), dont le pendage vers le nord (l'avant-pays) constitue une anomalie au sein du front de chevauchement varisque, toujours caractérisé par des réflecteurs à pendage sud (cf. article 4). Ces réflecteurs profonds tendent à devenir moins penté vers l'avant à proximité du réflecteur associé au niveau de décollement basal des unités chevauchantes varisques au mur du chevauchement frontal et vers l'arrière au niveau d'un réflecteur profond à faible pendage vers le sud. Par ailleurs, le niveau de décollement basal varisque apparaît replissé par des culminations de socle localisées à l'aplomb de ces réflecteurs profonds. Une telle géométrie suggère qu'il s'agit de rétro-chevauchements profonds qui viennent se brancher sur le niveau de décollement basal des unités para-autochtones formant la semelle du chevauchement frontal majeur, rétrochevauchements activés postérieurement (ou possiblement de façon quasi-synchrones) à la propagation des chevauchements au sein de l'avant-pays. Ce dispositif chevauchant à double vergence caractérise une zone de chevauchement triangulaire frontale, qui diffère cependant des géométries classiques dans la mesure où les chevauchements profonds sont à vergence vers l'arrière pays, et non vers l'avant-pays comme dans les cas classiques (Banks and Warburton, 1986; Vann et al, 1986). Ce type de zone triangulaire frontale est peu commun et à notre connaissance, a été décrite une seule fois auparavant, au front de l'Himalaya au Pakistan (Jadoon et Frisch, 1997).

Il est à noter que les réflecteurs profonds à pendage vers l'avant-pays tels que ceux observés sur le profil BM84G, ont déjà été décrits en profil sismique le long du front chevauchant varisque, par exemple sur les profils SWAT de Mer celtique, et interprétés comme la trace en profondeur de chevauchements calédoniens (Bois et al, 1994). Comme le montre la figure 1 de l'article 8 issus des travaux de Pharaoh et al (1993) sur les déformations calédoniennes de l'est de l'Angleterre, les fronts de déformation calédoniens et varisques arrivent en coïncidence au niveau du domaine Boulonnais-Artois. Il est ainsi probable que les rétrochevauchements profonds, impliqués dans la zone chevauchante triangulaire frontale de l'Artois, correspondent, en fait, à des chevauchements calédoniens frontaux, réactivés lors de la propagation du système varisque au sein de la marge continentale avalonienne.

Ce mécanisme d'interférence de deux fronts chevauchants à vergence opposée conduisant à la mise en place d'une zone triangulaire frontale a été testée par des expériences de modélisation analogique (stage de Master 1 de L. Folens suivi de travaux complémentaires hors-cursus). Là encore, l'ensemble des expériences n'a pas pu être totalement exploité pour l'instant. Les principes de la modélisation et les résultats de base sont, cependant, explicités dans l'article 8. Le point majeur de ces modélisations concerne la cinématique très particulière de ces systèmes chevauchants imbriqués. Nous montrons ici que la réactivation des rétrochevauchements de socle semble n'intervenir que lorsque l'extrémité du second front chevauchant (le front varisque) arrive en coïncidence avec le front antérieur (le front calédonien dans notre cas). Dès lors, on observe une partition du raccourcissement entre un unique chevauchement frontal, émergent sur l'avant-pays (l'analogue de la faille du Midi), et le système de rétrochevauchements profonds hérités, activé séquentiellement vers l'avant-pays du second front chevauchant (le Brabant dans le cas de la chaîne nord varisque). Cette séquence de déformation matérialise une propagation des chevauchements de type « gueule de crocodile » impliquant à la fois le charriage des unités allochtones frontales superficielles sur l'avant-pays et le sous-charriage séquentiel des unités profondes de l'avant-pays. Il est à noter, néanmoins, que plusieurs rétrochevauchements profonds peuvent être actifs en même temps une fois qu'ils ont été activés lors de la propagation du second front chevauchant. Cette imbrication des unités frontales conduit au redressement général des structures tant pro- que rétrochevauchantes et localise un bombement d'avant-pays juste à l'avant du chevauchement frontal majeur. Celui-ci induit une flexure extrêmement marquée à l'avant des unités chevauchantes coincées entre le bombement d'avant-pays et le chevauchement frontal majeur, localisant ainsi une sorte de fosse synclinale fortement déversée par le cisaillement vers l'avant associé au déplacement important sur le chevauchement frontal majeur (fig. 3 de l'article 8). Par ailleurs, la surrection localisée de l'avant-pays implique la réduction de la sédimentation du bassin d'avant-chaîne, juste au droit de l'émergence du chevauchement frontal.

Ces différents processus s'accordent parfaitement avec les caractéristiques structurales du front de chaîne mises en évidence sur le transect Boulonnais-Artois dont nous avions fait état plus haut dans ce paragraphe. Le modèle de zone frontale triangulaire profonde associée à l'interaction des fronts calédoniens et varisques semble, donc, dans l'état actuel des connaissances sur les domaines profonds de l'avant-pays varisque, rendre compte au mieux de la géométrie et de la cinématique du front chevauchant varisque Boulonnais-Artois. L'existence de chevauchements profonds (non émergents) au sud du massif du Brabant et la surrection associée de ce massif sur sa bordure sud, par ailleurs, ne contredisent en rien le fait que la déformation interne au sein de ce massif ait été acquise au cours des phases calédoniennes (Sintubin et al, 2009) comme le montrent, par exemple, les déformations internes enregistrées par les Massifs cristallins externes des Alpes (majoritairement varisques et non alpines). Enfin, pour expliquer l'évolution latérale du front de chaîne vers le segment ardennais, il est nécessaire d'envisager l'ennoiement vers le SE du bombement d'avant-pays et le transfert du déplacement associé aux rétrochevauchements vers des structures plus septentrionales ainsi que le suggère, sur les profils sismiques tranverses au front ardennais (e.g., Lacquement et al, 1999), la grande flexure de l'avant-pays limitant au nord le bassin houiller Nord-Pas de Calais. D'après l'analyse des anomalies gravimétriques, cette zone de transfert pourrait correspondre à une ligne transverse diffuse reliant grossièrement Lens à Lille (Minguely, 2007). Ce dispositif, quoiqu'encore grandement sous-contraint en profondeur entre Artois et bassin houiller Nord-Pas de Calais, montre nécessairement l'existence d'une segmentation du front de chaîne le long de son tracé. Ce thème sera abordé dans le chapitre suivant, en focalisant l'attention principalement sur des structures de second ordre accessibles à l'étude (affleurantes) le long du segment Avesnois-Ardennes.

Article 6.

Averbuch O. and Mansy J-L., 1998.- The “Basse-Normandie” duplex (Boulonnais, N France): evidence for an out-of-sequence thrusting overprint. J. Struct. Geol., 20, 33-42.

Pergamon

Journal of Structural Geology, Vol. 20, No. 1, pp. 33 to 42, 1998

0191–8141/98 $19.00 + 0.00

PII: S0191–8141(97)00078–3

The 'Basse-Normandie' duplex (Boulonnais, N France): evidence for an out-of-sequence thrusting overprint

O. AVERBUCH and J.-L. MANSY

Laboratoire de Sédimentologie et Géodynamique (URA CNRS 719), Université des Sciences et Technologies de Lille, 59 655 Villeneuve d'Ascq Cédex, France

(*Received* 5 *December* 1996; *accepted in revised form* 20 *September* 1997)

Abstract—The thrust-sheets outcropping in the 'Basse-Normandie' quarry (near the Hydrequent village, Boulonnais, N France) represents an exceptionally well exposed section of the NW European Variscan thrust front. These structures, developed in the footwall of the main Hydrequent thrust, have been often described as a classic example of a duplex structure. Only the lower part of the structure satisfies, however, the geometric and kinematic criteria defining a duplex (and more precisely an intraformational hinterland dipping duplex).

The upper thrust-sheets of the imbricate stack exhibit a much more complex pattern of deformation than a simple piggy-back duplication of the same rock sequence. Restoration of these thrust-sheets (based upon the definition of two marker beds as well as the analyses of fold–thrust relationships and strain markers) argues for a late NE verging thrust event that progressed within the thrust system from the tip of the upper thrust sheets towards the Hydrequent thrust in a local break-back style of thrust propagation. This out-of-sequence thrusting event induced refolding and cross-cutting of the forelimb of a hangingwall anticline developed previously above the footwall ramp of the NNE verging basal thrust of the structure. Within the whole thrust system, the lower duplex represents only a minor structure developed during the initial phase of thrusting in the foreland of the major anticline as a frontal second-order duplex.

The structural data presented in this paper illustrate the tectonic processes acting within the deformed zones lying in the footwall of major thrusts and emphasize the out-of-sequence style of thrust migration that arises from the sequential blocking of thrust propagation towards the foreland. © 1998 Elsevier Science Ltd.

INTRODUCTION

Duplex structures (Dahlstrom, 1970; Boyer and Elliott, 1982) have frequently been invoked in describing the geometry of thrust fronts within mountain belts. These structures, which imply the stacking of horses in between two thrust (or décollement) surfaces, are generally either evidenced by seismic imaging (Mitra, 1986) or inferred by map interpretation of branch lines of thrust systems and by balancing of cross-sections (for example Boyer and Elliott, 1982; Suppe, 1983; Bally *et al.*, 1986; Diegel, 1986; Butler, 1987; Graham *et al.*, 1987). Their recognition at outcrop scale is relatively rare. Few duplex structures have thus been observed directly in the field. Among these, some well known examples in Europe are the Foinaven (Boyer and Elliott, 1982) and the Moine thrust zone duplexes (Butler, 1987; Bowler, 1987) in the Scottish Caledonides, some flexural slip duplexes within fold limbs in N Devon (Tanner, 1992), the Cagalière duplex in the NE Pyrenean foreland (Averbuch *et al.*, 1992; Frizon de Lamotte *et al.*, 1997) and the 'Basse Normandie' duplex in the Boulonnais Variscan thrust front (N France) (Cooper *et al.*, 1983; Ramsay and Huber, 1987).

The latter exceptional imbricate stack exposed in the 'Basse-Normandie' quarry near the village of Hydrequent is the subject of this paper. It is the result of the juxtaposition of numerous decametric thrust sheets of limestones and dolostones of Visean age lying in the footwall of a major Variscan thrust, the Hydrequent thrust. Cooper *et al.* (1983) first recognized this thrust pattern. They interpreted the general geometry as the superposition of two duplexes: a lower one positioned in the more external part and affecting a 2 m thick calcareous sequence and an upper one, thrusted onto the back of the lower duplex, involving an older and thicker calcareous and dolomitic succession. However, they focused their work mainly on the precise restoration of the lower duplex. The latter is less internally deformed than the upper duplex so that it is possible to define and follow a marker bed only in the external part of this lower duplex. On the other hand, only the lower thrust sheets show a clearly exposed roof thrust.

While the duplex geometry of the lower imbricate stack is relatively clear, that for the upper thrust-sheets is not because the roof has been eroded. The piggy-back sequence of deformation imposed by the duplex interpretation of Cooper *et al.* (1983) is also a matter of debate and out-of-sequence movements along the Hydrequent thrust which overrides the upper thrust-sheets have recently been suggested by Mercier and Mansy (1995). These different points will be discussed below on the basis of new structural data acquired in the quarry and also in the adjacent Paleozoic massifs. These observations will lead us to propose an alternative model for the tectonic evolution of the 'Basse-Normandie' thrust complex suggesting that it results from the superimposition of out-of-sequence thrusting upon an earlier thrust-related anticline with a frontal second-order duplex (the lower duplex).

GEOMETRY AND KINEMATICS OF A DUPLEX STRUCTURE

A duplex corresponds geometrically to a set of imbricate horses bordered by two thrust or décollement surfaces: a floor one and a roof one (Fig. 1) (Boyer and Elliott, 1982). These horses result from the duplication of the same lithologic sequence so that the thrust flooring each horse of the duplex branches onto the same décollement zone. Considering an individual horse, the strata and the horse borders become folded as it moves over a thrust ramp (Fig. 1). The resulting geometry is directly dependent on (1) the ramp dip, (2) the amount of slip along the thrust with respect to the internal deformation and (3) the size of the horse. The final geometry of the imbricate stack and the shape of the roof of the duplex is thus primarily the result of the dips and spacing of the subsidiary thrusts as well as the displacement above each of them (Boyer and Elliott, 1982; Mitra, 1986; Mitra and Boyer, 1986; Butler, 1987). The ratio of displacement to the size of the horse is a critical parameter which controls the dip of the imbricates. This parameter is a primary consideration for duplex classification. Duplexes with horses dipping towards the inner part of the thrust system are termed hinterland dipping duplexes (Boyer and Elliott, 1982). Such a geometric pattern requires low displacement on each thrust with regard to the size of the corresponding horse. With increasing displacement, the adjacent horses tend to overlap in antiformal stacks then to slide along their forelimb part giving rise to foreland dipping duplexes (Boyer and Elliott, 1982). Various examples of these geometric patterns are provided by Mitra and Boyer (1986), Diegel (1986) and Butler (1987).

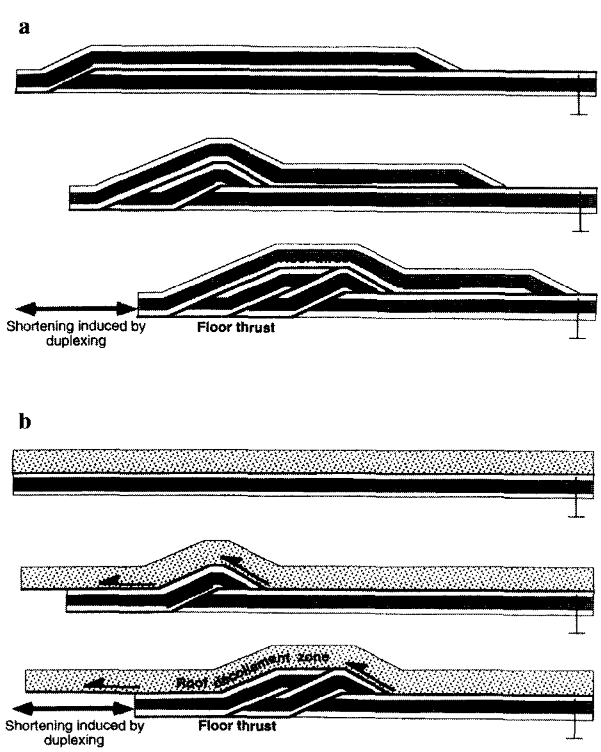

Fig. 1. Sketch diagram showing the sequential development of (a) an allochthonous roof duplex (modified from Boyer and Elliott, 1982) and (b) a para-autochthonous roof duplex with backwards activation of the roof décollement-zone (passive roof duplex).

The nature of the roof border of a duplex may also be various. The roof sequence may be allochthonous as initially described for duplexes (Boyer and Elliott, 1982) or para-autochthonous (for example Mitra, 1986; Kulander and Dean, 1986; Banks and Warburton, 1986; Geiser, 1988). In the first configuration, imbricate stacks develop beneath an initial major thrust (Fig. 1a). Kinematically, subsidiary thrusting above each thrust of the duplex is transferred forward by layer parallel slip along the upper flat. A part of the shortening may be also accommodated by internal deformation at the tip of the thrust (Cooper *et al.*, 1983; Mitra, 1986). In this kinematic evolution, the roof sequence situated above and at the back of the developing horse is pinned to this horse and passively folded. In interbedded imbricate horses, however, the roof border is a décollement zone localized in a particular ductile stratigraphic level situated in between the succession affected by the duplex and the para-autochthonous roof sequence. The kinematics of the roof décollement zone may either transfer displacement towards the foreland in the same manner as the above description (Kulander and Dean, 1986; Morley, 1986; Averbuch *et al.*, 1995) or towards the hinterland (Fig. 1b) (Fallot, 1949; Banks and Warburton, 1986; Price, 1986). The latter configuration has been termed a passive roof duplex (Banks and Warburton, 1986) or an intercutaneous wedge (Fallot, 1949).

The duplex classifications described above deal mostly with different geometrical patterns. A common feature for these geometries is the order in which the individual thrusts are activated. This parameter is very important in controlling the final geometry of the imbricate stack. A general opinion is that true duplexes occur in a foreland-progressing sequence of thrusting (Fig. 1) (Boyer and Elliott, 1982; Butler, 1987). This sequential activation implies the passive transport and folding of the hindward horses. Such a sequence is, however, generally difficult to establish in the field if the horses do not completely overlap. In this respect, it is worth noting that apparent duplex geometries may result from late crosscutting of an earlier fold–thrust situation (Butler, 1987). The sequence of deformation is thus critical in defining a duplex and has to be investigated even if the geometric characters of a duplex appear to be present.

GEOLOGICAL SETTING OF THE 'BASSE-NORMANDIE' THRUST-SHEETS

The 'Basse-Normandie' Variscan thrust sheets are situated in the Boulonnais area which lies in the northernmost part of France, along the eastern side of the English Channel (Fig. 2A). Geologically, the whole

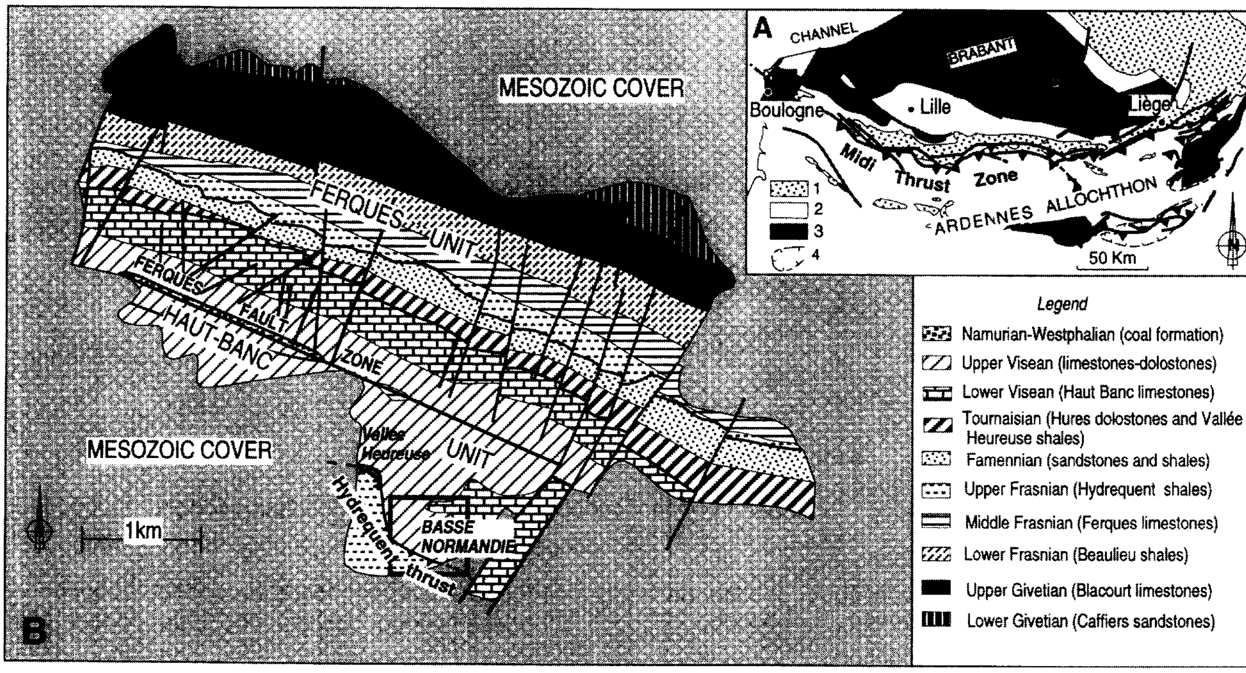

Fig. 2. (A) The location (black square) of the Boulonnais Paleozoic inliers within the tectonic framework of the Variscan thrust front of N France and Belgium. 1. Silesian basin. 2. Devonian to Visean. 3. Cambrian to Silurian rocks (Caledonian substratum). 4. Low-grade metamorphic area. (B) Geological map of the Paleozoic massif of the Boulonnais (after Mansy, in press). The rectangle locates the 'Basse-Normandie' quarry.

region today represents a wide faulted domal structure involving the Upper Cretaceous sedimentary rocks of the Paris Basin. This inverted Alpine domain exhibits within its core an unmetamorphosed Paleozoic sedimentary subtratum (Fig. 2B) folded and thrusted during the Variscan orogeny. The style of the folding-thrusting of this belt as well as the exposure of coal bearing Namuro-Westphalian rocks of a foreland basin setting type show that the Boulonnais massifs form the western tip of the French Variscan thrust front, which is well constrained in the Nord-Pas de Calais coal basin (Fig. 2A) (Bouroz, 1962). The major thrust front (the 'Midi fault' of the Nord-Pas de Calais coal basin) in classic interpretations lies a few kilometres south of the exposed Paleozoic levels, but its location remains poorly constrained. In this respect, the Boulonnais Paleozoic inliers can be considered as the deformed footwall of this major Variscan frontal thrust.

Structurally, the massif may be split into different tectonic units separated cartographically either by thrusts or by late vertical WNW–ESE trending strike-slip faults (Fig. 2B). This geometric configuration is primarily the result of the Variscan stacking of different thrust sheets as shown by an important set of drillholes and coal mining excavations (Fig. 3) (Olry, 1904; Pruvost and Delépine, 1921; Bonte, 1969; Wallace, 1983). The major décollement zone flooring these thrust sheets is likely to be situated within the thick incompetent Silurian shales recognized in the exposed core of the Landrethun culmination, on the Northern border of the Paleozoic massif. This structure, considered classically as autochthonous (for example Colbeaux and Leplat, 1985), is likely to form in fact a thrust related culmination resting upon the unfolded foreland of the London–Brabant massif. The so-defined thrust sheet constitutes the lowermost thrust unit exposed in the Boulonnais area known as the 'Ferques Unit'. To the south, this SW dipping unit ends against Visean subhorizontal layers along a Late Variscan vertical strike–slip fault of regional significance (the Ferques fault). At depth, drillholes show that these gently dipping Visean limestones (defining the 'Haut-Banc Unit') are in fact thrust onto the Namuro-Westphalian coal-bearing rocks roofing the 'Ferques Unit' (Olry, 1904; Pruvost and Delépine, 1921). The 'Haut-Banc' thrust sheet is itself overthrusted on its Southern boundary by the 'Hydrequent' thrust unit composed mainly of Upper Frasnian shales (Fig. 3) as confirmed by boreholes (Pasquet *et al.*, 1983). The contact between these two thrust sheets is defined as the Hydrequent thrust. This major fault contains in its footwall a hectometric deformation zone composed of Tournaisian lenses (in the 'Vallée Heureuse' quarry, W of the study area) and Visean slices which constitute the 'Basse-Normandie' imbricate stack.

In detail, the 'Basse-Normandie' fold–thrust system involves an about 40 m thick calcareous-dolomitic lithostratigraphic succession of Middle Visean age known as the 'Dolomie à *Siphonodendron martini*' (Hoyez, 1970; Colbeaux and Leplat, 1985; Prudhomme *et al.*, 1992). A detailed stratigraphic description has been made of this formation within the 'Basse-Normandie' quarry in the footwall of the imbrications forming the

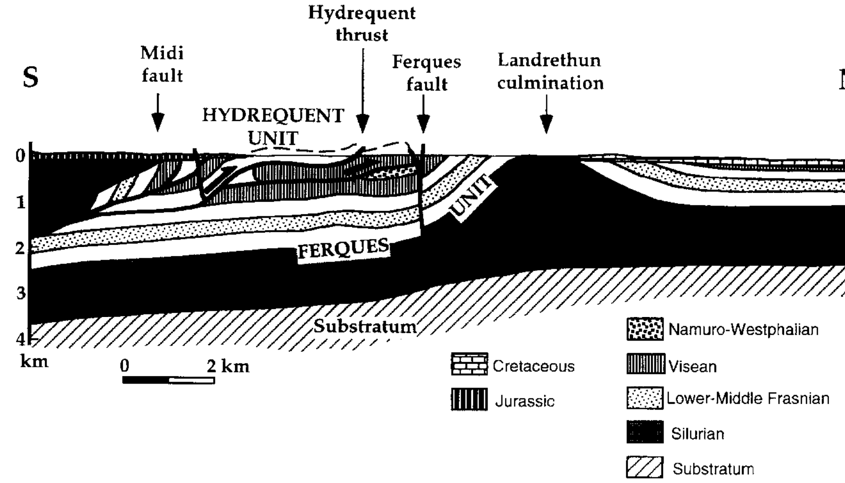

Fig. 3. Synthetic N–S cross-section through the Variscan thrust front of the Boulonnais area based on field and borehole data.

lower duplex (Figs 4 & 5) (Hoyez, 1970). Within the deformed zone, it is difficult to establish, with confidence, the precise stratigraphy due to an intense dislocation of beds. Marker beds have been recognized, however, in the thrust-sheets and in the reference cross section of the undeformed footwall allowing the reconstruction of the global geometry of the 'Basse-Normandie' thrust complex (Fig. 5).

GEOMETRY OF THE IMBRICATE STACK

As previously described by Cooper *et al.* (1983), two different thrust units may be defined within the 'Basse-Normandie' thrust complex (see the geometric reconstitution of Fig. 5 and the interpretative cross-section of Fig. 6). The lower unit (the lower duplex) consists of decametric imbrications of the same lithologic sequence (about 2 m thick) separated by SW dipping thrusts. These thrusts root backwards into a gently SW dipping floor thrust and branch upwards to a roof décollement zone thus defining a set of hinterland dipping intraformational duplications. The roof thrust exhibits a planar gently SW dipping attitude within its external part. Towards the inner part of the stack, it forms a pronounced culmination due to a greater amount of displacement along the underlying thrust surface. Within this zone, the precise geometry of the subsidiary thrusts of the duplex is difficult to decipher. However they seem to exhibit a steeper dip than the more external ones and branch onto the major thrust flooring the thickened zone. Above the roof décollement zone, just at the step surrounding the lower duplex major thickened zone, the roof sequence is affected by a system of NE and SW dipping decametric thrusts (the opposed dip complex of Cooper *et al.*, 1983) inducing its layer parallel shortening (Fig. 6).

The gently SW dipping thrust contact between the lower duplex and the upper thrust sheets (here defined as the upper thrust sheets (UTS) basal thrust) cannot be located precisely in the field. This poor exposure is explained partly by the fact that it branches very rapidly backwards to the lower duplex floor thrust forming the basal thrust of the whole structure and forward to the lower duplex roof décollement zone which forms its initial upper flat (Fig. 6). At the break point between the ramp and the upper décollement zone, the levels situated in the roof of the lower duplex fold into a subvertical wall. The location of this wall suggests that it probably represents the forelimb of a thrust-related anticline associated with the displacement above the UTS basal thrust. Its geometry is complicated by the existence of a complex thickened zone within the roof sequence (? in Figs 5 & 6).

It is not possible to determine the precise geometry of the Hydrequent thrust in the 'Basse-Normandie' quarry

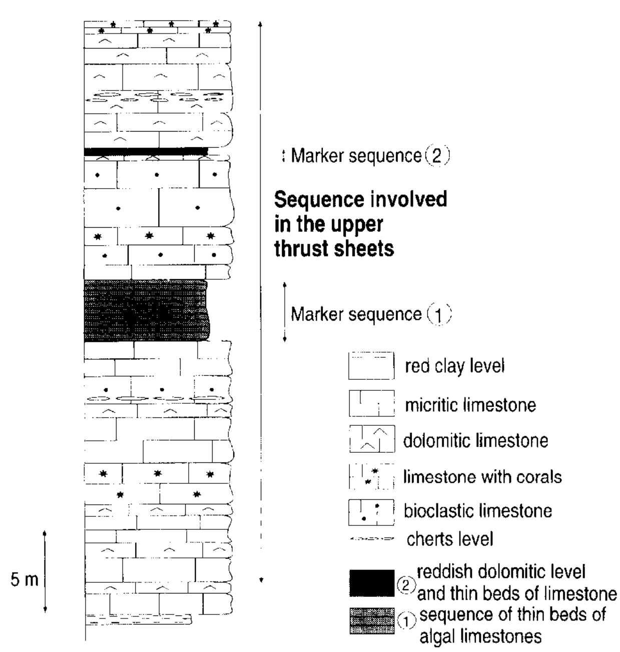

Fig. 4. Stratigraphic column of the sedimentary succession ('dolomie *a Siphonodendron martini*' formation) observed in the direct footwall of the 'Basse-Normandie' imbricate stack (redrawn from Hoyez, 1970).

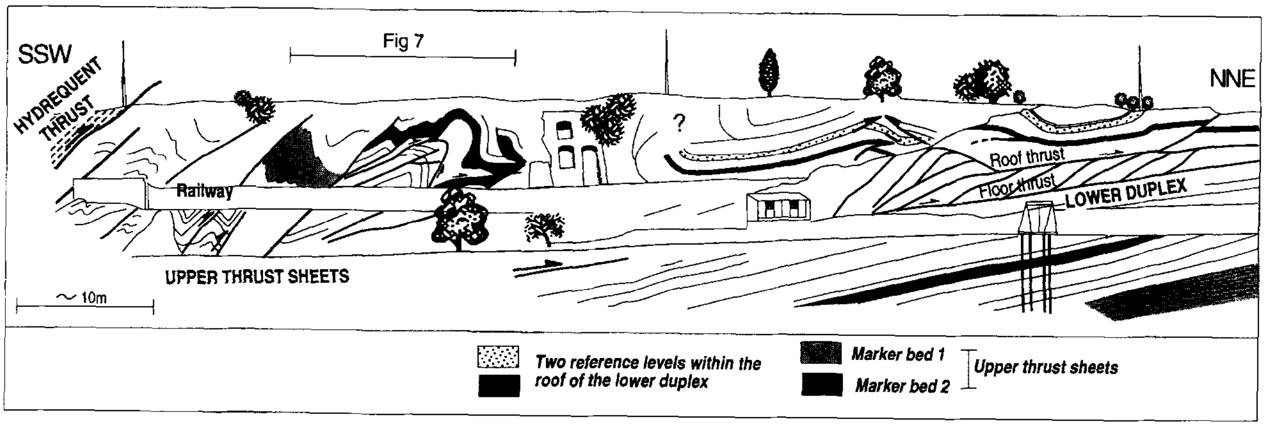

Fig. 5. Geometry of the 'Basse-Normandie' thrust-sheets (drawn from a photographic mossaic).

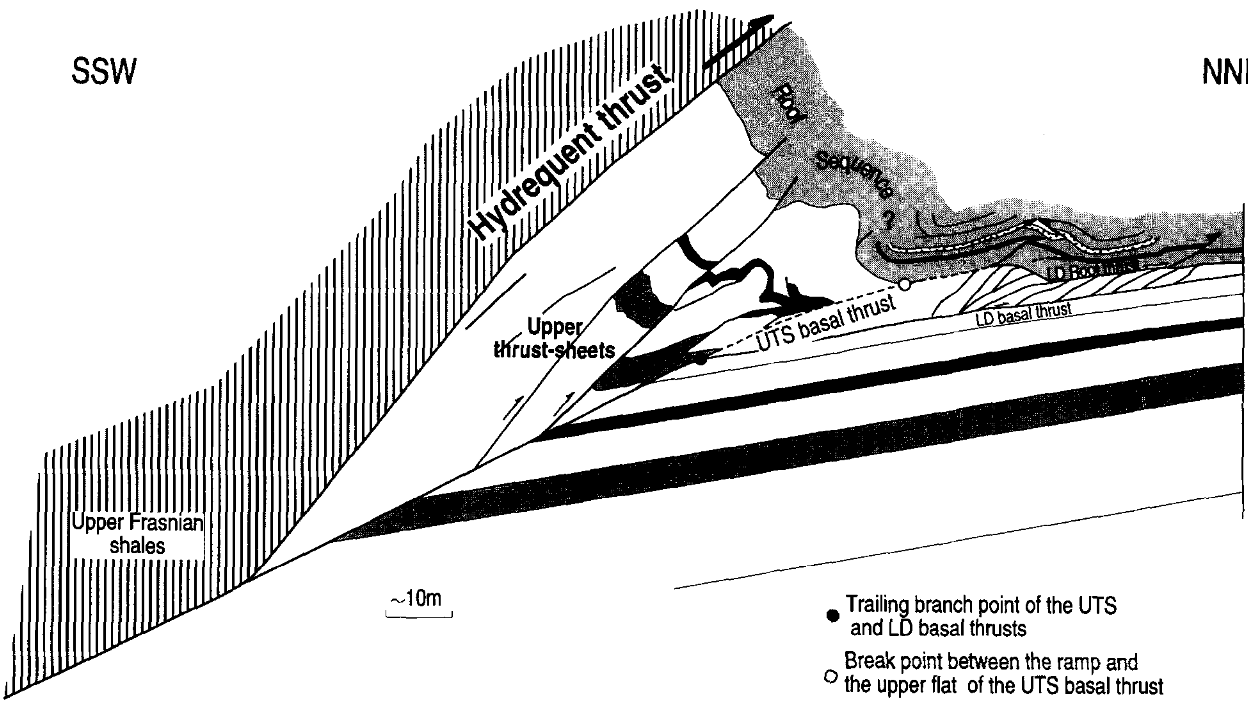

Fig. 6. Interpretative cross-section of the 'Basse-Normandie' thrust sheets.

as it is only observable at the back of the stack with a SW dipping attitude (Fig. 5). It is, however, clear in the exposed section that here is no leading branch line between the UTS basal thrust and the Hydrequent thrust as would be expected in the case of a classic allochthonous roof duplex geometry. This observation is also supported by the along-strike geometry of the Hydrequent thrust. Towards its western extension, within the 'Vallée Heureuse' quarry, it exhibits a southerly dip and affects some younger subhorizontal Visean limestones within its footwall (Pruvost and Delépine, 1921; Mansy, *in press*). Such a lateral attitude does not account for the previously proposed geometry (Cooper *et al.*, 1983), in which the Hydrequent thrust is resting horizontally, folded on top of the 'Basse-Normandie' thrust sheets. These data rather suggest that the SW dipping Hydrequent thrust crosscuts the whole series of the 'Haut-Banc Unit' (Fig. 6).

Within the upper thrust sheets located in between the UTS basal thrust and the Hydrequent thrust, the calcareous and dolomitic levels are highly dislocated and folded. The recognition of two marker beds in the thrust sheets and the undeformed footwall allows however a global geometric reconstruction (Fig. 5). Three major thrust-sheets may be distinguished, each separated by relatively planar SW dipping thrusts with decametric slip. They comprise as a whole a sequence about 35 m thick including the levels forming the lower duplex and the series lying just beneath them. In contrast to the lower duplex, however, the different UTS thrust sheets do not exhibit the same stratigraphic succession. The inner thrust-sheet of the UTS complex involves levels which are characteristic of the base of the sequence (some metres above the red clay level forming the bottom of the lithostratigraphic unit, see Fig. 4). The intermediate thrust-sheet is composed mainly of thin beds that characterize marker bed 1 situated in the middle of the sequence. The more external thrust-sheet of the UTS complex is made of a sequence about 15 m thick comprising the reddish dolomitic rocks of marker bed 2. This sequence and the roof levels of the lower duplex are globally conformable although separated by a badly exposed disharmonic zone. The complete stratigraphic succession is thus observed along the UTS complex with deeper levels being exposed towards the inner part of the stack. This configuration shows that the thrusts bounding the different upper thrust sheets can not be considered as the individual internal thrusts of a duplex. They instead seem to represent late features crosscutting and inducing the refolding of a previous NNE dipping fold limb (Fig. 6).

The geometric data discussed above show that although the duplex geometry of the lower thrust unit is well established, it is not the case for the upper thrust sheets. Indeed, more than a duplex, the geometry of the upper thrust sheets resembles more the forelimb of a hangingwall anticline developed above the UTS basal thrust, cut across by a system of late NE verging thrusts.

KINEMATICS OF THE THRUST SYSTEM

Thrust relationships

The relationships between the folds and thrusts and between the different internal thrusts of the 'Basse-Normandie' thrust sheets are investigated here to establish the kinematics of the resultant imbricate stack. When considering thrust relationships within superposed thrust units, two cases may be encountered:

(1) The upper unit is folded by an underlying frontal (Butler, 1987) or lateral ramp-related anticline (Averbuch *et al.*, 1993) implying a progressive thrusting towards the foreland;

(2) The basal thrust of the upper thrust unit truncates previously folded levels of the bottom thrust-sheet in a breaching style of thrust propagation (Butler, 1987; Morley, 1988).

These basic situations require that both thrusts are not active at the same time. A much more complex situation may evidently arise if the two thrust-sheets are developing synchronously (Morley, 1988; Boyer, 1992).

In any case, the conditions for deciphering the relationships between thrust units are not so common in the field. Concerning the major thrusts of the 'Basse-Normandie' imbricate stack, only the relationships between the two lower ones may be precisely analysed (see Fig. 6) since the Hydrequent unit is not visible at the top of the upper thrust sheets. As previously discussed, the upper thrust sheets basal thrust (the UTS basal thrust) branches forward onto the horizon localizing the lower duplex (LD) roof décollement zone. The latter is likely to resolve part of the UTS basal thrust displacement and to transfer it towards the foreland by layer parallel slip as shown by the NE verging thrusts affecting the roof sequence. It seems rather clear, however, that the shortening affecting the roof sequence in the foreland of the structure does not balance the total displacement above the UTS basal thrust. It appears, therefore, that some important part of the shortening has to be accommodated by internal deformation of the forelimb part of the developing anticline in a fault-propagation style of folding (Suppe and Medwedeff, 1990; Mercier and Mansy, 1995). The existence of the complex thickened zone affecting the roof sequence within the vertical wall (? in Figs 5 & 6) is another argument for such a tectonic style. Nevertheless, the LD roof décollement zone is clearly folded as developing the different imbrications of the lower duplex. On the other hand, no truncation is observed within the folded levels of the LD individual horses. It is thus clear that the UTS basal thrust has been activated mostly before the lower duplex developed in its direct footwall.

Within the lower duplex itself, the individual horses do not overlap except in its internal part where the structural thickness increases strongly. In this position, the subsidiary thrusts of the duplex seem to exhibit a steeper dip than the more external ones suggesting that they have been tilted during their rigid transport upon the lower ramps and thus indicating a progressive thrusting of the LD beds towards the foreland. Movement upon each subsidiary thrust is also only in part transferred to the LD décollement zone (less than 50% of the total shortening) as shown by Cooper *et al.* (1983), the other part being accommodated by layer parallel shortening of the LD beds. Above the décollement zone, just at the step surrounding the LD major thickened zone, the deformation zone with the double verging thrusts probably accommodates part of the shortening transferred from the lower duplex.

The geometric relationships between the Hydrequent thrust and the underlying upper thrust sheets cannot be observed in the 'Basse-Normandie' quarry. There is no leading branch line between the UTS basal thrust and the Hydrequent thrust. It is also not possible to define intersection relationships between the different upper thrust sheets as the bounding thrusts all dip in a similar manner towards the hinterland of the structure (Fig. 5).

In order to characterize the deformation sequence in the upper thrust sheets, fold-faults interactions have been investigated within the two more external thrust sheets. Figure 7 exhibits a scheme for the deformation observed within the latter. It is obvious that the rocks are more strained than within the lower duplex. In detail, rocks are intensively folded with asymmetrical folds showing steeper NE forelimbs. The style of the folds differs in relation to bed thickness. Second order chevron folds are

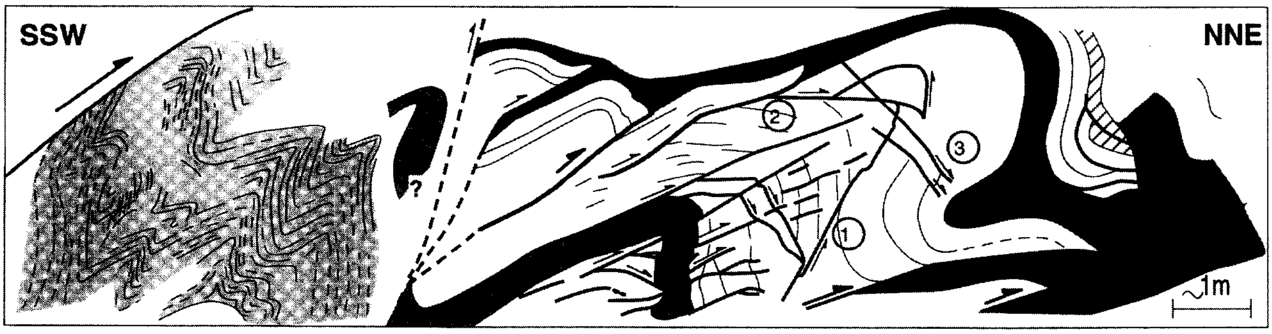

Fig. 7. Geometry of the external part of the upper thrust sheets (drawn from a photographic mossaic). Location is reported in Fig. 5. See text for comments.

thus observable within the thin dolomitic beds of marker bed 1. The most external part of the section is formed by a subvertical wall which represents the south–southwestwards extension of the forelimb of the UTS basal thrust hangingwall anticline. Towards the base of the section, the bedding rapidly becomes horizontal defining a pronounced disharmonic synclinal hinge. This structure develops above two gently SW dipping thrusts that we interpret here to be splays of the UTS basal thrust. These thrusts join in a high strain zone within a dolomitic succession (Fig. 7). This zone is the root of a nearly vertical SW verging backthrust which doubles the vertical wall of the ramp anticline. The core of the resultant structure is highly strained as indicated by minor intraformational thrusts. The global geometry represents a sort of decametric tectonic wedge initiated from the triple thrust junction zone acting as a buttress. This deformation pattern is likely to be indicative of difficulties in the forward propagation of displacement along the UTS basal thrust complex. As a result, numerous faults cross-cutting the folds are observed along the section. Three generations of faults have been defined (Fig. 7):

(1) The first set corresponds to thrusts affecting the limbs of the folds with antithetic vergence towards the hinge. These thrusts are syn-folding features resulting in the accentuation of the fold and thickening of the hinge zone. Such structures are common features in the Variscan folds of the Boulonnais Paleozoic massifs due to the ease in layer parallel displacement along the bedding discontinuities;

(2) The latter structures and the major fold are crosscut by a set of gently SW dipping thrusts. This thrusting event reflects a late NE verging component of shear which is likely to result from the blocking of the UTS basal thrust propagation as commonly observed in the late evolution of thrust-related folds (Butler, 1992; Frizon de Lamotte *et al.*, 1995). The minor thrusts branch onto the steeper thrust bounding at its back the thrust sheet producing a sort of imbricate fan that is interpreted, in such a context, to develop in a break-back sequence of thrusting;

(3) The last generation of faults are gently foreland-dipping normal faults with minor slip. It is worth noting that such faults are quite common in the Nord-Pas de Calais coal basin (Bouroz *et al.*, 1961) which is located within the direct footwall of the major out-of-sequence Midi thrust (Mansy and Meilliez, 1993). These structures are probably the result of the late loading and shearing of the area following the overthrusting of the Hydrequent nappe which represents the final thrust motion in the local break-back sequence of thrusting.

Within the upper thrust sheets, the deformation pattern thus argues for a more complex structural evolution than within the lower duplex. A late event of NE vergent thrusting is evidenced in relation to a change in the ease of forward thrust propagation along the UTS basal thrust zone. Although it is not posssible to determine the relationships between the higher thrusts, these data suggest, in agreement with the geometric considerations discussed above, that the upper thrust sheets are the result of out-of-sequence deformation of a previous fold forelimb.

Analysis of strain markers

In order to characterize better the kinematics of deformation, strain markers have been investigated within the upper thrust-sheets and the lower duplex. As only part of the structure is accessible, this study is not exhaustive (the UTS basal thrust displacement is, for example, not constrained).

No cleavage is visible along the 'Basse Normandie' section nor within the adjacent quarries of Visean limestone. Cleavage has only been observed in the 'Vallée Heureuse' quarry within Tournaisian calcareous shales situated in a mylonitic zone beneath the Hydrequent thrust. There, cleavage dips 65° towards the N215° (SW) and minor fold axes trend around N140°. Within the 'Basse-Normandie' thrust sheets, strain markers are mostly fold axes and bedding attitude as well as striations on fault planes (mostly shear fibres of calcite). These kinematic data are presented in Fig. 8. It is evident that there is little difference in movement direction between the upper thrust sheets and the lower duplex. In the lower duplex (Fig. 8a) and the upper thrust sheets (Fig. 8b),

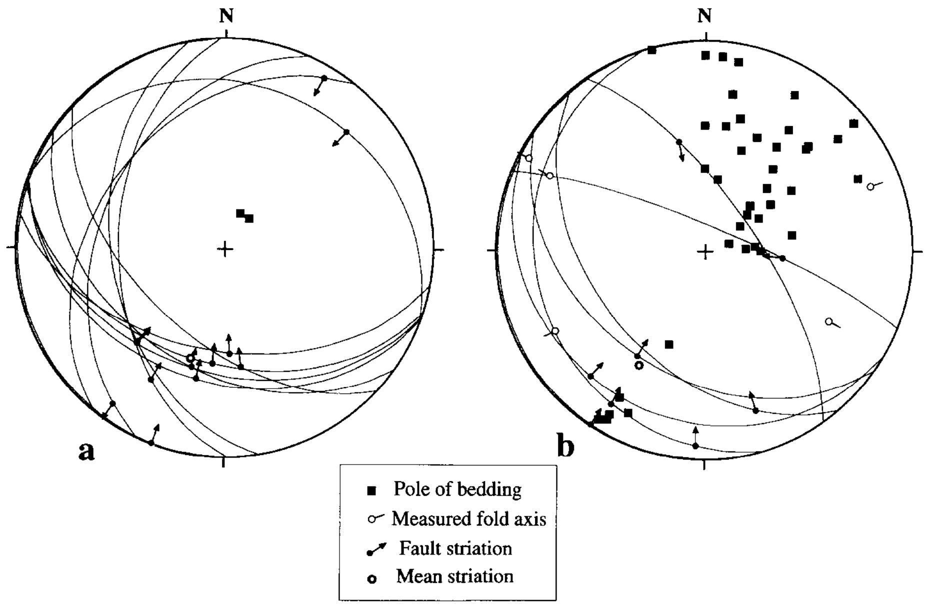

Fig. 8. Stereograms (lower hemisphere, equal area) of strain markers within (a) the lower duplex and (b) the upper thrust sheets.

kinematic data are relatively scattered showing N–S to NE–SW directions of movement. In the lower duplex, although these two directions are seen, the N–S to NNE–SSW movements (mean striation N195°) seem to be the most significant particularly along the SSW dipping subsidiary thrusts of the stack. In the upper thrust sheets, a complex distribution of the structural elements may be observed. Within the striation pattern, the NE–SW direction is more pronounced (mean N209°). Most bedding poles are distributed along this plane of movement in agreement with the orientation of the major fold axes (around N300°). A second population of compressive structures is, however, evident. The latter is characterized mostly by *ca* N070° trending folds which may explain the scatter of bedding poles towards the N–NNW direction (Fig. 8b). It is unclear whether these folds are second (or first) generation frontal folds or if they are only oblique–lateral structures in relation to the rapid plunge of the structure towards the NW. In any case, the major compressive event within the upper thrust-sheets is NE–SW directed, parallel to the orientation of shortening in the mylonitic zone beneath the Hydrequent thrust. Although the kinematic indicators do not give a clear picture, this direction seems slightly oblique to the thrust transport evidenced within the lower duplex which is more N–S directed.

We suggest here that such a slight deviation is the result of diachronous deformation within the lower duplex and the upper thrust sheets, the latter resulting from the late evolution of the hangingwall anticline developed above the UTS basal thrust. The induced clockwise rotation of thrust transport (from N–S to NE–SW) is consistent with the existence of Late Paleozoic left-lateral N110° trending faults (for example the Ferques fault) associated with a N060° direction of shortening.

DISCUSSION AND CONCLUSIONS

Although the 'Basse-Normandie' duplex is often cited as a classic duplex structure, the structural data presented here show that the tectonic development of the whole thrust stack is much more complex than a simple piggy-back duplication. The lower set of imbrications which was carefully analysed by Cooper *et al.* (1983) corresponds undoubtedly to an intraformational duplex structure but finally represents only a secondary structure with regards to the entire thrust complex. By contrast to this lower duplex, the upper thrust sheets of the 'Basse-Normandie' thrust complex exhibit neither the geometric nor the kinematic characters of a duplex. Instead they seem to represent the product of the late evolution of a NNE dipping forelimb of an hangingwall anticline developed above the basal thrust of the system. The lower duplex thus appears as a minor duplex developed in the frontal zone of a more important thrust related anticline accommodating displacement transferred towards the foreland (Fig. 9). During this event, the direction of transport is likely to be towards the NNE as indicated by striations recorded along the subsidiary thrusts of the duplex.

The main outcome of this study is the field evidence for the out-of-sequence evolution of the internal folds and thrusts of the upper thrust sheets and the Hydrequent thrust. Fold-thrust relationships as well as the deformation pattern observed within the upper thrust sheets argue for a local break-back sequence of thrusting in which thrusts sequentially cross-cut the forelimb of the basal thrust related anticline (Fig. 9). Such an evolution is likely to be linked to the difficulty of propagation of the upper thrust sheets basal thrust as shown by the intense deformation observed at its tip. The sequence of

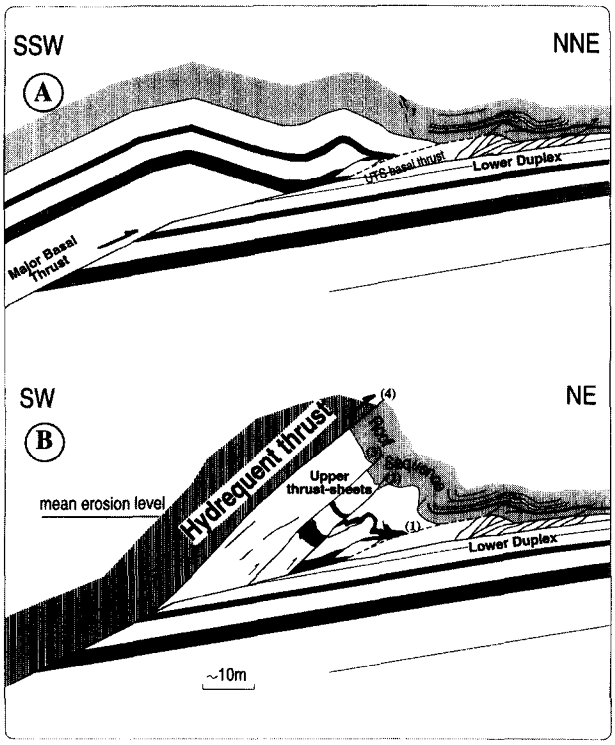

Fig. 9. A model for development of the 'Basse-Normandie' thrust-sheets. (A) Formation of an hangingwall anticline upon the basal thrust of the thrust system with a frontal second-order duplex accommodating forward transfer of displacement. (B) Out-of-sequence thrusting event within the upper thrust sheets and along the Hydrequent thrust inducing the refolding and cross-cutting of the previous situation.

thrusting is punctuated by the activation of the major Hydrequent thrust which emerged from the footwall ramp of the initial fold-thrust structure. Kinematic indicators argue for a late NE verging transport, slightly oblique to the initial shortening direction, which is believed here to be the result of a clockwise rotation of regional thrust transport.

This sequence of deformation, observed at the hectometric scale within the 'Basse-Normandie' thrust system, may well be representative of the processes acting along major Variscan structures such as the 'Midi thrust' as already suggested for other segments of the Western Europe Variscan thrust front (e.g. Mercier *et al.*, 1994). In such a respect, the UTS thrust-sheets could represent the equivalent of the thrust-sheets which appear systematically in a reverse position in the direct footwall of the 'Midi thrust' (Raoult and Meilliez, 1987).

In a more general way, the data presented here emphasize the out-of-sequence mode of thrust propagation which induces both the foreland migration of displacement by layer parallel slip and reactivation of transported fault zones. Such a sequence has been shown in recent times both by numerical modelling (Chalaron and Mugnier, 1993) and field work (e.g. Morley, 1988; Averbuch *et al.*, 1995) to be a widespread style of deformation in fold-thrust belts. Mechanical discontinuities of décollement zones as well as syntectonic sedimentation or erosion (Vinour *et al.*, 1996) are likely to be decisive parameters in controlling this sequence. These points require however further field characterization and modelling for a better understanding of fold-thrust belt kinematics.

Acknowledgements—This is a contribution from the URA CNRS 719 'Sédimentologie et Géodynamique'. The authors wish to thank the 'Vallée Heureuse' quarries for the permission to study the 'Basse-Normandie' section. We also thank A. Prudhomme, J. Lamarche, C. Phalempin and J.-D. Legrand for their help during the field work and M. Bocquet for technical support in the figures. D. Frizon de Lamotte, G. Manby, C. Morley, R. Lisle and an anonymous reviewer are gratefully acknowledged for their constructive comments on earlier versions of this paper and the improvement of the English.

REFERENCES

Averbuch, O., Frizon de Lamotte, D. and Kissel, C. (1992) Magnetic fabric as a structural indicator of the deformation path within a fold–thrust structure: a test case from the Corbières (NE Pyrénées France). *Journal of Structural Geology* **14**, 461–474.

Averbuch, O., Frizon de Lamotte, D., and Kissel, C. (1993) Strain distribution above a lateral culmination: an analysis using micro-faults and magnetic fabric measurements in the Corbières thrust belt (NE Pyrenees, France). *Annales Tectonicae* **VII**, 3–21.

Averbuch, O., Mattei, M., Kissel, C., Frizon de Lamotte, D. and Speranza, F. (1995) Cinématique des déformations au sein d'un système chevauchant aveugle: l'exemple de la 'Montagna dei Fiori' (front des Apennins centraux, Italie). *Bulletin de la Société géologique de France* **166**, 451–461.

Bally, A. W., Burbi, L., Cooper, C. and Ghelardoni, R. (1986) Balanced sections and seismic reflection profiles across the Central Apennines. *Memorie della Societa Geologica Italiana* **35**, 257–310.

Banks, C. J. and Warburton, J. (1986) 'Passive roof' duplex geometry in the frontal structures of the Kirthar and Sulaiman mountain belts, Pakistan. *Journal of Structural Geology* **8**, 229–237.

Bonte, A. (1969) Le Boulonnais. *Annales de la Société géologique du Nord* **89**, 23–46.

Bouroz, A. (1962) Contribution à l'étude de la structure du bassin houiller du Boulonnais. *Annales de la Société géologique du Nord* **82**, 27–37.

Bouroz, A., Chalard, J., Dalinval, A. and Stiévenard, M. (1961) La structure du bassin houiller du Nord de la France de Douai à la frontière belge. *Annales de la Société géologique du Nord* **81**, 173–220.

Bowler, S. (1987) Duplex geometry: an example from the Moine thrust zone. *Tectonophysics* **135**, 25–35.

Boyer, S. (1992) Geometric evidence for synchronous thrusting in the southern Alberta and northwest Montana thrust belts. In *Thrust Tectonics*, ed. K. R. McClay, Chapman and Hall, 377–390.

Boyer, S. and Elliott, D. (1982) Thrust systems . *American Association of Petroleum Geologists Bulletin* **66**, 1196–1230.

Butler, R. W. H. (1987) Thrust sequences. *Journal of the Geological Society of London* **144**, 619–634.

Butler, R. W. H. (1992) Structural evolution of the Chartreuse fold and thrust system, NW french Subalpine chains. in *Thrust Tectonics*, ed. K. R. McClay, Chapman and Hall, 287–298.

Chalaron, E. and Mugnier, J.-L. (1993) Séquence de propagation des failles dans un prisme d'accrétion: une modélisation numérique. *Bulletin de la Société géologique de France* **164**, 113–121.

Colbeaux, J. P. and Leplat, J. (1985) Le massif Paléozoïque du Bas-Boulonnais. Région de Marquise. in *Géologie du Boulonnais*, J. P. Colbeaux coord., Science et Nature n°3, Espace Naturel Régional, 176.

Cooper, M. A., Garton, M. R. and Hossack, J. R. (1983) The origin of the Basse-Normandie duplex, Boulonnais, France. *Journal of Structural Geology* **5**, 139–152.

Dahlstrom, C. D. A. (1970) Structural geology in the Eastern margin of the Canadian Rocky Mountains. *Bulletin of Canadian Petroleum Geology* **18**, 332–406.

Diegel, F. A. (1986) Topological constraints on imbricate thrust networks, examples from the Mountain City window, Tenessee, U.S.A *Journal of Structural Geology* **8**, 269–279.

Fallot, P. (1949) Les chevauchements intercutanés de Roya (A.-M.). *Annales Hébert et Hauy* **VII**, 161–169.

Frizon de Lamotte, D., Guézou, J. C. and Averbuch, O. (1995) Distinguishing lateral folds in thrust systems; examples from Corbières (SW France) and Betic Cordilleras (SE Spain). *Journal of Structural Geology* **17**, 223–245.

Frizon de Lamotte, D., Mercier, E., Dupré la Tour, A., Robion, P. and Averbuch, O. (1997) La cinématique du pli de Lagrasse (Aude, France). *Comptes Rendus de l'Académie des Sciences, Paris* **324**, 591–598.

Geiser, P. (1988) The role of kinematics in the construction and analysis of geological cross sections in deformed terranes. *Geological Society of America Special Paper* **222**, 47–78.

Graham, R., Hossack, J. Deramond, J. and Soula, J. C. (1987) Géométrie des surfaces de chevauchements. *Bulletin de la Société géologique de France* **III, 1**, 169–181.

Hoyez, B. (1970) Analyse séquentielle des calcaires viséeens du massif du Haut-Banc (Boulonnais). Unpublished thesis, Université de Lille, 174p.

Kulander, B. R. and Dean, S. L. (1986) Structure and tectonics of Central and Southern Appalachian Valley and Ridge and Plateau Provinces, West Virginia and Virginia. *American Association of Petroleum Geologists Bulletin* **70**, 1674–1684.

Mansy, J.-L. and Meilliez, F. (1993) Eléments d'analyse structurale à partir d'exemples pris en Ardenne-Avesnois *Annales de la Société géologique du Nord* **2**, 45–60.

Mansy, J.-L. (in press) Carte géologique de la France au 1/50 000 (feuille de Marquise). *B.R.G.M. ed.*

Mercier, E., DePutter, T., Mansy, J.-L. and Herbosch, A. (1994) L'écaille des Gaux (Ardennes belges): un exemple d'évolution tectono-sédimentaire complexe lors du développement d'un pli de propagation. *Geologische Rundschau* **83**, 170–179.

Mercier, E. and Mansy, J.-L. (1995) Le blocage du transport sur le plat de plis de propagation: une cause possible des chevauchements hors séquence. *Geodinamica Acta Paris* **8**, 199–210.

Mitra, G. and Boyer, S. (1986) Energy balance and deformation mechanisms of duplexes. *Journal of Structural Geology* **8**, 291–304.

Mitra, S. (1986) Duplex structures and imbricate thrust systems: geometry, structural position and hydrocarbon potential. *American Association of Petroleum Geologists Bulletin* **70**, 1087–1112.

Morley, C. K. (1986) A classification of thrust fronts. *American Association of Petroleum Geologists Bulletin* **70**, 12–25.

Morley, C. K. (1988) Out of sequence thrusts. *Tectonics* **7**, 539–561.

Olry, A. (1904) Travaux d'exploitation et de recherche exécutés dans le bassin houiller du Boulonnais et dans la région comprise entre le bassin du Pas de Calais et la mer. *Bulletin du Service de la Carte géologique de France* **100**(15), 131.

Pasquet, J.-F., Leplat, J. and Becq-Giraudon, J.-F. (1983) Premiers résultats du sondage de Réty-Rinxent (Massif paléozoïque de Ferques). *Memoire B.R.G.M.* **123**, 171–178.

Price, R. A. (1986) The southeastern Canadian Cordillera: thrust faulting, tectonic wedging and delamination of the lithosphere. *Journal of Structural Geology* **8**, 239–254.

Prudhomme, A., Vachard, D. and Mansy, J.-L. (1992) Séries carbonatées viséennes du Boulonnais (France): mise en évidence d'un diachronisme et conséquences structurales. *Comptes Rendus de l'Académie des Sciences, Paris.* **315**, 363–369.

Pruvost, P. and Delépine, G. (1921) Observations sur la faille d'Hydrequent et sur les couches de base du Carbonifère dans le Bas-Boulonnais. *Bulletin de la Société géologique de France* **21**, 189–206.

Ramsay, J. G. and Huber, M. (1987) *The Techniques of Modern Structural Geology, Vol 2: Folds and Fractures.* Academic Press, London.

Raoult, J.-F. and Meilliez, F. (1987) The Variscan front and the Midi fault between the Channel and the Meuse River. *Journal of Structural Geology* **9**, 473–479.

Suppe, J. (1983) Geometry and kinematics of fault-bend folding. *American Journal of Science* **283**, 684–721.

Suppe, J. and Medwedeff, D. A. (1990) Geometry and kinematics of fault-propagation folding. *Eclogae geologica Helvetica* **83**(3), 409–454.

Tanner, P. W. G. (1992) The duplex model: implications from a study of flexural-slip duplexes. in *Thrust Tectonics*, ed. K. R. McClay, Chapman and Hall, 201–208.

Vinour, P., Baby, P., Coletta B. and Mugnier, J.-L. (1996) Une modélisation analogique de l'influence de l'érosion et de la sédimentation sur la propagation des chevauchements. *Abstract 16 Réunion des Sciences de la Terre*, Société Géologique de France éd., 24.

Wallace, P. (1983) The subsurface Variscides of southern England and their continuation into continental Europe. in *The Variscan fold belt in the British Isles*, P. L. Hancock ed., Adam Hilger Ltd, Bristol, 198–208.

Article 7.

Averbuch O., Mansy J-L., Lamarche J., *Lacquement F.* and Hanot F. (2004). Geometry and kinematics of the Boulonnais fold-and-thrust belt (N France) : implications for the dynamics of the Northern Variscan thrust front. Geodinamica Acta 17, vol 2, 163-178.

Geodinamica Acta 17/2 (2004) 163–178

Geodinamica Acta

Geometry and kinematics of the Boulonnais fold-and-thrust belt (N France): implications for the dynamics of the Northern Variscan thrust front

Olivier Averbuch [a*], Jean-Louis Mansy [a], Juliette Lamarche [b*], Frédéric Lacquement [c], Franck Hanot [c]

[a] *UMR 8110, Processus et Bilans des Domaines Sédimentaires, Université de Lille 1, 59 655 Villeneuve d'Ascq cedex, France.*
[b] *Organische Geochemie und Kohlenwasserstoff-Systeme, GeoForschungsZentrum Potsdam, Telegrafenberg C, 14473 Potsdam, Germany.*
[c] *Bureau de Recherches Géologiques et Minières, 3 avenue C. Guillemin, BP 6009, 45060 Orléans cedex 2, France.*
[*] *Now at: Université de Provence, Centre Sed-Pal, 13331 Marseille cedex 3.*

Received : 06/02/2003, accepted : 21//11/2003

Abstract

Recent structural data obtained within the Boulonnais thrust belt along the Northern Variscan thrust front provide a new insight into the deformation history of the Variscan belt. The zone under study recorded the latest increments of inversion of the Rheno-hercynian basin in Late Westphalian—Early Stephanian times (ca 305 Ma). Thrusting within the southern margin of the "Old Red Sandstones Continent" propagated primarily in sequence up to the Brabant massif which acts as a significant buttress. This buttress effect, which we suggest to be due to the southward activation of deep-seated inherited Caledonian thrusts, resulted in the out-of-sequence dislocation of the thrust front. The associated localized thrust stack induced a sharp flexure of the underthrust block moulding the border of the molassic coal-bearing foreland basin. During this process, strain markers at the thrust front document an evolution of thrusting from a dominantly NNE to NE direction whereas more internal parts of the belt undergo dextral transcurrent deformations (e.g. the Bray fault zone). Such a partition of the deformation argues for a general transpressional setting of the SE England-Boulonnais orogenic belt acting as a relay zone between more frontal parts of the Variscan orogen (Ardenno-Rhenish and SW England segments). This mechanism highlights the segmented nature of the Variscan thrust front and points out the importance of the Devonian basin pre-structuration in the present-day arcuate shape of the Variscan belt. Late Variscan reactivation of the thrust network occured within a transtensional setting associated to a dominant NNW-SSE directed extension. This event induced the formation of local intramontane basins and contributed to the thinning and thermal restoration of the thickened external Variscan crust in Upper Stephanian—Middle Permian times.

Résumé

Des données structurales récentes acquises le long du front chevauchant varisque du Boulonnais (N France) permettent d'obtenir une nouvelle image de l'histoire de la déformation du domaine nord-varisque. Le secteur étudié retrace les derniers incréments de l'inversion tectonique du bassin rhéno-hercynien, durant la fin du Westphalien et le début du Stéphanien (aux alentours de 305 Ma BP). Il est montré que, dans un premier temps, l'écaillage de la marge sud du « Continent des Vieux Grès Rouges » intervient en séquence conforme jusqu'au massif du Brabant qui agit comme une zone de butoir majeure. Cet effet butoir, que nous interprétons comme le résultat de l'activation vers le sud de chevauchements profonds hérités des déformations calédoniennes, induit la dislocation hors-séquence du front de chevauchement. L'accumulation résultante d'écailles chevauchantes implique une flexuration importante du bloc crustal chevauché localisée sur l'extrémité nord du bassin d'avant-pays molassique à remplissage houiller. Au cours de cet épisode, les marqueurs de la déformation indiquent que le front de chaîne subit une déformation chevauchante avec une évolution de la direction de transport depuis

* Corresponding author.
E-mail address: Olivier.Averbuch@univ-lille1.fr

le NNE vers le NE alors que les zones plus internes comme le Pays de Bray sont soumises à des déformations décrochantes dextres. Cette partition de la déformation argumente un contexte général transpressif du domaine orogénique Boulonnais-SE de l'Angleterre agissant comme une zone de relais entre les domaines varisques plus frontaux que sont les segments Ardenno-rhénans et le sud-ouest de l'Angleterre. Ce mécanisme traduit le caractère segmenté du front de chevauchement varisque et illustre l'importance de la structure originelle du bassin dans la forme arquée actuelle de la chaîne. La réactivation des systèmes de chevauchement au cours d'un épisode tardi-varisque intervient dans un contexte transtensif impliquant une extension majeure orientée suivant une direction NNW-SSE. Cet événement induit la formation de bassins intra-montagneux très localisés et contribue dès le Stéphanien supérieur-Permien moyen à l'amincissement et au ré-équilibrage thermique de la croûte varisque externe surépaissie.

Keywords: Variscan thrust front; Late Variscan extension; Boulonnais; Fold-and-thrust belt; Transpression

Mots clé : Front de chevauchement varisque ; Extension tardi-varisque ; Boulonnais ; Chaîne de chevauchement-plissement ; Transpression

1. Introduction

The Western European Variscan belt is a major collisional orogen which developed in Upper Paleozoic times between Laurentia-Avalonia-Baltica (i.e. Old Red Sandstones Continent) and Gondwana margins. One of its major structural feature is a pronounced arcuate shape (Fig. 1), the origin of which still remains highly debated [1-7]. This peculiar geometry makes difficult the determination of the general kinematics of the belt and a major question is to understand for the present-day shape the partitioning between the original paleogeographic pattern of the Devonian-Carboniferous basins and a possible distortion due to oroclinal bending.

This problem is particularly well exemplified along the northern frontal zone of the Variscan belt which displays a pronounced change of structural trend. The latter occurs in connection with a major Variscan lineament, the Bray fault zone, accommodating an important shift of the northermost Variscan suture zone i.e. the suture of the Devonian Lizard-Rheno-hercynian ocean [8, 9] (Fig. 1). Within this area, the frontal part of the Variscan belt is classically assigned to the Rheno-hercynian domain as defined by Kossmat [10] and includes non-metamorphic to epimetamorphic sedimentary rocks of mostly Devonian-Carboniferous age. These rocks were deposited at the southern border of the "Old Red Sandstones" continent in a rifted continental margin-type environment. Rifting occured in Lower-Middle Devonian times when the Lizard-Rheno-hercynian ocean opened [9, 11]. Continental to shallow marine clastic sediments and carbonate platform deposits form most of sedimentary rocks involved in the Northern Variscan thrust front.

Along the SE England-Boulonnais segment, the thrust front displays a dominant NW-SE trend which turns to a NE-SW trend along the Ardennes-Rhenish segment (Fig. 2a). This change in direction occurs progressively within the Western Ardennes domain of northern France in association with second-order strike-deviated zones [12, 13]. The geometry and kinematics of the NE-SW trending branch is relatively well-known as it largely crops out within the Ardennes-Rhenish massifs. It is characterized by a thrust-wedge geometry developed above a crustal scale gently dipping basal thrust (Fig. 2b) [14-19], the emerging part of which is called the Midi thrust zone (MTZ) in northern France and southern Belgium. The latter thrust lies directly upon a Namurian-Westphalian coal-bearing molassic foreland basin inducing the complete dismembering of its southern border [16, 20, 21]. In the western Ardennes (Fig. 2b), the frontal thrust system accommodates a total displacement of about 70 km towards the NNW direction but towards the eastern Ardennes, the frontal throw tends to decrease to some 20-30 kilometers [19]. On the other hand, in the Western Ardennes, cross-cutting relationships show that a major part of the frontal displacement upon the MTZ is achieved during an out-of-sequence thrust activation which post-dates the Namurian-Westphalian foreland basin development. A pronounced flexure of the underthrust Brabant substratum is observed at the tip of the frontal thrust system resulting from the induced localized thrust stack.

Along the NW-SE trending segment of Northern France, the structure of the Variscan thrust front is less constrained due to its relatively poor exposure beneath the Mesozoic deposits of the Weald-Boulonnais basin. Subcrop data acquired during the coal exploration in the Artois Namurian-Westphalian molassic basin suggest a rather more complex situation than in the Ardennes-Rhenish belt with the existence of a system of *en-échelon* steeply dipping faults dissecting the thrust front (Fig. 2a) [22-24]. These faults strike parallel to the thrust front and to the more internal deep major discontinuities such as the Somme and the Bray fault zones [25]. During Late Paleozoic times, they display systematically down-faulted southern borders [22] which may localize few hundred of meters thick conglomeratic continental deposits [23, 26]. The latter lie unconformably on top of the Variscan thrust-units but their age is not precisely constrained. Reworked *microcodium* extracted recently from these deposits suggest a Middle Permian age for the upper part of the conglomeratic sequence [27]. These new data as well as close facies similarities suggest that the entire conglomeratic sequence could be a time-equivalent of the lower sequence of the early post-Variscan Exeter Group in south

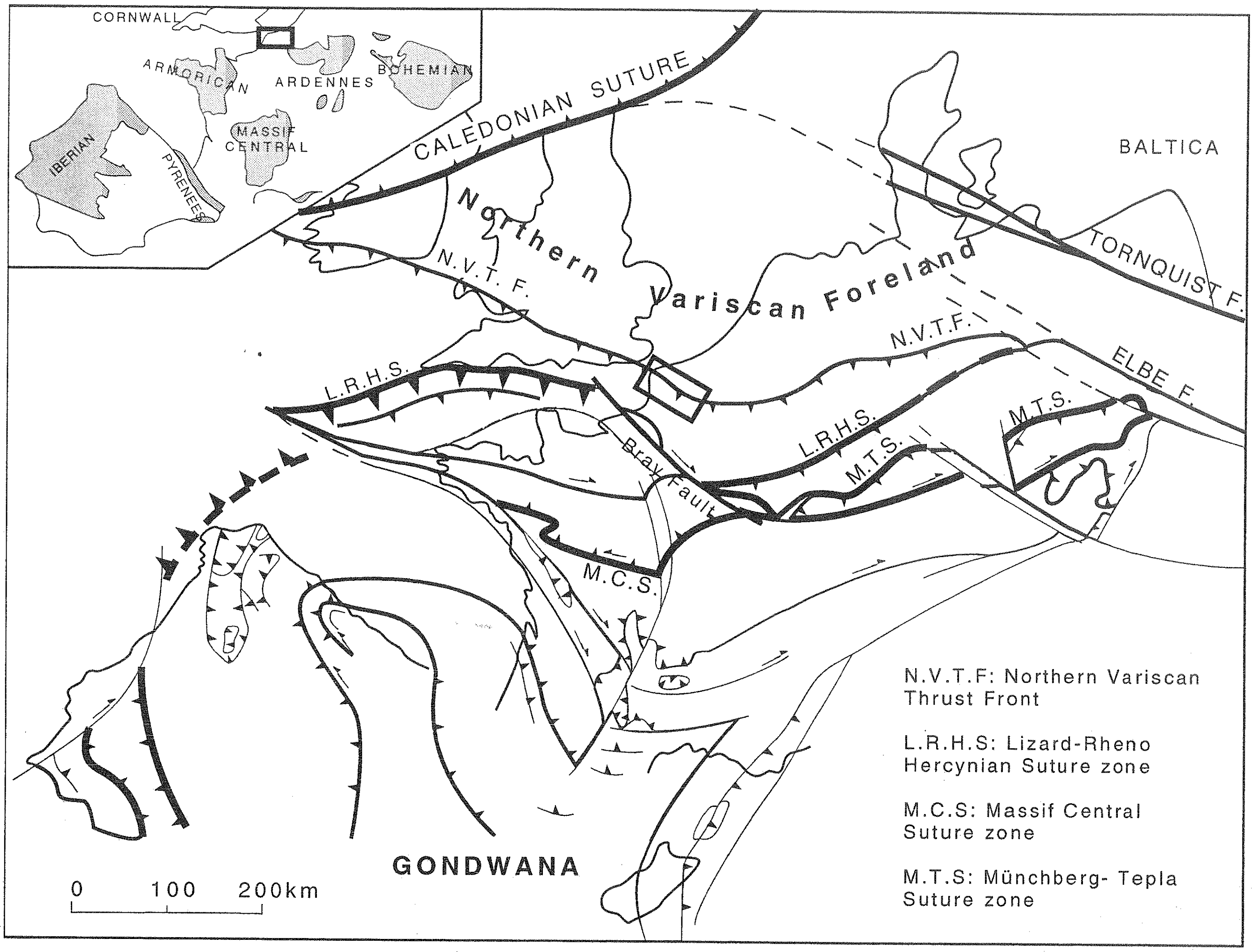

Fig. 1 Schematic structural map of the Western European Variscan belt (after [8]). The rectangles locate the study area. Thick lines correspond to the traces of the different Variscan suture zones.

Devon as defined by Edwards *et al.* [28] (i.e. Upper Stephanian-Middle Permian).

This system of sub-vertical faults has moreover been suggested to be part of a major "North Artois shear zone" [29] the geometry and kinematics of which remain highly unconstrained. A Late Carboniferous dextral motion has been postulated for this zone mainly based on similarities with the Bray fault zone situated in a more internal position with respect to the orogen. $^{39}Ar/^{40}Ar$ dating of metamorphic biotites collected within a mylonitic orthogneiss situated at depth along the Bray fault zone evidences a syn-metamorphic dextral wrenching event at ca 320 Ma BP (Namurian times) [30]. Such a transcurrent motion along the NW-SE trending segment of the Northern Variscan thust front is difficult to reconcile with the thrust tectonics pattern observed within structures like the well-known "Basse-Normandie" duplex in the Boulonnais area [31, 32].

To progress in the understanding of the Northern Variscan thrust front dynamics and in the documentation of the strain pattern along part of the Variscan arc, this paper aims to analyse the style and kinematics of the deformations within the Boulonnais Paleozoic massif which forms the primordial exposure along the NW-SE trending Variscan thrust front in Northern France. The data collected in the present study lead us to propose a model for the Late Carboniferous-Early Permian evolution of the Northern Variscan thrust front in NW Europe.

2. Geometry of the Boulonnais thrust front

2.1. General structure

On a present-day structural point of view, the Boulonnais area corresponds to an about 50 km wide E-W striking faulted antiform affecting the sedimentary series of the Weald-Boulonnais basin up to the Upper Cretaceous chalk formations (Fig. 3a). This recent uplift is related to tertiary contractional movements along localized fault zones of the basin that have been shown to parallel the basement structural framework [33, 34]. The process of basin inversion allowed the exhumation of the Paleozoic substratum in the northern part of the structure (i.e. the Ferques massif) (Fig. 3a).

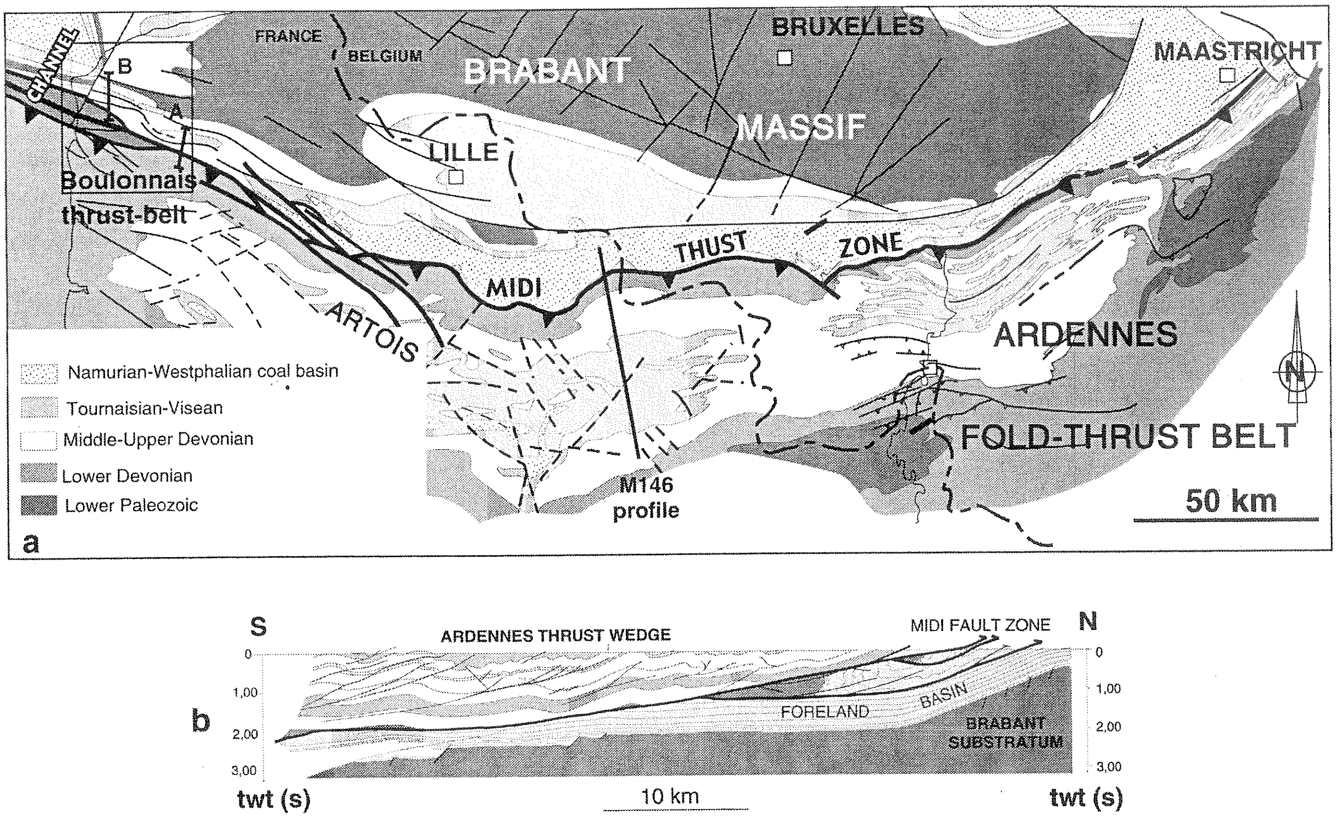

Fig. 2 (a) Structural map of the Northern France Variscan thrust front based on a synthesis of existing surface and subcrop data. Section A at the eastern border of the Boulonnais thrust belt refers to the seismic line 85A presented in Fig. 4; section **B** refers to the geological cross-section of the Boulonnais Paleozoic massif in Fig. 5. (b) Geometry of the Variscan thrust front along the M146 seismic profile across the Western Ardennes massif (after [16].

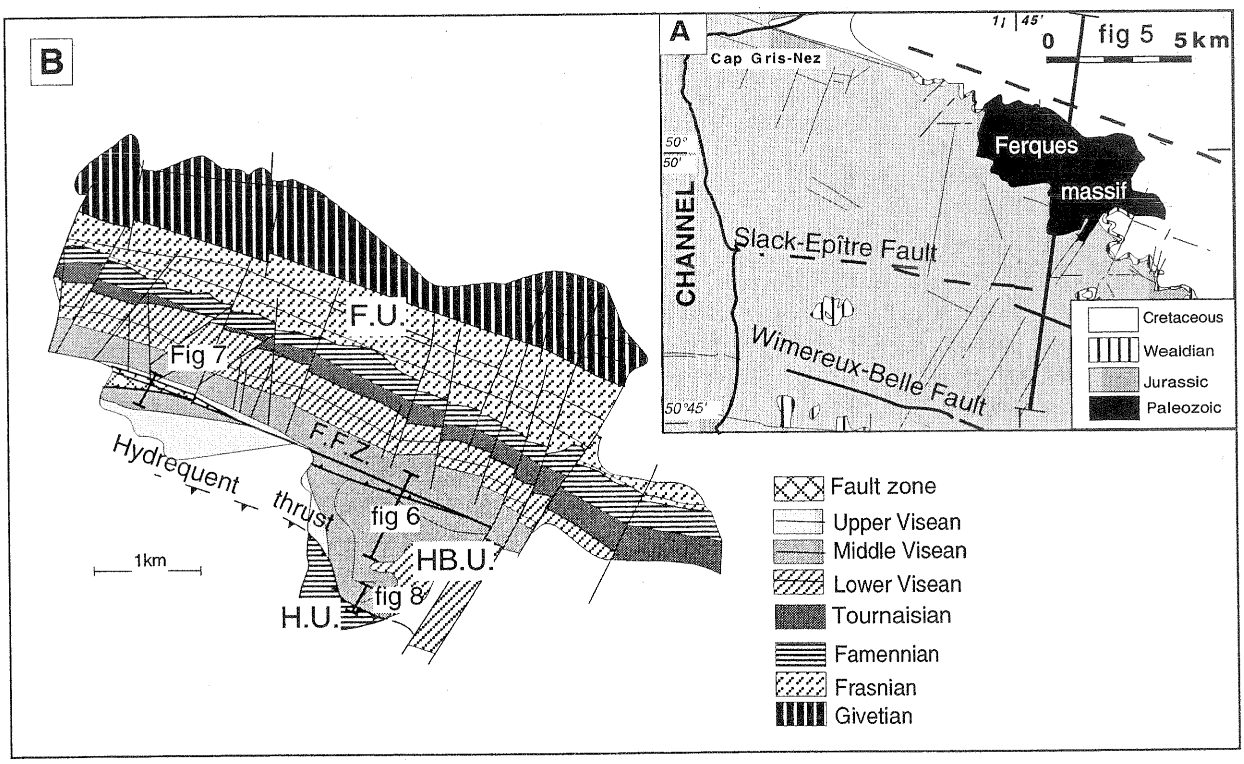

Fig. 3 (a) Schematic geological map of the Boulonnais area with the location of the general cross-section of Fig. 5. In black, the exhumed Paleozoic series (the Ferques massif) along the inverted northern border of the Boulonnais Mesozoic basin (b) Geological map of the Paleozoic Ferques massif with the location of exposed sections of Fig. 6, 7 and 8. F.U.: Ferques thrust unit; H.B.U.: Haut-Banc thrust unit; H.U.: Hydrequent thrust unit; F.F.Z.: Ferques fault zone.

The Paleozoic rocks include un-metamorphosed sedimentary series composed of Middle-Upper Silurian shales [35] slightly unconformably covered by a reduced sequence of Middle Devonian (Givetian) to Upper Carboniferous (Westphalian) rocks (Fig. 3b). This stratigraphic sequence with the hiatus of Lower Devonian rocks is characteristic for the northern part of the inverted Rheno-hercynian basin. Indeed, further south and east, in the Artois and the Ardennes regions, Lower Devonian shales and sandstones are observed directly on top of the Midi thrust i.e. the basal thrust of the Northern Variscan thrust wedge (Fig. 2). The general southward older age of the basal rocks and thickening of the Devonian-Carboniferous sequence reflects the rifted passive margin-type geometry of the Rheno-hercynian basin [11, 12, 36].

These paleogeographic considerations imply that the Boulonnais area corresponds to the very outer part of the northern Variscan thrust belt. This structural position is confirmed by the occurrence on top of the sedimentary sequence of Westphalian coal-bearing molassic levels of foreland basin setting type [37]. The latter are just very locally preserved due to their truncation by thrust faults and an intense post-orogenic erosion. Their maximum thickness known from boreholes reach 200 meters but should have been more important. Illite cristallinity and Tmax data from Upper Devonian shales situated in the outer part of the Boulonnais thrust belt suggest a minimum burial of *ca* 2,100 m [38] which in turn may imply a Westphalian molassic sequence about 1,000 m thick. The Boulonnais coal basin has been proposed to prolongate westward in a complex way through the Channel to connect the Kent basin on-shore Great-Britain [23, 33, 39]. The style of folding and thrusting within the remaining deposits of these basins suggests that they are situated few kilometres north of the major Variscan deformation front i.e. the Midi thrust zone in northern France and the Dorking-Biddenden structure in England [40].

2.2. *Seismic data*

No recently processed seismic profiles are available directly along the exposed Paleozoic massif of the Boulonnais. However, numerous boreholes drilled for to the coal exploration in the Namurian-Westphalian molasse of the foreland basin as well as an industrial reflection seismic profile (profile 85A) situated at the eastern border of the Boulonnais thrust belt (see location in Fig. 2a) seriously help to clarify the deep structure of the thrust front. The 12 km long NNE-SSW directed (normal to the front trend) seismic profile images the MTZ and its direct footwall. The investigated area is situated in a similar structural position than the Boulonnais exposed Paleozoic massif. The analysis of the profile 85A (stack SATAN processed) lead to the production of the line drawing section presented in Fig. 4a which depicts the geometry of significant seismic reflectors. The interpretation of the line drawing section (Fig. 4b) has been constrained by boreholes situated in the vicinity of the seismic line (2-7, 2-146, 2-155 and 2-156, after [41]) and projected onto the profile.

The Mesozoic cover is relatively thin in the study area but it is characterized by relatively strong sub-horizontal reflectors allowing a detailed observation of the Jurassic-Cretaceous basin geometry. Along the profile, a significant southward thickening of the Mesozoic series is noticed with a maximum thickness smaller than 200 m. The basin geometry is controlled by superficial syn-sedimentary faults displaying a strong dip to the south. This conspicuous geometry is explained by the fact that they branch at depth onto south slightly dipping Variscan thrust faults (Fig. 4b). Extensional reactivation of Variscan thrust ramps is shown to largely control the Mesozoic basin development in the Boulonnais area [see also 34].

The Paleozoic substratum is characterized by a very clear thrust pattern with two major planar, gently south dipping reflectors. The southernmost one is situated at the base of Lochkovian rocks (borehole 2-7) and is defined as the major Midi thrust zone (MTZ). The northern one, defined by the authors as the Quercamps thrust, floors at its tip some Famennian rocks (borehole 2-154) and is interpreted as a subsidiary thrust developed in the footwall of the MTZ. At depth (about 1,5 s twt), it displays a complex structure with the existence of a lens-shaped horse the origin of which is not fully understood. The lens is localized at a very subtle break in the dip of the thrust (which becomes more horizontal at depth) and thus could possibly be the remnant of the forelimb of a previous hangingwall anticline submitted to subsequent simple shear during an out-of-sequence reactivation of the thrust. In this respect, such horse could be the equivalent of thrust-sheets from the Ardennes thrust belt situated in an overturned position in the direct footwall of the MTZ [14]. At the northern tip of the Quercamps thrust, curved reflectors are branching on the latter planar thrust. They are interpreted as thrust zones lying on top of a folded sequence associated with deep-seated thrusts dying out in the Silurian shales. These points will be further discussed when correlated with the structure observed in the exposed Paleozoic massif of the Boulonnais area.

2.3. *Geometry of the exposed Paleozoic massif*

The geological map on Fig. 3b and the cross-section on Fig. 5, which provide a synthesis of up-to-date surface and subcrop data, illustrate the structure of the Paleozoic inliers of the Boulonnais area. The Boulonnais Paleozoic massif is classically divided into three major tectonic units (from north to south respectively the Ferques, Haut-Banc and Hydrequent thrust units) separated on the geological map either by thrust zones (the Hydrequent thrust in Fig. 3b) or by sub-vertical WNW-ESE trending faults (the Ferques fault zone (FFZ) in Fig. 3b). This structure is basically the result of the Variscan stacking of several thrust-sheets as shown by boreholes and coal-mining excavations [e.g. 37, 39, 42].

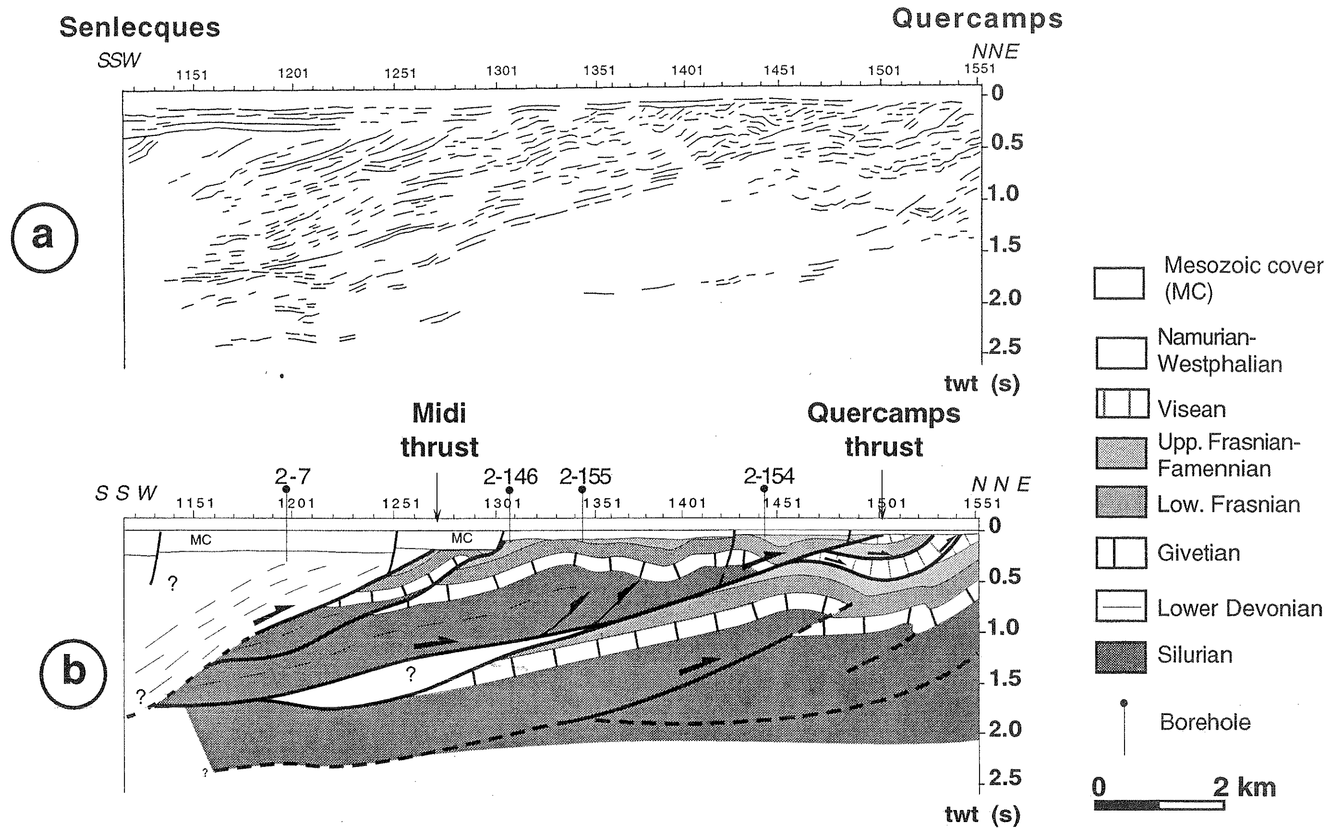

Fig. 4 (a) Line drawing of significant seismic reflectors along the line 85A (location in Fig. 2 (a)). (b) Interpreted seismic section of the profile 85A through the eastern border of the Boulonnais thrust belt. Boreholes 2-7, 2-146, 2-155 and 2-154 after [41].

The basal *décollement* zone of the imbricate stack is situated within the thick Silurian shales visible only locally (Caffiers railway cut) along the Landrethun culmination, on the northernmost border of the massif [35]. The emergence of the Middle-Upper Silurian substratum is interpreted as resulting from a thrust-related hangingwall anticline developed upon a blind thrust flooring the Boulonnais thrust-sheets, the Boulonnais basal thrust (BBT) (Fig. 5). This thrust-sheet, known as the Ferques unit, constitutes the lowermost thrust unit exposed in the Boulonnais massif. Displacement upon the BBT is suggested to be transferred forward by layer parallel slip on top of or within the Silurian shales. This thrust probably merges a few kilometres north of the Landrethun culmination on top of the slightly undeformed foreland of the Brabant massif as suggested by the subcrop geometry defined from boreholes [e.g. 39]. Borehole data furthermore suggest an important deepening of the base of the entire Devonian-Carboniferous cover south of the Landrethun culmination. This deepening is interpreted to result from the existence of a pronounced flexure of the Brabant foreland under the thick Variscan thrust stack forming the front of the belt. The flexure is highly localized and outlines the northern border of the crustal trough originating the Namurian-Westphalian foreland basin. Some south dipping normal faults that deforms the whole devono-carboniferous series along the backlimb of the Landrethun culmination (Fig. 5) could also accommodate part of the flexural behaviour of the crust.

At the surface, the south dipping basal unit ends against Visean carbonate layers from the Haut-Banc unit along a steep WNW-ESE striking fault zone i.e. the Ferques Fault Zone (FFZ) (Fig. 3b and Fig. 6) which can be tied to the system of sub-vertical fault zones observed in the Artois region (see Fig. 2b) [43]. At depth, boreholes show that the globally gently dipping Visean limestones forming the Haut-Banc Unit are however thrust onto the Namurian-Westphalian coal-bearing rocks situated on top of the Ferques unit (Fig. 5) [e.g. 37, 42]. The FFZ is thus cutting through both thrust units resulting in the uplift of the northern fault block. A vertical displacement of few hundred of meters may be inferred. On another hand, the location of the FFZ at the back-limb synclinal hinge of the Landrethun thrust-related anticline suggest that it branches at depth onto the base of the frontal ramp of the BBT. In detail, the map geometry of the FFZ shows that it forms a complex zone composed of numerous subvertical contacts (see the FFZ structure along its western segment in Fig. 7) which are laterally anastomosing (see the FFZ structure along its eastern segment in Fig. 6) [43]. Therefore, a kilometric scale vertical duplex structure can be deduced along the FFZ. The precise geometry of branching between the different tectonic contacts is however not possible to decipher due to the lack of good outcrops. In cross-section, the subsidiary faults involved in the FFZ display a diverging fan pattern (Fig. 7) that may be interpreted in terms of a flower

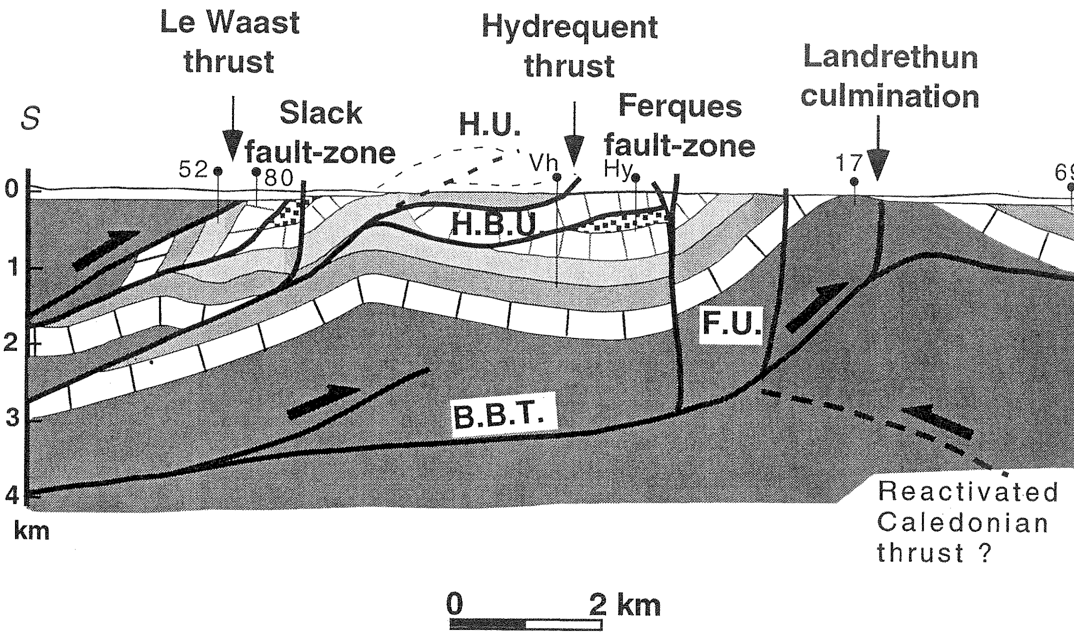

Fig. 5 Geological cross-section through the exposed Paleozoic massifs of the Boulonnais thrust belt based on field observations and borehole data. Same legend as in Fig. 4 (b). F.U.: Ferques thrust unit; H.B.U.: Haut-Banc thrust unit; H.U.: Hydrequent thrust unit; B.B.T.: Boulonnais basal thrust. Boreholes n° 52, 80, 17 and 69 refer to boreholes listed in Wallace [39]: 52: le Waast; 80: Surques; 17: Caffiers; 69: Pihen; Vh and Hy boreholes correspond respectively to the Vallée Heureuse and Hydrequent boreholes, after [37].

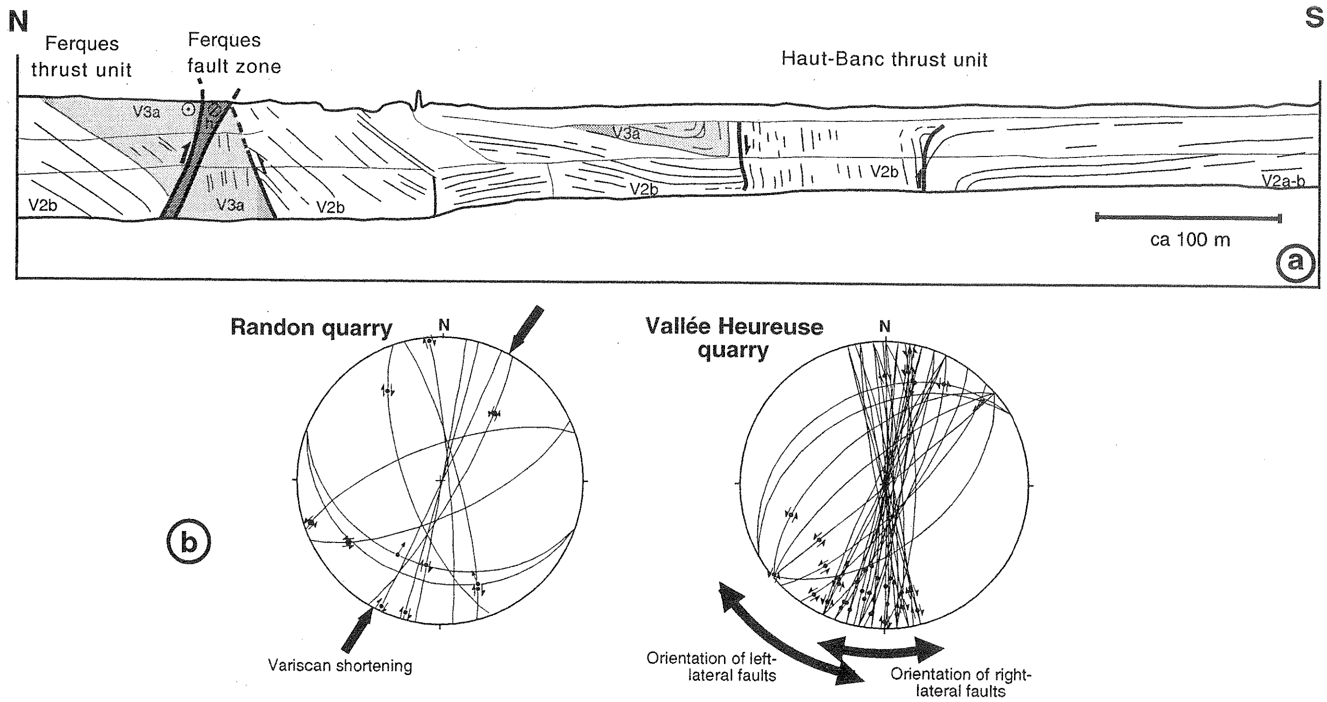

Fig. 6 (a) Sketch view (drawn from a photographic assemblage) of the geometry of Visean layers within the Haut-Banc thrust unit (Vallée Heureuse quarry) and its contact with the basal Ferques unit along the Ferques fault zone. V2a, V2b and V3a refer to different Visean layers, respectively Upper Arundian, Lower and Upper Holkerian levels. h refers to coal-bearing Westphalian molassic layers involved in the Ferques fault zone. (b) Stereodiagrams (lower hemisphere, equal area projection) showing the Variscan microfaults pattern within the Haut-Banc unit (southern part of Fig. 6a) and Ferques unit (northern part of Fig. 6a). Note the superposition of the orientations of dextral and sinistral faults suggesting a progressive change of shortening direction from N-S to NE-SW.

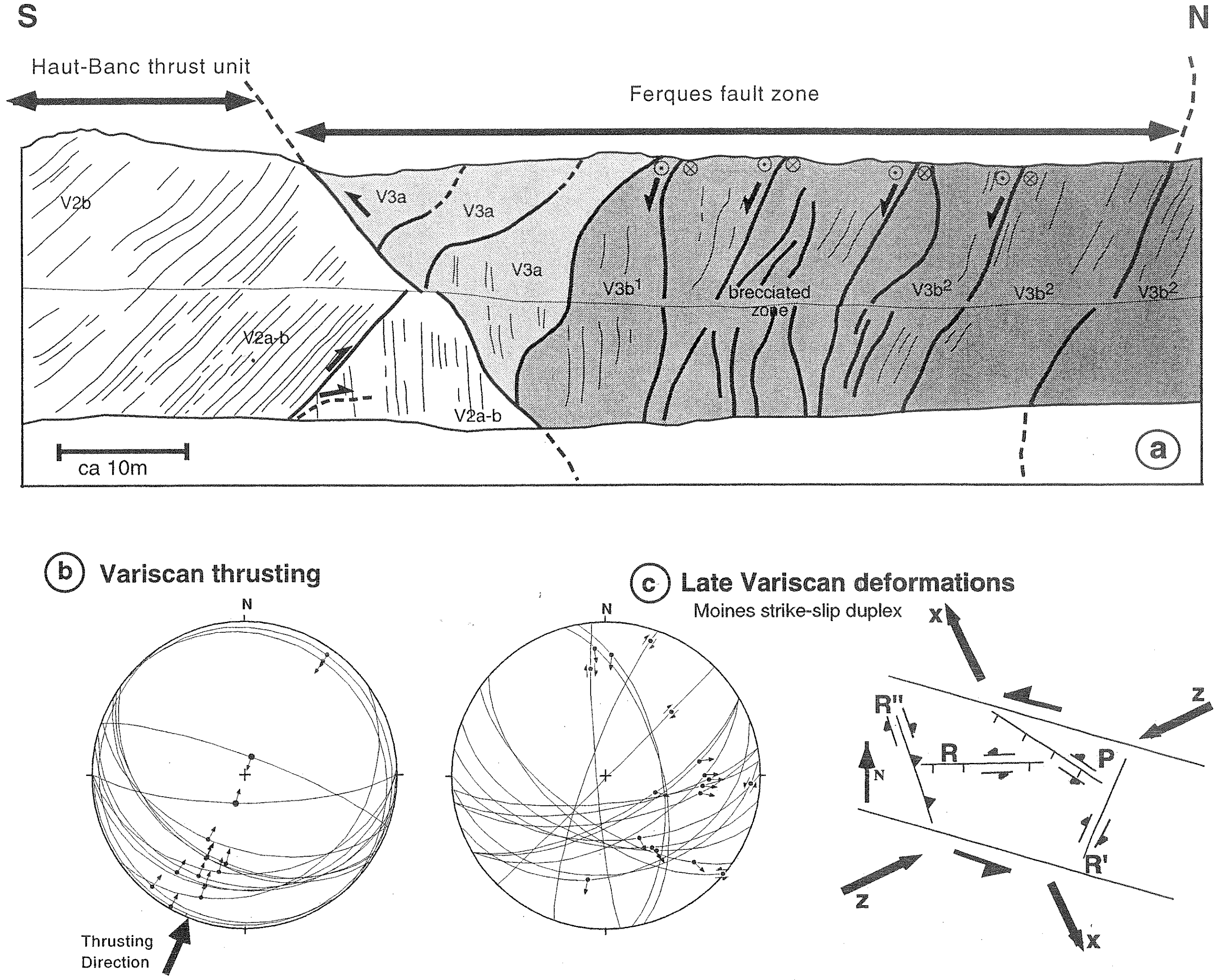

Fig. 7 (a) Sketch view (drawn from a photographic assemblage) of the attitude of the Visean layers at the tip of the Haut-Banc thrust zone (Moines quarry, location in Fig. 3b) and of the geometry of the cross-cutting Ferques Fault zone. V2a, V2b, V3a and V3b refer to Upper Arundian, Lower Holkerian, Upper Holkerian and Asbian levels respectively. (b) Stereodiagram (lower hemisphere, equal area projection) showing the striations along the forelimb thrusts dissecting the Variscan Moines frontal fold. (c) Stereodiagram (lower hemisphere, equal area projection) showing the microfaults measured within the Moines strike-slip duplex along the Late Variscan Ferques fault zone and integration in a model of Riedel type shear planes. R and P: synthetic Riedel planes showing a combined sinistral and normal displacement; R' and R'': antithetic dextral Riedel planes.

structure. Such geometry suggests a strike-slip displacement associated with the uplift of the northern border of the FFZ.

South of the FFZ, the Haut-Banc unit forms a gentle dome on top of Westphalian molassic layers of the basal Ferques unit as demonstrated by boreholes [e.g. 37]. It is affected however by hectometric fold structures associated with subsidiary thrusting due to the migration of décollement zones towards shallow interfaces. Folds, as exemplified in fig. 6, are characterized by very steep forelimbs, hinge convergent intra-formational thrusts and intense flexural slip as shown by the systematic striations observed upon the bedding planes. A fault-propagation mode of folding with transport upon the upper flat has been proposed for these structures [44]. The ease of layer-parallel slip within the finely bedded Visean limestones from the Haut-Banc unit may be a major controlling factor for such characteristic style of folding.

The Haut-Banc thrust-sheet is overthrust on its southern boundary by the Hydrequent thrust unit mainly composed of Upper Frasnian-Famennian shales. The latter is floored by the Hydrequent thrust that localizes in its footwall some hundred of meters wide slices of Tournaisian and Visean limestones (Fig. 8 and 9). The so-called "Basse-Normandie" thrust-sheets [31, 32] are composed of two sub-units. The lower one (lower duplex on Fig. 8 and 9) may be referred to as an intra-formational hinterland dipping duplex. It is developed in front of the upper thrust-sheets (UTS) which correspond to the dissected forelimb of a hangingwall anticline [32]. The latter formed above the basal thrust of the structure (UTS basal thrust on Fig. 8 and 9) which joins at depth the major Hydrequent thrust. The map (Fig. 3b)

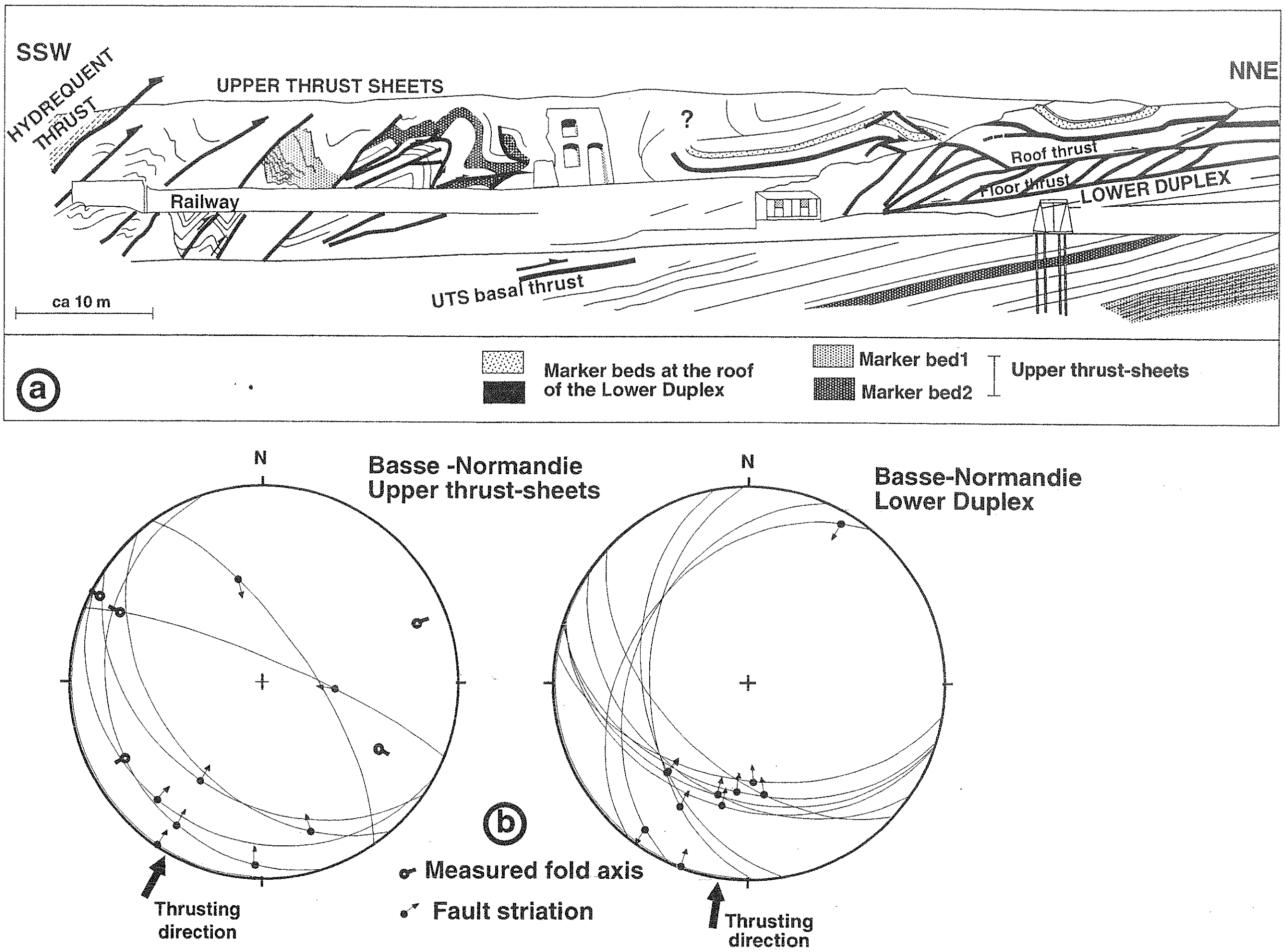

Fig. 8 (a) Sketch view (drawn from a photographic assemblage) of the geometry of the Basse-Normandie thrust-sheets in the footwall of the Hydrequent thrust (modified from [32]). b. Stereodiagrams (lower hemisphere, equal area projection) showing the strain markers (fold axes and microfaults) measured within the lower duplex and the upper thrust-sheets.

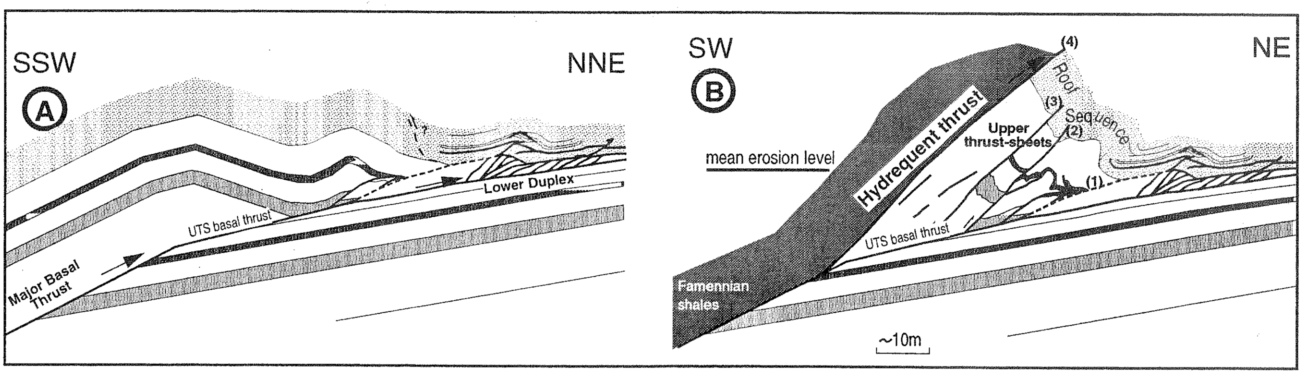

Fig. 9 Tectonic evolution of the Basse-Normandie thrust-sheets (modified from [32]): (1) Thrust-related hangingwall anticline developed above the Hydrequent basal ramp and lower duplex formation accommodating forward transfer of displacement; (2) Out-of-sequence activation of the Hydrequent thrust with deformation and dissection of the forelimb of the previous hangingwall anticline.

and the borehole data suggest that the Hydrequent thrust displays a curved synformal shape and deepens to the south along a south dipping thrust ramp. The latter localizes a steep multiphase fault zone (the Slack-Epitre fault) affecting Mesozoic rocks with a finite displacement inducing down-faulting of the southern fault block [34]. The geometry of the upper Hydrequent thrust and the Haut-Banc thrust (situated at the base of the the Haut-Banc unit) is very close to that observed along the northern part of the seismic profile 85A with the curved reflectors joining the major planar Quercamps thrust (Fig. 4b). We thus postulate that they form the same kind of imbricates with a curved thrust fan geometry cut through by a relatively planar south gently dipping thrust. In the Boulonnais massif, this structural pattern is not obvious from field observations due to a very bad exposure of the shaly Famennian rocks. On the other hand, such a geometry requires the existence of a deep-seated thrust-sheet which induced the folding of the superficial Hydrequent and Haut-Banc thrusts. This deep-seated culmination is very likely associated with the existence of a blind thrust zone which branches upon the BBT and roots within the Silurian shales of the substratum.

South of the Hydrequent thrust, the geometry is not so well constrained as it is only known from boreholes [39]. The MTZ, the emerging part of the major basal thrust of the allochthonous Variscan wedge, can not be precisely defined but, as classically observed along the allochthonous Rheno-hercynian units [e.g. 16], it likely corresponds to the emergence of Lower Devonian red sandstones some kilometres south of the outcropping Paleozoic rocks (Fig. 2a). Identification of Silurian rocks in Le Waast borehole directly south of the exposed Paleozoic massif imply the existence of a basement thrust-sheet on top of the Boulonnais thrust-system (floored by Le Waast thrust in Fig. 5). This structure probably corresponds to a basement slice deformed in the footwall of the MTZ. Moreover, the subcrop geometry beneath the Le Waast thrust (borehole 80 in Fig. 5) suggest the occurrence of an overturned thrust sheet composed of Upper Devonian and Lower Carboniferous rocks. This structure probably have a similar origin as the lens-shaped horse observed on seismic data i.e. the out-of-sequence dissection and simple shear of the forelimb of an hangingwall anticline. Such deformation argue for a significant out-of-sequence activation of the MTZ.

The cross-section of Fig. 10g illustrates the geometry of the Boulonnais thrust belt in the footwall of the MTZ reconstructed before the dissection by vertical faults. This cross-section is constructed parallel to the average thrust transport direction and supposes a reduced amount of lateral displacement associated to the Ferques fault zone. These classical assumptions of nearly plane strain, postulated at this point of our interpretation, will be argued in the following kinematic section.

Considering the final geometry of the Boulonnais thrust belt after the Variscan shortening, it is thus possible to draw significant differences compared with the situation observed in the Western Ardennes thrust belt (Fig. 2b). A major point to be emphasized is the reduced amount of allochthonous displacement upon the MTZ in the Boulonnais thrust belt and a somewhat bigger degree of truncation of the MTZ footwall thrust-sheets. Folding and thrusting in the Boulonnais foreland thrust belt accomodate a total shortening of about 52% of the external part of the northern Rheno-hercynian margin (Fig. 10g).

3. Kinematics of the Boulonnais thrust front

3.1. *Sequence of thrusting*

Concerning the propagation of thrusting in the Boulonnais thrust belt, a rather complex scenario may be emphasized. A striking characteristic of the exposed thrust units is that the *décollement* zone flooring each unit is situated within a different stratigraphic horizon: the Silurian shales for the Boulonnais basal thrust, the base of Carboniferous layers for the intermediate Haut-Banc thrust and the Upper Frasnian shales for the Hydrequent thrust (Fig. 5). As discussed previously, the two upper thrust-sheets (Haut-Banc and Hydrequent) branch very rapidly at depth onto the south dipping relatively planar thrust ramp merging at the back of both units (equivalent to the Quercamps thrust along the seimic profile). This forms an imbricate thrust fan in the footwall of the major planar thrust which probably dies out within Silurian shales and joins the MTZ at depth. The kinematics of the "Basse-Normandie" thrust-sheets, situated in the footwall of the Hydrequent thrust, help for discussing the thrust sequence within the thrust fan. Thrust relationships as well as the analysis of the internal deformation of thrust-sheets [32] document the out-of-sequence activation of the Hydrequent thrust with respect to the deformation of the Haut-Banc thrust unit (Fig. 9). The Hydrequent thrust is shown to cut through and to deform the forelimb of a previously developed hangingwall anticline associated with the forward propagation of displacement within the Visean carbonates of the Haut-Banc unit. These subsidiary structures, which are developed in the footwall of the Hydrequent thrust, thus argue for a break-backward sequence of thrusting of the whole thrust fan with first the activation of the Haut-Banc thrust and second that of the higher Hydrequent thrust. The sequence would end by thrusting along the Quercamps thrust and its equivalent in the exposed Paleozoic massif of the Boulonnais. Such an out-of-sequence thrusting could moreover well explain the lens-shaped horse located at depth at the base of the Quercamps thrust. As all thrusts branch onto the same major footwall ramp, it is suggested that they result from the sequential break-backward dissection of a previous major ramp-flat-shaped thrust structure the basal thrust of which would merge along the Haut-Banc thrust (Fig. 10d and e).

Such a scenario of deformation implies an initial foreland propagating thrusting at least up to the outer BBT (Fig. 10b and c) followed by the blocking of forward transfer of displacement inducing the out-of-sequence activation of the pre-existing thrust ramps at the back of the Haut-Banc thrust (Fig. 10d, e, f). Taking into account that the Haut-Banc and Hydrequent thrusts are folded on top of a deep-seated thrust that roots within the Silurian shales, it is inferred that the latter is developed lately, probably in response to the locking of movement along the BBT (Fig. 10g).

This whole sequence reveals some difficulties in the propagation of displacement towards the foreland. On the other hand, subsidiary back-thrusting along the relatively steeply dipping (ca 45°) back-limb of the Landrethun anticline [38] associated with south-vergent minor folds are additional indicators for a regional blocking of displacement towards the foreland of the northern Variscan thrust front along the Boulonnais segment. The reasons for such

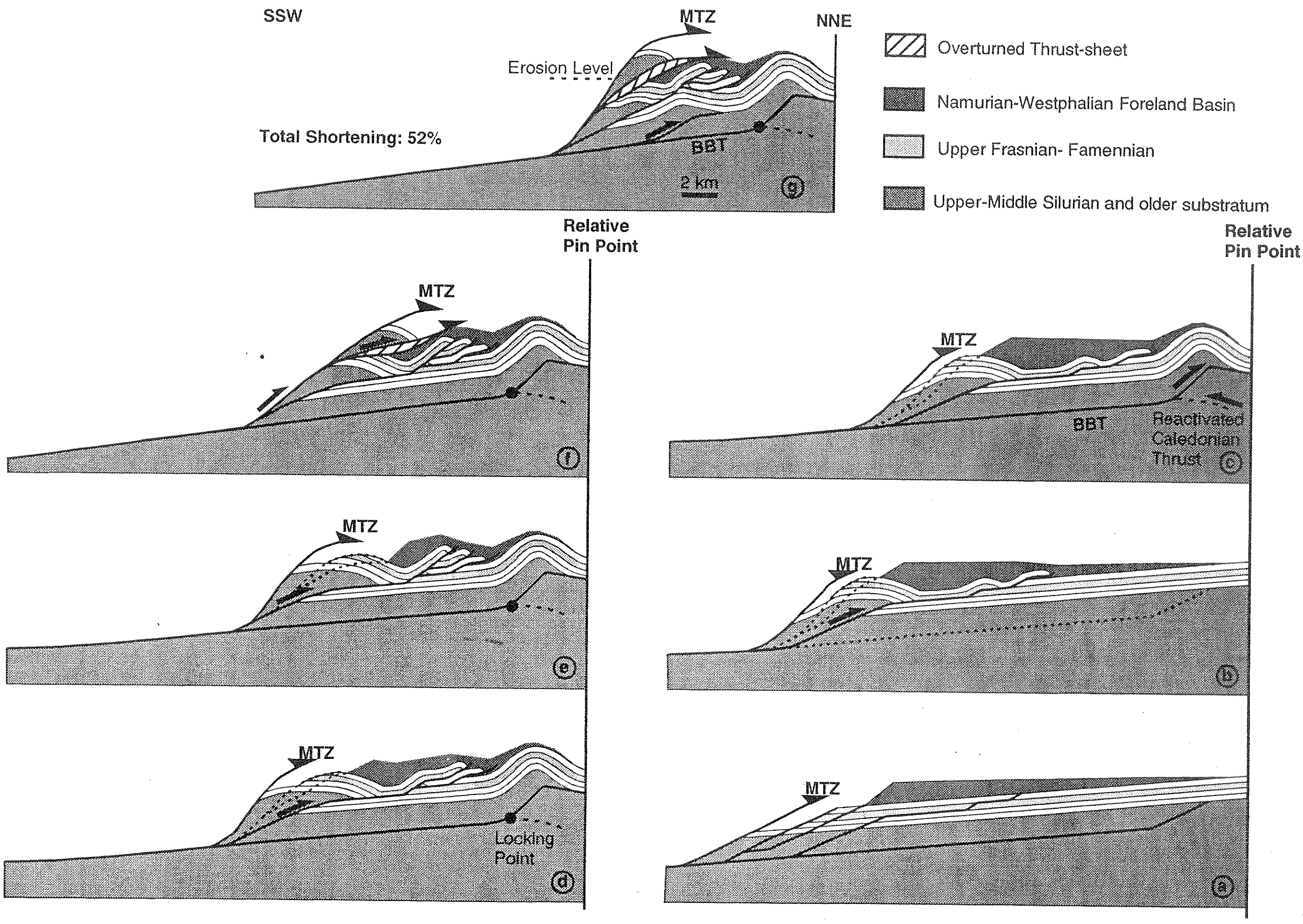

Fig. 10 A model for the sequential development of thrusting within the Boulonnais thrust-belt. Cross-sections are constructed parallel to the averaged thrust transport direction. Late strike-slip displacement along the Ferques fault zone is removed (see text for discussion). (a): initial state (mid-Westphalian); (b) and (c): piggy-back propagation of the thrusting with a frontal thrust wedge development (c) due to the reactivation of a deep-seated inherited thrust; (d), (e), (f) and (g): out-of-sequence thrusting due the locking of forward displacement inducing a localized thrust stack and the pronounced flexure of the underthrust unit. MTZ: Midi thrust zone; BBT: Boulonnais basal thrust.

a buttress effect of the Brabant massif is somewhat enigmatic. However, recent studies of potential field data along a Boulonnais-Brabant massif transect [45] suggest the existence of an inherited southward directed thrust zone within the Caledonian basement the reactivation of which during Variscan times could have form a sort of intracutaneous wedge hindering the northward propagation of Variscan thrust-sheets (Fig. 10c). Such deep-seated southward directed thrusts have also been observed at the southern edge of the Brabant massif along the ECORS "Nord de la France" seismic line [25]. The localized stacking of thrust-sheets induced by this frontal wedging process could explain the pronounced flexure of the substratum observed conspicuously along the Northern France Variscan thrust front [e.g. 16].

In terms of timing, the youngest molassic rocks imvolved in the exposed thrust structures in the Boulonnais are of Westphalian A age [23]. Further east, in the Artois region, Upper Westphalian rocks are deformed in the footwall of the MTZ [20]. As corroborated by the inclination data of syn-deformational remagnetizations compared to the reference curves of polar wander for the "Old Red Sandstones" Continent [6, 46], a Late Westphalian- Lower Stephanian age may be proposed for the whole thrust sequence along the frontal parts of the Northern Variscan thrust front.

As previously mentioned, subsequent to the thrusting event, the Boulonnais thrust units are cut through by steeply dipping faults localized along the ramp of previous thrust structure. For instance, the Ferques fault zone joins the base of the Boulonnais basal thrust frontal ramp and the Slack-Epitre fault is controlled by the ramp situated at the back of the Hydrequent thrust (Fig. 5). Both faults display a south down-faulted block and thus are likely to be associated with the steeply dipping fault system evident along the Artois thrust front. Within this *en-échelon* fault network, some faults such as the Slack-Epitre fault show a multiphase activation with significant Mesozoic and Cenozoic displacements [47]. Conversely, the Ferques fault zone is buried beneath a Middle Jurassic sedimentary cover implying no younger deformation event than Late Paleozoic to Early Mesozoic. North of the Ferques fault, associated subsidiary faults with a NNE-SSW trend (Fig. 3b) display karstic excavations fed with sands of Rhetian to Middle Jurassic age [e.g. 48]. Furthermore, paleomagnetic data from calcite veins related to the movement along the Ferques fault zone show the deformation to be older than Middle Triassic [49]. Considering the very likely Upper Stephanian-Middle Permian age of the conglomeratic sequence deposited along some comparable fault zones in the Artois region, we postulate the same age for the activation of the Ferques fault zone. These whole data thus argue for a Late Paleozoic (Upper Stephanian to Middle Permian) dissection of the Northern Variscan thrust front by a network of ENE-WSW striking sub-vertical faults.

3.2. Kinematics of small-scale deformations

The analysis of small-scale strain markers has been carried out within the Boulonnais Paleozoic massif. As currently observed in such outer parts of orogens, the deformation is mainly recorded by faulting and folding with few traces of internal deformation. Cleavage is thus expressed only very locally within shaly horizons in the vicinity of thrusts. For example, in a mylonitic zone within the direct footwall of the Hydrequent thrust [42], pressure solution cleavage is observed within Tournaisian shales dipping 65° towards the N215E. It is associated there with minor folds displaying about N140E trending axes.

Laterally, a few hundred of meters to the east, within the Basse-Normandie thrust-sheets, that developed within calcareous levels, shear fibres of calcite developed along the thrust planes document a general NNE-directed thrusting event (Fig. 8b). When looking these data further in detail, two groups of striations may be differenciated. One is associated to the south dipping internal thrust planes of the lower duplex, which is shown to develop before the upper thrust sheets. These striations document a dominantly N- to NNE-directed displacement (Fig. 8b). Within the upper thrust-sheets, kinematic data are evidently more scattered as they result from a multiphase deformation history but striations as well as minor fold axes show a dominant NE-SW oriented shortening, which is in good agreement with the cleavage and fold axes orientation observed laterally in the footwall of the Hydrequent thrust. Some ca N070E trending fold axes are also observed within the thrust-sheets (Fig. 8b). As such trending folds are restricted to a very local domain, it is inferred that they represent oblique folds connected to the rapid lateral plunge of the structure towards the west.

Within the Haut-Banc thrust unit, few minor fold-thrust structures crop out. The most prominent one is situated at the tip of the Haut-banc thrust (Fig. 7a). South of the Ferques fault zone, the Moines quarry displays a very sharp N120E trending anticline the vertical forelimb of which is dissected by an important set of out-of-sequence thrusts. In agreement with structures observed beneath the Hydrequent thrust, these late structures evidence a well-defined NE-directed (ca N025E) thrusting event (Fig. 7b).

Elsewhere in the Haut-Banc and Ferques units, Variscan deformation is mostly recorded by vertical conjugate strike-slip faults showing a consistent N-S to NE-SW shortening (Fig. 6b). However, we can observe a slight overlap in the direction of dextral and sinistral faults. This sort of inconsistency in the data set must be considered in the light of the kinematic data from the Basse-Normandie thrust-sheets which show a progressive change of the thrusting direction from N to NE between the lower and upper thrust-sheets. Accordingly, the directional overlap of dextral and sinistral faults may be interpreted as the result of a progressive rotation of the apparent Variscan shortening direction. Some additional complexity may also arise from late movements during the Tertiary inversion of the Boulonnais Mesozoic basin [47]. The contribution of these late movements to the bulk fault pattern is however very difficult to evaluate. Nevertheless, the whole kinematic data measured in Variscan structures from the Boulonnais massif are globally concordant and, combined with considerations upon the sequential development of thrusting, suggest a progressive evolution of thrust transport from dominantly N- to NE-directed.

The whole Variscan compressional structures are cut through by Late Paleozoic subvertical fault zones as exemplified by the Ferques fault zone. Locally, the latter involves a set of subsidiary faults defining vertical duplexing of the previously folded Visean layers (Fig. 7) [43]. The Visean limestones there exhibit particularly well developed brittle microstructures (Fig. 7c). Vertical duplexes are bordered by a set of about E-W trending irregular faults with a dominant steep southern dip. They mostly exhibit an oblique displacement with a left-lateral component associated with a normal one. The relative variations of left-lateral versus normal component of displacement is likely to characterize a mechanism of strain partitioning within a globally transtensional fault system as exemplified by sand-box modelling [e.g. 50]. Within individual duplexes, some antithetic dextral subvertical faults range from N160E to N045E. The great orientation scatter of minor faults within the fault zone is likely to be due to the rotational deformation during simple shear process and does not allow the application of classical tensorial analysis of fault populations. However, as classically observed in shear zones, microfaults are organized as Riedel systems of synthetic and antithetic shear planes (Fig. 7c) that consistently indicate a major left-lateral motion along the Ferques fault zone. Horizontal displacement is difficult to precisely quantify due to the lack of cartographic markers. However, taking into account the pitch of striations on fault planes synthetic to the general displacement (between 20 and 40° in average) and the observed vertical displacement (about 250 meters), it is possible to approximate an about 500 meters of horizontal displacement i.e. a reduced amount of lateral movement compared to the shortening accommodated by previous folding and thrusting.

4. A model for the evolution of the SE England-Boulonnais Northern Variscan thrust front in Late Paleozoic times

Structural data presented above allow a better definition of the tectonic evolution of the frontal parts of the SE England-Boulonnais segment of the Western European Variscan thrust belt. Within the study area, folding and thrusting occurred during Late Westphalian-Lower Stephanian times (ca 305 Ma BP after Menning's *et al.* time scale [51]) in response to the latest increments of inversion along the northern margin (or Brabant margin) of the Devonian Lizard-Rheno-hercynian oceanic basin. Closure of this ocean probably occured in Latest Devonian-Early Carboniferous times [e.g. 9, 52] and compressive deformations gradually progressed through its northern margin during Visean to basal Stephanian times. Thrusts developed in sequence towards the frontal parts of the belt upon a major crustal scale basal thrust i.e. the "Midi" thrust, the deformed footwall of which is observed in the Boulonnais thrust belt. Within the latter very frontal parts of the belt, an average top to the NNE displacement is evidenced during this primary in-sequence thrust activation (Fig. 11). An important out-of-sequence dislocation of the previous fold-thrust pattern is documented in the Boulonnais showing a general blocking of forward transfer of displacement towards the Caledonian Brabant massif. The induced deformation of the thrust front results in a strongly localized tectonic stack which implies a pronounced flexure of the underthrust crustal block. The buttress effect of the Brabant massif is suggested to be related to the reactivation of a deep-seated Caledonian north dipping thrust [45] forming an intracutaneous wedge in front of the northward propagating Variscan structures (Fig. 10). During this late event, thrust motion progressively tends to rotate clockwise towards the NE direction. Thrusting directions in the Boulonnais thrust belt thus significantly deviate from the top to the NNW directed displacement observed along the other segments of the thust front such as the Ardenno-Rhenish [12] and SW England [53, 54] massifs (Fig. 11).

Although no direct evidence of dextral wrenching can be observed along the frontal part of the belt, the existence of the Variscan dextral strike-slip Bray fault zone within more internal thrust units [30] argues for a general transpressional setting of the Northern France NW-SE trending Variscan belt. Such major wrench faults within the hinterland of thrust belts are very frequent in orogenic systems and are classically interpreted in terms of strain partitioning during an oblique collisional process [e.g. 55]. Likewise, we consider the association of the Boulonnais frontal thrust system and the hinterland dextral Bray fault zone to result from the strain partitioning of a general NNW-SSE directed convergence along an oblique NW-SE trending continental margin inherited from the Devonian geometry of the Lizard-Rheno-hercynian basin (Fig. 11). As previously stated by Rippon *et al.* [40], the SE England-Boulonnais thrust belt would

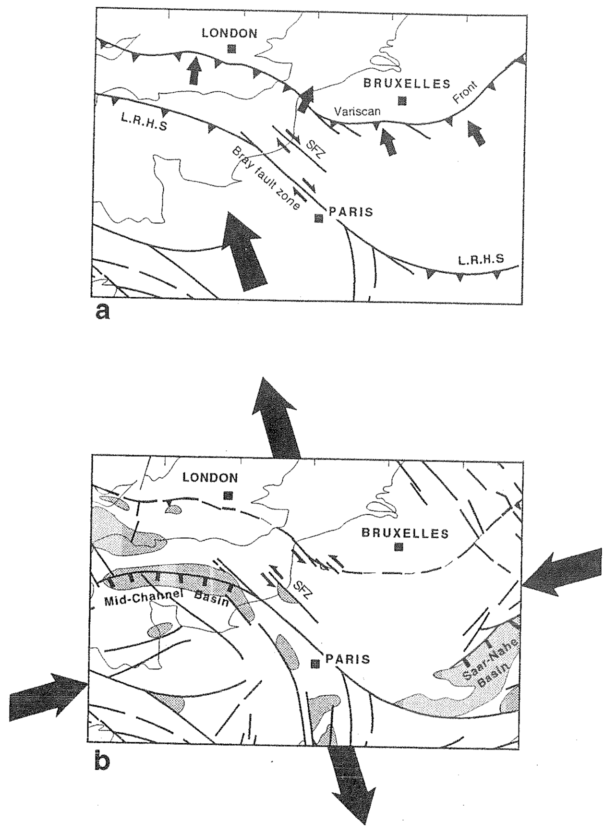

Fig. 11 A model showing (a) the Variscan (Late Westphalian-Lower Stephanian) and (b) the Late Variscan (Upper Stephanian-Middle Permian) kinematics of deformations along the Northern France Variscan thrust front. Structural framework modified from [65]. L.R.H.S.: Lizard Rheno-Hercynian Suture Zone. SFZ: Somme fault zone.

thus represent an oblique transfer zone between the Ardenno-Rhenish and SW England frontal belts. Therefore, the Northern Variscan thrust front appears as a highly segmented belt developed in response to an important Early Devonian basin pre-structuration. Structural inheritance is probably the fundamental parameter controlling the present-day arcuate shape of the Western European Variscan thrust front as also suggested by paleomagnetic data [6, 13, 46].

The Late Westphalian-Early Stephanian thrust front is shown to be cross-cut by a network of Late Paleozoic (Upper Stephanian-Middle Permian) WNW-ESE striking sub-vertical faults accommodating both vertical and strike-slip displacements. These faults reactivate the major Variscan footwall thrust ramps inducing systematic down-faulting of the southern fault blocks. Among this fault network, the Ferques fault zone displays a kilometric-scale strike slip duplex structure showing in cross-sections a flower-like geometry. Microfaults within this deformed zone document a left-lateral displacement associated with a normal component. The resultant transtensional deformation zone implies a NNW-SSE directed stretching and a ENE-WSW directed shortening. The orientation of the strain axes is corroborated by magnetic fabric data measured within some Upper Carboniferous coal-bearing layers involved in the Ferques fault zone [43].

This Late Paleozoic transtensional event is a very common structural feature of the northern Variscan thrust front as it is also evidenced by microfault analyses in the Artois Nord-Pas de Calais coal basin (Estevelles mine hole, [23]) as well as in some Stephanian-Permian basins from England [56, 57]. On the other hand, this deformation pattern well agrees with the existence of an about N-S directed post-Variscan and pre-Middle Permian extensional event in the Sarre-Nahe intramontane basin of NE France-SW Germany [58]. Considering more internal Variscan domains, it also fits the Late Variscan activation of widespread basin associated strike-slip fault zones in the French Massif Central [59, 60], the Western Alps [61], the Southern France [62, 63] and the Bohemian domains of Central Europe [64], which were all induced in a general about N-S trending stretching and E-W trending shortening. These data illustrate the systematic rotation of the shortening direction from a nearly N-S orientation during Variscan times (Visean up to Early Stephanian) to a nearly E-W orientation during Late Variscan times (Middle Stephanian-Early Permian) [e.g. 65].

Within the Northern Variscan framework, the system of WNW-ESE trending faults situated between the Bray fault zone area and the SE England-Boulonnais-Artois thrust front can be considered in Upper Stephanian-Early Permian times as a zone of left-lateral transtensional relay between the highly subsiding extensional basins from the Western Channel-Southern England [e.g. 28, 66] and Saar-Nahe region [58, 67] which display an orientation normal to the NNW-SSE extension direction active at that time (Fig. 11). This deformation pattern is likely to result from the accommodation of a nearly N-S directed extension by an already structured Variscan substratum, as shown by the moulding of Late Variscan structures upon the Variscan thrust pattern (Fig. 11). This mechanism contributed to the thinning and thermal restoration of the external parts of the thickened Variscan crust [68] and could possibly initiate the Paris basin subsidence as early as in Stephanian-Autunian times as suggested by subsidence-thermal modelling [69].

Acknowledgments

The authors wish to thank G. Manby, M. Everaerts, J. Chen, L. Csontos, M. Lewandowski, T. Pharaoh, F. Bergerat, D. Vachard and F. Meilliez for stimulating discussions either in the field or upon the general tectonics of the Boulonnais area. We also acknowledge the Carrières du Boulonnais, de la Vallée Heureuse and Randon for the permissions to enter the quarries. M. Faure and an anonymous reviewer are gratefully acknowledged for their pertinent comments on this study. This paper is a contribution of the "Atelier Manche-Mer du Nord" of the Unité Mixte de Recherches CNRS 8110 "Processus et Bilans des Domaines Sédimentaires".

References

[1] S. Eldredge, V. Bachtadse, R. Van der Voo, Paleomagnetism and the orocline hypothesis, Tectonophysics 119 (1985) 113-128.

[2] H. Perroud, Paleomagnetic evidence for tectonic rotations in the Variscan mountain belt, Tectonics 5 (1986) 205-214.

[3] V. Bachtadse, R. Van der Voo, Paleomagnetic evidence for crustal and thin-skinned rotations in the European Hercynides, Geophys. Res Let. 13 (1986) 161-164.

[4] R. Dias, A. Ribeiro, The Ibero-Armorican Arc: A collision effect against an irregular continent?, Tectonophysics 246 (1994) 113-128.

[5] A.B. Weil, R. Van der Voo, B.A. Van der Pluijm, J.-M. Parès, The formation of an orocline by multiphase deformation: a paleomagnetic investigation of the Cantabria-Asturias Arc (northern Spain), Journal of Structural Geology 22 (2000) 735-756.

[6] E. Marton, J-L. Mansy, O. Averbuch, L. Csontos, The Variscan belt of Northen France—Southern Belgium: geodynamic implications of new paleomagnetic data, Tectonophysics 324 (2000) 57-80.

[7] J-B. Edel, The rotations of the Variscides during the carboniferous collision: paleomagnetic constraints from the Vosges and the Massif Central (France), Tectonophysics 332 (2001) 69-92.

[8] P. Matte, Accretionary history and crustal evolution of the Variscan belt in Western Europe., Tectonophysics (1991) 196, 309-337.

[9] W. Franke, The mid-European segment of the Variscides: Tectonostratigraphic units, terrane boundaries and plate tectonic evolution. In Orogenic processes: quantification and modelling in the Variscan Belt, W. Franke, V. Haak, O. Oncken and D. Tanner (Eds.), Geological Society of London Spec. Pub. 179 (2000) 35-61.

[10] F. Kossmat, Gliederung des varistischen Gebirgsbaues, Abhandlungen des Sächsischen Geologischen Landesamtes 1 (1927) 1-39.

[11] F. Meilliez, L. André, A. Blieck, W. Fielitz, O. Goffette, L. Hance, A. Khatir, J-L. Mansy, P. Overlau, J. Verniers, Ardenne-Brabant, Sci. Géol. Bull. 44 (1991) 3-29.

[12] F. Lacquement, L'Ardenne varisque. Déformation progressive d'un prisme sédimentaire pré-structuré, de l'affleurement au modèle de chaîne. Publication de la Société géologique du Nord 29 (2001) 285p.

[13] O. Averbuch, F. Lacquement, R. Szaniawski, J-L. Mansy, M. Lewandowki, Segmentation of the Variscan thrust front (N France-S Belgium): insights into the geometry of the Devonian Rheno-hercynian basin, Contributions to the Geology of Belgium and Northwest Europe, Degryse P. and Sintubin M. (Eds.), Aardk. Mededel. 12 (2002) 89-92.

[14] J-F. Raoult, F. Meilliez, The Variscan front and the Midi fault between the Channel and the Meuse River, Journal of Structural Geology 9 (1987) 473-479.

[15] M.A. Houchen, Structural modelling of the external Variscides of France and Belgium, unpublished pHD thesis, National University of Ireland, (1988) 227p.

[16] F. Lacquement, J-L. Mansy, F. Hanot, F. Meilliez, Retraitement et interprétation d'un profil sismique pétrolier méridien au travers du massif paléozoïque ardennais (Nord de la France), C.R. Acad. Sci. Paris 329 (1999) 471-477.

[17] A. Plesch, O. Oncken, Orogenic wedge growth during collision - constraints on mechanics of a fossil wedge from its kinematic record (Rhenohercynian FTB, Central Europe), Tectonophysics 309 (1999) 117-139.

[18] R. Adams, N. Vandenberghe, The Meuse section across the Condroz-Ardennes (Belgium) based on a predeformational sediment wedge, Tectonophysics 309 (1999) 179-195.

[19] O. Oncken, A. Plesch, J. Weber, W. Ricken, S. Schrader, Passive margin detachment during arc-continent collision (Central european Variscides), in Orogenic processes: quantification and modelling in the Variscan Belt, W. Franke, V. Haak, O. Oncken and D. Tanner (Eds.), Geological Society of London Spec. Pub. 179 (2000) 199-216.

[20] A. Bouroz, J. Chalard, A. Dalinval, M. Stiévenard, La structure du bassin houiller du Nord de la France de Douai à la frontière belge. Annales de la Société géologique du Nord 81 (1961) 173-220.

[21] B. Le Gall, Deformation of the Nord-Pas de Calais Carboniferous coalfield (France) in the Variscan frontal tectonic pattern, in Hydrocarbon and Petroleum geology of France, A. Mascle (Ed.), Springer Verlag (1994) 379-398.

[22] A. Bouroz, La structure du bassin houiller du Pas-de-Calais à l'ouest du méridien de Lens, Annales Société géologique Nord 68 (1948) 93-105.

[23] J-F. Becq-Giraudon, Synthèse structurale et paléogéographique du bassin houiller du Nord et du Pas-de-Calais, Mem. BRGM 123 (1983) 68p.

[24] M. Everaerts, J-L. Mansy, Le filtrage des anomalies gravimétriques: une clé pour la compréhension des structures tectoniques du Boulonnais et de L'Artois (France), Bull. Soc. géol. France 172 (2001) 267-274.

[25] M. Cazes, A. Mascle, G. Toreilles, C. Bois, B. Damotte, P. Matte, J-F. Raoult, V.N. Pham, A. Hirn, A. Galdeano, Large Variscan overthrusts beneath the Paris basin, Nature, 323 (1986) 144-147.

[26] E. Mériaux, Observations sur les conglomérats et marbres rouges de l'Artois, Ann. Soc. Géol. Nord 81 (1961) 65-71.

[27] J-L. Mansy, L. Csontos, D. Rolin, F. Hanot, F. Bergerat, D. Vachard, Variscan structures and their reactivation in Artois (N France), EGS-AGU-EUG meeting, Nice, Geophysical Research Abstracts 5 (2003) 01985.

[28] R.A. Edwards, G. Warrington, R.C. Scrivener, N.S. Jones, H.W. Haslam, L. Ault, The Exeter Group, south Devon, England: a contribution to the early post-Variscan stratigraphy of northwest Europe, Geol. Mag. 134 (1997) 177-197.

[29] J-P. Colbeaux, L'évolution structurale du sud de la Belgique et du nord de la France: sa relation avec la dérive des continents – quelques hypothèses, Bull. Soc. belge Géol. 93 (1984) 71-78.

[30] P. Matte, J.-P. Respaut, H. Maluski, J. Lancelot, M. Brunel, La faille NW-SE du Pays de Bray, un décrochement ductile dextre hercynien: déformation à 330 Ma d'un granite à 570 Ma dans le sondage Pays de Bray 201, Bull. Soc. géol. France 8 (1986) 69-77.

[31] M.A. Cooper, M.R. Garton, J-R. Hossack, The origin of the Basse-Normandie duplex, Boulonnais, France, Journal of Structural Geology 5 (1983) 139-152.

[32] O. Averbuch, J-L. Mansy, The "Basse-Normandie" duplex: evidence for an out-of-sequence thrusting overprint, J. Struct. Geol. 20 (1998) 33-42.

[33] E.R. Shephard-Thorn, R.D. Lake, E.A. Atitullah, Basement control of structures in the Mesozoic rocks in the Strait of Dover region, and its reflexion in certain features of the present land and submarine topography, Phil. Trans. Roy. Soc. London 272 (1972) 99-113.

[34] J-L. Mansy, G.M. Manby, O. Averbuch, M. Everaerts, F. Bergerat, B. Van Vliet-Lanoe, J. Lamarche, S. Vandycke, Dynamics and inversion of the Mesozoic basin of the Weald-Boulonnais area: role of basement reactivation, Tectonophysics 373 (2003) 161-179.

[35] J-M. Dégardin, J-L. Mansy, A. Le Hérissé, T. Servais, P. Steemans, J. Verniers, Identification du Silurien par Acritarches et Chitinozoaires dans le Boulonnais (Nord de la France): implcations géodynamiques et paléogéographiques, Early Paleozoic Paleogeography of Western Europe and North Africa, Université de Lille (2001) 18.

[36] O. Oncken, C. v. Winterfeld, U. Dittmar, Accretion of a rifted passive margin—the Late Paleozoic Rhenohercynian fold and thrust belt (Mid-european Variscides), Tectonics 18 (1999) 75-91.

[37] A. Bouroz, Contribution à l'étude de la structure du bassin houiller du Boulonnais. Annales de la Société géologique du Nord 82 (1962) 27-37.

[38] A. Lefrancois, J-F. Deconinck, J-L. Mansy, J-N. Proust, Structure, sédimentologie et minéralogie des argiles des formations de Beaulieu et d'Hydrequent (Dévonien supérieur du Bas Boulonnais), Annales Société géologique Nord 2 (1993) 123-135.

[39] P. Wallace, The subsurface Variscides of southern England and their continuation into continental Europe, in The Variscan fold belt in the British Isles, P.L. Hancock (Ed.), Adam Hilger Ltd, Bristol (1983) 198-208.

[40] J.H. Rippon, R.A. Gayer, M. Miliorizos, Variscan structures in the Kent coaldfield, southeast England, and their regional significance, Geol. Mag. 134 (1997) 885-867.

[41] A. Bonte, J. Leplat, J. Sommé, Carte géologique de Desvres (1/50 000), B.R.G.M. editions, Orléans (1982).

[42] P. Pruvost, G. Delépine, Observations sur la faille d'Hydrequent et sur les couches de base du Carbonifère dans le Bas-Boulonnais, Bulletin de la Société géologique de France 21 (1921) 189-206.

[43] O. Averbuch, J-L. Mansy, J. Lamarche, Déformations tardi-paléozoïques au front septentrional de la chaîne varisque: l'exemple des massifs paléozoïques du Boulonnais (N France), Annales Société géologique Nord 9 (2001) 13-25.

[44] E. Mercier, J-L. Mansy, Le blocage du transport sur le plat de plis de propagation: une cause possible des chevauchements hors séquence, Geodinamica Acta 8 (1995) 199-210.

[45] J. Chen, J-L. Mansy, M. Everaerts, J.-L. Wang, Application of normalized total gradient method to tectonic research, Bulletin de la Société géologique de France, submitted.

[46] R. Szaniawski, M. Lewandowski, J-L. Mansy, O. Averbuch, F. Lacquement, Syn-folding remagnetizations in the French-Belgium Variscan thrust front as markers of the fold-and-thrust belt kinematics, Bull. Soc. géol. France 174 (2003) 511-523.

[47] J. Lamarche, F. Bergerat, J-L. Mansy, Déformation cassantes et plicatives dans le Jurassique du Boulonnais, influence lithostructurale et héritage paléozoïque. Compte Rendu Académie Sciences Paris 326 (1997) 57-63.

[48] J-L. Mansy, F. Amedro, J-P. Auffret, P. Guennoc, J. Lamarche, D. Lefevre, F. Robaszynski, J. Sommé, J-P. Vidier, Carte géologique de Marquise (1/50000), 2nd edition, B.R.G.M. editions, Orléans (in press).

[49] M. Lewandowski, J. Lamarche, J-L. Mansy, O. Averbuch, R. Szaniawski, Palaeomagnetic dating of brittle tectonics structures: case studies on Ferques Fault (Boulonnais, France) and two faults from the Holy Cross Mountains (Poland). Compte Rendu Académie Sciences Paris 329 (1999) 495-502.

[50] P. Richard, P. Cobbold P., Experimental insights into partitioning of fauult motions in continental convergent wrench zones, Annales Tectonicae 4 (1990) 35-44.

[51] M. Menning, D. Weyer, G. Drozdzewski, H.W.J. Van Ameron, I. Wendt, A Carboniferous time Scale 2000: discussion and use of geological parameters as time indicators from Central and Western Europe, Geol. J.-B., A156 (2000) 3-44.

[52] J. Rollet, B. Le Gall, J-R. Darboux, P. Thonon and M. Gravelle, L'évolution géodynamique dévono-carbonifère de l'extrémité occidentale de la chaîne hercynienne d'Europe sur le transect Armorique-Cornwall, Bull. Soc. Géol. France 8 (1986) 43-54.

[53] D.M. Hobson, D.J. Sanderson, Variscan deformation in Southwest England, in The Variscan Fold Belt in the British Isles, P.L. Hancock (Ed.), Adam Hilger Ltd Bristol (1983) 108-129.

[54] M.T. Holder, B.E. Leveridge, A model for the tectonic evolution of south Cornwall, Journal of the Geological Society of London 143 (1986) 125-134.

[55] F. Roure, P. Choukroune, R. Polino, Deep seismic reflection data and new insights on the bulk geometry of mountain ranges, Compte Rendu Académie Sciences Paris 322 (1996) 345-359.

[56] C. Hibsch, M. Cushing, J. Cabrera, J. Mercier, P. Prasil, J.-J. Jarrige, Évolution des paléo-contraintes en Grande-Bretagne du Permien au Cénozoïque : approche géodynamique de l'évolution des bassins méridionaux du Royaume Uni, Bull. Centres Rech. Explor.-Prod. Elf Aquitaine 17 (1993) 304-330.

[57] R.K. Shail, A.C. Alexander, Late Carboniferous to Triassic reactivation of Variscan basement in the western English Channel: evidence

from onshore exposures in south Cornwall, J. Geol. Soc. London 154 (1997) 163-168.

[58] M. Donsimoni, Le bassin houiller lorrain, synthèse géologique, Mémoire B.R.G.M. n° 117 (1981) 102 p.

[59] B. Vallé, L. Courel, J-P. Gélard, Les marqueurs de la tectonique synsédimentaire et syndiagénétique dans le bassin stéphanien à régime cisaillant de Blanzy-Montceau (Massif Central, France), Bull. Soc. géol. France 8 (1988) 529-540.

[60] M. Faure, J-F. Becq-Giraudon, Sur la succession des épisodes extensifs au cours du désépaississement carbonifère du Massif Central français, Compte Rendu Académie Sciences Paris 316 (1993) 967-973.

[61] M.R. Handy, L. Franz, F. Heller, B. Janott, R. Zurbriggen, Multistage accretion and exhumation of the continental crust (Ivrea section, Italy and Switzerland), Tectonics 18 (1999) 1154-1177.

[62] J-C. Soula, Genèse de bassins sédimentaires en régime de cisaillement transcurrent: modèles expérimentaux et exemples géologiques, Bull. Soc. belge Géol. 93 (1984) 83-104.

[63] A. Genna, P.J. Debriette, Structures en fleur dans le bassin houiller d'Alès. Implications structurales, Compte Rendu Académie Sciences Paris 318 (1994) 977-984.

[64] F. Mattern, Permo-Silesian movements between Baltica and Western Europe: tectonics and "basin families", Terra Nova 13 (2001) 368-375.

[65] P.A. Ziegler, Geological Atlas of Western and Central Europe, Shell Internationale Petroleum Maatschappij B.V. (1990) 239 p.

[66] T.J. Chapman, The Permian to Cretaceous structural evolution of the Western Approaches Basin (Melville sub-basin), UK, in Cooper M.A., Williams G.D. (Eds), Inversion Tectonics, Geological Society Special Publication 44 (1989) 177-200.

[67] R.J. Korsch, A. Schäfer, The Permo-Carboniferous Saar-Nahe Basin, south-west Germany and north-east France: basin formation and deformation in a strike-slip regime, Geol. Rundsch. 84 (1995) 293-318.

[68] J-P. Lefort, M. Jaffal, Les témoins de l'extension post-hercynienne dans la croute inférieure litée de la Manche Occidentale et de la Mer celtique. Bull. Centres Rech. Explor.-Prod. Elf Aquitaine 18 (1991) 421-436.

[69] C. Prijac, M-P. Doin, J-M. Gaulier, F. Guillocheau, Subsidence of the Paris basin and its bearing on the Late Variscan lithosphere evolution : a comparison between Plate and Chablis models, Tectonophysics 323 (2000) 1-38.

Article 8.

Minguely B., Folens L., Averbuch O. and Vendeville B.C., 2008. Formation of deep-seated triangle zones by interaction between two orogenic thrust fronts having opposite vergence : structural evidence from the Caledonian-Variscan system in Northern France and preliminary analogue modelling. Bolletino di Geofisica teorica ed applicata, 49-2, 242-246.

Bonnet, C., Malavieille J., and Mosar J.; 2007: Interactions between tectonics, erosion, and sedimentation during the recent evolution of the Alpine orogen: Analogue modelling insights, Tectonics, 26, TC6016, doi:10.1029/2006TC002048.

Bonnet, C., Malavieille, J., & Mosar, J. ; 2008 : *Surface processes versus kinematics of thrust belts : impact on rates of erosion, sedimentation, and exhumation – Insights from analogue models.* Bull. Soc. géol. Fr., 2008, t. 179, no 3, pp. 179-192

Dahlen F.A., Suppe J. & Davis D.M.; 1984: *Mechanics of fold and thrust belts and accretionary wedges: Cohesive Coulomb theory.* J. Geophys. Res., 89, 10087-10101.

Faure, M. and Cottereau N.; 1988: *Données cinématiques sur la mise en place du dôme migmatitique carbonifère moyen de la zone axiale de la Montagne Noire (Massif Central français),* C.R. Acad. Sci. Paris, 2, 307, p. 1787-1794.

Gutscher M.-A., Kukowski N., Malavieille J. & Lallemand S.; 1996: *Cyclical behavior of thrust wedges: Insights from high basal friction sandbox experiments.* Geology, 24, 2, 135-138.

Konstantinovskaia, E., and Malavieille, J.; 2005: *Erosion and exhumation in accretionary orogens : Experimental and geological approaches.* Geochemistry, Geophysics, Geosystems, Vol. 6, Number 2, 25pp.

Malavieille, J., Lu, C-Y., Chang, K-J., Konstantinovskaia, E. ; 2007 : *From oceanic to continental subduction in Taiwan: Dynamics of a growing accretionary wedge.* Subduction Zone Geodynamics Conference, June 4 to 7, 2007, Montpellier, France.

Naylor M. & Sinclair. H.D.; 2007: *Punctuated thrust deformation in the context of doubly-vergent thrust wedges: implications for the localization of uplift and exhumation,* Geology, v. 35 ; no. 6 ; p. 559-562.

Simoes M., Avouac, J.P., Beyssac, O., Goffe, B., Farley, K.A., Chen, Y.-G.; 2007: *Mountain building in Taiwan: a thermokinematic model.* Journal of Geophysical Research, 112, 2007.

Van den Driessche, J., Brun, J.P.; 1992: *Tectonic evolution of the Montagne Noire (French Massif Central): a model of extensional gneiss dome.* Geodinamica Acta 5, 85-99.

FORMATION OF DEEP-SEATED TRIANGLE ZONES BY INTERACTION BETWEEN TWO OROGENIC THRUST FRONTS HAVING OPPOSITE VERGENCE: STRUCTURAL EVIDENCE FROM THE CALEDONIAN-VARISCAN SYSTEM IN NORTHERN FRANCE AND PRELIMINARY ANALOGUE MODELLING

B. Minguely, L. Folens, O. Averbuch, B.C. Vendeville

Géosystèmes, Université de Lille 1, 59 655 Villeneuve d'Ascq cédex (France)

Summary

At the border between Northern France and Southern Belgium, the North-verging Variscan thrust front and the South-verging Caledonian thrust front are closely juxtaposed geographically, but how these two fronts may have interacted has not, however, been considered so far. We present here new interpretations of seismic-reflection profiles along the Variscan thrust front in Northern France providing evidence for the existence of a deep-seated triangle zone induced by the reactivation of deep Caledonian thrusts below the propagating Variscan thrust system. These deep back-thrusts branch upward into the main Variscan décollement zone, folding and uplifting the former tip of the foreland propagated thrust front and inducing its general out-of-sequence dislocation. To get further insights on the kinematics of such unusual triangle zones, we conducted several analogue experiments modelling the interaction between two subsequent thrust fronts having opposite vergence. Preliminary results show that the triangle zone initiates when the frontal thrust reaches the buried tip of the inherited basement thrust system. From this time onward, thrusting propagates towards the foreland by synchronous forethrusting along one localized superficial thrust and deep underthrusting by sequential reactivation of the inherited basement thrusts. Such progressive thrust imbrication at the thrust front induces the general backward rotation and steepening of both the deep backthrusts and the superficial forethrust, which generates an uplifted foreland bulge in front of the main emergent forethrust.

Introduction

The Variscan (ca. 300 Ma) thrust front in Northern France extends, below the thin Mesozoic sedimentary cover of the Paris Basin, from the English Channel to the west, to the Ardennes massif to the east (Figure 1). Outcrops located at both extremities (Boulonnais and Ardennes areas), as well as seismic profiles and numerous boreholes show that the frontal thrust system is characterized by one major crustal-scale thrust zone dipping gently Southward and whose emergence corresponds to a large out-of-sequence thrust, the Midi thrust zone (e.g., Averbuch et al., 2004). Analysis of recent seismic data suggests that the total amount of slip along the Midi thrust zone could be as much as 70 km in the North in the Western Ardennes area (Lacquement et al., 1999), thereby strongly dissecting the South border of the coal-bearing molassic foreland basin of Namurian-Westphalian age. This foreland basin (up to 3-4 km thick) formed at the top of a reduced Devonian-Carboniferous sedimentary sequence resting unconformably on a Lower Paleozoic substratum, which crops out a few tens of km North of the Variscan thrust front, in the Belgian Brabant Massif. The Brabant Massif extends further North into Eastern England and was deformed during Caledonian times (Late Silurian, ca. 415 Ma), forming the Southeastern front of the Anglo-Brabant deformation belt (Pharaoh et al., 1993). Significant North-dipping crustal reflectors, evidenced on the BIRPS seismic profiles in the Celtic Sea and the southern North Sea as well as the ECORS Northern France seismic line, image the traces of the South-verging Caledonian thrust in the direct footwall of the Variscan thrust front (Bois et al., 1994) thus suggesting the direct juxtaposition of these two Paleozoic fold-and-thrust belts having opposite vergence (Figure 1)(Mansy et al., 1999). Reactivation of the Caledonian thrusts was considered to be likely (Bois et al., 1994), but, so far, this scenario had not been investigated in detail. In this article, we present new interpretations of unpublished industrial seismic data acquired along the Variscan thrust front in the Artois area (Northern France) that argue for the existence of a deep-seated triangle zone (or thrust wedge) caused by the interaction between these two thrust fronts. To our knowledge, this type of deep frontal triangle zone has been described only once, in the Himalayan foreland in Pakistan (Jadoon and Frisch, 1997). Therefore, the detailed kinematics of such unusual thrust stack is rather unclear. Moreover, in our study area, the kinematic evolution cannot be constrained properly at depth using only cross-sectional geometry alone. We thus conducted a series of analogue experiments to better understand the complex thrusting kinematics inherent to such buried frontal triangle zones. We present preliminary results of experiments in which we modelled the interaction between two subsequent orogenies having opposite vergence.

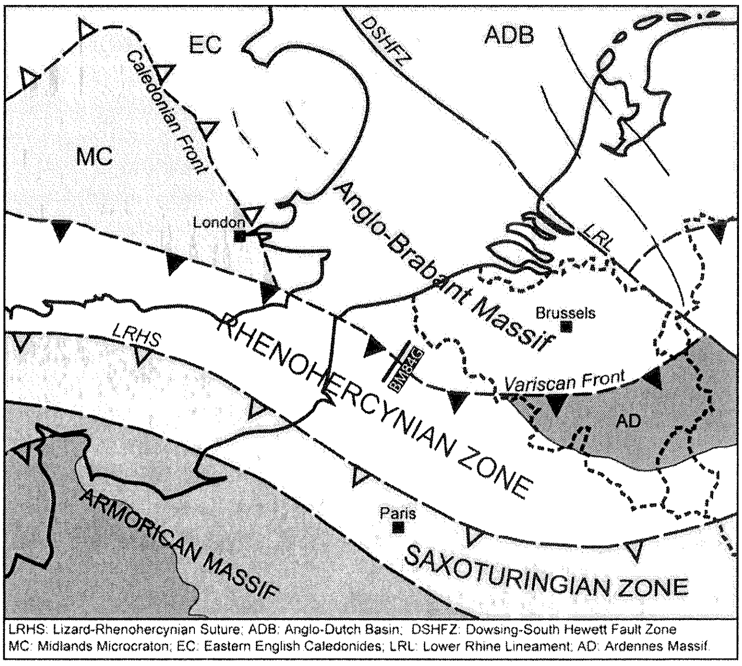

Figure 1. Tectonic sketch map at the border of Variscan and Caledonian thrust fronts in Northern France - Southern Belgium - Southern Britain area (modified from Pharaoh et al., 1993) showing the location of Seismic Profile BM84G shot in the Artois area (Northern France).

Structural evidence for a deep-seated triangle zone at the Variscan thrust front

The Boulogne-Maubeuge industrial seismic survey was conducted in 1984-1985 throughout the Northern France Variscan thrust front but particularly focused on the Artois area (Figure 1). A set of 14 seismic profiles shot either perpendicularly or parallel to the regional trend of the thrust front were analyzed, allowing us to define a consistent 3-D geometry of Variscan fold-thrust structures at depth. Interpretations of seismic lines are constrained by borehole data and gravity modelling (Minguely, 2007). As exemplified by the Profile BM84G (Figure 2), a prominent reflector corresponds to the main frontal thrust (the Midi thrust zone) dipping south to about 2.5 s TWT at the southern end of the section (6-7 km depth, considering seismic velocities in the area). The Midi thrust placed Latest-Silurian shales and a thick Lower-Devonien sequence above the reduced Upper-Devonian- Lower-Carboniferous series that overly unconformably the Lower Paleozoic Brabant massif (dominanted thick Silurian shales in the cross section). The degree of allochtony upon this main thrust is difficult to assess precisely, but 20 km of displacement can be considered as a minimum value. The footwall of this main thrust exhibits a somewhat folded and thrusted Devonian-Carboniferous sequence (the Paleozoic inliers cropping out further to the west in the Boulonnais (Averbuch et al, 2004)) with a basal décollement zone located at the interface with the Lower Paleozoic substratum. Consistently, along the different seismic profiles across the thrust front, this basal décollement zone is folded by culminations of the substratum systematically floored by discontinuous North-dipping reflectors. On the Profile BM84G, these deep reflectors seem to flatten upwards in the vicinity of the base Upper Devonian décollement zone and backwards onto another deep reflector dipping slightly to the South. We interpret these reflectors as basement backthrusts branching upward onto the basal Variscan décollement zone and thus forming a deep triangle zone at the front of the Variscan thrust system. Such a very unusual geometry at a thrust front is likely to be related to the pre-existence at depth of South-verging Caledonian thrusts, thrusts that were reactivated when the Variscan thrust front propagated northward onto the Brabant foreland. Likely, the reactivated basement thrusts in the Variscan foreland acted as significant buttresses that hindered the northward propagation of the Variscan thrusts, thereby inducing a strong out-sequence dislocation of the foreland basin. However, it is not possible to decipher the precise kinematics of this intercutaneous wedge using only the data from the on cross-sections.

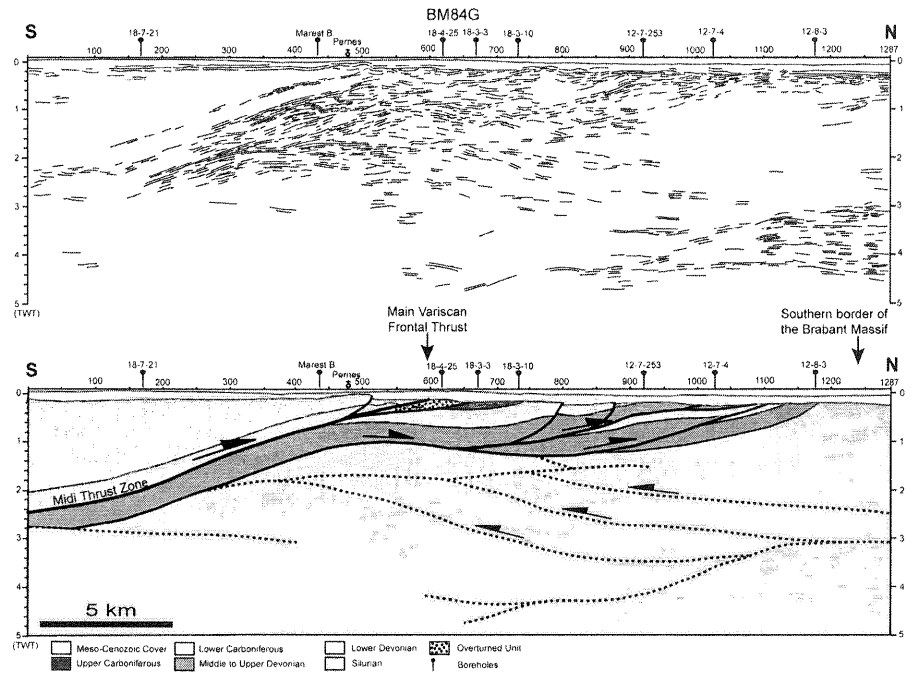

Figure 2. Line drawing showing prominent reflectors of Seismic Profile BM84G (Artois area; see location in Figure 1) and interpreted geological cross section constrained by borehole data and gravity modelling (Minguely, 2007).

Analogue modelling: preliminary results

We designed a set of analogue experiments in order to investigate the interaction between two thrust systems having different ages of formation and opposite vergence. We conducted these experiments at the tectonic modelling laboratory of the University of Lille 1. The general set up was as follows. All models were constructed using brittle, cohesionless, dry, porous materials (sand glass microbeads). All models were built, then deformed above a flat, horizontal, rigid base. Here, we illustrate the results of only one experiment. In this experiment, the model comprised a 5-mm-thick décollement layer made of glass microbeads overlain by a "stronger" cover of dry sand (2.5-cm thick). The model was initially 110-cm long.

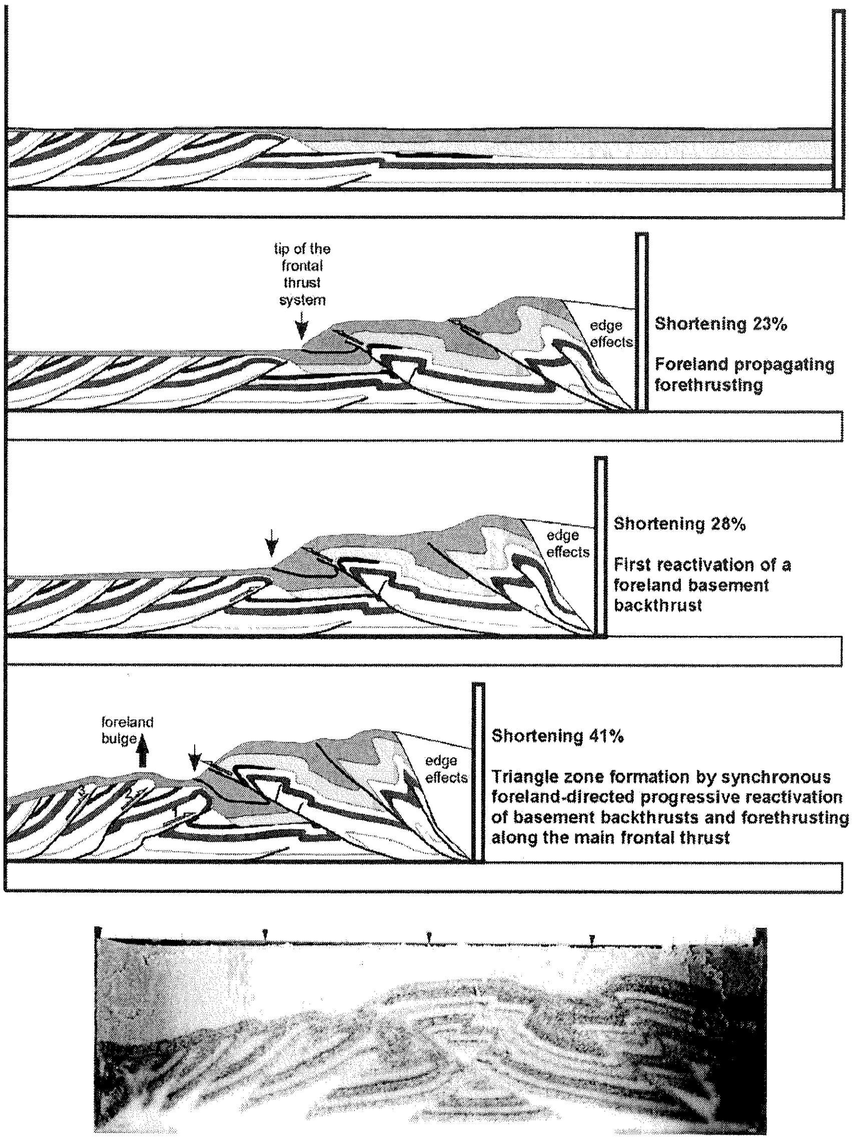

Figure 3. A: Line drawing from photographs through the sidewalls showing an analogue model simulating the formation of deep frontal triangle zones related to the interaction of two successive thrust fronts having opposite vergence. B: Photograph of a section cut near the model's centre. Scale in centimetres.

The entire model was subjected to one first phase of shortening by moving progressively the left-hand wall until a value of 39% bulk shortening was reached. That stage simulated the Caledonian orogeny. An orogenic wedge formed against the moving wall, then propagated progressively rightward by formation of new forethrusts and by bulk thickening of the wedge itself. Five emergent thrusts and one external blind thrust formed during that stage (Figure 3). Shortening stopped, and post-tectonic layers were deposited in the foreland area, covering the top of the two frontal thrusts. Farther in the hinterland, most of the fold-and-thrust belt was eroded then buried under a thin (5-mm thick) post-tectonic layer. The post-tectonic sedimentation included no décollement. The model was then subjected to a second phase of shortening by moving the right-handed wall, simulating the later Variscan orogeny. The additional shortening amounted up to a final value of 41%. As shown in figure 3, during the early stages of the second phase of shortening (up to 24% shortening), folds and thrusts propagated according to a classical piggy-back into the cover that did not comprise any pre-existing thrusts dating from the first shortening phase. Reactivation of older antithetic basement thrusts occurred only once the tip of the younger frontal thrust system reached the first pre-existing basement thrust of the older belt. From this time on, shortening was partitioned between a main forethrust localizing the foreland-directed advance (a possible analogue to the Midi thrust zone in Northern France) and a system of inherited basement thrusts accommodating progressive underthrusting of the foreland (a "crocodile" type of thrust propagation). In the latter thrust system, deformation sequentially propagates towards the older hinterland of the thrust system but it is worth noting, however, that different backthrusts remained active at the same time. Such a progressive thrust imbrication at the thrust front induces the general backward rotation and steepening of both the deep backthrusts and the shallower, younger forethrust (Figure 3) and creates a foreland bulge in front of the main emergent forethrust. The latter phenomenon is likely to produce a reduction in the thickness of foreland basin deposits above the bulge and, applied to Northern France, it could therefore explain the reduced coal-bearing Namurian-Westphalian molasse deposits, as is observed in the Artois area, in the foreland of the main Variscan thrust.
This first experiment emphasizes the peculiar style of thrust propagation in such triangle zones, and especially, it explains the existence of numerous reactivated basement backthrusts in the Variscan foreland, as well as the general geometry and kinematics of the thrust front. To account, however, for a stronger "out of sequence" dislocation of the thrust front, further modelling experiments must be conducted (work in progress), particularly some experiments that investigate the role of an intermediate décollement zone at the base of the "second phase" sedimentary cover.

REFERENCES

Averbuch O., Mansy J-L., Lamarche J., Lacquement F. and Hanot F.; 2004: *Geometry and kinematics of the Boulonnais fold-and-thrust belt (N France): implications for the dynamics of the Northern Variscan thrust front.* Geodinamica Acta, 17, 163-178.

Bois C., Cazes G., Choukroune P., Gariel O., Hirn A., LeGall B., Lefort J-P., Matte P. and Pinet B.; 1994: *Seismic reflections images of the Pre-Mesozoic crust in France and adjacent areas.* In: Keppie J.D. (ed), Pre-Mesozoic geology in France and related areas, Springer-Verlag Berlin Heidelberg, pp. 3-48.

Jadoon I.A.K. and Frisch W.; 1997: *Hinterland-vergent tectonic wedge below the Riwat thrust, Himalayan foreland, Pakistan; implications for hydrocarbon exploration.* A.A.P.G. Bull., 81, 3, 438-448.

Lacquement F., Mansy J-L., Hanot F. and Meilliez F.; 1999: *Retraitement et interpretation d'un profil sismique pétrolier méridien au travers du massif paléozoïque ardennais (N de la France).* C.R.Geosciences, 329, 471-477.

Mansy J-L., Everaerts M. and Devos W.; 1999: *Structural analysis of the adjacent Acadian and Variscan fold belts in Belgium and Northern France from geophysical and geological evidence.* Tectonophysics, 309, 99-116.

Minguely B.; 2007: Caractérisation géométrique 3-D de la couverture sédimentaire méso-cénozoïque et du substratum varisque dans le Nord de la France. PhD Thesis, University of Lille 1, 226pp.

Pharaoh T.C., Molyneux S.G., Merriman R.J., Lee M.K. and Verniers J.; 1993: *The Caledonides of the Anglo-Brabant Massif reviewed.* Geol. Mag., 130, 561-562.

3.B. Segmentation et courbure du front de chaîne dans le nord de la France : l'impact de la pré-structuration du bassin rhéno-hercynien.

Ainsi que nous l'avons vu précédemment, le front de chaîne varisque septentrional du Nord de la France change significativement d'orientation et de style structural entre la partie Boulonnais-Artois WNW-ESE (en moyenne N110) et la partie Ardennes ENE-WSW (en moyenne N060-N070). Cette déflexion des structures de premier ordre se met en place au niveau de la zone bassin houiller Nord-Pas de Calais-Avesnois à la faveur de virgations secondaires dont la géométrie reste, pour l'heure, grandement méconnue. Afin de progresser dans la compréhension de l'évolution latérale du front de chaîne, nous avons mis en place une étude couplant l'analyse des déformations (analyse structurale et étude de la fabrique magnétique) à des études paléomagnétiques. Cette approche, que j'avais particulièrement développée au cours de ma thèse, nécessite, bien sur, l'accès à des affleurements paléozoïques impliqués dans le front de chaîne ce qui réduit *de facto* son extension aux massifs paléozoïques, affleurant dans le nord de la France : le massif du Boulonnais à l'extrémité occidentale du front varisque dans le nord de la France et le massif des Ardennes à son extrémité orientale. L'étude paléomagnétique de ces deux massifs a été menée dans le cadre de deux collaborations sucessives, tout d'abord avec E. Marton du laboratoire paléomagnétique de l'Institut de géophysique de Budapest, puis avec M. Lewandowski du laboratoire paléomagnétique de l'Institut de Géophysique de Varsovie. La première de ces études a été menée à grande échelle le long du front de chaîne avec une résolution toutefois relativement faible (cf. article 9); la seconde a fait l'objet d'une étude plus localisée (les Ardennes et quelques affleurements très localisés en Artois, cf. la carte géologique de l'article 4) mais plus poussée en ce qui concerne le signal paléomagnétique, ceci dans le cadre de la thèse en cotutelle de R. Szaniawski (2004)(cf. article 10).

Je ne reviendrai pas, ici, en détail, sur ces études paléomagnétiques qui, même si elles n'abordent pas, avec la même résolution, la complexité du signal paléomagnétique des formations paléozoïques étudiées, convergent au final sur les principaux résultats. Au sein des différentes formations étudiées, les séries carbonatées du Givétien et du Carbonifère présentent les résultats les plus significatifs, le signal paléomagnétique, quoique toujours secondaire, étant notablement plus stable qu'au sein des formations gréso-pélitiques rouges du Dévonien inférieur. Deux composantes de réaimantations principales, contemporaines des déformations varisques, ont pu être individualisées au sein des différents sites étudiés : la première, assez précoce vis à vis du plissement, résulterait de l'enfouissement des séries sédimentaires dévono-carbonifères sous l'épais bassin molassique namuro-westphalien d'avant-chaîne (3-4 km d'épaisseur au front des Ardennes) ; la seconde, au contraire tardive vis à vis du plissement, pourrait être associée à la phase générale de dissection « hors-séquence » du front de chaîne. Indépendemment de l'âge des réaimantations, les données disponibles ne montrent pas de variation significative de déclinaison paléomagnétique associée à la virgation de premier ordre entre la branche Boulonnais-Artois et la branche Ardennes, ni entre les unités allochtones et l'avant-pays brabançon représentatif du continent des Vieux Grès Rouges (ou Laurussia)(cf. article 9). Ce résultat, quoique significatif à l'échelle des sites étudiés, nécessite, cependant, d'être nuancé compte-tenu du peu de sites accessibles le long de l'allochtone sur le segment Boulonnais-Artois (Szaniawski, 2004). Au sein des structures plissées-faillées des unités allochtones ardennaises, les données paléomagnétiques sont beaucoup plus nombreuses même si leur localisation n'est pas distribuée de façon homogène (article 10). Elles confirment néanmoins l'absence de rotation d'ensemble du segment ardennais (d'orientation N060-070) par rapport au continent stable des Vieux Grès Rouges. Par ailleurs, les données paléomagnétiques acquises le long des structures ardennaises argumentent l'existence de rotations horaires localisées au sein de virgations structurales secondaires telles que celles de la Vallée de l'Ourthe dans la région de Liège (Belgique) ou de la Vallée de la Meuse dans la région de Givet (France) et Dinant (Belgique)(cf. fig. 7 de l'article 10).

Cette dernière illustre, à mes yeux, de façon particulièrement parlante les processus contrôlant l'évolution latérale du front de chaîne et un accent particulier sera mis, dans ce paragraphe, sur l'étude des déformations impliquées dans sa formation, étude explicitée dans les articles 11 et 12. Cette étude synthétise les travaux que j'ai menés avec F. Lacquement (2001) et R. Szaniawski (2004) au cours de leurs thèses.

Au sein d'un couloir, orienté NW-SE, d'une quarantaine de kilomètres de large, centré sur la vallée de la Meuse, les axes des structures de chevauchement-plissement présentent un changement significatif d'orientation passant de la direction ardennaise classique (WSW-ENE, autour de N060) à une direction E-W voire localement NW-SE (Fig. 1 de l'article 11). Cette virgation structurale affecte l'ensemble de l'allochtone ardennais jusqu'au chevauchement frontal (du Midi) et est particulièrement explicite dans la région de Givet, au niveau de la retombée avant de la culmination de socle du massif de Rocroi (Fig. 3 de l'article 11). Cette dernière peut être interprétée comme une accumulation d'écailles de substratum paléozoique inférieur (principalement cambrien), plissé et schistosé dans des conditions de faible métamorphisme (cf. article 13 pour une description détaillée de la déformation interne du massif), accumulation développée à l'aplomb d'une rampe majeure du chevauchement basal ardennais. A l'avant du massif de Rocroi, le déplacement le long du chevauchement basal est transféré vers l'avant-pays à la base des niveaux de couverture dévono-carbonifères dans le niveau de décollement localisé dans les formations schisteuses, fortement incompétentes, du Dévonien basal (Lochkovien). La retombée nord de la culmination implique une série dévonienne épaisse, à pendage général assez fort vers le nord, affectée de nombreux replis fortement déversés et chevauchements secondaires à vergence nord. Dans la région de Givet, ce dispositif général vient buter sur une zone de rétrochevauchements complexe, le rétrochevauchement de Givet (Fig. 3 et 4 de l'article 11). Celui-ci s'enracine manifestement sur le chevauchement de base ardennais et émerge au sein des unités schisteuses du Frasnien supérieur-Famennien, qui forment un niveau de décollement intermédiaire particulièrement marqué au sein des séries ardennaises. Dans ces séries faiblement résistantes vis à vis de la déformation, le déplacement sur le rétrochevauchement de Givet est transféré sur différents accidents secondaires et est absorbé par une intense déformation interne des roches. Au toit du rétrochevauchement (cartographiquement, au nord), on note un découplage majeur de la déformation matérialisé par un changement drastique du style structural, s'exprimant en particulier par des plis polyharmoniques à plan axial subvertical caractéristiques d'un mécanisme de raccourcissement parallèle aux couches.

Au sein de la virgation, la déflexion des structures est particulièrement marquée au niveau de la barre carbonatée givétienne, qui s'étend avec une orientation générale ENE-WSW, oblique à la chaîne, sur plus de quarante kilomètres (Fig. 3 de l'article 11). Ce large flanc oblique est affecté de replis d'échelle kilométrique présentant une augmentation graduelle de plongement axial vers l'est (de 5° à Givet à 50° au sud du sondage de Focant). Cette augmentation du plongement axial s'accompagne d'une déviation progressive de la direction des plis (jusqu'à 70° de déviation par rapport à la direction ardennaise) et localement, d'un basculement de la schistosité vers le nord ou vers l'est.

En profondeur, les données du forage profond de Focant (Boulvain et Coen-Aubert, 1997 ; Han et al, 2003) et les profils de sismique rélexion (Raoult, 1986) montrent que l'amplitude du raccourcissment le long du rétrochevauchement de Givet augmente vers l'est de la zone de virgation (cf. les coupes géologiques en Fig. 4 de l'article 11). Par ailleurs, ainsi que l'a montré Raoult (1986) à partir de l'interprétation des lignes sismiques de la Famenne (Fig. 5), la profondeur du chevauchement basal ardennais subit des variations latérales majeures à l'aplomb de la zone de virgation. En tenant compte des lois de vitesse classique, le chevauchement basal passe d'environ 7 km de profondeur à l'ouest de la virgation à 5 km à l'est de celle-ci, ainsi qu'il a été montré au niveau du forage profond d'Havelange (Raoult, 1986). Cette variation importante de profondeur du niveau de décollement basal du système chevauchant ardennais caractérise une rampe latérale majeure au sein du système chevauchant ardennais. L'analyse des réflecteurs au mur du chevauchement basal (le réflecteur Y de Raoult, 1986) montre que cette rampe latérale se superpose à une discontinuité initiale (faille normale profonde) d'orientation transverse aux structures ardennaises. Ainsi que l'illustre le modèle géométrique 3D présenté en Fig. 5 de l'article 11, il est proposé que cette faille normale profonde, qui a contrôlé la profondeur et l'épaisseur des séries dévono-carbonifères au sein du prisme sédimentaire rhénohercynien initial, localise la rampe latérale du chevauchement basal ardennais et de fait, implique, de part et d'autre, une propagation différentielle des chevauchements. Ces données suggèrent, ainsi, que la virgation de la vallée de la Meuse matérialise un système de déformation transpressif agissant comme une zone distribuée de transfert entre des domaines ouest est ardennais, individualisés lors de la segmentation initiale de la marge rhéno-hercynienne.

Les données de fabrique magnétique (ou d'anisotropie de susceptibilité magnétique) mésurées sur 35 sites distribués sur l'ensemble de la structure (Fig. 6 et 7 de l'article 11) combinées aux données paléomagnétiques compilées sur le secteur d'étude (Fig. 8 et 9 de l'article 11) permettent de caractériser de façon plus précise la cinématique des déformations au sein de cette zone transpressive, particulièrement complexe. Une évolution significative des fabriques magnétiques est mise en évidence au sein de la virgation : les zones les plus occidentales, caractérisées par des plongements axiaux faibles, ne montrent pas de variation significative de la fabrique par rapport aux zones d'orientation ardennaise classique, si ce n'est un basculement globalement vers l'est et une déviation en sens horaire de la fabrique syn-pli ; à l'inverse, dans les secteurs orientaux où les plongements axiaux des plis augmentent jusqu'à 50°, on observe une réorganisation notable de la fabrique magnétique avec la surimposition d'une foliation subverticale d'orientation NNW-SSE sur la fabrique classique syn-pli. Cette seconde foliation implique l'existence d'un raccourcissement ENE-WSW (sub-perpendiculaire au transport tectonique général) qui augmente en direction de l'extrémité orientale de la virgation. Ce gradient de racourcissement latéral corrobore les observations faites sur le rétrochevauchement de Givet qui absorbe également un raccourcissement plus important vers l'est de la virgation (dans la région de Focant) et documente une sorte d'effet butoir de la rampe latérale localisée sous la partie orientale de la virgation (cf. le modèle cinématique 3D de la Fig. 10). Les données paléomagnétiques à plus grande échelle (12 sites au sein de la virgation et 5 sites avec une orientation ardennaise classique) mettent en évidence une déviation systématique en sens horaire des déclinaisons au sein de la zone de virgation. L'amplitude de la rotation ne se corrèle cependant pas de façon directe avec l'amplitude de déviation des structures plissées. En particulier, les sites présentant une déviation d'axe de plus de 30° par rapport à l'orientation ardennaise standard, ne montrent pas de rotation supérieure à 30°. Ces données suggèrent qu'au sein de la zone de virgation de la Meuse, les plis se soient développés dès le départ de façon oblique aux structures générales puis aient été accentués par rotation en sens horaire à mesure que se développait le cisaillement dextre associé au transfert de déplacement de part et d'autre de la zone latérale (cf. le modèle cinématique en Fig. 10). Il est à noter que les zones occidentales, les moins déviées de la virgation, ont subi une rotation horaire en rapport avec la déviation des plis ce qui implique que la zone de virgation se soit élargie au cours du temps lors de la propagation des chevauchements.

Les résultats, issus de cette étude de détail autour de la zone de virgation de la Meuse (dite aussi virgation de Dinant), permettent, de façon générale, de mieux contraindre les mécanismes de déformation associés aux limites latérales des écailles chevauchantes. Plus particulièrement, ils illustrent l'impact des variations d'épaisseur sédimentaire au sein d'un système chevauchant (et donc des variations latérales de profondeur des niveaux de décollement) sur la propagation différentielle des unités chevauchantes (cf. Liu Huiqi et al, 1992 ; Marshak et al, 1992 ; Philippe, 1995 pour la modélisation analogique de ce processsus). Ce mécanisme résulte dans le développement, au toit de la rampe latérale, d'une zone de transfert complexe entre les deux unités différenciées absorbant de façon hétérogène un cisaillement normal aux couches (dextre dans le cas de la Vallée de la Meuse) et un raccourcissement oblique au transport tectonique contrôlé par l'effet butoir exercé par la discontinuité latérale profonde.

Dans le cas du front de chaîne varisque septentrional, cette étude montre l'existence d'une segmentation importante du front chevauchant associée à la géométrie initiale des séries sédimentaires déposées sur la marge rhénohercynienne. A l'aplomb de la virgation de la Meuse, un système de failles normales profondes d'orientation générale NW-SE et de pendage vers le SW, induit un décalage vertical d'environ 2 km du décollement basal des unités situées de part et d'autre de la discontinuité profonde. A partir des relations définies ici entre zone de virgation et failles normales profondes synsédimentaires, l'article 12 extrapole ce dispositif aux autres virgations secondaires observées au sein des unités allochtones ardennaises (celles de Valenciennes, de Beaumont et de l'Ourthe), définissant ainsi un réseau de failles normales profondes transverses contrôlant l'évolution latérale de la géométrie du bassin rhénohercynien avant son inversion dès la fin du Viséen. A plus grande échelle, en accord avec les données paléomagnétiques présentées plus haut, ces études le long du front ardennais montre l'impact du dispositif hérité de la marge rhénohercynienne sur la géométrie actuelle du front de chaîne varisque. Le segment Boulonnais-Artois, d'orientation générale WNW-ESE, peut ainsi être considéré comme un analogue à grande échelle des couloirs transpressifs observés le long des Ardennes. Sur ce modèle, l'association des chevauchements frontaux à vergence vers le NE observés dans le Boulonnais et de failles décrochantes dextres majeures au niveau de l'arrière-pays (la faille décrochante du Pays de Bray par exemple) matérialiserait une partition de la déformation associée à un mécanisme de convergence oblique le long de la marge Boulonnais-Artois (cf. Fig. 11 de l'article 7). Dans ce contexte, le segment Boulonnais-Artois représenterait une zone de transfert oblique entre les systèmes frontaux ardenno-rhénan et du sud-ouest de l'Angleterre à vergence vers le NNW. En premier ordre, la forme actuelle du front de chaîne varisque peut ainsi être considérée comme le résultat du moulage des déformations compressives sur une marge rhénohercynienne fortement pré-structurée. L'héritage structural apparaît donc comme un paramètre de contrôle fondamental sur la forme arquée actuelle du front de chaîne dans le nord de la France.

Article 9.

Marton E., Mansy J-L., Averbuch O. and Csontos L., 2000- The Variscan belt of N France-S Belgium: geodynamic implications of new paleomagnetic data. Tectonophysics, 324, 57-80.

ELSEVIER

Tectonophysics 324 (2000) 57–80

TECTONOPHYSICS

www.elsevier.com/locate/tecto

The Variscan belt of Northern France–Southern Belgium: geodynamic implications of new palaeomagnetic data

Emő Márton [a,*], Jean-Louis Mansy [b], Olivier Averbuch [b], László Csontos [c]

[a] *Eötvös Loránd Geophysical Institute of Hungary, Palaeomagnetic Laboratory, Columbus u. 17-23, H-1145 Budapest, Hungary*
[b] *Université Lille I, Sciences de la Terre, Villeneuve d'Ascq, 59655, France*
[c] *Eötvös Loránd University, Geol. Dept., Múzeum krt 4/a, H-1088 Budapest, Hungary*

Received 22 June 1999; accepted for publication 10 April 2000

Abstract

Palaeomagnetic investigations were carried out in Devonian–early Carboniferous rocks of the Variscan foreland chain of Northern France–Southern Belgium in order to reveal the origin of its arcuate shape. The Brabant Parautochthon was sampled in the Boulonnais (near Calais) and near Tournai, while the Ardenne Allochthon was sampled near Maubeuge and in the Givet area. All the sampled localities yielded characteristic remanent magnetization as a result of stepwise demagnetization and component analysis. Fold or tilt tests were possible for three localities, with negative results indicating pervasive remagnetization. The tectonic position was sub-horizontal at two localities, while the tilt was monoclinal for the rest. Therefore, the acquisition time of the magnetic signals was estimated by comparing the palaeolatitude computed from each magnetic component to the palaeolatitudes of Variscan Europe calculated after Van der Voo (1993).

Three components showing: A, a southern B, a near-Equatorial, and C, a northern palaeolatitude are recognized from our data. Since a pre-Variscan age of component A (observed only in Boulonnais, at 10 sites) is not supported by data, it is assigned to an early phase of deformation. Component B (16 sites) was acquired during the peak of the Variscan tectonics (late Westphalian), while component C (five sites) originated during Permian times.

Regardless of the palaeolatitudes, declinations fall between 190 and 210°, thus being conformable with the declinations expected for Variscan Europe. The declinations show no correlation with the arcuate shape of the belt, neither are they different in the Paraauthochthon and in the Allochthon, nor in the different components.

Arc formation by moulding of the Allochthon on the Brabant Parautochthon is, therefore, not supported by these data, since this mechanism requires substantial (opposed) rotations on both wings of the arc. The available palaeomagnetic data are conformable with a pre-formed arc, simply docking to the Brabant obstacle of similar shape. Variable offsets along a main thrust could support a third model, which slightly unfolds the former passive arc.

Keywords: geodynamic implication; palaeomagnetism; Palaeozoic; Variscan belt

* Corresponding author. Tel.: +36-319-3203; fax: +36-319-2303.
E-mail address: h11000mar@ella.hu (E. Márton)

0040-1951/00/$ - see front matter
PII: S0040-1951(00)00109-8

1. Introduction

The northern front of the Variscan orogen in central and western Europe is conventionally located in the Rhenohercynian tectono-metamorphic zone (Kossmat, 1927). This zone was first defined from field studies in the Harz, Rhenish and Ardenne massifs and subsequently extented westwards to the British Isles by several authors (e.g., Matthews, 1984a,b; Franke and Engel, 1986; Matte, 1986; Bois et al., 1994). The Ardenne massif is classically divided into two main units separated by a major fault, the Midi Fault (Gosselet, 1888), which overthrusts the Coal Basin (Figs. 1 and 2). North of this fault, the Brabant Massif and its cover crop out in the Boulonnais, Tournai and Coal Basin areas. They constitute the weakly deformed Brabant Parautochthon formerly called the Namur syncline (Fourmarier, 1922). South of the Midi Fault, the more intensely deformed Ardenne Allochthon (Meilliez and Mansy, 1990; Meilliez et al., 1991) crops out in the Avesnois region and near the Meuse valley, corresponding broadly to the formerly defined Dinant synclinorium (Fourmarier, 1922).

Displacement on the Midi Fault varies along the strike, from a few kilometres near Aachen and Liège (Winterfeld and Walter, 1993; Laloux et al., 1997) to more than 50 km in the central part of the Coal basin (Raoult and Meilliez, 1987; Mansy et al., 1997). The main shortening deformation began in Late Visean in the Ardenne Allochthon and in the Late Westphalian time in the Brabant Parautochthon.

The southern allochthonous elements record low-grade (higher epizone) metamorphism with

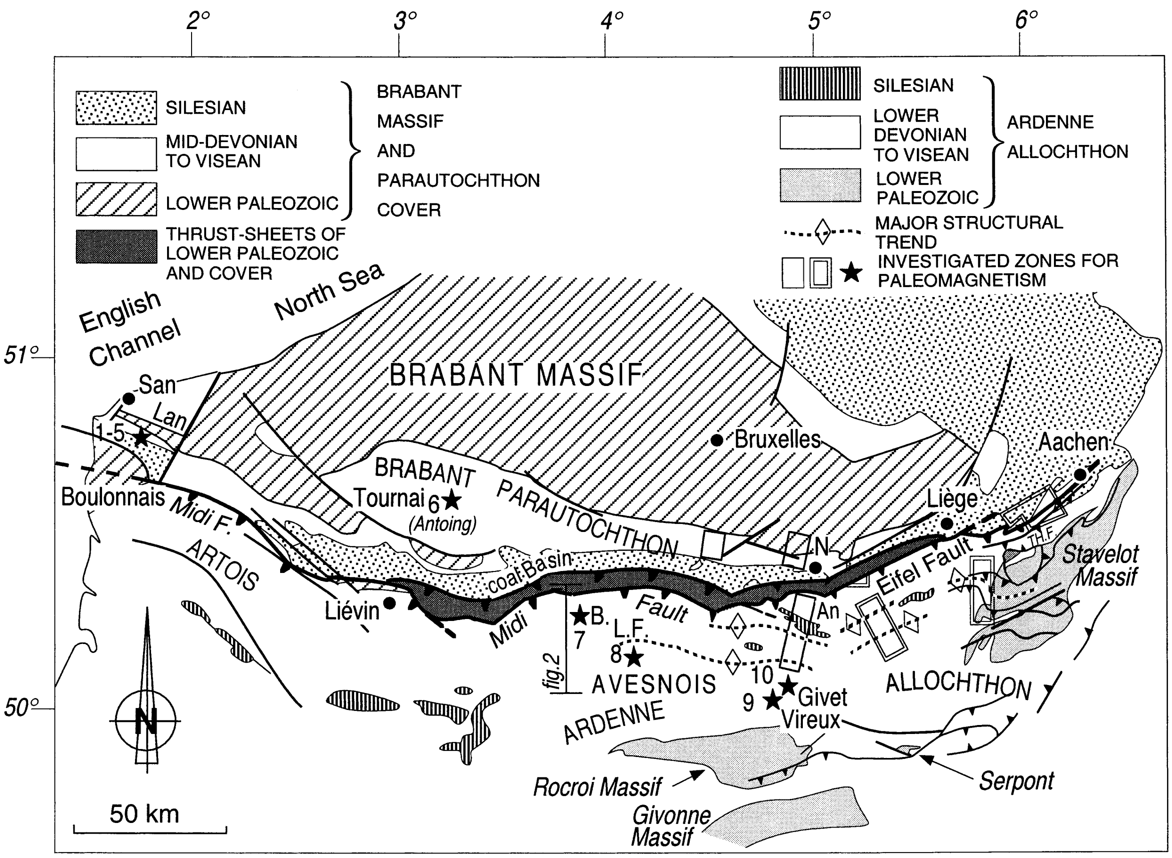

Fig. 1. Location map and structural outlines of the study area.

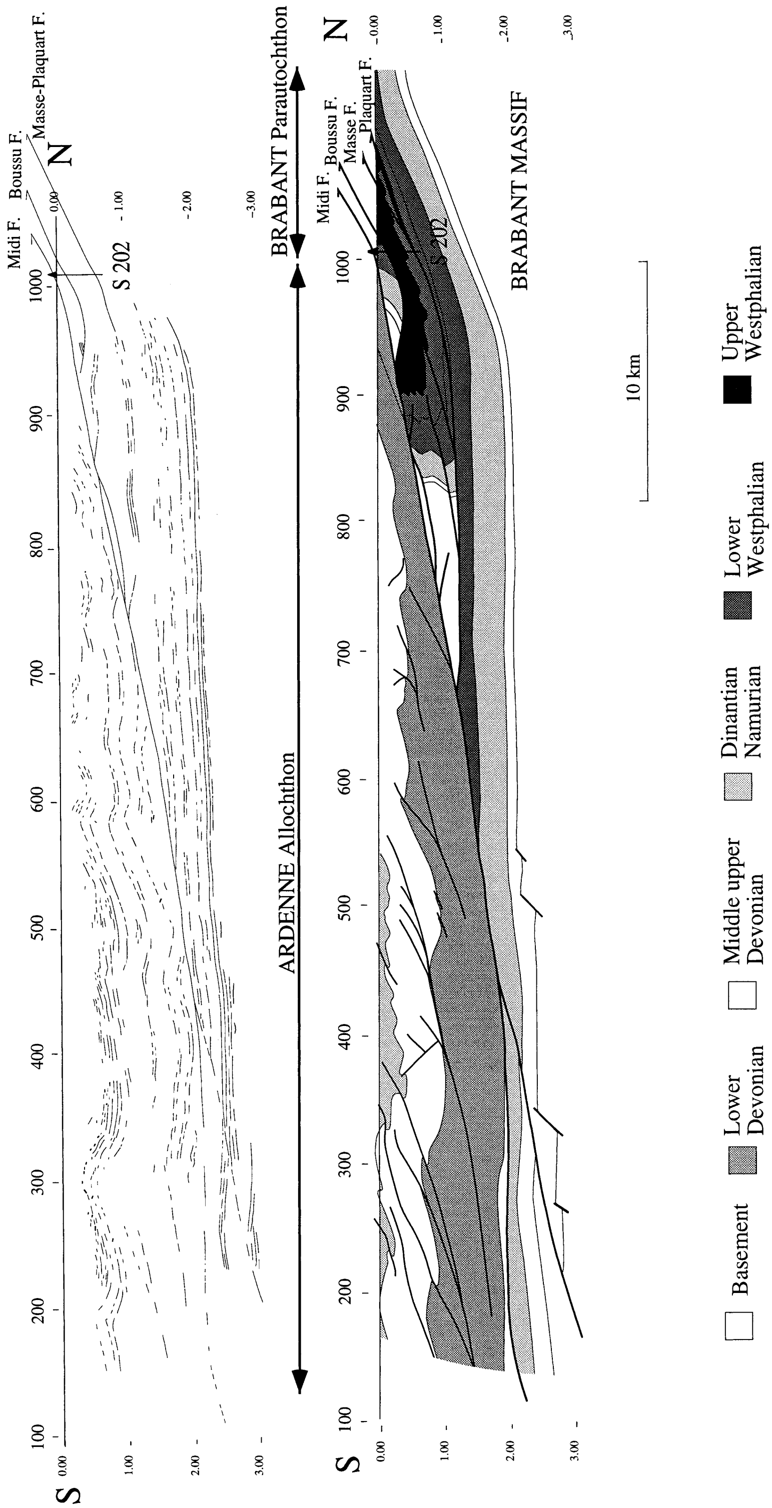

Fig. 2. Schematic cross-section of the central part of the study area based on seismic profiles (after Lacquement et al., 1999).

temperatures not exceeding 400°C (Potdevin and Goffette, 1991; Chamley et al., 1997), while the localities sampled in this study show temperatures that did not exceed 300°C. The Parautochthon records only diagenetic conditions (Fielitz and Mansy, 1999).

The Boulonnais-Ardenne segment of the Variscan chain is classically described as a bent orogen, with structural trends of major fold axes varying from N110° in the Boulonnais to N70° in the Ardenne. Based on palaeomagnetic data, this has already been interpreted as an arched orogen by Perroud (1986), Edel and Coulon (1986), and Thominski et al. (1993), though observations were made only in the eastern part of the Ardenne.

This paper presents the first palaeomagnetic observations from the Boulonnais and new data from the Tournai, Avesnois and Meuse valley regions. Combined with the previously published palaeomagnetic and structural data, an attempt is made to relate palaeomagnetic events to the structural evolution and general kinematics of the chain.

2. Geological overview

2.1. Brabant Parautochthon

The basement (Brabant Massif) is composed of Early Palaeozoic rocks, folded and metamorphosed in the early Devonian (Acadian time). To the northeast and to the south, it is bounded by laterally variable continental to marine sediments of Givetian to Dinantian age. Early Devonian deposits are lacking in most regions, whereas Middle Devonian clastic and Dinantian carbonate sediments form a sedimentary cover with few gaps and increasing thicknesses towards the borders of the Massif (Bless et al., 1980; Muchez, 1989; Meilliez et al., 1991). From the Boulonnais (in France) to the Aachen area (in Germany), a succession of Namurian to Westphalian coal-bearing clastic sequence represents the foreland coal basin of the northwards migrating deformational front. In all exposed areas, cleavage is either very weak or absent.

The WNW–ESE-oriented Boulonnais area (Fig. 3) is situated in the SW margin of the Brabant unit along the eastern side of the English Channel, as an extension of the Variscan structures of Southern England. The Boulonnais region presently represents a faulted inverted structure involving, in addition, Jurassic and Upper Cretaceous sedimentary rocks. Within the core of the massif, there are unmetamorphosed Devono-Carboniferous sedimentary rocks lying unconformably on Silurian shales. The whole sequence was folded and thrusted after mid-Westphalian times. The cover-basement succession can be divided into three structural subunits: the lowest and northernmost Ferques, the intermediate Haut Banc, and the uppermost and southernmost Hydrequent units (Figs. 3 and 4). The style of the NNE vergent folds and thrusts faults (for example Averbuch and Mansy, 1998) shows that the Boulonnais Palaeozoic area forms the westernmost extension of the French Variscan thrust front, which is well constrained in the Nord-Pas de Calais coal basin (Bouroz et al., 1962). The major thrust zone, the Midi Fault, in classical interpretations, lies a few kilometres south of the exposed Palaeozoic strata. The Boulonnais Palaeozoic can thus be considered as the deformed footwall of this major Variscan thrust. In the Boulonnais, the Midi Fault is a complex, rather than a singular, fault zone, and it does not represent the emergent front of the Variscan orogen. Some of the Variscan faults are reactivated during Mesozoic times (e.g., Landrethun Fault, Figs. 1, 3, and 4), while others are sealed by undisturbed Middle Jurassic deposits (e.g., Ferques Fault, Fig. 3., Mansy et al., in press).

The Tournai Palaeozoic massif is situated in a more intermediate section of the Northern France–Southern Belgium Variscan front with a general E–W trend (see Fig. 1), some tens of kilometres north of the major Midi Fault Zone. It is dominantly a Carboniferous carbonate cover affected by very gentle folding and contractional faults with little offset (Hennebert, 1998).

The Coal Basin crops out south of the Tournai area with a thick and in places intensely deformed Namuro-Westphalian coal sequence. The onset of shortening was characterized by the development of metric to kilometric ramps and contractional faults that became folded as deformation proceeded (Humblet, 1941; Chalard, 1945).

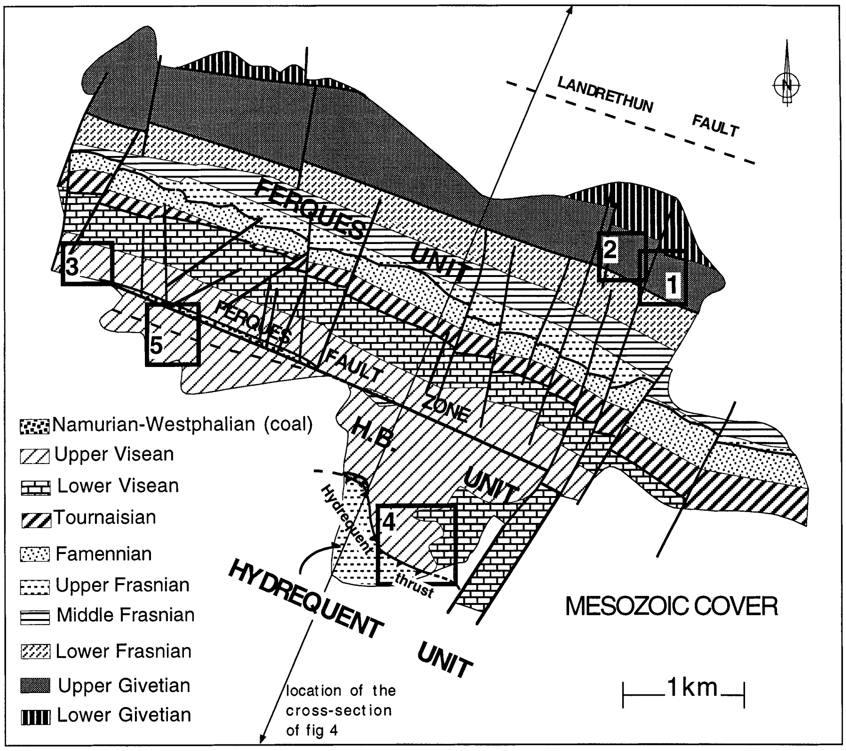

Fig. 3. Location map and simplified geological map of the Boulonnais area (after Mansy et al, in press).

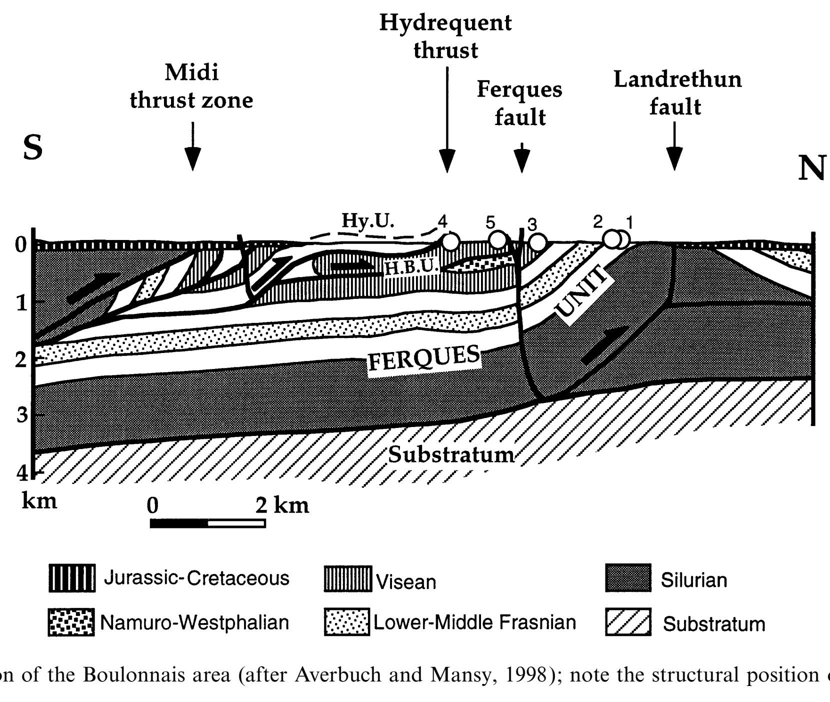

Fig. 4. Cross-section of the Boulonnais area (after Averbuch and Mansy, 1998); note the structural position of the sampled sites.

Superimposed on these early folded and faulted structures is a succession of out-of-sequence thrust faults that often have kilometric displacements (Mansy et al., 1997; Hance et al., 1999). The deformation in the Coal Basin suggests that the Variscan front lies several kilometres to the north.

2.2. Ardenne Allochthon

In the Rocroi, Givonnne and Stavelot massifs (Fig. 1), parts of the Ardenne Allochthon, Lower Devonian strata unconformably overlie strongly folded lower Palaeozoic rocks.

The Lower to Middle Devonian cover lies unconformably and without décollement or detachment on this basement (Meilliez et al., 1994). It consists of a fining-upwards clastic group deposited in a continental to marine environment. The Middle Devonian rocks accumulated on a carbonate platform grading southwards into a slope. In Late Devonian times, a strongly differentiated clastic and carbonate shelf developed. This was succeeded by a condensed carbonate platform sequence in Early Carboniferous times. The late Early Carboniferous is characterized by strongly differentiated facies distribution. The Late Carboniferous clastics are interpreted as a basin fill that developed in front of the emerging Variscan nappes.

The Variscan shortening gave rise to a system of folds and faults, which record a progressive deformation (Mansy and Meilliez, 1993; Mansy et al., 1995). Irrespective of the scale, the shortening is expressed as asymmetrical north verging folds with short steep limbs commonly cut by flat to shallow dipping faults. In the whole Allochthon, a penetrative cleavage is observed, which affects both the Lower Palaeozoic and its unconformable Devonian–Carboniferous cover. In southern parts, the cleavage is post-folding. In some places, a second crenulation cleavage can be observed. In the central part of the Ardenne Allochthon, tectonic transport is directed northward, although in detail, variations in fold trends and cleavage strike orientations from N70 to N120° are found.

The basement and the cover of the southern margin of the Rocroi Massif record an epizonal metamorphism that decreases in intensity both to the north and to the south. Ages obtained from chlorite flakes constituting the schistosity range from 315 Ma in the south to 290 Ma in the north (Piqué et al., 1984), similar to the trend observed in Germany (Ahrendt et al., 1983). The general northwards younging of deformation is also corroborated by Uppermost Visean sedimentological features such as slumps and megabreccias.

In the southern part of the Ardenne Allochthon, illite crystallinity indicates anchizonal burial. In some places, clay assemblages show that burial and metamorphism were weak (Chamley et al., 1997). This observation suggests that Devonian rocks had only a moderate overburden (2–4 km) and that they were rapidly uplifted during Late Visean–Early Namurian times (Mansy et al., 1995). Helsen (1992, 1995) has measured CAI values between 3.0 and 3.5 (i.e., 100–150°C) on the northern flank of the Rocroi massif, and values of 4.5–5.0 (250–300°C) have been obtained near the Stavelot Massif (Fielitz and Mansy, 1999).

The Avesnois region is located to the NW of the Rocroi Massif in the area affected mainly by diagenesis to anchizonal metamorphism. It is composed of different north-vergent, internally deformed thrust-sheets, involving 3 km thick Lower Devonian to Visean sequence (Khatir, 1990). The sampled Givet region of the Meuse valley is located to the north of the Rocroi massif and has the same structural and diagenetic–metamorphic conditions as the Avesnois region.

3. Palaeomagnetic sampling

In the framework of a French–Hungarian Intergovernmental Project (Balaton Project F-45/96), a total of 144 samples were drilled at 10 Palaeozoic localities (Fig. 1, Table 1) and oriented in situ by magnetic compass during two field campaigns in 1996–1997. The sampling localities are within the exposed NW, central and eastern parts of the Variscan chain of Northern France–Southern Belgium, namely the Boulonnais (five localities), the Tournaisis (one locality), the Avesnois (two localities) and the Ardennes-Meuse valley (two localities) areas. Sampling was not extended east of the Givet region since recent

Table 1
List of the palaeomagnetic localities

	Locality	Latitude	Longitude	Magnetic declination	Age
Boulonnais - Ferques Unit					
1	Griset	50°50′00	1°47′30	−2.9°	Upper Givetian: 374–380 Ma
2	Banc Noir	50°50′00	1°47′30	−2.9°	Upper Givetian: 374–380 Ma
3	Leulinghen	50°48′30	1°46′00	−3.0°	Visean: 333–352 Ma
Boulonnais - Haut-Banc Unit					
4	Basse-Normandie	50°48′00	1°46′30	−3.0°	Visean: 333–352 Ma
5	Moines	50°48′30	1°46′00	−3.0°	Visean: 333–352 Ma
Tournaisis					
6	Antoing	50°37′00	3°20′00	−2.0°	Tournaisian: 352–360 Ma
Avesnois					
7	Bettrechies	50°13′20	3°43′00	−2.1°	Givetian: 374–380 Ma
8	Limont-Fontaine	50°12′00	3°48′00	−2.0°	Visean: 333–352 Ma
Ardennes					
9	Vireux	50° 5′00	4°42′30	−1.7°	Lower Emsian: 387–394 Ma
10	Givet	50°7′30	4°50′00	−1.7°	Givetian: 374–380 Ma

palaeomagnetic data are available for this part of the Ardennes (Thominski et al., 1993; Molina Garza and Zijderveld, 1996).

3.1. Brabant Parautochthon

3.1.1. Boulonnais region

There are several quarries in the Palaeozoic of Boulonnais. Most of them were visited, but only a few appeared to be suitable for palaeomagnetic investigation. Three localities, Griset, Banc Noir and Leulinghen quarries (respectively points 1, 2 and 3 in Fig. 3) of Upper Givetian and Visean age, have been sampled in the lowermost thrust unit known as the Ferques Unit (see the structural positions of the sites in Fig. 4).

In Griset, a thick sequence of dark grey Givetian limestones and shales is quarried. Locally, beds rich in corals and other reef-building organisms can be found, especially towards the top of the exposed series. In the quarry, three sites were sampled with different lithologies and in different stratigraphic positions: dark grey marl, black marl, black shale-silt and silty limestone. The sites represent about 100 m in stratigraphic thickness.

In the Banc Noir quarry, a Givetian dark limestone–shale sequence is exposed. A green index horizon was sampled, consisting of clays, which could be of volcanic origin, and a reddish marl intercalated with the black–grey limestones.

In the Leulinghen quarry, the sampled material comes from a part of the quarry lying at a considerable distance from the Ferques fault. The Early Visean rock consists of cycles of dark, 0.5–1 m thick dolomitic limestone beds topped generally by a few centimetres of thin reddish, marly-clayey material. The latter may be of palaeo-soil or tuff origin. The sampled rocks are reddish palaeo-soils with dolomitic debris and dark dolomitic beds with small pebbles. The facies is interpreted as a shallow carbonate platform.

Two other localities [Basse-Normandie (point 4 in Fig. 3) and Moines quarries (point 5 in Fig. 3)] have been sampled within the Visean limestones–dolostones of the intermediate Haut-Banc unit (see Table 1). In the Basse Normandie quarry, the wall near the railroad cut was sampled, where a fold and ramp is exposed. The structure has been analysed by Cooper et al. (1983), Averbuch and Mansy (1998). The fold was not accessible, and samples were collected from the footwall of the large ramp, 4 m beneath the duplex horizon. Here, the beds were monoclinal with a southerly dip and consisted of metre-thick light grey limestone beds, that alternate with thin marly–sandy layers. Some of these have oxidized to a secondary red colour.

There are also some clayey beds that may also have an original red colour. Several sites were sampled in red clays–shales, in dark grey–brownish siltstones and dark, thin limestone intercalations.

In the Moines quarry, Early Visean limestones intercalated with thin marls or shales are exposed. Thin intercalations of limestones and fine-grained sandstones–shales, all dark grey in colour, were sampled.

3.1.2. Tournai area

In the Tournai area, one locality, the Antoing quarry, has been investigated (point 6 in Fig. 1), where subhorizontal black Tournaisian marly limestones are exploited. The quarry yards are cross-cut by major faults, and the rigid material is also frequently fractured. The samples are from the eastern yard. The black, often fossiliferous, rock is composed of thick limestone and thin shale layers. Both marly limestone and thinner shale intervals were sampled.

3.2. Ardenne Allochthon

3.2.1. Avesnois area

Two folded sequences have been investigated: one in the Givetian marly limestones, in the Bettrechies syncline lying a few kilometres south of the Midi Fault (point 7, in Fig. 1; see also Fig. 2), and the other from the synclinally folded Visean limestones in the Avesnes thrust unit (Limont-Fontaine quarry, point 8, in Fig. 1).

In the Bettrechies quarry, the Late Devonian dark carbonate consists of regular alternations of 30–80 cm thick limestones, marly limestones and 5–10 cm thick black shales, marls. Both rocks can be fossiliferous. Penetrative or weaker cleavage, depending on clay content, affects both rocks. Frequently, the limestone beds are cross-cut by white calcite veins, and both rock varieties are also fractured. Layer-parallel slip, sometimes filled by calcite veins, is also very frequently observed, especially within thicker shale horizons. The quarry exposes a kilometric syncline, the southern limb of which is more deformed, than the northern limb (Mansy et al. 1995). The structure is truncated on the top by subhorizontal Cenomanian and younger beds. Seven sites were drilled on the two limbs of the Palaeozoic syncline in sectors that seemed less deformed and farther from detachments. Limestones, marly limestones and dark shales were collected.

This quarry is especially valuable, since geotemperature studies were carried out, using different methods. Fluid inclusions in the calcite veins (Kenis et al., 2000) suggest a stepwise decrease in temperature from 300 to 70°C that is related to different tectonic events. Vitrinite reflectance values (Degardin, pers. commun.) range between 4 and 3.5 and indicate the same range of temperature. The CAI (Conodont Alteration Index) values (Helsen 1995) are between 5 and 4.5, corresponding to temperatures of 300 and 250°C.

The Limont-Fontaine quarry exploits mid-Visean limestones. The dark carbonate consists of a cyclic alternation of thicker limestone layers, often dolomitized, and thinner, sometimes reddish marly–shaley horizons, interpreted as palaeosoils. Hectometric slumps are frequent. Smaller limestone beds immediately below the red clays may contain intraclasts or brecciated layers, while the bulk of the limestone is composed of micrite. No cleavage is apparent in the sampled rocks. The quarry exposes a syncline, two flanks of which were sampled.

3.2.2. Meuse valley, Givet area

Two localities were investigated in the region of Givet in anchi-metamorphosed Devonian rocks of the northern limb of the Rocroi massif (Fig. 1): one in the north-dipping Lower Emsian sandstones of the Vireux quarry and another in subvertical Givetian limestones in the vicinity of Givet.

In the Vireux quarry, the rocks are thick, brownish, massive sandstones, often showing ripple marks, and thinner, very compact, black shales. A strong cleavage is observed in the latter. Dark shales in several beds were sampled, but in the same structural position, with a northerly dip.

The locality near Givet is in a road cut on the eastern flank of the Meuse, near a small bridge, on the French side. The sampled rock was a Givetian black, sometimes dolomitic limestone in 20–10 cm thick beds, with a few intercalations of clay and fine-grained limestone. The sequence is cut by calcite veins and cracks. Two of the thin dark limestone beds from the steep (75°) overturned limb were sampled.

4. Rock magnetic properties and palaeomagnetic analysis

The standard-sized specimens cut from the drillcores were subjected to magnetic susceptibility anisotropy (AMS) measurements in Lille (KLY-2 Kappabridge), NRM (Natural Remanent Magnetization) measurements and demagnetization in increments by an AF (alternating field) or thermal method or by the combination of the two in Budapest (JR-4 magnetometers, two axes Cryogenic magnetometer, Schonstedt oven, Schonstedt AF demagnetizer and AF demagnetizer built at the Technical University, Budapest peak field 0.24T). Magnetic minerals were also identified in Budapest by IRM (Isothermal Remanent Magnetization) acquisition characteristics (Pulse Magnetiser, Molspin) and by stepwise thermal demagnetization of the three-component IRM (Lowrie, 1990).

4.1. Intensity of the magnetic signal and AMS analysis

The magnetic susceptibility and the initial NRM intensity of the samples were variable, depending on the sedimentary facies. For instance, in the Boulonnais area, the samples from the Visean carbonate platform (Basse-Normandie, Moines, Leulinghen and Limont-Fontaine quarries) had negative bulk susceptibilities and very weak remanences (Fig. 5). In these cases, the calcite matrix may be the major contributor to the magnetic susceptibility, and the AMS results display a large scatter of the principal axes.

Rocks deposited in more restricted environments (black shaley limestones and siltstones) as well as the red clay levels display rather weak positive susceptibilities and relatively high NRM intensities. In these rocks, the AMS is likely to be of ferromagnetic origin. In contrast, green clay levels from the Banc Noir quarry and grey shales from the Griset quarry are characterized by relatively high positive susceptibilities and low NRM intensities (Fig. 5). This is likely to be due to a dominant paramagnetic contribution to the magnetic susceptibility from the clay minerals.

A significant mean AMS ellipsoid could only be determined for the sites with a positive magnetic susceptibility. The anisotropy parameter, P (K_{max}/K_{min}), depends on the lithology and the tectonic context but never exceeds 1.05 (maximum value in the Vireux quarry). The low values indicate that the rocks have suffered little internal deformation, and consequently, the direction of remanent magnetization is not biased. Magnetic fabrics are generally triaxial with a significant component of tectonic-induced linearity (Fig. 6a). Within localities, the anisotropy parameters and the shape of the AMS ellipsoid may vary strongly. This feature is particularly clear within the Bettrechies syncline. There, the degree of anisotropy and the planar/linear tendency of the fabric vary with the sedimentary facies (limestones exhibit dominantly prolate AMS ellipsoid, whereas shales show more planar fabrics). The general anticorrelation between the magnetic susceptibility and the anisotropy degree (Fig. 6b) may be explained by the variable amount of secondary, post-deformational, weakly anisotropic pyrite observed under the microscope.

In the majority of sites, the minimum susceptibility axes cluster close to the bedding pole, suggesting an inherited sedimentary fabrics (see Fig. 7c). In the sites from the Bettrechies syncline and from the Givet area, some minimum susceptibility axes deviate from the bedding pole and define a subtle girdle-like distribution around the maximum susceptibility axes (Fig. 7a, b, and d). The latter are generally well clustered within the bedding, defining a magnetic lineation that, in most cases, can be related to the observed structural markers.

The relations of anisotropy lineations and structures are basically of two types. The first type is characterized by lineation perpendicular to the shortening, like in the sites from Tournai, Bettrechies, Vireux and the southern part of the Griset quarry. Such a magnetic fabric, with an intersection-type lineation within the bedding, has been frequently observed in folded rock sequences

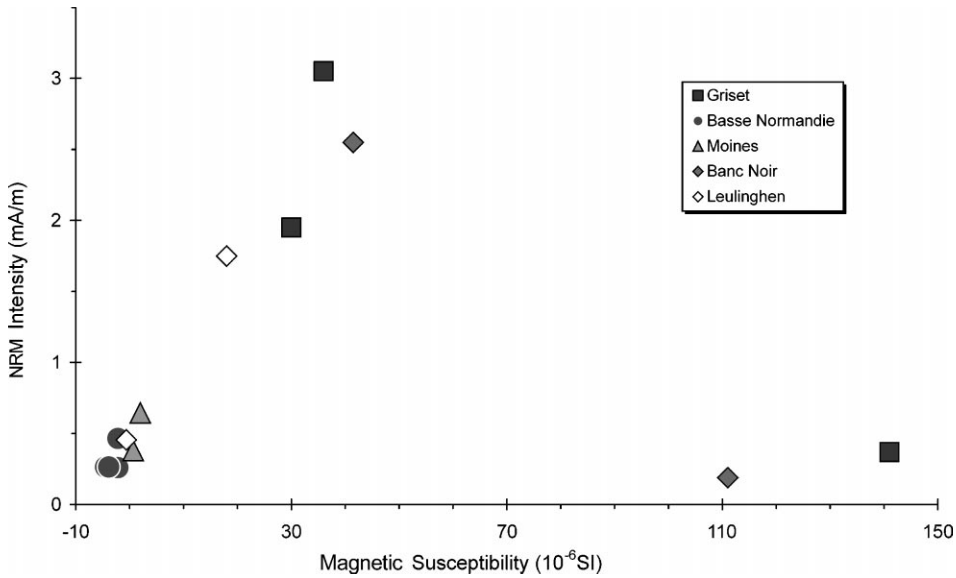

Fig. 5. Correlation diagram between the intensity of Natural Remanent Magnetization/Magnetic Susceptibility in the Boulonnais area.

(see Borradaile and Tarling, 1981; Kligfield et al., 1981; Kissel et al., 1986; Averbuch et al., 1995, for example) and can be interpreted as a composite feature due to the superposition of the tectonic fabric upon the sedimentary fabric. It is interesting to note that in Bettrechies, the magnetic lineation is normal to the late Variscan direction of shortening (NE–SW; see Fig. 7a and b) that postdates

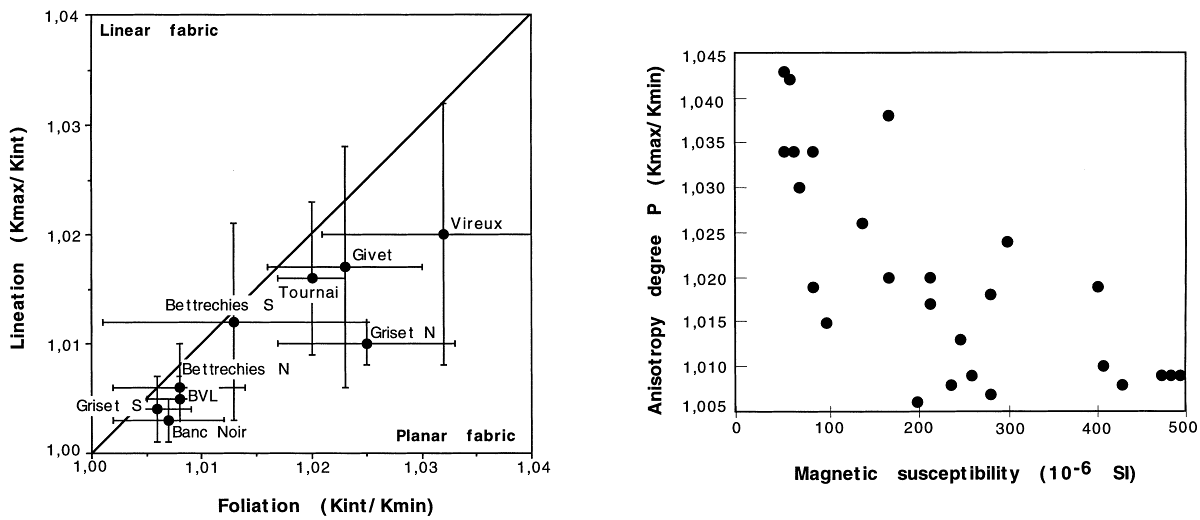

Fig. 6. Magnetic fabric parameters within the study area. (a) Diagram reporting the mean values of magnetic lineation, L (K_{max}/K_{int}) versus magnetic foliation, F (K_{int}/K_{min}). Site means are arithmetic means. Bars represent standard deviation on each parameter. The line $L=F$ separates an upper domain of dominantly linear magnetic fabrics ($L>F$) from a lower domain of dominantly planar magnetic fabrics ($F>L$). BVL: Boulonnais Visean Limestones. (b) Diagram showing the degree of anisotropy, P (K_{max}/K_{min}) versus the mean magnetic susceptibility for all samples from the Bettrechies quarry. Note the general anticorrelation of these parameters due to the influence of weakly anisotropic paramagnetic pyrite.

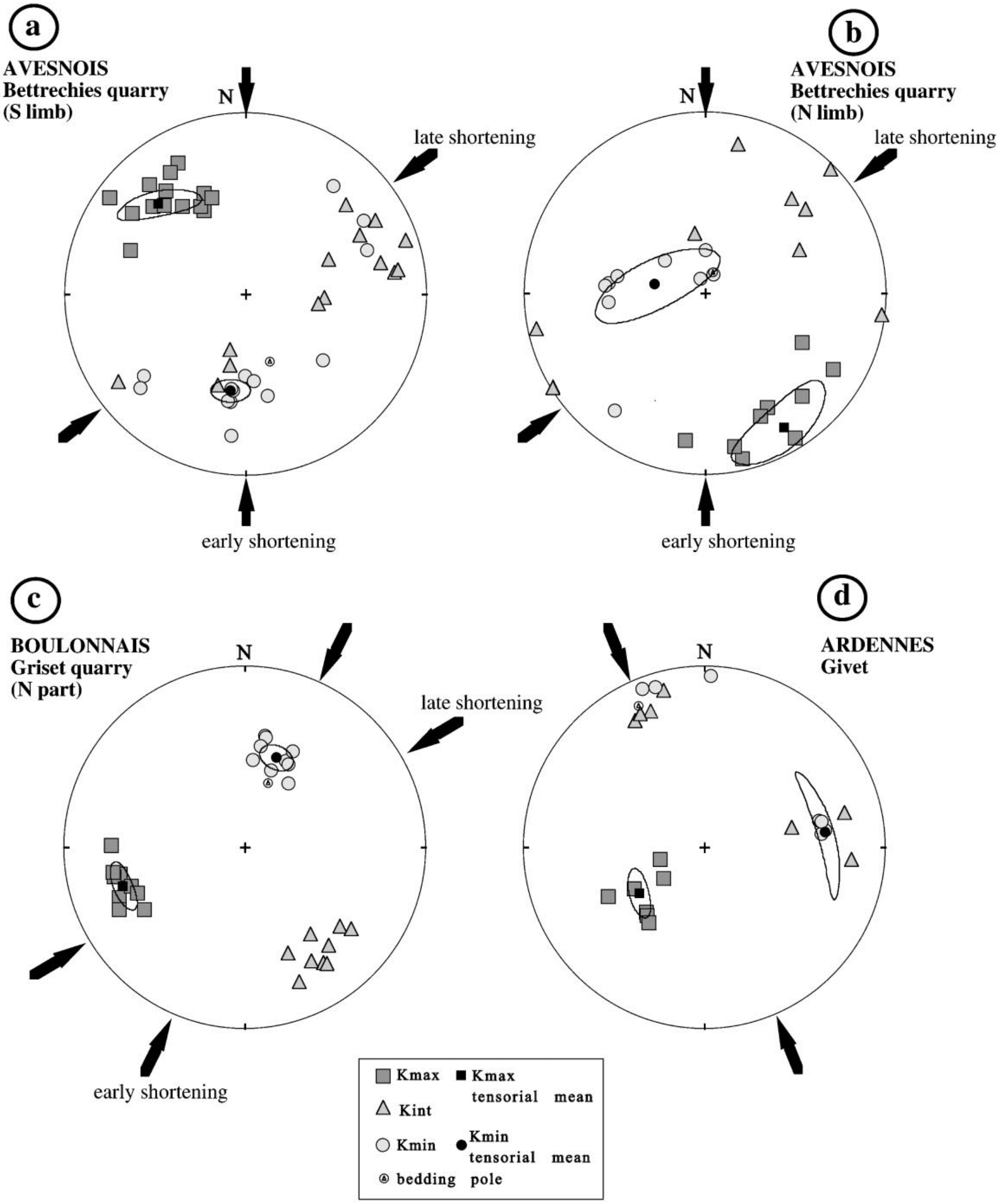

Fig. 7. Stereoplots (lower hemisphere, equal area) of representative magnetic fabrics from the area. The ellipses represent the confidence angle around the mean direction of each principal susceptibility axis.

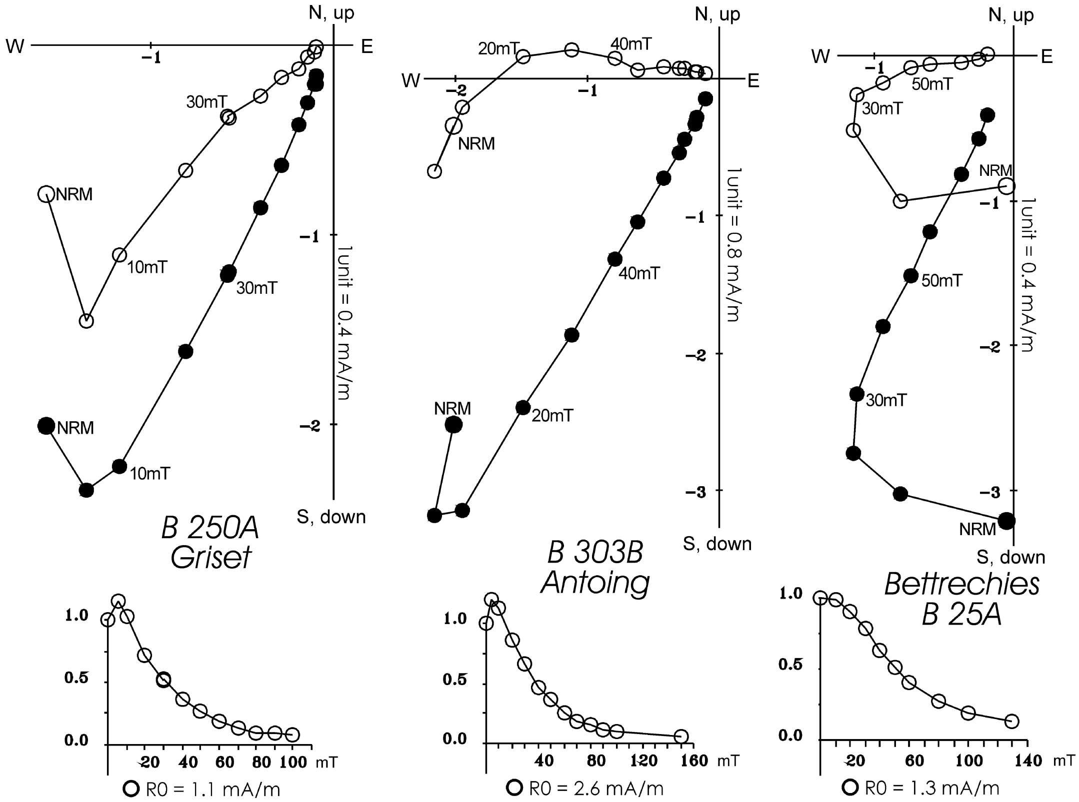

Fig. 8. Typical demagnetization curves for soft remanence. Upper row: Zijderveld diagrams. Open/solid symbols are projections on the vertical/horizontal plane. Lower row: normalized intensity versus demagnetizing field diagrams.

the major folding. A late reorganization of the fabric is also suggested by the formation of late pyrite. The second type of relationship between lineation and structures is observed at the northern part of the Griset and in the Banc Noir quarries. Here, the magnetic lineation strikes NNE–SSW to ENE–WSW (Fig. 7c), parallel to the tectonic transport directions evidenced in the Boulonnais (Averbuch and Mansy, 1998). Although an orientation of the magnetic lineation of depositional origin cannot be excluded, it seems more reasonable to interpret it as a tectonic transport-parallel lineation related to layer-parallel shear of the sedimentary sequence. The mechanisms for such a preferred orientation pattern still remain to be understood.

The site of Givet is a kind of exception, in which a well-developed lineation cannot be readily related to structural features (Fig. 7d).

4.2. Magnetic mineralogy and behaviour of NRM on demagnetization

The lithologic groups defined above were characterized by different magnetic signal intensities and also behaved differently during demagnetization.

The dark grey marls of Griset, Antoing and Bettrechies (Fig. 8) were completely demagnetized in AF fields of a maximum of 200 mT, while the other rock types needed thermal treatment for defining the components of the NRM. The positive response of the dark grey marls to AF treatment was very welcome since, during thermal treatment, above 400°C, their susceptibility rapidly increased as a result of newly formed magnetite, thus making the measurement of the NRM difficult. The softness of the magnetic material in the dark grey marls of the above mentioned three localities is corroborated

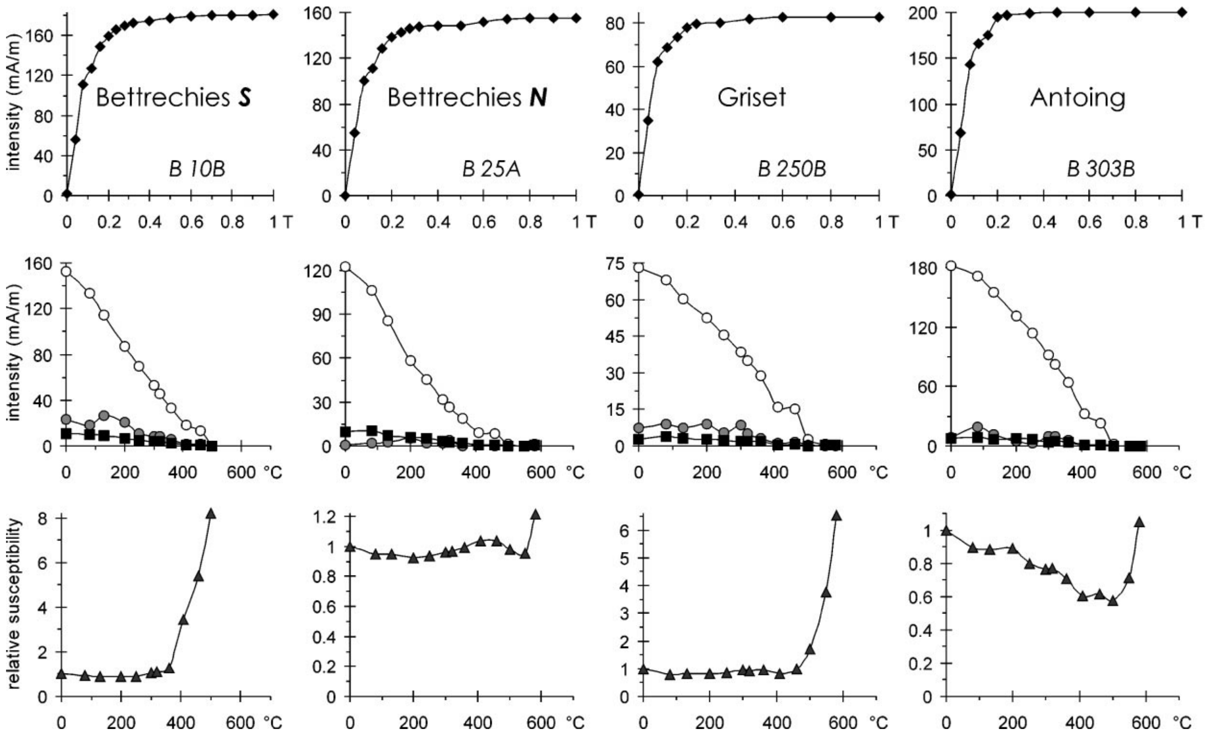

Fig. 9. Identification of magnetic minerals. First row: isothermal remanence (IRM) acquisition characteristics. Second row: thermal demagnetization of the three-component IRM; intensity versus temperature diagrams. Open symbols represent the softest component, dots the medium hard component, and squares the hardest component. Third row: behaviour of the magnetic susceptibility on heating.

by the easy saturation of the IRM acquisition curves (Fig. 9). Stepwise thermal demagnetization of specimens with dominant soft magnetic minerals eliminates the softest component (acquired in a field of 200 mT) of the three-component IRM by 500°C. The demagnetization curves also exhibit an inflexion at about 400°C, suggesting that ferrimagnetic iron sulphides and magnetite together may be present in these specimens. The presence of iron sulphide is further supported by increasing susceptibility from 400°C on. The medium hard (acquired in a field of 360 mT) and hardest (acquired in a field of 1.0 T) components in these specimens are really subordinate. They exhibit a noisy behaviour on thermal demagnetization, yet, in some cases, the trend in their decay clearly corresponds to that of the softest component (e.g., B10b, B303b, B250b in Fig. 9).

For the other rock types, typical thermal demagnetization curves are shown in Fig. 10. For them, saturation of the IRM is not achieved at 1 T, indicating the general high coercitive nature of the magnetic fraction. A subordinate soft magnetic fraction is locally associated with the dominant hard magnetic mineral (for example in Limont-Fontaine). The hard and dominant magnetic mineral is haematite, as shown by the three-axis and classical IRM thermal demagnetization curves (Fig. 11). Exceptions occur in the Moines quarry, where a drastic decrease of the IRM is observed at about 100°C, indicating the existence of goethite (B 52a in Fig. 11).

As a result of the analysis of the stepwise thermal or AF demagnetization of the NRM, the components of the NRM were defined for each specimen (Kent et al., 1983), and the site and locality palaeomagnetic mean directions were calculated (Tables 2 and 3). Most of the NRM demagnetization curves, apart from a small, recently acquired overprint component, exhibit single component NRM. In Limont-Fontaine and

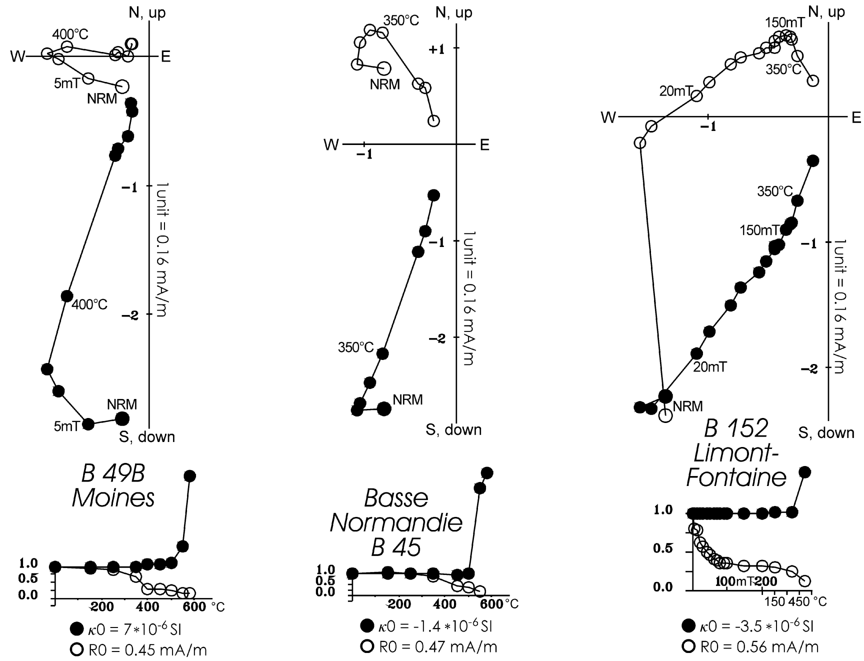

Fig. 10. Typical demagnetization curves for hard remanence. Upper row: Zijderveld diagrams. Open/solid symbols are projections on the vertical/horizontal plane. Lower row: intensity (circles) and susceptibility (dots) versus temperature curves.

Basse Normandie, both low- and a high-blocking NRM components were recognized occasionally.

Concerning the actual carriers of the remanence, there is a good agreement between the decay of the NRM and that of the three component IRM on thermal demagnetization, except in the case of the Moines quarry, where the goethite is not indicated by the decay of the NRM on heating.

5. Assessment of the palaeomagnetic directions

Several samples from each locality yielded characteristic remanent magnetization (ChRM), which is suitable for tectonic interpretation (Tables 2 and 3). The age of the acquisition of the ChRM is not, however, directly related to the stratigraphic age of the rocks.

In three cases, it was possible to sample folded structures or strata with different tilts, so that fold- or tilt-tests could be carried out on a locality level. For two such localities (Limont-Fontaine and Griset), the test is definitely negative, so the acquisition of magnetization must post-date the folding event. Therefore, these palaeomagnetic directions will be interpreted without tilt correction. For Bettrechies, partial unfolding provides the most consistent direction. This remanent magnetic signal is thus interpreted to be related to a remagnetization process acquired during a late syn-folding event.

For the other sites, which are either subhorizontal or exhibit a uniform bedding attitude within each locality, there are few arguments in favour of, or against, the pre-tectonic age of the magnetizations, except the palaeolatitude indicated by them. This aspect of the ChRM directions will be discussed later. However, it is possible to reject a pre-tectonic age for the ChRMs in the Banc Noir, Leulinghen and Moines sites in the Boulonnais due to their oversteepened negative inclinations in bedding corrected coordinates that would imply too high northern palaeolatitudes in pre-Westphalian times. As a consequence, the hard component of NRM measured within the Griset site exhibits a similar direction to that defined in the red clay samples from the Banc Noir quarry (close to the Griset quarry), is suggested to have

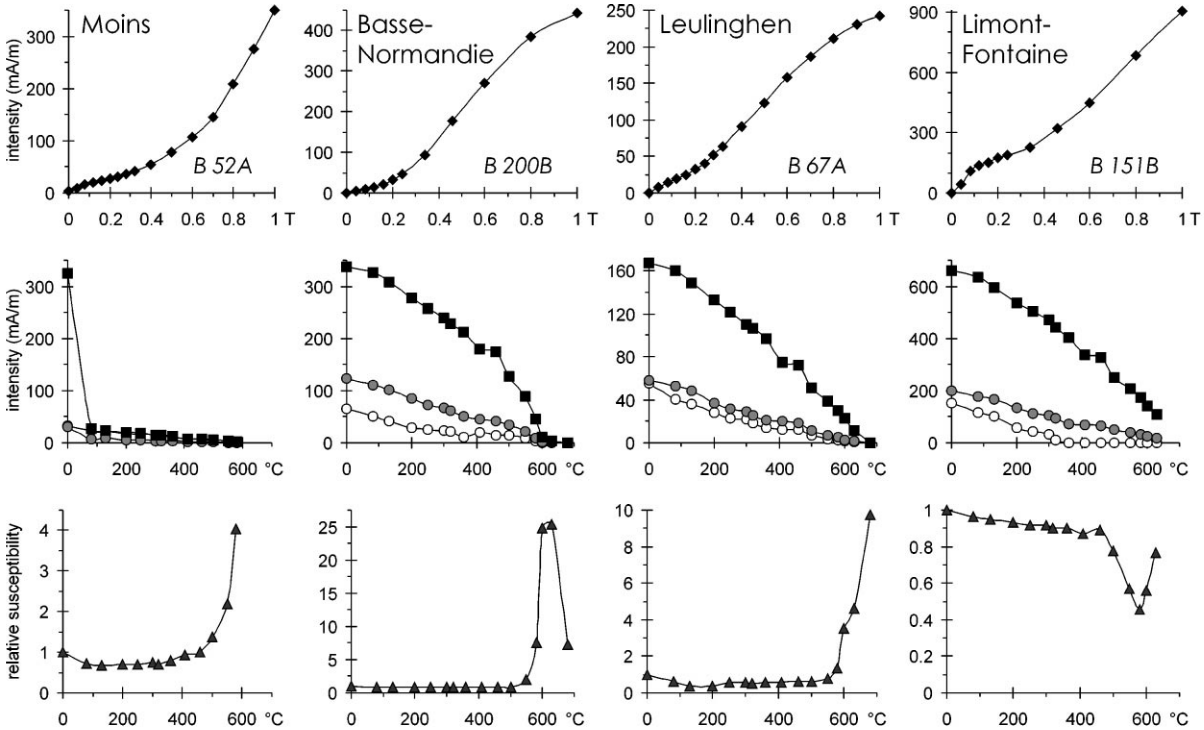

Fig. 11. IRM acquisition curves for slowly saturating samples and thermal demagnetization of the three-component IRM. Explanation as in Fig. 9.

also a post-tectonic origin. Such interpretation may be extrapolated to the extremely hard components of the NRM observed at Limont Fontaine and Basse Normandie sites.

In the Vireux and Givet sites in the Meuse valley area, where the sampled strata are tilted by the same angle within each locality, the ChRM directions are quite similar before, and widely different after, tilt correction. It is also known that these localities represent an area where metamorphic temperatures may have reached 300°C. During thermal demagnetization, the NRM signal is lost by 400°C. All these point to the post-tectonic age of the NRM in both localities.

6. Discussion of the palaeomagnetic data

6.1. Discussion of inclination data

Van der Voo (1993) compiled palaeomagnetic data for Palaeozoic time and plotted a palaeolatitude-versus-time curve for Variscan Europe. This suggests that Variscan Europe travelled from high southerly to very low southerly latitudes from Silurian through Late Devonian time. After the Late Devonian, the movement seemed to slow down, and the equator was crossed by the Armorican Massif during the Carboniferous.

Similar figures were constructed for the study area north of the Armorican Massif. As a reference framework for the new results, the expected palaeolatitudes were calculated from North European poles published by Van der Voo (1993) (his table 5.1) for several time intervals in the Palaeozoic. The general tendency shown by the black bars is that all expected palaeolatitudes are southerly until the culmination of the Variscan orogeny, followed by a sudden shift to the N during the orogeny. Afterwards, the movement to the N continued until the area probably reached 20°N by the end of the Permian (Fig. 12).

The palaeolatitudes obtained for the different components of our sites in the parautochthon

Table 2
Palaeomagnetic results from the Parautochthon[a]

Locality	n/no	$D°$	$I°$	k	$\alpha_{95}°$	$D_C°$	$I_C°$	k	$\alpha_{95}°$	Dip
Boulonnais *Ferques Unit*										
1. Griset B239–264										
B239–243 grey silty marl	5/5	206.6	+7.5	36	12.9	207.3	−23.1			200/31
B244–249 grey sandy marl	6/6	203.0	+12.1	31	12.2	203.2	−18.7			200/31
B250–253 dark grey clay	4/4	200.3	+16.8	81	10.3	200.1	−1.1			198/18
B254–257 black marl	4/4	200.7	+14.2	221	6.2	200.5	−3.7			198/18
B258–264 black shale	7/7	202.0	+17.2	1006	1.9	201.8	−3.8			201/21
Griset locality mean	26/26	202.7	+13.7	63	3.6	202.7	−10.4	38.1	4.7	
2. Banc Noir B265–275										
B271–275 purple marl component C	4/5	197.5	−22.6	62	12.0	196.0	−45.5			205/23
3. Leulinghen B59–67										
B59–61 mix of dolomite and red clay	3/3	196.9	−1.4	142	10.4	190.8	−25.1			191/24
B62–64 red clay	3/3	199.1	−10.5	104	12.1	201.2	−34.0			191/24
B65–67 dark grey dolomite	3/3	193.4	−6.3	241	8.0	194.2	−30.2			191/24
Leulinghen locality mean	9/9	196.5	−6.1	118	4.8	197.8	−29.8			
Boulonnais *Haut-Banc Unit*										
4. Basse Normandie B36–48, B199–207										
B36–40 pinkish grey limestone	5/5	181.9	+15.3	51	11	183.1	+8.5			227/9
B41–44 red limestone	3/4	169.9	+12.2	54	17	177.0	+6.1			227/9
B45–48 silty limestone	4/4	187.8	+23.8	62	12	190.5	+21.4			262/7
B199–204 grey limestone	4/6	209.5	+31.4	31	17	210.4	+23.6			226/8
B205–207 grey limestone	3/3	195.8	+24.5	26	25	297.2	+17.3			226/8
Basse Normandie locality mean	19/22	189.6	+21.8	23	7	191.3	+15.7	22	7	
Basse Normandie component C	3	202.1	−33.6	221	8	199.2	−40	113	12	
5. Moines B49–58										
B49–51, sandstone	3/3	192.6	−2.1	477	6	184.2	−40.3			220/43
B52–58 limestone	6/6	195.8	+27.3	88	6	197.8	−13.2			220/43
Tournaisis										
6. Antoing B303–314										
B303–308 black marl	6/6	210.3	−5.4	643	3	210.1	−5.6			295/2
B309–314 black marl	4/6	207.9	−3.3	208	6	207.7	−3.5			295/2
Antoing locality mean	10/12	209.3	−4.5	359	3	209.2	−4.8			

[a] n/no: number of used/collected samples $D°$, $I°$: palaeomagnetic declination and inclination before tilt correction. $D_C°$, $I_C°$: palaeomagnetic declination and inclination after tilt correction. k and $\alpha 95°$ are Fisher's (1953) precision parameter and the radius of the 95% cone of confidence, respectively.

(Fig. 12a) and the allochthon (Fig. 12b) are plotted according to the stratigraphic age of the rock. It is clear from these diagrams that some of the components define southerly latitudes (Component A), others show latitudes close to the equator (Component B) and the rest indicate northerly latitudes (Component C). This marked difference in palaeolatitudes of the components allows an age to be assigned to the acquisition of the different magnetic components in comparison with the reference palaeolatitudes.

In two cases (1A, 4A, on Fig. 12a), the age assigned by the palaeolatitude is in accordance with the stratigraphic age, yet a negative fold test indicates that one of them (Griset) is not primary. Nevertheless, the expected palaeolatitude remains almost identical for a long period, during which remagnetization could have occurred. In the rest of the components, the acquisition clearly postdates deposition. Most of them must have been acquired during the orogeny (Components B), and the rest (Components C) well after the orogeny.

Table 3
Palaeomagnetic results from the Allochthon[a]

Locality	n/no	D°	I°	k	α_{95}°	D_C°	I_C°	k	α_{95}°	Dip
Avesnois										
7. Bettrechies B10–35										
B10–13 S. limb, limestone	3/3	208.2	−7.9	377	4.7	209.4	+13.5			344/31
B14–18 S. limb, shale	5/5	210.0	−7.2	1251	2.2	211.3	+15.5			344/31
B19–23 S. limb, limestone	5/5	211.6	−10.5	350	4.1	211.4	+9.9			344/31
S. limb mean	14/14	210.1	−8.6	425	1.9	211.8	+12.3			
B24–26 N. limb, limestone	3/3	204.8	+4.0	355	6.6	205.0	−11.8			197/16
B27–28 N. limb, limestone	2/2	202.9	−0.5			203.4	−16.4			197/16
B29–32 N. limb, shale	4/4	205.2	0.0	166	7.1	205.5	−15.7			197/16
B33–35 N. limb, limestone	3/3	205.4	−0.2	1235	3.5	205.9	−15.9			197/16
N. limb, mean	12/12	204.8	+0.9	334	2.4	205.2	−14.9			
Bettrechies locality mean	26/26	207.6	−4.2	140	2.4	208.2	−0.3	37	5.2	
Bettrechies[b] locality mean	7/7	206.9	−3.1	170	4.6	206.6	−3.2	590	2.6	
Avesnois										
8. Limont Fontaine B147–157										
B147–151	5/5	195.1	+1.9	39	12.4	224.0	+34.1			11/57
B152–157	5/6	213.6	+15.2	68	9.4	200.7	−58.3			170/72
Limont Fontaine locality mean	10/11	204.3	+8.7	26	9.7	195.3	+12.1	2.7	36.5	
Limont Fontaine component C	4	199.8	−33.8	113	8.7	229.0	−26.0	1.8		
Ardennes										
9. Vireux B108–116										
B108–110, 111–116	7/9	196.2	−27.4	18	14.5	190.8	+4.8	21	13.6	336/44 342/36
10. Givet B117–124										
B117–120, 121–124	5/8	193.1	−15.5	25	15.7	237.1	+51.7			155/75 overturned

[a] Variables as for Table 2.
[b] Palaeomagnetic direction at 26% unfolding.

This latter component is invariably resides in haematite.

Since there is a general tendency of a northward shift with age, we might interpret the slight differences between palaeolatitudes of components B as a slightly older magnetization in the Allochthon and a younger magnetization in the Autochthon. If the magnetization were due to tectonic events, the above sequence of remagnetization would also correspond to the known sequence of tectonic evolution (Mansy and Meilliez, 1993).

Comparing the reference palaeolatitudes (Van der Voo, 1993) and those calculated from the present study to previously published data sets from the Namur-Brabant and Ardenne areas (Molina Garza and Zijderveld 1996; shaded stripes on Fig. 12), it can be concluded that in the new data set, there seem to be magnetizations that are older, and also younger, than previously published values.

6.2. Discussion of declination data

The expected declinations in different times are plotted (Fig. 13) for the study area from data by Van der Voo (1993) together with the new declinations. The diagram suggests a broad agreement between the two data sets, since the declinations fall between 190 and 210°, but on closer examination, the declinations for group C are all far from the declinations expected from the stratigraphic age of the rocks. If these directions are moved to their estimated age of remagnetization (based on the palaeolatitudes), the declinations come quite close to those expected. The declinations for age group B display a relative scattering with sites

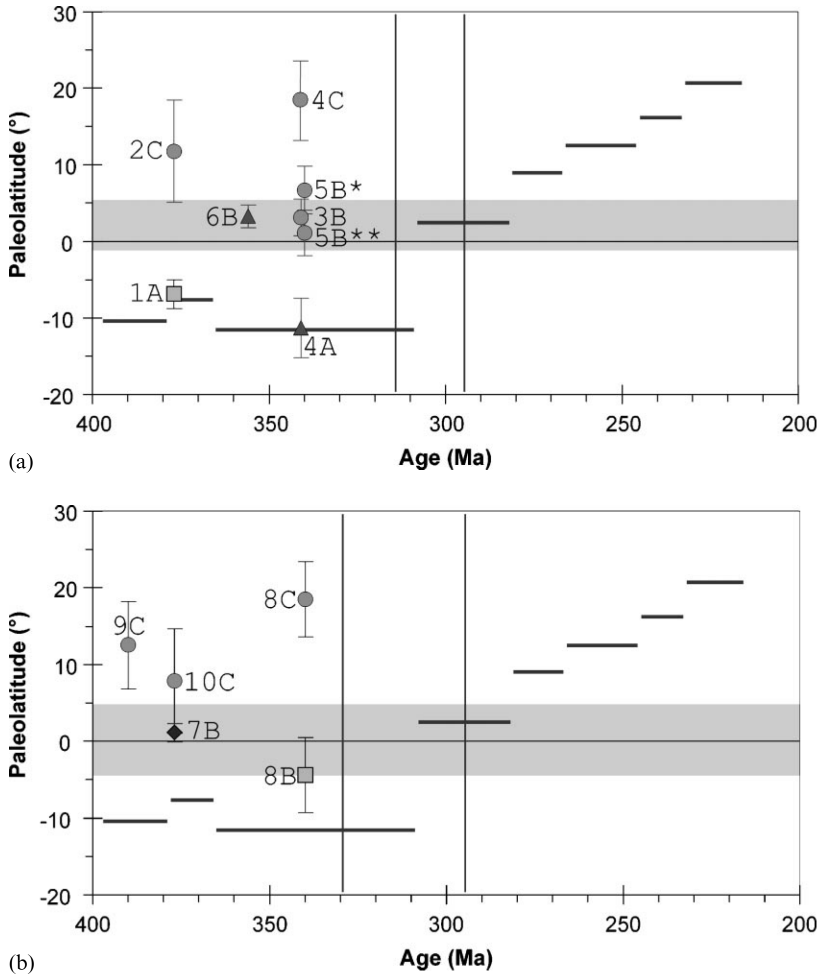

Fig. 12. Comparison of palaeolatitudes from new data with those for stable Europe. (a) Palaeolatitudes of the Parautochthon. (b) Palaeolatitudes of the Allochthon. Expected palaeolatitudes (Van der Voo, 1993) are horizontal bars; numbers refer to the localities of the present study, upper-case letters to the components of different ages. Squares are for localities with post-folding remanence, triangles for those with subhorizontal tilt, and diamonds for synfolding remanence. Dots represent localities, where, applying the tilt correction, the palaeolatitude would be too high for a Palaeozoic age of aquisition of the remanence (i.e., unrealistic). Vertical lines are the time limits for the Variscan compressive deformation in the corresponding area. The grey zone represents the interval defined by the mean palaeolatitudes of the low- and high-temperature components identified by Molina Garza and Zijderveld (1996).

showing directions close to those expected for the age of remagnetization and others closer to that expected for the stratigraphic age [for example, Antoing (6B), Bettrechies (7B) and Limont-fontaine (8B)]. Despite these small deviations from the expected declinations for the estimated age of the aquisition of the remanence, neither systematic rotation of the measured parts with respect to the reference declinations nor any difference along the studied belt can be found in these data. It is therefore concluded that the differences in declination are best explained by a moderate scatter around the mean value of 200° both in the Parautochthon and in the Allochthon, partly due to the different ages of remagnetizations.

The earliest remagnetizations (age group A) show interesting results: the Griset soft component (1A in Fig. 13a) has declinations that fall near to

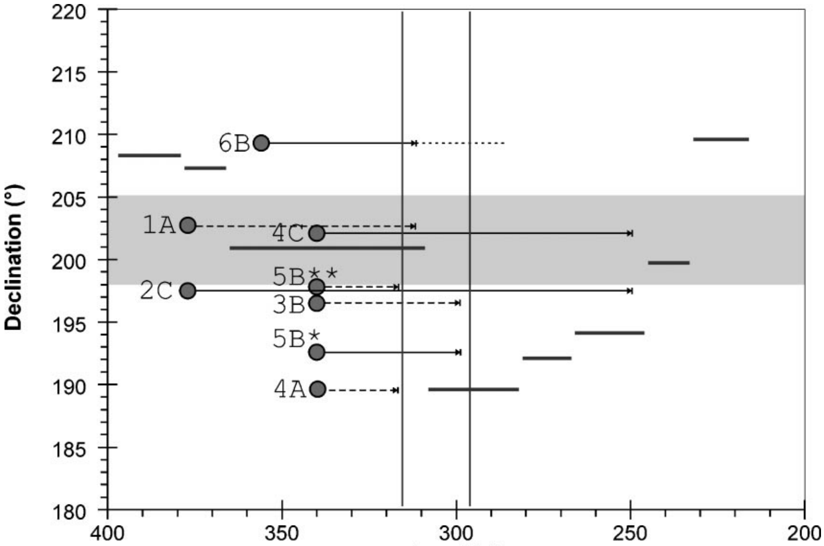

(a)

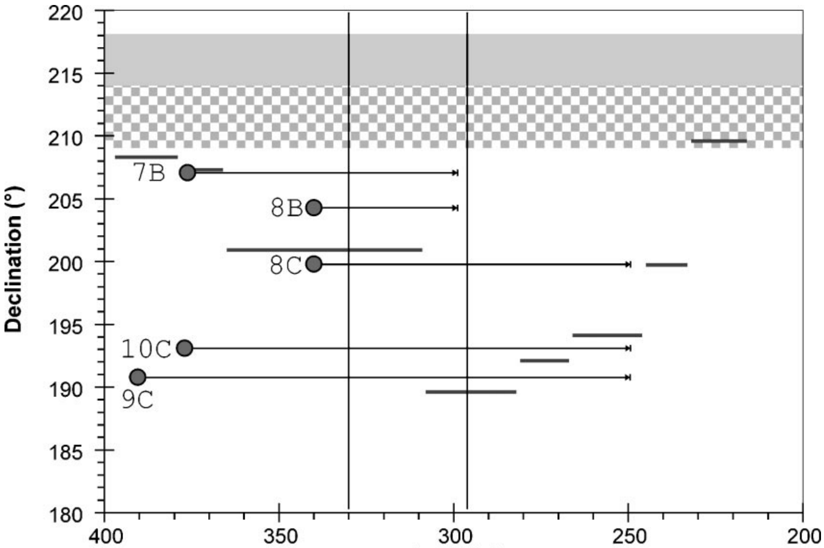

(b)

Fig. 13. Comparison of palaeodeclinations from new data with those for stable Europe. (a) Palaeodeclinations of the Paraautochthon. (b) Palaeodeclinations of the Allochthon. Expected palaeodeclinations (Van der Voo, 1993) are horizontal bars; numbers refer to the localities of the present study, upper-case letters to the component of different ages. Light and broken horizontal lines extend from the stratigraphic ages to the estimated ages of the acquisition of the remanence. Vertical lines are the time limits for the Variscan compressive deformation in the corresponding area. The grey zone represents the interval defined by the mean palaeodeclinations of the low- and high-temperature components identified by Molina Garza and Zijderveld (1996). In the Parautochthon, the declinations of the low-temperature components fall between 181 and 208°, and that of the high-temperature component between 179 and 216°. The same values for the allochthon are 211–230 and 210–234°, respectively. From the data set by Thominski et al. (1993), the mean declinations for the lower Devonian through lower Carboniferous age groups define the checked interval.

the expected declinations, suggesting litte rotation. The soft component of Basse Normandie (4A in Fig. 13a), however, shows a difference of 10–15° from the expected declination. This locality is in the same area as Griset, but in an upper tectonic slice, at the footwall of the Midi Fault. The confidence circles of the two palaeomagnetic directions overlap, i.e., the two declinations do not differ in a significant way. Nevertheless, they might be regarded as indicating a 10–15° counterclockwise rotation of Basse Normandie with respect to the non-rotating Griset and reference frame.

Assessment of previously published declination data is somewhat difficult because different authors suggested different remagnetization ages and published different declination values for the same Ardenne area. Molina Garza and Zijderveld (1996) suggested a 15° clockwise rotation of the Ardenne Allochthon with respect to the Brabant Parautochthon, which was recorded in both their high- and low-temperature components. This rotation is thus younger than 300 Ma. All the other authors interpreted slightly larger (20–30°) clockwise rotations in both their earlier and later remagnetizations.

In contrast, Givet and Vireux localities (component C) of the present study, in the same Ardenne region, show no significant rotation. This contradiction is even more interesting if we note that in the Parautochthon, the new declination data scatter around those of the mean declinations of the high- and low-temperature components of Molina Garza and Zijderveld (1996), i.e the older and new data sets are not different (Fig. 13).

In conclusion, the declination data obtained here do not indicate any significant rotation along the central and western portions of the Variscan chain of Southern Belgium–Northern France with respect to its foreland. Therefore, it is reasonable to compute palaeomagnetic pole positions from the overall mean directions of component A, B, and C, respectively (Table 4). There is perhaps one exception. The small (10–15°) counterclockwise deviation of the declination of the upper tectonic slices of the Boulonnais (Brabant Parautochthon) with respect to the foreland may have some tectonic significance.

7. Discussion on geodynamic models

The Variscan front of NW Europe exhibits a progression of deformation events. First, the Southern part of the Allochthon was deformed in Late Visean time with folding, cleavage formation and thrust faulting progressing northward during Late Carboniferous time. Fold axes are generally oriented NE–SW in the eastern Ardenne, and E–W in the central Avesnois. This deformation is accompanied in the Parautochthon by the formation of a foreland basin where thick molasse deposits (coal measures) accummulated. Folding in the middle part of the Parautochthon appears slightly later than Westphalian D. Fold axes in the Parautochthon generally follow the strike of the deformation front and fold axes in the Allochthon. In the Boulonnais (part of the Parautochthon), fold axes strike NW–SE. The structural directions of the Variscan front thus define an arc concave towards the north.

Table 4
Palaeomagnetic overall-mean directions and pole positions for components of early Variscan (A), main Variscan (B) and post-Variscan, probably Permian (C) age[a]

	N	$D°$	$I°$	k	$\alpha_{95}°$	Pole		δp	δm
						Longitude	Latitude		
Component A	10	195.5	+17.8	35	8.2	166	29	4.4	8.5
Component B	16	203.4	−2.9	72	4.4	154	37	2.2	4.4
Component C	5	197.6	−26.6	94	7.9	154	51	4.6	8.6

[a] N: number of sites. $D°$, $I°$: palaeomagnetic declination and inclination in the geographic system. k, $\alpha_{95}°$ as in Table 2. δp and δm are the semi-axes of the 95% confidence ellipse associated with the mean poles (Fisher, 1953).

The main Midi Fault is an out-of-sequence fault that cuts folds, implying Westphalian C, as well as cutting faults of the Parautochthon, and has a variable offset along its strike. Near Aachen, the displacement does not exceed a few kilometres, in the central part of the arc (near Bettrechies) it is at least 80 km (Mansy et al., 1997), and in the western segment of the arc (Boulonnais-Artois), the displacement is at least 15–20 km, while in southern England it is not known.

Several models possibly explain the present arcuate shape of the Variscan front of Southern Belgium–Northern France. The first (oroclinal bending; Fig. 14a) implies a wedge-shaped obstacle or promontory at the Brabant margin, on which a linear orogen is moulded. In this model the originally parallel, linear structures are rotated as the allochthon moves northward until they become (grosso modo) parallel with the margins of the obstacle. This model would imply clockwise and counterclockwise rotation of declination directions on the western and eastern branches of the chain, respectively. The amount of rotation would depend on the angular difference between the linear chain and the margins of the obstacle.

The second model (inherited shapes, Fig. 14b)

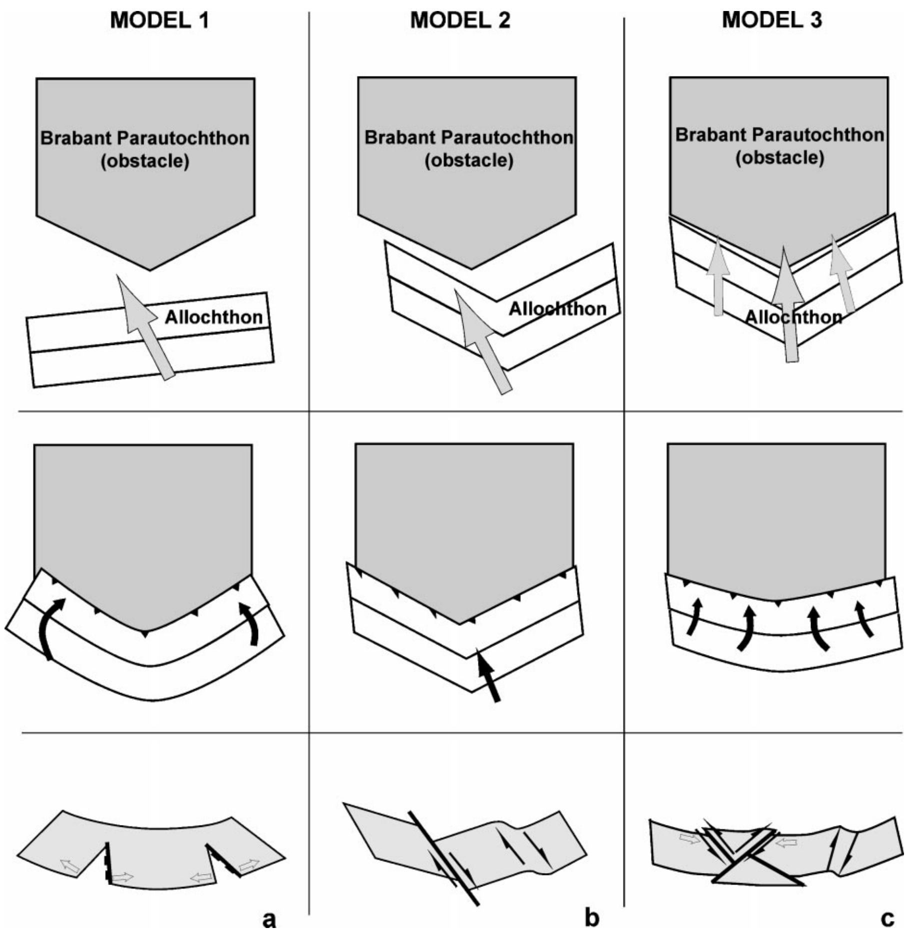

Fig. 14. Possible geodynamic models explaining the curvature of the Northern France–Southern Belgium Variscan thrust front. (a) Moulding of an originally linear orogen. (b) Collision of an originally arched orogen. (c) Unfolding of an originally arched orogen with the help of a variable offset thrust fault. Upper row: before orogeny. Arrows indicate future movements. Middle row: after orogeny. Black arrows indicate induced rotations. Lower row: sketch of internal deformations induced by the models.

presumes an originally arcuate shape of the Allochthon, which has the shape of the obstacle. When deformed, these would produce structures parallel to the margin of the Brabant obstacle, regardless of the tectonic transport directions. In this case, the structures were originally arranged in an arcuate pattern with no significant rotation in either branch of the chain. During progressive deformation, the shape of the original arc may be accommodated by strike-slip fault zones according to local space problems. A limited amount of rotation is possible along these zones.

In the third model (Fig. 14c), an original arcuate shape of the arc is again postulated, similar to the second model, but with the curvature diminishing with time. The decrease in curvature is accommodated by thrust-faulting, the offset of which varies from nil at both ends to maximal in the central part. The thrust-faulting would imply opposed, clockwise and counterclockwise rotations in the eastern and western branches, respectively. In models 1 and 3, the induced rotations imply orogen-parallel elongation or shortening. These deformations may be accommodated by structures at a high angle to the orogenic front.

The presently available palaeomagnetic data do not support the first model. The data set of the present study shows no significant rotation either in the time interval when the components of different ages (age groups A, B, C) were acquired, or along the chain, though age group B data correspond in age to those of Thominski et al. (1993) and Molina Garza and Zijderveld (1996). Arc forming would be best seen with the help of pre-tectonic declination directions. In the eastern Ardenne sector, there are no such data so far, as the only available declinations are syn- to post-tectonic. In the western sector, however, early tectonic declinations (Griset, Basse Normandie) are present and do not show any rotation.

The second model explains rather well the lack of significant palaeomagnetic rotations, and it needs only secondary deformation zones to explain the measured small rotations. The Meuse valley segment, measured by Molina Garza and Zijderveld (1996), is interpreted as a NW–SE-oriented dextral shear zone, creating the observed 15° clockwise rotation (Fig. 1). Here, near Givet, axial planes of folds are also rotated, cleavage is tilted and folds are refolded (Lacquement et al., 1997). Other smaller rotations would be also explained by local, late, accommodating strike-slip zones.

Model 3 could explain the clockwise rotation of the eastern Ardenne segment, together with the increased offsets observed along the Midi Fault from the east towards the central part. A symmetrical model would imply a small counterclockwise rotation in the western, Boulonnais segment and a decrease in the offsets of the Midi Fault from the center towards the west as well. The more daring interpretation of the Boulonnais palaeomagnetic data could support some limited counterclockwise rotation, but there is no information on the amount of offset along the western, covered segments of the Midi Fault. In this model, the orogen-parallel shortening could be accommodated by conjugate sets of strike-slip faults, along which material would be extruded to the north or south.

Acknowledgements

This work was partly sponsored by a Hungarian–French intergovernmental project (Balaton F-49/95) and by the Hungarian Science Research Found (OTKA, No. T029805). We are grateful to Prof. D.H. Tarling and an anonymous reviewer for useful comments. F. Bergerat from Université Paris VI. (France) and S. Vandycke from Mons University (Belgium) are thanked for field assistance and organization. The quarry owners and staff in the Boulonnais, Tournai area and Avesnois are thanked for their kind cooperation and local guidance.

References

Ahrendt, H., Clauer, N., Hunziker, J.C., Weber, K., 1983. Migration of folding and metamorphism in the Rheinische Schiefergebirge deduced from K–Ar and Rb–Sr age determinations. In: Martin, H., Eder, F.W. (Eds.), Intracontinental Fold Belts. Springer, Berlin, pp. 323–338.

Averbuch, O., Mattei, M., Kissel, C., Frizon de Lamotte, D., Speranza, F., 1995. Cinématique des déformations au sein d'un système chevauchant aveugle: l'exemple de la Montagna dei Fiori (front des Apennins centraux, Italie). Bull. Soc. géol. Fr. 166, 451–461.

Averbuch, O., Mansy, J.-L., 1998. The 'Basse-Normandie' duplex (Boulonnais, N France): evidence for an out-of-sequence thrusting overprint. J. Struct. Geol. 20, 33–42.

Bless, M.J.M., Bouckaert, J., Paproth, E., 1980. Environmental aspects of some Pre-Permian deposits in NW Europe. Meded. Rijks Geol. Dienst 32 (1), 3–13.

Bois, Ch., Cazes, M., Choukroune, P., Gariel, O., Hirn, A., Le Gall, B., Lefort, J.P., Matte, P., Pinet, B., 1994. Seismic reflexion images of the Pre-mesozoic crust in France and adjacent areas. In: Pre Mesozoic in France and Related Areas. Springer, Berlin, pp. 3–48.

Borradaile, G.J., Tarling, D., 1981. The influence of deformation mechanisms on magnetic fabrics in weakly deformed rocks. Tectonophysics 77, 151–168.

Bouroz, A., Chalard, J., Dalinval, A., Stievenard, M., 1962. La structure du bassin houiller du Nord de la région de Douai à la frontière belge. Ann. Soc. géol. Nord LXXXI, 173–220.

Chalard, J., 1945. La faille de Vicoigne du terrain houiller du Nord de la France. Ann. Soc. géol. Nord LXV, 177–196.

Chamley, H., Proust, J.N., Mansy, J.L., Boulvain, F., 1997. Diagenetic and paleogeographic significance of clay and other sedimentary components in the middle Devonian limestones of Western Ardenne, France. Palaeogeogr., Palaeoclimatol., Palaeoecol. 129, 369–385.

Cooper, M.A., Garton, M.R., Hossack, J.R., 1983. The origin of the Basse-Normandie duplex, Boulonnais, France. J. Struct. Geol. 5, 139–152.

Edel, J.B., Coulon, M., 1986. Mise en évidence de rotations tardihercyniennes à partir d'un profil paléomagnétique à travers l'Ardenne et le Brabant. Ann. Soc. géol. Nord 105, 139–144.

Fielitz, W., Mansy, J.-L., 1999. Pre- and synorogenic burial metamorphism in the Ardenne and neighbouring areas (Rhenohercynian zone, Central European Variscides). Tectonophysics 309, 227–256.

Fisher, R., 1953. Dispersion on a sphere. Proc. R. Soc. Lond., Ser. A 217, 295–305.

Fourmarier, P., 1922. Tectonique générale des terrains paléozoiques de la Belgique. C.G.I., Livret-guide pour la XIII° session, Belgique. Exc. C2.

Franke, W., Engel, W., 1986. Synorogenetic sedimentation in the Variscan belt of Europe. Bull. Soc. Géol. Fr. 1 (8), 25–33.

Gosselet, J., 1888. L'Ardenne. Mém Carte Géol. Fr. Baudry, Paris. 881 pp

Hance, L., Ghysel, P., Laloux, M., DeJonghe, L., Mansy, J.L., 1999. Influence of heterogeneous layering on orogenic deformation in the Variscan front zone (eastern Belgium). Tectonophysics 309, 161–177.

Helsen, S., 1992. Conodont colour alteration maps for palaeozoic strata in Belgium, northern France and westernmost Germany. Preliminary results. Ann. Soc. géol. Belg. 115 (1), 135–143.

Helsen, S., 1995. Burial history of Palaeozoic strata in Belgium as revealed by conodont colour alteration data and thickness distributions. Geol. Rundschau 84, 738–747.

Hennebert, M., 1998. L'anticlinal faillé du Mélantois-Tournaisis fait partie d'une structure en fleur positive tardi-varisque. Ann. Soc. géol. Nord 6, 65–78.

Humblet, E., 1941. Le Bassin houiller de Liege. Revue Universelle des Mines 17 (12), 357–377.

Kenis, I., Muchez, P., Sintubin, M., Mansy, J.-L., Lacquement, F., 2000. Thermal constraints on the progressive deformation in the frontal area of the variscan Ardenne Allochthon (Bettrechies, France). J. Struct. Geol. 22, 589–602.

Kent, J.T., Briden, J.C., Mardia, K.V., 1983. Linear and planar structure in order multivariate data as applied to progressive demagnetization of paleomagnetic remanence. Geophys. J. R. Astr. Soc. 75, 593–621.

Khatir, A., 1990. Structuration et déformation progressive au front de l'allochtone ardennais (Nord de la France). Publ. Soc. Géol. Nord 18, 293 pp.

Kissel, C., Barrier, E., Laj, C., Lee, T.Q., 1986. Magnetic fabric in undeformed marine clays from compressional zones. Tectonics 5, 769–781.

Kligfield, R., Owens, W.H., Lowrie, W., 1981. Magnetic susceptibility anisotropy, strain and progressive deformation in Permian sediments from the Maritime Alps (France). Earth Planet. Sci. Lett. 55, 181–189.

Kossmat, F., 1927. Gliederung des varistischen Gebirgsbaues. Abh. Sachs. geol. Landesamt heft 1, 1–39.

Lacquement, F., Mansy, J.-L., Mercier, E., Averbuch, O., Meilliez, F., 1997. Mécanismes de plissement disharmonique dans le Paléozoique ardennais. Aardkundige Mededelingen 8, 119–122.

Lacquement, F., Mansy, J.-L., Hanot, F., Meilliez, F., 1999. Retraitement et interprétation d'un profil sismique pétrolier méridien au travers du Massif Paléozoique ardennais (Nord de la France). C. R. Acad. Sci., Paris 329, 471–477.

Laloux, M., DeJonghe, L., Ghysel, P., Hance, L., Mansy, J.L., 1997. Nouveaux concepts tectoniques à partir de la révision des cartes Fléron-Verviers et Limbourg-Eupen (Est de la Belgique). Ann. Soc. géol. Nord 5, 23–46.

Lowrie, W., 1990. Identification of ferromagnetic minerals in a rock by coercivity and unblocking temperature properties. Geophys. Res. Lett. 17, 159–162.

Mansy, J.L., Meilliez, F., 1993. Eléments d'analyse structurale à partir d'exemples pris en Ardenne–Avesnois. Ann. Soc. géol. Nord 2, 45–60.

Mansy, J.-L., Meilliez, F., Mercier, E., Khatir, A., Boulvain, F., 1995. Le rôle du plissement disharmonique dans la tectogenese de l'allochtone ardennais. Bull. Soc. géol. Fr., Paris 166 (83), 295–302.

Mansy, J.L., Lacquement, F., Meilliez, F., Hanot, F., Everaerts, M., 1997. Interprétation d'un profil sismique pétrolier, sur le méridien de Valenciennes (Nord de la France). Aardk. Mededel. 8, 127–129.

Mansy, J.L., Amedro, F., Auffret, J.P., Guennoc, P., Lamarche, J., Lefevre, D., Robaszinski, F., Somme, J., Vidier, J.P., press. Carte géologique de Marquise (50000eme). second ed., BRGM, Orléans. in press.

Matte, P., 1986. Tectonics and plate tectonic model for the Variscan belt of Europe. Tectonophysics 126, 329–374.

Matthews, S.C., 1984a. Tectonic antecedence of Variscan geology in Belgium. Bull. Soc. belge géol., Bruxelles 93, 33–44.

Matthews, S.C., 1984b. Northern margins of the variscides in the North Atlantic region: comments on the tectonic context of the problem. In: Hutton, D., Sanderson, D. (Eds.), Variscan Tectonics of the Atlantic Region, Geol. Soc. Spec. Publ., pp. 71–85.

Meilliez, F., Mansy, J.L., 1990. Déformation pelliculaire différenciée dans une série lithologique hétérogene: Le Dévono-Carbonifère de l'Ardenne. Bull. Soc. géol. Fr., VI 1, 177–188.

Meilliez, F., Andre, L., Blieck, A., Fielitz, W., Goffette, O., Hance, L., Khatir, A., Mansy, J.L., Overlau, P., Verniers, J., 1991. Ardenne-Brabant. Sci. Géol. Bull. 44, 3–29.

Meilliez, F., Fielitz, W., Laduron, D., Mansy, J.L., Manby, J.L., 1994. The deep structure of the Ardennes Variscan thrust belt from structural and ECORS seismic data: Discussion. J. Struct. Geol. 16 (3), 431–432.

Molina Garza, R.S., Zijderveld, J.D.A., 1996. Paleomagnetism of Palaeozoic strata, Brabant and Ardennes Massifs, Belgium: Implications of prefolding and postfolding Late Carboniferous secondary magnetizations for European apparent polar wander. J. Geophys. Res. 101, 15799–15818.

Muchez, P., 1989. Comparison of the Visean strata north and south of the London–Brabant Massif. Bull. Soc. Belg. Géol. 98, 155–162.

Perroud, H., 1986. Paleomagnetic evidence for tectonic rotations in the Variscan mountain belt. Tectonics 5, 205–214.

Piqué, A., Huon, S., Clauer, N., 1984. La schistosité hercynienne et le métamorphisme associé dans la vallée de la Meuse, entre Charleville-Mèziéres et Namur (Ardennes franco-belges). Bull. Soc. Belge Géol. 93, 55–70.

Potdevin, J.L., Goffette, O., 1991. Les assemblages métamorphiques du filon de diabase de la Grande Commune (Massif Rocroi), des témoins d'une évolution rétrograde varisque en Ardenne. C. R. Acad. Sci. Paris 312 (2), 1545–1550.

Raoult, J.-F., Meilliez, F., 1987. The Variscan front and the Midi fault between the Channel and the Meuse River. J. Struct. Geol. 9, 473–479.

Thominski, H.P., Wohlenberg, J., Bleil, U., 1993. The remagnetization of Devono-Carboniferous sediments from the Ardenno-Rhenish Massif. Tectonophysics 225, 411–431.

Van der Voo, R., 1993. Paleomagnetism of the Atlantic Tethys and Iapetus Oceans. Cambridge University Press, Cambridge. 411 pp

Winterfeld, C.V., Walter, R., 1993. Die varisziche Deformations front des nordwestlichen Rheinischen Schiefergebirges—Ein bilanziertes geologisches Tiefenprofil über die Nordeifel. N. Jb. Geol. Paläont. Mh. 1993 (5), 305–320.

Article 10.

Szaniawski R., Lewandowski M., Mansy J-L., Averbuch O. and *Lacquement F.* (2003). Syn-folding remagnetization events in the French-Belgium Variscides as markers of the fold-thrust belt kinematics. Bulletin Société géologique de France, 174, 511-523.

Bull. Soc. géol. Fr., 2003, t. 174, n° 5, pp. 511-523

Syn-folding remagnetization events in the French-Belgium Variscan thrust front as markers of the fold-and-thrust belt kinematics

RAFAL SZANIAWSKI[1,2], MAREK LEWANDOWSKI[1], JEAN-LOUIS MANSY[2],
OLIVIER AVERBUCH[2*] and FREDERIC LACQUEMENT[2]

Key words. – Ardennes, Paleomagnetism, Variscides, Fold test, Remagnetizations, Tectonic rotations.

Abstract. – New paleomagnetic studies have been carried out within the Ardennes segment of the N France - S Belgium Variscan fold-and-thrust belt to set constraints on the fold-thrust belt kinematics and reveal the casual relationships between vertical-axis rotations and major strike deviated zones localised along the general trend of the belt. Magnetite-bearing Devonian and Carboniferous limestones yielded two characteristic, secondary components of the natural remanent magnetization : a low temperature component recorded most probably during the late stages of folding and a high temperature component, acquired during incipient stages of deformation. Both post- and synfolding magnetizations were identified in the Lower Devonian hematite bearing sandstones. Ages of magnetization, inferred from the analysis of characteristic remanence inclinations compared to the reference curves for the stable parts of the Old Red Sandstones Continent (ORC), suggest the previous remagnetization event to be due to the burial of sedimentary rocks under the thick molassic foreland basin of Namurian-Westphalian age and the second to the final out-of-sequence activation of the thrust front in Stephanian times. Irrespective of the age of the magnetizations, orientations of paleomagnetic directions are dominantly governed by second-order structural trends. Clockwise rotations are observed in relatively narrow zones featuring deviated orientations of fold axes, other sites show paleomagnetic directions akin to those known from the ORC. We interpret this feature as a result of local transpressive deformations and related rotations, which occurred at lateral borders of propagating thrust-sheets. The latter deformation zones are suggested to be controlled by deep-seated discontinuities inherited from the Devonian Rheno-hercynian basin development. The Ardennes thrust belt was thus not rotated as a whole unit with respect to the ORC after the Namurian, preserving the initial orientation of the continental margin.

Réaimantations syn-cinématiques au front de la chaîne varisque franco-belge : apports à la cinématique des structures plissées-faillées

Mots clés. – Ardennes, Paléomagnetisme, Varisque, Test du pli, Réaimantations, Rotations.

Résumé. – De nouvelles données paléomagnétiques ont été acquises dans le massif des Ardennes (N France-S de la Belgique), au front septentrional de la chaîne varisque, afin d'établir des contraintes temporelles sur les déformations plissées-faillées et mettre en évidence d'éventuelles rotations autour d'axes horizontaux associées à l'existence de virgations majeures le long de la chaîne.

Les calcaires dévoniens et carbonifères présentent deux composantes de réaimantation portées par de la magnétite : une composante de relativement basse température enregistrée très probablement au cours des dernières phases de plissement et une composante de haute température acquise au tout début des déformations plissées. Des réaimantations post-pli et syn-pli sont également observables dans les grès rouges du Dévonien inférieur à hématite. L'âge des réaimantations, établi à partir des inclinaisons caractéristiques mesurées comparées aux courbes de référence pour les zones stables du Continent des Vieux Grès Rouges, suggère que le premier épisode régional de réaimantation résulte de l'enfouissement des séries sous l'épais bassin molassique d'avant-pays d'âge Namurien-Westphalien et que le second soit enregistré lors de l'activation finale du front de chaîne (Stéphanien d'après les données d'inclinaison) lors de la reprise hors-séquence des chevauchements majeurs.

Indépendamment de l'âge des réaimantations, les directions des vecteurs paléomagnétiques sont principalement contrôlées par l'orientation des structures. Des rotations horaires d'une amplitude maximale de 40° sont localisées le long des virgations des structures chevauchantes. Les zones, présentant l'orientation classique du segment ardennais, ne montrent aucune rotation par rapport aux domaines stables du continent des Vieux Grès Rouges. Il est suggéré que la torsion des structures se développent au sein de zones transpressives dextres mises en place aux limites latérales d'écailles chevauchantes majeures, ces dernières étant probablement contrôlées par des discontinuités profondes héritées de la géométrie du bassin rhéno-hercynien. La chaîne de chevauchements des Ardennes n'a ainsi pas subi de rotation d'ensemble par rapport au continent des Vieux Grès Rouges postérieurement au Namurien, conservant l'orientation initiale de la paléo-marge continentale.

[1] Institute of Geophysics of the Polish Academy of Sciences, Ks. Janusza 64, 01-452 Warsaw, Poland.
[2] UMR 8110, Processus et Bilans des Domaines Sédimentaires, Université de Lille 1, 59655 Villeneuve d'Ascq, France.
* Corresponding author, E-mail : rafsz@igf.edu.pl, fax : +48 22 6915915.
Manuscrit déposé le 30 octobre 2002 ; accepté après révision le 31 mars 2003.

INTRODUCTION

The northern rim of the Variscan orogenic belt extends from eastern Europe to the Iberian Peninsula, displaying a distinctly curved trend [Perroud, 1986 ; Eldredge *et al.*, 1985 ; Bachtadse and Van der Voo, 1986 ; Dias and Ribeiro, 1994 ; Weil *et al.*, 2000 ; Matte, 1991, 2001]. One of the basic problems concerned with the curved shape of the outer Variscides is to what extent the present-day structural pattern is governed by the original shape of the Devonian - Carboniferous sedimentary basins, and what impact does oroclinal bending have on the shape of the Variscan fold belt. In this study, we applied the paleomagnetic method to set time-constraints on the different stages of tectonic development in the northern France - Belgium segment of the belt, focusing on a better understanding of the origin of strike variations in a context of oroclinal bending/primary basin shape alternatives. Special attention is given to regional-scale tectonic rotations related to the process of thrusting [e.g. Allerton, 1998], as well as to the nature of the locally observed strike disturbances with respect to the general trend of the belt. We also used information from structural geology, attempting a more interdisciplinary approach. Providing new information, our results are complementary to the outcomes obtained so far.

Previous paleomagnetic studies in the N France-S Belgium part of the Variscan fold belt (FBVB) have been performed by Nowaczyk and Bleil [1985] ; Edel and Coulon [1987] ; Thominski *et al.* [1993] ; Molina Garza and Zijderveld [1996] and Marton *et al.* [2000]. They were concentrated mainly in the eastern part of this orogen i.e. the Ardennes thrust belt. All these authors reported on the presence of characteristic secondary components of the natural remanent magnetization (NRM), recorded at different stages of the tectonic evolution. Described pre-, syn- or post-folding components were generally dated between late Carboniferous and Permian in age. In sites situated in the Brabant Massif and the Namur Syncline (Parautochthonous units *sensu* Meilliez and Mansy [1990]), directions akin to those known from stable Europe were observed. In turn, in the Dinant Syncline (Allochthonous unit *sensu* Meilliez and Mansy [1990]), most of the authors noted paleomagnetic rotations [Edel and Coulon, 1987 ; Thominski *et al.*, 1993 ; Molina Garza and Zijderveld, 1996].

A two components nature of NRM in Ardennes was described so far only by Edel and Coulon [1987], and Molina Garza and Zijderveld [1996]. In these studies most of the paleomagnetic sampling sites were localised in the vicinity of the Meuse and Ourthe river valleys. However, since these rivers cut through the thrust units along specific zones of strike deviation [Lacquement, 2001], the obtained data cannot be considered as representative for the entire Ardennes segment of the FBVB.

GEOLOGICAL OVERVIEW

Paleozoic structures of northern France and Belgium show a multi-stage tectonic development. At the Silurian/Devonian boundary, the region was situated at the southern margin of the Old Red Sandstones Continent (ORC) [e.g. Cook *et al.*, 1997, Meilliez *et al.*, 1991] that formed by collage of the Laurentia, Avalonia and Baltica continents in mid-Paleozoic times. An early Devonian rifting event generated extensional deformations in this area [Meilliez *et al.*, 1991 ; Franke, 1992, 2000 ; Lacquement, 2001] and resulted in the formation of a rifted sedimentary basin (the Rheno-Hercynian basin) characteristic for a continental passive margin. Subsidence and deposition were controlled by normal faulting of the Lower Paleozoic basement and led to the formation of several independent blocks bordered by a set of NW-SE and NE-SW fault zones [Meilliez *et al.*, 1991].

Development of the southward dipping subduction of the Rheno-Hercynian domain initiated the Variscan orogenic wedge, with a progressive northward propagation of thrusting and folding [e.g. Plesch and Oncken, 1999]. In Upper Carboniferous times, sedimentary rocks from the Rheno-Hercynian margin were transported towards the north-northwest and formed a typical thrust weddge upon a major crustal scale, southward dipping, décollement zone (fig. 1) [e.g. Lacquement *et al.*, 1999]. The frontal zone of the main Variscan basal thrust is represented by the Midi Fault zone, that separates the so-called allochthonous units (Ardennes thrust belt) to the south from the parautochthonous units to the north on top of which lie the residual parts of a molassic coal-bearing Namurian-Westphalian foreland basin (see cross-section in figure 1, definition of units after Meilliez and Mansy, 1990]. The parauthochthonous unit, that was only partially mobilised and deformed, forms the cover of the Caledonian Brabant Massif [e.g. Lacquement *et al.*, 1999].

Thrusting within the Ardennes belt was influenced both by the basement geometry, inherited from the extensional period of basin development, and differences in thickness of sedimentary series [Meilliez *et al.*, 1991]. Variscan shortening in the region under study led to gently dipping thrusts and asymmetric folds with a general north vergence [Mansy *et al.*, 1995]. Despite the general NNW direction of the tectonic transport and shortening in the allochthonous units, related structural trend, expressed by cleavage and fold axes orientations, displays distinct local variations. Magnitude of these deviations reaches up to 70 degrees in some places. Along the general NE-SW regional tectonic trend, we can thus observe local E-W to NW-SE aberrant orientations of structures in the region of Meuse and Ourthe rivers (fig. 1a).

At the scale of the whole Ardennes thrust-belt, strain markers as well as fold-thrust relationships document a general migration of the deformation towards the foreland [Mansy *et al.*, 1995 ; Lacquement *et al.*, 1997]. The frontal parts of the belt display however a conspicuous out-of-sequence dislocation of the primary thrust structures [e.g. Averbuch and Mansy, 1998] that possibly implies a final buttress effect of the Brabant Caledonian massif. Nevertheless, structures display generally younger ages towards the Midi Fault, as it is indirectly evidenced by radiometric data obtained for the chlorite minerals grown within the cleavage. Their estimated ages vary between 315 Ma in the southern region up to 297 Ma in the northern one [Piqué *et al.*, 1984]. Migration of the deformation front toward the N-to-NNW is also attested by paleontological dating within the Namurian-Westphalian synorogenic deposits [Meilliez *et al.*, 1991 ; Engel and Franke, 1983].

The sequence of tectono-thermal events in the allochthonous units can be reconstructed on the basis of the low-grade metamorphic evolution [see Fielitz and Mansy, A

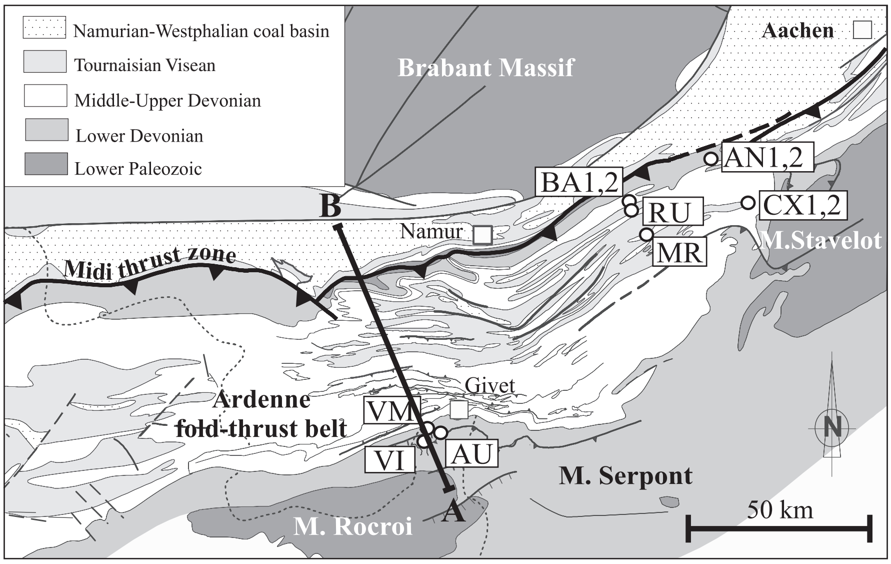

B

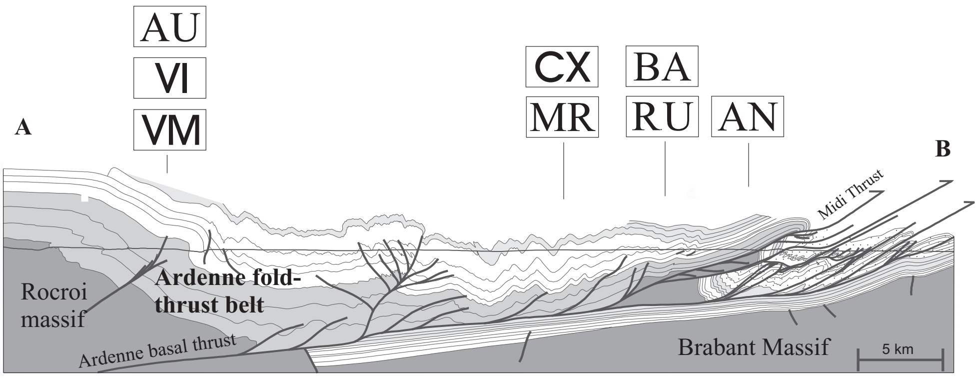

FIG. 1. – A. Geological map of study area showing location of paleomagnetic sampling sites (for abbreviations see table I).
B. Structural cross-section [after Lacquement, 2001] throughout the FBVB ; labels refer to site localities (see table I for explanations).
FIG. 1. – A. *Carte géologique de la zone d'étude montrant la localisation des sites d'échantillonnage pour le paléomagnétisme (pour les abbréviations voir table I).*
B. *Coupe géologique du front chevauchant varisque franco-belge [d'après Lacquement, 2001] reportant la position structurale des sites échantillonnés (descriptions en table I).*

1999 ; Kenis *et al.*, 2000]. The first thermal event was related to the general burial of the sedimentary cover during basin subsidence. Its magnitude, controlled by extensional faults, increased generally towards the south [e.g. Meilliez *et al.*, 1991]. The Devonian-Carboniferous rocks of the allochthonous units situated north of the Lower Paleozoic Massifs [Dinant synclinorium according to Fourmarier, 1922], show a maximum degree of metamorphism in its southern part, locally reaching anchi-metamorphic conditions [e.g. Fielitz and Mansy 1999 ; Robion *et al.*, 1999].

The second phase of metamorphism, developed during the main Variscan orogenic deformations when the foreland basin accumulated molasse-type sediments, originated from the already uplifted zones to the south. As a consequence of the northward foreland basins migration, a variation in the time of acquisition of the metamorphic overprint is recorded [Han *et al.*, 2000]. Within the Ardennes belt, the highest thermal overprint is observed in the central part of the allochthonous complex (up to 200-300 ^{o}C, dated around 300 Ma), probably as the result of maximum burial under the thick molassic cover [see Chamley *et al.*, 1997 ; Han *et al.*, 2000].

SAMPLING AND LABORATORY METHODS

A total of 58 oriented hand samples were collected. The samples were set in plaster of Paris and drilled to give cores of 24 mm diameter. These were sliced into standard specimens of 22 mm length. Smaller 8 mm right-cylindrical cores were drilled for thermomagnetic analysis prior to demagnetization.

Identification of the magnetic minerals in the rocks was done by thermomagnetic analysis [e.g. Kadzialko-Hofmokl and Kruczyk, 1976]. The specimen was saturated in a magnetic field of ca. 1T to produce a saturated induced remanent magnetization (SIRM). It was then continuously heated in a zero magnetic field in a furnace combined with a spinner magnetometer. During the experiment, the unblocking temperature spectrum (Tub) was plotted against the decaying SIRM.

Thermal demagnetization was carried out using a magnetic measurements MM-1 furnace. Each specimen was heated stepwise up to 650 ^{o}C and cooled in a zero magnetic field. After each demagnetization step, the remaining remanence was measured with a 2G SQUID cryogenic magnetometer with a residual internal of < 3 μA/m and noise level of about 5 µA/m. Both the furnace and magnetometer were operated inside Helmholz coils, diminishing the ambient geomagnetic field by ~ 95 %. The experiment continued until the remanence intensity dropped down to magnetometer noise level unless a spurious magnetization appeared in the specimen. Alternating field (AF) cleaning was performed by means of demagnetization coils integrated with the 2G SQUID magnetometer. Magnetic susceptibility was monitored after subsequent steps of thermal cleaning in order to identify mineralogical changes. Specimens which displayed strong change in magnetic susceptibility combined with significant shift in remanence orientation were rejected from further analysis.

Orthogonal projections of the remanence vector endpoints during stepwise demagnetization were plotted for each specimen. Paleomagnetic data analysis (PDA) software by Lewandowski *et al*. [1997], employing principal component analysis (PCA [Kirschvink, 1980]), was used to calculate characteristic NRM components (ChRM) from the demagnetization data and to plot the demagnetization diagrams. Standard Fisher [1953] statistics were used to calculate characteristic mean directions for each sub-populations.

We used the fold test of McFadden and Jones [1981] as well as inclination-only test using procedure of Enkin and Watson [1996]. The softwares by McFadden [1990] and Enkin [1994] were used for performing the tests. Reference paleomagnetic data for the Old Red Sandstones Continent were taken from Van der Voo [1993].

All sampling sites of rocks for paleomagnetic study are situated within the allochthonous units. We preferred locations that had not been yet investigated paleomagnetically and we avoided areas of uncertain structural coherence. Special attention was given to sampling different limbs of kilometric to hectometric folds in the sites representative for the different structural trends along the allochthonous unit (fig. 1a).

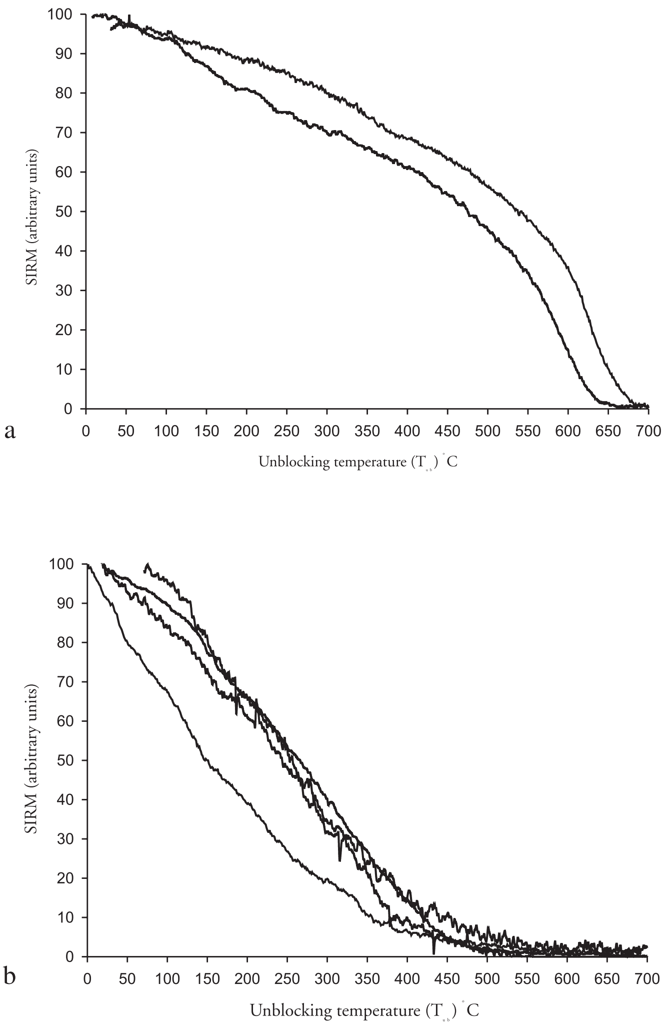

FIG. 2. – Thermomagnetic analysis of carbonates (a) and red beds (b). SIRM = saturation isothermal remanent magnetization. Each curve corresponds to a single sample.

FIG. 2. – *Analyse thermomagnétique des carbonates* (a) *et des niveaux clastiques rouges* (b) *étudiés. SIRM = aimantation rémanente isotherme à saturation. Chaque courbe correspond à un échantillon.*

PALEOMAGNETIC RESULTS

Devonian and Carboniferous limestones

Six sites have been investigated in carbonate rocks of Givetian and Visean age (CX1, CX2, BA1, BA2, RU, MR – see fig. 1a and table I for details). Thermomagnetic curves for carbonates (fig. 2a) show a progressive decrease of the magnetic signal, with maximum unblocking temperatures (Tub) around 500 °C-550 °C. Such Tub range is characteristic for magnetite [Lowrie and Heller, 1982], which was the only magnetic carrier identified in the rocks.

TABLE I. – Summary of paleomagnetic sites.
Dir/dip – is direction of the dip and dip ; N/n ratio of rock samples and specimens.

TABL. I. – *Description synthétique des sites paléomagnétiques. Dir/dip : azimut de la ligne de plus grande pente et valeur du pendage ; N/n : nombre de blocs orientés sur le nombre total d'échantillons.*

Site	Locality	Lithology	Age	Dir/dip	N/n
CX2	Chanxhe	crinoid limestone	Visean	171/61	6/15
CX1	Chanxhe	crinoid limestone	Visean	350/58	7/17
RU	Roiseux	crinoid limestone	Visean	157/41	6/11
MR	Petite Avins	crinoid limestone	Visean	334/67	4/12
BA2	Barse	lamin. limestone	Givetian	350/15	5/9
BA1	Barse	lamin. limestone	Givetian	157/47	5/14
VM	Vireux-Molhain	red sandstone	Emsian	350/105	7/12
VI	Vireux	red sandstone	Emsian	150/25	4/7
AU	Aubrives	red sandstone	Emsian	320/77	4/10
AN2	Angleur	red sandstone	Emsian	11/53	5/10
AN1	Angleur	red sandstone	Emsian	170/80	5/8

NRM of the carbonates displays a multicomponent behaviour during demagnetization and shows a strong variation of the initial intensity between 0.1 and 15 mA/m. AF method of demagnetization in spectrum fields up to 20 mT (fig. 3a) removes a weak, northerly directed, normal polarity component with moderately high positive inclination. While this component, most probably of recent origin, is being removed, the resultant vector moves along a great-circle plane towards a reversed polarity component with shallow inclination, the remanence intensities gradually increasing (fig. 3a). In AF fields ranging from 30 to 50 mT the reversed polarity component decays to the origin of Zjiderveld diagram, suggesting the univectorial nature of this remanence. More detailed analysis indicates, however, that for most of the samples the inclination displays small, but successive changes in progressive demagnetization

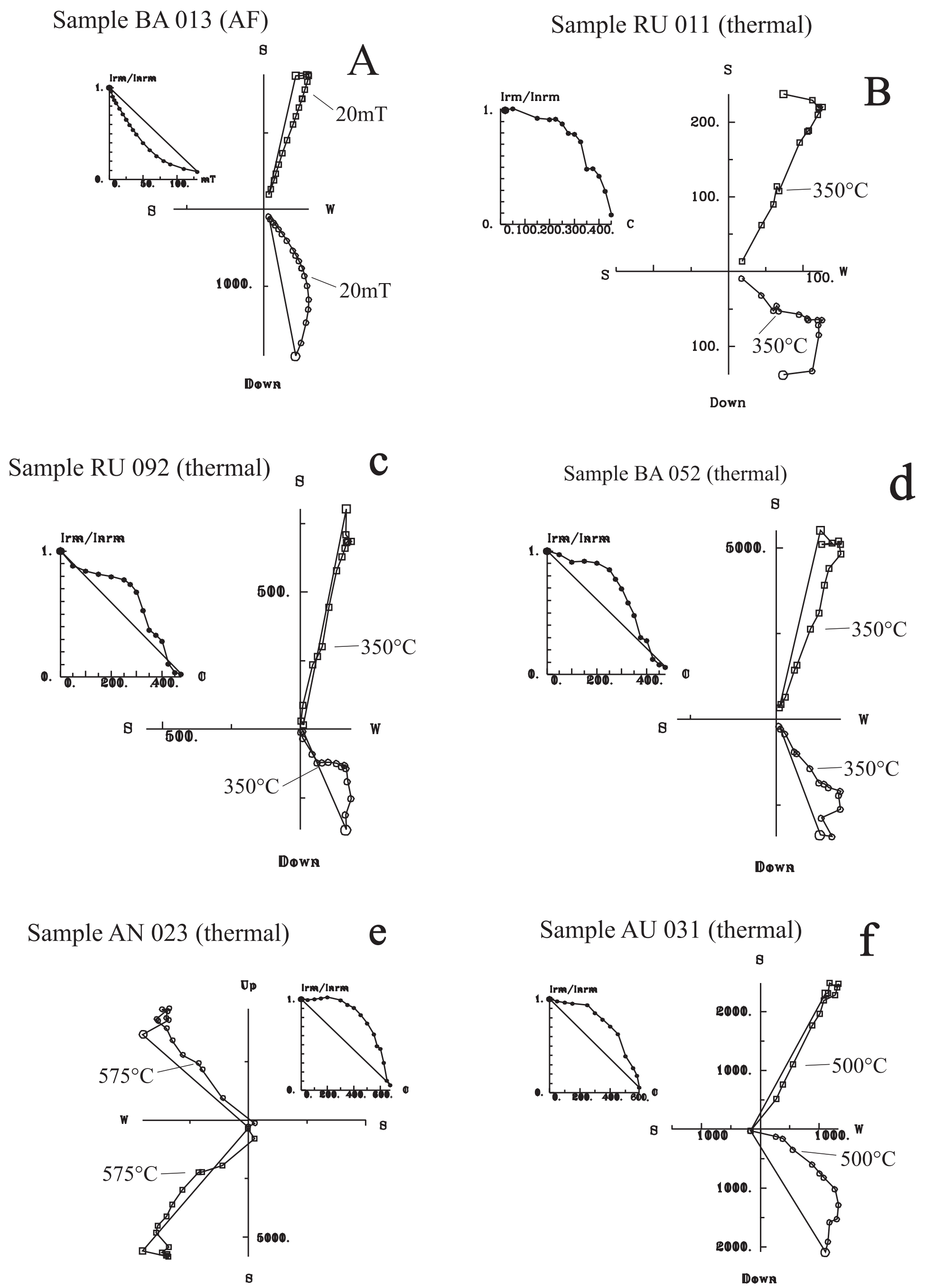

FIG. 3. – Thermal (b, c, d, e, f) and alternative field (AF) (a) demagnetization results. Specimens of limestones (a, b, c, d) and clastics (site AN – e ; AU – f). Units at Zijderveld diagrams expressed in µA/m. Irm/Inrm = normalized intensity of remanent magnetization/intensity of initial NRM. In situ position.
FIG. 3. – *Résultats des désaimantations thermiques* (b, c, d, e, f) *et en champ alternatif* (a). *Échantillons carbonatés* (a, b, c, d) *et clastiques (site AN* - e *; AU* - f*). Les unités des diagrammes de Zijderveld sont exprimées en µA/m. Irm/Inrm = intensité normalisée de l'aimantation rémanente/intensité de l'aimantation rémanente naturelle initiale. Report en position in situ.*

(fig. 3a). This observation suggests that the investigated reversed polarity remanence is in fact composed of two characteristic components with strongly overlapping coercivity spectra.

The multicomponent nature of the ChRM is confirmed by the results of thermal cleaning (fig. 3b, c, d), which proved to be more efficient in separation of the NRM components. Low temperatures of demagnetization effectively remove the component directed towards the recent magnetic field, akin to the one observed in the low fields of AF cleaning. At higher temperatures, usually two characteristic components were observed. The low temperature component (LT), demagnetised between 250 °C and 350 °C, is characterised by generally SSW declination and horizontal inclination (before tectonic correction). In temperatures over 375 °C, when the LT component is finally removed, the remaining component (high temperature component - HT) exhibits an univectorial behaviour, going to the origin of the Zijderveld diagram. The HT component, with Tub ca. 550 °C, shows generally SW to SSW declinations with shallow positive to horizontal inclinations after bedding correction.

Devonian clastic red beds

Five sites have been investigated in clastic rocks of Lower Devonian age (AN1, AN2, VI, VM, AU). Their location is reported in figure 1a and their geological characteristics are listed in table I.

The red beds of Lower Devonian age contain hematite as the main magnetic carrier. The presence of hematite can be inferred from the thermomagnetic analysis, which points to a magnetic phase with Tub as high as 650 °C (fig. 2b), as well as from a weak response of NRM to AF demagnetization.

The structure of the NRM record is different in investigated localities. In the Emsian sandstones from the Angleur anticline (sites AN1, AN2, fig 3e), a soft component is removed after cleaning up to 300 °C. A single, stable component is demagnetised in subsequently higher temperatures, showing trends towards the origin of the Zijderveld diagram up to 550 °C, when artificially induced magnetization prevents further thermal cleaning. In turn, the Emsian sandstones from the Chooz Formation (sites VM, VI, AU fig. 3f) yielded a characteristic component that could be defined up to 600 °C. Generally, the magnetic record from the red beds is of moderate-to-low quality, frequently showing saw-shaped demagnetization paths. Although in several cases the presence of two components with strongly overlapping blocking temperatures cannot be excluded, in most specimens high Tub ChRM display univectorial behaviour.

Apart from the red beds, greenish to grey Devonian clastics containing magnetite were also investigated, but no reliable results were obtained.

FOLD TESTS, RELATIVE AGE AND ORIGIN OF REMAGNETIZATIONS

Devonian and Carboniferous limestones

It should be mentioned first that in both carbonate and clastic rocks we have observed a relatively low degree of anisotropy of magnetic susceptibility. Therefore we postulate that tectonic deformation had little influenced on CHRM which is a necessary condition for the fold tests to be performed [see Stamatakos and Kodama, 1991].

We have applied a fold test for a kilometric scale fold with parallel striking limbs (sites CX1, CX2 in Chanxhe locality) and a local, small scale anticline (sites BA1, BA2 in Barse locality), within the southern limb of a regional-scale anticlinal structure. Results are shown in the figure 4 a, b and 4 c, d respectively. In both cases the HT component indicated an early synfolding origin, displaying a maximum k parameter [Fisher, 1953], as well as a minimum f parameter [McFadden and Jones, 1981] for 80 % (CX1, CX2) and 70 % (BA1, BA2) of unfolding. In turn, the LT component displays best grouping in the initial stage of unfolding for both sites. In this case, however, the variability of statistic parameters is smaller.

In cases where sampling sites were situated in structures featuring different tectonic trends, we applied an inclination-only test using the Enkin and Watson [1996] procedure. The inclination-only test was performed under the assumption, that the axes of the tectonic rotations were vertical so that tectonic dips and paleomagnetic inclinations remained unchanged. For data combined from sites CX1, CX2, BA1, BA2, MR, RU we have found (fig. 5 a) that the best grouping, expressed by maximum value of precision parameter k appeared after 83 % and 12 % of unfolding for HT and LT, respectively. For these optimal degrees of untilting we have found a 95 per cent confidence intervals : 78 % to 88 % of untilting for HT component and 12 % to 26 % of untilting for LT component. We observed also similar results including data of Molina Garza and Zijderveld [1996] (sites characterised by significant plunging of the fold axes are not considered) (fig. 5 b). In this case, the maximum k occurs at 89 % of unfolding for HT and 8 % for LT with 95 per cent confidence intervals 86 %-91 % and 5 %-12 %, respectively.

This outcome is in line with previously published data [Molina Garza and Zijderveld, 1996], where the classical McElhinny [1964] fold test was performed at the site level giving a maximum for κ at 90 % and 10 % of unfolding for the HT and LT components, respectively. However maximum κ for HT and LT components did not pass the test at the 95 % significance level and therefore both components were interpreted as pre-and postfolding origin, respectively [see Molina Garza and Zijderveld, 1996].

In our study, paleomagnetic results indicate the early synfolding (HT components) and late synfolding (LT components) character of the magnetizations. It is worth noting however that for the LT component, estimated optimal degrees of untilting are very close to zero. Therefore, we postulate that the HT and LT components are of secondary origin. The HT component, being older, had been acquired at the incipient stage of structural development, while the LT component (younger) has been recorded during the final stage or just after the deformations.

For our final tectonic interpretation, we have taken into account also the site-mean directions presented by Molina Garza and Zijderveld [1996], which were formerly considered of pre- and postfolding origin. Following the results presented above, we have finally considered them of synfolding origin and therefore we calculated the paleomagnetic directions with the tectonic corrections, deduced from the fold test performed by these authors (i.e. 90 % and 10 % of untilting for HT and LT respectively).

Some evidences for the age of the remanence can be obtained by comparing measured inclinations with reference data recalculated from the apparent polar wander path (APWP) for the Old Red Sandstones Continent at the geographic position of the study sites. For both HT and LT components (see table II), observed inclinations range typically from -10^{o} to $+10^{o}$ (reversed polarity), being typically somewhat shallower for the LT component. This suggests an Upper Carboniferous age for both HT and LT components acquisition. The reversed polarity of both components points to Kiaman reversed polarity superchron. Taking into account that values of paleomagnetic inclinations generally decrease with age for ORC in the Carboniferous-Permian time interval, we may only estimate the time of the

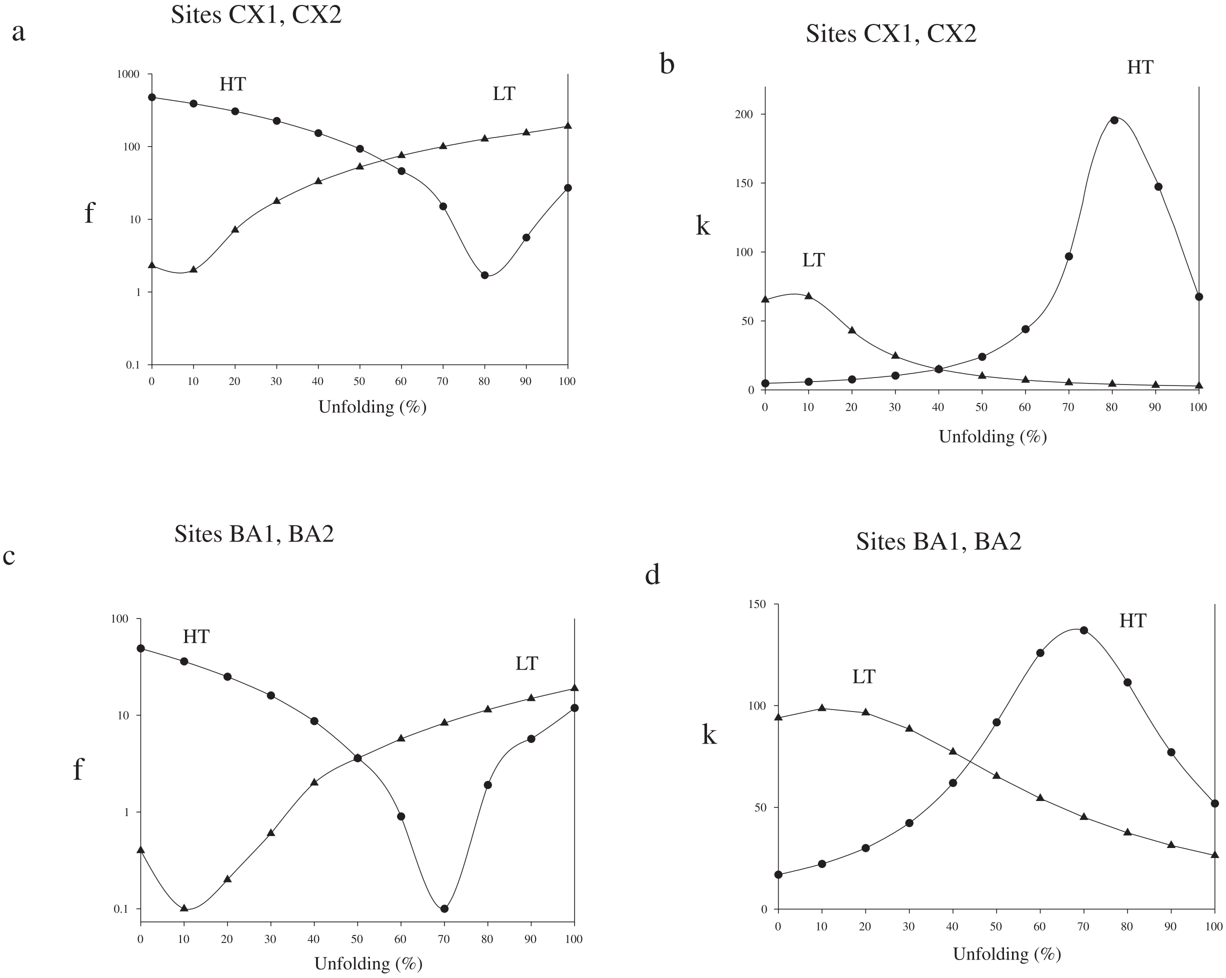

FIG. 4. – Fold test results for Devonian and Carboniferous limestones : (a, c) – following McFadden and Jones's procedure [1981] ; (b, d) – kappa versus per cent of untilting plot ; (a, b) – local fold test for sites CX1 and CX2 (Chanxhe fold). (c, d) – local fold test for sites BA1, BA2 (Barse fold). f = observed value of F distribution, k = fisherian precision parameter. HT = high temperature component ; LT = low temperature component.
FIG. 4. – *Résultats des tests du pli pour les calcaires dévoniens et carbonifères : (*a, c*) – suivant la procédure de McFadden et Jones [1981] ; (*b, d*) – diagramme reportant k en fonction du pourcentage de débasculement ; (*a, b*) – test du pli local pour les sites CX1 et CX2 (pli de Chanxhe). (*c, d*) – test du pli local pour les sites BA1 et BA2 (pli de Barse).* f = *valeur observée de la distribution F,* k = *paramètre de précision de la statistique fisherienne.* HT = *composante haute température ;* LT = *composante de relativement basse température.*

remanence acquisition to be Namurian/Westphalian for HT and Stephanian for LT components, bearing in mind that the latter is younger and displays slightly shallower inclinations.

It is worth noting that this method of remanence dating is very sensitive to even small errors in inclination estimations. In our fold test, we have unfolded two limbs of a fold symmetrically with respect to the axial plane, which may not mimic real kinematics of these structures [Shipunov, 1997 ; Setiabudidaya *et al*., 1994]. Moreover, we cannot exclude small-scale tilting of the whole of the structure during thrusting. This and the unfolding procedure may have some bearing on observed between-site dispersion of inclination, while in-site clustering of NRM components is very good.

Assuming that the process of unfolding did not imply a significant inclination error, then a Namurian-Westphalian age is very likely for the early folding HT component and a Stephanian one can be proposed for the late folding LT component. Taking into account the tectono-thermal evolution of rocks involved in the Ardennes thrust belt, we can relate the first event to the general burial of the Devonian-Carboniferous limestones under the 3-4 kilometers thick [Han *et al*., 2000] Namurian-Westphalian molassic foreland basin and the second to the final activation of the frontal thrust zone in early Stephanian times. The precise mechanisms by which the Ardennes limestones have been remagnetized are however poorly constrained. Chemical as well as thermo-viscous remanent overprints can commonly operate in fold-thrust belts during foreland basin-induced burial (first event) and frontal thrust-sheet stacking (second event) [see for example Enkin *et al*., 2000]. Based on SEM observations, Molina-Garza and Zijderveld [1996] suggested a chemical origin of both Ardennes limestones remagnetization events due to the formation of secondary "diagenetic" magnetite. Enkin *et al*. [2000], in the southern Canadian Cordillera, interpreted the same scenario of remagnetizations that we observed in the Variscan frontal thrust belt (e.g, an early folding and a late folding overprint) as the result of successive chemical and thermo-viscous remagnetization events. In the absence of more precise petrological and geochemical data on the Ardennes Devo-

TABLE II. – (a, b) Paleomagnetic data from carbonates.
D_0/I_0 - declination and inclination of ChRM *in situ* ; % - percent of untilting that yields best grouping direction in terms of McFadden and Jones (1981) test; D/I – mean declination and inclination in synfolding position from McFadden and Jones [1981], * - from inclination only test [Enkin and Watson 1996] ; κ, α - statistical parameters calculated at the sample level, N – number of independently oriented hand samples employed for calculations.
TABL. II. – (a, b) *Données paléomagnétiques pour les sites carbonatés.* D_0/I_0 *- déclination et inclinaison de l'aimantation rémanente caractéristique in situ ; % - pourcentage de débasculement donnant le meilleur groupement au sens de McFadden et Jones (1981) ;* D/I *– déclinaison et inclinaison moyenne après débasculement optimal suivant McFadden et Jones [1981], * - à partir uniquement du test d'inclinaison [Enkin et Watson, 1996] ; κ, α - paramètres de quantification de l'analyse statistique, N – nombre de blocs orientés indépendants utilisés lors du calcul.*

CARBONATES HT

Site	D_0/I_0	N	κ	α	%	D/I	κ	α
CX2	222.7/40.7	6	139.4	5.7	80	**209.5/2.7**	195.8	3.0
CX1	220.3/-32.1	7	355.9	3.2				
RU	212.4/24.5	6	215.8	4.6	-	**205.6/4.0***	215.8	4.6
MR	210.3/-37.2	4	96.6	9.4	-	**195.5/-0.2***	96.6	9.4
BA2	194.2/-0.8	4	69.7	11.1	70	**193.6/8.6**	137.5	4.4
BA1	201.4/34.5	5	277.8	4.6				

CARBONATES LT

Site	D_0/I_0	N	κ	α	%	D/I	κ	α
CX2	193.8/4.4	5	91.9	8.0	10	**197.1/0.9**	67.6	6.3
CX1	201.2/-1.5	4	61.5	11.8				
RU	203.8/3.3	6	82.4	7.4	-	**203.7/-2.4***	82.4	7.4
MR	199.0/-28.5	4	51.9	12.9	-	**195.0/-18.7***	51.9	12.9
BA2	197.0/1.8	4	92.9	9.6	10	**196.9/2.3**	97.9	5.2
BA1	197.0/5.2	5	82.1	8.5				

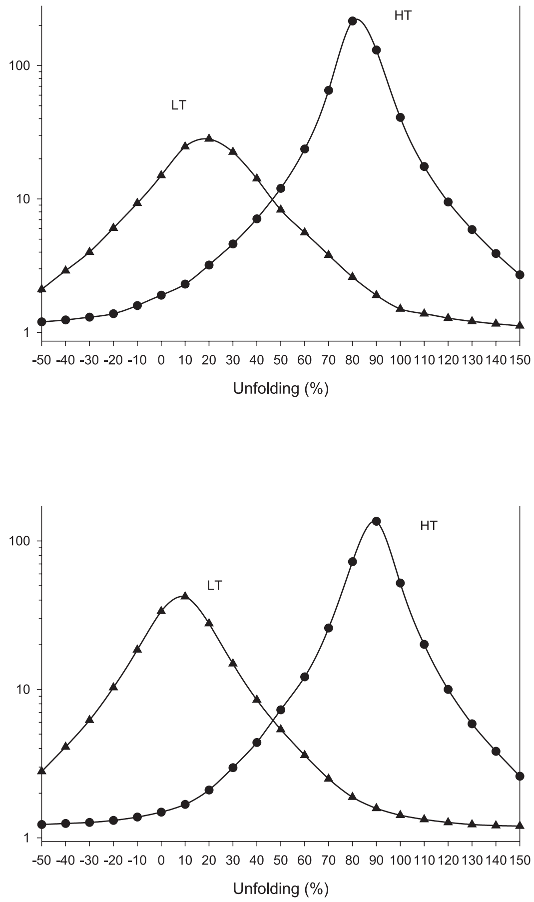

FIG. 5. – Inclination-only tilt tests following Enkin and Watson's procedure [1996]. (a) – taking into account only carbonate sites of this study (CX1, CX2, BA1, BA2, RU and MR), (b) – including carbonate sites of Molina-Garza and Zijderveld [1996]. Other explanations are the same as in the figure 4.
FIG. 5. – *Tests de débasculement d'inclinaison suivant la procédure d'Enkin et Watson [1996].* (a) *– prenant en compte uniquement les sites carbonatés de cette étude (*CX1, CX2, BA1, BA2, RU et MR*), (*b*) – incluant les sites carbonatés de l'étude de Molina-Garza et Zijderveld [1996]. Autres explications identiques à la figure 4.*

nian and Carboniferous limestones, we cannot discriminate between these two mechanisms for the sites studied in this paper. However, as proposed for other foreland thrust belts [Setiabudidaya *et al.*, 1994 ; Enkin *et al.*, 2000], we subscribe to the idea that hot fluid flows expelled ahead of the deformation front are likely to contribute to the process of remagnetization in the French-Belgium Variscan thrust belt. Pervasive dolomitization events observed in the carbonate rocks from the Ardennes thrust belt are also likely to reflect such regional fluid migrations during thrust belt development as suggested by petrological and fluid inclusion studies [e.g. Goudalier, 1998].

Devonian clastic red beds

A fold test was performed in two distant locations : the Angleur anticline situated close to the Midi Fault (fig. 1 a, site AN1, AN2) and in the northern forelimb of the Rocroi culmination (sites VM, VI and AU, fig. 1 a), characterised by various bedding strikes and dips. Results from Angleur indicate synfolding magnetization (fig. 6a, b), while within sites VM, AU, VI, the best grouping of paleomagnetic directions was observed without tectonic correction (fig. 6c, d).

Analysis of paleomagnetic inclinations (see table III) and their comparison with Devonian-Carboniferous inclinations for ORC suggest an older age for the postfolding than for the synfolding component of NRM. Such an apparent paradox, however, may be explained by the progressive migration of the thrusting towards the foreland (see isochrones

TABLE III. – Paleomagnetic data from clastics.
D_0/I_0 - declination and inclination of ChRM in situ; % - percent of untilting that yields best grouping direction in terms of McFadden and Jones [1981] test; D/I – mean declination and inclination in synfolding/postfolding position from McFadden and Jones [1981]; , α - statistical parameters calculated at the sample level, N – number of independently oriented hand samples employed for calculations.
TABL. III. – *Données paléomagnétiques pour les échantillons clastiques.*
D_0/I_0 *- déclinaison et inclinaison de l'aimantation rémanente caractéristique in situ; % - pourcentage de débasculement donnant le meilleur groupement au sens de McFadden et Jones [1981] ;* D/I *– déclinaison et inclinaison moyenne après débasculement optimal suivant McFadden et Jones [1981] ; κ, α - paramètres de quantification de l'analyse statistique*, N *– nombre de blocs orientés indépendants utilisés lors du calcul.*

CLASTICS

Site	D_0/I_0	N	κ	α	%	D/I	κ	α
VM	205.2/13.8	7	44.6	9.1	0	**207.2/11.0**	32.3	6.8
AU	203.5/3.3	4	67.4	11.3				
VI	214.9/13.7	4	18.7	21.8				
AN2	214.1/-40.7	5	114.8	7.2	60	**209.4/-10.4**	67.0	5.9
AN1	215.2/26.3	5	40.7	12.1				

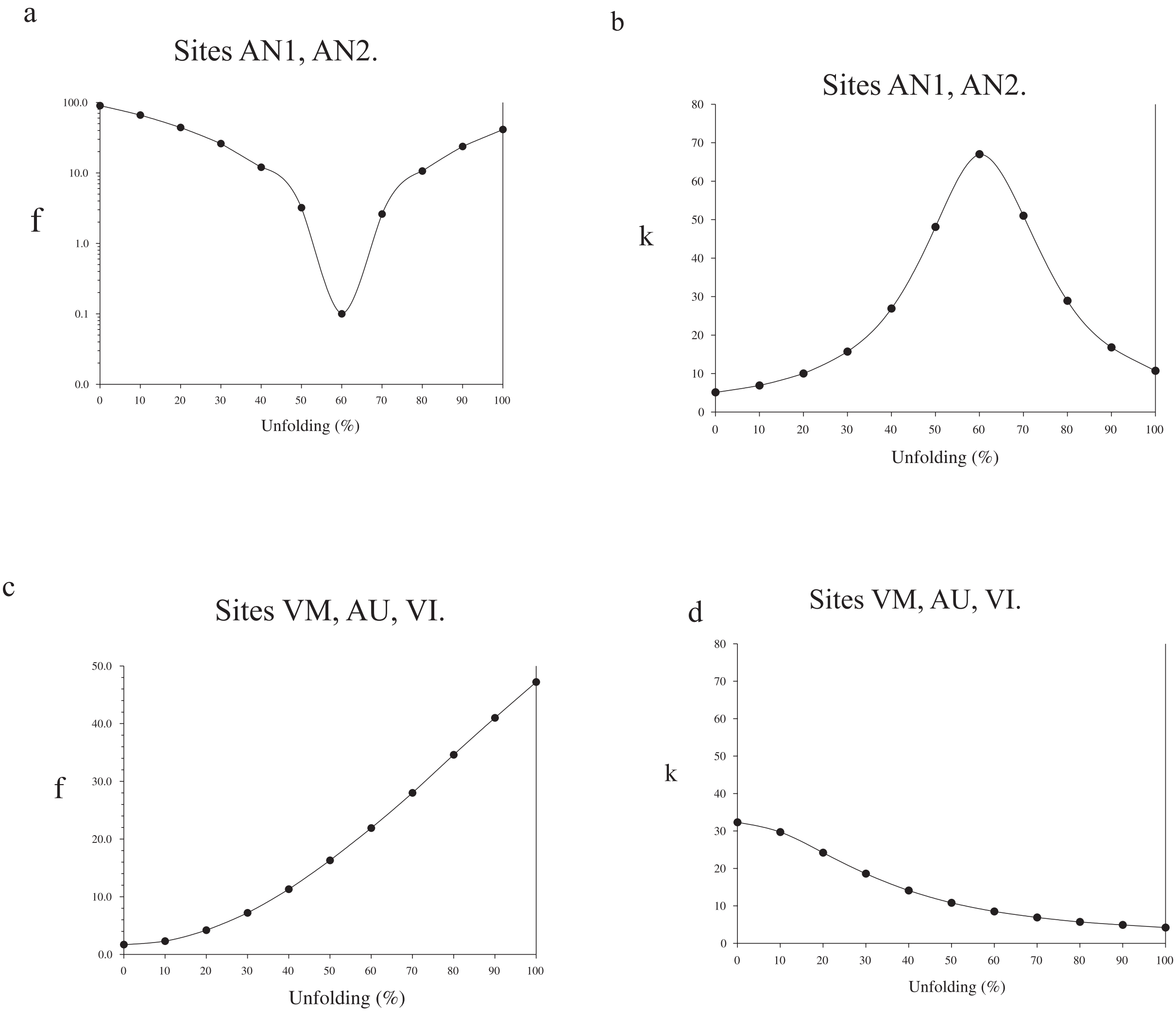

FIG. 6. – Fold test results for Lower Devonian clastic sites. (a, c) – following McFadden and Jones's procedure [1981], (b, d) – kappa versus per cent of untilting plot. (a, b) – local fold test for sites AN1 and AN2 (Angleur fold). (c, d) – local fold test for sites VM, AU, VI (forelimb of the Rocroi anticline). Other explanations are the same as in the figure 4.

FIG. 6. – *Résultats des tests du pli pour les sites clastiques du Dévonien inférieur (*a, c*) – d'après la procédure de McFadden et Jones [1981], (*b, d*) – diagramme reportant* k *en fonction du pourcentage de débasculement (*a, b*) – test du pli local pour les sites AN1 et AN2 (pli d'Angleur). (c, d) – test du pli local pour les sites* VM, AU, VI *(retombée avant de l'anticlinal de Rocroi). Autres explications identiques à la figure 4.*

from fig. 7). Structural data suggest that the sampling area situated to the south of the allochthonous units (sites VM, VI, AU) had already been folded and uplifted when the regions located to the north (site AN1, AN2) were still undeformed and covered by molasse. This scenario of tectonic development is also reflected in the burial history and patterns of radiometric and paleontological dating [Chamley *et al.*, 1997 ; Han *et al.*, 2000 ; Plesch and Oncken, 1999]. Devonian and Carboniferous limestones investigated in this study as well as the Angleur clastic rocks were sampled along the youngest isochrone of deformations (circa 300Ma – see fig. 7). The Angleur synfolding magnetization can thus be dated as late Westphalian to early Stephanian. The Lower Devonian sandstones sampled in the southern parts of the fold-belt did not record however the same deformation history. The latter are involved in the forelimb of the Rocroi thrust ramp anticline (fig. 1) [e.g. Lacquement, 2001] and were deformed very likely in Upper Visean times. They are the only one in our data set to have experienced anchi-metamorphic conditions due to tectonic burial under the thick Rocroi massif thrust wedge [e.g. Robion *et al.* 1999]. In this zone, remagnetizations thus probably occurred during this process (i.e. in late Visean times).

TECTONIC INTERPRETATION OF PALEOMAGNETIC DECLINATIONS

Combined together, the ChRM declinations of this study and the results of Molina Garza and Zijderveld [1996] are shown on a geological map (fig. 7) in order to compare obtained paleomagnetic declinations with structural trends in the FBVB. It is clear that declinations for HT component are similar to directions known for the Upper Paleozoic of the ORC in regions of NE-SW orientation of fold axes. Conversely, areas characterised by E-W to WNW-ESE trends show ChRMs rotated clockwise. Similar dependence can be

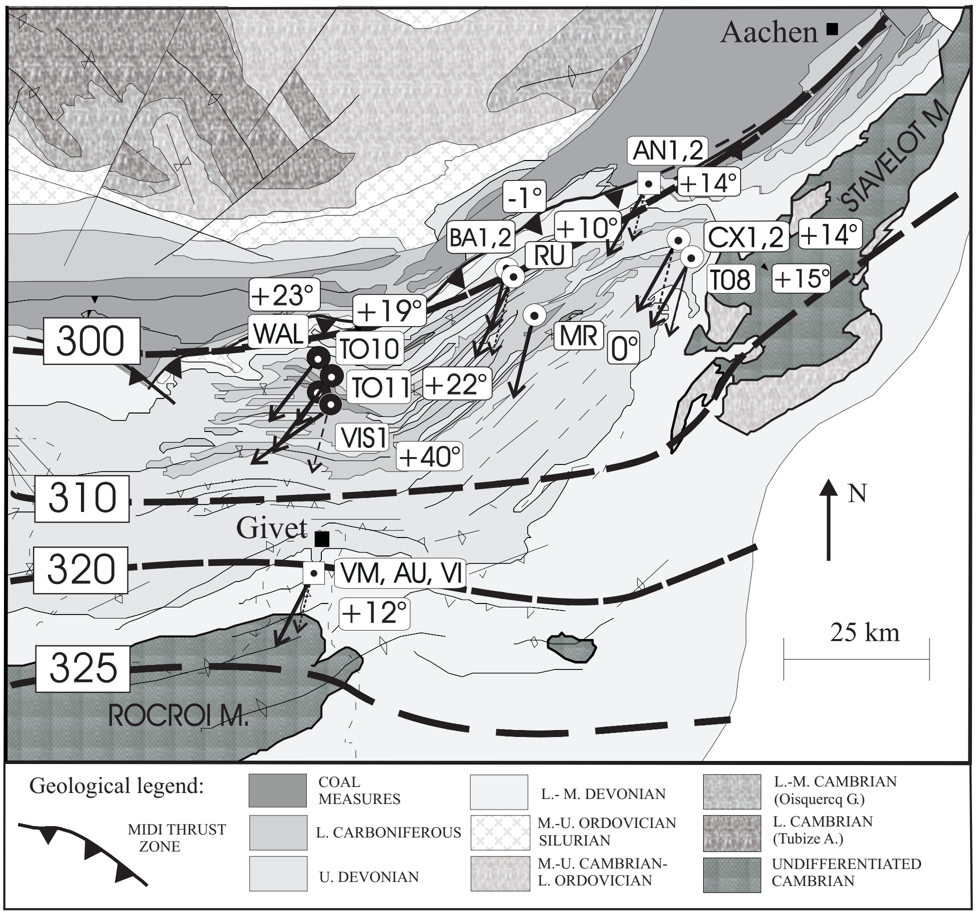

a

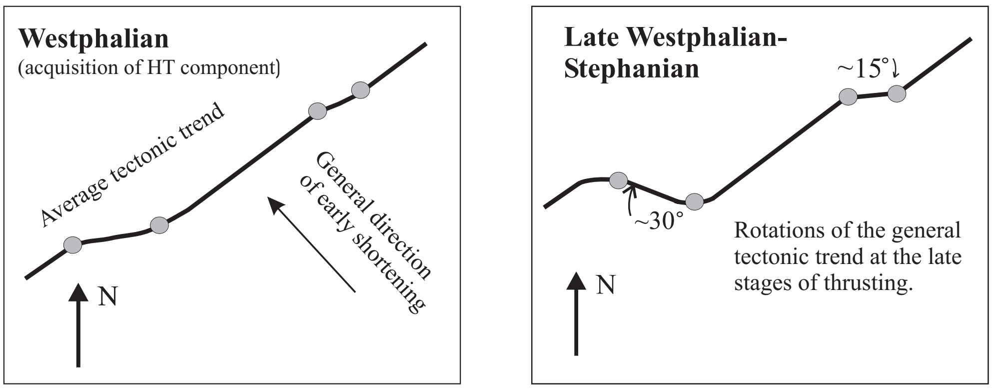

b

FIG. 7. – a. Geological map of the study area [after Lacquement, 2001] showing the paleomagnetic declinations for HT components at different sites. The horizontal projection of the paleomagnetic vector is shown by a black arrow, the reference direction for stable ORC is shown by a dashed arrow, the angular deviation at each site is reported (see text for more explanations).
Paleomagnetic data:
this study: ⊙ – carbonates, ⊡ – clastics;
study of Molina Garza and Zijderveld [1996] : ● – carbonates
300 – Isochrones (Ma) of progressive deformation [after Plesch and Oncken,1999].
b. Schematic diagrams illustration the evolution of the general tectonic trend during the different stages of shortening.

FIG. 7. – a. Carte géologique du secteur d'étude [d'après Lacquement, 2001] montrant la déclinaison paléomagnétique pour la composante de haute température au niveau des différents sites. La composante horizontale du vecteur paléomagnétique est reportée par une flèche noire, la direction de référence pour le continent stable (ORC) est reportée en pointillée, la déviation angulaire à chaque site est reportée (voir le texte pour plus d'explications).
Données paléomagnétiques :
Cette étude : ⊙ – carbonates, ⊡ – niveaux clastiques;
Etude de Molina Garza et Zijderveld [1996] : ● – carbonates
300 – Isochrones de déformation (Ma) montrant la migration du front chevauchant [d'après Plesch et Oncken, 1999]
b. Diagrammes schématiques illustrant la torsion localisée des structures au cours du raccourcissement.

observed for the LT component, but in this case magnitude of the deviation of paleomagnetic declination from the reference directions for ORC is generally smaller and correlation of strike and declinations more dispersed (fig. 8a, b). Paleomagnetic declinations obtained for clastics display orientations deviated from the reference directions from ORC in the same way going with a corresponding pattern for carbonates (fig. 7). It should be pointed out, that such correlation of paleomagnetic declinations from carbonates with structural trends was noted also by Thominski *et al.* [1993]. However, using AF method for paleomagnetic cleaning, these authors did not discriminate between HT and LT components.

Presented declination data thus support the local oroclinal bending origin of strike deviations observed in the Ardennes thrust-belt (fig. 7b). However, as shown by the slope of the linear correlation estimated between declination anomalies and strike deviations (fig. 8), observed rotations do not account for the total fold axes deviations. We suggest that clockwise rotations of the structures occur as the result of distributed dextral transpressive deformations, that took place within the lateral boundaries of propagating thrusts sheets (fig. 9) [Lacquement, 2001 ; Averbuch *et al.*, 2002]. HT and LT components, acquired at different steps of structural development and exhumation process, recorded successive stages of bending within the developing fold belt. Notable rotations within the thrust-sheet, inferred from declinations of the presumably late-synfolding LT component, indicate that evidenced shear zones were active late in the process of thrusting. Geometry in cross-sections and depth map of the basal décollement zone [Lacquement, 2001 ; Averbuch *et al.*, 2002] moreover suggest that such narrow shear zones are localized by a system of NW-SE trending deep-seated basement discontinuities inherited from the Lower Devonian Rheno-Hercynian basin geometry (fig. 9).

GENERAL CONCLUSIONS

Paleomagnetic results from FBVB indicate the existence of two main episodes of regional remagnetization acquired at different stages of the deformation process. Fold tests applied for sites situated at different distances from the main frontal thrust (Midi thrust) evidenced a first episode of remagnetization which is coeval with the onset of deformation within the central and northern part of the allochthonous unit. Based on inclination data compared with reference directions for ORC [recalculated from Van der Voo, 1993], we suggest a Namurian-Westphalian age for this remagnetization event. Taking into account only reversed polarity for ChRM components in our studies and those of Molina Garza and Zijderveld [1996], we can furthermore constrain a time of remanence acquisition to the Kiaman reverse superchron. We relate the remagnetization event to the general burial of the FBVB under a thick molassic foreland basin (up to 4 km thick), as evidenced by fluid inclusions [Kenis *et al.*, 2000] and illite cristallinity data [Han *et al.*, 2000].

The second remagnetization event affected FBVB carbonates at a late stage of folding, as could be evidenced in the central and northern part of the thrust-and-fold belt. Inclination data indicate a Stephanian age for this remagnetization episode. We suggest this second event to be related with the final activation of the Midi frontal thrust zone which has been shown to occur as an out of sequence thrust system when the frontal parts of the belt were almost completely emplaced [e.g. Averbuch et Mansy, 1998 ; Lacquement *et al.*, 1999].

The distribution of paleomagnetic directions implies the existence of localized domains of tectonic rotations associated to strike deviated zones along the belt. Within these narrow zones, declination data evidence clockwise rotations of maximum 40 degrees whereas the zones trending NE-SW

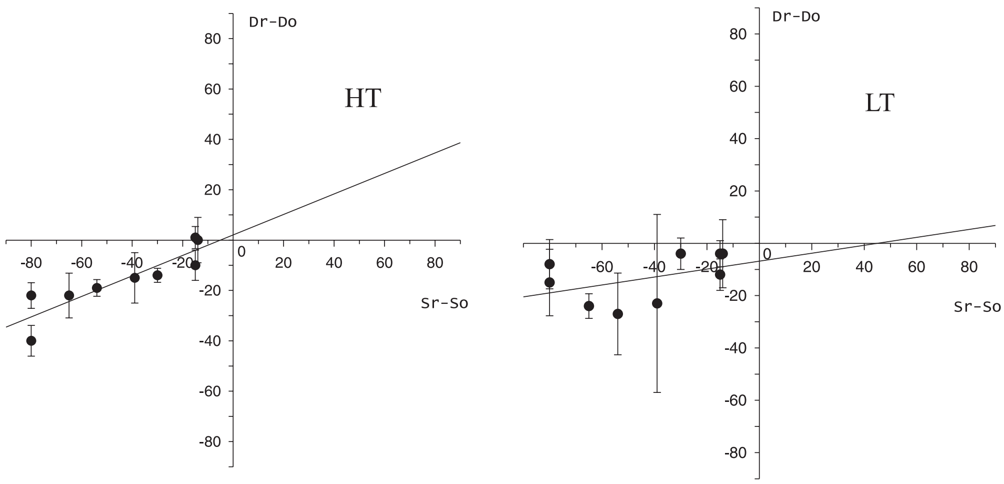

FIG. 8. – Diagram reporting strike deviations (Sr-So) with respect to declination deviations (Dr-Do) for HT and LT components. Reference strike (Sr) is 50°E for both diagrams, while reference declination Dr for ORC is 195°E for HT (Namurian-Westphalian) and 193°E for LT (Stephanian). Do – measured declination, So – observed strike. Solid line is the best fitted line for the data sets. Note the poor correlation of LT component directions with structural trends.

FIG. 8. – *Diagramme reportant la déviation d'orientation des structures (*Sr-So*) en fonction de la déviation de déclinaison (*Dr-Do*) pour les composantes de haute température (*HT*) et de basse température (*LT*). La direction de référence (*Sr*) est 50°E pour les deux diagrammes, la déclinaison de référence (*Dr*) pour ORC est 195°E pour la composante de haute température* HT *d'âge namurien-westphalien et de 193°E pour la composante de plus basse température* LT *d'âge stéphanien.* Do – *déclinaison mesurée,* So – *direction des structures observée. La droite en trait plein est la droite de corrélation optimale pour les deux ensembles de données. A noter une moins bonne corrélation pour les composantes de basse température* LT.

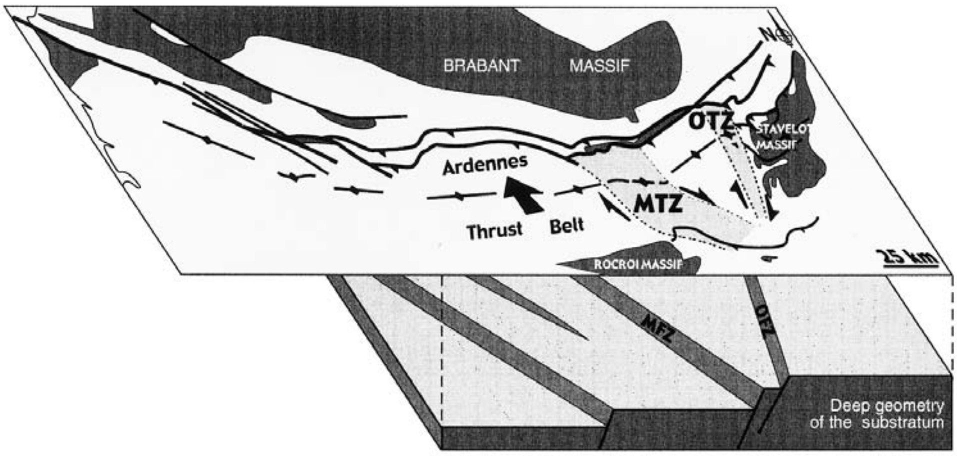

Fig. 9. – Schematic 3D view illustrating the development of clockwise rotated corridors due to distributed dextral transpressive deformation at lateral borders of propagating thrust-sheets. Note that this zones are controlled by deep-seated footwall discontinuities inherited from the Lower Devonian basin development [modified from Lacquement, 2001 and Averbuch *et al*., 2002]. MTZ : Meuse Valley transpressive zone ; OTZ : Ourthe Valley transpressive zone ; MFZ : Meuse Valley footwall fault zone ; OFZ : Ourthe Valley footwall fault zone.

FIG. 9. – *Vue 3D schématique illustrant le développement de couloirs de rotation en sens horaire associés à une déformation distribuée à caractère transpressif dextre en bordure latérale d'écailles chevauchantes. Il est à noter que ces zones sont contrôlées par des discontinuités profondes du substratum héritées du développement du bassin au cours du Dévonien inférieur [modifié de Lacquement, 2001 et Averbuch* et al., *2002].* MTZ *: zone transpressive de la Vallée de la Meuse;* OTZ *: zone transpressive de la Vallée de l'Ourthe;* MFZ *: zone faillée au mur des chevauchements associée à la zone de la vallée de la Meuse;* OFZ *: zone faillée au mur des chevauchements associée à la zone de la vallée de l'Ourthe.*

exhibit no rotations compared to the ORC. Rotation magnitude correlates well with the degree of strike deviation but does not account for the entire shape of the bent structures. We suggest that these rotations occurred within dextral transpressive zones located at lateral borders of thrust-sheets. The latter are likely to be controlled by pre-existing discontinuities inherited from the early Devonian basin evolution as shown by drastic variations in the depth of the base of the Devonian-Carboniferous cover [Lacquement, 2001 ; Averbuch *et al.*, 2002]. On the other hand, as parts of these rotations are recorded by the late remagnetization event, we may infer that the transpressive system was active until late in the deformation history.

At a more regional scale, it is worth noting that the zone displaying the general NE-SW trend of the Ardenno-Rhenish segment of the Variscan arc preserved the original orientation of the sedimentary basin. This indicates that the study area was not rotated as a whole unit with respect to the ORC since the high temperature component was acquired (i.e. Namurian/Westphalien). This result contrasts with previous paleomagnetic interpretations [Edel and Coulon, 1987 ; Thominski *et al.*, 1993 ; Molina Garza and Zijderveld, 1996] and has thus to be considered regarding the origin of the arcuate shape of the western European Variscan belt (Ibero-Armorican arc).

Acknowledgments. – This study was supported by grants founded by the Ministry of Foreign Affairs of France and Ministry of National Education of Poland. It is a contribution of the "Atelier Nord" of the UMR CNRS 8110, Processus et Bilans des Domaines Sédimentaires. A.Blieck and Y.Van Brabant are greatly thanked for their help during the fieldwork. We also thank R. Enkin and P. Robion for their constructive reviews of the paper.

References

ALLERTON S. (1998). – Geometry and kinematics of vertical-axis rotations in fold and thrust belts. – *Tectonophysics,* **299**, 15-30.

AVERBUCH O. & MANSY J.L. (1998). – The Basse-Normandie duplex (Boulonnais, N France) : evidence for an out-of-sequence thrusting overprint. – *J. Struct. Geol.,* **20**, 33-42.

AVERBUCH O., LACQUEMENT F., SZANIAWSKI R., MANSY J.L. & LEWANDOWSKI M. (2002). – Segmentation of the Variscan thrust front (N France-S Belgium) : insights into the geometry of the Devonian Rheno-Hercynian basin. Contributions to the geology of Belgium and Northwest Europe. – *Degryse P. and Sintubin M. eds, Aardk. Mededel.* **12**, 89-92.

BACHTADSE V. & VAN DER VOO R. (1986). – Paleomagnetic evidence for crustal and thin-skinned rotations in the European Hercynides. – *Geophys. Res Let.,* **13**, 161-164.

CHAMLEY H., PROUST J.N., MANSY J.L. & BOULVAIN F. (1997). – Diagenetic and paleogeographic significance of clay and other sedimentary components in the middle Devonian limestones of western Ardennes, France. – *Palaeogeogr. Palaeoclimatol. Palaeoecol.,* **129**, 369-385.

COOK L.R.M., MCKERROW W.S. & VAN STAAL C.R. (1997). – The margins of Avalonia. – *Geol Mag.*, **134** (5), 627-636.

DIAS R. & RIBEIRO A. (1994). – The Ibero-Armorican arc : A collision effect against an irregular continent ? – *Tectonophysics,* **246**, 113-128.

EDEL J.B. & COULON M. (1987). – A paleomagnetic cross-section through the Ardennes and Brabant Massifs (France-Belgium). – *J. Geophys.,* **61**, 21-29.

ELDREDGE S., BACHTADSE V. & VAN DER VOO R. (1985). – Paleomagnetism and the orocline hypothesis. – *Tectonophysics,* **119**, 113-128.

ENKIN R.J. (1994). – A computer program package for analysis and presentation of paleomagnetic data.

ENKIN R.J. & WATSON G.S. (1996). – Statistical analysis of paleomagnetic inclination data. – *Geophys. J. Int.,* **126**, 495-504.

ENKIN R.J., OSADETZ K.G., BAKER J. & KISILEVSKY D. (2000). – Orogenic remagnetizations in the Front Ranges and Inner Foothills of the southern Canadian Cordillera : Chemical harbinger and thermal handmaiden of Cordilleran deformation. – *Geol. Soc. Amer. Bull.*, **112**, 6, 929-942.

ENGEL W. & FRANKE W. (1983). – Flysch-sedimentation : its relations to tectonism in the European Variscides. *In* : H. MARTIN & F.W. EDER (Eds.), Intracontinental fold belts. Case studies in the Variscan Belt of Europe and the Damara Belt in Namibia. – Springer, Berlin, 289-321.

FIELITZ W. & MANSY J.L. (1999). – Pre- and synorogenic burial metamorphism in the Ardenne and neighbouring areas (Rhenohercynian zone, central European Variscides). – *Tectonophysics*, **309**, 227-256.

FISHER R.A. (1953). – Dispersion on a sphere. – *Proc. R. Soc. London,* A **217**, 295-305.

FOURMARIER P. (1922). – Tectonique générale des terrains paléozoïques de la Belgique. – CGI, Livret-guide pour la XII session, Belgique. Exc C2.

FRANKE W. (1992). – Phanerozoic structures and events in central Europe. *In* : D. BLUNDELL, R. FOREMAN & S. MUELLER (Eds), A continent revealed, the European Geotraverse. – Cambridge Univ. Press, 164-180.

FRANKE W. (2000). – The mid-European segment of the Variscides : Tectonostratigraphic units, terrane boundaries and plate tectonic evolution. – *Geol. Soc. Spec. Pub.,* **179**, 35-61.

GOUDALIER M. (1998). – Dolomitisation des calcaires du Frasnien moyen en Belgique : contrôles sédimentaire, diagénétique et tectonique. – Thèse de doctorat de l'Université de Lille, 185 p.

HAN G., PREAT A., CHAMLEY H., DECONINCK J.F. & MANSY J.L. (2000). – Palaeozoic clay mineral sedimentation and diagenesis in the Dinant and Avesnes Basins (Belgium, France) : relationships with Variscan tectonism. – *Sed. Geol.*, **136**, 217-238.

KENIS I., MUCHEZ P., SINTUBIN M., MANSY J.L. & LACQUEMENT F. (2000). – The use of a combined structural, stable isotope and fluid inclusion study to constrain the kinematic history at the northern Variscan front zone (Bettrechies, northern France). – *J. Struct. Geol.*, **22**, 589-602.

KIRSCHVINK J.L. (1980). – The least-square line and plane and the analysis of paleomagnetic data. – *J. R. Astr. Soc.*, **62**, 699-718.

KADZIALKO-HOFMOKL M. & KRUCZYK J. (1976). – Complete and partial self-reversal of natural remanent magnetization of basaltic rocks from Lower Silesia, Poland. – *Pure Appl. Geophys.*, **110**, 2031-2040.

LACQUEMENT F., MANSY J.L., MERCIER E., AVERBUCH O. & MEILLIEZ F. (1997). – Mécanismes de plissement disharmonique dans le Paléozoïque ardennais. – *Aardk. Meded.* **8**, 119-122.

LACQUEMENT F., MANSY J.L., HANOT F. & MEILLIEZ F. (1999). – Retraitement et interprétation d'un profil sismique pétrolier méridien au travers du Massif paléozoïque ardennais (Nord de la France). – *C. R. Acad. Sci.,* Paris, **329**, 471-477.

LACQUEMENT F. (2001). – L'Ardenne varisque. Déformation progressive d'un prisme sédimentaire pre-structuré, de l'affleurement au modèle de chaîne. – *Soc. Géol. Nord Publ.*, **29**, 285.

LEWANDOWSKI M., WERNER T. & NOWOZYNSKI K. (1997). – PDA, a package of FORTRAN programs for paleomagnetic data analysis. – *Inst Geoph, Pol. Acad. Sc. manuscript*, 18 p.

LOWRIE W. & HELLER F. (1982). – Magnetic properties of marine limestones. – *Rev. Geophys. Space Phys.*, **20**, 2, 171-192.

MANSY J.L., MEILLIEZ F., MERCIER E., KHATIR A. & BOULVAIN F. (1995). – Le rôle du plissement disharmonique dans la tectogenèse de l'allochtone ardennais. – *Bull. Soc. géol. Fr.,* **166**, 295-302.

MANSY J.L., EVERAERTS M. & DE VOS W. (1999). – Structural analysis of the adjacent Acadian and Variscan fold belts in Belgium and northern France from geophysical and geological evidence. – *Tectonophysics*, **309**, 99-116.

MARTON E., MANSY J.L., AVERBUCH O. & CSONTOS L. (2000). – The Variscan belt of northern France – Southern Belgium : geodynamic implications of new paleomagnetic data. – *Tectonophysics,* **324**, 57-80.

MATTE P. (1991). – Accretionary history and crustal evolution of the Variscan belt in western Europe. – *Tectonophysics*, **196**, 309-337.

MATTE P. (2001). – The Variscan collage and orogeny (480-290) and the tectonic definition of the Armorica microplate : a review. – *Terra Nova*, **13** n° 2, 122-128.

MC ELHINNY M.W. (1964). – Statistical significance of the fold test in paleomagnetism. – *Geophys. J. R. Astron. Soc.,* **8**, 338-340.

MC FADDEN P.L. & JONES D.L. (1981). – The fold test in paleomagnetism. – *Geophys. J. R. Astron. Soc.*, **67**, 53-58.

MC FADDEN P.L. (1990). – A computer program package for analysis of paleomagnetic data.

MEILLIEZ F. & MANSY J.L. (1990). – Déformation pelliculaire différenciée dans une série lithologique hétérogène : le Dévono-Carbonifère de l'Ardenne. – *Bull. Soc. géol. Fr.*, **8**, 177-188.

MEILLIEZ F., ANDRÉ L., BLIECK A., FIELITZ W., GOFFETTE O., HANCE L., KHATIR A., MANSY J.L., OVERLAU P. & VERNIERS J. (1991). – Ardenne-Brabant. – *Sci. Géol. Bull.*, **44**, 3-29.

MOLINA GARZA R. & ZIJDERVELD J.D.A. (1996). – Paleomagnetism of Paleozoic strata, Brabant and Ardennes Massifs, Belgium : Implications of prefolding and postfolding late Carboniferous secondary magnetizations for European apparent polar wander. – *J. Geophys. Res.*, **101** (B7), 15779-15818.

NOWACZYK N. & BLEIL U. (1985). – Paleomagnetic reconnaissance study of Paleozoic rocks from the Hohes Venn area (West Germany). – *Neues Jahrb. Geol. Palaontol. Abh.*, **171**, 351-362.

PERROUD H. (1986). – Paleomagnetic evidence for tectonic rotations in the Variscan mountain belt. – *Tectonics*, **5**, 205-214.

PIQUÉ A., HUON S. & CLAUER N. (1984). – La schistosité hercynienne et le métamorphisme associé dans la vallée de la Meuse. – *Bull. Soc. Belg. Géol.,* **l93**, 55-70.

PLESCH A. & ONCKEN O. (1999). – Orogenic wedge growth during collision – constraints on mechanics of a fossil wedge from its kinematic record (Rhenohercynian FTB, Central Europe). – *Tectonophysics*, **309**, 117-139.

ROBION P., AVERBUCH O. & SINTUBIN M. (1999). – Fabric development and metamorphic evolution of the Paleozoic slaty rocks from the Rocroi massif (French-Belgian Ardennes) : new constrains from magnetic fabrics, phyllosilicate preferred orientation and illite crystallinity. – *Tectonophysics*, **309**, 257-273.

SETIABUDIDAYA D., PIPER J.D.A. & SHAW J. (1994). – Paleomagnetism of the (early Devonian) Lower Old Red sandstones of south Wales : Implications to Variscan overprinting and differentional rotations. – *Tectonophysics* **231**, 257-280.

SHIPUNOV S.V. (1997). – Synfolding magnetization : detection, testing and geological applications. – *Geophys. J. Int.*, **130**, 405-410.

STAMATAKOS J. & KODAMA K.P. (1991). – Flexural flow folding and the paleomagnetic fold test : an example of strain reorientation of remanence in the Mauch Chunk formation. – *Tectonics*, 10 (5), 807-819.

THOMINSKI H.P., WOHLENBERG J. & BLEIL U. (1993). – The remagnetization of Devono-Carboniferous sediments from the Ardennes-Rhenish Massif, Germany. – *Tectonophysics*, **225**, 411-431.

WATSON G.S. & ENKIN R.J. (1993). – The fold test in paleomagnetism as a parameter estimation problem. – *Geophys. Res. Lett.*, **20**, 2135-2137.

WEIL A.B., VAN DER VOO R., VAN DER PLUIJM B.A. & PARÈS J.M. (2000). – The formation of an orocline by multiphase deformation : a paleomagnetic investigation of the Cantabria-Asturias Arc (northern Spain). – *J. Struct. Geol.,* **22**, 735-756.

VAN DER VOO R. (1993). – Paleomagnetism of the Atlantic, Tethys and Iapetus Oceans. – Cambridge University Press, 411 pp.

Article 11.

Lacquement F., Averbuch O., Mansy J-L., *Szaniawski R.* and Lewandowski M. (2005). Transpressional deformations at lateral boundaries of propagating thrust-sheets : the example of the Meuse Valley Recess within the Ardennes Variscan fold-thrust belt (N France-S Belgium). Journal of Structural Geology 27, 1788-1802.

ELSEVIER

Journal of Structural Geology 27 (2005) 1788–1802

JOURNAL OF STRUCTURAL GEOLOGY

www.elsevier.com/locate/jsg

Transpressional deformations at lateral boundaries of propagating thrust-sheets: the example of the Meuse Valley Recess within the Ardennes Variscan fold-and-thrust belt (N France–S Belgium)

F. Lacquement[a,b], O. Averbuch[b,*], J.-L. Mansy[b], R. Szaniawski[b,c], M. Lewandowski[c]

[a]*Bureau de Recherches Géologiques et Minières, 3 Av. C. Guillemin, 45000 Orléans, France*

[b]*Université de Lille 1, Processus et bilans en domaines sédimentaires, UMR 8110, 59655 Villeneuve d'Ascq cédex, France*

[c]*Institute of Geophysics of the Polish Academy of Sciences, Ks. Janusza 64, 01-452 Warsaw, Poland*

Received 17 June 2004; received in revised form 5 April 2005; accepted 8 May 2005
Available online 9 August 2005

Abstract

The 3D kinematics of the fold–thrust structures within the Meuse Valley Recess (MVR) (Ardennes Variscan thrust belt, N France–S Belgium) have been investigated using an integrated approach combining geological mapping, cross-section analyses and studies of magnetic fabrics and paleomagnetic data at a total of 52 sites distributed within the study area. Fold–thrust geometries, strain distribution and thrust-sheet rotational patterns lead to a conceptual structural model illustrating natural deformation processes at lateral boundaries of propagating thrust-sheets. The MVR is shown to result from distributed transpressional deformation of the Ardennes Basal Thrust hanging wall above a buried lateral/oblique ramp inherited from the Lower–Middle Devonian extensional tectonics of the sedimentary wedge. This deep lateral/oblique discontinuity basically controls the thickness and basal friction of the Ardennes thrust wedge, thus resulting in contrasting thrust propagation west and east of the MVR. Out-of-plane strain within the transfer zone includes some varying components of normal-to-bedding shear and lateral shortening depending on the proximity with the buried lateral discontinuity. A gradient of lateral shortening is evidenced towards this discontinuity, thus acting as a buttress zone. We emphasize the high friction conditions prevailing along the lateral borders of the thrust sheets, which potentially result in drag effects during foreland-directed thrust propagation. Such additional shear strain is suggested to be accommodated by late pervasive thrust-sheet rotation and lateral broadening of the deformed zone subsequent to oblique folding close to the lateral/oblique boundary.

Keywords: Fold-and-thrust belt; Lateral/oblique ramp; Transpression; Ardennes; Variscan thrust front

1. Introduction

Lateral boundaries of fold–thrust structures within the outer parts of orogenic belts have been shown to develop complex 3D kinematics resulting in significant structural strike deviation and relatively steeply dipping axial plunges (e.g. Apotria, 1995; Frizon de Lamotte et al., 1995; Wilkerson et al., 2002). On the basis of analog modeling experiments, such along-strike geometrical evolutions have been generally attributed to either displacement gradients due to lateral variations in the strength of the underlying décollement zone or lateral changes in the thickness of the thrust wedge (either combined or in isolation) (Dixon and Liu, 1992; Marshak et al., 1992; Calassou et al., 1993; Philippe, 1995; Macedo and Marshak, 1999; Paulsen and Marshak, 1999). These changes in the mechanical properties of the thrust wedge can be continuous along strike, or be localized to a very narrow domain. The latter situation involves a sharp, steeply dipping discontinuity oriented parallel or oblique to the thrusting direction transferring differential movements between adjacent thrust units having different mechanical behavior, i.e. a lateral/oblique ramp (e.g. Dahlstrom, 1970; Butler, 1982; Schirmer, 1988). Obviously, these lateral changes primarily result from the inherited basin geometry. Basement normal-fault zones coeval with the basin development form strong mechanical

* Corresponding author. Fax: +33 320 43 49 10.
E-mail address: olivier.averbuch@univ-lille1.fr (O. Averbuch).

0191-8141/$ - see front matter © 2005 Elsevier Ltd. All rights reserved.
doi:10.1016/j.jsg.2005.05.017

heterogeneities in the sedimentary wedge and thus have been shown both by modeling experiments and structural studies to control the location of future footwall thrust ramps (Wiltschko and Eastman, 1982; Thomas, 1990; Frizon de Lamotte et al., 1995; Philippe, 1995; Tavarnelli, 1996). Thrust-sheet motion along such lateral/oblique ramp-flat system has been shown to induce variable amounts of out-of-plane strain of the hanging wall block including layer-normal simple shear and lateral/oblique shortening owing to buttressing effect of the ramp (Coward and Potts, 1983; Hyett, 1990; Apotria et al., 1992; Averbuch et al., 1993; Apotria, 1995; Holl and Anastasio, 1995). Within lateral boundaries of thrust-sheets, such a mechanism generally results in distributed transpressional deformation expressed by a complex pattern of fold–faults interaction accommodating thrust-sheet rotation around vertical axes (Apotria, 1995; Allerton, 1998; Bayona et al., 2003), tear faulting (Donzeau et al., 1993) and oblique layer-parallel shortening (Averbuch et al., 1993; Apotria, 1995).

This paper aims to address the problem of 3D kinematics of fold–thrust structures using a multidisciplinary structural study of the Meuse Valley Recess (MVR) within the Ardennes fold-and-thrust belt (N France–S Belgium Variscan thrust front). Fold–thrust geometries, strain distribution and thrust-sheet rotational patterns are investigated using an integrated approach coupling geological mapping, cross-section analyses and studies of magnetic fabrics and paleomagnetic data at a total of 52 sites distributed along the MVR. These data are finally integrated in a structural model illustrating natural deformation processes at lateral boundaries of propagating thrust sheets.

2. The Ardennes fold-and-thrust belt: geological overview

The Ardennes fold-and-thrust belt (N France–S Belgium) represents the northern thrust front of the western European Variscan orogenic belt (Fig. 1a), which resulted from the collision of the Laurentia–Avalonia–Baltica (i.e. Old Red Sandstones Continent) and Gondwana margins in Upper Paleozoic times. It includes non-metamorphic to epimetamorphic sedimentary rocks of mostly Devonian–Carboniferous age (Fig. 2) deposited at the southern border of the 'Old Red Sandstones' continent in a rifted continental margin-type environment (Rheno–Hercynian basin).

Structurally, the N France– S Belgium Variscan thrust front is a composite feature (Fig. 1b) that extends from the Channel–Boulonnais thrust belt (Averbuch et al., 2004) to the Ardennes thrust belt changing progressively strike from NW–SE to NE–SW. This large-scale strike change is accommodated by second-order curved thrust zones, relaying in a complex way within the Western Ardennes fold-and-thrust belt. Such segmentation is exemplified by the map geometry of the 'Midi Thrust Zone' (Mansy et al., 1999), which corresponds to the emergence of the Ardennes Basal Thrust (ABT), a crustal-scale, gently south-dipping décollement zone accommodating a general NNW-directed displacement. The Midi Thrust Zone separates the Ardennes Belt, displaying a classic thrust-wedge geometry from the underthrusted Namurian–Westphalian coal-bearing, foreland basin, heavily dismembered along its southern border (Fig. 1c). This up to 4-km-thick basin lies on top of the Brabant massif basically structured in Caledonian times and surrounded by a reduced Upper Devonian–Carboniferous sedimentary cover. A recent interpretation of a seismic profile across the Western Ardennes belt (Fig. 1c) shows that the minimum total displacement along the basal thrust system is approximately 70 km and that a major part of this displacement occurred by out-of-sequence thrusting after deposition of the Namurian–Westphalian molasse (Lacquement et al., 1999). A pronounced flexure of the underthrust Brabant foreland is visible at the tip of the frontal thrust system resulting from the localized load, coeval with the out-of-sequence thrust stack (Averbuch et al., 2004).

Unlike the Brabant foreland, the Ardennes thrust belt displays a thick Lower Devonian sequence composed of alternating shale and sandstone (Fig. 2). The thick shaly layers at the base of this sequence act as a major décollement level that localized the ABT in its outer part. The general southward increase in thickness of the Devonian–Carboniferous sedimentary sequence and associated facies changes suggest a rifted passive margin type geometry of the Rheno–Hercynian basin (e.g. Meilliez et al., 1991; Franke, 2000; Oncken et al., 2000; Lacquement, 2001). As proposed by Oncken et al. (2000) for the Eastern Ardennes belt, overturned basement-involved thrust sheets (OTS in Fig. 1c) in the footwall of the Midi Thrust Zone are likely to represent the result of the short-cut dissection and transport upon the upper flat of the rift shoulders that formed the northern extension of the Lower Devonian deposits. These structures illustrate the strong segmentation of the basin that in turn controlled the depth and extension of the potential décollement levels within the inverted Variscan belt. Based on depositional facies variations, syn-sedimentary fault zones active during the Lower–Middle Devonian rifting event have been shown to display dominant ENE–WSW and NW–SE trends (Meilliez et al., 1991), i.e. roughly normal and parallel to the Variscan thrusting directions. Therefore, these early structures are likely to have localized the frontal and lateral ramps in the Ardennes thrust wedge.

3. The Meuse Valley Recess: geometry and 3D structural model

Within an about 40-km-wide NW–SE-trending corridor centered on the Meuse river valley, the axial trace of the fold–thrust structures display pronounced strike deviations (Fig. 1b). The general ENE–WSW trend of the Western Ardennes thrust belt (average N070) turns clockwise to a

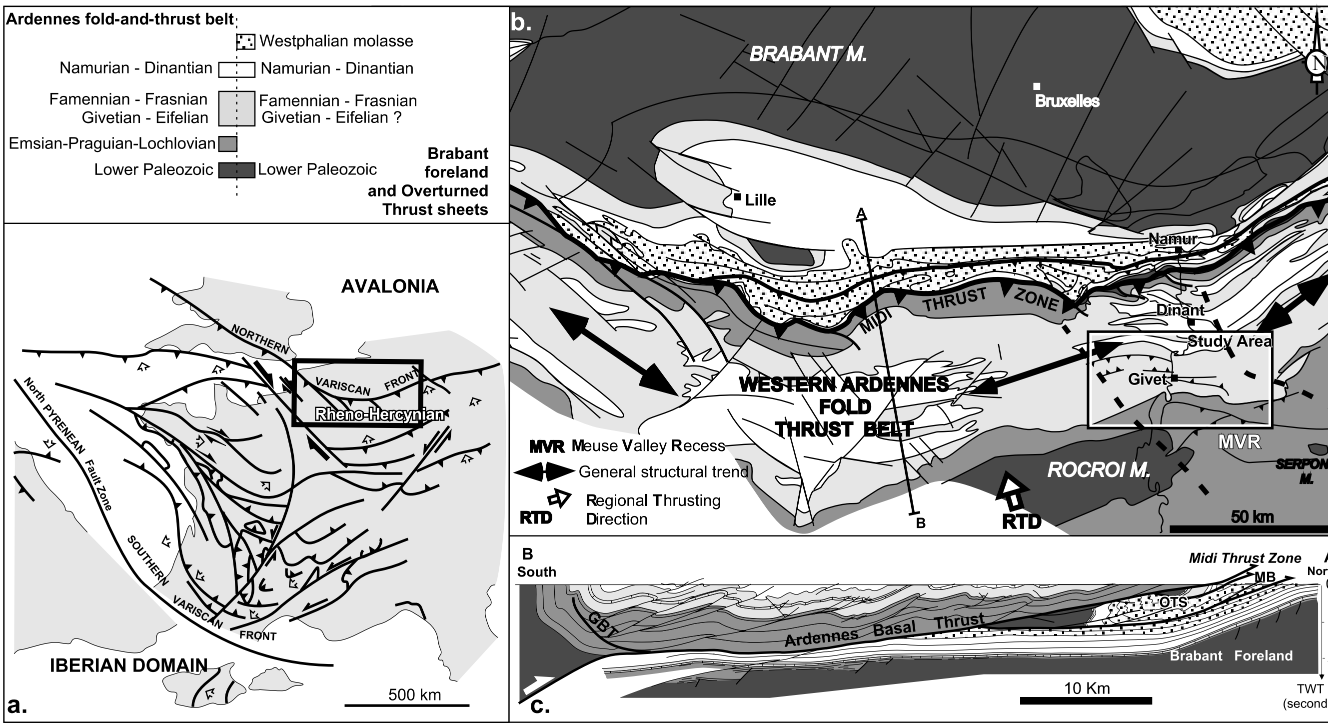

Fig. 1. (a) A tectonic map of the Western European Variscan belt (after Ledru et al., 2001). The rectangle locates the map in (b); (b) Subcrop map of the Northern France–Southern Belgium Variscan thrust front. The borders of the Meuse Valley Recess are emphasized by dashed lines. The specific study area is shown by a rectangle (map of Fig. 3). Section A–B refers to the M146 seismic line presented in (c); (c) A seismic cross-section (M146 profile) through the Western Ardennes thrust belt; OTS, Overturned thrust sheets; MB, Molassic basin; note the classical thrust wedge geometry of the Ardennes thrust belt upon a crustal scale S-dipping basal thrust.

WNW–ESE trend in the center of the corridor then turns back to a NE–SW trend towards the Eastern Ardennes belt (average N050). This progressive change in structural trend draws a concave-toward-the-foreland curvature defined here as the Meuse Valley Recess (MVR).

This strike deviation is particularly well represented within the southern part of the Ardennes thrust belt (Fig. 3). This zone corresponds to the northern forelimb of a major basement culmination (the Rocroi culmination) (Fig. 1b), which exposes in its core, a thick turbiditic series of Cambrian–Ordovician age submitted to very low grade metamorphism. This culmination can be interpreted as a large thrust-related anticlinal stack developed above a major footwall ramp of the ABT (Fig. 1c). North-northwestward displacement is transferred towards the foreland upon the base Lower Devonian décollement zone gently dipping to the south. The forelimb of the Rocroi culmination includes a thick Devonian–Carboniferous cover with a general steep northern dip (see the geological map of Fig. 3 and the cross-sections of Fig. 4). In the Givet area, it is affected by a complex out-of-the-syncline backthrust zone, the Givet backthrust zone (GBT) that roots at depth onto the ABT. It climbs southward through the Devonian series and emerges within the thick Frasnian–Famennian shaly layers situated just at the forelimb synclinal hinge. Due to the particularly weak behavior of the Frasnian–Famennian sequence, which potentially acts as a roof décollement level, displacement along the GBT is distributed into subsidiary thrusts and accommodated by intense folding and internal deformation.

From a structural point of view, two very different domains can be defined on both sides of the GBT (Lacquement, 2001): (1) the southern one corresponds to the steep forelimb of the Rocroi basement anticline, which involves the Lower–Middle Devonian series. This general north-dipping limb includes numerous second-order north-verging recumbent folds that display gently south-dipping axial plane cleavage. Folds are systematically dissected by NNW-verging forelimb thrusts indicating a general top-to-the-north simple shear of the fold–thrust structures; (2) north of the GBT, structures are characterized by polyharmonic upright folds with sub-vertical pressure-solution cleavage. This deformation pattern indicates bulk pure shear and layer-parallel shortening of the Upper Devonian–Carboniferous cover likely to be the result of a buttressing effect in front of the North-northwestward propagating Rocroi thrust-sheet (Fig. 4, sections a–c.).

Likewise, within the MVR, deformation is strongly heterogeneous, and strike-changes are accommodated in different ways, depending on their location with respect to the GBT. South of the GBT, the 400-m-thick competent Givetian limestone unit is involved in an about 50-km-wide oblique limb developed at the lateral tips of thrusts cross-cutting the Rocroi basement anticline and its Lower Devonian cover (Figs. 3 and 4). This large oblique

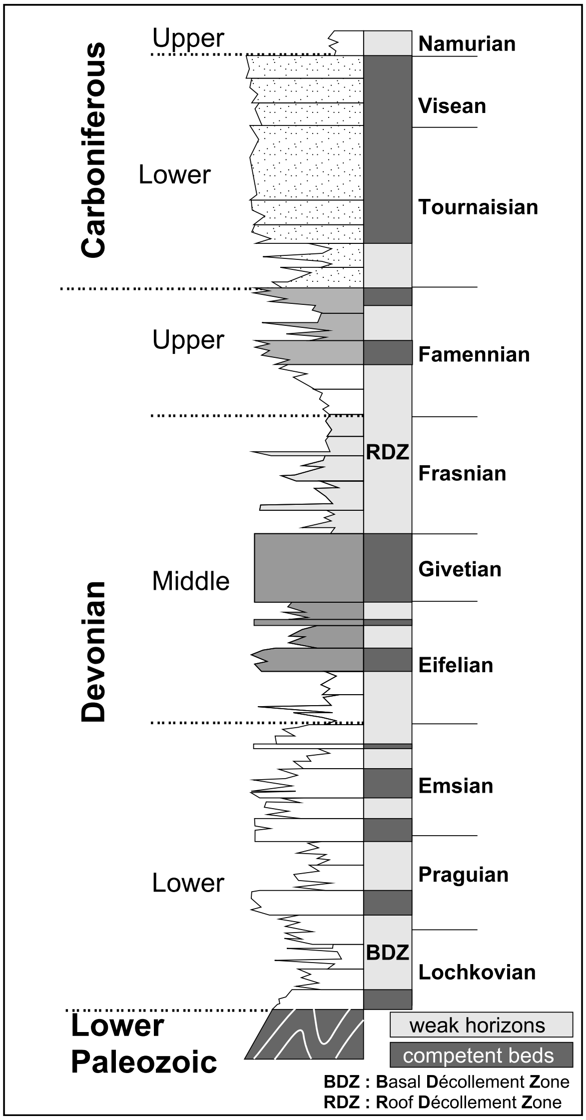

Fig. 2. Stratigraphy and rheological properties of Devonian–Carboniferous rocks involved in the Ardennes thrust belt. Note the existence of two main décollement-zones in the thrust wedge: a basal one within the Lochkovian shales and an upper one within the Frasnian–Famennian shales.

culmination wall is affected by kilometer-scale minor folds exhibiting a gradual increase in axial plunge (from 5 to about 50°) towards the inner parts of the MVR. Increase in the plunge of fold axes is associated with a progressive clockwise deviation of their strike (up to about 70°) (Fig. 3). An interesting point to be noticed is that the area of both maximum axial plunges and strike deviation is not located in the center of the corridor but is offset towards its eastern boundary. As proposed by Wilkerson et al. (2002) on the basis of ramp-related fold modeling, such high plunges and strong deviations of fold terminations suggest the existence of a buried lateral/oblique ramp beneath the inner parts of the strike-deviated corridor. Alternatively, the oblique culmination wall displays in specific deformation zones a significant cleavage tilt either towards the NNE or towards the E (Fig. 3). Like fold axial plunge, the amplitude of cleavage tilt within these zones globally increases towards the east. However, it is worth noting that areas of tilted cleavage are restricted to the central part of the oblique culmination wall and are not observed in the easternmost part of the MVR.

Within the Frasnian–Famennian sequence involved in the large syncline at the roof of the GBT, deformation is characterized by approximately 10 km scale en-échelon folds (Fig. 3). These folds are closely related to steep subsidiary back-thrusts branching on the GBT (see cross-sections in Fig. 4). Towards the north, the amplitude of such folds gradually decreases, indicating a general strain gradient towards the GBT. These second-order folds fade out northwards and the major fold structures display gently curved axes in the northern part of the study area.

Beneath the MVR, the geometry at depth can be constrained using both deep boreholes (the Focant and Rosée boreholes; see location in Fig. 3) (Boulvain and Coen-Aubert, 1997; Han et al., 2003) and a set of previously published seismic profiles from the Famenne area (e.g. Raoult, 1986; Goudalier, 1998), along the eastern boundary of the recess (the inner zones). The Focant borehole is particularly interesting because it is situated in the inner zones of the strike-deviated corridor, a few hundred meters north of the GBT emergence. As shown on cross-section (c) in Fig. 4, the Focant borehole surprisingly encountered 3000 m of strongly deformed Frasnian series (e.g. Raoult, 1986), which usually have thicknesses of about 400 m. This geometry has been interpreted as the result of the existence of a very deep and tight syncline bordered by sub-vertical limbs and dissected by numerous thrust faults. The GBT is encountered at about 2000 m showing its global sub-vertical attitude (i.e. parallel to the oblique wall of the Rocroi culmination). An E–W seismic profile through the GBT within the eastern part of the deformed corridor (Goudalier, 1998) suggests that this thrust branches rapidly laterally onto the ABT cutting through the Givetian limestone unit involved in an apparent westward thrusting (cross-section (d) in Fig. 4). This geometry points to a significant component of shortening at high angle to the regional thrusting direction inducing the upward lateral expulsion of a restricted thrust sheet in the innermost zone of the MVR.

On the other hand, previous interpretations of the network of N–S and E–W seismic profiles within the eastern part of the Meuse valley recess help to further constrain the deep geometry of the ABT as well as the structure of the ABT footwall units. As shown by Raoult (1986), seismic depth maps of the well-resolved ABT reflector display strong lateral variations from west to east in the investigated area (Fig. 5). The ABT lies at about 2.5 s two way time travel (TWT) in the central part of the recess (about 7–8 km depth following classical seismic velocity values within the Ardennes belt (Lacquement, 1997)) and climbs progressively eastward to about 1.8 s TWT east of the recess (about 5 km depth as shown by the Havelange

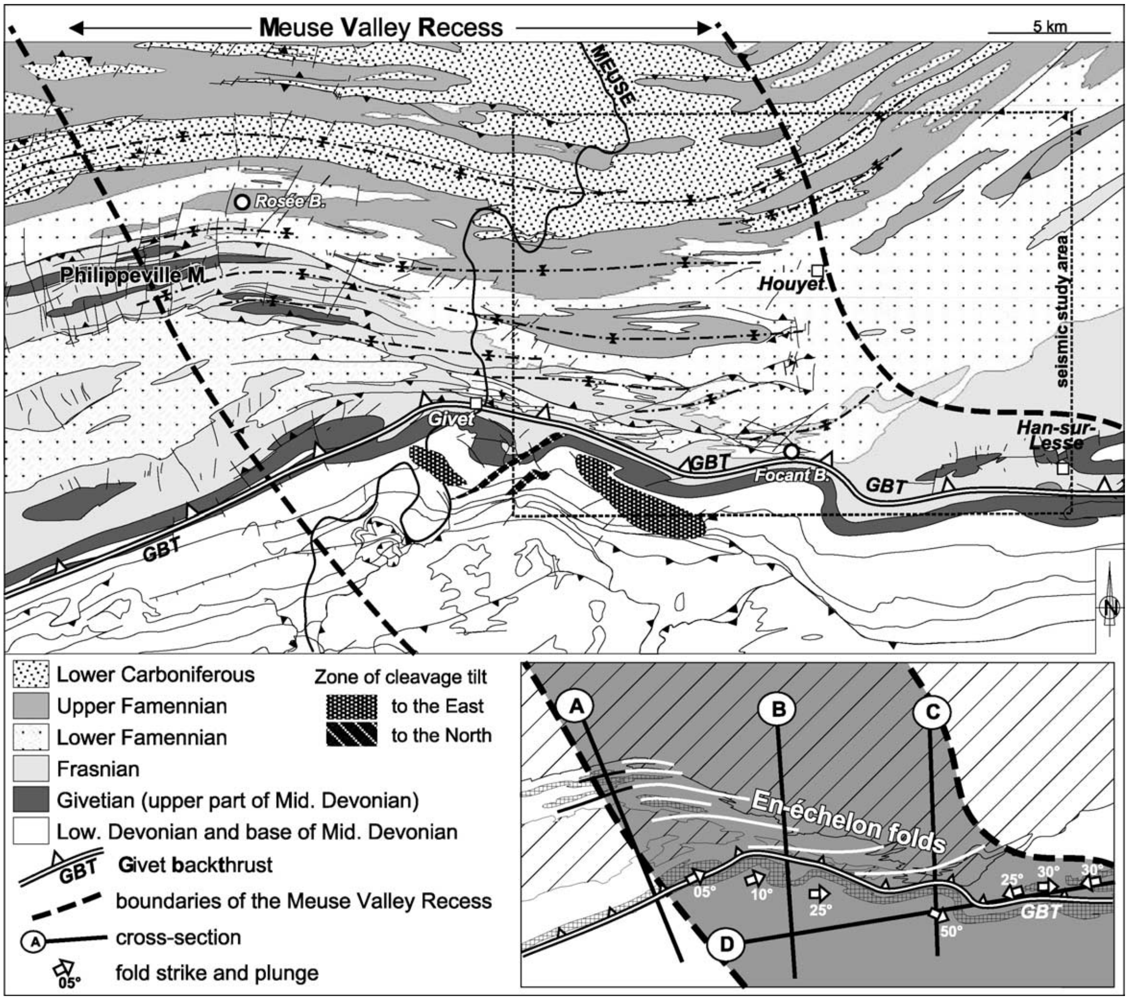

Fig. 3. (a) Geological map of the northern forelimb of the Rocroi basement culmination along the Meuse river valley. Note the progressive structural strike deviation characteristic of the Meuse Valley Recess (MVR) and also the existence of a significant back-thrust zone (GBT) along the Givetian limestone unit involved in the culmination wall. The zones of occurrence of cleavage tilt are reported on the map. Note the locations of the Focant and Rosée deep boreholes. (b) A schematic structural map of the study area showing the fold geometries along the MVR, and localizing the cross-sections of Fig. 4. Note the increase in fold strike deviation and plunges (up to 50°) towards the inner parts of the recess.

deep borehole (Raoult, 1986)). The interpreted seismic depth isovalues present a general NW–SE trend, almost parallel to the boundary of the corridor but slightly oblique to the regional thrusting direction. Moreover, these variations roughly parallel the lateral changes of the depth of a prominent reflector in the footwall of the ABT (the Y reflector of Raoult (1986) supposed to be the top of the Lower Paleozoic basement). Despite the relatively low resolution of the 3D seismic data, this geometric pattern shows that the structural strike variations observed in the Devonian–Carboniferous cover within the MVR are localized by a pronounced lateral step in the depth of the ABT. It forms a major buried lateral/oblique ramp in the thrust wedge as exemplified by cross-section (d) in Fig. 4, perpendicular to the regional thrusting direction. As shown on the large-scale map of Fig. 1, this lateral ramp clearly limits the eastward extension of the Rocroi basement culmination, thus decoupling two major thrust units, west and east of the MVR. Therefore, the MVR can be considered as the distributed hanging wall signature of a buried transfer zone between the Western and Eastern Ardennes thrust sheets. The seismic data moreover suggest that this lateral/oblique ramp is controlled by the ABT footwall topography, i.e. the geometry of the Brabant substratum. Considering the highly segmented nature of the Ardennes thrust wedge, the most satisfactory explanation for such basement topography is the existence, at depth, of a regional syn-sedimentary fault zone, inherited from the Devonian basin development (see the sketch 3D structural model presented in Fig. 5).

4. Magnetic fabric analysis

To further document the strain pattern within the MVR, we carried out a magnetic fabric analysis on 35 sites

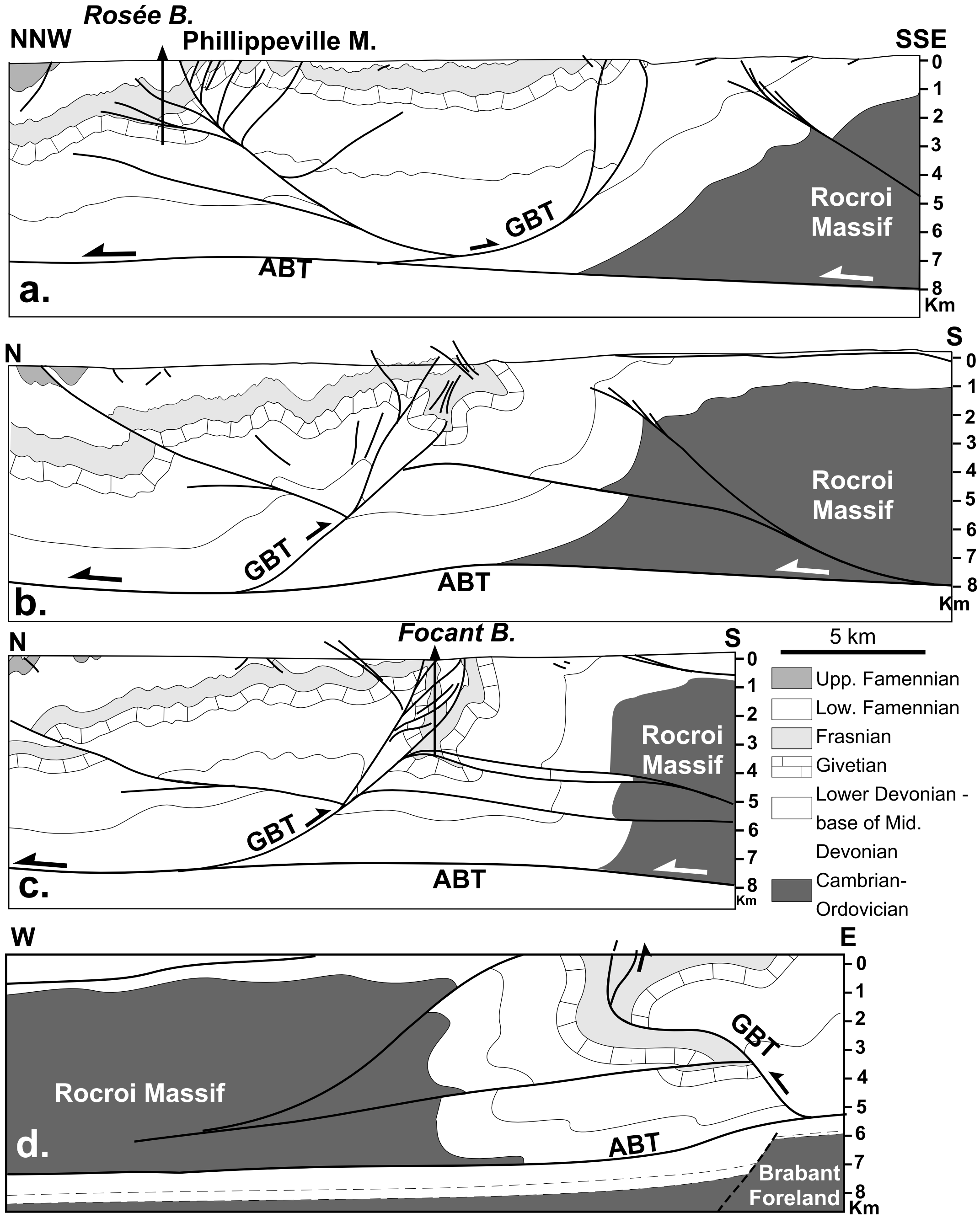

Fig. 4. Cross-sections through the forelimb of the Rocroi culmination: (a) parallel to the regional thrusting direction (RTD); (b) and (c) oblique to RTD; (d) perpendicular to RTD. See locations in Fig. 3b.

distributed within the structure. This method, based on the analysis of the anisotropy of the magnetic susceptibility (AMS), has been widely shown to represent a semi-quantitative strain indicator (see reviews in Tarling and Hrouda (1993) and Borradaile and Henry (1997)), particularly efficient in weakly deformed areas, such as foreland fold-and-thrust belts where few strain markers are available (Averbuch et al., 1992; Parès et al., 1999). AMS reflects the preferred orientation of grains and/or crystal lattices of all the minerals that contribute to the magnetic susceptibility (essentially ferro- and paramagnetic minerals). It can be described by an ellipsoid characterized by the orientation and the relative magnitude of three principal axes, a maximum axis, K_{max}, an intermediate axis K_{int} and a minimum axis K_{min}. The shape of the ellipsoid is described by the AMS shape parameter T (Jelinek, 1981), with $0<T\leq 1.0$ for oblate ellipsoids (dominantly planar fabrics) and $-1.0\leq T<0$ for prolate ellipsoids (dominantly linear fabrics) (Fig. 6). Strength of anisotropy is described by the anisotropy degree P (see Jelinek, 1981) (Fig. 6).

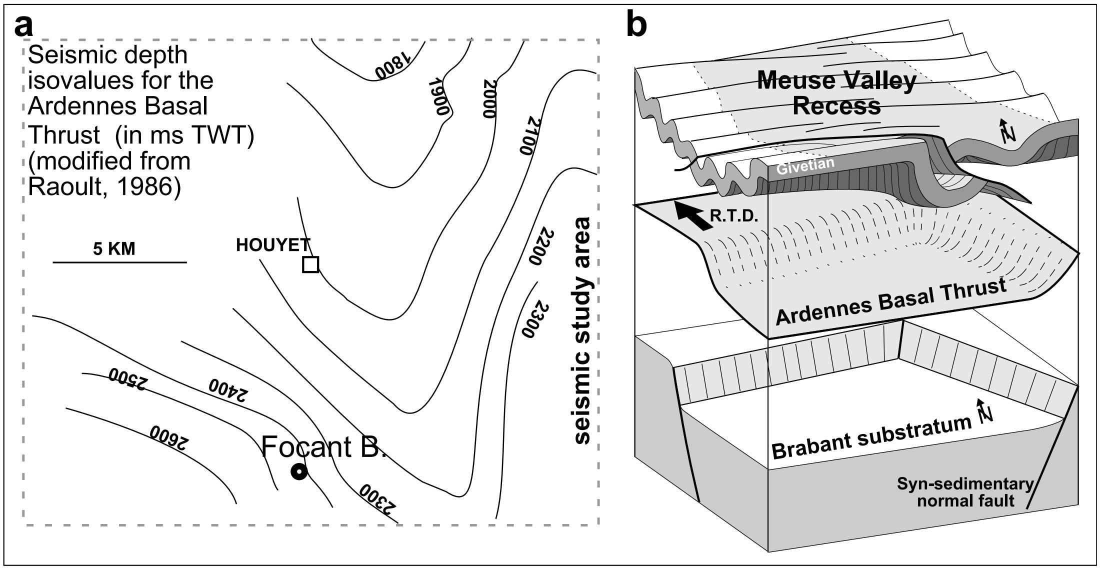

Fig. 5. (a) Seismic depth isovalues (in milliseconds two way time travel (TWT)) for the Ardennes Basal Thrust (ABT) along the eastern part of the Meuse Valley Recess (MVR) (modified from Raoult, 1986). Note the pronounced NW–SE-trending step in the depth of the ABT. (b) A 3D sketch structural model showing the close relationships between the MVR within the Ardennes thrust belt and the lateral variations in the geometry of the Ardennes basal thrust. Note that the buried lateral/oblique ramp localizing the MVR is controlled by the basement topography inherited from the Rheno–Hercynian basin development.

To provide the best possible distribution within the structure, sites having different lithologies (carbonates, shales and sandstones, except for red beds) and age (Praguian to Famennian) were sampled (see sample distribution in Fig. 7). The site-mean magnetic susceptibilities (K_m) are globally low (below 500×10^{-6} SI) (Fig. 6a) indicating a potentially combined paramagnetic (clay minerals) and ferromagnetic (iron oxides or sulfides) source for the magnetic anisotropy. Site-mean anisotropy degrees (P_m) are also globally low (below 1.15) indicating

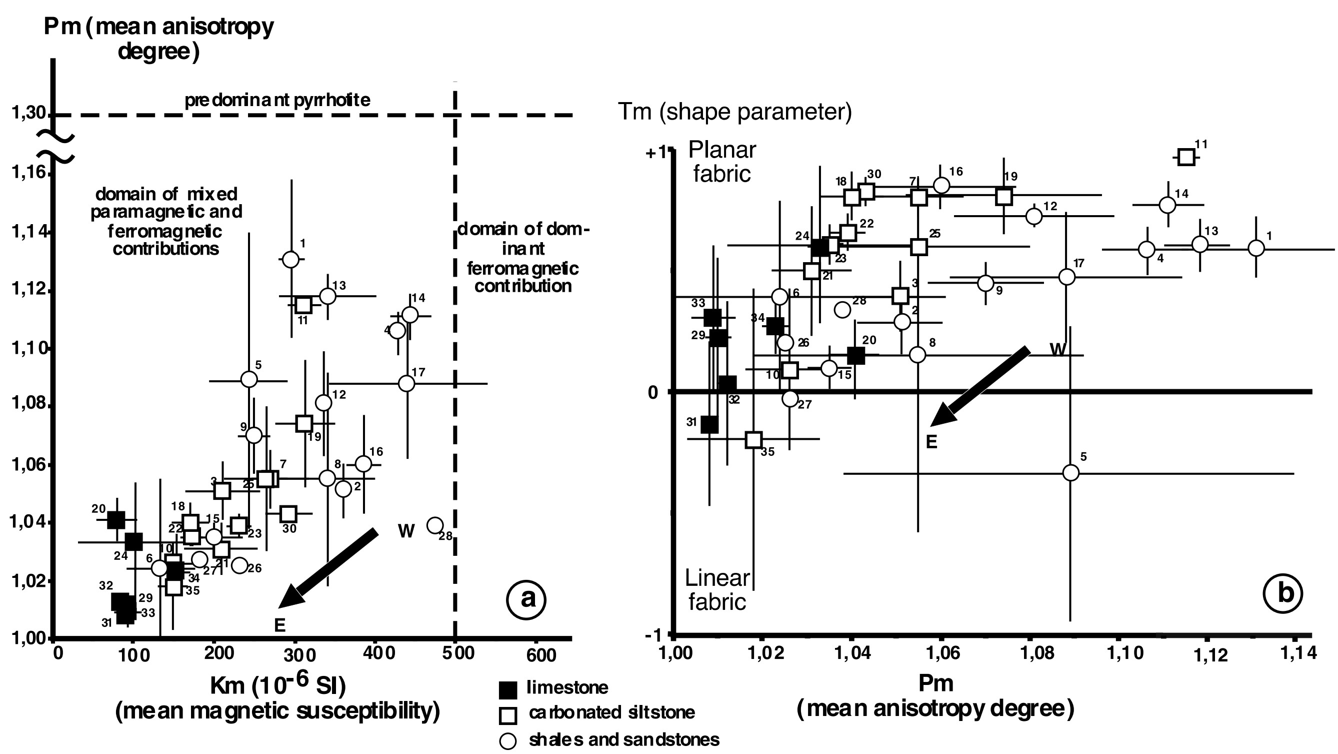

Fig. 6. Evolution of site-mean parameters of the anisotropy of magnetic susceptibility (AMS) along the Meuse Valley Recess. Numbers refer to sampling sites located in Fig. 7. (a) Diagram reporting the anisotropy degree P_m versus magnetic susceptibility K_m. (b) Diagram reporting the AMS shape parameter T_m versus the anisotropy degree P_m.

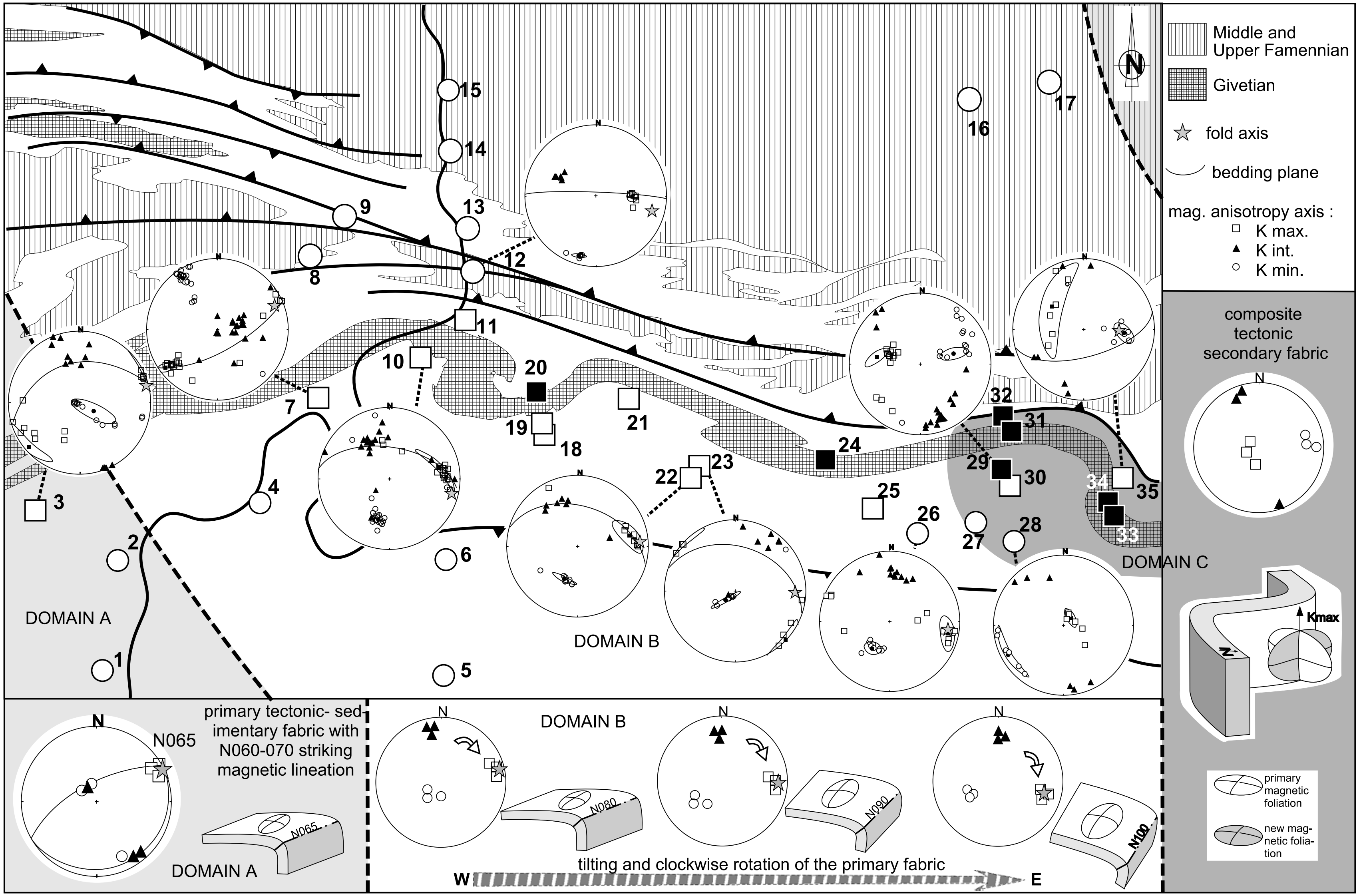

Fig. 7. Sketch geological map with the location of sites sampled for the magnetic fabric analysis (black squares refer to limestones, white squares to calcareous shales and white circle to shales and sandstones). The stereoplots (lower hemisphere, equal area) show the orientation of principal axes of the ellipsoid of anisotropy of magnetic susceptibility for representative sites along the Meuse Valley Recess. Black squares correspond to the orientation of the tensorial mean maximum axis K_{max} and black circles to the tensorial mean minimum axis K_{min}. Ellipses correspond to the confidence angles around the mean directions. Note the progressive evolution of the magnetic fabric from west (domain A) to east (domain C). See explanations in text.

that ferromagnetic iron sulfides (pyrrhotite) do not contribute significantly to the AMS (Rochette et al., 1992; Robion et al., 1999). Alternatively, the somewhat reducing conditions associated with the dark gray to green color of sampled shales and sandstones (we avoided red beds in sampling) suggest that magnetite and clays form the dominant contributions to the magnetic anisotropy. A combination of magnetite grain shapes and phyllosilicate crystallographic preferred orientations is thus likely to be responsible for the bulk magnetic anisotropy. Contrasting rheological properties of studied rocks, as well as the relative amounts of both these contributions to the sampling set, induce significant variations of the mean magnetic susceptibilities and anisotropy degrees. Shaly and sandy rocks have susceptibilities and anisotropies significantly higher than carbonate-bearing rocks (Fig. 6a). The global correlation of magnetic susceptibility and degree of anisotropy exemplifies the control exerted by the lithology and the magnetic mineralogy on the AMS (Rochette et al., 1992). If we consider, however, dominant lithologies separately, it is worth noting the persistence of significant variations of the anisotropy degree that can be related to the structural position of the sampled site (Figs. 6 and 7). Sites from the most deformed zone of the recess (the eastern sites of our distribution) display surprisingly low anisotropies compared with sites located outside the MVR or towards more external parts (the western sites of our distribution).

Site-mean shape parameters, T_m (Fig. 6b) display the same type of distribution with a significant structurally-related evolution from strongly planar to slightly linear fabrics. This evolution correlates well with the anisotropy degree showing that the most anisotropic fabrics from the western zones are dominantly planar, whereas the less anisotropic fabrics from the inner zone of the MVR are triaxial or slightly linear. As frequently observed in complex tectonic zones, this paradox suggests the composite nature of magnetic fabrics observed in the inner zone, owing to the superimposition of two non-coaxial planar sub-fabrics (Housen et al., 1993; Parés et al., 1999; Robion et al., 1999).

The orientation of principal axes of magnetic susceptibility corroborates this interpretation. Outside the MVR (domain A in Fig. 7), classical fabrics from foreland fold-and-thrust belts can be observed: K_{min} axes are clustering along the bedding-pole (or sometimes along the cleavage pole, depending on the lithology). Within this magnetic foliation, maximum susceptibility axes (magnetic lineation) cluster horizontally parallel to the fold axis (at the outcrop-scale, the cleavage–bedding intersection), here about N060–N070. This common type of fabric has been largely shown to result from the interference between growing pressure-solution cleavage surfaces and inherited bedding planes (Borradaile and Tarling, 1981; Kligfield et al., 1981; Averbuch et al., 1995; Parés et al., 1999). In these zones, magnetic fabrics thus evidence a shortening oriented about N330–340, i.e. parallel to the average thrusting direction. Such a type of fabric is also characteristic of the outer parts of the MVR (domain B in Fig. 7); it is worth noting, however, that with alike fold axes, the magnetic lineations tend to plunge eastward and progressively deviate towards an E–W to NW–SE direction.

In the easternmost part of the MVR (domain C in Fig. 7), the fabric is completely different from the other parts of the Ardennes belt. Regardless of the bedding attitude, a steep magnetic foliation striking about NNW–SSE to N–S can be observed. It is associated with a sub-vertical to steeply dipping magnetic lineation. As suggested by their low anisotropy degrees and slightly linear character, these fabrics have likely been reworked by superimposition of an incipient NNW–SSE tectonic foliation upon the primary tectonic–sedimentary fabric of type similar to those observed in other parts of the belt (Fig. 7). The sub-vertical magnetic lineation would thus correspond to the intersection between these two vertical foliations. Such a late NNW–SSE penetrative tectonic foliation implies a WSW–ENE shortening, i.e. a lateral shortening normal to the general thrusting direction. This lateral shortening is mostly localized within the eastern part of the MVR, as is also demonstrated by the Famenne seismic sections. In the more external parts, as also evidenced by the specific occurrence of zones of cleavage tilt (Fig. 3), out-of-plane deformation is expressed by the tilting and deviation of the initial fabric without any strong penetrative reworking (domain B in Fig. 7).

5. Rotational behavior of thrust-sheets

To constrain the rotational behavior of the tectonic units under study, we made a synthesis of up-to-date paleomagnetic data from the Ardennes thrust belt. Numerous recent paleomagnetic data are available in the Meuse Valley region (Molina Garza and Zijderveld, 1996; Marton et al., 2000; Szaniawski et al., 2003; Zegers et al., 2003) because it provides a natural cross-section through the folded Paleozoic series of the northern Variscan thrust front. Sites with contrasted deviated strike have thus been preferentially analyzed. Although fewer sites with the classical Ardenno–Rhenish ENE–WSW trend have been investigated, there are, however, sufficient data to discuss possible relative rotations associated with the MVR development (Szaniawski et al., 2003). The paleomagnetic sites distribution is reported in Fig. 8. Magnetite-bearing limestones of Middle Devonian and Carboniferous age are dominantly represented in the data set because they have been shown to display remanent magnetizations more stable than Lower or Upper Devonian red–green sandstones or siltstones. These whole sites have been shown to be remagnetized at different episodes of the deformation process but always with a reverse polarity (Kyaman superchron) (Szaniawski et al., 2003). Incremental untilting test procedures in different regional folds have evidenced a high temperature remagnetization component to occur at the incipient stages of folding probably due to the burial of

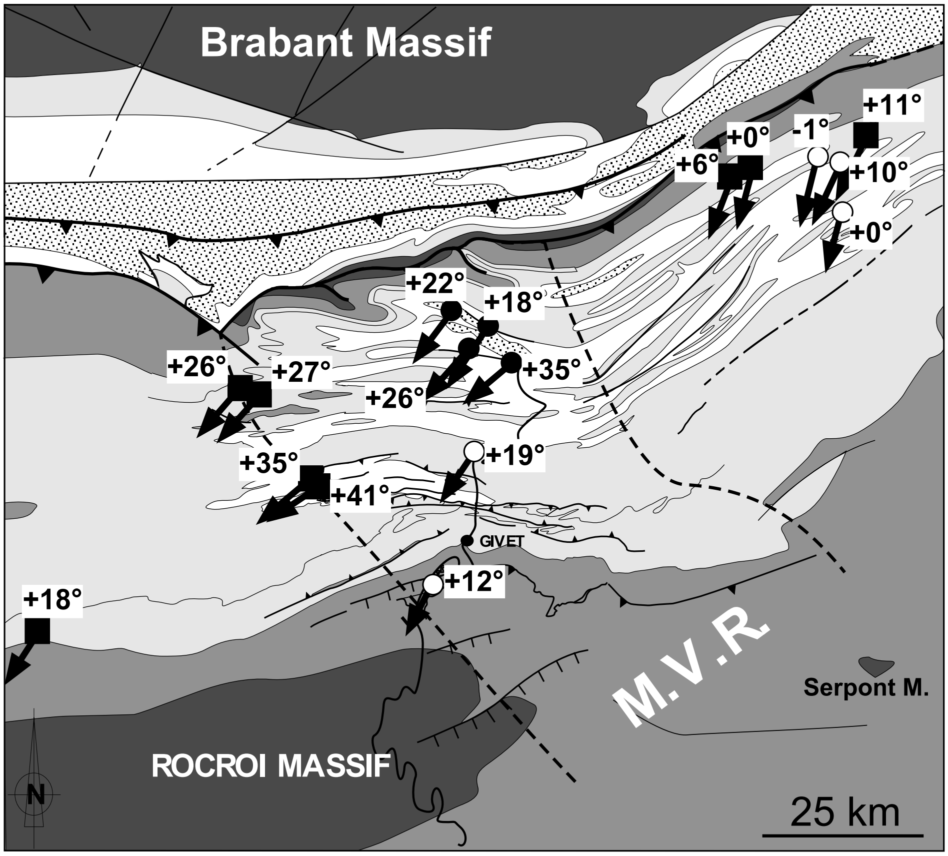

Fig. 8. Paleomagnetic results from relevant published sites within the Ardennes thrust belt (same geological map legend as Fig. 1). Black circles refer to paleomagnetic data from Molina Garza and Zijderveld (1996), white circles to data from Szaniawsky et al. (2003) and black squares to data from Zegers et al. (2003). The arrow corresponds for the majority of sites to the measured declination of the HT component of the remanent magnetization of some Givetian and Carboniferous limestones. For the few sites in Devonian siliciclastics, the arrow corresponds to the measured declination of the characteristic remanent magnetization (see text for discussion). Numbers correspond to the deviations with the expected declination for the Ardennes thrust belt based on the Westphalian paleopole for the stable 'Old Red Sandstones' continent of Van der Voo (1993).

sedimentary rocks under the thick molassic foreland basin of Namurian–Westphalian age. This remagnetization event occurred before most of the compressive deformation proceeded. Rotations around the vertical axis of the thrust sheets involved in the MVR are thus expected to have been recorded by the deviations of the site-mean remanence declinations with respect to that expected for the stable domain of the 'Old Red Sandstones continent' (here N195 following the Wespthalian paleopole of Van der Voo (1993)). Such an interpretation is not so evident for the Lower Devonian red beds from the southern part of the belt, within the forelimb of the Rocroi massif (Fig. 8), because they display syn- to post-folding remagnetizations. Nevertheless, we calculated the declination deviations for 17 published relevant sites distributed along the Ardennes thrust belt based on previous paleomagnetic studies of Molina-Garza and Zijderveld (1996), Zegers et al. (2003) and Szaniawski et al. (2003). Declination directions along with their deviations to the expected data are reported on a Variscan subcrop tectonic map in Fig. 8. Regardless of the age of the magnetization, these data show a permanent clockwise rotation of strike deviated sites from the MVR compared with zones showing the general trend of the Ardenno–Rhenish segment. The quantitative relationship between the amount of rotation and the local strike deviation at the study site compared with an average reference strike of N060E is plotted in Fig. 9. A clear linear correlation with a slope of 1 can be suggested for sites having strike deviation up to about 35°, indicating the pure rotational origin (orocline type) of the curvature. For sites having strikes deviated more than 35°, rotation does not increase more than about 30–40°. This suggests that rotation around vertical axes, particularly for zones of important strike deviation, does not account for the entire curvature. Instead, rotation increases some previous strike-deviated structures developed as oblique folds at the lateral boundary of the propagating Western Ardennes thrust-sheet.

6. A model for the development of the Meuse Valley Recess

Structural data presented above allow discussion of

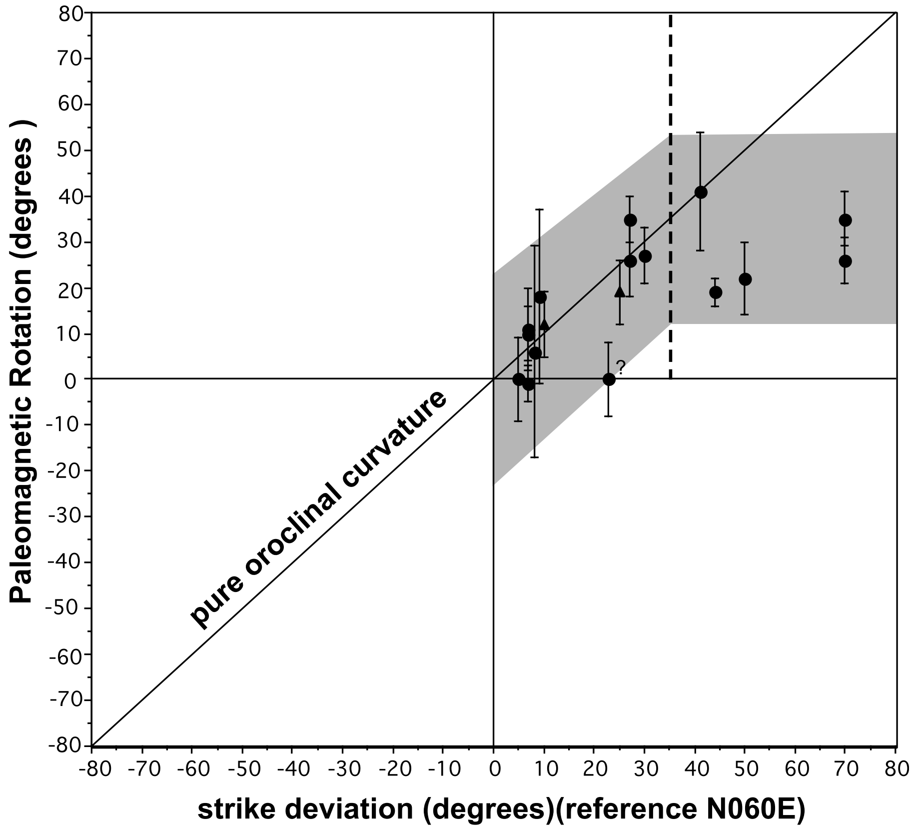

Fig. 9. Diagram showing the paleomagnetic rotation (deviation of declination) versus the strike deviation considering a reference strike of N060E. Black circles: Givetian and Carboniferous limestones; black triangles: Devonian siliciclastics.

geometrical and deformational features associated with the development of the MVR. One of the main results of our 3D structural analysis is that the MVR developed above a deep-seated lateral/oblique ramp controlling changes in the depth of the ABT. About 2 km of vertical offset can be suggested from west to east of the recess based on the roughly depth-converted seismic data. The data, however, do not have enough resolution and geographic coverage necessary to precisely define the geometry of this lateral step. It is unlikely that the 2 km offset would be accommodated by a single lateral/oblique ramp as shown on our simplified model in Fig. 5. Complex relay zones are likely, but are impossible to precisely define at depth. Despite this relatively low resolution, seismic data clearly show that the structure is mould on the basement topography, thus illustrating the control of the basin's early geometry on the thrust wedge development. As suggested by the occurrence of numerous syn-sedimentary normal faults controlling facies changes in the study area (Meilliez et al., 1991), the buried lateral ramp beneath the MVR is likely to be localized by a network of basement fault zones inherited from the Lower Devonian Rheno—Hercynian rifting event. These data thus corroborate observations by Hollmann and Von Winterfeld (1999) in the Western Rhenish massif, east of the Ardennes thrust belt.

A direct consequence of this geometry is that the belt involves a much thicker sedimentary sequence in the Western Ardennes area compared with the Eastern Ardennes which, as it has been shown by analog modeling experiments (e.g. Liu Huiqi et al., 1992; Marshak et al., 1992; Philippe, 1995), results in differential thrust propagation onto the foreland and thrust spacing within the wedge. Moreover, the increased thickness of the Lower Devonian shales at the base of the wedge, combined with enhanced pore-fluid pressure along the décollement zone due to increased overburden thickness are likely to decrease the friction at the base of the Western Ardennes thrust wedge compared with that in the Eastern Ardennes area (Henry and Le Pichon, 1991; Cobbold et al., 2001). Both mechanisms can combine to produce differential thrusting and thrust propagation, west and east of the Meuse Valley Recess. Regardless of its origin, this lateral variation in thrusting should result, in the hanging wall of the Ardennes basal thrust, in a somewhat distributed component of normal-to-bedding simple shear within the transfer zone. Moreover, as suggested by Hyett (1990) and Dixon and Liu (1992), additional shear strain may arise from drag effects against the lateral/oblique boundary during thrust propagation.

Paleomagnetic data within the MVR show that distributed thrust-sheet rotation account for only part of this deformation process. In the zones of maximum fold-strike

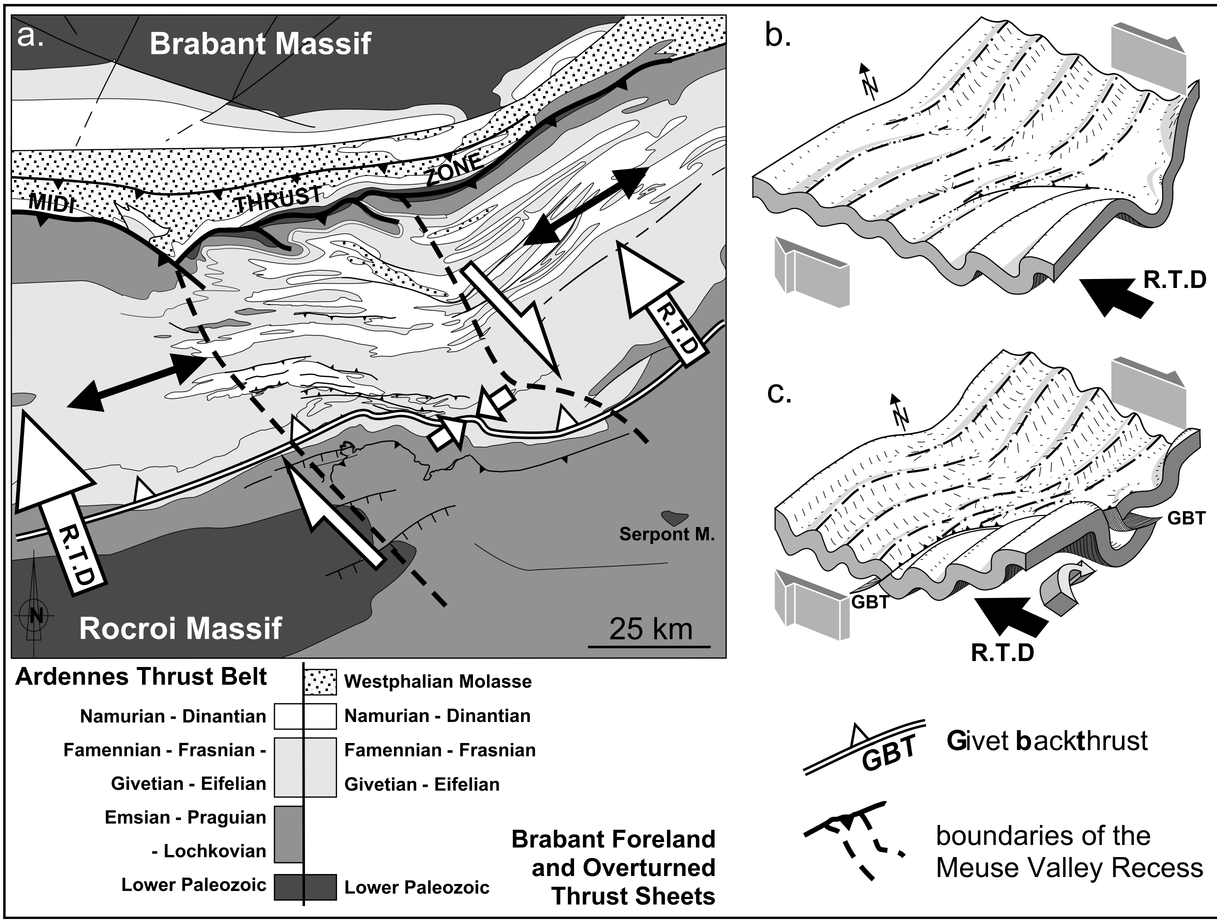

Fig. 10. (a) Structural map showing the kinematics of the Meuse valley transfer zone between the Western and Eastern Ardennes thrust belt. (b) and (c) A 3D model exemplifying the kinematics of deformation at the lateral boundaries of thrust sheets based on the Meuse Valley Recess development. (b) Oblique folding of the Ardennes basal thrust hanging wall above the buried lateral/oblique ramp. (c) Increase of lateral shortening against the lateral discontinuity (buttress effect) and late pervasive thrust-sheet rotation accommodating enhanced shear strain during basal thrust propagation. Note the outward propagation of the transfer zone with increased displacement towards the foreland.

deviation (up to 70°), paleomagnetic data record a maximum of 30–40° clockwise rotation around vertical axes compared with structural domains outside the recess. Conversely, zones which deviate less than 30° from the regional strike display almost pure rotational behaviour (Fig. 9). These data thus show that hanging wall structures situated in the direct vicinity of the lateral/oblique ramp (the eastern part of the MVR) originated as oblique folds (Fig. 10b) that rotated subsequently clockwise as shear strain increased with the propagation of displacement towards the foreland (Fig. 10c). It is worth noting that the width of the strike-deviated zone should have increased during this late process as suggested by the pure rotational behavior of domains deviated less than 30°. This point is corroborated by the occurrence of localized zones of tilt of the early pressure-solution cleavage that are geographically restricted to the external parts of the MVR. The clear asymmetric character of strains within the Meuse Valley corridor show that shear strain propagated dominantly westward along the MVR (i.e. in the direction opposite to that of the buried lateral discontinuity). This deformation scenario is in good agreement with previous strain studies on oblique fold–thrust structures, such as the Wyoming Salient, USA, where rotation was the stage of deformation latest recorded (Apotria, 1995). It moreover satisfies the results of theoretical analytical modeling along transverse zones in thrust belts suggesting the progressive rotation of obliquely-initiated folds towards the orientation of the underlying lateral/oblique discontinuity (Philippe, 1995).

Along the MVR, the component of shortening oblique to the regional top-to-NNW thrusting direction is strongly heterogeneous depending on the rheological properties of deformed units. Thick shaly layers (Frasnian–Famennian unit) develop an en-échelon fold pattern, whereas the competent Givetian limestone unit deforms in a wide oblique culmination wall affected by second-order folds. Decoupling of both mechanical units is accommodated by a complex backthrust zone (the Givet Backthrust Zone). In the inner parts of the MVR, these whole folds exhibit a progressive axial plunge increase up to 50° and displacement along the oblique backthrust zone increases (Fig. 10c). Accordingly, magnetic fabric analyses show a strain evolution towards inner zones of the MVR characterized by the progressive superimposition of a sub-vertical, broadly NNW–SSE-trending, cleavage plane upon the classical fold-type magnetic fabric characteristic of the general Ardennes fold-and-thrust-belt. Elsewhere in the MVR, the magnetic fabric and the initial pressure-solution cleavage are tilted and deviated with respect to their regional orientation without any significant reworking. The incipient vertical cleavage responsible for the magnetic fabric reworking document an ENE–WSW contraction episode localized predominantly along the eastern border of the MVR. Along with the increase in displacement along the Givet Backthrust Zone, these data demonstrate the presence of a gradient of lateral/oblique shortening towards the area localizing the major lateral discontinuity at depth (Fig. 10). The latter thus clearly acted as a buttress at the lateral boundary separating the Western and Eastern Ardennes foreland propagating thrust sheets.

7. Conclusions

Data presented above illustrate the complex 3D fold–thrust pattern at lateral boundaries of thrust sheets. The MVR results from the distributed transpressional deformation of the ABT hanging wall above a buried lateral/oblique ramp. The ramp acted as a transfer zone between two major NNW-directed thrust sheets of different thickness and having possibly varying basal friction. The resultant out-of-plane deformation includes some heterogeneous components of normal-to-bedding shear and lateral shortening, depending on the structural position within the recess. Normal-to-bedding shear is distributed within the MVR, whereas lateral shortening predominantly occurs along its eastern border, which localizes the deep-seated lateral/oblique discontinuity. Along the MVR, shear strain is expressed by distributed rotation of hanging wall folds with no significant trace of tear faulting. Thrust-sheet rotation around vertical axes does not account, however, for the total strike deviation. In the inner zone of the recess, only about 50% of the strike deviation (about 30–40°) is accommodated by thrust-sheet rotation, the remaining part resulting from initial oblique folding. Thrust-sheet rotation thus appears as a late effect of shear strain during differential thrust propagation. The pure rotational origin of strike deviation within the outer zones (sites deviated less than 30°) as well as the tilting of early strain markers suggest that the transfer zone broadened and propagated laterally outward (i.e. towards the west) during ongoing foreland-directed thrusting. Alternatively, lateral shortening clearly increases towards the eastern border of the MVR. The zone localizing the deep lateral discontinuity thus acted as a buttress likely due to edge effects against the buried lateral/oblique ramp. During propagation of thrusting, our data analysis thus emphasizes the high friction conditions prevailing along the lateral/oblique transfer zone. Drag effects along this discontinuity are therefore very likely with increased displacement along the basal thrust zone. Such a mechanism would result in enhanced shear strain that could account for the late thrust sheet rotation of the hanging wall folds and lateral outward broadening of the transfer zone.

Acknowledgements

This work has been conducted during the PhD theses of F.L. and R.S. at the University of Lille 1. It is a contribution of the 'Atelier Nord' of the UMR CNRS 8110 and of the Institute of Geophysics of the Polish Academy of Sciences. Additional financial support has been provided by the Bureau de Recherches Géologiques et Minières (France geological map project, P. Rossi coord.). We thank B. Vendeville and D. Frizon de Lamotte for friendly reviews of an early version of the text. The two journal reviewers, Y. Philippe and D. Wiltschko, are greatly thanked for their constructive remarks that strongly improved the previous version of this article.

References

Allerton, S., 1998. Geometry and kinematics of vertical-axis rotations in fold and thrust belts. Tectonophysics 299, 15–30.

Apotria, T.G., 1995. Thrust sheet rotation and out-of-plane strains associated with oblique ramps: an example from the Wyoming salient, USA. Journal of Structural Geology 17, 647–662.

Apotria, T.G., Snedden, W.T., Spang, J.H., Wiltscko, D.V., 1992. Kinematic models of deformation at an oblique ramp. In: McClay, K. R. (Ed.), Thrust Tectonics. Chapman and Hall, London, pp. 141–154.

Averbuch, O., Frizon de Lamotte, D., Kissel, C., 1992. Magnetic fabric as a structural indicator of the deformation path within a fold–thrust structure: a test case from the Corbières (NE Pyrenees, France). Journal of Structural Geology 14, 461–474.

Averbuch, O., Frizon de Lamotte, D., Kissel, C., 1993. Strain distribution above a lateral culmination: an analysis using microfaults and magnetic fabric measurements in the Corbières thrust belt (NE Pyrenees, France). Annales Tectonicae VII, 3–21.

Averbuch, O., Mattei, M., Kissel, C., Frizon de Lamotte, D., Speranza, F., 1995. Cinématique des déformations au sein d'un système chevauchant aveugle: l'exemple de la Montagna dei Fiori (front des Apennins centraux, Italie). Bulletin de la Société Géologique de France 166, 451–461.

Averbuch, O., Mansy, J-L., Lamarche, J., Lacquement, F., Hanot, F., 2004. Geometry and kinematics of the Boulonnais fold-and-thrust belt (N France): implications for the dynamics of the Northern Variscan thrust front. Geodinamica Acta 17/2, 163–178.

Bayona, G., Thomas, W.A., Van der Voo, R., 2003. Kinematics of thrust-sheets within transverse zones: a structural and paleomagnetic investigation in the Appalachian thrust belt of Georgia and Alabama. Journal of Structural Geology 25, 1193–1212.

Borradaile, G.J., Henry, B., 1997. Tectonic applications of magnetic susceptibility and its anisotropy. Earth Science Reviews 42, 49–93.

Borradaile, G.J., Tarling, D.H., 1981. The influence of deformation mechanisms on magnetic fabric in weakly deformed rocks. Tectonophysics 77, 151–168.

Boulvain, F., Coen-Aubert, M., 1997. Le sondage de Focant: lithostratigraphie et implications structurales, Memoirs of the Geological Survey of Belgium, vol. 43 1997. 74pp.

Butler, R., 1982. Hanging wall strain: a function of duplex shape and footwall topography. Tectonophysics 88, 235–246.

Calassou, S., Larroque, C., Malavieille, J., 1993. Transfer zones of deformation in thrust wedges: an experimental study. Tectonophysics 221, 325–344.

Cobbold, P.R., Durand, S., Mourgues, R., 2001. Sandbox modeling of thrust wedges with fluid-assisted detachments. Tectonophysics 334, 245–258.

Coward, M.P., Potts, G.J., 1983. Complex strain patterns developed at the frontal and lateral tips to shear zones and thrust zones. Journal of Structural Geology 5, 383–399.

Dahlstrom, C.D.A., 1970. Structural geology in the eastern margin of the Canadian Rocky Mountains. Bulletin of Canadian Petroleum Geology 18, 332–406.

Dixon, J.M., Liu, S., 1992. Centrifuge modeling of the propagation of thrust faults. In: McClay, K.R. (Ed.), Thrust Tectonics. Chapman and Hall, London, pp. 53–69.

Donzeau, M., Gamond, J.-F., Mugnier, J.-L., 1993. Evolution latérale et amortissement d'une structure chevauchante, un exemple du Nord Vercors. Compte Rendus Geosciences Paris 317, 1675–1682.

Franke, W., 2000. The mid-European segment of the Variscides: Tectonostratigraphic units, terrane boundaries and plate tectonic evolution. In: Franke, W., Haak, V., Oncken, O., Tanner, D. (Eds.), Orogenic Processes: Quantification and Modeling in the Variscan Belt Geological Society of London Special Publication, vol. 179, pp. 35–61.

Frizon de Lamotte, D., Guezou, J-C., Averbuch, O., 1995. Distinguishing lateral folds in thrust-systems: examples from Corbières (SW France) and Betic Cordilleras (SE Spain). Journal of Structural Geology 17, 223–244.

Goudalier, M., 1998. Dolomitisation de calcaires du Frasnien moyen de la Belgique: contrôle sédimentaire, diagénétique et tectonique. PhD thesis, Université de Lille 1, France.

Han, G., Yans, J., Goudalier, M., Lacquement, F., Corfield, R.M., Mansy, J.-L., Boulvain, F., Préat, A., 2003. Recognition and implication of tectonic loading-induced reheating in the northern Variscan front (Belgium and northern France), based on an illite Kübler index and oxygen isotope study. International Journal of Earth Science 92, 348–363.

Henry, P., Le Pichon, X., 1991. Fluid flow along a décollement layer: a model applied to the 16°N section of the Barbados accretionary wedge. Journal of Geophysical Research 96, 6507–6528.

Holl, J.E., Anastasio, D.J., 1995. Kinematics around a large-scale oblique ramp, southern Pyrenees, Spain. Tectonics 14, 1368–1379.

Hollmann, G., Von Winterfeld, C., 1999. Laterale strukturvariationen eines Vorlandüberschiebungs-gürtels. Zeitschrift der Deutschen Geologischen Gesellschaft 150, 431–450.

Housen, B.A., Richter, C., Van der Pluijm, B.A., 1993. Composite magnetic anisotropy fabrics: experiments, numerical models and implications for the quantification of rock fabrics. Tectonophysics 220, 1–12.

Hyett, A.J., 1990. Deformation around a thrust tip in Carboniferous limestone at Tutt Head, near Swansea, south Wales. Journal of Structural Geology 12, 47–58.

Jelinek, V., 1981. Characterization of the magnetic fabric of rocks. Tectonophysics 79, 63–67.

Kligfield, R., Owens, W.H., Lowrie, W., 1981. Magnetic susceptibility anisotropy, strain and progressive deformation in Permian sediments from the Maritime Alps (France). Earth and Planetary Science Letters 55, 181–189.

Lacquement, F., 1997. Retraitement du profil sismique M146, nord de de la France. Unpublished report, Compagnie Générale de Géophysique-Université de Lille.

Lacquement, F., 2001. L'Ardenne Varisque. Déformation progressive d'un prisme sédimentaire pré-structuré, de l'affleurement au modèle de chaîne. Publication de la Société Géologique du Nord 29.

Lacquement, F., Mansy, J.-L., Hanot, F., Meilliez, F., 1999. Retraitement et interprétation d'un profil sismique pétrolier méridien au travers du massif paléozoïque ardennais (nord de la France). Compte Rendus Geosciences Paris 329, 471–477.

Ledru, P., Faure, M., Bouchot V., 2001. Le Massif Central, témoin de la chaîne varisque ouest européenne. In: Géologue, Spécial Massif Central, no. 130–131, pp. 30–44.

Liu Huiqi, McClay, K.R., Powell, D., 1992. Physical models of thrust wedges. In: McClay, K.R. (Ed.), Thrust Tectonics. Chapman and Hall, London, pp. 71–81.

Macedo, J., Marshak, S., 1999. Controls on the geometry of fold–thrust belt salients. Geological Society of America Bulletin 111, 1808–1822.

Mansy, J.-L., Everaerts, M., De Vos, W., 1999. Structural analysis of the adjacent Acadian and Variscan fold belts in Belgium and northern France from geophysical and geological evidence. Tectonophysics 309, 99–116.

Marshak, S., Wilkerson, M.S., Hsui, A.T., 1992. Generation of curved fold–thrust belts: insight from simple physical and analytical models. In: McClay, K.R. (Ed.), Thrust Tectonics. Chapman and Hall, London, pp. 83–92.

Marton, E., Mansy, J.L., Averbuch, O., Csontos, L., 2000. The Variscan belt of Northen France–Southern Belgium: geodynamic implications of new paleomagnetic data. Tectonophysics 324, 57–80.

Meilliez, F., André, L., Blieck, A., Fielitz, W., Goffette, O., Hance, L., Khatir, A., Mansy, J.L., Overlau, P., Verniers, J., 1991. Ardenne-Brabant. Sciences Géologiques Bulletin 44, 3–29.

Molina-Garza, R., Zijderveld, J.D.A., 1996. Paleomagnetism of Paleozoic strata, Brabant and Ardennes Massifs, Belgium: implications of prefolding and postfolding late Carboniferous secondary magnetizations for European apparent polar wander. Journal of Geophysical Research 101 (B7), 15779–15818.

Oncken, O., Plesch, A., Weber, J., Ricken, W., Schrader, S., 2000. Passive margin detachment during arc-continent collision (Central European Variscides). In: Franke, W., Haak, V., Oncken, O., Tanner, D. (Eds.), Orogenic Processes: Quantification and Modeling in the Variscan Belt Geological Society of London Special Publications, vol. 179, pp. 199–216.

Parès, J.M., van der Pluijm, B.A., Dinarès-Turell, J., 1999. Evolution of magnetic fabrics during incipient deformation of mudrocks (Pyrenees, northern Spain). Tectonophysics 307, 1–14.

Paulsen, T., Marshak, S., 1999. Origin of the Uinta recess, Sevier fold–thrust belt, Utah: influence of basin architecture on fold-thrust belt geometry. Tectonophysics 312, 203–216.

Philippe, Y., 1995. Rampes latérales et zones de transfert dans les chaînes plissées: géométrie, conditions de formation et pièges structuraux associés. PhD thesis, Université de Savoie, France.

Raoult, J.-F., 1986. Le front varisque du Nord de la France d'après les profils sismiques, la géologie de surface et les sondages. Revue de géologie dynamique et de géographie physique 27, 247–288.

Robion, P., Averbuch, O., Sintubin, M., 1999. Fabric development and metamorphic evolution of the Paleozoic slaty rocks from the Rocroi massif (French–Belgian Ardennes): new constrains from magnetic fabrics, phyllosilicate preferred orientation and illite crystallinity. Tectonophysics 309, 257–273.

Rochette, P., Jackson, J., Aubourg, C., 1992. Rock magnetism and the interpretation of anisotropy of magnetic susceptibility. Review of Geophysics 30, 209–226.

Schirmer, T.W., 1988. Structural analysis using thrust-fault hanging-wall sequence diagrams: Ogden duplex, Wasatch Range, Utah. American Association of Petroleum Geologists Bulletin 72, 573–585.

Szaniawski, R., Lewandowski, M., Mansy, J.-L., Averbuch, O., Lacquement, F., 2003. Syn-folding remagnetization events in the French–Belgium Variscan thrust front as markers of the fold-and-thrust belt kinematics. Bulletin de la Société Géologique de France 174, 511–523.

Tarling, D.H., Hrouda, F., 1993. The Magnetic Anisotropy of Rocks. Chapman and Hall, London. 217pp.

Tavarnelli, E., 1996. Ancient synsedimentary structural control on thrust ramp development; an example from the Northern Apennines. Terra Nova 8, 65–74.

Thomas, W.A., 1990. Controls on locations of transverse zones in thrust belts. Eclogae Geologicae Helvetica 83, 727–744.

Van der Voo, R., 1993. Paleomagnetism of the Atlantic, Tethys and Iapetus Oceans. Cambridge University Press, Cambridge. 411pp.

Wilkerson, S., Apotria, T., Farid, T., 2002. Interpreting the geologic map expression of contractional fault-related fold terminations: lateral/oblique ramps versus displacement gradients. Journal of Structural Geology 24, 593–607.

Wiltschko, D.V., Eastman, D.B., 1982. Role of basement warps and faults in localizing thrust-fault ramps. Geological Society of America Memoir 158, 177–190.

Zegers, T., Dekkers, M.J., Bailly, S., 2003. Late Carboniferous to Permian remagnetization of Devonian limestones in the Ardennes: role of temperature, fluids and deformation. Journal of Geophysical Research 108 (B7), 2357.

Article 12.

Averbuch O., *Lacquement F., Szaniawski R.,* Mansy J-L. and Lewandowski M., 2002.- Segmentation of the N France-S Belgium Variscan thrust front : insights into the geometry of the Devonian Rheno-hercynian basin. Contributions to the geology of Belgium and Northwest Europe, P. Degryse and M. Sintubin eds., Aardk. Mededel. 12 , 89-92.

Proceedings of the first Geologica Belgica International Meeting, Leuven, 11-15 September 2002
Aardk. Mededel., 2002, **12**, 89-92

Segmentation of the Variscan thrust front (N France, S Belgium): insights into the geometry of the Devonian Rheno-Hercynian Basin

***O. Averbuch*[1], *F. Lacquement*[2], *R. Szaniawski*[3], *J.-L. Mansy*[1] & *M. Lewandowski*[3]**

1. *Processus et bilan des Domaines sédimentaires, Université de Lille 1, 59655 Villeneuve d'Acsq cédex, France, Olivier.Averbuch@univ-lille1.fr*
2. *BRGM, 3, avenue C. Guillemin, BP6009, 45060 Orléans cédex 2, France, f.lacquement@brgm.fr*
3. *Institute of Geophysics of the Polish Academy of Sciences, Ks. Janusza 64, 01-452 Warsaw, Poland, rafszt@igf.edu.pl*

ABSTRACT

The structure of the Variscan thrust front (N France, S Belgium) has been investigated with a special emphasis on the lateral discontinuities affecting the thrust wedge and associated structural strike deviations. We focused on the geometry and kinematics of the Dinant virgation zone (DVZ) using structural, magnetic fabric and palaeomagnetic data. Results show that it forms a major transpressive zone submitted to strain partitioning between dextral simple-shear and shortening normal to the deformed zone. Such corridor of deformation is localized upon deep-seated basement discontinuities inherited from the Rheno-hercynian basin development in Lower-Middle Devonian times. This study suggests that at a larger scale, the Variscan thrust front is segmented and locally curved due to the existence of a system of dominantly northwest-southeast trending inherited basement fault zones, that basically control the depth and location of the basal Ardennes décollement zone.

KEYWORDS

Ardennes, Rheno-Hercynian Basin, transpression, Variscan thrust front

Introduction

The Variscan thrust front (N France, S Belgium) is a composite structural feature that extends from the Channel-Boulonnais region to the Ardennes massif changing progressively strike from northwest-southeast to northeast-southwest. This large-scale strike variation occur in relation with second-order virgations zones relaying in a complex way through lateral discontinuities within the fold-thrust belt (Fig. 1). Such segmentation of the belt may also be observed on the « Midi thrust zone » (Mansy *et al.*, 1999) which corresponds to the emergence of the main Ardennes basal thrust, a crustal-scale gently south dipping décollement zone accommodating a general northnorthwest directed displacement of more than 70 km (Lacquement *et al.*, 1999). The « Midi thrust zone » separates the Ardennes Allochthonous Units that display a classical thrust-wedge geometry from the underthrusted Namurian-Westphalian coal-bearing foreland basin, partly dismembered along its southern border (Fig. 1)(e.g. Lacquement *et al.*, 1999). This basin lies on top of the Brabant massif basically structured in Caledonian times and surrounded by a reduced Devonian sedimentary sequence characterized by the lack of Lower Devonian rocks.

At the opposite, the Allochthonous Units display a thick Lower Devonian sequence. The general southward increase of the thickness of the sedimentary pile and associated facies changes argue for a rifted passive margin type geometry of the Devonian Rheno-hercynian basin (e.g. Meilliez *et al.*, 1991; Franke, 2000). Therefore, during its Devonian development, it must have been strongly compartimented by syn-sedimentary fault zones. Their geometry is not precisely constrained but it shoud have had a great importance in the segmentation and the present-day shape of the inverted Variscan belt (see for example the east-west cross-section of Fig. 2 showing changes in the depth of the basal décollement zone in relation with inherited basin structures).

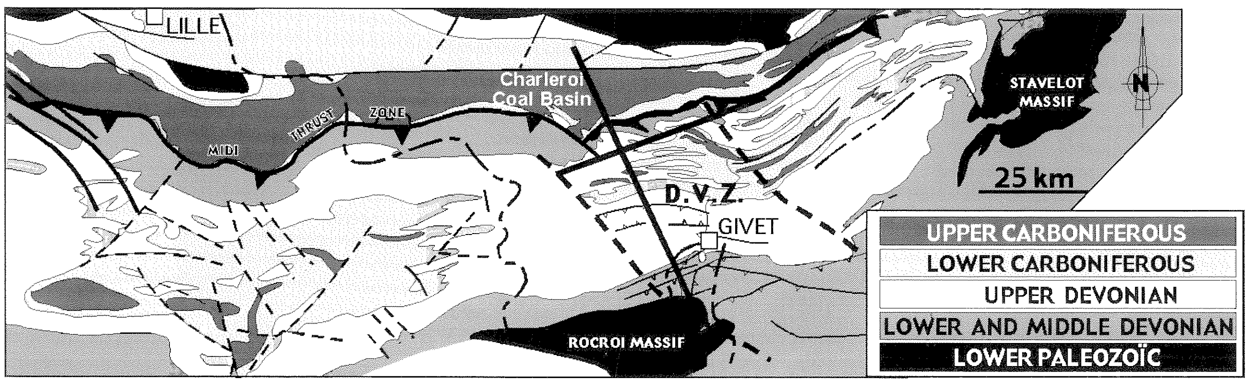

Fig. 1. Subcrop map showing the geometry of the Variscan thrust front(N France, S Belgium) with emphasis on structural strike deviations along northwest-southeast trending corridor.

For example, inherited faults are particularly important in the localization of lateral ramps of thrust sheets (e.g. Frizon de Lamotte *et al*, 1995).
To progress in the knowledge of such inherited discontinuities within the Ardennes thrust belt, we carried out combined structural, magnetic fabric and palaeomagnetic studies within one of the major lateral discontinuities of the belt: the Dinant virgation zone. The conclusions of this work are extrapolated to other zones of the belt showing important strike variations leading to a model for the geometry of the deep discontinuities in the substratum of the Rheno-hercynian basin.

The Dinant virgation zone

Structural framework

Within the Ardennes fold-and-thrust belt, the Givet-Dinant area displays an about 30 km large northwest-southeast striking corridor where the strike of fold-thrust structures progressively deviates from the general eastnortheast-westsouthsest to an eastsoutheast-westnorthwest orientation (Fig. 1). Along the steep northern forelimb of the basement culmination of the Rocroi massif (Givet area), this general strike variation is accommodated from the western part of the corridor towards its eastern boundary by the progressive deviation and gradual plunge increase (from 10 to 50°) of the fold axes. Within this zone, cleavage appears locally tilted dominantly towards the northeast quadrant

Strain distribution

Strain distribution was investigated using magnetic fabric analyses (e.g. Averbuch *et al.*, 1992; Borradaile & Henry, 1997). Apart from a dominant lithological control upon the magnetic anisotropy degree, it is possible to detect a conspicuous tendency for an eastward decrease of the magnetic anisotropy degree. Parallel to that decrease, the global planar character of the magnetic fabric diminishes towards the eastern part of the area and locally tends to be slightly linear. In such cases, the fabric is strongly reworked compared to the general situation with a resulting vertical magnetic lineation. This composite fabric is interpreted as the superimposition of an incipient northnorthwest-southsoutheast trending vertical tectonic foliation upon the bedding or cleavage parallel planar fabric with a fold axis parallel magnetic lineation. The incipient tectonic fabric argues for a late eastnortheast-westsouthwest lateral shortening mostly active within the eastern part of the corridor. In the central part of the virgation zone, this late deformation is recorded by the tilting and rotation of the initial fabric without any strong reworking.

Palaeomagnetic data

To constrain the rotational behaviour of the tectonic units under study, we carried out palaeomagnetic work at a slightly larger scale i.e. from the Dinant virgation zone (DVZ) to the Ourthe virgation zone (OVZ) in the Liège area (Szaniawski *et al.*, in press). Sites with the dominant eastnortheast-westsouthwest trend as well as sites with deviated strike were analyzed and compared to published data (Molina Garza & Zijderveld, 1996).

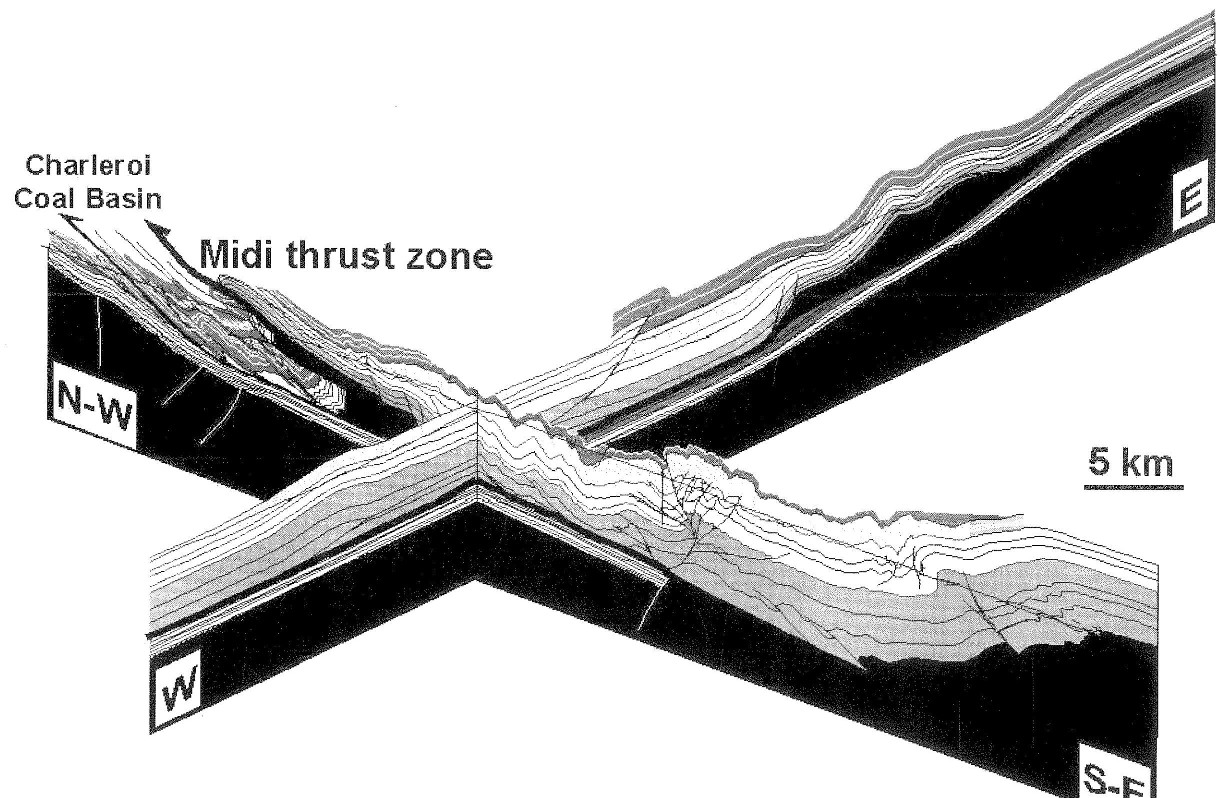

Fig. 2. Parallel and normal to the thrusting direction cross-sections through the thrust front in the Dinant Virgation Zone area. Same legend as in Fig. 1.

Although remagnetised at different steps of the Variscan deformation process, the sites display varying declinations of the characteristic remanent magnetisation according to their structural position. Sites situated within the Ourthe and Dinant virgation zones show 15-35° clockwise deviated declinations compared to that with the general Ardennes trend (that do not show any rotation compared to stable Old Red Continent). The measured rotations do not account, however, for the total strike deviation observed in the virgation zones.

Conclusion

The data presented above suggest that the Dinant virgation zone (DVZ) results from distributed transpressive deformation at the lateral boundary of a major northnorthwest directed thrust sheet. Structures within this zone would have originated as oblique folds and were subsequently strongly exaggerated. This late event implies a partitioning of the deformation with a component of dextral simple-shear inducing an about 20-30°of clockwise rotation and a component of lateral shortening normal to the orientation of the deformed zone. Geometry in cross-sections and depth map of the basal décollement zone (Lacquement, 2001) show that the Dinant virgation zone is localized by a system of northwest-southeast trending deep-seated basement discontinuities inherited from the Lower-Middle Devonian basin geometry.

We suggest that at a larger scale, the other zones of strike deviation affecting the north France – south Belgium Variscan thrust front (i.e. the Artois, Valenciennes, Beaumont and Ourthe zones) are the results of transpressional deformations above deep-seated syn-sedimentary faults of the Rheno-hercynian basin. This lead us to consider the Variscan thrust front to be segmented in response to the footwall pre-structuration along different fault zones i.e. the inner Dinant, Beaumont, Valenciennes and Ourthe fault zones (Fig. 3). This network of basement faults dominantly display a northwest-southeast trend as already noticed by Meilliez (1989) on the basis of sedimentary facies variations.

References

AVERBUCH O., FRIZON DE LAMOTTE D. & KISSEL C. 1992. Magnetic fabric as a structural indicator of the deformation path within a fold-thrust structure: a test case from the Corbières (NE Pyrénées, France). *J. Struct. Geology* **14**, 461-474.

BORRADAILE, G. & HENRY B. 1997. Tectonic applications of magnetic susceptibility and its anisotropy. *Earth Science Reviews* **42**, 49-93.

FRANKE W. 2000. The mid-european segment of the Variscides: tectonostratigraphic units, terrane boundaries and plate tectonic evlution. In: Franke W., Haak V., Oncken O. & Tanner D. (Eds.) Orogenic processes: quantification and modelling in the Variscan belt. *Geological Society of London Special Publications* **179**, 35-61.

FRIZON DE LAMOTTE D., GUEZOU J-C. & AVERBUCH O. 1995. Distinguishing lateral folds in thrust-systems; examples from Corbières (SW France) and Betic Cordilleras (SE Spain). *J. Struct. Geology* **17**, 233-244.

LACQUEMENT, F. 2001. L'Ardenne varisque. Déformation progressive d'un prisme sédimentaire pré-structuré, de l'affleurement au modèle de chaîne. *Publications Soc. Géol. Nord* **29**, 285 pp.

LACQUEMENT F.., MANSY J-L., HANOT F. & MEILLIEZ F. 1999. Retraitement et interprétation d'un profil sismique pétrolier au travers du Massif paléozoïque ardennais. *C. R. Acad.* Sci. Paris **329**, 471-477.

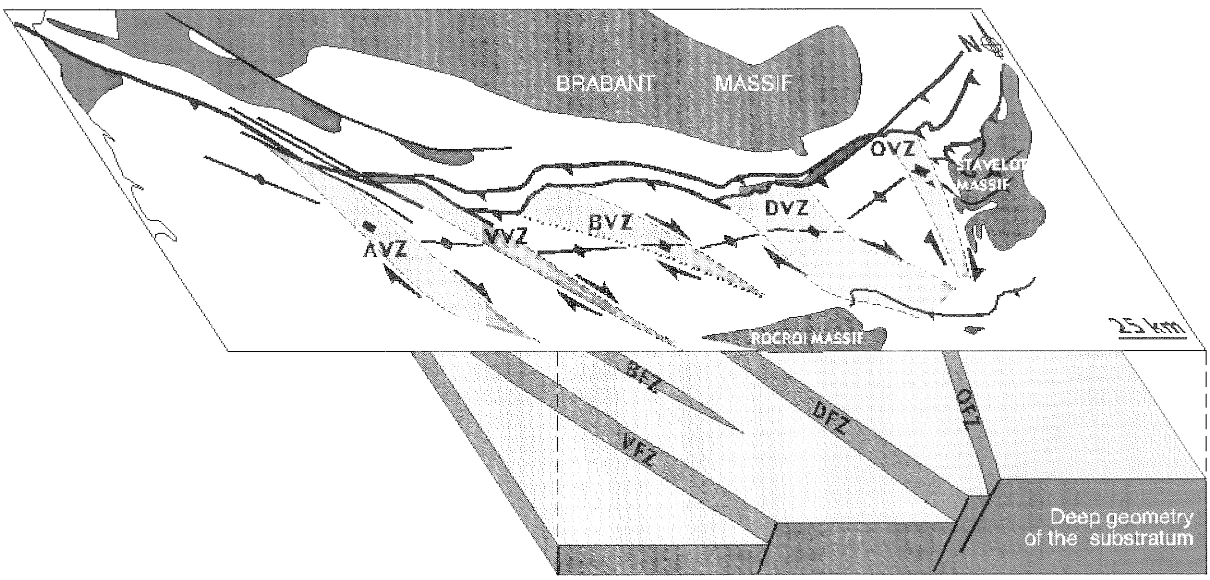

Fig. 3. Schematic 3D view showing the segmentation of the Variscan thrust front (N France, S Belgium) and location of associated basement fault zone. AVZ, VVZ, BVZ, DVZ and OVZ respectively Artois, Valenciennes, Beaumont, Dinant and Ourthe virgation zones. VFZ, BFZ, DFZ, OFZ respectively Valenciennes, Beaumont, Dinant and Ourthe footwall fault zones.

MANSY J-L., EVERAERTS M. & DE VOS W. 1999. Structural analysis of the adjacent Acadian and Variscan fold belts on Belgium and Northern France from geophysical and geological evidence. *Tectonophysics* **309**, 99-116.

MEILLIEZ F. 1989. Importance de l'événement calédonien dans l'allochtone ardennais; essai sur une cinématique paléozoïque de l'ardenne dans la chaîne varisque. *Unpublshed Doctoral Thesis, Université du Maine.*

MEILLIEZ F., ANDRE L., BLIECK A., FIELITZ W., GOFETTE O., HANCE L., KHATIR A., MANSY J-L., OVERLAU P. & VERNIERS J. 1991. Ardenne-Brabant *Sci. Géol. Bull.* **44**, 3-29.

MOLINA-GARZA R. & ZIJDERVELD J.D.A. 1996. Paleomagnetism of the Paleozoic Brabant and Ardennes massifs (Belgium): implications of prefolding and postfolding Late carboniferous secondary magnetisation for European apparent polar wander. *J. Geophys. Res.* **101**, 15779-15818.

SZANIAWSKI R., LEWANDOWSKI M., MANSY J-L., AVERBUCH O. & LACQUEMENT F. In press. Syn-folding magnetisations in the French-Belgium Variscides as a marker of the fold belt tectonic evolution. *International Journal of Earth Sciences*.

Article 13.

Robion P., Averbuch O. and Sintubin M., 1999. Fabric development and metamorphic evolution of the Paleozoic slaty rocks from the Rocroi massif (French-Belgian Ardennes): new constraints from magnetic fabrics, phyllosilicate preferred orientation and illite cristallinity data. Tectonophysics 309, 257-273.

ELSEVIER

Tectonophysics 309 (1999) 257–273

TECTONOPHYSICS

www.elsevier.com/locate/tecto

Fabric development and metamorphic evolution of lower Palaeozoic slaty rocks from the Rocroi massif (French–Belgian Ardennes): new constraints from magnetic fabrics, phyllosilicate preferred orientation and illite crystallinity data

P. Robion [a,*], O. Averbuch [b], M. Sintubin [c]

[a] *Département des Sciences de la Terre (CNRS ESA 7072), Université de Cergy-Pontoise, 8, Le Campus, 95031 Cergy-Pontoise cédex, France*
[b] *Laboratoire de Sédimentologie et Géodynamique, URA 719, Université de Lille 1, 59655 Villeneuve d'Acsq cédex, France*
[c] *Laboratorium voor Algemene Geologie, Katholieke Universiteit Leuven, Redingenstraat 16, B-3000 Leuven, Belgium*

Accepted 9 April 1999

Abstract

This paper presents new results of a petrofabric study from Cambrian slates cropping out within the anchi–epimetamorphic core of the Rocroi massif (Ardennes Variscan fold-thrust belt of northern France and southern Belgium). This study includes measurements of the Anisotropy of the Isothermal Remanent Magnetisation (AIRM) and the phyllosilicate preferred orientation. It completes the previous results of Anisotropy of Magnetic Susceptibility (AMS) and of magnetic mineralogy which were obtained in 47 sites situated in and around this massif. These new data allow the characterisation of the different subfabrics carried by the ferromagnetic minerals (metamorphic pyrrhotite and magnetite) and the paramagnetic matrix (Fe-rich phyllosilicates). Combined with some illite crystallinity data measured throughout the massif, the petrofabric measurements evidence a polyphase tectonometamorphic evolution. A major Variscan compressional event is evidenced inducing the growth of highly anisotropic pyrrhotite, coarse-grained hematite and phyllosilicates. By contrast, the magnetite grains display a less well-organised fabric due to the existence of an inherited orientation pattern. In agreement with recent metamorphic studies, it argues for an early diastathermal metamorphic event developed during a Devonian crustal-scale extension.

Keywords: Ardennes; Variscan; magnetic fabrics; phyllosilicate preferred orientation; illite crystallinity; anisotropy of isothermal remanence magnetization

1. Introduction

Magnetic anisotropy has been shown in the last 20 years to be a powerful tool for petrofabric analysis of rocks both in sedimentary and crystalline domains (see the recent review of Borradaile and Henry, 1997). In numerous tectonic studies, the anisotropy of low field magnetic susceptibility (AMS) ellipsoid has been evidenced to be coaxial with the finite strain ellipsoid in such a way that the maximum axis of susceptibility $K1$ is parallel to the structural lineation and the minimum axis of susceptibility $K3$ is nor-

* Corresponding author. E-mail: robion@u-cergy.fr

0040-1951/99/$ – see front matter
PII: S0040-1951(99)00142-0

mal to the structural foliation (for example Graham, 1954; Kligfield et al., 1981; Averbuch et al., 1992). However, because AMS measurements reflect a bulk contribution of all the minerals of a rock, its interpretation may not be straightforward (Borradaile, 1988; Rochette et al., 1992; Aubourg et al., 1995). Concentrations, size, intrinsic anisotropic properties and subfabrics of each constituent are parameters that can significantly influence orientation and intensity of the AMS ellipsoid (see for example Daly and Zinsser, 1973; Borradaile and Tarling, 1981; Housen and Van der Pluijm, 1991; Housen et al., 1993; Borradaile and Henry, 1997). In such cases, the identification of the sources of magnetic susceptibility and the separation of the different anisotropic contributions are thus essential for a better constraint of the deformation pattern.

This is particularly evident in domains that suffered a polyphase deformation history like the lower Palaeozoic siliciclastic rocks of the Ardennes massif (northern France and southern Belgium). A previous AMS study within 47 sites sampled throughout the slaty rocks of the Rocroi massif has shown that both the direction and magnitude of the magnetic fabric were controlled by increasing metamorphic grade as well as by the change of deformational style which occur within the massif (Robion et al., 1995, 1997). In order to better constrain the fabric development of the Palaeozoic rocks of the Rocroi massif, we carried out complementary studies including the determination of the anisotropy of the ferromagnetic fraction by measurement of the anisotropy of isothermal remanent magnetisation (AIRM) and the characterisation of the phyllosilicate preferred orientation. These analyses have been conducted within selected sites from the Cambrian core of the Rocroi massif in order to separate possible superimposed fabrics carried by the ferromagnetic grains (both oxides and sulphides) and by the paramagnetic constituents of the rock (for example phyllosilicates and other Fe-rich silicates). The petrofabric investigations have been completed by measurements of illite crystallinity in all the sites investigated for AMS. The latter data will be used as an independent indicator of the degree of metamorphism and will be compared to the magnetic fabric data.

This will finally enable a discussion on the relationships between the fabric acquisition and the metamorphic evolution and point out the consequences concerning the tectonic evolution of the Rocroi massif.

2. Geological setting

The Rocroi massif represents a wide culmination of lower–middle Palaeozoic rocks cropping out within the southern part of the Ardennes Variscan Fold-and-Thrust Belt (Fig. 1A). This major Variscan E–W striking anticline (Fig. 1B and Fig. 2) involves an anchi–epimetamorphic siliciclastic sedimentary sequence composed of Cambro–Ordovician slates and quartzites unconformably overlain by a thick Devonian cover. The latter includes at the base Pridolian conglomerates that grade upward into shales and a thick sandstone sequence.

Evolutions in the sedimentary facies from north to south of the massif as well as a drastic southward increase of the thickness of the Devonian series give evidence for an important Devonian crustal extensional event in the Ardennes area (Meilliez, 1989; Meilliez et al., 1991). The related emplacement of a regional thermal dome is suggested to produce an epizonal diastathermal metamorphism centred on the southern border of the massif (Beugnies, 1986; Potdevin and Goffette, 1991; Fielitz, 1995, 1997). Coeval magmatic activity is attested by the existence, in the central part of the massif, of microgranite and diabase dykes swarm of Middle Devonian age (Goffette et al., 1991).

The well-exposed unconformity situated at the base of the Lower Devonian rocks forms another significant structural feature of the massif. It seems now largely admitted, although interpreted by some authors as a major Variscan detachment zone (Le Gall, 1992), that the unconformity is mainly of sedimentary origin, unravelling a Caledonian orogenic process (Meilliez et al., 1994). Non-coaxial Caledonian and Variscan folds interact within the Cambro–Ordovician substratum inducing a complex structural pattern that remains highly debated (Hugon, 1982; Delvaux de Fenffe and Laduron, 1984, 1991; Belanger and Epard, 1997). An ubiquitous south-dipping slaty cleavage, that affects both the Cambro–Ordovician and Devonian rocks, argues however for a major Variscan overprint. The Variscan origin of

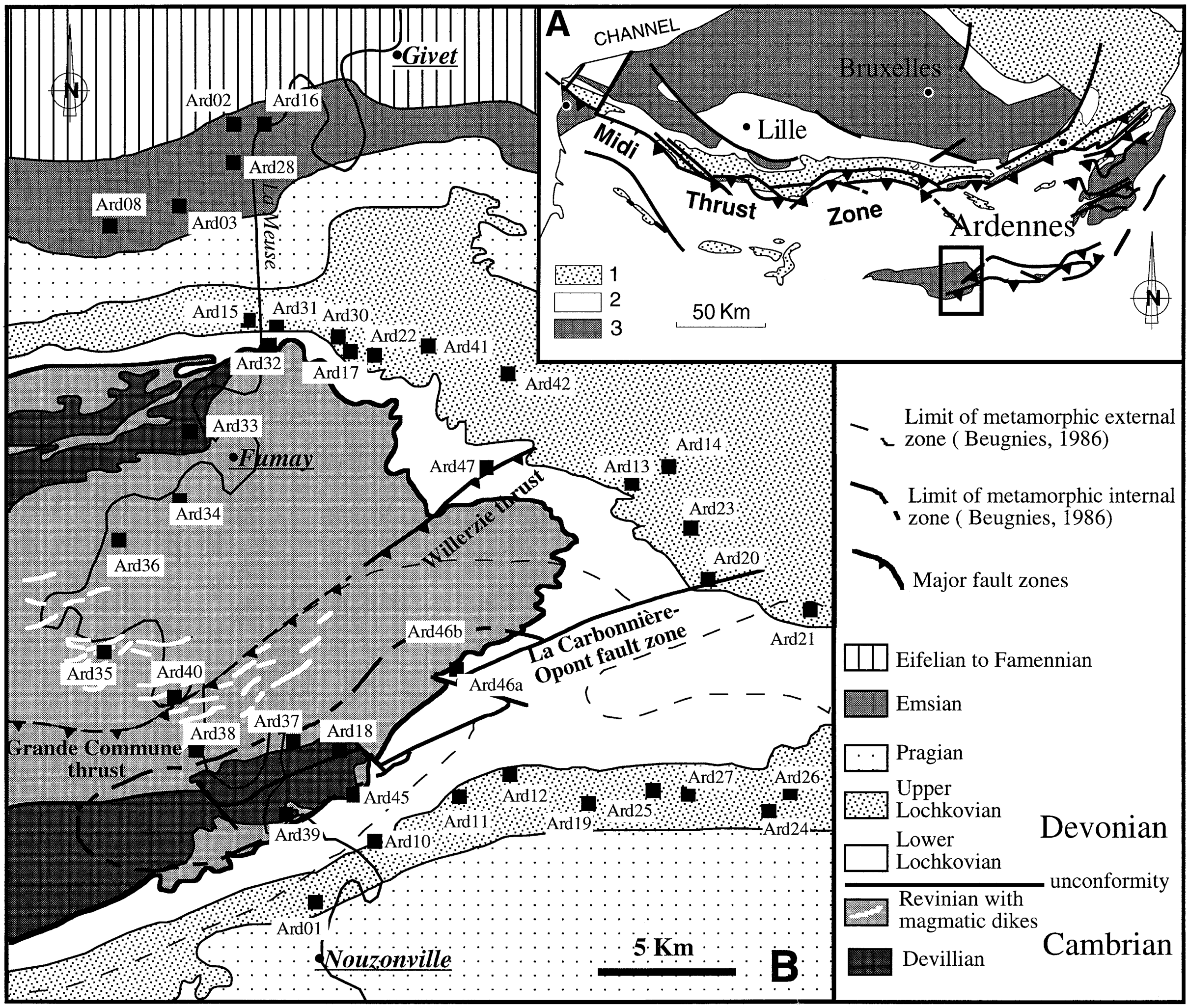

Fig. 1. (A) The general Variscan tectonic framework of northern France and southern Belgium (after Mansy and Averbuch, 1996). The rectangle locates the eastern Rocroi massif. *1* = Silesian coal basin; *2* = Devono-Carboniferous sedimentary rocks; *3* = lower Palaeozoic basement. (B) Geological sketch map of the Rocroi massif with location of studied sites (modified from Robion et al., 1995).

the penetrative deformation is attested by the age of phyllite flakes grown within the cleavage (between 339 and 300 Ma) (Piqué et al., 1984). Such syn-deformation metamorphic minerals are likely to develop in a general low-grade retromorphic context as suggested by studies conducted in some Middle Devonian dykes (Potdevin and Goffette, 1991). The Variscan event led to the general tectonic framework of the massif and is responsible for the Rocroi culmination associated with the northwards directed stack of thrust units above the major Midi thrust (see Fig. 2) (Raoult and Meilliez, 1987).

3. Previous rock magnetic results

The previous AMS studies gave evidence of an evolution in the fabric intensity and orientation from north to south of the massif in connection with the change of both magnetic mineralogy and style of deformation with increasing metamorphism (Robion et al., 1995). The magnetic fabric is essentially expressed in the southern epimetamorphic domain by tectonically induced magnetic foliations (planar fabric parallel to the cleavage) and N–S lineations parallel to the transport direction. In this zone, the

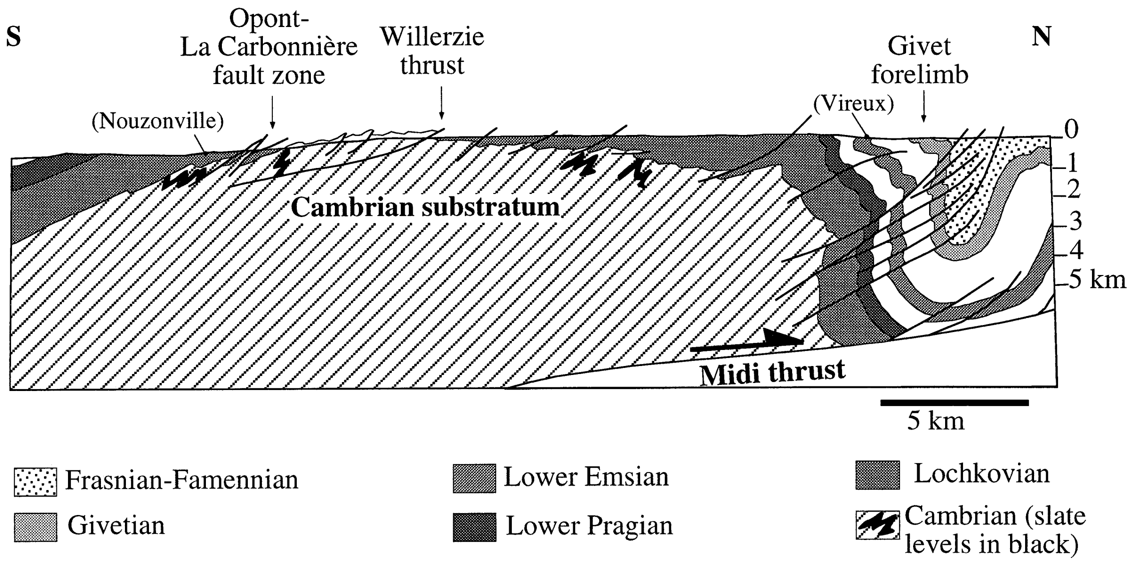

Fig. 2. Schematic cross-section of the studied area (after Raoult and Meilliez, 1987).

magnetic mineralogy study has shown the wide occurrence of a, to date unrecognised, mineralogical phase: pyrrhotite (Robion et al., 1997). This metamorphic mineral is well expressed in the Cambrian rocks of the massif as well as in the Lochkovian rocks of its southern border inferring a wider distribution of metamorphism than the one previously proposed by Beugnies (1986) on the basis of different iron-oxides occurrences. Relationships of pyrrhotite with the different metamorphic iron-oxide phases are however difficult to specify on the basis of these previous data. On the other hand, chlorite and other Fe-rich phyllosilicates are also probably in part responsible for the magnetic anisotropy but this paramagnetic contribution is so far not well constrained.

In the northern practically unmetamorphosed margin of the massif, the magnetic anisotropy is due in most cases to the hematite preferred crystallographic orientation of sedimentary-diagenetic origin (Robion et al., 1995). In this folded and thrust domain, the tectonic fabric is not strong enough to completely overprint the primary sedimentary fabric. The superimposition of two sub-fabrics gives rise to a more linear anisotropy with an intersection type lineation, perpendicular to the shortening direction. It is worth to note that the inferred shortening direction is oriented NW–SE, oblique with respect to the transport direction evidenced in the south of the massif. Both directions of shortening have also been shown by structural data in the region of Givet, some few kilometres north of the investigated zone (Lacquement et al., 1997). It remains unclear however whether the variation in the shortening direction results from a local reorientation due to an inherited geometry or from two non-coaxial increments of compressional deformation.

4. Methodology

The different studies that we have carried out within the Rocroi massif (Robion et al., 1995, 1997) included a set of 47 sites sampled throughout the Cambrian basement and in the Lochkovian and Emsian cover. At each site, a mean of 10 samples have been drilled and oriented in situ. Their location is reported in the sketch map of Fig. 1B.

4.1. Magnetic fabrics analysis

In order to extract the ferromagnetic s.l. fabric and compare it to AMS, the anisotropy of remanence was studied using isothermal remanent magnetisation (so-called AIRM). On the basis of the previous magnetic mineralogy studies (Robion et al., 1995, 1997), 36 specimens were selected in 6 sites from the Cambrian basement: 12 samples within pyrrhotite-rich sites (Ard35 and Ard36), 18 samples within the magnetite-rich sites (Ard18, Ard32 and Ard39) and 6 samples within a site (Ard38) exhibiting a mixed magnetic mineralogy (pyrrhotite and magnetite). The procedure that we used here to determine AIRM has been developed by Jelinek (1993) and stipulates that under the condition that magnetisation takes place in the Rayleigh region, anisotropic behaviour of isothermal remanent magnetisation can be represented by a second-order tensor.

Measurement of AIRM requires the application of successive magnetisations of the standard cylindrical specimen (22 mm height $\times$ 25 mm diameter) in six directions and subsequent measurement of its remanent magnetisation. Before each magnetisation in a new direction, the specimen is demagnetised using a tumbling a.f. demagnetiser with a maximum peak of 80 mT. In order to avoid imperfectly demagnetised remanences induced in a previous direction, the specimen is magnetised commutatively; the field changes between zero, $+B$, $-B$, $\ldots$, $+B$, and zero in the case of a positive orientation, while it changes between zero, $-B$, $+B$, $\ldots$, $-B$ and zero in the case of a negative magnetic field orientation. The intensity of the magnetising direct field is 15 mT. After each magnetisation, the remanent magnetisation was measured with a spinner magnetometer JR-5.

As demonstrated by Jelinek (1993), in the range of magnetising direct field lower than 20 mT, the anisotropy of the remanent magnetisation refers to the eigenvectors and eigenvalues of the remanence tensor $[R]$ characterised by three principal axes $R1 > R2 > R3$. It should be noted that such representation of AIRM is similar to the representation of AMS tensor $[K]$ with its three principal axes $K1 > K2 > K3$. Principal magnitude and direction of $[R]$ has been calculated using the eigenvalue decomposition on an average susceptibility tensor (Jelinek, 1978). To define the magnitude and shape of the ellipsoid, we used four parameters (see Hrouda (1982) for an exhaustive description of these parameters). The intensity of the AIRM fabric may be characterised by the degree of anisotropy P $(R1/R3)$. The changes of the shape of the ellipsoid are visualised by the T parameter. When $-1 < 0$, the AIRM ellipsoid is mostly prolate and when $0 < 1$, the ellipsoid is mostly oblate. Thus, the horizontal line passing through 0 separates the field of flattening from that of constriction (Hrouda, 1982). In a similar manner, the foliation parameter F $(R2/R3)$ indicates the degree of oblateness and the lineation parameter L $(R1/R2)$ the degree of prolateness of the AIRM ellipsoid.

4.2. Phyllosilicate preferred orientation

The preferred orientation of mica (001) (d = 10 Å) and chlorite (002) (d = 7 Å) has been measured on an X-ray pole figure goniometer, using Fe-filtered CoKα-radiation (40 kV $\times$ 30 mA). Measurements were performed in transmission geometry. Complete, normalised, pole figures were obtained by combining incomplete pole figure measurements on three, mutually perpendicular, sections of the cylindrical specimen. Phyllosilicate preferred orientations are evidenced using contoured orientation distributions (lower-hemisphere equal-area projections). Contours represent 'multiples of a random distribution' (m.r.d.). The interpretation of the pole figures is, on the one hand, based on the pole figure pattern (cf. Sintubin, 1994), taking into account the symmetry of the orientation distribution and its angular relationship with the distinct fabric elements (bedding, cleavage, . . .), and, on the other hand, on the degree of preferred orientation.

4.3. Illite crystallinity

The illite crystallinity parameter corresponds to the half peak width of the 10 Å Illite X-ray diffraction peak (Kübler, 1967). Although some problems still remain in its interpretation (see e.g. Nieto and Sanchez-Navas, 1994; Barrenechea et al., 1995), this parameter has been widely shown to be a marker of the variations of metamorphic conditions within the anchi–epimetamorphic domains matching the progressive transformation of illite into muscovite (Kübler, 1967; Frey, 1987; Warr et al., 1991; Merriman, 1991).

The illite crystallinity (IC) has been measured for each of the sites sampled for the magnetic fabric analysis allowing a relatively precise spatial distribution of this parameter within the Rocroi massif. It has been measured on ethylene-glycol treated clay preparations in the Laboratory of Sedimen-

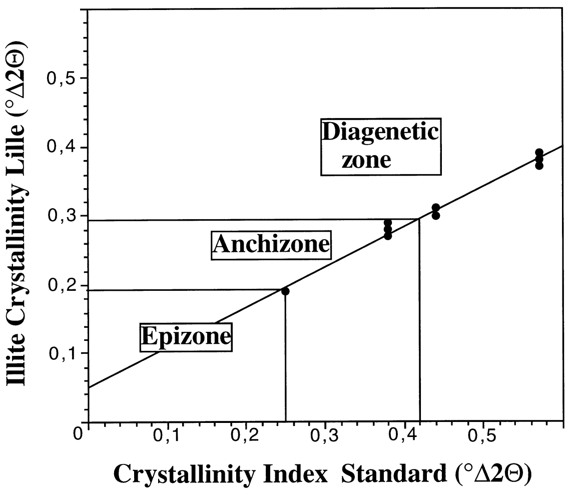

Fig. 3. Calibration of the Lille illite crystallinity data with respect to the international calibrated index CIS (Warr and Rice, 1994); limits for diagenetic, anchi- and epizones are taken from Kübler (1967).

tology and Geodynamics of the University of Lille using a Philips PW1730 DX diffractometer. The precise methodology used for the measurements can be found in Holtzhapffel (1985). As the measurement processing and the sample preparation have been shown to strongly influence the results (Kisch, 1991; Krumm and Buggisch, 1991), some standard specimens have been measured at the same time allowing the calibration of the presented illite crystallinity data with respect to an international calibrated index of illite crystallinity (CIS of Warr and Rice, 1994) (Fig. 3).

5. Results and discussion

5.1. Magnetic fabric studies

5.1.1. The bulk remanence vs the bulk susceptibility

When studying magnetic anisotropy, one has to consider a variable mineralogical composition of the rocks (see general discussion in Rochette et al., 1992; Borradaile and Henry, 1997). The AMS tensor represents the summation over the tensor of each constituent of the rocks:

$$[K]_0 = [K]_d + \alpha[K]_p + \beta[R]$$

$[K]_0$ is the tensor of the anisotropy of the low field magnetic susceptibility (AMS tensor), $[K]_d$ is the diamagnetic contribution and is generally negligible and $[K]_p$ is the paramagnetic contribution with the fraction α. Diamagnetic and paramagnetic contribution are usually termed as the matrix contribution. $[R]$ is the ferromagnetic s.l. contribution with the fraction β. The whole anisotropy (i.e. the magnetic fabric) of a rock is thus controlled by the relative abundance of each constituent, their intrinsic susceptibility and anisotropy and the way by which they are submitted to a deformation. Because intrinsic susceptibility of ferromagnetic phases are between 10 and 10^5 times higher than intrinsic susceptibility of the paramagnetic one, a small change of the concentration of the former could significantly affect the values of $[K]_0$. It is thus fundamental to know the main constituents of the sample to interpret correctly its magnetic fabric. In our previous AMS study (Robion et al., 1995), we have shown a correlation between bulk susceptibility K_m $(K1+K2+K3/3)$ and the anisotropy degree P indicating the dependence of AMS on rock composition. In order to further constrain this magnetic mineralogical influence, the bulk remanence R_m $(R1 + R2 + R3/3)$, which takes into account only the ferromagnetic contribution, has been compared to the bulk magnetic susceptibility K_m which is influenced by the whole magnetic constituents of the rock, i.e. matrix contribution and ferromagnetic contribution.

The observation of R_m vs K_m plot enables the separation of two domains (Fig. 4A): the first one associated with dominant magnetite-bearing rocks in the lower part of the plot and the second one associated with pyrrhotite-bearing rocks in the upper part. This is particularly well exemplified in site Ard38 where both pyrrhotite-rich samples and magnetite-rich samples were identified (Robion et al., 1997). The former domain corresponds to $K_m > 5 \times 10^{-4}$ SI and $R_m > 1 \times 10^{-4}$ A m^{-1} and the second one corresponds to $K_m < 5 \times 10^{-4}$ SI and $R_m < 1 \times 10^{-4}$ A m^{-1}. When pyrrhotite is the dominant ferromagnetic phase (sites Ard35 and Ard36 with values of K_m above 5×10^{-4} SI and R_m above 2×10^{-4} A m^{-1}), a positive correlation is observed between R_m and K_m (Fig. 4A). This trend indicates that the magnetic susceptibility in this domain is totally controlled by the ferromagnetic concentration in the rocks. Below this limit, the decrease of R_m is steeper than K_m and

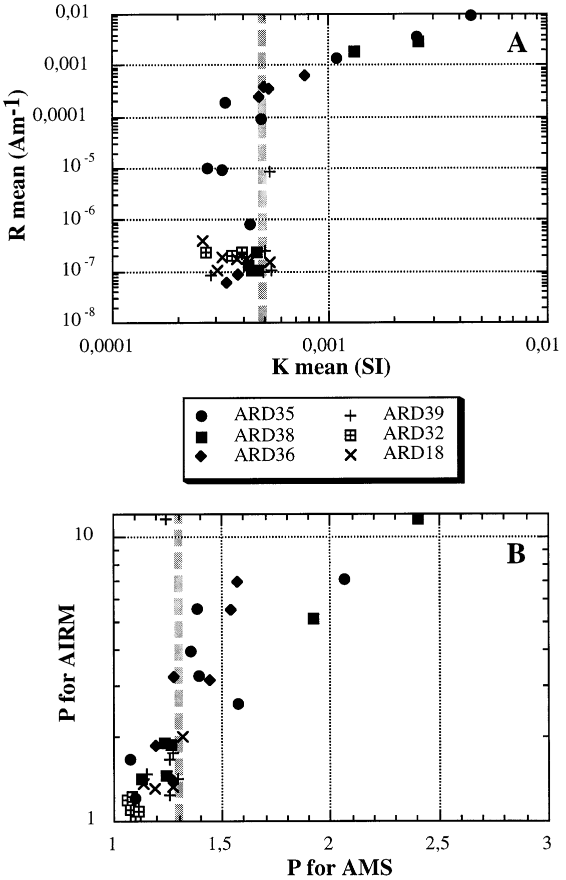

Fig. 4. Correlation of magnetic anisotropy parameters for AMS and AIRM. (A) Bulk remanence R_m versus bulk susceptibility K_m. (B) AIRM anisotropy degree P ($P_{AIRM} = R1/R3$) versus AMS anisotropy degree P ($P_{AMS} = K1/K3$). The dashed lines represent the limits above which ferromagnetic carriers are supposed to be dominant in the AMS signal ($K = 500$ μSI and $P = 1.3$, after Rochette et al., 1992).

the trend of the data joins progressively the magnetite domain. Because we did not put in evidence the presence of magnetite in sites Ard35 and Ard36, we interpret this result as an effect of decreasing of the pyrrhotite amount.

For the magnetite-rich sites (Ard18, Ard32, Ard39), a relatively poor correlation appears between K_m and R_m. Most of the samples show a bulk susceptibility K_m lower than 6×10^{-4} SI and a bulk remanence R_m lower than 1×10^{-5} A m^{-1}. In this domain, increasing of K_m is not accompanied by an increase of R_m. As suggested by Rochette et al. (1992), the common K_m value of 5×10^{-4} SI indicates, within low-grade metamorphic rocks, the upper limit of the paramagnetic contribution in the whole magnetic signal. In the case of the Ardennes rocks, the absence of a clear positive correlation in the magnetite-bearing rock domain suggests that the evolution of K_m mainly reflects the change of the matrix contribution in the sample. The investigation of R_m vs K_m gives thus the evidence for a mineralogical control of the magnetic signal: in pyrrhotite-bearing rocks, high values of R_m indicate that AMS is mainly controlled by ferromagnetic fraction; in magnetite-bearing rocks low values of R_m and absence of positive correlation between R_m and K_m argues for a matrix control of the AMS tensor.

5.1.2. The anisotropy degree P

The same mineralogical control is recorded in the change of the magnitude of the anisotropy (P) of both AIRM and AMS ellipsoids (Fig. 4B). Within the magnetite-rich sites (Ard32, Ard39, Ard18), P values for AIRM are lower than 2 (except for one sample reaching $P = 12$ in site Ard39) and P for AMS is lower than 1.3. For pyrrhotite-bearing rocks (Ard36, Ard35) P_{AIRM} higher than 2 are current values (up to $P = 12$) and P_{AMS} is higher than 1.3. Within site Ard38 (where pyrrhotite and magnetite were identified), pyrrhotite-rich samples exhibit P_{AIRM} values higher than 5 and magnetite-rich samples show P_{AIRM} values lower than 2. The samples shown on the basis of R_m/K_m to display a dominant paramagnetic anisotropy (values of $R_m < 5 \times 10^{-4}$ A m^{-1} and $K_m < 500$ μSI) cluster in a domain characterised by $P_{AIRM} < 3$ and $P_{AMS} < 1.35$. Above these limits, the anisotropy of the ferromagnetic pyrrhotite governs the whole anisotropy. These results thus show a clear mineralogical control of P, which makes its use difficult for a semi-quantitative strain analysis.

5.1.3. The shape parameter T

The main part of the AIRM and AMS ellipsoids are in the field of the oblate shape ($T > 0$) reflecting the dominant cleavage-parallel fabric of the samples. The mean of T parameters is globally more oblate for AMS than for AIRM (Fig. 5) reflecting the relative more planar intrinsic anisotropy of the phyllosilicate fraction. For magnetite-bearing rocks, the increase of metamorphic grade induces a very

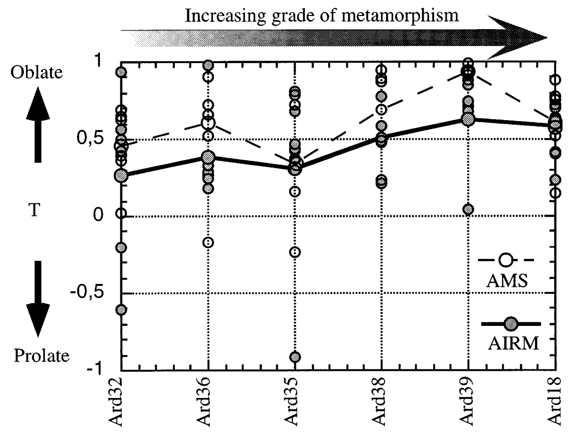

Fig. 5. Evolution of shape parameter T for AMS and AIRM fabrics with respect to the structural position of the site. The lines join the mean T parameter calculated for the whole samples of each site. T parameter is calculated by using the Jelinek expression: $T = [2\ln(K2/K3)/\ln(K1/K3)] - 1$ (Hrouda, 1982).

clear increase of the oblateness of the fabrics. For example, the T parameter measured for AMS within magnetite-bearing rocks from the internal zone of metamorphism (Ard38, Ard39) are close to perfectly oblate shape. Such a pattern is likely to reflect the high degree of alignment of the phyllosilicate matrix, which controls the AMS in these sites. The T parameters measured for AIRM are, however, also very high within these sites. The oblate shape of the AIRM ellipsoid of these magnetite-rich sites reflects the important planar distribution of the magnetite grains. As the intrinsic shape anisotropy of the magnetite has generally a relatively prolate component, this pattern also indicates a very low degree of alignment of the long axes of the magnetite grains within the cleavage. By contrast, pyrrhotite-bearing rocks display a much more linear fabric both for AMS and AIRM. Such an unexpected linear component of pyrrhotite has already been mentioned by Rochette (1988) and Borradaile and Sarvas (1990) in pyrrhotite-bearing shales. The elongated form of some pyrrhotite aggregates parallel to a syn-metamorphic stretching direction or the disposition of pyrrhotite along the zone axis of an L-fabric (Borradaile and Henry, 1997) may explain this linear anisotropy.

These results thus underline the contrasting behaviours of metamorphic pyrrhotite and magnetite grains during the development of the fabric. Such a difference is likely to be related to different mechanisms of preferred orientation (oriented growth versus passive rotation) and thus to questions about the relative age of the two minerals.

5.1.4. Orientation of the principal axes of AMS and AIRM

In Figs. 6 and 7, the stereographic distribution of both AIRM and AMS principal axes within the Cambrian pyrrhotite- and magnetite-rich sites of the Rocroi massif are shown. The mean directions are calculated by the statistics of Jelinek (1978) which takes into account the degree of anisotropy of each sample.

In all the studied sites, the mean direction of the minimum axis of remanence $R3$ is close to that of magnetic susceptibility $K3$ and corresponds to the cleavage pole. By contrast, the directions of the maximum axes of remanence $R1$ are not directly linked to those of magnetic susceptibility $K1$. They are distributed in the cleavage plane depending on the nature of the main ferromagnetic phase.

Within site Ard38, which displays both magnetite- and pyrrhotite-rich samples, two clusters of $R1$ are observed (Fig. 6): two samples exhibit N–S AIRM maximum axes parallel to AMS axes; the other four directions of maximum remanence are oriented NE–SW clearly oblique to the AMS axes (marked by a star). The two first samples, close to the N–S orientation, correspond to a bulk magnetisation R_m higher than 2×10^{-4} A m^{-1} and were defined in the previous section as the pyrrhotite-rich samples. The other samples, with R_m lower than 2×10^{-4} A m^{-1}, correspond to magnetite-rich samples.

Within pyrrhotite-rich sites (sites Ard35 and Ard36), the most part of the samples show N–S AIRM maximum axes directions in good agreement with those of Ard38 pyrrhotite-rich samples (Fig. 6). As in site Ard38, the control of the $R1$ axes orientation by the intensity of R_m is observed within site Ard36 for which the lowest values of R_m exhibit maximum axes rotating from the N–S to the NW–SE direction. This mineralogical control induces a relative scattering of the maximum axis, variable from one site to the other. However, the mean direction is always oriented N–S within the cleavage plane and is parallel to the AMS $K1$ mean orientation.

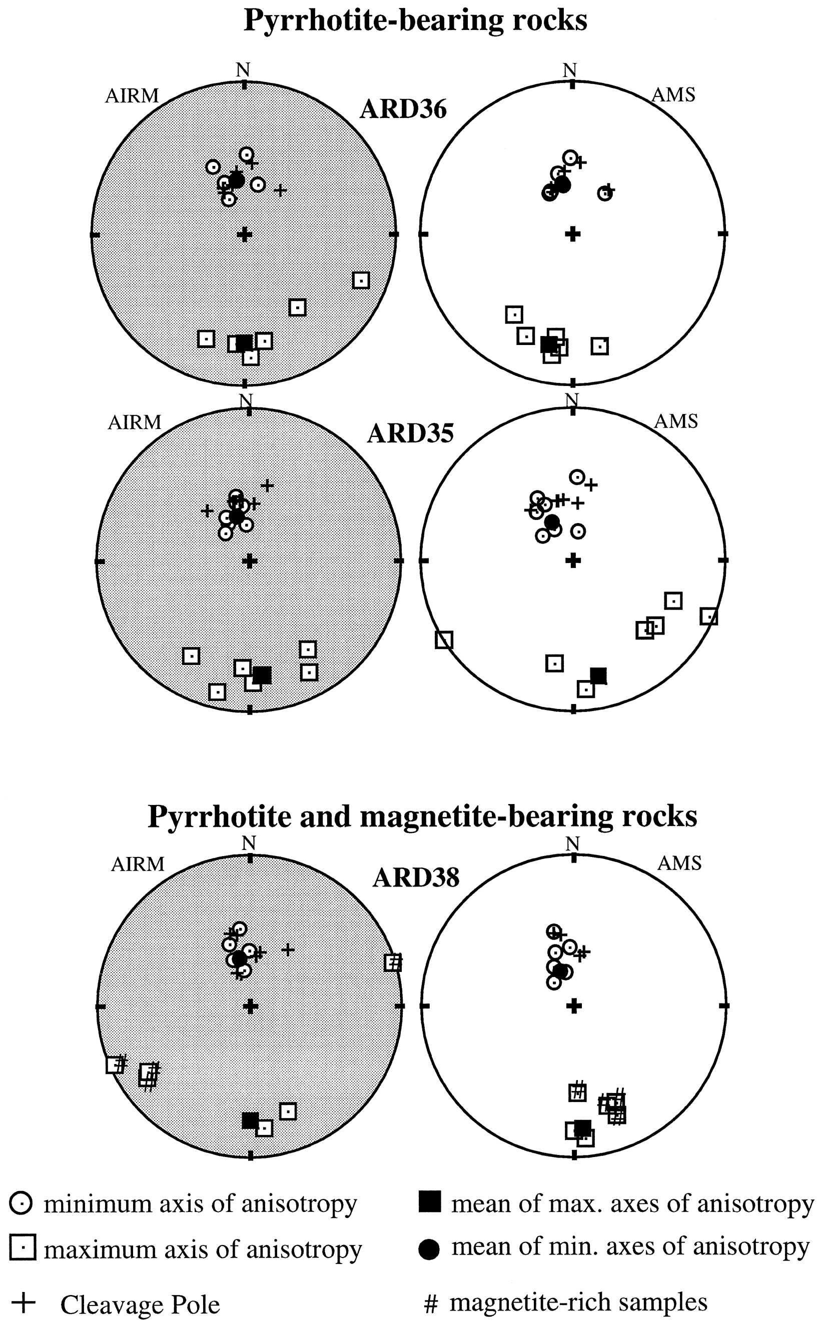

Fig. 6. Equal-area lower-hemisphere stereoplot showing the distribution of AIRM (left dashed stereoplots) and AMS (right stereoplots) principal axes for Cambrian pyrrhotite-bearing rocks of the Rocroi massif. In Ard38 stereoplots, magnetite-rich samples are represented by a star.

Thus, pyrrhotite exhibits both a well-defined planar distribution within the cleavage plane and a linear anisotropy parallel to the thrusting-induced stretching direction. This well developed fabric may result from the oriented growth of pyrrhotite aggregates during Variscan deformation.

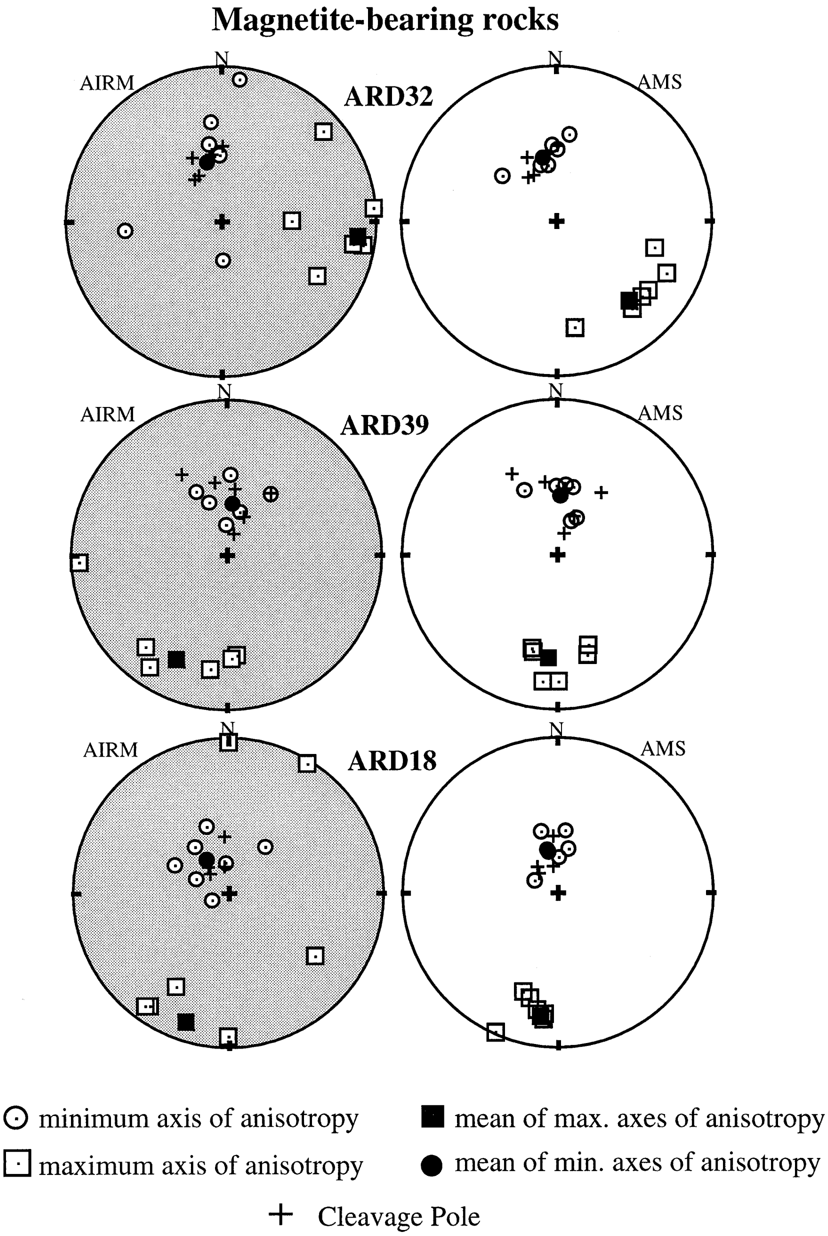

Fig. 7. Equal-area lower-hemisphere stereoplot showing the distribution of AIRM (left dashed stereoplots) and AMS (right stereoplots) principal axes for Cambrian magnetite-bearing rocks of the Rocroi massif.

In the magnetite-rich sites Ard18 and Ard39 in the southern part of the Rocroi massif, AIRM fabric shows maximum axes distributed between the NE–SW and N–S directions (Fig. 7). It is worth noting that the former direction corresponds to the AIRM direction seen in the magnetite-rich samples of site Ard38 (Fig. 6) and the second direction is close to the AMS lineation in these sites. Thus, the mean $R1$ direction results from a composite feature and deviates from the mean AMS maximum axis. For the magnetite-rich site Ard32, located in the northern part of the Rocroi massif, the AIRM lineation

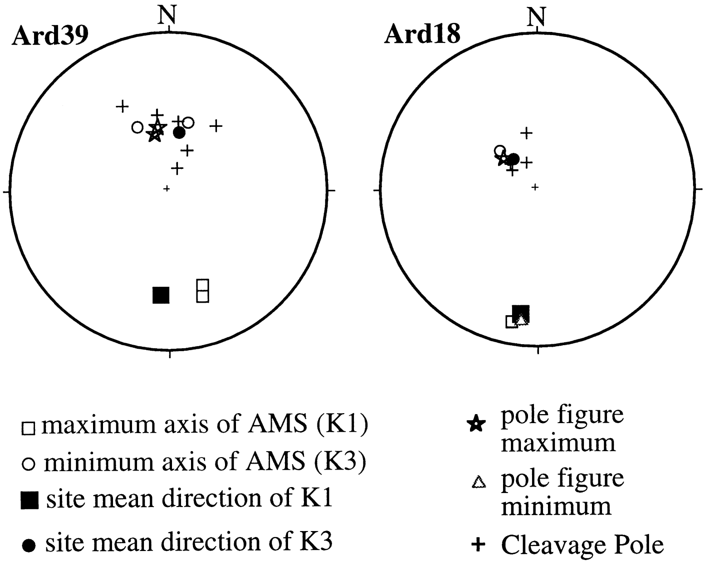

Fig. 8. Equal-area lower-hemisphere stereoplot of pole figure maximum and minimum of the measured phyllosilicate preferred orientation of some magnetite-bearing samples from sites Ard39 and Ard18. For site Ard39 the phyllosilicate texture shows an axially symmetrical orientation distribution. The results are presented with the corresponding maximum and minimum axes of the AMS ellipsoid and the cleavage poles measured in the field. Samples used to determine phyllosilicate texture are not treated with AIRM method and thus do not appear in Fig. 7.

is nearly E–W and oblique to the NW–SE AMS lineation.

In contrast to pyrrhotite, these data show that the magnetite grains do not display a strong preferred alignment within the cleavage plane. Only part of the magnetite seems to be oriented parallel to the N–S general stretching direction. This pattern suggests that the magnetite orientation results from an incomplete reorganisation of an inherited fabric. The mechanism for such a reorganisation would be the passive rotation of the magnetite porphyroblasts during Variscan deformation. This interpretation is furthermore supported by the thin section observation of clearly defined rotational structures around the magnetite porphyroblasts (for example Zwart and Oele, 1966; Hugon, 1982; Piqué et al., 1984).

5.2. Preferred orientation and crystallinity of the phyllosilicate fraction

5.2.1. The phyllosilicate preferred orientation

The phyllosilicates preferred orientation (PPO) has been determined on three selected samples from magnetite-bearing Cambrian slates of the southern part of the Rocroi massif (two from site Ard39 and one from site Ard18). The PPO pole figure maxima and minima are presented in the stereographic plot of Fig. 8. They are plotted along with the AMS principal axes of the same samples and the poles of macroscopic cleavage measured in the field.

For the two samples from site Ard39, the phyllosilicate preferred orientation shows an axially symmetrical orientation distribution about the cleavage pole with a high degree of preferred orientation. The pole figure maximum is close to the $K3$ ASM axes and parallel to the cleavage pole. These results perfectly agree with the high degree of oblateness of the magnetic fabric at this site (see Fig. 5).

The phyllosilicate fabric for site Ard18 shows an orientation distribution related to the cleavage pole. The pole figure maximum is parallel to $K3$ (and the cleavage pole) and the pole figure minimum of the orthorhombic orientation distribution is close to $K1$. The orthorhombic symmetry indicates that the phyllosilicate fabrics developed under apparent flattening deformation regime with N–S stretching in the cleavage plane. The inferred lineation accounts for the well defined AMS N–S lineation evidenced at this site, where the paramagnetic fraction has been shown to control the AMS signal. The phyllosilicate

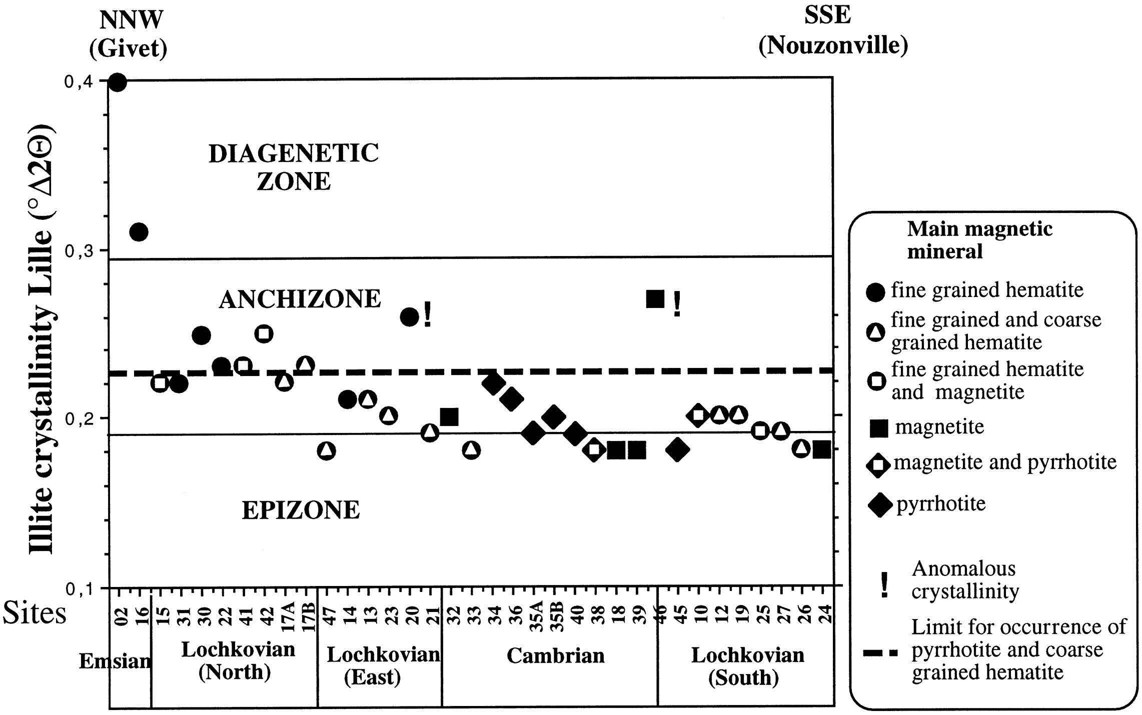

Fig. 9. Evolution of the measured illite crystallinity data as a function of the structural position of the sampling site (see Figs. 1 and 10 for location). The main magnetic mineralogy observed at each site is also reported (data from Robion et al., 1997).

lineation is furthermore consistent with the AIRM lineations carried by pyrrhotite at sites Ard38, Ard35 and Ard36.

A general accordance is thus observed between both the shapes and directions of the magnetic and the phyllosilicate fabrics. It is worth to note that the variation of the phyllosilicate preferred orientation between sites Ard39 and Ard18 and the parallel evolution of the magnetic fabrics (decreasing T shape parameter and better defined lineation) are significant indicators of a change in the deformation regime, from pure flattening at site Ard39 to apparent flattening with N–S stretching in the cleavage plane at site Ard18.

5.2.2. Illite crystallinity data and their relationships with the magnetic fabric development

The composition of the clay fraction as recognised by X-ray diffraction diagrams remains relatively constant over the whole study area and includes almost exclusively illite and chlorite. The relative amount of illite and chlorite is however variable depending on the nature and structural position of the rock. Paragonite and pyrophyllite that can potentially induce an enlargement of the 10 Å peak width (Barrenechea et al., 1995) have not been observed in significant quantity in the studied sites.

As already discussed by Dandois (1981), a general increase in the degree of crystallinity of illite has been observed from the northern part of the massif (within the diagenetic to anchizonal facies) towards its southern border (within the epizonal domain) (Fig. 9). The spatial distribution of illite crystallinity fits relatively well the zoning established on the basis of magnetite and hematite occurrences (Fig. 10) except within the SE part of the massif where the zone of maximum metamorphism has to be slightly extended. However, within the southern epimetamorphic domain, two data of anomalously low crystallinity can be recognised (Ard20 and Ard46a). It is worth to note that both sites are the only ones to exhibit a clay mineralogy composed exclusively of illite. Both are situated along the 'La Carbonnière-Opont' fault zone (Fig. 1) which is a major compos-

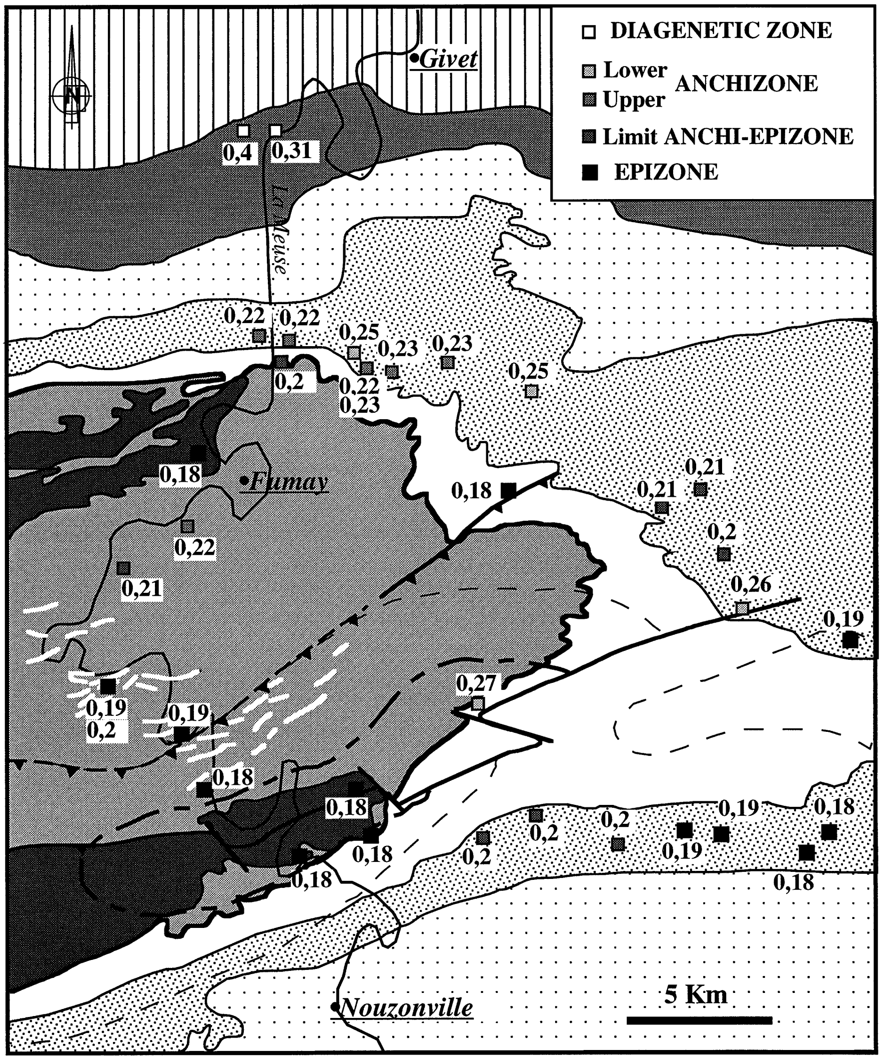

Fig. 10. Sketch map of the Rocroi massif (same legend as in Fig. 1B) showing the spatial distribution of the illite crystallinity. The limits for the metamorphic zonation of the samples are obtained by calibration with the international index CIS (Warr and Rice, 1994; see text and Fig. 3). Dashed lines correspond to metamorphic zonation after Beugnies (1986).

ite structural feature of late Variscan age (Beugnies, 1983; Fielitz, 1997). These anomalous data thus are likely to be the result of the late crystallisation of illite during the activation of this fault zone in a general retrograde metamorphic context.

Although the metamorphic occurrence of the magnetic minerals depends on the initial sedimentary facies (Robion et al., 1997), a clear IC upper limit for appearance of pyrrhotite and coarse-grained hematite may be defined (Fig. 9). This limit is about the same for both minerals and is situated within the lower part of the anchizone (IC values on the order of 0.22 in the Lille IC scale). Pyrrhotite and coarse-grained hematite thus seem to occur within the same spectrum of P–T conditions but in different p_{O_2} conditions.

This interpretation is also supported by the comparison of the magnetic fabric parameters with the illite crystallinity. The AMS parameters — the foliation parameter $F = K2/K3$ (Fig. 11) and the

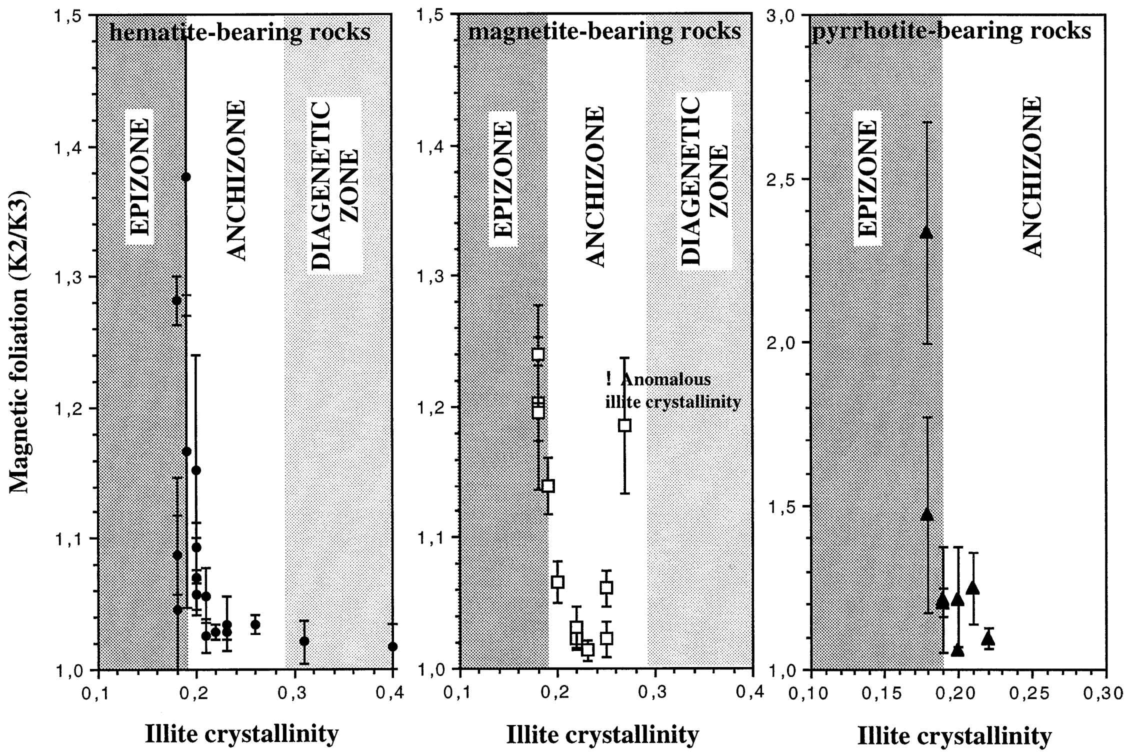

Fig. 11. Diagrams showing the evolution of the AMS mean foliation parameter ($F = K2/K3$) versus the illite crystallinity for pyrrhotite, hematite and magnetite-rich sites. Bars represent standard deviations associated to the determination of the AMS mean parameter.

lineation parameter $L = K1/K2$ (Fig. 12) — exhibit a global correlation with the illite crystallinity within the same site. The degree of correlation is however variable depending on the anisotropy parameter (lineation or foliation) and the nature of the magnetic carrier.

For pyrrhotite-bearing rocks and to a lesser extent hematite-bearing rocks, for which the magnetic susceptibility is shown to be controlled by the ferromagnetic phase (this study and Robion et al., 1995, 1997), a very clear correlation is established between both foliation and lineation parameters and IC. This correlation confirms the coeval development of pyrrhotite and coarse-grained hematite during the same Variscan tectonometamorphic event that crystallised the phyllosilicates.

For magnetite-bearing rocks, in which paramagnetic phases control AMS, the foliation parameter correlates significantly with IC in contrast to the lineation parameter. This is consistent with a low linear intrinsic anisotropy of the paramagnetic phyllosilicate fraction. Furthermore, as shown by the AIRM results, this lack of correlation exemplified the low degree of linear anisotropy of the magnetite grains. Although preferentially oriented within the cleavage plane, the latter do not exhibit a higher preferential alignment as the metamorphic grade increases suggesting that metamorphic magnetite may pre-date the major Variscan deformational event.

6. Conclusions

Both the ferromagnetic fabric and the phyllosilicate preferred orientation isolated subfabric contribution to the whole rock AMS fabric. In the pyrrhotite-bearing rocks, AMS and AIRM lineations are subparallel due to the high concentration and anisotropy of the ferromagnetic phase. Within the magnetite-bearing rocks of the southern part of the Cambrian massif, AIRM directions are clearly oblique to the N–S AMS lineations. As suggested by the phyl-

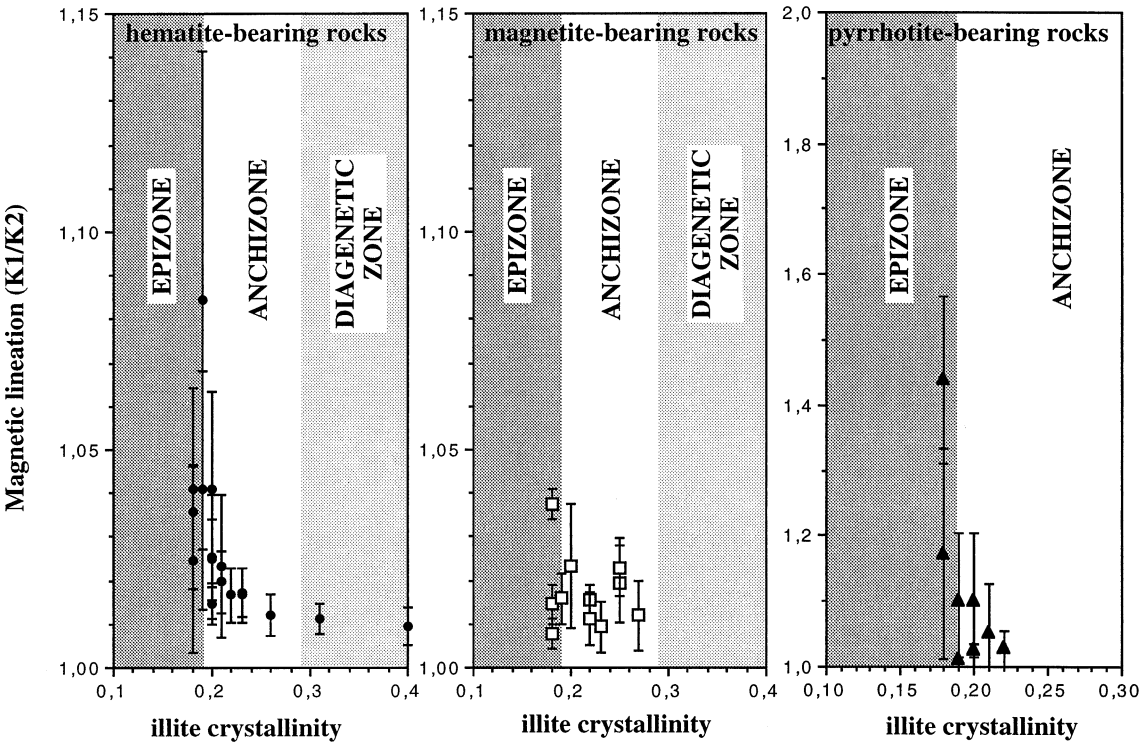

Fig. 12. Diagrams showing the evolution of the AMS mean lineation parameter ($L = K1/K2$) versus the illite crystallinity for pyrrhotite, hematite and magnetite-rich sites. Bars represent standard deviations associated to the determination of the AMS means parameter.

losilicate preferred orientation and the low values of the bulk AIRM, the AMS fabric is controlled by the preferred orientation of the phyllosilicate matrix minerals. Elsewhere, this N–S lineation is consistent with that of the pyrrhotite-rich samples, suggesting that pyrrhotite grew coeval with the phyllosilicates. The great variation of the ferromagnetic maximum direction carried by magnetite as well as the relatively oblate character of the AIRM ellipsoids argue for a feeble fabric due to the existence of a pre-Variscan subfabric in the Cambrian rocks.

In agreement with recent studies conducted in Devonian magmatic dykes (Potdevin and Goffette, 1991), the present data favour polyphase tectonometamorphic evolution for the Rocroi massif. Metamorphic magnetite is likely to have occurred during a prior event of diastathermal origin related to a Devonian lithospheric extension (Fielitz, 1995, 1997). The oriented growth within the cleavage of pyrrhotite, coarse-grained hematite and phyllosilicates (chlorites, illites) argues for a second retrograde metamorphic event associated with the Variscan Upper Carboniferous thrusting deformation. The crystallisation of pyrrhotite in non-coaxial deformation circumstances, resulting from a N–S thrusting-induced shear, may explain the magnetic lineations observed both by AMS and AIRM (Werner and Borradaile, 1996). This succession of events implies for magnetite-bearing rocks a composite fabric reflecting the superimposition of the Variscan compressional anisotropy (N–S lineation and cleavage-parallel foliation) on an inherited, weak preferred orientation. In this respect, the existence of NE–SW trending intersection-type AIRM lineations within some magnetite-rich rocks suggests that the variation of thrust transport direction from north to south of the massif might result from two successive compressional events, the N–S direction of thrust transport due to a late reactivation of the southern flank of the Rocroi massif.

Acknowledgements

The authors wish to thank D. Frizon de Lamotte and C. Kissel for their constant support, the colleagues from Lille and Cergy-Pontoise for discussions about the different aspects of this study and P. Recourt and D. Malengros (University of Lille) for the X-ray diffractometry measurements. G. Borradaile and W. Fielitz are gratefully acknowledged for constructive reviews that helped to improve the first draft of this paper. M. Sintubin is Postdoctoral Fellow of the F.W.O.-Vlaanderen (Belgium).

References

Aubourg, C., Rochette, P., Bergmüller, F., 1995. Composite magnetic fabric in weakly deformed black shales. Phys. Earth Planet. Inter. 87, 267–278.

Averbuch, O., Frizon de Lamotte, D., Kissel, C., 1992. Magnetic fabric as a structural indicator of the deformation path within a fold-thrust structure: a test case from the Corbières (NE Pyrenees, France). J. Struct. Geol. 14, 461–474.

Barrenechea, J.F., Rodas, M., Mas, J.R., 1995. Clay mineral variations associated with diagenesis and low-grade metamorphism of Early Cretaceous sediments in the Cameros basin, Spain. Clay Miner. 30, 119–133.

Belanger, I., Epard, J.-L., 1997. Modelling of the southern border of the Rocroi massif (Belgian–French Ardenne). Aardkd. Mededel. 8, 7–10.

Beugnies, A., 1983. Structure de l'aire anticlinale de l'Ardenne à l'ouest du méridien de Libramont. Ann. Soc. Geol. Nord 102, 165–173.

Beugnies, A., 1986. Le métamorphisme de l'aire anticlinale de l'Ardenne. Hercynica 2, 17–33.

Borradaile, G.J., 1988. Magnetic susceptibility, petrofabric and strain: a review. Tectonophysics 156, 1–20.

Borradaile, G.J., Henry, B., 1997. Tectonic applications of magnetic susceptibility and its anisotropy. Earth Sci. Rev. 42, 49–93.

Borradaile, G.J., Sarvas, P., 1990. Magnetic susceptibility fabric in slates: structural mineralogical and lithological influence. Tectonophysics 172, 215–222.

Borradaile, G.J., Tarling, D.H., 1981. The influence of deformation mechanisms on magnetic fabric in weakly deformed rocks. Tectonophysics 77, 151–168.

Daly, L., Zinsser, H., 1973. Etude comparative des anisotropies de susceptibilité et d'aimantation rémanente isotherme. Conséquences pour l'analyse structurale et le paléomagnétisme. Ann. Géophys. 29, 189–200.

Dandois, P., 1981. Diagénèse et métamorphisme des domaines calédonien et hercynien de la vallée de la Meuse entre Charleville–Mézières et Namur. Bull. Soc. Belge Géol. 90, 229–316.

Delvaux de Fenffe, D., Laduron, D., 1984. Analyse structurale au bord sud du Massif de Rocroi (Ardennes françaises). Bull. Soc. Belge Géol. 93 (1–2), 11–26.

Delvaux de Fenffe, D., Laduron, D., 1991. Caledonian and Variscan structures in the Rocroi–Ardenne Lower Paleozoic basement. Ann. Soc. Belge Géol. 114, 141–162.

Fielitz, W., 1995. Epizonal to lower mesozonal diastathermal metamorphism in the Ardennes (Rhenohercynian belt of western central Europe). Terra Nostra 95 (8), 95.

Fielitz, W., 1997. Inversion tectonics and diastathermal metamorphism in the Serpont Massif area of Variscan Ardenne (Belgium). Aardkd. Mededel. 8, 79–82.

Frey, M., 1987. Very low-grade metamorphism of clastic sedimentary rocks. In: Frey, M. (Ed.), Low Temperature Metamorphism. Blackie, Glasgow, pp. 9–58.

Goffette, O., Liégeois, J.P., André, L., 1991. Age U–Pb sur zircon dévonien moyen supérieur du magmatisme bimodal du Massif de Rocroi (Ardenne, France): implications géodynamiques. C. R. Acad. Sci. Paris 2, 1155–1161.

Graham, J.W., 1954. Magnetic susceptibility anisotropy: an unexploited element of petrofabric. Bull. Geol. Soc. Am. 65, 1257–1258.

Holtzhapffel, T., 1985. Les minéraux argileux. Publ. Soc. Géol. Nord 12, 136 pp.

Housen, B.A., Van der Pluijm, B.A., 1991. Slaty cleavage development and magnetic anisotropy fabrics. J. Geophys. Res. 96, 9937–9946.

Housen, B.A., Richter, C., Van der Pluijm, B.A., 1993. Composite magnetic anisotropy fabrics: experiments, numerical models and implications for the quantification of rock fabrics. Tectonophysics 220, 1–12.

Hrouda, F., 1982. Magnetic anisotropy of rocks and its application in geology and geophysics. Geophys. Surv. 5, 37–82.

Hugon, H., 1982. Structures et déformations du massif de Rocroi (Ardennes). Approche géométrique, quantitative et expérimentale. Thèse, Université de Rennes.

Jelinek, V., 1978. Statistical processing of anisotropy of magnetic susceptibility measured on group of specimen. Stud. Geophys. Geod. 22, 50–62.

Jelinek, V., 1993. Theory and measurement of anisotropy of isothermal magnetisation of rocks. Trav. Geophys. 37, 27–134.

Kisch, H.J., 1991. Illite crystallinity: recommendations on sample preparation, X-ray diffraction settings and interlaboratory samples. J. Metamorph. Geol. 9, 665–670.

Kligfield, R., Owens, W.H., Lowrie, W., 1981. Magnetic susceptibility anisotropy, strain and progressive deformation in Permian sediments from the Maritime Alps (France). Earth Planet. Sci. Lett. 55, 181–189.

Krumm, S., Buggisch, W., 1991. Sample preparation effects on illite crystallinity measurement: grain-size gradation and particle orientation. J. Metamorph. Geol. 9, 671–677.

Kübler, B., 1967. La cristallinité de l'illite et les zones tout à fait supérieures du métamorphisme. In: Coll. Neuchâtel, Etages tectoniques, pp. 105–122.

Lacquement, F., Mansy, J.-L., Mercier, E., Averbuch, O., Meil-

liez, F., 1997. Mécanismes de plissement disharmonique dans le Paléozoïque Ardennais. Aardkd. Mededel. 8, 119–122.
Le Gall, B., 1992. The deep structure of the Ardennes Variscan thrust belt from structural and ECORS seismic data. J. Struct. Geol. 14, 431–446.
Mansy, J.-L., Averbuch, O., 1996. Le duplex de Basse-Normandie (Boulonnais, N France): une nouvelle interprétation. 16e R.S.T., Orléans, Soc. Géol. Fr., 29.
Meilliez, F., 1989. Tectonique distensive et sédimentation à la base du Dévonien, en bordure NE du massif de Rocroi (Ardenne). Ann. Soc. Géol. Nord 57, 281–295.
Meilliez, F., Andrè, L., Blieck, A., Fielitz, W., Goffette, O., Hance, L., Kathir, A., Mansy, J.L., Overlau, P., Verniers, J., 1991. Ardenne–Brabant. Sci. Géol. Bull. 44, 3–29.
Meilliez, F., Fielitz, W., Laduron, D., Mansy, J.-L., Manby, G., 1994. The deep structure of the Ardennes Variscan thrust belt from structural and ECORS seismic data: discussion. J. Struct. Geol. 16, 431–432.
Merriman, R.J., 1991. Phyllosilicates as indicators of very low-grade metamorphism and diagenesis: introduction. J. Metamorph. Geol. 9, 663–664.
Nieto, F., Sanchez-Navas, A., 1994. A comparative XRD and TEM study of the physical meaning of the white mica 'crystallinity' index. Eur. J. Mineral. 6, 611–621.
Piqué, A., Huon, S., Clauer, N., 1984. La schistosité hercynienne et le métamorphisme associé dans la vallée de la Meuse entre Charleville-Mézières et Namur. Bull. Soc. Belge Géol. 93, 55–70.
Potdevin, J.-L., Goffette, O., 1991. Les assemblages métamorphiques du filon de diabase de la Grande-Commune (Massif de Rocroi); des témoins d'une évolution rétrograde varisque en Ardenne. C. R. Acad. Sci. Paris 312, 1545–1550.
Raoult, J.-F., Meilliez, F., 1987. The Variscan Front and the Midi Fault between the Channel and the Meuse River. J. Struct. Geol. 9, 473–479.
Robion, P., Frizon de Lamotte, D., Kissel, C., Aubourg, C., 1995. Tectonic versus mineralogical contribution to the magnetic fabric of epimetamorphic slaty rocks: an example from the Ardennes massif (France–Belgium). J. Struct. Geol. 17, 1111–1124.
Robion, P., Kissel, C., Frizon de Lamotte, D., Lorand, J.P., Guézou, J.-C., 1997. Magnetic mineralogy and metamorphic zonation in the Ardennes Massif (France–Belgium). Tectonophysics 271, 231–248.
Rochette, P., 1988. La susceptibilité anisotrope des roches faiblement magnétiques: origines et applications. Thèse, Univ. de Grenoble, 211 pp.
Rochette, P., Jackson, J., Aubourg, C., 1992. Rock magnetism and the interpretation of anisotropy of magnetic susceptibility. Rev. Geophys. 30, 209–226.
Sintubin, M., 1994. Texture types in shales and slates. In: Bunge, H.J., Siegesmund, S., Skrotski, W., Weber, K. (Eds.), Textures of Geological Materials. DGM Informationgesellschaft Verlag, pp. 221–229.
Warr, L.N., Rice, A.H., 1994. Interlaboratory standardization and calibration of clay mineral crystallinity and crystallite size data. J. Metamorph. Geol. 12, 141–152.
Warr, L.N., Primmer, T.J., Robinson, D., 1991. Variscan very low-grade metamorphism in southwest England: a diastathermal and thrust related origin. J. Metamorph. Geol. 9, 751–764.
Werner, T., Borradaile, G.J., 1996. Dispersion of paleoremanences across a transpressed Archean terrain: deflection by anisotropy of remanence or by late tectonic stress. J. Geophys. Res. 101, 5531–5545.
Zwart, H.J., Oele, J.A., 1966. Rotated magnetite crystals from the Rocroi Massif (Ardennes). Geol. Mijnbouw 45, 70–74.

4. Impact de la surrection initiale de la chaîne varisque sur le climat et les environnements terrestres à la limite Frasnien-Famennien.

Le volet, présenté ici, considère la géodynamique de la chaîne varisque sous un angle plus global que ceux étudiés jusqu'alors, à travers les relations qu'il peut y avoir, entre la mise en place de reliefs montagneux de grande extension (les grands épisodes orogéniques) et les variations des environnements terrestres et du climat (e.g., Ruddiman, 1997).

En effet, ces vingt dernières années, en échos aux problèmes de rejets anthropiques des gaz à effet de serre déstockés du réservoir rocheux, une grande réflexion a été menée sur les processus naturels conduisant à une modification de la répartition des différents stocks de carbone à l'échelle géologique. Il a été montré que la dynamique interne de la Terre, *via* les éruptions volcaniques (dégazage de CO_2 mantellique) et la formation des chaînes de montagne (altération chimique de la croûte continentale, transfert de carbone organique vers les océans), pouvait sur le long terme avoir une répercussion importante sur la teneur en CO_2 de l'atmosphère et donc, par l'intermédiaire de l'effet de serre, induire des variations significatives et globales du climat. Les perturbations associées des environnements océaniques et continentaux, couplées aux variations climatiques globales engendrées, peuvent conduire à des pertes significatives de biodiversité sur des périodes relativement courtes, i.e. les périodes de crise biologique.

En ce qui concerne l'impact des orogenèses, la communauté scientifique, jusqu'alors, s'est focalisée principalement sur les périodes relativement récentes en vue d'expliquer le refroidissement climatique graduel observé depuis environ 40 Ma. Une attention particulière a été portée sur le couplage potentiel de la surrection des grandes chaînes de montagne tertiaires (système Alpes-Himalaya) avec l'évolution du climat (*e.g.* Raymo, 1991; France-Lanord and Derry, 1997; François and Goddéris, 1998; Zachos and Kump, 2005; Garzione, 2008; Gaillardet and Galy, 2008).

Or, comme nous avons pu le voir au long de ce mémoire, le Paléozoïque supérieur correspond également à une période orogénique majeure, comparable en terme de reliefs créés à la période tertiaire; c'est en effet à cette époque (globalement entre le Dévonien supérieur et le Carbonifère terminal) que s'édifient de nombreux systèmes montagneux, résultats de l'accrétion progressive des continents qui culminera au Permien avec la formation du supercontinent pangéen (cf. le modèle géodynamique présenté dans l'article 1). Cette période, caractérisée également par la formation épisodique de calottes de glace sur les pôles (au moins le pôle sud), peut donc être en quelque sorte considérée comme un analogue des temps récents tout du moins pour ce qui concerne les aspects paléotopographiques et paléoclimatiques. Dans la mesure où l'évolution de ces systèmes montagneux a été beaucoup plus poussée que le système Alpes-Himalaya, qui est encore dans un stade relativement précoce de son évolution (il reste encore de grands bassins océaniques non résorbés au cœur du domaine montagneux, en particulier les bassins méditerrannéens), la compréhension du système Terre au Paléozoïque supérieur peut nous donner des informations précieuses sur l'évolution naturelle du climat pour les millénaires à venir.

Les premiers effets de cette grande période orogénique sont enregistrés dès le Dévonien supérieur au passage entre le Frasnien et le Famennien (*ca* 375 Ma) avec le soulèvement de cordillères montagneuses péri-équatoriales s'étendant d'Asie centrale à l'Amérique du Nord, résultats du début de la collision entre Sibérie, Kazakhstan, Laurussia et Gondwana (comme nous l'avons vu, l'océan marginal Lizard-Rhénohercynien reste à refermer au nord du bloc armoricain, cf. la reconstruction paléo-tectonique de l'article 18). Cet événement orogénique majeur est, bien sûr, dénommé différemment dans la littérature selon le tronçon de chaîne étudié, ce qui rend difficile son analyse à grande échelle. Dans la littérature, il peut être appelé néoacadien dans les Appalaches septentrionaux (e.g. Van Staal et al, 2009), ligérien, éovarisque (ou éohercynien) (e.g. Ballèvre *et al*, 1994 ; Echarfaoui *et al*, 2002) voire médio-varisque (Ledru *et al*, 1989) ou simplement varisque (Souquet *et al*, 2003) dans les chaînes paléozoïques d'Europe ou d'Afrique du Nord. Il a également été évoqué sans dénomination précise, par exemple, dans le sud de l'Oural (e.g. Matte, 1995; Puchkov, 1997 ; 2009) ou en Asie centrale (Sengör et Natal'in, 1996). La collision de ces blocs majeurs est contemporaine de l'accrétion de « terranes » en bordure des continents comme c'est le cas dans l'ouest et le nord du continent nord-américain (les systèmes orogéniques des Antler (e.g. Johnson et Pendergast, 1981) et Ellesmerides dans l'Arctique canadien (e.g. Embry, 1991)) ou dans le domaine Proto-andin en Amérique du Sud (les Bolivianides, e.g. Vincente, 1975 ; Ramos, 1988). Dans la suite de ce mémoire, par souci de simplicité, j'appellerai « éovarisque » cet événement orogénique du Dévonien supérieur, même s'il dépasse de loin les contours de la chaîne varisque d'Europe et d'Afrique du Nord.

Cette période du Dévonien supérieur est marquée également par une chute significative de la biodiversité (une des 5 grandes crises du Phanérozoïque, celle de la limite Frasnien-Famennien) et par des changements environnementaux drastiques contemporains d'un refroidissement global du climat conduisant à la mise en place de calottes de glace aux hautes latitudes au Famennien supérieur (e.g. Isaacson *et al*, 1999 ; Streel *et al*, 2000). Cette période glaciaire, qui va se poursuivre globalement jusqu'à la fin du Permien, semble s'accompagner

d'une baisse drastique de la teneur en CO_2 de l'atmosphère ainsi que le suggèrent les mesures indirectes de la pCO_2 atmosphérique (*e.g.* Royer, 2006).
L'impact de la surrection de la chaîne « éovarisque » sur les paléoenvironnements a été abordé au sein d'un groupe pluridisciplinaire de chercheurs, structuré autour d'un projet Eclipse financé par le CNRS. Ce programme, que j'ai coordonné sur 3 ans entre 2001 et 2003, a permis l'organisation de 5 missions de terrain au Maroc, aux USA et en Allemagne. Ce projet a été structuré en quatre axes majeurs :
(1) Géométrie et cinématique de la chaîne éovarisque et dynamique de l'érosion sur les continents.
(2) Evolution des paléoenvironnements océaniques à la limite Frasnien-Famennien.
(3) Evolution de la biosphère au cours de la crise du Frasnien-Famennien.
(4) Modélisation du cycle du carbone au cours de la crise du Frasnien-Famennien.

Le second de ces axes a servi de support à trois thèses :

- celle d'Anne-Christine Da Silva à l'Université de Liège sur l'évolution de la production carbonatée sur la plate-forme frasnienne en Belgique (encadrant : F. Boulvain, soutenue en juin 2004) ;
- celle de Laurent Riquier à l'Université de Lille sur la caractérisation par la géochimie inorganique et le magnétisme des roches des perturbations environnementales à la limite Frasnien-Famennien (encadrants : O. Averbuch, N. Tribovillard, soutenue en novembre 2005) ;
- et enfin celle d'Ivan Berra à l'Université libre de Bruxelles sur l'analyse couplée des faciès sédimentaires et de la géochimie isotopique du Sr et et du C dans les séries du Frasnien-Famennien des Rocheuses canadiennes et américaines (encadrant : A. Préat, soutenue en novembre 2008).

Le quatrième axe du projet a servi de support à la thèse de Vincent Lefebvre sur la modélisation du cycle du carbone et du climat au cours du Dévonien supérieur et de l'Ordovicien supérieur (co-direction : O . Averbuch-T. Servais). Cette thèse (soutenue en juillet 2009) a été menée dans le cadre d'un projet commun aux deux unités de recherches en géosciences de Lille (le laboratoire de Paléontologie du Paléozoïque et le laboratoire Processus et Bilans en Domaines Sédimentaires) et s'est faite en collaboration (et en cotutelle) avec Louis Francois du Laboratoire de Physique Atmosphérique et Planétaire de l'Université de Liège.

Les articles, présentés ici, illustrent d'une part les changements environnementaux globaux enregistrés à la transition entre le Frasnien et le Famennien, d'autre part intègrent ces changements dans le cadre d'un modèle ayant comme moteur de base la surrection de l'orogène éovarisque.

Dans les domaines marins épicontinentaux, situés sur les marge océaniques passives ne jouxtant pas directement les domaines orogéniques, il est montré que le Frasnien terminal correspond à une période de stockage accru de carbone organique et de carbonates non construits (niveaux Kellwasser inférieur et supérieur) suite à une augmentation significative de la productivité marine et à la mise en place de conditions disoxiques à anoxiques assez largement répandues dans les mers du Frasnien terminal (en particulier, en bordure de l'océan Prototéthys)(articles 14 et 15). De façon plus précise, les données géochimiques suggèrent un premier événement (Kellwasser inférieur) principalement contrôlé par une hausse de la productivité primaire en bordure des continents alors que le second (Kellwasser supérieur) serait plutôt une conséquence de bouffées d'anoxie des eaux de fond se propageant ensuite sur les domaines de marge (article 15). Cette période correspond également à une baisse importante des apports détritiques vers ces bassins non péri-orogéniques, aussi bien sur la marge nord-gondwanienne (Montagne Noire, Maroc central) que la marge sud-laurussienne (Massif schisteux rhénan, Ardennes, Pologne), ainsi que le montrent, de façon récurrente, les variations de la susceptibilité magnétique dans les séries du Frasnien-Famennien (articles 16 et 17).

A l'inverse, la base du Famennien est marquée par une recrudescence généralisée des apports détritiques en contexte de bas niveau marin (chute du niveau marin de plus de 75m à la limite Frasnien-Famennien selon Haq et Schutter, 2008). Ces variations, liées à l'évolution à grande échelle des conditions d'érosion sur les continents et aux variations du niveau de base, ont été interprétées comme le résultat d'un changement climatique majeur avec des conditions particulièrement chaudes et humides au Frasnien terminal (optimum climatique dévonien) et des conditions beaucoup plus froides et sèches au Famennien basal (article 17).

Un modèle couplant ce changement climatique abrupt à la surrection de la chaîne éovarisque a été proposé (article 18) et testé par une modélisation couplée du cycle du carbone et du climat (article 19). L'augmentation drastique au Frasnien supérieur de l'érosion chimique sur les domaines en cours de surrection, augmentation marquée par une anomalie positive du rapport isotopique du strontium (e.g. Chen et al, 2005; Berra, 2008), aurait induit un transfert accru de nutriments vers les bassins épicontinentaux générant ainsi une plus forte productivité marine. La réduction des communications océaniques franches entre Panthalassa et Paléotéthys suite à la collision entre le bloc gondwan et le bloc laurussien aurait induit un confinement plus important des bassins, contribuant ainsi à l'enfouissement généralisé de matière organique marine au Frasnien terminal. Dans notre modèle, altération continentale accrue et stockage massif de matière organique auraient formé une pompe efficace de CO_2 atmosphérique au Frasnien terminal conduisant à un refroidissement significatif au Famennien, prémisse de l'englaciation d'une partie du Gondwana au Famennien supérieur. La fin du Dévonien correspondrait ainsi à une période de transition climatique majeure sous contrôle orogénique avec le passage d'un climat chaud et humide de type « greenhouse » au Frasnien à un climat globalement plus froid et plus sec de type « icehouse » au cours du Dévonien terminal et du Carbonifère.

Pour valider ce modèle conceptuel, l'impact climatique de l'augmentation de l'altération continentale, associée à la surrection de la chaîne, ainsi que de la la réduction des communications océaniques entre Panthalassa et Prototéthys, a fait l'objet d'une modélisation numérique (thèse de Vincent Lefebvre, 2009)(article 19). Il s'agit là, à notre connaissance, de la première tentative de modélisation directe de l'impact des flux d'érosion orogéniques sur le cycle du carbone. Le modèle créé à cette intention est un modèle géochimique de boîtes couplé au modèle climatique de type EBM à une dimension (la latitude) conçu par Francois et Walker (1992). Le modèle géochimique de base est issu des travaux de l'équipe de Louis François à Liège et a été utilisé dans sa version classique pour modéliser différentes périodes de crise environnementale au cours du Phanérozoïque (la limite Permien-Trias, Grard et al, 2000; les événements climatiques du Miocène, Diester-Haas et al, 2009 ; la glaciation de la fin de l'Ordovicien, Lefebvre et al, 2010). La version de modèle utilisée ici comprend deux évolutions majeures : (1) une régionalisation latitudinale des processus d'érosion et d'altération permettant d'augmenter les flux d'érosion sur une zone particulière (la zone soumise à surrection, dans le cas qui nous concerne la zone péri-équatoriale entre 30°N et 30°S) ; (2) le couplage des différents cycles géochimiques classiques avec le cycle de l'oxygène. Ce dernier est, en effet, nécessaire pour mettre en place des milieux océaniques disoxyques ayant des répercussions importantes sur les flux de stockage de carbone dans les domaines marins. La mise en place de ce cycle implique, cependant, d'importantes rétroactions vis à vis des différents processus impliqués dans le modèle et a, donc, nécessité une attention particulière vis à vis de la quantification de la dépendance de ces processus par rapport à l'oxygène. Les lois d'altération utilisées dans le modèle, permettant, en particulier, de coupler érosion mécanique et altération chimique, sont issues des études de bilans géochimiques réalisés dans les grands bassins versants actuels (Gaillardet et al, 1999 ; Millot et al, 2002).

Le modèle, étalonné sur l'actuel, a été calibré de façon à atteindre un équilibre pré-perturbation caractéristique du système Terre au Dévonien moyen. A cet effet, le modèle a été configuré sur une paléographie représentative du Dévonien moyen permettant, en particulier, de définir la part respective de surfaces continentales et océaniques dans chaque bande de lattitude. La configuration des différentes boîtes océaniques a été également calqué sur la paléogéographie du Dévonien moyen avec un océan Protéthys, faiblement mixé, en communication avec un océan Panthalassa ouvert, avec une circulation thermo-haline efficace (cf. la partie calibration de l'article 19).

Pour simuler l'augmentation de l'érosion associée à la surrection éovarisque, nous nous sommes basés sur les concepts classiques de soulèvement orogénique intégrant une phase transitoire de surrection de la surface terrestre avant que le chaîne n'atteigne un état topographique stationnaire global (e.g., Burbank et Anderson, 2001). Au cours de cette phase transitoire, les taux d'érosion augmentent au sein de la chaîne jusqu'à venir équilibrer les taux de soulèvement. L'augmentation du taux d'érosion (du flux clastique dans le modèle) a été considéré linéaire dans cette étude jusqu'à atteindre un plateau, valeur maximale d'érosion qui reste constante pendant la phase stationnaire de mise en place du relief montagneux (10 Ma dans nos simulations). La durée de la phase transitoire de soulèvement (et, de fait, de l'augmentation de l'érosion) est difficile à apréhender directement dans les chaînes anciennes mais elle peut être approchée à partir de la dynamique du bassin d'avant-chaîne. En effet, on considère classiquement qu'elle coincide avec la transition récurrente, dans les bassins d'avant-chaîne, entre des conditions de sous-alimentation marquées par des faciès marins profonds (fyschs) et des conditions de sur-alimentation marquées par des dépôts marins peu profonds ou fluviatils (molasse)(e.g., Covey, 1986). Le bassin d'avant-chaîne taiwanais est, très certainement, l'endroit où l'on peut appréhender la durée de cette phase transitoire avec la plus grande résolution puisque la chaîne de Taiwan résulte de la collision la plus récente sur Terre (collision initiée il y a environ 6,5 Ma selon Lin et al, 2003). Les données de modélisation de la subsidence au sein du bassin d'avant-chaîne taiwanais montrent que la période transitoire de remplissage accéléré du bassin s'est faite sur environ 1,5 Ma, ce qui correspond à la période nécessaire pour atteindre la géométrie stationnaire du bassin (Simoes et Avouac, 2006). A Taiwan, à une latitude donnée, l'état d'équilibre entre soulèvement et érosion a donc été atteint en 1,5 Ma ce qui représente un temps très court en regard de la durée d'existence de la topographie d'une chaîne de montagne (30-40 Ma par exemple pour les chaînes alpines et himalayennes). Cette durée significative a été utilisée comme modèle de base pour notre modélisation (au cours de la simulation de référence, les taux d'érosion sont augmentés sur 2 Ma). Pour évaluer l'impact de cette phase transitoire sur les résultats, des simulations ont aussi été réalisées pour des durées de 1 et 3 Ma.

L'augmentation de l'érosion associée à la surrection de la chaîne a été simulée en augmentant le flux clastique uniquement sur les zones soumises à une surrection (entre 30°N et 30°S dans le cas de la chaîne éovarisque). A partir de l'état d'équilibre pré-perturbation du Dévonien moyen (30% du flux clastique actuel), le flux clastique a été augmenté dans la bande de latitude 30°N et 30°S de différents facteurs au cours de la simulation (60%, 90% et 120% du flux clastique actuel) simulant ainsi une orogénèse qui aurait conduit à des flux d'érosion inférieurs (60%), sensiblement égaux (90%) ou légèrement supérieurs (120%) à l'actuel. On peut rappeler ici que le flux clastique global actuel n'est pas contraint et donc, que toute quantification directe d'un flux clastique orogénique (via des surfaces orogéniques définies et des taux d'érosion classiques) ne peut être utilisé ici car impossible à comparer au flux global actuel.

De la même façon, l'impact de la réduction des communications entre Panthalassa et Prototéthys a été testé en diminuant les flux de transfert entre les deux domaines océaniques à la fois pour les réservoirs de surface et thermocline. Là encore, le « timing » et l'intensité de cette réduction est difficile à préciser dans le cas de la collision éovarisque et des tests ont donc été effectués pour préciser l'impact des variations d'intensité et de durée des différents flux de transfert de surface et thermocline entre Prototéthys et Panthalassa.

Enfin, ces deux mécanismes majeurs résultant du soulèvement initial de la chaîne varisque ont été couplés pour évaluer leurs éventuelles interactions et au final, donner probablement l'idée la plus fine de ce qu'ont pu être les variations environnementales et climatiques au cours de la phase de soulèvement de la chaîne. Cependant, l'évolution dans le temps de ces phénomènes (synchronisme ou déphasage), leur intensité relative ainsi que leur durée respective peuvent jouer un rôle non négligeable sur les processus de couplage. Dans l'article 19, des ajustements ont été donc fait sur ces paramètres afin de « fitter » au mieux l'évolution du $\delta_{13}C$ au cours de la crise Frasnien-Famennien avec deux pics significatifs séparés d'environ 1 Ma, correspondant aux deux évenements Kellwasser inférieur et supérieur tels que compilés par Goddéris et Joachimski (2004).

Au final, ces expériences de modélisation numérique confortent grandement le modèle conceptuel de l'article 18 considérant le soulèvement de la chaîne varisque (l'événement éovarisque) comme un moteur possible de la crise environnementale, climatique et biologique de la transition Frasnien-Famennien au Dévonien supérieur. Nous montrons, en particulier, qu'un processus orogénique, considéré souvent comme long-terme en ce qui concerne les processus géologiques, peut provoquer des perturbations très rapides (de l'ordre de 1 à 2 Ma) des environnements terrestres lors de la phase transitoire d'édification du relief. Cette phase transitoire qui coincide avec une augmentation drastique des flux d'érosion dans le domaine soumis à l'orogenèse aura un impact d'autant plus grand qu'elle se situe en milieu péri-équatorial chaud et humide et que les bassins océaniques en bordure de chaîne subissent un confinement important suite à la réduction des communications océaniques franches aux limites du système. Par ailleurs, nos études montrent que le couplage entre l'augmentation de l'érosion mécanique et le confinement des marges prototéthysiennes peut conduire au développement de deux événements de stockage accru de carbone organique sur une période d'environ 2 Ma: (1) le premier contrôlé par l'augmentation de l'érosion (et de l'altération associée) au sein de la chaîne induit une fertilisation de grande extension des espaces océaniques limitrophes et l'enfouissement accru de carbone en écho à la sur-productivité marine ; (2) le second, en rétroaction du premier, correspond au développement de bouffées disoxyques au sein des espaces océaniques favorisant le stockage de matière organique dans les sédiments de profondeur. Dans le cas du système éovarisque au Dévonien supérieur, il est proposé que ces processus puissent correspondre aux deux niveaux Kellwasser du Frasnien terminal. Les expériences de modélisation numérique montrent que l'enfouissement associé de carbone organique couplé avec l'augmentation de l'altération des silicates au sein de la chaîne peut induire une chute très importante de la pression de CO_2 atmosphérique en 2 Ma (de 3100 à 760 ppmv) ce qui correspond à une baisse d'environ 6° des températures moyennes équatoriales sur la base du module climatique EBM couplé avec le modèle géochimique. Ces valeurs sont en très bon accord avec les données existantes pour le Dévonien supérieur tant pour les estimations de PCO_2 (Royer, 2006) que pour celles de chute de température à la limite Frasnien-Famennien (Joachimski and Buggisch, 2002). De telles valeurs peuvent permettre l'initiation de calottes de glace sur le sud du Gondwana dès la base du Famennien ainsi que le suggèrent, par exemple, Streel et al (2000) sur la base d'études palynologiques. Selon nos études, la transition Frasnien-Famennien serait ainsi une crise climatique abrupte sous contrôle orogénique, crise initiale du passage à l'ère glaciaire et montagneuse du Carbonifère et du Permien.

Article 14.

Riquier L., Tribovillard N., Averbuch O., Joachimski M., Racki G., Devleeschouwer X., El Albani A. and Riboulleau A. (2005). Productivity and bottom water redox conditions at the Frasnian-Famennian boundary on both sides of the Eovariscan belt : constraints from trace-element geochemistry. In : Understanding Late Devonian and Permian-Triassic Biotic and Climatic Events : Towards an Integrated Approach, P. Wignall, J. Morrow and J. Over eds., Developments in Palaeontology and Stratigraphy, Elsevier, vol. 20, 199-224.

Chapter 8

Productivity and bottom water redox conditions at the Frasnian–Famennian boundary on both sides of the Eovariscan Belt: constraints from trace-element geochemistry

Laurent Riquier[a,*], *Nicolas Tribovillard*[a], *Olivier Averbuch*[a], *Michael M. Joachimski*[b], *Grzegorz Racki*[c], *Xavier Devleeschouwer*[d], *Abderrazzak El Albani*[e] *and Armelle Riboulleau*[a]

[a]*Laboratoire des Processus et Bilans des Domaines Sédimentaires, CNRS UMR 8110 & FR 1818, Université Lille 1, bâtiment SN5, F-59655 Villeneuve d'Ascq cedex, France*
[b]*Institute of Geology and Mineralogy, University of Erlangen-Nürnberg, Schlossgarten 5, D-91054 Erlangen, Germany*
[c]*Department of Palaeontology and Stratigraphy, University of Silesia, Bedzinska Str. 60, PL 41-200 Sosnowiec, Poland*
[d]*Geological Survey of Belgium, Rue Jenner 13, B-1000 Brussels, Belgium*
[e]*Laboratoire Hydrogéologie, Argiles, Sols et Altérations., CNRS UMR 6532, Université Poitiers, 40, Avenue du Recteur Pineau, F-86022 Poitiers cedex, France*

Abstract

The Late Devonian Frasnian–Famennian (F–F) mass extinction event coincides in many places with the deposition of C_{org}-rich "Kellwasser" facies. Four F–F boundary sections representative of platform and basin environments from widely separated locations (Morocco, Germany, and France) were analysed for inorganic geochemistry, especially trace elements (redox and productivity proxies), in order to describe paleodepositionnal environments for the Kellwasser horizons. Ni/Co, V/Cr, U/Th, and V/(V+Ni) ratios, as well as redox trace metal concentrations indicate that oxygen-depleted conditions existed during the times of Kellwasser facies deposition. In platform settings, dysoxic conditions seem to be limited to the Late Frasnian. In basinal settings, oxygen depletion was stronger and persisted into the Early Famennian. Enrichments of Ba, Cu, Ni, that are limited to the Late Frasnian, show that surface productivity was relatively high and organic matter could accumulate, especially in the deeper environments. The stratigraphical distribution of several geochemical markers are linked with two positive excursions of the $\delta^{13}C_{carb}$ signal that result from enhanced organic matter burial. Reducing conditions likely resulted from high productivity of Late Devonian marine ecosystems. Intense nutrient supply resulted probably from the biogeochemical recycling of nutrients, and/or runoff from emerged lands. Coupled with other factors, such as rapid sea-level fluctuations and climatic changes, oxygen-depleted conditions and eutrophication would have modified Late Devonian environments and could be possible factors in the F–F mass mortality.

Keywords: Late Frasnian; inorganic geochemistry; anoxia; primary productivity; eutrophication

1. Introduction

The Late Devonian Frasnian–Famennian (F–F) boundary (374.5 Ma; Kaufmann et al., 2004) represents one of the five most severe biological crises of the Phanerozoic

*Corresponding author. Fax: +33-320-43-49-10. *E-mail address*: Laurent.Riquier@ed.univ-lille1.fr (L. Riquier).

(Sepkoski, 1986; Copper, 1986; McGhee, 1989, 1996; Hallam and Wignall, 1997; House, 2002). The biodiversity decrease particularly affected marine shallow-water tropical faunas of epicontinental reefal carbonate platforms. In outer shelfal (ca. 100–200 m depth) and epicontinental basin settings, the Upper Frasnian extinction interval is characterized by the occurrence of two distinctive black-coloured units, i.e., the so-called "Kellwasser" horizons (Schindler, 1990). The top of the Upper Kellwasser horizon usually marks the F–F boundary. These two beds have been recognized in various places, located on the borders of Laurussian (N. America, N. Europe) (Sandberg et al., 1989; Schindler, 1990, 1993; Buggisch, 1991) and Gondwanian (S. Europe, S. America, Africa) blocks (Feist, 1990; Wendt and Belka, 1991). They have generally been attributed to episodes of enhanced organic carbon preservation under pervasive anoxic bottom conditions (Joachimski and Buggisch, 1993; Joachimski et al., 2001) or increased carbon flux to the sea floor driven by high surface water productivity (May, 1995; Caplan and Bustin, 1998), or combinations of these processes (Murphy et al., 2000b). This paper presents the inorganic geochemistry record for four F–F boundary sequences deposited in different paleogeographic units on both sides of the incipient Eovariscan orogenic belt. The sections studied are distributed from platform to basin settings. Geochemical signatures of Gondwanian (Morocco and France) and Laurussian (Germany) sections were analysed, specially focussing on redox and productivity indicators. The purpose of this study is to provide insight to the paleoenvironmental conditions existing in marine setting and leading to organic matter (OM) accumulation. The results are compared with those obtained for time-equivalent deposits in the detailed studies of Joachimski et al. (2001, 2002), Racki et al. (2002), Yudina et al. (2002) and Bond et al. (2004) to establish a wider paleoenvironmental reconstruction.

2. Investigated sections

The four sections investigated, Bou-Ounebdou, Anajdam, La Serre, and Aeketal, are well-known F–F boundary localities (Fig. 1). During the last decade, detailed investigations of sedimentary sequences and faunas have been performed, particularly within the IGCP projects 216 on "Global biological events in Earth History" (Walliser, 1996) and 421 on "North Gondwanian Mid-Paleozoic bioevent/biogeography patterns in relation to crustal dynamics" (El Hassani and Tahiri, 1999) and by the Subcommission on Devonian Stratigraphy in order to supplement the F–F stratotype section at Coumiac. These studies allowed paleoenvironments assessment and precise dating using conodont biostratigraphy.

2.1. Bou-Ounebdou and Anajdam (Western Meseta, Morocco)

The Bou-Ounebdou and Anajdam sections are located in the M'rirt area, in the eastern part of central Morocco (western Meseta). Both sections are in the Azrou-Kenifra Basin, located at subtropical palaeolatitudes (15–30°S) on the northern margin of Gondwana during the Late Devonian (Fig. 2). The Anajdam and Bou-Ounebdou sections were described in detail by Lazreq (1992, 1999), Becker and House (2000), Walliser et al. (2000), and Chakiri (2002). The interval considered in this study records condensed sedimentation, spanning from the Late Frasnian (*rhenana* Zone) to Early Famennian (*triangularis* Zone). The Early

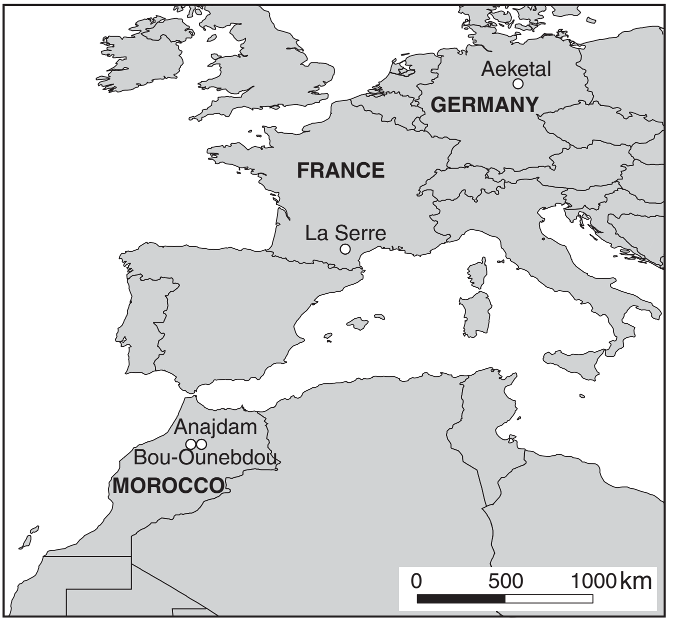

Figure 1. Index map of Western Europe and North Africa, showing several locations of studied sections in Germany, France, and Morocco.

triangularis Zone may be absent in the Bou-Ounebdou section (Lazreq, 1992; Becker, pers. comm.). The sequences mainly consist of a succession of cephalopod limestone beds (wackestone) with intercalated calcareous shale levels. In the upper Frasnian, two dark-coloured (supposedly organic C-rich) horizons were biostratigraphically identified as the Lower and Upper Kellwasser horizons, respectively (Lazreq, 1992). The Lower and Upper dark-coloured Kellwasser horizons are about 25 and 40 cm thick, respectively (Fig. 3). The faunal associations of conodonts, tentaculitids, ammonoids, trilobites, bivalves, and ostracods characterize deep, off shore platform settings where the majority of Kellwasser fossils are pelagic, such as *Manticoceras* ammonoids, orthocone nautiloids, bivalves of the *Buchiola*-group, conodonts, and tentaculitids (Lazreq, 1999; Chakiri, 2002).

2.2. Aeketal (Harz Mountains, Germany)

The Aeketal section is located in the north-western part of the Harz Mountains, included in the Rhenohercynian zone of the German Variscides. The Harz area is believed to have occupied a subtropical position (0–15°S) on the southern margin of Laurussia during deposition of Late Devonian sediments (Fig. 2). The Aeketal section, studied in details by Schindler (1990, 1993) and Feist and Schindler (1994), records condensed sedimentation spanning from Late Frasnian (*rhenana* Zone) to Early Famennian (*triangularis* Zone). The section mainly exposes light-grey limestones (calcilutites) and two black horizons of limestones and marls. The Upper Kellwasser horizon is 90 cm thick (Fig. 3). Diversified faunas, such as trilobites, ostracods, echinoderms, and ammonoids, have been found and both

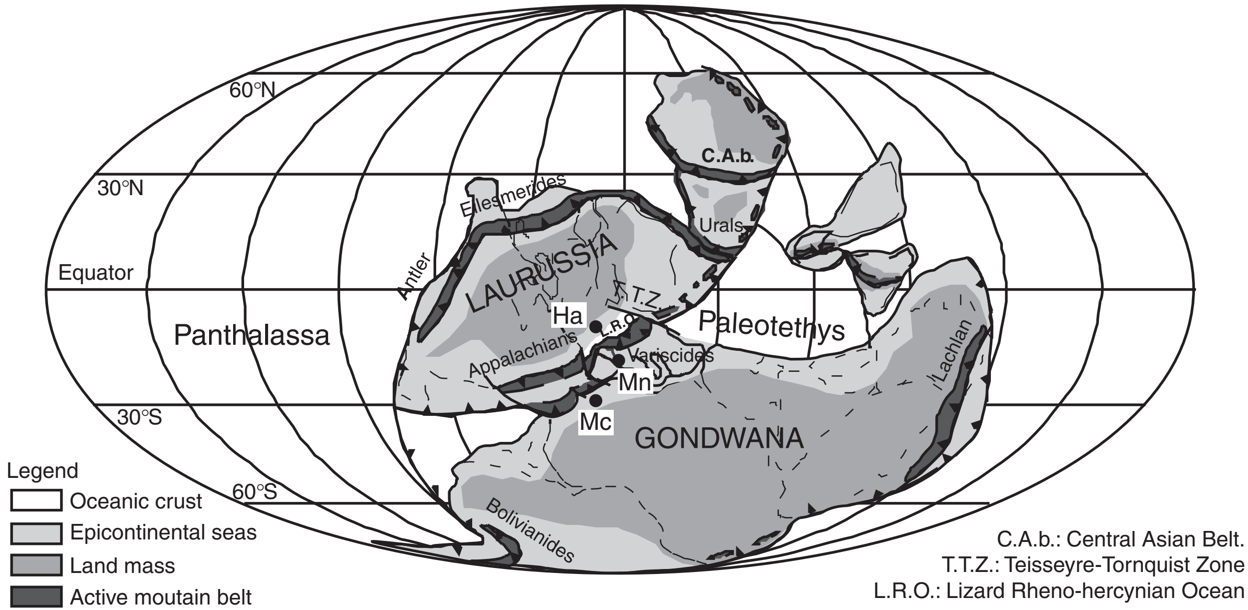

Figure 2. Schematic paleogeographic reconstruction for the Frasnian–Famennian boundary times showing main geological structures and the approximate location of studied areas. Mc: Maroc central (Central Morocco); Mn: Montagne Noire (France); Hz: Harz Mountains (Germany) (Modified from Averbuch et al., 2005).

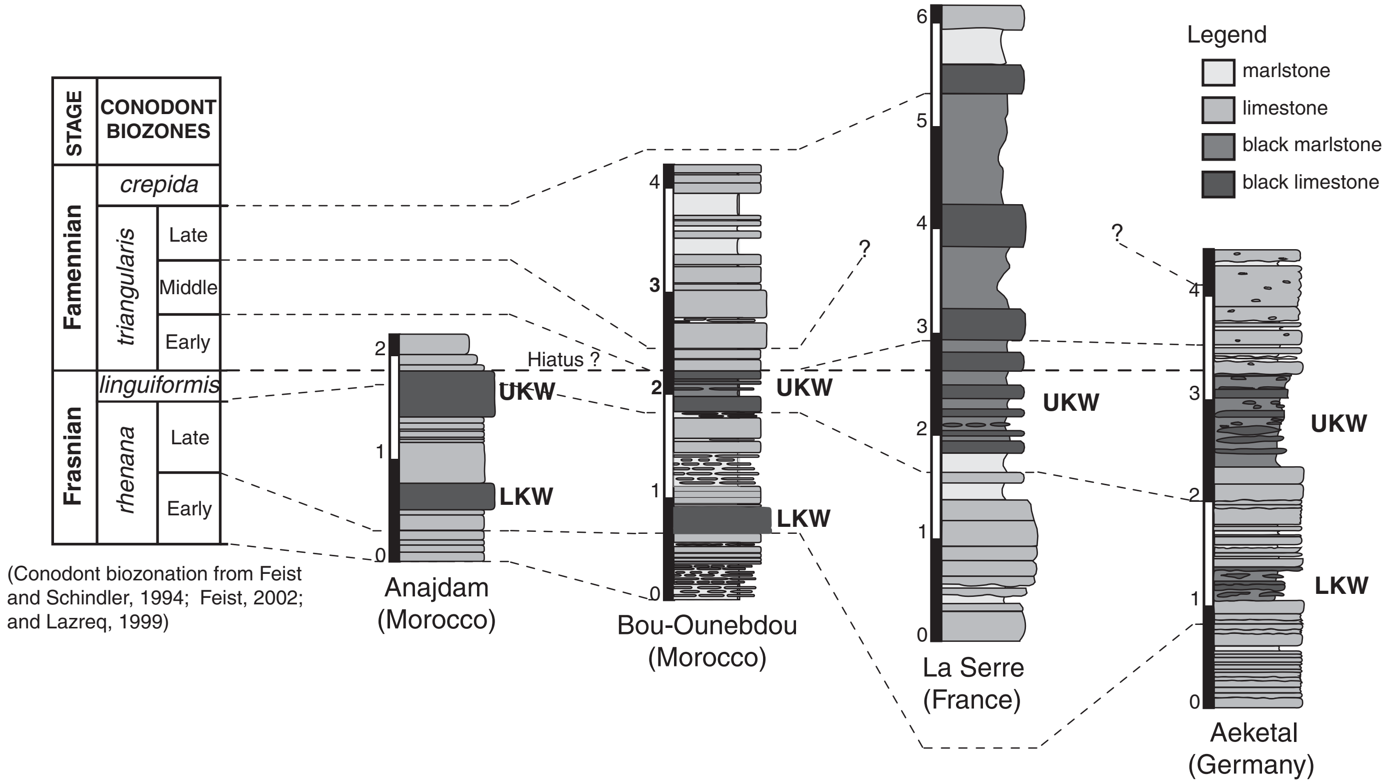

Figure 3. Simplified stratigraphic columns of the Frasnian–Famennian boundary sequence of the sections studied and biocorrelations. LKW: Lower Kellwasser, UKW: Upper Kellwasser, scale in meters.

Kellwasser horizons are dominated by pelagic fossils, such as conodonts, homoctenid cricoconarids, orthocone nautilids, and bivalves of the *Buchiola*-group. The Aeketal section is thought to correspond to a submarine-rise setting in a pelagic realm (Schindler, 1990).

2.3. La Serre (Montagne Noire, France)

The La Serre (Trench C) section is located on the southern slope of the La Serre hill, 2.4 km from Cabrières (Montagne Noire). Paleogeographically, the Montagne Noire area was located at paleolatitudes between 15 and 30°S (Fig. 2). This section displays a complete succession without sedimentary gaps. The interval considered in this study starts with light-grey pyritic calcilutites rich in pelagic and benthic biota that are abruptly overlain by an alternating sequence of dark brownish and black, fissile marls, and platy thin-bedded bituminous marly limestones. The levels at the base of this alternation are considered to be equivalent to the Upper Kellwasser horizon (Schindler, 1990; Girard and Albarède, 1996; Devleeschouwer, 1999). The C_{org}-rich Kellwasser facies prevailed for longer time periods than the Kellwasser horizon duration, and ended in the early Famennian *crepida* Zone (Fig. 3). At La Serre, the fine-grained, laminated sediments contain exclusively pelagic, nekto-planktonic biota of small size, characterized by homoctenids, conodonts, entomozoan ostracods, and buchiolid bivalves, but no cephalopods, in contrast to the normally much coarser-grained, cephalopod-rich Kellwasser limestone of the western Meseta and Aeketal sections. Based on palaeoecological criteria, the depositional environment of the La Serre section is interpreted as corresponding to an offshore basin (Feist, 1985; Paris et al., 1996; Lethiers et al., 1998).

3. Methods

For each section, about 20 bulk-rock samples of limestones to marls were analysed for major (Al, Fe, K, Mn, Ti, Si) and trace elements (Ba, Co, Cr, Cu, Mo, Ni, Pb, U, V, Zn). Elemental analyses were performed by ICP-AES (major or minor elements) and ICP-MS (trace elements), at the spectrochemical laboratory of the Service d'Analyse des Roches et des Minéraux of the Centre National de la Recherche Scientifique (Vandœ uvre-les-Nancy, France). The samples were prepared by fusion with $LiBO_2$ and HNO_3 dissolution. Precision and accuracy were both found to be better than 1% (mean 0.5%) for major–minor elements, 5% for Cr, Pb, U, V, and Zn, and 10% for Ba, Co, Cu, Mo, and Ni as checked by international standards (Carignan et al., 2001) and analysis of replicate samples, respectively. Calcium carbonate ($CaCO_3$) content was determined using a Bernard calcimeter (acid digestion). Total carbon was measured with a Leco CS-125 analyser (combustion at 1200°C) and total organic carbon (TOC) was calculated as the difference between total carbon and inorganic carbon, deduced from calcium carbonate content. A few tests of Rock Eval pyrolysis were also performed on the Morocco and Germany samples to compare the TOC values, using the Delsi Instrument 'Oil Show Analyser' of the Earth Sciences Department of Pierre et Marie Curie – Paris VI University.

The trace metal data are reported here as metal/aluminium ratios in order to eliminate the dilution effect of the biogenic phase (calcium carbonate and OM) and to compare different environmental settings with regard to variations in trace-element contents

(Brumsack, 1989; Arthur et al., 1990; Calvert and Pedersen, 1993). Higher element/Al ratios will indicate synsedimentary additions, if a constant composition of the background is assumed. Variations of the Al content in relation with diagenetic formation of clay minerals is unlikely, because in the present study Al is positively correlated with Ti ($R^2 = 0.99$ for each section) that is not incorporated during authigenic clay–mineral formation (Pratt et al., 1986), an indication that Al is a reliable detrital proxy. All trace elements concentrations are reported as Al-normalized values, instead of Ti-normalized because Al-normalization is more usual in the literature, and facilitates comparisons.

4. Results

4.1. Carbon concentrations

The four sections studied are composed of pure to shaly limestones. Carbonate contents mostly vary from 50 to 99% $CaCO_3$ (Figs. 4–7). At Anajdam, both Upper and Lower Kellwasser horizons are made of massive limestone; at Bou-Ounebdou, only the Lower Kellwasser horizon is made of massive limestone. In the other sections studied, the Kellwasser horizons correspond to marl–limestone alternations (Figs. 4–7). In Moroccan platform sections, no enrichment of TOC is recorded in the Kellwasser horizons. At Aeketal, samples from the grey limestone sequence are devoid of organic carbon, whereas the TOC content can reach 1.5 wt% in the Kellwasser horizons. At La Serre, the TOC content varies from 0 to 3.7 wt%, maximal values are recorded in the Early and Middle *triangularis* zones. Except for the La Serre section, all the sections studied belong to heavily tectonised and/or buried areas, and the OM endured severe loss and transformations. Consequently, the major part of the residual organic carbon is 'graphitic' carbon, and the TOC values have little significance (see Section 5). Conversely, in the case of the La Serre section and the Kowala section used for comparison (Joachimski et al., 2001, 2002), TOC values can be used directly because of (very) low thermal alteration (Devleeschouwer, 1999).

4.2. Trace metal concentrations

Enrichment factors (EF) for selected trace elements were determined by comparing Al-normalized trace element ratio to those of average shale (Wedepohl, 1971, 1991). The enrichment factor for any element (e), hereafter $EF_{(e)}$, is equal to $(e/Al)_{sample}/(e/Al)_{shale}$. In plots of stratigraphical variations of normalized elements concentration, the ratio calculated for the average shale (Wedepohl, 1971) is indicated by a dashed line to provide the baseline for which $EF_{(e)} = 1$.

In the outer platform environments of Anajdam, Bou-Ounebdou, and Aeketal, the concentrations of redox-sensitive metals (Mo, U, V, Cr, Cu, Ni, Zn, and Pb), as well as markers of productivity (Ba) and OM-related trace elements (Cu, Ni, Zn), are generally elevated throughout the black-coloured Kellwasser horizons relative to overlying and underlying strata. Most of the trace metal elements, particularly U and Cu, show a relatively monotonous distribution in strata overlying and underlying the Kellwasser horizons. $EF_{(U)}$ and $EF_{(Cu)}$ have average values of 2.4 and 1.5, respectively. The Lower Kellwasser horizon is

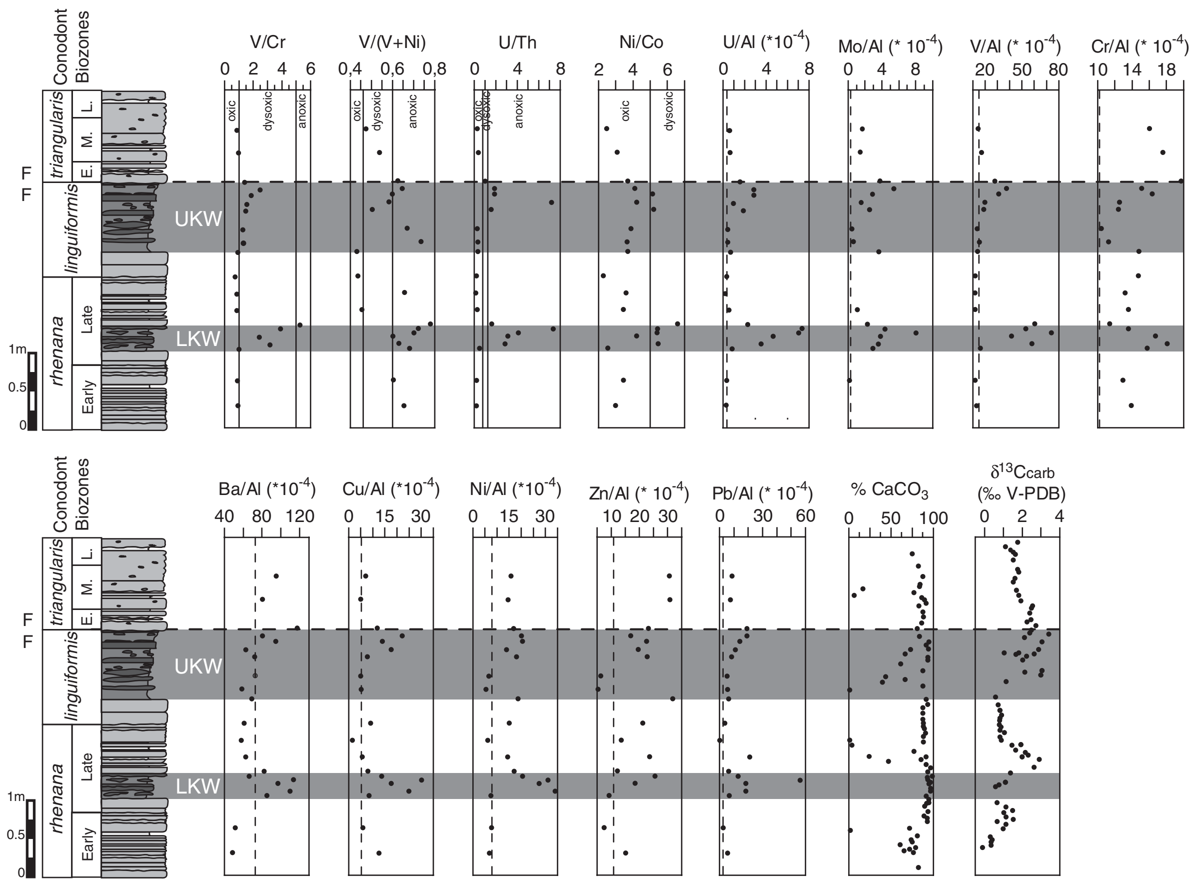

Figure 4. Stratigraphic distribution of carbonate content, $\delta^{13}C_{carb}$, Al-normalised trace-element concentrations and geochemical indices for the Aeketal section. Dashed lines indicate the metal/aluminium concentration ratios for average shales (Wedepohl, 1971, 1991) and the boundary of redox zones for V/Cr, Ni/Co, U/Th (from Jones and Manning, 1994) and V/(V+Ni) (from Hatch and Leventhal, 1992). Dark grey background corresponds to the black shale and limestone facies.

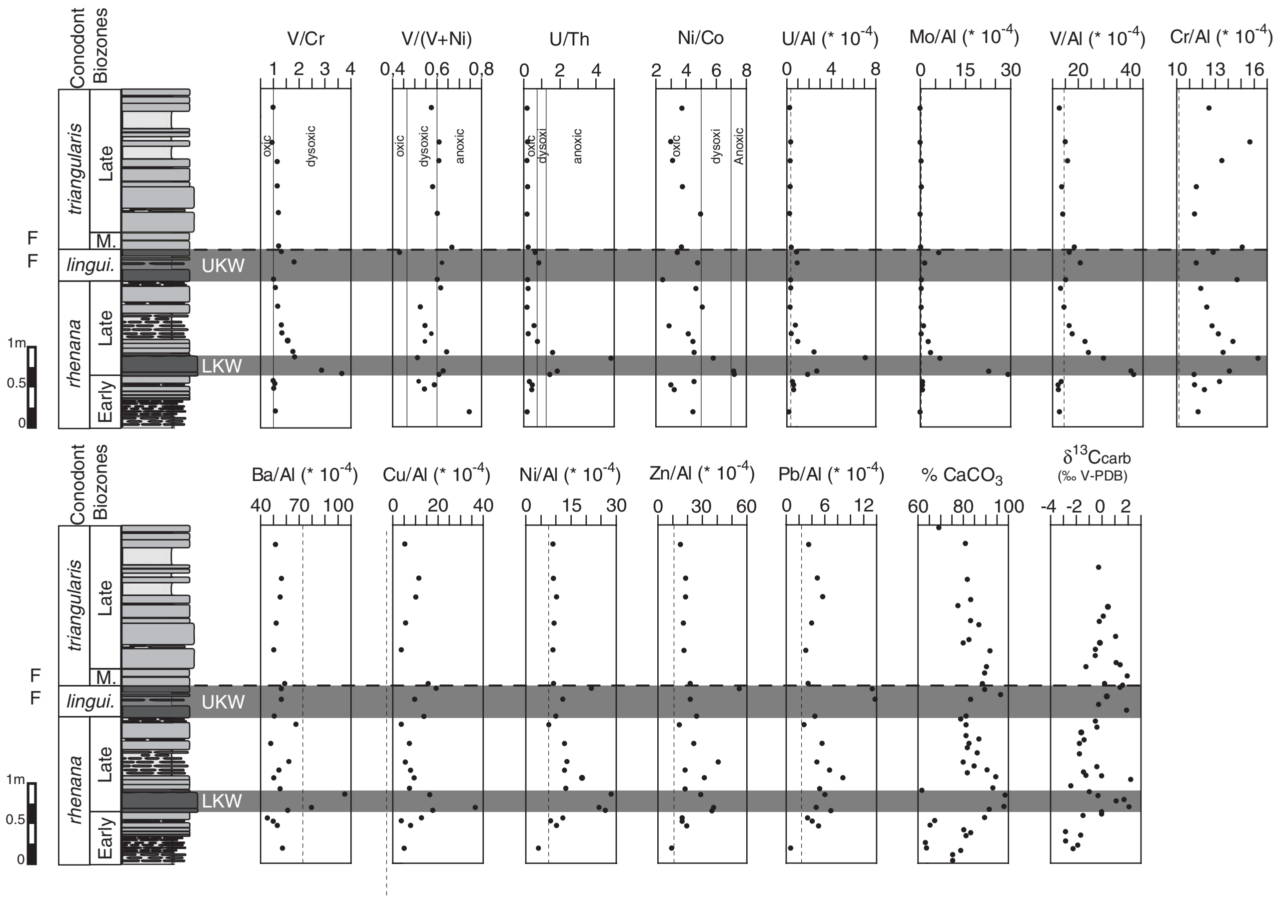

Figure 5. Stratigraphic distribution of carbonate content, $\delta^{13}C_{carb}$, Al-normalised trace-element concentrations and geochemical indices for the Bou-Ounebdou section. Dashed lines indicate the metal/aluminium concentration ratios for average shales (Wedepohl, 1971, 1991) and the boundary of redox zones for V/Cr, Ni/Co, U/Th (from Jones and Manning, 1994) and V/(V+Ni) (from Hatch and Leventhal, 1992). Dark grey background corresponds to the black shale and limestone facies.

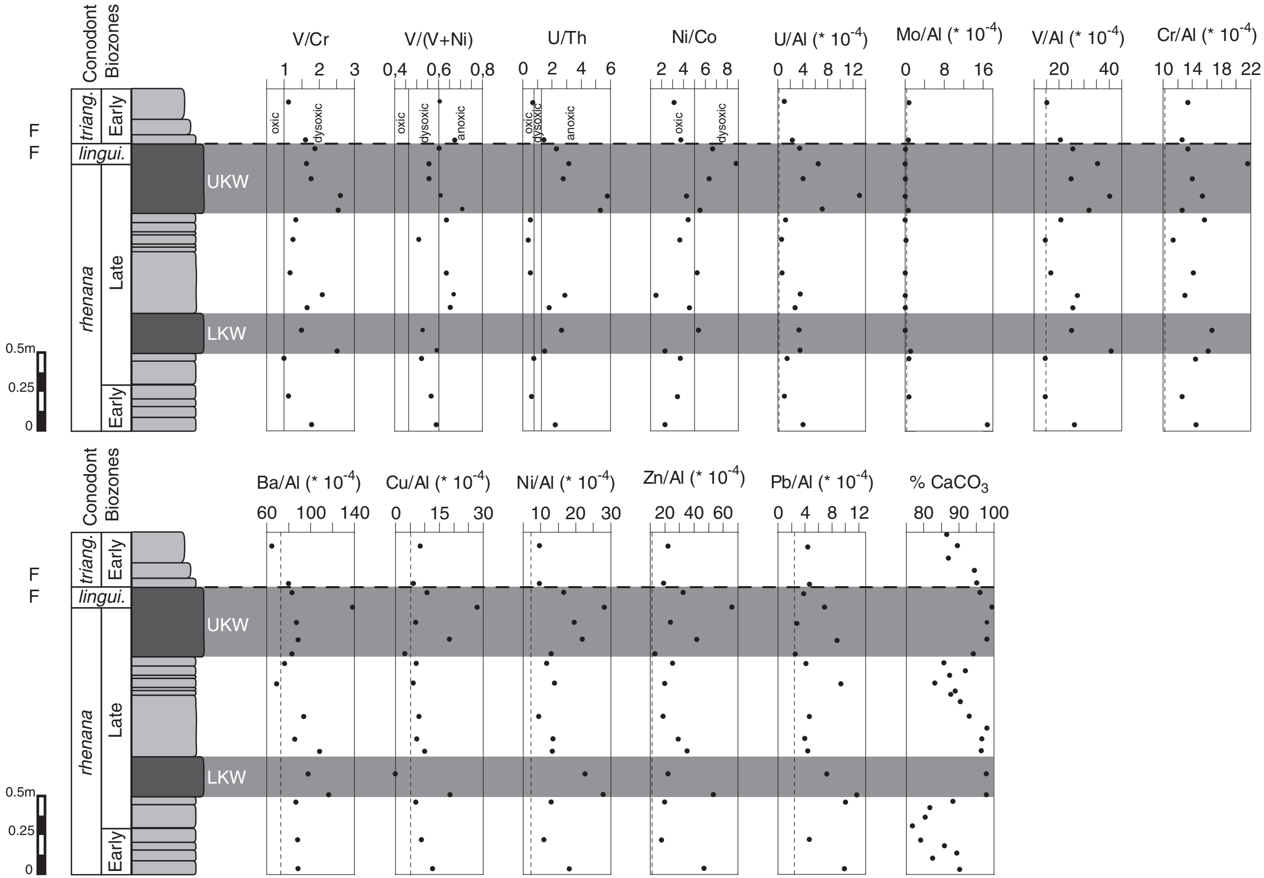

Figure 6. Stratigraphic distribution of carbonate content, Al-normalised trace-element concentrations and geochemical indices for the Anajdam section. Dashed lines indicate the metal/aluminium concentration ratios for average shales (Wedepohl, 1971, 1991) and the boundary of redox zones for V/Cr, Ni/Co, U/Th (from Jones and Manning, 1994) and V/(V+Ni) (from Hatch and Leventhal, 1992). Dark grey background corresponds to the black shale and limestone facies.

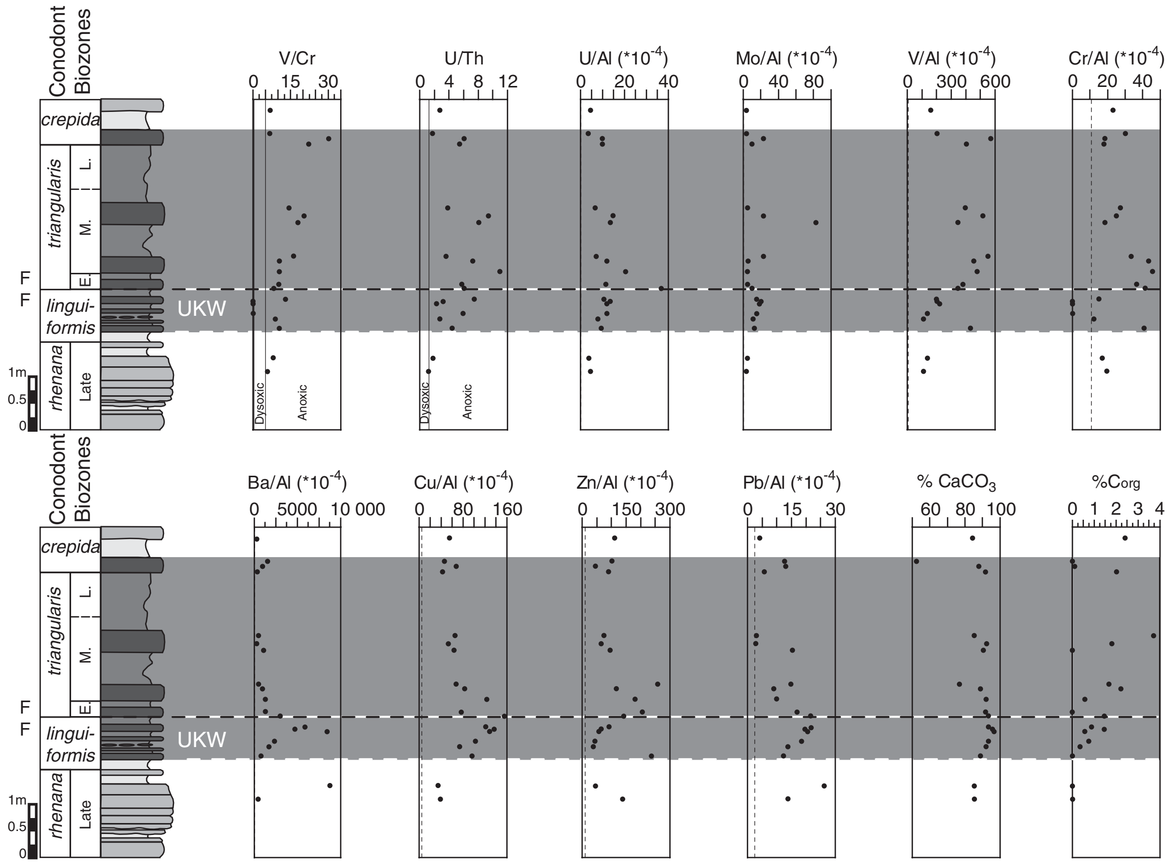

Figure 7. Stratigraphic distribution of carbonate content, Al-normalised trace-element concentrations and geochemical indices for the La Serre section. Dashed lines indicate the metal/aluminium concentration ratios for average shales (Wedepohl, 1971, 1991) and the boundary of redox zones for V/Cr, Ni/Co, U/Th (from Jones and Manning, 1994) and V/(V+Ni) (from Hatch and Leventhal, 1992). Dark grey background correspond to the black shale and limestone facies and white dashed lines indicate the time-equivalent upper Kellwaser horizon.

marked by a short positive peak of these ratios. The maximum $EF_{(U)}$ of the peaks varies between 10 at Anajdam and 23 at Bou-Ounebdou. $EF_{(Cu)}$ ranges from 3 to 7. The Upper Kellwasser horizon records a gradual and moderate rise of the ratios. $EF_{(Cu)}$ is about 3 in the three sections. At Aeketal and Bou-Ounebdou, samples from the *linguiformis* Zone are weakly to moderately enriched in U ($3 < EF_{(U)} < 8$), whereas at Anajdam $EF_{(U)}$ can reach 38. For the other trace elements, comparable trends are observed (Figs 4–6).

In the basinal environments at La Serre, trace metal elements are always highly enriched with respect to average shales, in contrast to the outer platform sections that exhibit relatively low EF. This concentration contrast is particularly exhibited with barium. Due to analytical problems and low sample quantities, Ni data are not available for this section. In Bou-Ounebdou, Anajdam, and Aeketal sections, the Kellwasser horizons are marked by a slight increase of barium ($EF_{(Ba)} < 2$), whereas in the La Serre section, $EF_{(Ba)}$ shows a remarkable increase from the base of the Upper Kellwasser horizon to the F–F boundary. $EF_{(Ba)}$ values rise up to 120, a few cm below the F–F boundary in the *linguiformis* Zone (Fig. 7). At La Serre, the concentrations of the other trace metals (Mo, U, V, Cr, Cu, and Zn) fluctuate widely through the F–F sequence. Peak values are observed immediately above the F–F boundary, in the Early to Middle *triangularis* Zone, $EF_{(U)}$ and $EF_{(Cu)}$ reach 109 and 30, respectively.

In the recent literature (Hatch and Leventhal, 1992; Jones and Manning, 1994), V/Cr, V/(V+Ni), Ni/Co, and U/Th indices have been used to derive information on paleo-oxygenation in the depositional environment. The four ratios show similar trends of higher values in the dark-coloured Kellwasser samples relative to overlying and underlying strata (Figs. 4–7); the highest values were recorded in the basinal La Serre section. In addition, the distribution of the four redox indices seems to confirm the diachronism of positive peaks between platform and basin settings observed with the trace metal concentrations. In platform environments, maximal values are recorded in the Kellwasser horizons during Late Frasnian. In the distal La Serre section, the samples of the time-equivalent Upper Kellwasser horizon (*linguiformis* Zone) do not show peak values; the highest values are found within the C_{org}-rich facies in the Early Famennian Early *triangularis* Zone.

4.3. Summary

The stratigraphical variations of the redox indices U/Th, V/Cr, Ni/Co, and V/(V+Ni) as well as the trace element concentrations show consistent fluctuations in space and time. Firstly, in the basinal environment at La Serre, the EF of trace elements are always higher than those recorded in outer platforms. Thus, the magnitude of trace metal enrichments varies with respects to the depositional setting. Secondly, the redox indices and the trace element concentrations are the highest within the black Kellwasser intervals. Moreover, it is noteworthy that in each platform setting, where the two Kellwasser horizons are found, the Lower Kellwasser records a rapid shift toward the highest values for most geochemical indices, particularly in central Morocco, whereas the Upper Kellwasser horizon is marked by a minor but more durable enrichment. In basinal setting, where only one prolonged interval of Kellwasser facies deposition is recognized, the increases of the redox indices are not limited to Late Frasnian times and extends into the Famennian strata. In contrast to other trace elements, Ba enrichments seem to be limited to Late Frasnian in all studied sections, both in proximal and distal settings. The element abundance lowers immediately above the F–F boundary.

5. Interpretation

Illite Crystallinity Index Standard (CIS) obtained from clay mineral analyses (unpublished data), indicate that the investigated sections have been affected by a pronounced diagenesis, especially in Germany. Illite CIS ranges from 0.30 to 0.41, which correspond to a maximal temperature of 300°C (Han et al., 2000). Nevertheless, the correlative geochemical trends observed in different lithologies and distant sites suggest that primary environmental signals were not significantly altered by diagenetic overprint, except for the organic-carbon content. In addition, Mongenot et al. (1996) have shown that strong thermal evolution of an OM-rich formation does not alter the trace-metal distribution in a detectable way, even in the case of severe OM destruction.

5.1. Paleo-oxygenation

For each section, it is clear that the Kellwasser horizons are levels enriched in Mo, U, V, Cu, Cr, and Ni. These elements can be fixed in high amounts in sediments under reducing conditions (Brumsack, 1989; Hatch and Leventhal, 1992; Calvert and Pedersen, 1993). They may either be precipitated as autonomous sulphides, coprecipitated with iron sulphides, or bound to organic matter. Among the studied trace metals, V, U, and Mo are reputed as sensitive redox markers (a very large literature is devoted to the trace metals used as redox proxies, see Crusius et al., 1996; Helz et al., 1996; Dean et al., 1997; Zheng et al., 2000; Adelson et al., 2001; Lyons et al., 2003; Rimmer, 2004; Rimmer et al., 2004; Tribovillard et al., 2004a,b among recent papers with thorough presentations of these elements). At La Serre (distal setting), the enrichment in these elements is very strong, indicating the rapid development of reducing conditions in the sediments. Anoxia could have affected the water column itself as indicated by the ostracod fauna (Lethiers et al., 1998; Tribovillard et al., 2004a), which is in agreement with the high trace-element concentrations at La Serre. In outer platforms, where the increase of Al-normalized trace elements is obviously lower than in distal settings, the Kellwasser events seem to coincide with a period of oxygen decreasing, probably corresponding to dysoxic conditions only, and not to anoxic conditions. For instance, considering molybdenum abundance, the La Serre section shows much higher enrichments than the other sections studied. Following the papers by Helz et al. (1996), Zheng et al. (2000), Adelson et al. (2001), Vorlicek et al. (2002, 2004), and Lyons et al. (2003), it is currently admitted that Mo enrichment is tied to sulphidic conditions. It is inferred that, if sulphidic conditions unambiguously developed at La Serre, the depositional conditions for the other sections studied were probably no more severe than dysoxic.

Depositional conditions are assessed by cross-ploting of redox parameters V/Cr, V/(V+Ni), Ni/Co, and U/Th (Fig. 8). In this study, we use threshold values proposed by Hatch and Leventhal (1992) for V/(V+Ni) and by Jones and Manning (1994) for V/Cr, Ni/Co, and U/Th (Table 1). However, it must be kept in mind that these thresholds must be cautiously used because they were not specifically determined for Devonian environments, and thus the relative variations are of safer use. For each of the indices used, the Kellwasser samples show higher values and the data plot within the dysoxic and anoxic fields for proximal sections. In platform settings U/Th values indicate predominantly anoxic conditions for the dark-coloured horizons and oxic conditions below, between, and above the

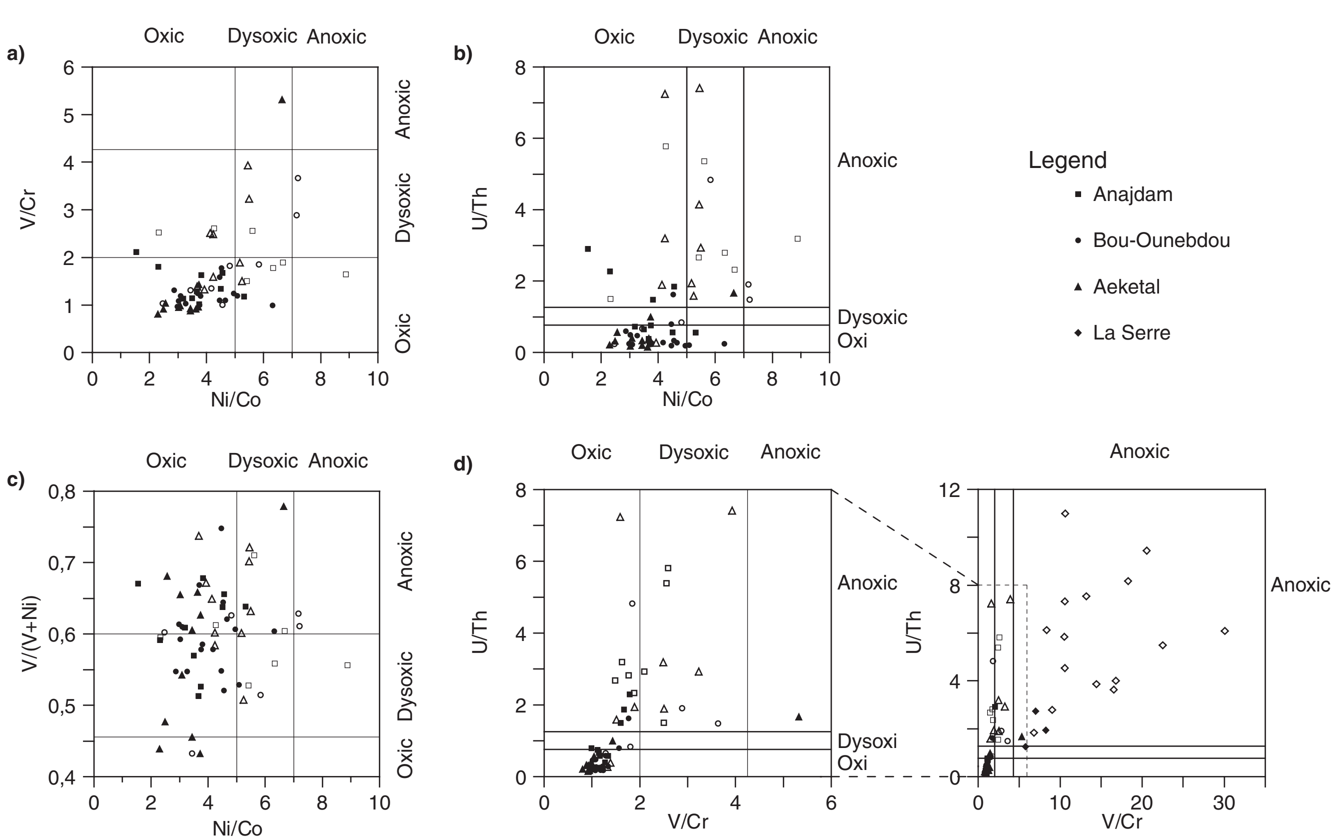

Figure 8. Crossplots of trace-elements ratios used as paleoredox proxies. (a) V/Cr vs. Ni/Co, (b) U/Th vs. Ni/Co, (c) V/(V+Ni) vs. Ni/Co, and (d) U/Th vs. V/Cr. Ranges for V/Cr, U/Th, and Ni/Co are from Jones and Manning (1994); ranges for V/(V+Ni) are from Hatch and Leventhal (1992). Ni concentrations not available for the La Serre section. Open symbols: Kellwasser samples.

Table 1. Summary of correlations between trace element ratio values and redox zones.

	Oxic zone (8.0–2.0 mlO_2/l)	Dysoxic zone (2.0–0.2 mlO_2/l)	Anoxic zone (0.0 mlO_2/l)
U/Th[a]	<0.75	0.75–1.25	>1.25
V/Cr[a]	<2.00	2.00–4.25	>4.25
Ni/Co[a]	<5.00	5.00–7.00	>7.00
V/V+Ni[b]	<0.46	0.46–0.60	0.54–0.82

[a] Jones and Manning (1994).
[b] Hatch and Leventhal (1992).
Note : Bottom water oxygen levels from Tyson and Pearson, (1991).

Kellwasser levels. The V/Cr and Ni/Co ratio indicate oxic to dysoxic conditions for the Kellwasser interval and oxic conditions elsewhere. V/(V+Ni) ratio does not show clear distinctions between the two Kellwasser horizons and the other beds. Dysoxic to anoxic conditions for all sequences are suggested by V/(V+Ni) ratio. The chemical data indicate two pulses of bottom water dysoxia, coeval with the Kellwasser horizons in platform environments. Conversely, in the basinal La Serre section, the highest values of V/Cr and U/Th indicate that reducing conditions were more pronounced in deeper settings of the Gondwanan margins and anoxia was not limited to the Late Frasnian, but extended into the Early Famennian (*crepida* Zone; see also Tribovillard et al., 2004a). Thus, it clearly appears that the intensity and duration of bottom water oxygen depletion varied according to the paleodepth of deposition. Our data are in agreement with published ones concerning other F–F boundary sequences. In subpolar Ural area, Yudina et al. (2002) documented dysoxic conditions from the Early *rhenana* Zone to the Late *triangularis* Zone with a euxinic pulse in the Late *linguiformis* Zone. In Germany, the Steinbruch Benner section records two anoxic episodes in an otherwise well-oxygenated sequence (Bond et al., 2004), whereas in Poland, the basinal Kowala section records oxygen-depleted condition across the F–F boundary (Joachimski et al., 2001; Racki et al., 2002; Bond et al., 2004). In addition, Marynowski et al. (2000) and Joachimski et al. (2001) observed the presence of chlorobiacean pigment molecular markers at Kowala, an indication that anoxia rose into the photic zone.

5.2. Paleoproductivity

Ba/Al, as well as Ni/Al, Cu/Al, and Zn/Al, shows noticeable variations from the Late Frasnian to Early Famennian. The distribution of dissolved Ba in the ocean appears to be related to biological production in surface water as Ba is incorporated in photosynthetic organisms (Dymond et al., 1992; MacManus et al., 1998). During decay, Ba can be partly released and recycled. It is supplied to the sediment and preserved primarily in the form of barite ($BaSO_4$) (Dymond et al., 1992). Ba abundance is commonly used as a paleoproductivity markers even if the interpretation is not always straight forward because barite can be dissolved in case of intense sulphate-reduction (McManus et al., 1998; Jacot des Combes et al., 1999). In that case, Ba can be released to pore waters, migrate with them, and re-precipitate when less reducing conditions are met. Thus barite migration fronts are formed (e.g. McManus et al., 1998). The distribution of dissolved Ni, Cu, and Zn in the ocean appears to be related to settling organic debris, since Ni, Cu, and Zn behave as micronutrients (Calvert and Pedersen, 1993; Algeo and Maynard, 2004). These elements are readily adsorbed onto organic particles settling through the water column. So, decaying OM easily forms organo-metal complexes that can be incorporated to the sediment (Algeo and Maynard, 2004; Tribovillard et al., 2004b). Thus, these elements are usually trapped with organic particles and are incorporated into iron sulphides during diagenesis. Consequently, they are preserved in the sediment even in case of complete OM remineralisation as well as in the case of marked thermal evolution (Mongenot et al., 1996). Thus, Ni, Cu, and Zn serve as indicators of organic inputs (Tribovillard et al., 2000, 2004b), and, in the present case, Cu abundance is a better proxy to OM inputs than TOC.

The highest values of paleoproductivity (Ba) and OM input (Cu) tracers are recorded in the basinal sequence at La Serre. As said above, reducing conditions developed at La Serre. Consequently, Ba diagenetical release and migration can be suspected. It implies that the strong Ba enrichments can be interpreted as an indication that barite was brought to the sediment by increased export production, but Ba can have been moved and concentrated after deposition. The level the richest in Ba are not necessarily precisely those recording the highest productivity. However, the Ba and Cu enrichments are observed in the same strata. As Cu is not known to be moved during early diagenesis, the good Ba–Cu covariations are an indication that Ba content was probably not deeply affected by post-deposition migrations. An independent indication of marked productivity at La Serre is reported by Paris et al. (1996) who based their interpretation on chitinozoan overabundance. The enrichment of these productivity tracers is outstanding compared to platform environments. However, in the La Serre section and in less distal settings, the increased abundance of Ba, and Cu is limited to the Late Frasnian. Consequently, it may be thought that the Late Frasnian, more particularly the Kellwasser intervals, are characterized by a rise in productivity and by enhanced OM accumulation. These conclusions agree with results obtained from carbon isotopic signal by Joachimski et al. (1994, 2002) on the sections studied here. These data are illustrated with Figures 4 and 5. In the Bou-Ounebdou and Aeketal sections, as well as in other F–F boundary sections in many places (Australia, Austria, Canada, China, France, Germany, Poland, USA; Joachimski et al., 2002), two positive excursions of $\delta^{13}C_{carb}$ with amplitude of around 3.5% have been recorded (Figs. 4 and 5). In the two sections considered here, a first excursion starts just above the base of the Late *rhenana* Zone and coincides with the deposition of the Lower Kellwasser horizon. Between the two Kellwasser horizons, $\delta^{13}C_{carb}$ values decrease toward the pre-excursion background level. The second excursion occurs below the base of the Upper Kellwasser horizon. This increase in $\delta^{13}C_{carb}$ starts in the uppermost Late *rhenana* Zone at Bou-Ounebdou and at the base of the *linguiformis* Zone at Aeketal. In both sections, the maximum $\delta^{13}C_{carb}$ values are recorded several centimetres above the top of the Kellwasser horizons. Then, a gradual decrease toward lighter values is recorded in the *triangularis* Zone. The two Late Frasnian positive shifts in $\delta^{13}C$ are explained by an increase in the organic carbon burial rate (Joachimski et al., 2002). This phenomenon may be due to either better preservation of organic matter, as a consequence of reducing conditions, and/or high primary productivity. A productivity increase results from higher concentration of PO_4^{3-} and NO_3^- that are biolimiting nutrients, and possibly of iron (Martin, 1990; Falkowski et al., 1998). The nutrient supply can originate from recycling processes such as upwelling, basinal turnover, P regeneration from anoxic sediments (Ingall and Van Cappellen, 1990; Murphy et al., 2000a) or continental runoff (Peterhänsel and Pratt, 2001). Reactive iron can be also significantly brought by winds, e.g. as clay-mineral coatings.

The contrasting record of paleoproductivity between deep and shallower water settings may be explained by environmental conditions. Generally speaking, organic productivity on platforms may be high as a consequence of an enhanced nutrient flux from continental weathering and, possibly, upwelling, which may favour the onset of dysoxic conditions and OM burial (Tyson and Pearson, 1991). Nevertheless, higher oxygenation levels and sensitive sea-level fluctuations in proximal environments generally do not allow good accumulation and preservation of OM. Platform settings do not allow favourable conditions for OM burial, particularly during sea-level lowstands (see discussion about this aspect in Tyson and Pearson, 1991). In basins, where terrestrial inputs are lower, primary productivity was seemingly high during the Kellwasser interval. OM preservation was high due to a marked oxygen deficiency, in addition to high productivity and relatively reduced sedimentation rate.

To conclude, it seems that the record of primary production was potentially related to the depositional setting, with deep-water environments showing the highest record for water mass fertility (geochemical data and independent paleoecological data). The sediments have recorded productivity indications in conjunction with favourable, oxygen-deficient paleoenvironmental conditions affecting basinal settings. In all studied sections, pulses of recorded productivity seem to be limited to the Late Frasnian. Similar trends have been observed for the Polish and Ural sections (Racki et al., 2002; Yudina et al., 2002). There, the highest concentrations of productivity proxies are recorded below and within the F–F boundary strata.

6. Discussion

Numerous authors have postulated that the usually organic C-rich Kellwasser horizons resulted from enhanced preservation of OM (Buggisch, 1991; Joachimski et al., 1994, 2002), under O_2-depleted conditions and high primary productivity (this study; Paris et al., 1996; Racki, 1998, 1999; Racki et al., 2002; Filipiak, 2002; Giles et al., 2002; Murphy et al., 2000a), presumably linked to short-term transgressive–regressive pulses (Buggisch, 1991; Sandberg et al., 2002) and an incipient climate cooling (Copper, 1986). Primary productivity and thus levels of dissolved oxygen in marine domains are controlled by nutrient availability in surface waters. The nutrients can be delivered mainly by vertical convection currents during oceanic overturn and fluvial runoff, together with submarine hydrothermalism and volcanism. The respective contributions of these various environmental nutrient sources, which associate several transport processes (fluvial, eolian, marine currents), depend on geographic context and consequently may vary locally (Mutti and Hallock, 2003).

The onset of eutrophic (namely, rich in nutrients) conditions triggers enhanced marine production. A high rate of primary production increases the accumulation of organic matter and accelerates consumption of oxygen within the bottom water. On platforms, anoxia develops in the bottom water when the respiratory demands of heterotrophic activity, i.e., OM degradation mainly carried out by aerobic bacteria, exceeds the supply of dissolved oxygen derived from photosynthetic activity and exchanges with the atmosphere (Brasier, 1995). Other processes, such as thermohaline stratification and restricted lateral circulation in the deep-water column, are generally invoked to explain the development of anoxic conditions (Cruse and Lyons, 2004). From these observations, several hypotheses and models have been developed to explain the onset of eutrophication in surface water and the development of bottom water anoxia during the time slice encompassing the F–F boundary.

6.1. Anoxia

Late Devonian anaerobic environments are thought to have developed because of water stratification in basinal settings, that may have resulted from the formation of a halocline associated with repeated spills of warm, saline surface water generated by evaporation on sub-tropical platforms (Joachimski and Buggisch, 1993; Hallam and Wignall, 1997; Claeys et al., 1996; Marynowski et al., 2000; Joachimski et al., 2001). High evaporation rates caused an increase of water salinity, producing denser saline waters that subsequently sunk down and were carried to bottom waters in distal settings. Water stratification induced in turn bottom water anoxia. In modern shallow environments, water is usually mixed down to a depth of about 150–200 m by wind energy and diffusion, preventing the onset of water stratification and anoxia formation. In such conditions, the redox boundary or chemocline is situated at the sediment surface or, more frequently, within the sediment (the reader is referred to the articles of the volume edited by Tyson and Pearson, 1991). Consequently, most of OM is not accumulated in sediment because of aerobic degradation within the water column and at the sediment–water interface. Water stratification may take place in relatively shallow environments during sea-level rise, as it possibly occurred for the two Kellwasser events (e.g., Wignall and Newton, 2001). During transgression, former shallow continental areas were probably flooded, which increased the formation of warm, saline, and dense water masses by evaporation on sub-tropical platforms (Hallam and Wignall, 1997). The oxic–anoxic interface rose in the water column and previously well-oxygenated platform environments were covered by anoxic waters (Joachimski and Buggisch, 1993; Walliser, 1996). The lateral migration of oxygen-depleted water onto shelves in response to eustatic transgressions certainly led to reduced availability of ecological niches, potentially causing the death of nektobenthic organisms. In deeper, quiet water environments, water stagnation, density contrast, and thus anoxia, were relatively stable. Thus, reducing conditions could prevail in the basin depositional environments during F–F transition and could last until early Famennian (this study, Lethiers et al., 1998; Joachimski et al., 2001; Racki, 1998; Tribovillard et al., 2004a), whereas in platform environments, oxygen-depletion could develop only during the two pulses of sea-level rise corresponding to the Kellwasser horizons.

6.2. Nutrient recycling

Water stratification and anoxia were perhaps not permanent because of episodic oceanic turnover or stratification disruption (Wilde and Berry, 1984; Halas et al., 1992; Becker and House, 1994; Racki et al., 2002). Long-term water stratification and bottom water anoxia development could facilitate the preferential release of P and N from OM during carbon oxidation (Ingall and Jahnke, 1997; Murphy et al., 2000a). Another source of nutrients in bottom water may be hydrothermal megaplumes (Vogt, 1989). According to some authors (Racki, 1998, 1999; Racki et al., 2002; Yudina et al., 2002), Variscan submarine volcanic eruptions may have episodically released Fe, P, and other trace elements, such as V and Cr. Upon release, episodic water mixing would have brought nutrient-rich bottom waters up into the photic zone, establishing eutrophic conditions and stimulating temporarily phytoplankton productivity. The transfer of dissolved P from anoxic bottom water to ocean surface creates a positive feedback loop between high surface productivity, anoxia and P regeneration in bottom water (Ingall and Jahnke, 1997). Intensification of upwelling can be caused by changes in water circulation and by wind-stress, in response to climatic or sea-level variations. The incipient climatic cooling, which destabilized the greenhouse climate during the Late Devonian (Copper, 1986; Buggisch, 1991), favoured seasonality contrasts and the effectiveness and the frequency of water mixing increased (Sageman et al., 2003). During the Kellwasser events, deepening phases probably prevented mixing in bottom water and enhanced water stratification whereas the shallowing phases, recorded at the end of the dark-coloured horizons, would have increased stratification disruptions.

6.3. Terrestrial nutrient inputs

Based on isotopic C composition, Joachimski et al. (2001, 2002) suggest that upwelled nutrient-rich deep waters were not the only cause for eutrophication and that during the Kellwasser events, the productivity must have been stimulated by an enhanced input of continent-derived nutrient under greenhouse conditions (Algeo et al., 1995; Algeo and Scheckler, 1998; Joachimski et al., 2001; Girard and Lecuyer, 2002; Chen et al., 2002; Martin, 2003). Evidence of large-scale high continental input into the ocean is suggested by the strontium $^{87}Sr/^{86}Sr$ isotope signal (Veizer et al., 1997; Goddéris and Veizer, 2000), by the rare earth element distribution (Girard and Lécuyer, 2002), and by the distribution of the magnetic parameters of the formations that were deposited close to the paleo-reliefs (Devleeschouwer, 1999; Crick et al., 2002). Weathering of aluminosilicate rocks supplies nutrients and high continental weathering rates are controlled by enhanced humidity conditions and sea level falls (François et al., 1993; Royer et al., 2001; Berner and Kothavala, 2001). In addition, mountain uplift automatically enhances the erosion/weathering intensity and is thus considered to increase the nutrient flux to the seas independent of the sea-level fluctuations: Racki (1998), Gibbs et al. (1999), Peterhänsel and Pratt (2001), Tribovillard et al. (2004a), and Averbuch et al. (2005) suggest that tectonic activity must have been a factor enhancing long-term nutrient flux to the oceans at the Frasnian/Famennian boundary. Increases in seafloor spreading rates enhance volcanism and mountain building, and potentially control sea-level fluctuations (Racki, 1998). This mechanism would result in a higher supply of nutrients to shallow water environments. Volcanic activity is indicated by some bentonite layers, found between the two Kellwasser horizons at Steinbruch Schmidt (Germany) and in other localities (USA) (Tucker et al., 1998; Kaufmann et al., 2004). Volcanic ashes have a high fertilization potential. According to Racki et al. (2002) and Yudina et al. (2002), nutrients, supplied in Urals and Polish areas, resulted from replenishing by volcanism and hydrothermal activity. Variscan volcanism influence may not be excluded, particularly in the Laurussian margin as a nutrient source. However, the traces of volcanism remain relatively scarce. The onset and the acceleration of Ellesmerian–Eovariscan orogenic

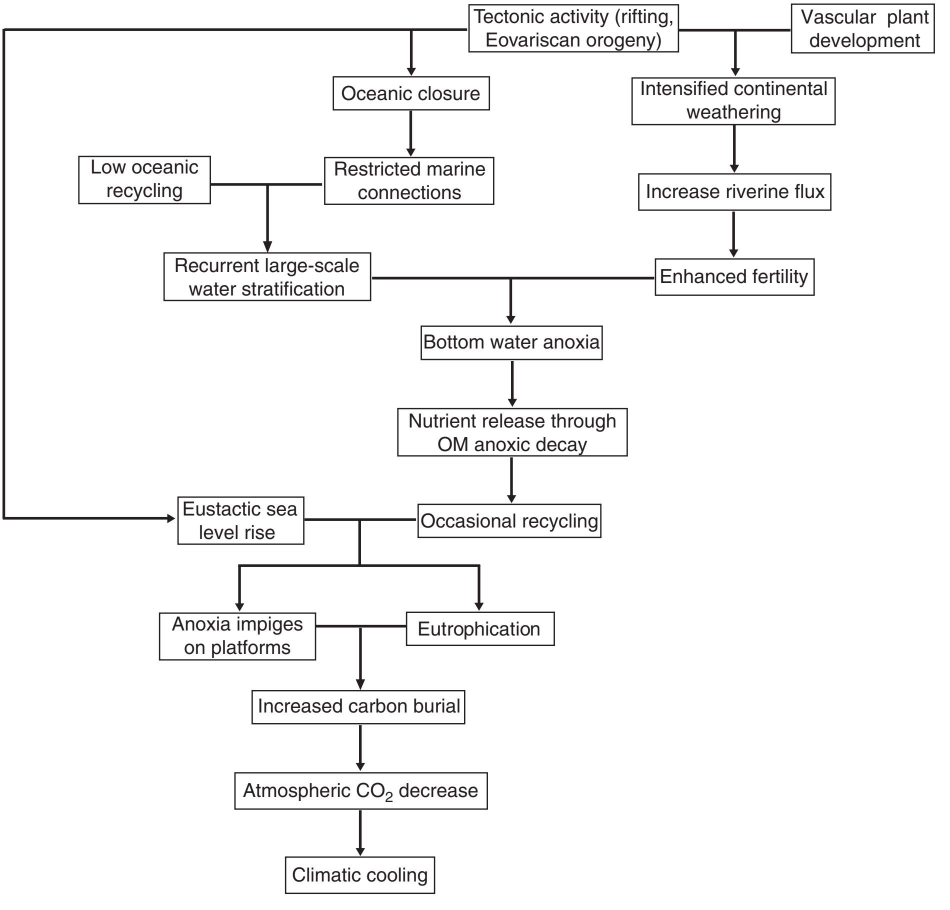

Figure 9. Flowchart illustrating possible links between several environmental processes during Late Devonian.

activities probably stimulated weathering on emerged landmasses. In addition, mountain building might modify atmospheric circulations and collision of Laurussia and northwestern Gondwana may cause changes in oceanic water circulations (Copper, 1986). Reduced circulation slows the ventilation of deep water.

Algeo et al. (1995) have proposed to link the enhanced continental weathering with the development of vascular land plants. Palaeobotanical innovations, i.e. arborescence, advanced roots systems as well as the seed habit, are believed to have led to an intensification of pedogenesis and enhanced chemical weathering by humic acid leaching (Retallack, 1997). The terrestrial nutrient hypothesis is interesting for long-term supply of continent-derived nutrients. Rejuvenation of continental rocks via repeated uplift associated with vascular plant development would ensure continued supply of nutrients in the Late Devonian.

Accompanying this long-term trend that can explain the long-term OM enrichment in basinal settings, the short-term Kellwasser events can be explained by two additional pulses of sea-level variation that would have allowed increased nutrient-cycling and thus anoxia to impinge on platforms and end with the deposition of the Kellwasser horizons (Fig. 9).

6.4. Climatic consequences

Silicate alteration, enhanced by large uplifting starting during Frasnian, and the burial of large quantities of OM by the end of Frasnian, resulting from high primary production and reducing conditions, stimulated CO_2-pumping. The decreased concentration of this greenhouse gas could have resulted in climatic cooling (Berner, 1997; Berner and Kothavala, 2001; Royer et al., 2001). Basing on conodont apatite $\delta^{18}O$ signatures, Joachimski and Buggisch (2002) proposed a temperature decrease of 5–7°C for tropical sea-surface during the Kellwasser horizons. The cooling of sea water, which could not be tolerated by many organisms has been postulated as a factor involved in the Kellwasser crisis (Copper, 1986). The extinction of the Late Frasnian carbonate-producing reef ecosystem may have reduced CO_2 concentration in surface water (Copper, 2002). The climatic cooling may have caused a sea-level fall, recorded at the end of the Kellwasser deposition that led to emergence of platform and reduction of ecological niches.

7. Conclusions

The geochemical study of four F–F boundary sections located on both sides of the Eovariscan belt shows that the depositional conditions of the Kellwasser horizons were strongly influenced by productivity and anoxia. The geographical distribution of the studied sections indicates that it was not just local conditions. In basinal environments of La Serre and Kowala, reducing conditions developed in a dominant, but probably not permanent manner, and these conditions extended into the early Famennian, at least to the *crepida* Zone. In platform settings (Aeketal, Anajdam, and Bou-Ounebdou), dysoxic–anoxic conditions developed only twice (Late *rhenana* and *linguiformis* zones). The oxygen-depleted conditions probably developed in response to sustained productivity, coupled to recurrent water stratification and possible reduction of sedimentation rates during sea-level rises. The pulse of productivity, recorded in the Late Frasnian, is interpreted as sustained primarily mostly by an increased land-derived nutrient flux, enhanced by the weathering of the incipient Eovariscan belt uplift. This primary nutrient input is probably reinforced by episodes of marine nutrient recycling. The ‘chain of reactions’ is illustrated with Figure 9. Lastly, it can be hypothesized that OM storage and atmospheric pCO_2 drawdown of the Late Devonian induced a global climate cooling culminating with Devonian glaciations.

Acknowledgements

We thank Nezha Lazreq, Catherine Crônier, Ivan Berra, Said Chakiri, and Alain Herbosh for their assistance during field work, Jacques Morel for the ICP-MS measurements at CRPG-CNRS (Vandœuvre-les-Nancy, France), and François Baudin for the Rock Eval pyrolysis. We thank Walter Dean and an anonymous reviewer who helped to improve this paper considerably. We thank D. Jeffrey Over for his comments and corrections. This is a contribution to the ‘Eclipse’ Program of the CNRS-INSU.

References

Adelson, J.M., Helz, G.R., Miller, C.V., 2001. Reconstructing the rise of recent coastal anoxia; molybdenum in Chesapeake Bay sediments. Geochim. Cosmochim. Acta 65, 237–252.

Algeo, T.J., Berner, R.A., Maynard, J.B., Scheckler, S.E., 1995. Late Devonian oceanic anoxic events and biotic crises: rooted in the evolution of vascular land plants? GSA Today 5, 64–66.

Algeo, T.J., Scheckler, S.E., 1998. Terrestrial-marine teleconnections in the Devonian: links between the evolution of land plants, weathering processes, and marine anoxic events. Philos. Trans. R. Soc. London, B 353, 113–130.

Algeo, T.J., Maynard, J.B., 2004. Trace-element behavior and redox facies in core shales of Upper Pennsylvanian Kansas-type cyclothems. Chem. Geol. 206, 289–318.

Arthur, M.A., Jenkyns, H.C., Brumsack, H.J., Schlanger, S.O., 1990. Stratigraphy, geochemistry, and paleoceanography of organic carbon-rich Cretaceous sequences. In: Ginsburg, R.N., Beaudoin, B. (Eds), Cretaceous Resources, Events and Rhythms. Kluwer Academic Publishing, Amsterdam, pp. 75–119.

Averbuch, O., Tribovillard, N., Devleeschouwer, X., Riquier, L., Mistiaen, B., van Vliet-Lanoë, B., 2005. Mountain building-enhanced continental weathering and organic carbon burial as major causes for climatic cooling at the Frasnian–Famennian boundary (ca 376 Ma BP). Terra Nova 17(1), pp. 33–42.

Becker, R.T., House, M.R., 1994. Kellwasser events and goniatite successions in the Devonian of Montagne Noire with comments on possible causations. Cour. Forsch. Inst. Senckenb. 169, 45–77.

Becker, R.T., House, M.R., 2000. Sedimentary and faunal succession of the allochtonous Upper Devonian at Gara d'Mrirt (Eastern Moroccan Meseta). Notes Mém. Serv. Géol. Maroc 399, 109–114.

Berner, R.A, 1997. The rise of plants and their effects on weathering and atmospheric CO_2. Science 276, 544–546.

Berner, R.A., Kothavala, Z., 2001. Geocarb III: a revised model of atmospheric CO_2 over Phanerozoic times. Am. J. Sci. 301, 182–204.

Bond, D., Wignall, P.B., Racki, G., 2004. Extent and duration of marine anoxia during the Frasnian–Famnennian (Late Devonian) mass extinction in Poland, Germany, Austria and France. Geol. Mag. 141, 173–193.

Brasier, M.D., 1995. Fossil indicators of nutrient levels. 1: Eutrophication and climate change. In: Bosence, D.W.J., Allison, P.A. (Eds), Marine palaeoenvironmental analysis from fossils. Geol. Soc. London Spec. Publ. 83, pp. 113–132.

Brumsack, H.J., 1989. Geochemistry of recent TOC-rich sediments from the Gulf of California and the Black Sea. Geol. Rundsch. 78, 851–882.

Buggisch, W., 1991. The global Frasnian–Famennian "Kellwasser Event". Geol. Rundsch. 80, 49–72.

Calvert, S.E., Pedersen, T.F., 1993. Geochemistry of recent oxic and anoxic marine sediments: implications for the geological record. Mar. Geol. 113, 67–88.

Caplan, M.L., Bustin, R.M., 1998. Paleoceanographic controls on geochemical characteristic of organic-rich Exshaw mudrocks: role of enhanced primary productivity. Org. Geochem. 30, 161–188.

Caplan, M.L., Bustin, R.M., 1999. Devonian–Carboniferous Hangenberg mass extinction event, widespread organic-rich mudrocks and anoxia: causes and consequences. Palaeogeogr. Palaeoclimatol. Palaeoecol. 149, 187–207.

Carignan, J., Hild, P., Morel, J., Yeghicheyan, D., 2001. Routine analyses of trace elements in geochemical samples using flow injection and low pressure on-line liquid chromatography coupled to ICP-MS: a study of geochemical reference materials BR, DR-N, UB-N, AN-G and GH. Geostand Newslett. 25, 187–198.

Chakiri, S., 2002. Sédimentologie et géodynamique du Maroc Central Hercynien pendant le Dévonien. Unpublished PhD thesis, Ibn Tofail University, Kenitra.

Chen, D., Tucker, M.E., Shen, Y., Yans, J., Préat, A., 2002. Carbon isotope excursions and sea-level change: implication for the Frasnian–Famennian biotic crisis. J. Geol. Soc. 159, 623–626.

Claeys, P., Kyte, F.T., Herbosch, A., Casier, J.-G., 1996. Geochemistry of the Frasnian–Famennian boundary in Belgium: mass extinction, anoxic oceans, and microtektite layer, but no much iridium? Geol. Soc. Am. Spec. Pap. 307, 491–504.

Copper, P., 1986. Frasnian/Famennian mass extinction and cold-water oceans. Geology 14, 835–839.

Copper, P., 2002. Reef development at the Frasnian–Famennian mass extinction boundary. Palaeogeogr. Palaeoclimatol. Palaeoecol. 181, 27–65.

Crick, R.E., Ellwood, B.B., Feist, R., El Hassani, A., Schindler, E., Dreesen, R., Over, D.J., Girard, C., 2002. Magnetostratigraphy susceptibility of the Frasnian/Famennian boundary. Palaeogeography, Palaeoclimatology, Palaeoecology, 181, 67–90.

Cruse, A.M., Lyons, T.W., 2004. Trace metal records of regional paleoenvironmental variability in Pennsylvanian (Upper Carboniferous) black shales. Chem. Geol. 206, 319–345.

Crusius, J., Calvert, S., Pedersen, T., Sage, D., 1996. Rhenium and molybdenium enrichments in sediments as indicators of oxic, suboxic, and sulfidic conditions of deposition. Earth Planet. Sci. Let. 145, 65–78.

Dean, W.E., Gardner, J.V., Piper, D.Z., 1997. Inorganic geochemical indicators of glacial-interglacial changes in productivity and anoxia on the California continental margin. Geochim. Cosmochim. Acta 61, 4507–4518.

Devleeschouwer, X., 1999. La transition Frasnien/Famennien (Dévonien sup.) en Europe : sédimentologie, stratigraphie séquentielle et susceptibilité magnétique. Unpublished PhD thesis, FreeUniversity, Brussels.

Dymond, J., Suess, E., Lyle, M., 1992. Baryum in deep-sea sediments: a geochemical proxy for paleoproductivity. Paleoceanography 7, 163–181.

El Hassani, A., Tahiri, A., 1999. Excursion guide book. Sub-commission Devonain Stratigraphy- IGCP 421 Morrocco Meeting. April-Mai – Rabat-Errachidia, 160 pp.

Falkowski, P.G., *Barber*, R.T., Smetacek, V., 1998, Biogeochemical controls and feedbacks on ocean primary production. *Science* 281**,** 200–206.

Feist, R., 1985. Devonian stratigraphy of the South-eastern Montagne Noire (France). Cour. Forsch. Inst. Senckenb. 75, 331–352.

Feist, R., 1990. The Frasnian–Famennian boundary and adjacent strata of the eastern Montagne noire, France, IUGS Subcommission on Devonian Stratigraphy, Field Meeting 1990, Guide Book. Montpellier, 69 pp.

Feist, R., 2002. Montagne Noire 25–28 June 2002.–IGCP 421: North Gondwana mid-Paleozoic biodynamics and ECOS VIII: 8th European Conodont Symposium—Guidebook of the Field Excursion. Institut des Sciences de l'Evolution, University of Montpellier II, Montpellier, pp. 1–85.

Feist, R., Schindler, E., 1994. Trilobites during the Frasnian Kellwasser Crisis in European Late Devonian cephalopod limestones. Cour. Forschung. Inst. Senckenb. 169, 195–223.

Filipiak, P., 2002. Palynofacies around the Frasnian–Famennian boundary in the Holy Cross Mountains, southern Poland. Palaeogeogr,. Palaeoclimatol., Palaeoecol. 181, 313–324.

François, L., Walker, J.C.G., Opdyke, B.N., 1993. The history of global weathering and the chemical evolution of the ocean-atmosphere system. Geophys. Monogr. 74, vol.14, 143–159.

Gibbs, M.T., Bluth, G.J., Fawcett, P.J., Kump, L.R., 1999. Global chemical erosion over the last 250 My: variations due to changes in paleogeography, paleoclimate and paleogeology. Am. J. Sci. 299, 611–651.

Giles, K.A., McMillan, N.J., McCarson, B.L., 2002. Geochemical analysis and paleoecological implications of phosphatic microspherules (otoliths?) from Frasnian–Famennian boundary strata in the Great Basin, USA. Palaeogeogr. Palaeoclimatol. Palaeoecol. 181, 111–125.

Girard, C., Albarède, F., 1996. Trace elements in conodont phosphate from the Frasnian/Famennian boundary. Palaeogeogr. Palaeoclimatol. Palaeoecol. 126, 195–209.

Girard, C., Lécuyer, C., 2002. Variations in Ce anomalies of conodonts through the Frasnian–Famennian boundary of Poland (Kowala – Holy Cross Mountains): implications for the redox state of seawater and biodiversity. Palaeogeogr. Palaeoclimatol. Palaeoecol. 181, 299–311.

Goddéris, Y., Veizer, J., 2000. Tectonic control of chemical and isotopic composition of ancient oceans: the impact of continental growth. American Journal of Science, 200, 434–461.

Godderis and Veizer, as well as Crick et al, are not in the reference list.

Here are the complete references:

Goddéris Y., Veizer J., 2000. Tectonic control of chemical and isotopic composition of ancient oceans: the impact of continental growth. American Journal of Science, 200, 434-461.

Halas, S., Balinski, A., Gruszczynski, M., Hoffman, A., Malkowski, K., Narkiewicz, M., 1992. Stable isotope record at the Frasnian/Famennian boundary in southern Poland. N. Jb. Geol. Paläontol. Mh. 3, 129–138.

Hallam, A., Wignall, P.B., 1997. Mass extinctions and sea-level changes. Earth. Sci. Rev. 48, 217–250.

Han, G., Preat, A., Chamley, H, Deconinck, J.-F., Mansy, J.-L., 2000. Palaeozoic clay mineral sedimentation and diagenesis in the Dinant and Avesnes Basins (Belgium, France): relationships with Variscan tectonism. Sed. Geol. 136, 217–238.

Hatch, J.R., Leventhal, J.S., 1992. Relationship between inferred redox potential of the depositional environment and geochemistry of the Upper Pennsylvanian (Missourian) Stark Shale Member of the Dennis Limestone, Wabaunsee County, Kansas, U.S.A. Chem. Geol. 99, 65–82.

Helz, G.R., Miller, C.V., Charnock, J.M., Mosselmans, J.L.W., Pattrick, R.A.D., Garner, C.D., Vaughan, D.J., 1996. Mechanisms of molybdenum removal from the sea and its concentration in black shales: EXAFS evidences. Geochim. Cosmochim. Acta 60, 3631–3642.

House, M.R., 2002. Strength, timing, setting and cause of mid-Palaeozoic extinctions. Palaeogeogr. Palaeoclimatol. Palaeoecol. 181, 5–25.

Ingall, E.D., Van Cappellen, P., 1990. Relation between sedimentation rate and burial of organic phosphorus and organic carbon in marine sediments. Geochim. Cosmochim. Acta 54, 1219–1234.

Ingall, E., Jahnke, R., 1997. Influence of water-column anoxia on the elemental fractionation of carbon and phosphorus during diagenesis. Mar. Geol. 139, 219–229.

Jacot des Combes, H., Caulet, J. – P., Tribovillard N., 1999. Pelagic productivity changes in the equatorial area of the NW Indian Ocean during the last 400 kyr. Mar. Geol. 158, 27–55.

Joachimski, M.M., Buggisch, W., 1993. Anoxic events in the late Frasnian – Causes of the Frasnian–Famennian faunal crisis? Geology 21, 675–678.

Joachimski, M.M., Buggisch, W., 2002. Conodont apatite $\delta^{18}O$ signatures indicate climatic cooling as a trigger of the Late Devonian mass extinction. Geology 30, 711–714.

Joachimski, M.M., Buggisch, W., Anders, T., 1994. Mikrofazies, Conodontenstratigraphie und Isotopengeochimie des Frasne/Famenne Grenzprofils Wolayer Gletscher (Karnische Alpen). Abh. Geol. Bundesanst. Wien 50, 183–195.

Joachimski, M.M., Ostertag-Henning, C., Pancost, R.D., Strauss H., Freeman, K.H., Littke, R., Sinninghe Damsté, J.S., Racki, G., 2001. Water column anoxia, enhanced productivity and concomitant changes in ^{13}C and ^{34}S across the Frasnian–Famennian boundary (Kowala Holy Cross Mountains/Poland). Chem. Geol. 175, 109–131.

Joachimski, M.M., Pancost, R.D., Freeman, K.H., Ostertag-Henning, C., Buggisch, W., 2002. Carbon isotope geochemistry of the Frasnian–Famennian transition. Palaeogeogr. Palaeoclimatol. Palaeoecol. 181, 91–109.

Jones, B., Manning, D.A.C., 1994. Comparison of geochemical indices used for the interpretation of palaeoredox conditions in ancient mudstones. Chem. Geol. 111, 111–129.

Kaufmann, B., Trapp, E., Mezger, K., 2004. The numerical age of the Late Frasnian (Late Devonian) Kellwasser horizons – a new U-Pb zircon date from Steinbruch Schmidt (Kellerwald, Germany). J. Geol. 112, 495–501.

Lazreq, N., 1992. The upper Devonian of M'rirt (Morocco). Cour. Forsch. Inst. Senckenb. 154, 107–123.

Lazreq, N., 1999. Biostratigraphie des conodontes du Givétien au Famennien du Maroc Central. Biofaciès et événement Kellwasser. Cour. Forsch. Inst. Senckenb. 214, 1–111.

Lethiers, F., Baudin, F., Casier, J.-G., 1998. Ostracodes de la limite Frasnien–Famennien en environnement anoxique (La Serre, Montagne Noire, France). Rev. Micropal. 41, 321–336.

Lyons, T.W., Werne, J.P., Hollander, D.J., Murray, R.W., 2003. Contrasting sulfur geochemistry and Fe/Al and Mo/Al ratios across the last oxic-to-anoxic transition in the Cariaco Basin, Venezuela. Chem. Geol. 195, 131–157.

McGhee, G.R., 1989. The Frasnian–Famennian event. In: Donovan, S.K. (Eds), Mass Extinction: Processes and Evidences. Belhaven Press, London, pp. 133–151.

McGhee, G.R., 1996. The Late Devonian Mass Extinction. The Frasnian–Famennian Crisis. Columbia University Press, New York.

McManus, J., Berelson, W.M., Klinkhammer, G.P., Johnson, K.S., Coale, K.H., Anderson, R.F., Kumar, N., Burdige, D.J., Hammond, D.E., Brumsack, H.-J., McCorkle, D.C., Rushdi, A., 1998. Geochemistry of barium in marine sediments: implications for its use as a paleoproxy. Geochim. Cosmochim. Acta 62, 3453–3473.

Martin, J.H., 1990. Glacial–interglacial CO_2 change: the iron hypothesis. Paleoceanography 5, 1–13.

Martin, R.E., 2003. The fossil record of biodiversity: nutrients, productivity, habitat area and differential preservation. Lethaia 36, 179–194.

Marynowski, L., Narkiewicz, M., Grelowski, C., 2000. Biomarkers as environmental indicators in a carbonate complex, example from the Middle to Upper Devonian, Holy Cross Mountains, Poland. Sediment. Geol. 137, 187–212.

May, A., 1995. Relationship among sea-level fluctuation, biogeography and bioevents of the Devonian: an attempt to approach a powerful, but simple model for complex long-range control of biotic crises. Geolines 3, 38–49.

Mongenot, T., Tribovillard, N.-P., Desprairies, A., Lallier-Vergès, E., Laggoun-Defarge, F., 1996. Trace elements as palaeoenvironmental markers in strongly mature hydrocarbon source rocks: the Cretaceous La Luna Formation of Venezuela. Sediment. Geol. 103, 23–37.

Murphy, A.E., Sageman, B.B., Hollander, D.J., 2000a. Eutrophication by decoupling of the marine biogeochemical cycles of C, N and P: a mechanism for the Late Devonian mass extinction. Geology 28, 427–430.

Murphy, A.E., Sageman, B.B., Hollander, D.J., Lyons, T.L., Brett, C.E., 2000b. Black shale deposition and faunal overturn in the Devonian Appalachian Basin: clastic starvation, seasonal water-column mixing, and efficient biolimiting nutrient recycling. Paleoceanography 15, 280–291.

Mutti, M., Hallock, P., 2003. Carbonate systems along nutrient and temperature gradients: some sedimentological and geochemical constraints. Int. J. Earth Sci. 92, 465–475.

Paris, F., Girard, C., Feist, R., Winchester-Seeto, T., 1996. Chitinozoan bio-event in the Frasnian–Famennian boundary beds at La Serre (Montagne Noire, Southern France). Palaeogeogr. Palaeoclimatol. Palaeoecol. 121, 131–145.

Peterhansel, A., Pratt, B.R., 2001. Nutrient-triggered bioerosion on a giant carbonate platform masking the post-extinction Famennian benthic community. Geology 29, 1079–1082.

Pratt, L.M., Claypool, G.E., King, J.D., 1986. Geochemical imprint of depositional conditions on organic matter in laminated-bioturbated interbeds from fine-grained marine sequences. Mar. Geol. 70, 67–84.

Racki, G., 1998. Frasnian–Famennian biotic crisis: undervalued tectonic control? Palaeogeogr. Palaeoclimatol. Palaeoecol. 141, 177–198.

Racki, G., 1999. Silica-secreting biota and mass extinctions: survival patterns and processes. Palaeogeogr. Palaeoclimatol. Palaeoecol. 154, 107–132.

Racki, G., Racka, M, Matyja, H., Devleeschouwer, X., 2002. The Frasnian/Famennian boundary interval in the South Polish-Moravian shelf basins: integrated event-stratigraphical approach. Palaeogeogr. Palaeoclimatol. Palaeoecol. 181, 251–297.

Retallack, C.J., 1997. Early forest soils and their role in Devonian global change. Science 276, 583–585.

Rimmer, S.M., Thompson, J.A., Goodnight, S.A., Robl, T.L., 2004. Multiple controls on the preservation of organic matter in Devonian–Mississippian marine black shales: geochemical and petrographic evidence. Palaeogeogr., Palaeoclimatol., Palaeoecol. 215, 125–154

Rimmer, S.M., 2004. Geochemical paleoredox indicators in Devonian–Mississippian black shales, Central Appalachian Basin (USA). Chem. Geol. 206, 373–391.

Royer, D.L., Berner, R.A., Beerling, D.J., 2001. Phanerozoic atmospheric CO_2 change: evaluating geochemical and paleobiological approaches. Earth-Sci. Rev. 54, 349–392.

Sageman, B.B., Murphy, A.E., Werne, J.P., Ver Straeten, C.A., Hollander, D.J., Lyons, T.W., 2003. A tale of shales: the relative roles of production, decomposition, and dilution in the accumulation of organic-rich strata, Middle-Upper Devonian, Appalachian basin. Chem. Geol. 195, 229–273.

Sandberg, C.A., Poole, F., Johnson, J.G., 1989. Upper Devonian of the western United States. In: McMillan, N.J., Embry, A.F., Glass, D.J. (Eds), Devonian of the World, Vol. I. Regional Syntheses, Proceedings of the 2nd International Symposium on the Devonian System, Calcary, Canada. Can. Soc Petrol. Geol. pp. 183–220 (imprinted 1988).

Sandberg, C.A., Morrow, J.R., Ziegler, W., 2002. Late Devonian sea level changes, catastrophic events and mass extinctions. Geol. Soc. Amer. Spec. Pap. 356, 473–487.

Schindler, E., 1990. Die Kellwasser Krise (hohe Frasne-Stufe, Ober Devon). Gött. Arb. Geol. Paläeontol. 46 1–125.

Schindler, E., 1993. Event-stratigraphic markers within the Kellwasser Crisis near the Frasnian/Famennian boundary (Upper Devonian) in Germany. Palaeogeogr. Palaeoclimatol. Palaeoecol. 104, 115–125.

Sepkoski, J.J., 1986. Phanerozoic overview of mass extinctions. In: Raup, D.M., Jablonski, D. (Eds). Patterns and Processes in the History of Life. Springer, Berlin, pp. 277–295.

Streel, M., Caputo, M.V., Loboziak, S., Melo, J.H.G., 2000. Late Frasnian–Famennian climates based on palynomorph analyses and the question of the Late Devonian glaciations. Earth-Sci. Rev. 52, 121–173.

Tribovillard, N., Desprairies, A., Lallier-Vergès, E., Bertrand, P., Moureau, N., Ramdani, A., Ramanampisoa, L., 1994. Geochemical study of organic-matter rich cycles from the Kimmeridge clay formation of Yorkshire (UK): productivity versus anoxia. Palaeogeogr. Palaeoclimatol. Palaeoecol. 108, 165–181.

Tribovillard, N., Dupuis, C., Robin, E., 2000. Sedimentological and diagenetical conditions of the impact level of the Cretaceous/Tertiary boundary in Tunisia: no anoxia required. Bull. Soc. Géol. Fr. 171, 629–636.

Tribovillard, N., Averbuch, O., Devleeschouwer, X., Racki, G., Riboulleau, A., 2004a. Deepwater anoxia at the Frasnian–Famennian boundary (La Serre, France): a tectonically-induced Late Devonian oceanic anoxic event? Terra Nova, 16, 288–295.

Tribovillard, N., Ramdani, A., Trentesaux, A., 2004b. Controls on organic accumulation in Late Jurassic shales of Northwestern Europe as inferred from trace-metal geochemistry. In: Harris, N. (ed.), The Deposition of Organic-Carbon-Rich Sediments: Models, Mechanisms, and Consequences. SEPM Spec. Public., 82, 145–164.

Tucker, R.D., Bradley, D.C., Ver Straeten, C.A., Harris, A.G., Ebert, J.R., Mc Cutcheon, S.R., 1998. New U-Pb zircon ages and the duration and division of Devonian time. Earth Planet. Sc. Lett. 158, 175–186.

Tyson, R.V., Pearson, T.H., 1991. Modern and ancient continental shelf anoxia: an overview. In: Tyson, R.V., Pearson, T.H. (Eds), Modern and Ancient Continental Shelf Anoxia. Spec. Publ. Geol. Soc. 58, pp. 1–24.

Tyson, R.V., Pearson, T.H., 1991. Modern and ancient continental shelf anoxia. Geol. Soc. Spec. Publ.58, p. 470.

Veizer, J., Buhl, D., Diener, A., Ebneth, S., Podlaha, O.G., Bruckschen, P., Jasper, T., Korte, C., Schaaf, M., Ala, D., Azmy, K., 1997. Strontium isotope stratigraphy: potential resolution and event correlation. Palaeogeogr. Palaeoclimatol. Palaeoecol. 132, 65–77.

Vogt, P.R.,1989.Volcanogenic upwelling of anoxic, nutrient-rich water: a possible factor in carbonate-bank/reef demise and benthic faunal extinction? Geol. Soc. Am. Bull. 101, 1225–1245.

Vorlicek, T.P., Helz, G.R., 2002. Catalysis by mineral surfaces: implications for Mo geochemistry in anoxic environments. Geochim. Cosmochim. Acta 66, 3679–3692.

Vorlicek, T.P., Kahn, M.D., Kasuza, Y., Helz, G.R., 2004. Capture of molybdenum in pyrite-forming sediments: role of ligand-induced reduction by polysulfides. Geochim. Cosmochim. Acta 68, 547–556.

Walliser, O.H., 1996. Global events and event stratigraphy in the Phanerozoic: results of international interdisciplinary cooperation in the IGCP Project 216 “Global Biological Events in Earth History”: Springer, Heidelberg, p. 333.

Walliser, O.H., El Hassani, H., Tahiri, A., 2000. Mrirt: a key area for the Variscan Meseta of Morocco. Notes Mém. Serv. Géol. Maroc 399, 93–108.

Wedepohl, K.H., 1971. Environmental influences on the chemical composition of shales and clays. In: Ahrens, L.H., Press, F., Runcorn, S.K., Urey, H.C. (Eds), Physics and chemistry of the Earth, Pergamon, Oxford, pp. 305–333.

Wedepohl, K.H., 1991. The composition of the upper Earth’s crust and the natural cycles of selected metals. In: Merian, E. (Ed.), Metals and their Compounds in the Environment, VCH-Verlagsgesellschaft, Weinheim, pp. 3–17.

Wendt, J., Belka, Z., 1991. Age and depositional environment of Upper Devonian (Early Frasnian to Early Famennian) black shales and limestones (Kellwasser Facies) in the eastern Anti-Atlas, Morocco. Facies, 25, 51–90.

Wignall, P.B., Newton, R., 2001. Black shales on the basin margin: a model based on examples from the Upper Jurassic of the Boulonnais, northern France. Sedim. Geol. 144, 335–356.

Wilde, P., Berry, W.B.N., 1984. Destabilization of the oceanic density structure and its significance to marine “extinction” events. Palaeogeogr. Palaeoclimatol. Palaeoecol. 48, 143–162.

Yudina, A.B., Racki, G., Savage, N.S., Racka, M., Malkowski, K., 2002. The Frasnian–Famennian events in deep-shelf succession, Subpolar Urals: biotic, depositional and geochemical records. Acta Palaeontol. Pol. 47, 355–372.

Zheng, Y., Anderson, R.F., van Geen, A., Kuwabara, J., 2000. Authigenic molybdenium formation in marine sediments: a link to pore water sulfide in the Santa Barbara Basin. Geochim. Cosmochim. Acta 64, 4165–4178.

Article 15.

Riquier L., Tribovillard N., Averbuch O., Devleeschouwer X. and Riboulleau A. (2006). The Late Frasnian Kellwasser horizons of the Harz mountains (Germany) : two oxygen-deficient periods resulting from contrasting mechanism. Chemical Geology, 233, 137-155.

Chemical Geology 233 (2006) 137 – 155

CHEMICAL GEOLOGY
INCLUDING
ISOTOPE GEOSCIENCE

www.elsevier.com/locate/chemgeo

The Late Frasnian Kellwasser horizons of the Harz Mountains (Germany): Two oxygen-deficient periods resulting from different mechanisms

Laurent Riquier [a,*], Nicolas Tribovillard [a], Olivier Averbuch [a], Xavier Devleeschouwer [b], Armelle Riboulleau [a]

[a] *Laboratoire des Processus et Bilans des Domaines Sédimentaires, CNRS UMR 8110 and FR 1818, Université Lille 1, bâtiment SN5, F-59655 Villeneuve d'Ascq cedex, France*

[b] *Royal Belgian Institute of Natural Sciences, Dpt VII: Geological Survey of Belgium, Rue Jenner 13, B-1000 Brussels, Belgium*

Received 1 September 2005; received in revised form 10 February 2006; accepted 20 February 2006

Abstract

In the Harz Mountains (Germany), three Late Devonian sections, Aeketal, Hühnertal and Kellwassertal, were analyzed for major- and trace-element concentration. The inorganic geochemical data were used to determine the environmental conditions, associated with the deposition of the two Late Frasnian black Kellwasser horizons in a submarine-rise environment. Low Ti/Al and Zr/Al values and slight enrichment in nutrient- and organic matter-related trace elements (e.g., Ba, Cu, and Ni) suggest that the Kellwasser horizons were deposited during two periods of minimum detrital input but relatively elevated primary production. Enrichments in U, V, and Mo in both black Kellwasser horizons and values of redox indices, including U/Th, V/Cr, and Ni/Co, indicate oxygen-restricted conditions prevailed during the Late Frasnian times. Under oxygen-depleted conditions, reductive diagenesis caused precipitation of iron sulphides, such as pyrite, that are observed with SEM. However, variations in major and trace element concentrations are not similar in the two Kellwasser horizons, particularly regarding redox markers. The Lower Kellwasser horizon seems to be more O_2-depleted than the Upper Kellwasser horizon in some German sections.

On the basis of these results, we propose that the two Kellwasser horizons are not caused by identical conditions. The Lower Kellwasser horizon results from increased primary productivity, enhanced by land-derived nutrient-loading and which triggered the anoxic conditions recorded in drowned platform setting. In contrast, the Upper Kellwasser horizon results from the onset of oxygen-impoverished bottom water in the deepest part of the ocean, due to episodic water stratification during maximum Frasnian flooding. Oxygen-depleted water may have impinged shallower environment during the *linguiformis* transgressive pulse. Nutrients would have been released from organic matter decay under reducing conditions and brought up to the photic zone during episodic water mixing.

Keywords: Late Frasnian; Kellwasser horizons; Harz mountains; Trace metals; Anoxia; Productivity; Pyrite

1. Introduction

The well-known Late Frasnian Kellwasser (KW) horizons are two black, bituminous decimetre-thick

* Corresponding author. Fax: +33 3 20 43 49 10.
E-mail address: Laurent.Riquier@univ-lille1.fr (L. Riquier).

0009-2541/$ - see front matter © 2006 Elsevier B.V. All rights reserved.
doi:10.1016/j.chemgeo.2006.02.021

sequences relatively rich in carbonate (shale-limestone facies) (e.g., Buggisch and Clausen, 1972; Schindler, 1990; Buggisch, 1991; Walliser, 1996). They are well exposed in the Harz Mountains area (Germany), where they were first described in 1850 by Roemer. They are frequently interpreted as resulting from episodes of increased organic-matter (OM) preservation and burial (e.g., Buggisch, 1991; Joachimski et al., 1994, 2002). Coeval with the Frasnian–Famennian (F–F) mass extinction event (Sepkoski, 1986; Copper, 1986; McGhee, 1989, 1996; Hallam and Wignall, 1997; House, 2002), these black horizons have also been observed in numerous shelfal- to basinal settings in North America, Europe, North Africa and South China (e.g., Feist, 1985; Wendt and Belka, 1991; Lazreq, 1992; Ettensohn, 1998; Lazreq, 1999; Yudina et al., 2002; Chen et al., 2005).

To explain the coeval occurrence of black facies and a decrease in biodiversity, several causes have been proposed (Joachimski and Buggisch, 1993; Becker and House, 1994; Algeo et al., 1995; Racki, 1998; Caplan and Bustin, 1999; Murphy et al., 2000a; Joachimski and Buggisch, 2002; Godderis and Joachimski, 2004). The formation of black sedimentary facies is commonly thought to be mainly controlled by oxygen (O_2) level in bottom waters and nutrient concentration in surface water. They may result from either (1) improved preservation of organic matter (OM) due to onset of an anoxic water column (preservation model of Demaison and Moore, 1980), or (2) increased marine production, induced by enhanced inputs of nutrients (productivity model of Pedersen and Calvert, 1990); the nutrients may be either delivered with the terrestrial run-off or recycled in situ (e.g., by up-welling or anoxia-induced benthic regeneration of P; see Ingall and Jahnke, 1997; Murphy et al., 2000a). According to the model considered, anoxic conditions are either a consequence or a cause of enrichment in OM. In the last decades, it has been documented that other factors, such as the clastic influx of terrigenous elements, linked to sea-level fluctuations and/or climatic conditions, or oceanic circulation, may also influence the formation of these peculiar facies (Arthur and Sageman, 1994; Murphy et al., 2000a,b; Joachimski et al., 2002; Sageman et al., 2003; Joachimski et al., 2004; Arthur and Sageman, 2004; Tribovillard et al., 2004b; Averbuch et al., 2005; Riquier et al., 2005).

In this paper, we present the results obtained for three sections of the Harz Mountains area, exposing the two KW horizons, based on inorganic geochemistry. Elemental concentrations (major and trace elements) have been measured in order to evaluate the fluctuations in bottom-water O_2 level, sea-surface primary productivity and detrital inputs in the marine environments at the F–F boundary along the south Laurussian margin. These data have been complemented by scanning electron microscopy (SEM) observations on polished thin sections that particularly focused on the morphologies and sizes of iron sulphide minerals. The implications of these results for the formation of the KW horizons will be considered at both local and regional scales to assess (1) the possible consequences of early diagenetic perturbations on the depositional record, and (2) possible models concerning the extensive development of black facies during Late Devonian times.

2. Geological background

The Harz Mountains are some of the main outcropping Palaeozoic massifs of northern Germany. They form part of the Rheno-Hercynian fold Belt of the German Variscides. This foreland belt evolved from a rifted passive continental margin during the Early Devonian to an orogenic belt in Upper Carboniferous times (e.g., Franke, 2000). During the Late Devonian, the Harz Mountains were located along the southern border of the Laurussian continent, close to the equator (around 15°S according to paleogeographical reconstructions, Golonka et al., 1994; Scotese, 1997; Averbuch et al., 2005). Sedimentation occurred on the gently subsiding northern passive margin of the Lizard-Rhenohercynian Ocean (e.g., Franke, 2000) and is, thus, little influenced by the tectonics of the Eovariscan mountain belt under incipient uplift, some few thousand of kilometres south of the area under study.

The studied three sections, Aeketal, Hühnertal and Kellwassertal, are located in the Upper Harz, i.e., the north-western part of the Harz Mountains (Schindler, 1990) (Fig. 1a). The Upper Harz area is mainly composed of three units (Fig. 1b). The Devonian Anticline consists of Devonian limestones, sandstones and clay schists. The Clausthal Fold Zone is mainly composed of Early Carboniferous graywackes, siliceous schists and clay schists. Lastly, the Acker Bruchberg Zone contains Late Devonian siliceous schists and graywackes and Early Carboniferous quartzites (Gabriel et al., 1997). The Aeketal and Hühnertal sections occur in the Devonian Anticline, whereas the Kellwassertal section occurs in the Claustal Fold Zone. In more detail, the Aeketal and Kellwassertal sections are respectively situated about 10 km and 2 km north of the town of Altenau, whereas the Hühnertal section is situated 1.5 km north-east of the town of Hahnenklee (Fig. 1b). The lithologic and faunal characteristics of the

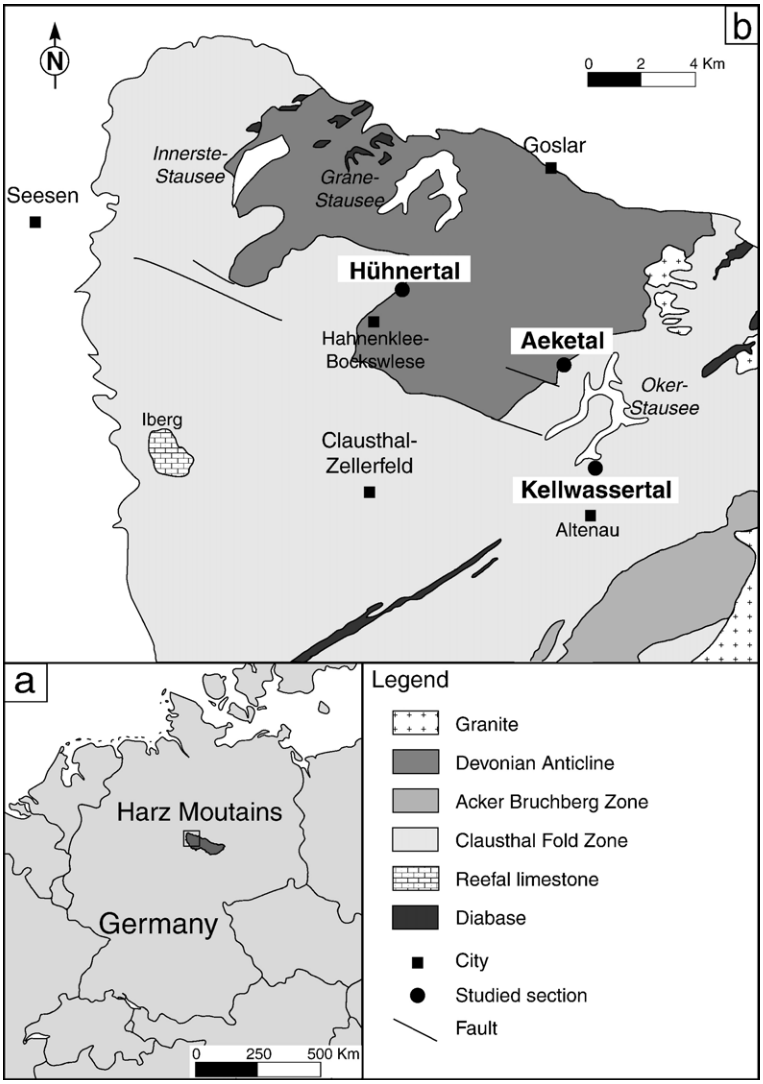

Fig. 1. Location of the studied area (a), and geological sketch of the sampling area in the Harz Mountains (modified from Alberti and Walliser, 1977; Schindler, 1990) (b).

Aeketal, Hühnertal and Kellwassertal sections were described in detail by Schindler (1990, 1993), and Feist and Schindler (1994). The sampled interval records condensed carbonate sedimentation from the Middle Frasnian *jamieae* conodont zone to the Early Famennian Upper *crepida* zone (Fig. 2), but we mainly focus our attention on the time interval from the Lower *rhenana* zone to the Upper *triangularis* zone.

The Late Devonian sequence is about 3.5 to 4.5 m thick and exposes a succession of cephalopod limestone beds, with intercalated calcareous shale levels (Fig. 2). The carbonate content mainly ranges from 60% to 100% for the Hühnertal and Aeketal sections. In the Kellwassertal section, the fluctuations in the carbonate content are more pronounced (5% to 100%) and many marlstone beds are present. The three sections present two black laminated horizons, corresponding to the Lower Kellwasser (LKW) and the Upper Kellwasser (UKW) horizons, which occur at the base of the Upper *rhenana* and in the upper part of the *linguiformis* zones, respectively. The KW horizons may consist of either pure black limestones with the highest % $CaCO_3$ contents, as observed for the LKW horizon in Aeketal and the UKW horizon in Hühnertal, or lenticular lenses of black limestones, alternating with black marls, as observed in the LKW horizon in Kellwassertal and the UKW horizon in Aeketal. Whereas the LKW horizon is about 40-cm thick in each section, the thickness of the

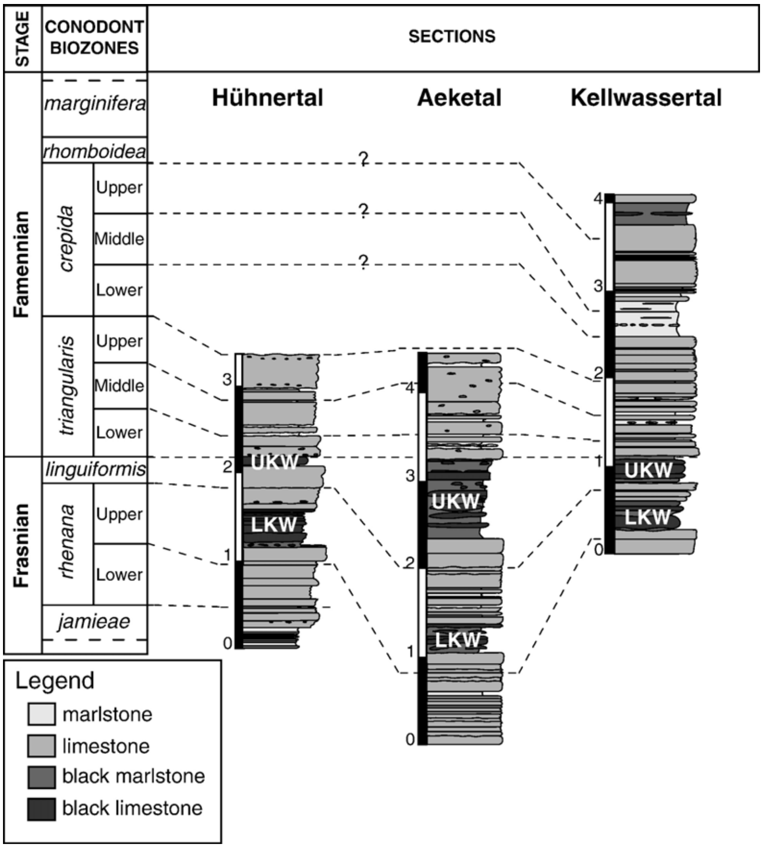

Fig. 2. Lithology, conodont biozonation (from Schindler, 1990) and biostratigraphical correlations between the studied three sections. Scale in meters. LKW and UKW stand for Lower Kellwasser horizon and Upper Kellwasser horizon, respectively.

UKW horizon is more variable, ranging from about 20-cm thick in the Hühnertal section to 90 cm in the Aeketal section. The three sections are thought to correspond to a submarine-rise setting in a pelagic realm, because of the diversified faunas, such as trilobites, ostracods, echinoderms and ammonoids observed in the sedimentary beds. The Hühnertal section is thought to represent the shallowest environment (Schindler, 1990).

3. Methods

3.1. Inorganic geochemical analyses

Major- and trace-element analyses were performed on selected samples using ICP-AES and ICP-MS, respectively, at the spectrochemical laboratory of the Service d'Analyse des Roches et des Minéraux of the Centre National de la Recherche Scientifique (Vandœuvre-les-Nancy, France). From the three sections, a total of 51 samples were prepared by fusion with $LiBO_2$ and HNO_3 dissolution. Precision and accuracy were both found to be better than 1% (mean 0.5%) for major–minor elements, 5% for Cr, Pb, U, V and Zn, and 10% for Ba, Co, Cu, Mo, and Ni as checked by international standards and analysis of replicate samples, respectively.

Sedimentary rocks usually have variable proportions of phases, often biogenic that "dilute" the trace-element abundance relative to crustal averages and mechanisms of enrichment. The most typical biogenic dilutants are calcium carbonate and opal. Thus, to be able to compare trace-element proportions in samples with variable carbonate and opal contents, it is recommended to normalize the trace-element concentration, most commonly to the aluminum content (e.g., Calvert and Pedersen, 1993). For the great majority of sedimentary deposits, aluminum can be considered as an indicator of the aluminosilicate fraction of the sediments, with very little ability to move during diagenesis (Brumsack, 1989; Calvert and Pedersen, 1993; Morford and Emerson, 1999; Piper and Perkins, 2004). However, although Al-normalization is an attractively quick and easy way to normalize chemical data and to present Al-normalized element concentrations in sediment profiles, it must be noted that this methods also present some pitfalls. Van der Weijden (2002) demonstrated that uncorrelated variables (trace metal concentrations) may acquire "spurious" correlations when normalized, and that normalization can also increase, decrease, change sign of, or even blur the correlations between unmodified variables. This is all the more so when the coefficient of variation (standard deviation divided by the mean) of Al concentration is large compared to the variation coefficients of the other variables (Van der Weijden, 2002). In addition, there are also distinct instances when Al should not be used for normalization (Murray and Leinen, 1996). This is the case of marine sediments with a detrital fraction lower than 3–5% and a relative excess of aluminum compared to e.g., titanium (Kryc et al., 2003). The excess Al may be scavenged as hydroxides coated to biogenic particles (Murray and Leinen, 1996; Dymond et al., 1997; Yarincik et al., 2000; Kryc et al., 2003). A part of the excess Al could also result from an authigenic clay mineral formation (Timothy and Calvert, 1998). Nevertheless, such sediments with so reduced detrital fractions are not common.

Van der Weijden (2002) also showed that the comparison to average shale values might raise some complications. The composition of the commonly used standard shale and, consequently, the reference values of normalized elements are not necessarily representative of the local/regional sediments in the study area. This fact may complicate the comparison of the chemical composition of geological formations that are geographically and/or stratigraphically distinct.

To summarize, Al normalization of element concentrations in usual marine sediments may be considered to be a valuable method to estimate the enrichment in an element relative to a reference sediment, but cannot be used alone to identify and quantify contributions by sediment components other than the detrital fraction (Van der Weijden, 2002). Because the reference shales commonly used to calculate enrichment factors (EF) also present a diagenetic component, the use of EF to estimate limited enrichment/depletion may be delicate. However, when EF show values significantly higher than 1 (from ten- to thousand-fold enrichment), elemental enrichment may be unambiguously deduced. Lastly, the best way to get rid of the normalization bias is–whenever possible–to examine the stratigraphical variations in the EF or the Al-normalized element contents rather than the absolute values, provided the coefficient of variation in Al is not too large, which is generally the case with studies involving high-resolution sampling on stratigraphically limited sequences.

3.2. Rock-Eval pyrolysis

Rock-Eval parameters, such as total organic carbon (TOC) content, Hydrogen Index (HI) and T_{max} (Espitalié et al., 1986), were determined using a Delsi Oil Show Analyser at the Earth Science Department of Paris VI-Pierre et Marie Curie University.

3.3. SEM analyses

Six samples from the KW Horizons were studied in polished thin sections using an FEI Quanta 200 environmental scanning electron microscope (SEM), operated at low vacuum (about 0.70 Torr and 20.0 kV). The SEM is coupled to an energy-dispersive X-ray spectrometer (EDS) (XFlash 3001), allowing elemental analysis.

4. Results

4.1. Geochemistry

According to several authors (e.g., Brumsack, 1989; Werne et al., 2002; Sageman et al., 2003; Algeo and Maynard, 2004; Tribovillard et al., 2005, in press, and references therein), the sedimentary geochemical signal records the influence of three types of fractions: (1) a detrital fraction derived from terrigenous (fluvial, eolian, volcanogenic) sources, the main proxies of which are Ti, Zr, Th, and Cr, (2) a biogenic fraction, composed of carbonate, silica or OM, the main proxies of which are Ba, Ni, and Cu, and (3) an authigenic fraction, mainly composed of sulphides and insoluble oxyhydroxides, the main proxies of which are Mo, V, and U.

To determine the origin of the elements studied here (clastic or biogenic supply, authigenic enrichment), the major and trace element abundances were cross-correlated with Al abundance, used here as a proxy for the land-derived aluminosilicate fraction of the sediments. From the r values (Table 1), it clearly appears that (1) Si, Fe, Mg, Na, K, Ti, Ba, Cr, Ni, V, Th and Zr are strongly correlated with Al ($0.90<r<0.99$), (2) Co, Cu Pb, Zn are moderately correlated with Al ($r<0.90$), (3) Mn, Mo and U are poorly to not correlated with Al ($r<0.75$), and (4) both Ca and Sr are negatively correlated versus Al ($r>0.85$). Consequently, most of the major elements (Si, Mg, Na, K and Ti) and some minor/trace elements (Zr, Th and Cr) have a siliciclastic origin and their fluctuations can be related to variations in the detrital influx. Moreover, the anti-correlation existing between Ca and Sr vs. most of major and minor

Table 1
Correlation coefficients (r) between Al and selected major and trace elements and level of significance of correlations (p, expressed in %)

	Aeketal (n=21)		Hühnertal (n=15)		Kellwassertal (n=16)	
	r	p	r	p	r	p
Major elements (%)						
Si	0.99	<0.1	0.99	<0.1	0.99	<0.1
Fe	0.96	<0.1	0.99	<0.1	0.96	<0.1
Mn	0.06	n.s.	0.47	n.s.	0.06	n.s.
Mg	0.97	<0.1	0.90	<0.1	0.91	<0.1
Ca	0.99	<0.1	0.99	<0.1	0.99	<0.1
Na	0.96	<0.1	0.87	<0.1	0.98	<0.1
K	0.99	<0.1	0.99	<0.1	0.99	<0.1
Ti	0.99	<0.1	0.99	<0.1	0.99	<0.1
Trace elements (ppm)						
Ba	0.99	<0.1	0.98	<0.1	0.80	<0.1
Co	0.95	<0.1	0.74	<1.0	0.61	<5.0
Cr	0.99	<0.1	0.99	<0.1	0.99	<0.1
Cu	0.64	<1.0	0.85	<0.1	0.54	<5.0
Mo	0.52	<5.0	0.11	n.s.	0.38	n.s.
Ni	0.96	<0.1	0.99	<0.1	0.78	<0.1
Pb	0.56	<5.0	0.79	<0.1	0.59	<5.0
Sr	0.59	<5.0	0.89	<0.1	0.79	<0.1
Th	0.99	<0.1	0.99	<0.1	0.99	<0.1
U	0.52	<5.0	0.72	<1.0	0.61	<1.0
V	0.96	<0.1	0.94	<0.1	0.73	<1.0
Zn	0.84	<0.1	0.48	n.s.	0.73	<1.0
Zr	0.97	<0.1	0.98	<0.1	0.98	<0.1

elements can be interpreted as dilution of geochemical signal by carbonate production. The stratigraphic distribution of some selected elements (Al-normalized) is illustrated in Fig. 3. Broadly speaking, and consistently with the fact that most elements are strongly tied to Al abundance, the distribution of element/Al ratios are rather uniform, but some variations are visible for the KW horizons. In all sections, the stratigraphic profiles of all the redox-sensitive trace elements (Mn, U, Mo and V) and paleoproductivity tracers (Ba, Cu, Ni) exhibit moderate to high enrichments in both KW horizons, relative to the other parts of the sections, where the samples have element/Al ratios at or near average shale values (Fig. 3). Thus, the two KW horizons correspond to the analytical points showing the poorest correlation vs. Al concentration. These enrichments are particularly well expressed within the LKW horizon of the Aeketal section, where the highest values are recorded. Fig. 3 also shows that only the top part of the UKW shows any enrichment in redox and paleoproductivity ratios; the lower portion of the UKW horizon, for the most part, looks like background level. Concerning the lateral variations in elemental concentrations, it is noteworthy that the redox-sensitive metal/Al ratios in the KW horizons of Hühnertal are twice lower than those of the KW horizons of Aeketal. The Kellwassertal section shows intermediate values comparing to the other two sections.

The other major and trace elements have less contrasting fluctuations during the Late Frasnian–Early Famennian times. Ti and Zr are two markers of the detrital fraction of sediments (r=0.99 with Al). In the studied three sections, they show rather uniform stratigraphic distributions with the lowest values corresponding to the two KW horizons (Fig. 3). This phenomenon is more accentuated in the Hühnertal and Aeketal sections. Among the detrital proxies, Si is the only major element that shows a well-marked positive peak within the LKW horizon in Aeketal. Iron shows slightly higher Fe/Al values in the KW horizons. Potassium shows similar behaviour.

To summarize, in the three sections, the geochemical composition of the rocks is strongly influenced by the detrital supply, but some elements shows more or less marked enrichment or depletion in the KW horizons (depleted in Ti and Zr, enriched in redox and productivity proxies).

In addition to element/Al ratios, some redox indices (U/Th, V/Cr, Ni/Co, and V/(V+Ni)) have been calculated and reported as cross-plots in Fig. 4. In the literature (Hatch and Leventhal, 1992; Jones and Manning, 1994), these geochemical indices have been used to derive information on the paleo-oxygen level of the depositional environments (Table 2). For all four indices, the highest values are recorded within the two KW horizons. Nevertheless, the contrast between the samples from the KW horizons and those from the rest of the section varies according to the considered indices. In each section, the samples of the KW horizons have values of the V/Cr and U/Th ratios above 1.25, whereas the non-KW horizons have values that rarely exceed 1 and 0.6, respectively. For the V/(V+Ni) and Ni/Co ratios, the distinction is not as clear. Nevertheless, most of the samples of the KW horizons are characterized by V/(V+Ni)>0.60 and Ni/Co>4. Nevertheless, as discussed by Rimmer (2004), it is not recommended to focus on the absolute values of these elemental ratios, but rather on their relative variations.

4.2. Rock-Eval data

The Rock-Eval parameters indicate that the TOC is ranging between 0% and 2%, most values being below 0.5%. Consequently, the other parameters, T_{max} and HI, cannot be used confidently (Espitalié et al., 1986), hence they are of no help to determine the type of OM (II or

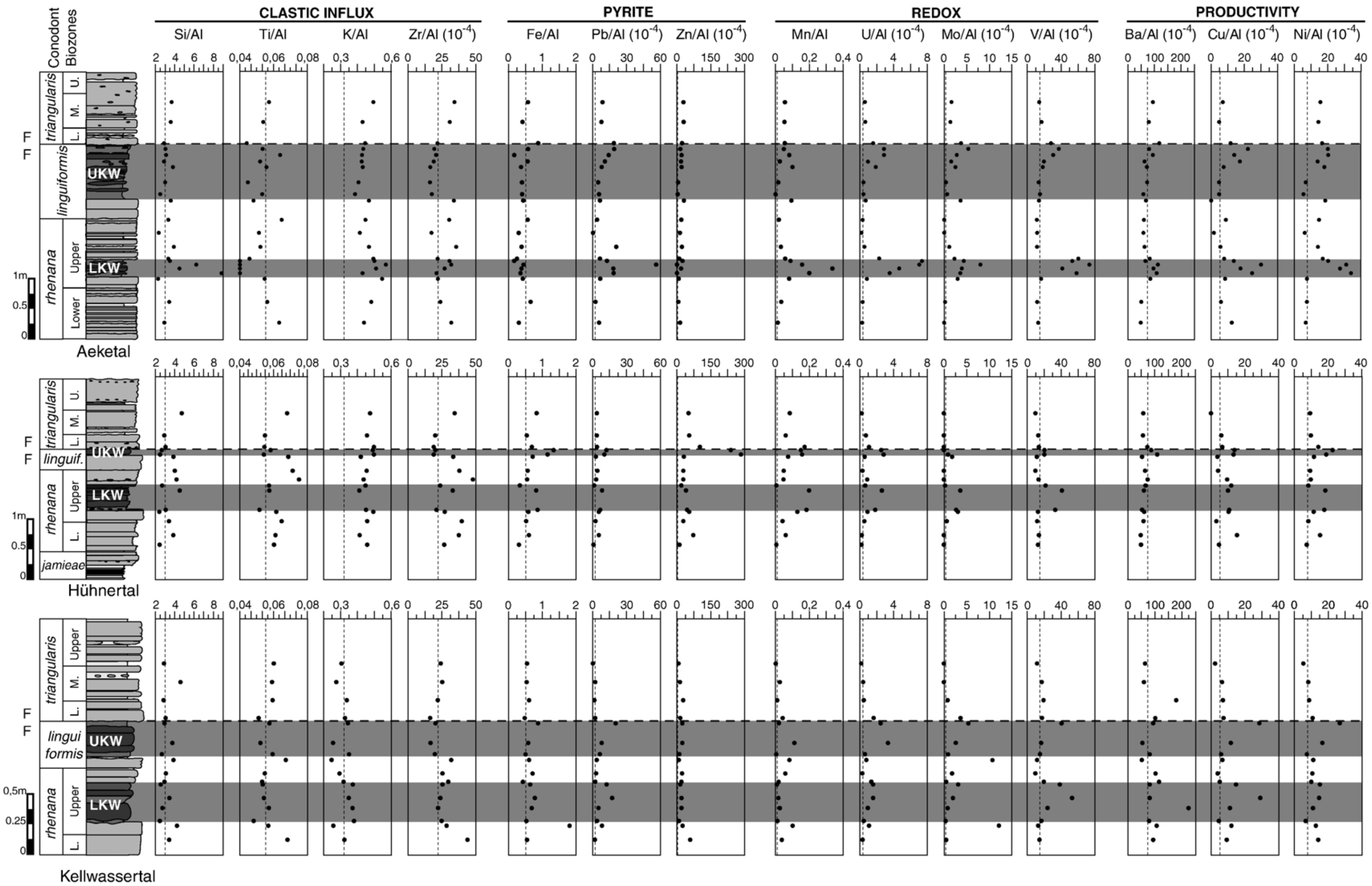

Fig. 3. Normalized metal concentrations in the Aeketal, Hühnertal and Kellwassertal sections. The dashed lines indicate the metal/Al concentration ratios for average shales (Wedepohl, 1971, 1991). Major element/Al ratios are given as weight-ratios and trace element/Al ratios as weight-ratios multiplied by 10^4. The two shaded bands correspond to the KW horizons.

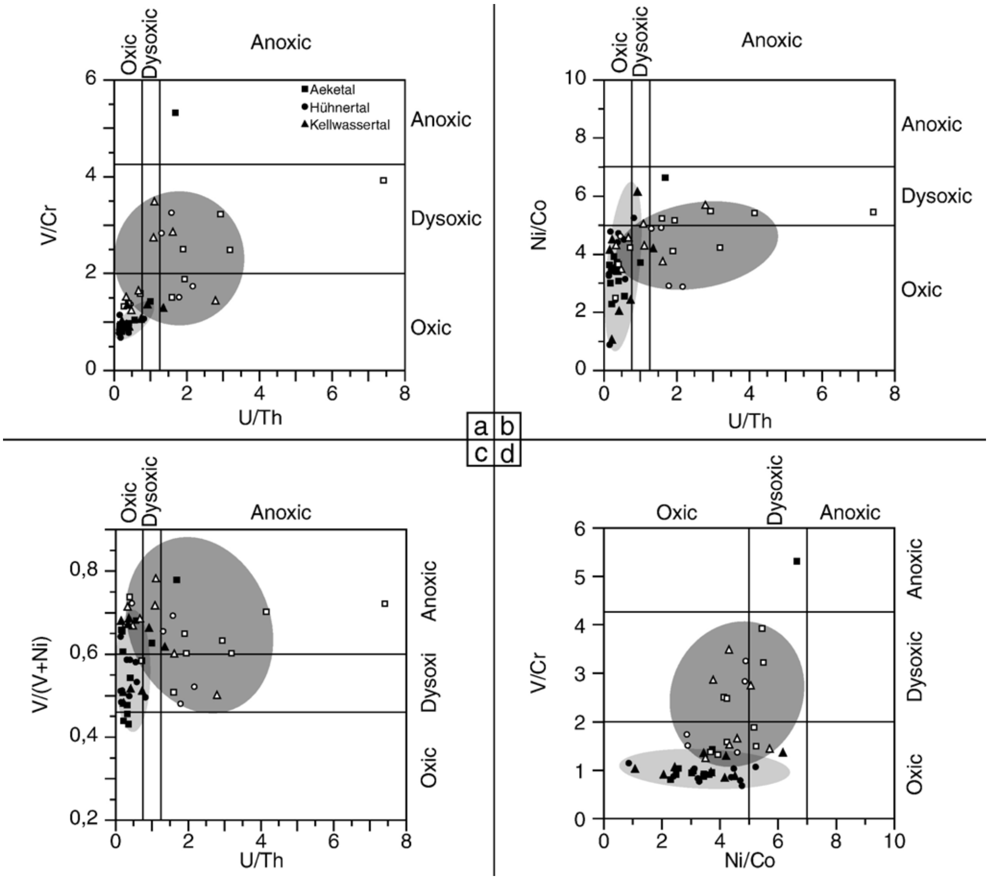

Fig. 4. Crossplot of redox indices. V/Cr vs. U/Th (a), Ni/Co vs. U/Th (b), V/(V+Ni) vs. U/Th (c) and V/Cr vs. Ni/Co (d). Ranges for V/Cr, U/Th and Ni/Co are from Jones and Manning (1994); ranges for V/(V+Ni) are from Hatch and Leventhal (1992). Open symbols: Kellwasser horizon samples. The dark shaded area corresponds to cluster of the KW samples, whereas the light shaded area corresponds to cluster of the no-KW samples.

III). The few samples with TOC above detection value show high T_{max} values (T_{max}>460 °C), indicating that OM is mature. The marked maturation may be ascribed to regional tectonic history (thrusting or heat flow), and may be held responsible for the destruction of a part of the OM content. However, according to Mongenot et al. (1996), the trace-metal content is not markedly affected in sedimentary rocks with strong over maturation (in the case of the elements studied here). Thus, the geochemical message must have been preserved.

4.3. SEM–EDS results

SEM observations coupled to EDS microprobe analyses on polished thin sections reveal that framboidal and, very scarce euhedral, pyrite minerals are the most significant iron-bearing phases in the KW horizons. The sizes of framboidal and euhedral pyrites are variable. In each section, the framboidal pyrites are larger than the euhedral pyrites: framboidal pyrites ranging from 2 to 15 μm and most of them being around 8 μm, whereas the euhedral specimens range from 1 to 7 μm, with an average value of 4 μm (Fig. 5a–b). Comparatively, detrital iron oxides (very likely magnetite) are only scarce. An additional point to be noticed is that most framboids are partly or totally weathered to iron oxides but their morphology has been preserved (Fig. 5c).

5. Interpretation

5.1. Clastic inputs

In the studied three sections, the good correlations of Si, K, Ti, Zr, Fe, Cr vs. Al (r>0.95) (Table 1), and the rather uniform stratigraphic distribution of K/Al and Fe/Al and, to a lesser degree Si/Al, suggest a rather homogeneous nature for the detrital supply. However, the Ti/Al and Zr/Al ratios show the lowest values for both KW horizons. Ti and Zr are frequently enriched in

Table 2
Correlations between trace-element ratio values and redox zones (bottom-water oxygen levels from Tyson and Pearson, 1991)

	Oxic zone (8.0–2.0 ml O_2/l)	Dysoxic zone (2.0–0.2 ml O_2/l)	Anoxic zone (0.0 ml O_2/l)
U/Th [a]	<0.75	0.75–1.25	>1.25
V/Cr [a]	<2.00	2.00–4.25	>4.25
Ni/Co [a]	<5.00	5.00–7.00	>7.00
V/V+Ni [b]	<0.46	0.46–0.60	0.54–0.82

[a] Jones and Manning (1994).
[b] Hatch and Leventhal (1992).

the presence of accessory minerals, such as ilmenite, rutile, zircon and augite that are usually associated with the coarser-grained part of fine-grained siliciclastic sediments (Brumsack, 1986, 1989; Calvert et al., 1996; Caplan and Bustin, 1999). The relatively low abundance of Ti and Zr in the KW horizons could thus indicate a decrease in the grain size of the land-derived supply. This grain size decrease could accompany the sea-level rise frequently suggested for the two KW horizons (Girard and Feist, 1997; Hallam and Wignall, 1999; Sandberg et al., 2002; Chen and Tucker, 2003; Godderis and Joachimski, 2004; see discussion in Chen and Tucker, 2004).

Alternatively, Ti and Zr are also two elements frequently referred to as tracers of airborne or eolian detrital supplies (Rachold and Brumsack, 2001). Their relative low abundance could reflect a decrease in eolian supply during the deposition of the KW horizons. This second interpretation is plausible but it demands more hypotheses about the sources of eolian dust, the dominant-wind patterns, and the location of high-pressure cells that one is unable to discuss with the present knowledge about global circulations during the Late Devonian.

The Si/Al ratio shows relatively low values in the KW horizons of the Hühnertal and Kellwassertal sections. This is consistent with both hypotheses: decreased grain size of the detrital supply, including quartz grains, or decrease in the airborne quartz silt abundance (e.g., Tribovillard et al., 2005). However, this Si/Al decrease is not observed in the Aeketal section. In contrast, a strong Si/Al increase is marked for the LKW horizon of the Aeketal section. In that case, the increased presence of SiO_2 could be explained by an increase in biogenic SiO_2 (silica-secreting organisms) recorded locally (Racki, 1999; see discussion below about the increase in productivity).

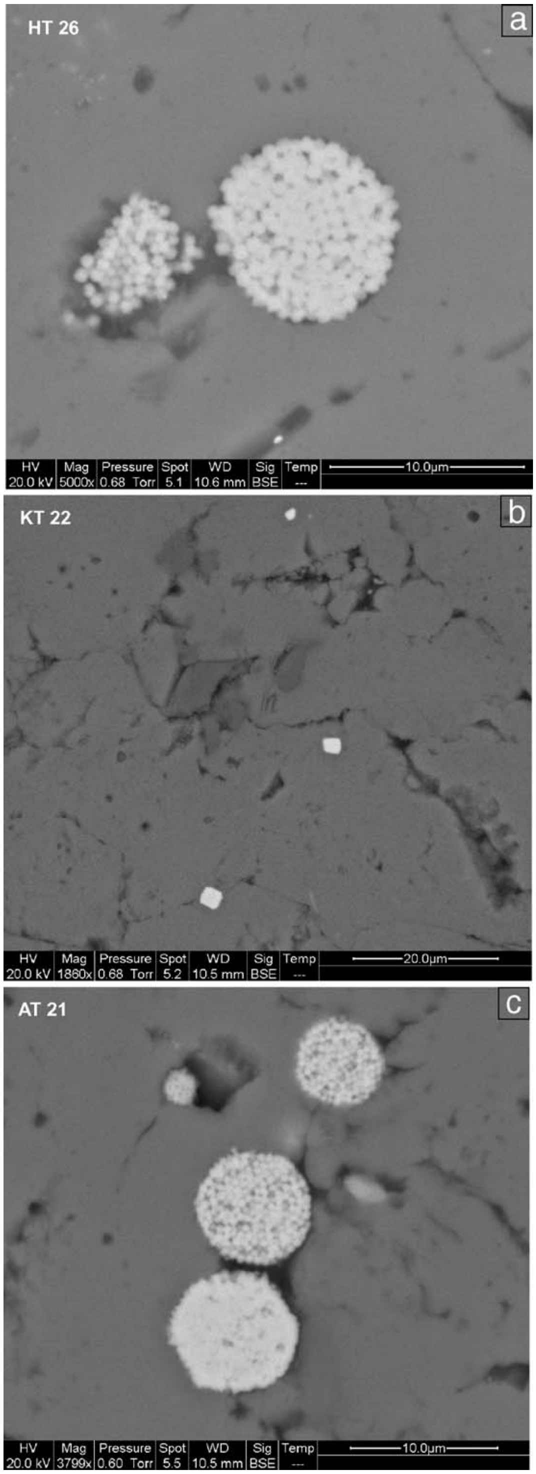

Fig. 5. Backscattered electron microphotographs of framboidal pyrite (sample HT 26, LKW horizon of Hühnertal) (a) and of euhedral pyrite (sample KT 22, UKW horizon of Kellwassertal) (b). (c) Four framboids from sample AT 21 (LKW horizon of Aeketal): two unweathered large ones above and, bottom, a large framboid converted to iron oxides. There is no evidence that the oxidation processes induced a variation in the size of the framboids.

5.2. Redox conditions

For each section, the KW horizons are enriched in Mo, U, V, Cu, Cr, and Ni. These elements that are redox sensitive and/or sulphide forming, and also possible indicators of the OM flux to the sediments (Ni and Cu) can be fixed in high amounts in sediments under reducing conditions (Brumsack, 1986, 1989; Hatch and Leventhal, 1992; Calvert and Pedersen, 1993; Lipinski et al., 2003; Algeo and Maynard, 2004; Meyers et al., 2005; Tribovillard et al., 2005, in press). They may either be precipitated as autonomous sulphides (Co, Zn and Pb), coprecipitated with iron sulphides (V, Ni and Cu), and/or bound to organic matter (V, Mo, Ni, Cu and U). Among the studied trace metals, V, U, and Mo are reputed as redox-sensitive markers (Crusius et al., 1996; Helz et al., 1996; Dean et al., 1997; Zheng et al., 2000; Adelson et al., 2001; Lyons et al., 2003; Algeo et al., 2004, Cruse and Lyons, 2004; Rimmer, 2004; Rimmer et al., 2004; Tribovillard et al., 2004a,b, 2005; Algeo and Lyons, in press). In all three sections, Mo and U are the most enriched elements in the KW horizons compared to the average shale values (entire LKW and upper part of UKW; Figs. 3 and 6). The enrichment in

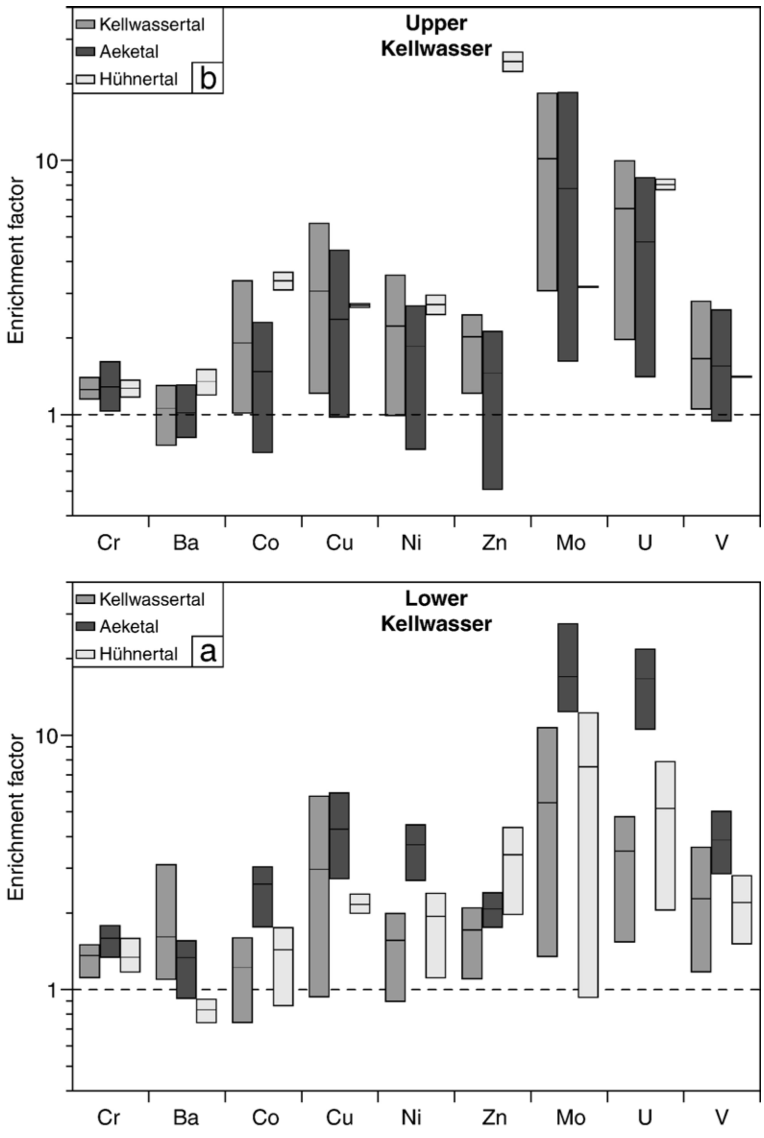

Fig. 6. Comparison of enrichment factor of some trace metals for the two Kellwasser horizons of the studied three sections. The extent of the boxes corresponds to the range of values (min–max) and the inner line to the average value. The enrichment factor for any element (e), $EF_{(e)}$, is equal to $(e/Al)_{sample}/(e/Al)_{shale}$. The dashed line indicates the value for which there is no enrichment/depletion with regards to average shale composition.

Mo and U within the black horizons indicates that the sediments were likely depleted in O_2 at the time of deposition of the KW horizons. Between these two redox-sensitive elements, enrichment in Mo within the KW horizons is the highest (Figs. 3 and 6), suggesting the possible presence of dissolved sulphide close to the sediment–water interface (Lyons et al., 2003; Algeo and Maynard, 2004; Tribovillard et al., 2005).

In addition, some redox indices, such as U/Th, V/Cr, Ni/Co and V/(V+Ni), were used. According to Jones and Manning (1994) and Rimmer (2004), these various ratios cannot be used reliably individually, but rather must be considered collectively. In the present case, these proxies behave consistently and show their highest values for samples of the Kellwasser horizons. It means that the most oxygen-poor conditions were met during the KW deposition. However, it is observed that only the upper part of the UKW records oxygen-restricted conditions, whereas the LKW integrally indicates O_2-restriction (Figs. 3 and 4). According to the considered ratio, the values point to dysoxic (Ni/Cr, V/Cr) or anoxic (U/Th) conditions. U/Th and V/(V+Ni) are the most and least discriminating proxies, respectively (Fig. 4). Nevertheless, following Rimmer's conclusion (2004), we do not pay too confident attention to the threshold values, and conclude from the ratios with oxygen-restricted conditions for the LKW and the upper part of the UKW horizons.

To summarize, our geochemical data (Al-normalized trace metal abundance and redox ratios) indicate two pulses of bottom water dysoxia to anoxia, coeval with the KW horizons in the drowned platform environments studied here (the entire LKW and the upper part of the UKW horizons).

Lastly, information concerning O_2 levels can also be deduced from the Mn/Al ratio. Manganese is frequently depleted in sediments in dysoxic to anoxic environment because manganese oxyhydroxides undergo reductive dissolution and are remobilized as soluble elements (Mn^{2+}) (Calvert and Pedersen, 1996; Tribovillard et al., in press). In contradiction to the above interpretation, Mn is relatively enriched in the KW horizons, notably in the Aeketal and Hühnertal sections. The Mn enrichment may be accounted for by the authigenic precipitation of manganese carbonates such as rhodochrosite ($MnCO_3$) or kutnahorite ($Ca(Mn,Mg,Fe)(CO_3)_2$) (Calvert and Pedersen, 1996). These minerals can form where carbonate supersaturation is reached in presence of solubilized Mn^{2+} ions in pore waters. These minerals are thought to form close to the sediment–water interface, in marine anoxic sediments, overlain by oxic bottom waters (Calvert and Pedersen, 1996). In the Aeketal and Hühnertal sections, the KW horizons mainly correspond to pure limestone units, most of samples have $CaCO_3$ content higher than 90%. Good to moderate correlations between Mn/Al and Ca/Al are obtained ($0.69 < r < 0.94$), confirming that Mn could be potentially fixed in carbonate phases.

To summarize, in the drowned platform environments studied here, the two KW horizons correspond to sediments deposited in reducing environments, as indicated by the trace-metal parameters. However, the simultaneous enrichment in redox-sensitive, sulphide-forming elements, and Mn indicate that the sediments must have been reducing and that the redox chemocline (i.e., the boundary between oxidizing and reducing conditions) must have resided within the sediments or, at most, at the sediment–water interface. The chemocline can not have risen durably into the water column, because no such Mn enrichment could have been recorded. Thus, in agreement with Murphy et al. (2000a,b) and Racki et al. (2002), our observations are incompatible with a permanently stratified basin model.

5.3. Pyrite framboid size

Our results point out a slight Fe enrichment in the KW horizons unrelated to Al or Ti abundance. Such enrichment may be caused by the presence of syngenetic pyrite (e.g., Werne et al., 2002; Lyons et al., 2003; and references herein). Sedimentary pyrite forms as a consequence of bacterially mediated sulphate-reduction reactions generating sulphide ions (HS^-/H_2S) that combine with reactive iron (Berner, 1970, 1984). Several pathways are possible for sedimentary pyrite formation, but, most frequently, pyrite forms via a metastable "FeS" precursor. The transformation of FeS to FeS_2 needs the reaction of FeS with intermediate sulphur species such as S^0 and S_x^{2-} and has been documented in the laboratory (Rickard, 1975; Schoonen and Barnes, 1991a,b; Wilkin and Barnes, 1996).

The oxidized intermediate S species may be produced by H_2S oxidation near the redox boundary by oxidants such as O_2, NO_3^-, MnO_2, FeOOH (Middelburg, 1991; Suits and Arthur, 2000; Schippers and Jørgensen, 2001). In natural environments, the intervention of oxidized intermediate S species appears to be fundamental, and is consistent with the observation that for many environments, the majority of pyrite forms early, near the redox boundary, either in the water column (in euxinic settings) or within the sediments (Goldhaber and Kaplan, 1974; Calvert and Karlin, 1991; Middelburg, 1991; Canfield et al., 1992;

Lyons, 1997; Raiswell and Canfield, 1998; Hurtgen et al., 1999; Wijsman et al., 2001; Lyons et al., 2003; Allen, 2003).

Recent studies of pyrite framboid diameters from a variety of modern and past environments have provided a potential tool to distinguish ancient euxinic conditions from dysoxic–anoxic (non-sulphidic) conditions (Wilkin et al., 1996, 1997; Wignall and Newton, 1998; Taylor and Macquaker, 2000; Lyons et al., 2003; Bond and Wignall, 2005; Wignall et al., 2005). The basic idea is that pyrite growth requires the presence of (partially) oxidized S species (S^0) that can be found only close to the redox boundary. Thus, for anoxic sediments found beneath oxic or dysoxic bottom waters, the oxidants required for pyrite growth are supplied by diffusion from bottom waters to the sediment, bioturbation and burrow penetration into the underlying sulphate reduction zone. In a euxinic water column the only favourable place for framboid formation is within the water column, immediately beneath the redox boundary (Wilkin et al., 1996, 1997; Wignall and Newton, 1998; Wignall et al., 2005). In the water column, the pyrite particles sink to the seafloor before they reach appreciable diameters (only small euhedral crystals and small-sized framboid, i.e., a few micrometers large, can form) and no enlargement is observed after deposition (Wilkin et al., 1996, 1997; Wignall and Newton, 1998). Consequently, according to these authors, "euxinic" framboids are smaller and more constant in diameter than framboids formed within sediments underlying oxic or suboxic bottom waters.

Our SEM observations of the KW samples (Fig. 5) reveals the presence of dispersed pyrite framboids, more abundant in the Aeketal and Kellwassertal sections than in the Hühnertal section. The framboid diameters fall within the 2–15-μm range, which are rather considerable sizes. These observations indicate that pyrite growth occurred in presence of relatively abundant S^0, allowing the framboid to reach a large size. It is inferred that the paleoenvironmental conditions were not euxinic and that the redox boundary was probably lying close to sediment–water interface. The pyrite data thus confirm the interpretations derived from the geochemical data.

Lastly, the SEM–EDS analyses and observations reveal that pyrite framboids are partly oxidized, with a marked departure of S, indicating that they suffered from severe post depositional alteration. This strong oxidation is most probably attributable to late-diagenesis processes, in an intrusively tectonized area. The results show the partial or total departure of S from the pyrite framboids. It may be inferred that the trace metals, usually associated with pyrite (Ni, Cu, Co, Zn, Mo and Cr) may have also been leached from iron sulphides (at least partly). Consequently, the trace metal concentrations observed here must be looked at as minimum values, probably below the original concentrations at the time of sulphide precipitations.

5.4. Productivity conditions

Both KW horizons record increased Cu/Al and Ni/Al ratios in the three sections. These elements are usually enriched in reduced sediments (Brumsack, 1989; Calvert and Pedersen, 1993). Recent studies (Algeo and Maynard, 2004; Tribovillard et al., 2005) emphasized the fact that Ni and Cu are mainly brought to the sediment in associations with OM and they are retained in the sediment within sulphides (usually solid solution within pyrite) even in the case of complete OM remineralization Thus, Ni and Cu are considered to be reliable tracers of the OM delivery to the sediment (Riboulleau et al., 2003; Algeo and Maynard, 2004; Tribovillard et al., 2005, in press). Thus, the positive peaks of the Ni/Al and Cu/Al ratios recorded here indicate that the KW horizons are interpreted as corresponding to episodes of increased OM influx, possibly recording increased productivity.

Barium is usually considered as a productivity proxy when brought to the sediment as barite (e.g., Dymond et al., 1992; McManus et al., 1998; Tribovillard et al., in press). However, barite ($BaSO_4$) may be sensitive to severe sulphate-reducing conditions (McManus et al., 1998). In the present case, Ba shows subtle enrichments in the KW horizons. These enrichments are coeval to those of Cu and Ni (Fig. 3). These observations suggest some increased productivity at the time of deposition of the KW horizons. However, the relatively low Ba enrichment, compared to Ni and Cu, could indicate Ba remobilization and loss after barite dissolution, as a consequence of the development of strongly reducing conditions below the sediment–water interface. This interpretation is, however, in contradiction with the Mn enrichment, indicating that oxidizing conditions were probably met close to the sediment–water interface. Consequently, the relatively low Ba concentrations are rather interpreted as resulting from moderate productivity increases. The slight increases of productivity resulted in increased delivery of OM and thus Ni and Cu. These elements could be trapped thanks to sulphide precipitation induced by the reducing conditions, the latter being partly induced by the increase OM influx. These interpretations underline the usually intertwined relationships between OM productivity and reducing conditions development. Lastly, a Si/Al peak is marked for the LKW horizon of the Aeketal section (Fig. 3), without coeval peaks of clastic proxies (Ti and Zr). The increased Si abundance must be the echo of a local increased biogenic productivity by silica-secreting organisms, consistent with the coeval enrichment in the abundance of the productivity proxies (Ni, Cu and Ba).

5.5. Summary

Our geochemical data indicate that the two KW horizons correspond to episodes of development of reducing conditions, but the chemocline probably remained at small distance below the sediment–water interface. We have no indications that the redox conditions were constantly reducing, we shall interpret them as dominantly reducing. The LKW event seems to be more intense than the UKW, notably in the Aeketal and Hühnertal sections. The development of reducing conditions is attributed to moderate increases in surface-water productivity during periods of detrital influx decrease that probably reflect the transgressive nature of the KW horizons. These results from inorganic data, presented here, are in agreement with those obtained by Joachimski et al. (1994) concerning the $\delta^{13}C_{carb}$ isotopic signal in the studied three sections.

6. Discussion

6.1. The contrasting record of the two Late Frasnian anoxic events

According to previous studies, mainly based on geochemical data (Bond et al., 2004; Riquier et al., 2005; Pujol et al., in correction), the onset of reducing conditions during the deposition of both black KW facies at the F–F boundary seems to be a widespread phenomenon, at least in European and North African areas, on both sides of the Eovariscan Belt. Nevertheless, some authors evidenced the diachroneity of the LKW that is sometimes not developed (e.g., in the Great Basin of the USA; Schindler, 1990, 1993; Crick et al., 2002).

Our results about the Harz sections show that the LKW horizon coincides with the development of dysoxic–anoxic conditions. They are consistent with those of Bond et al. (2004) and Riquier et al. (2005) that demonstrate that the early Upper *rhenana* anoxic event, corresponding to the LKW horizon, is strongly marked in some German sections (e.g., Steinbruch Schmidt) and Moroccan sections (e.g., Anajdam and Bou-Ounebdou), corresponding to submarine rise and platform settings, respectively. However, this anoxic event was not extended to the whole marine domain, as it is not clearly recorded in basinal environments, such as in Kowala (Poland) and La Serre (France) (Bond et al., 2004).Thus, the early Upper *rhenana* anoxic event, corresponding to the LKW horizons, appears to be limited to shallower environments.

In contrast to this first Late Frasnian anoxic event, the *linguiformis* anoxic event, corresponding to the UKW horizon, is recorded in platform and submarine rise settings, as well as in basinal settings (Joachimski et al., 2002; Racki et al., 2002; Yudina et al., 2002; Bond et al., 2004; Tribovillard et al., 2004b; Riquier et al., 2005; Pujol et al., in correction). In many submarine rise and platform sections (e.g., Aeketal, Hühnertal, Bou-Ounebdou), the inorganic geochemical data seem to indicate that the UKW horizon is less enriched in redox proxies (i.e., Mo, U, V), suggesting less reducing paleoenvironments, compared to the LKW horizon. Dysoxic conditions could prevail during the deposition of the second KW horizons in the more proximal settings. In the deepest sections (e.g., La Serre, Kowala Quarry), the oxygen-depleted conditions were strongly marked and could persist up to the Early Famennian (Upper *triangularis*) (Bond et al., 2004; Tribovillard et al., 2004b). According to these statements, it may be supposed that both anoxic events could have had different causes.

6.2. The possible causes of the two Late Frasnian anoxic events

Nowadays, it is frequently considered that the F–F boundary represents an interval of eutrophication and major anoxic events in the oceans, during a “greenhouse” type period (Murphy et al., 2000a,b; Racki et al., 2002; Joachimski et al., 2002; Bond et al., 2004; Tribovillard et al., 2004b; Riquier et al., 2005; but see Ginter, 2002 for the opposite idea and discussion in Sandberg et al., 2002). Environmental changes led to widespread accumulation of organic-rich sediments, the Lower and Upper KW horizons and episode of major biotic turnover (McGhee, 1996). According to several authors (Algeo et al., 1995; Racki, 1998; Murphy et al., 2000a,b; Peterhansel and Pratt, 2001; Joachimski et al., 2002; Racki et al., 2002; Tribovillard et al., 2004b; Averbuch et al., 2005; Riquier et al., 2005), the transition from oxic to anoxic sediments at the F–F boundary occurred in several sedimentary basins all over the world (North America, Europe, China, North Africa) in response to increasing productivity resulting from the Frasnian sea-level rise and corresponding increase in surface water nutrient availability. Additional processes, such as thermohaline stratification and restricted lateral circulation in deep-water settings, are generally invoked to explain the development of oxygen-restricted conditions (e.g., Cruse and Lyons, 2004; Averbuch et al., 2005).

6.2.1. The influence of productivity

Based on the geochemical indices used here, it appears that the conditions during accumulation of the both KW horizons were most likely dysoxic, with possible intermittent periods of anoxic conditions, the LKW horizons probably representing the most O_2-depleted interval in shallow environments. In addition, the LKW horizon is characterized by periods of relatively increased productivity. For the LKW horizons, where positive peaks of redox indices and productivity markers are recorded, the "productivity" model (Pedersen and Calvert, 1990) could be applied to the drowned platform settings. Increased surface water productivity causes bottom water anoxia by driving benthic O_2 demand to exceed O_2 supply by water column mixing. According to the model of Algeo et al. (1995) and Joachimski et al. (2002), the primary productivity increase may have been induced by enhanced delivery of terrestrially derived nutrients by rivers. Basing on isotope arguments, Joachimski et al. (2002) rule out any marked influence of upwelling systems for the nutrient supply. Eutrophication would occur in more proximal environments, like platform in Germany and Morocco. The materials (sediments and nutrients) supplied by continental influx are usually deposited or consumed in nearshore environments and consequently the productivity should be limited in remote-offshore settings, far from riverine influx. This may explain why the Upper *rhenana* anoxic event, corresponding to the LKW horizons, is poorly recorded in basinal setting. The low concentration of terrigenous materials in distal setting should have been enhanced by the marine transgression associated with the deposition of the LKW horizon.

For the UKW horizon, where increases of productivity are coeval with milder O_2-depletion, compared to the LKW horizons, the application of the "productivity" model may be problematic. Surface productivity did not cause the onset of truly anoxic conditions, in that anoxic conditions only developed below the sediment–water interface, and in the upper part of the UKW horizon. So, it could be envisioned that surface water productivity was not the only triggering factor of reducing conditions in drowned platform setting. The main problem concerning the UKW horizon is that in deeper setting, such as La Serre, peaks of productivity higher than those recorded in platform environments, are recorded within the UKW horizon before the F–F boundary (Tribovillard et al., 2004b; Riquier et al., 2005). Peaks of O_2-depleted conditions are also higher than those recorded in platform environments and are observed few cm above the F–F boundary. For distal and deeper parts of basinal settings, the terrestrial influence is minimal and the concentration of terrigenous nutrients should be low. The source of nutrient has to be autochthonous and, thus, likely results from nutrients released from OM decomposition under reducing conditions. Some authors (Murphy et al., 2000a; Riquier et al., 2005) proposed the onset of positive feedback between anoxia–eutrophication–OM decay, based on the model of Ingall and Jahnke (1997) to account for productivity increases within the UKW horizon. So, unlike the Upper *rhenana* anoxic event during which productivity increase, coupled with sea-level rises, was probably the main cause of reducing conditions, the *linguiformis* anoxic-event productivity increase would be one of the consequences of the onset of anoxic conditions in bottom water. Of course, nutrients released from emerged land could have been added to those recycled by OM remineralization (Racki, 1998; Joachimski et al., 2002; Tribovillard et al., 2004b; Averbuch et al., 2005).

6.2.2. The influence of sea-level fluctuations

The sea-level change is considered as a major factor for the deposition of black horizons (e.g., Tyson and Pearson, 1991; Arthur and Sageman, 1994; Wignall, 1994; Arthur and Sageman, 2004). During periods of sea-level rise, the depocenters shift landward and the inputs of terrigenous material to deep marine environments are diminished. A decreased dilution of the sedimentary OM by the terrigenous fraction could be a possible factor triggering enhanced OM accumulation. For the last decades, it has been widely accepted that the formation of both KW horizons is linked to short-term transgressive–regressive pulses (Johnson et al., 1985; Sandberg et al., 1988, 2002; Buggisch, 1991). Deposition of both KW horizons occurred during a global Frasnian sea-level rise and corresponded to highstand periods of two punctuated transgressive phases (Johnson et al., 1985; Hallam and Wignall, 1999; Chen and Tucker, 2003, 2004).

In Germany and other areas, representing shallow marine environments (e.g., Morocco), the UKW horizon could result from the progressive impingement of anoxic water from deeper environment onto platform settings. The rise of bottom-water anoxia from deep to shallower setting may have been favoured by the pulse of sea-level rise during the *linguiformis* zone. Anoxia would thus originate from the deep parts of the ocean. The *linguiformis* transgressive phase may have allowed the onset of water stratification in the deepest settings, causing the establishment of anoxic conditions (Tyson and Pearson, 1991). Frequent mixing in platform environments would have cycled nutrients back into sea surface, stimulating higher productivity and introducing dissolved O_2 into bottom water. This may explain the observed record toward less reducing conditions during the *linguiformis* anoxic event, compared to the Upper *rhenana* anoxic event.

In platform settings, the UKW facies ended with the beginning of a well-marked Early Famennian sea-level fall (Devleeschouwer et al., 2002; Sandberg et al., 2002); more frequent water mixing and better oxygenation caused the end of deposition of black facies, and this process affected first the more proximal settings. In deeper environments, water stagnation, density contrast, and thus anoxia, were relatively more stable. Thus, reducing conditions could prevail in the basinal environments during F–F transition and could last until early Famennian (Lethiers et al., 1998; Racki, 1998; Joachimski et al., 2001; Bond et al., 2004; Tribovillard et al., 2004b, Riquier et al., 2005).

7. Conclusion

Our results allow us to suggest that the formations of the KW horizons occurred during times of oxygen-depletion at or slightly below the water–sediment interface in the relatively shallow environment of present-day Harz Mountains (Germany). Some differences exist between the two black KW horizons. In platform setting, the LKW horizon corresponds to dysoxic to anoxic conditions, whereas the UKW horizon seems to be mainly characterized by dysoxic conditions only. In basinal settings, the contrary is observed. From these statements, two kinds of processes are used to account for the two Late Frasnian black facies. The LKW horizon, corresponding to the Upper *rhenana* anoxic event, and recorded in platform settings, would result from increased productivity in shallow environments, whereas basinal settings kept on with oxygenated conditions. The nutrients causing the increased productivity originated from emerged lands. The UKW horizon corresponds to the *linguiformis* anoxic event and is markedly recorded in basinal environments and, to a lesser degree, in platform environments. In basinal settings, the development of reducing conditions was more drastic with euxinic conditions rising into water column, and lasted longer that in shelfal environments. The basinal settings also recorded more intense episodes of surface-water productivity than the platforms. Thus, the UKW event has mechanisms other than the LKW event. The onset of reducing conditions on the platforms may have two (complementary) causes. The first cause could be the raise of anoxic waters higher up in the water column in response to a marked sea-level rise and their impingement of platforms. The second cause could be the development of eutrophic conditions in basinal environments according to the model by Ingall and Jahnke (1997) of phosphorus regeneration under anoxic conditions (see also Murphy et al., 2000a). The eutrophication could cause the expansion of anoxic conditions in the water column, temporarily reaching and invading shelfal environments. After the contraction of the anoxic water mass, anoxia could still prevail in bottom environments but oxygenated conditions resumed on the platforms.

Acknowledgements

This study has been funded by the Eclipse program of the C.N.R.S.-I.N.S.U. (leader: O. Averbuch) and is a contribution of the UMR PBDS 8110. We greatly thank J. Morel and L. Sevrin for the ICP analyses in CRPG (Nancy) and F. Baudin (Paris VI University) for Rock-Eval analyses. We also thank M. Vandaele for the preparation of polished thin sections and P. Recourt for technical assistance for SEM analysis. Thanks are also for M. Frere, L.M. Bernard and D. Malengros (Lille 1 University) for technical assistance. We thank P. Wignall, T. Becker and P. Königshof for their much-appreciated advices. We are grateful to Lynn Walter (Chemical Geology editor) and two anonymous reviewers who helped improve considerably this paper. **[LW]**

References

Adelson, J.M., Helz, G.R., Miller, C.V., 2001. Reconstructing the rise of recent coastal anoxia; molybdenum in Chesapeake Bay sediments. Geochim. Cosmochim. Acta 65, 237–252.

Alberti, H., Walliser, O.H., 1977. Überblick über die paläogeographische und tecktonishe Entwicklung des Westharzes.-Exkursionsführer Geotagung 77, I, Exk. H: 172–178, 3 Abb., Göttingen (Geol.-Paläontol. Inst.).

Algeo, T.J., Maynard, J.B., 2004. Trace-element behavior and redox facies in core shales of Upper Pennsylvanian Kansas-type cyclothems. Chem. Geol. 206, 289–318.

Algeo, T.J., Lyons, T.W., in press. Mo-TOC covariation in modern anoxic marine environments: implication for analysis of paleoredox and -hydrographic conditions. Paleoceanography.

Algeo, T.J., Berner, R.A., Maynard, J.B., Scheckler, S.E., 1995. Late Devonian oceanic anoxic events and biotic crises: “rooted” in the evolution of vascular land plants? GSA Today 5, 64–66.

Algeo, T.J., Schwark, L., Hower, J.C., 2004. High-resolution geochemistry and sequence stratigraphy of the Hushpuckney Shale (Swope Formation, eastern Kansas): implications for climato-environmental dynamics of the Late Pennsylvanian Midcontinent Seaway. Chem. Geol. 206, 259–288.

Allen, R.E., 2003. Role of diffusion–precipitation reactions in authigenic pyritization. Chem. Geol. 182, 461–472.

Arthur, M.A., Sageman, B.B., 1994. Marine black shales: a review of depositional mechanisms and significance of ancient deposits. Annu. Rev. Earth Planet. Sci. 22, 499–551.

Arthur, M.A., Sageman, B.B., 2004. Sea-level control on source-rock development: perspectives from the Holocene Black Sea, the Mid-Cretaceous Western Interior Basin of North America, and the Late Devonian Appalachian Basin. In: Harris, N. (Ed.), The Deposition of Organic-Carbon Rich Sediments: Models, Mechanisms, and Consequences. SEPM Spec. Public., vol. 82, pp. 35–59.

Averbuch, O., Tribovillard, N., Devleeschouwer, X., Riquier, L., Mistiaen, B., van Vliet-Lanoe, B., 2005. Mountain building-enhanced continental weathering and organic carbon burial as major causes for climatic cooling at the Frasnian–Famennian boundary (ca 376 Ma BP). Terra Nova 17, 25–34.

Becker, R.T., House, M.R., 1994. Kellwasser events and goniatite successions in the Devonian of the Montagne Noire with comments on possible causations. Cour. Forschungsinst. Senckenberg 199, 129–146.

Berner, R.A., 1970. Sedimentary pyrite formation. Am. J. Sci. 268, 1–23.

Berner, R.A., 1984. Sedimentary pyrite formation: an update. Geochim. Cosmochim. Acta 48, 605–615.

Bond, D., Wignall, P.B., 2005. Evidence for the Late Devonian (Kellwasser) anoxic events in the Great Basin, western United States. In: Over, D.J., Morrow, J.R., Wignall, P.B. (Eds.), Understanding Late Devonian and Permian–Triassic Biotic and Climatic Events: Towards an Integrated Approach: Developments in Palaeontology and Stratigraphy, vol. 20, pp. 225–262.

Bond, D., Wignall, P.B., Racki, G., 2004. Extent and duration of marine anoxia during the Frasnian–Famnennian (Late Devonian) mass extinction in Poland, Germany, Austria and France. Geol. Mag. 141, 173–193.

Brumsack, H.J., 1986. The inorganic geochemistry of Cretaceous black shales (DSDP leg 41) in comparison to modern upwelling sediments from the Gulf of California. In: Summerhayes, C.P., Shackleton, N.J. (Eds.), North Atlantic Palaeoceanography. Geol. Soc. Spec. Publ., vol. 21, pp. 447–462.

Brumsack, H.J., 1989. Geochemistry of recent TOC-rich sediments from the Gulf of California and the Black Sea. Geol. Rundsch. 78, 851–882.

Buggisch, W., 1991. The global Frasnian–Famennian “Kellwasser Event”. Geol. Rundsch. 80, 49–72.

Buggisch, W., Clausen, C.-D., 1972. Conodonten- und Goniatiten-Faunen aus dem oberen Frasnium und unteren Famennium Marokkos (Tafilalt, Antiatlas). N. Jb. Geol. Paläont. Abh. 141, 137–167.

Calvert, S.E., Karlin, R.E., 1991. Relationships between sulfur, organic carbon and iron in the modern sediments of the Black Sea. Geochim. Cosmochim. Acta 55, 2483–2490.

Calvert, S.E., Pedersen, T.F., 1993. Geochemistry of recent oxic and anoxic marine sediments: implications for the geological record. Mar. Geol. 113, 67–88.

Calvert, S.E., Pedersen, T.F., 1996. Sedimentary geochemistry of manganese: implications for the environment of formation of manganiferous black shales. Econ. Geol. 91, 36–47.

Calvert, S.E., Bustin, R.M., Ingall, E.D., 1996. Influence of water column anoxia and sediment supply on the burial and preservation of organic carbon in marine shales. Geochim. Cosmochim. Acta 60, 1577–1593.

Canfield, D.E., Raiswell, R., Bottrell, S., 1992. The reactivity old sedimentary iron minerals toward sulfide. Am. J. Sci. 292, 659–683.

Caplan, M.L., Bustin, R.M., 1999. Devonian–Carboniferous Hangenberg mass extinction event, widespread organic-rich mudrocks and anoxia: causes and consequences. Palaeogeogr. Palaeoclimatol. Palaeoecol. 149, 187–207.

Chen, D., Tucker, M., 2003. The Frasnian-Famennian mass extinction: insights from high-resolution sequence stratigraphy and cyclostratigraphy in South China. Palaeogeogr. Palaeoclim. Palaeoecol. 193, 87–111.

Chen, D., Tucker, M., 2004. Palaeokarst and its implication for the extinction event at the Frasnian–Famennian boundary (Guilin, South China). J. Geol. Soc. 161, 895–898.

Chen, D., Qing, H., Li, R., 2005. The Late Devonian Frasnian/Famennian (F/F) biotic crisis: insights from $\delta^{13}C_{carb}$, δ^{13}Corg and $^{87}Sr/^{86}Sr$ isotopic systematics. Earth Planet. Sci. Lett. 235, 151–166.

Copper, P., 1986. Frasnian/Famennian mass extinction and cold-water oceans. Geology 14, 835–839.

Crick, R.E., Ellwood, B.B., Feist, R., El Hassani, A., Schindler, E., Dreesen, R., Over, D.J., Girard, C., 2002. Magnetostratigraphy susceptibility of the Frasnian/Famennian boundary. Palaeogeogr. Palaeoclimatol. Palaeoecol. 181, 67–90.

Cruse, A.M., Lyons, T.W., 2004. Trace metal records of regional paleoenvironmental variability in Pennsylvanian (Upper Carboniferous) black shales. Chem. Geol. 206, 319–345.

Crusius, J., Calvert, S., Pedersen, T., Sage, D., 1996. Rhenium and molybdenum enrichments in sediments as indicators of oxic, suboxic, and sulfidic conditions of deposition. Earth Planet. Sci. Lett. 145, 65–78.

Dean, W.E., Gardner, J.V., Piper, D.Z., 1997. Inorganic geochemical indicators of glacial–interglacial changes in productivity and anoxia on the California continental margin. Geochim. Cosmochim. Acta 61, 4507–4518.

Demaison, G.J., Moore, G.T., 1980. Anoxic environments and oil source bed genesis. Am. Assoc. Pet. Geol. Bull. 64, 1179–1209.

Devleeschouwer, X., Herbosch, A., Préat, A., 2002. Microfacies, sequence stratigraphy and clay mineralogy of a condensed deep-water section around the Frasnian–Famennian boundary (Steinbruch Schmidt, Germany). Palaeogeogr. Palaeoclimatol. Palaeoecol. 181, 171–193.

Dymond, J., Suess, E., Lyle, M., 1992. Barium in deep-sea sediments: a geochemical proxy for paleoproductivity. Paleoceanography 7, 163–181.

Dymond, J., Collier, R., McManus, J., Honjo, S., Manganini, S., 1997. Can the aluminium and titanium contents of ocean sediments be used to determine the paleoproductivity of the oceans? Paleoceanography 12, 586–593.

Espitalié, J., Deroo, G., Marquis, F., 1986. La pyrolyse Rock-Eval et ses applications, 3$^{\text{ème}}$ partie. Rev. Inst. Fr. Pet. 41, 73–89.

Ettensohn, F.R., 1998. Compressional tectonic controls on epicontinental black-shale depositions: Devonian–Mississipian examples from North America. In: Schieber, J., Zimmerle, W., Sethi, P.S. (Eds.), Shales and Mudstones, vol. 1, pp. 109–128.

Feist, R., 1985. Devonian stratigraphy of the South-eastern Montagne Noire (France). Cour. Forschungsinst. Senckenberg 75, 331–352.

Feist, R., Schindler, E., 1994. Trilobites during the Frasnian Kellwasser Crisis in European Late Devonian cephalopod limestones. Cour. Forschungsinst. Senckenberg 169, 195–223.

Franke, W., 2000. The mid-European segment of the Variscides: tectonostratigraphic units, terrane boundaries and plate tectonic evolution. In: Franke, W., Haak, V., Oncken, O., Tanner, D. (Eds.), Orogenic Processes: Quantification and Modelling in the Variscan Belt. Spec. Publ. Geol. Soc. London, vol. 179, pp. 35–61.

Gabriel, G., Jahr, T., Jentzsch, G., Melzer, J., 1997. Deep structure and evolution of the Harz Mountains: result of three-dimensional gravity and finite element modelling. Tectonophysics 270, 279–299.

Ginter, M., 2002. Chondrichthyan fauna of the Frasnian–Famennian boundary beds in Poland. Acta Palaeontol. Pol. 47, 329–338.

Girard, C., Feist, R., 1997. Eustatic trends in conodont diversity across the Frasnian–Famennian boundary in the stratotype area, Montagne Noire, Southern France. Lethaia 29, 329–337.

Godderis, Y., Joachimski, M.M., 2004. Global change in the Late Devonian: modelling the Frasnian–Famennian short-term carbone isotope excursions. Palaeogeogr. Palaeoclimatol. Palaeoecol. 202, 309–329.

Goldhaber, M.B., Kaplan, I.R., 1974. The sulfur cycle. In: Goldberg, E.D. (Ed.), The Sea, vol. 5. Wiley-Interscience, New York, pp. 569–655.

Golonka, J., Ross, M., Scotese, C.R., 1994. Phanerozoic paleogeographic and paleoclimatic modeling maps. In: Embry, A.F., Beauchamp, B., Glass, D.J. (Eds.), Global Environments and Resources. Canadian Society of Petroleum Geologists, Memoir, vol. 17, pp. 1–47.

Hallam, A., Wignall, P.B., 1997. Mass Extinction and their Aftermath. Oxford University Press, Oxford. 330 pp.

Hallam, A., Wignall, P.B., 1999. Mass extinctions and sea-level changes. Earth. Sci. Rev. 48, 217–250.

Hatch, J.R., Leventhal, J.S., 1992. Relationship between inferred redox potential of the depositional environment and geochemistry of the Upper Pennsylvanian (Missourian) Stark Shale Member of the Dennis Limestone, Wabaunsee County, Kansas, U.S.A. Chem. Geol. 99, 65–82.

Helz, G.R., Miller, C.V., Charnock, J.M., Mosselmans, J.L.W., Pattrick, R.A.D., Garner, C.D., Vaughan, D.J., 1996. Mechanisms of molybdenum removal from the sea and its concentration in black shales: EXAFS evidences. Geochim. Cosmochim. Acta 60, 3631–3642.

House, M.R., 2002. Strength, timing, setting and cause of mid-Palaeozoic extinctions. Palaeogeogr. Palaeoclimatol. Palaeoecol. 181, 5–25.

Hurtgen, M.T., Lyons, T.W., Ingall, E.D., Cruse, A.M., 1999. Anomalous enrichments of iron monosulfide in euxinic marine sediments and the role of H_2S in iron sulfide transformations: examples from Effingham Inlet, Orca Basin, and the Black Sea. Am. J. Sci. 299, 556–588.

Ingall, E., Jahnke, R., 1997. Influence of water-column anoxia on the elemental fractionation of carbon and phosphorus during diagenesis. Mar. Geol. 139, 219–229.

Joachimski, M.M., Buggisch, W., 1993. Anoxic events in the late Frasnian—causes of the Frasnian–Famennian faunal crisis. Geology 21, 675–678.

Joachimski, M.M., Buggisch, W., 2002. Conodont apatite $\delta^{18}O$ signatures indicate climatic cooling as a trigger of the Late Devonian mass extinction. Geology 30, 711–714.

Joachimski, M.M., Buggisch, W., Anders, T., 1994. Mikrofazies, Conodontenstratigraphie und Isotopengeochimie des Frasne/Famenne Grenzprofils Wolayer Gletscher (Karnische Alpen). Abh. Geol. Bundesanst. Wien 50, 183–195.

Joachimski, M.M., Ostertag-Henning, C., Pancost, R.D., Strauss, H., Freeman, K.H., Littke, R., Sinninghe Damsté, J.S., Racki, G., 2001. Water column anoxia, enhanced productivity and concomitant changes in $\delta^{13}C$ and $\delta^{34}S$ across the Frasnian–Famennian boundary (Kowala Holy Cross Mountains/Poland). Chem. Geol. 175, 109–131.

Joachimski, M.M., Pancost, R.D., Freeman, K.H., Ostertag-Henning, C., Buggisch, W., 2002. Carbon isotope geochemistry of the Frasnian–Famennian transition. Palaeogeogr. Palaeoclimatol. Palaeoecol. 181, 91–109.

Joachimski, M.M., van Geldern, R., Breisig, S., Buggisch, W., Day, J., 2004. Oxygen isotope evolution of biogenic calcite and apatite during the Middle and Late Devonian. Int. J. Earth Sci. 93, 542–553.

Johnson, J.G., Klapper, G., Sandberg, C.A., 1985. Devonian eustatic fluctuations in Euramerica. Geol. Soc. Amer. Bull. 96, 567–587.

Jones, B., Manning, D.A.C., 1994. Comparison of geochemical indices used for the interpretation of palaeoredox conditions in ancient mudstones. Chem. Geol. 111, 111–129.

Kryc, K.A., Murray, R.W., Murray, D.W., 2003. Al-to-oxide and Ti-to-organic linkage in biogenic sediments: relationship to paleo-export production and bulk Al/Ti. Earth Planet. Sci. Lett. 211, 125–141.

Lazreq, N., 1992. The upper Devonian of M'rirt (Morocco). Cour. Forschungsinst. Senckenberg 154, 107–123.

Lazreq, N., 1999. Biostratigraphie des conodontes du Givétien au Famennien du Maroc Central. Biofaciès et événement Kellwasser. Cour. Forschungsinst. Senckenberg 214, 1–111.

Lethiers, F., Baudin, F., Casier, J.-G., 1998. Ostracodes de la limite Frasnien–Famennien en environnement anoxique (La Serre, Montagne Noire, France). Rev. Micropaléontol. 41, 321–336.

Lipinski, M., Warning, B., Brumsack, H.-J., 2003. Trace metal signatures of Jurassic/Cretaceous black shales from the Norwegian Shelf and the Barent Sea. Palaeogeogr. Palaeoclimatol. Palaeoecol. 190, 459–475.

Lyons, T.W., 1997. Sulfur isotope trends and pathways of iron sulfide formation in upper Holocene sediments of the anoxic Black Sea. Geochim. Cosmochim. Acta 61, 3367–3382.

Lyons, T.W., Werne, J.P., Hollander, D.J., Murray, R.W., 2003. Contrasting sulfur geochemistry and Fe/Al and Mo/Al ratios across the last oxic-to-anoxic transition in the Cariaco Basin, Venezuela. Chem. Geol. 195, 131–157.

McGhee, G.R., 1989. The Frasnian–Famennian event. In: Donovan, S. K. (Ed.), Mass Extinction: Processes and Evidences. Belhaven Press, London, pp. 133–151.

McGhee, G.R., 1996. The Late Devonian Mass Extinction. The Frasnian–Famennian Crisis. Columbia University Press, New York.

McManus, J., Berelson, W.M., Klinkhammer, G.P., Johnson, K.S., Coale, K.H., Anderson, R.F., Kumar, N., Burdige, D.J., Hammond, D.E., Brumsack, H.-J., McCorkle, D.C., Rushdi, A., 1998. Geochemistry of barium in marine sediments: implications for its use as a paleoproxy. Geochim. Cosmochim. Acta 62, 3453–3473.

Meyers, S.R., Sageman, B.B., Lyons, T.W., 2005. Organic carbon burial rate and the molybdenum proxy: theoretical framework and application to Cenomanian–Turonian oceanic event 2. Paleoceanography 20, PA2002. doi:10.1029/2004PA001068.

Middelburg, J.J., 1991. Organic carbon, sulphur and iron in recent semi-euxinic sediments of Kau Bay, Indonesia. Geochim. Cosmochim. Acta 55, 815–828.

Mongenot, T., Tribovillard, N.-P., Desprairies, A., Lallier-Vergès, E., Laggoun-Defarge, F., 1996. Trace elements as palaeoenvironmental markers in strongly mature hydrocarbon source rocks: the Cretaceous La Luna Formation of Venezuela. Sediment. Geol. 103, 23–37.

Morford, J.L., Emerson, S., 1999. The geochemistry of redox sensitive trace metals in sediments. Geochim. Cosmochim. Acta 63, 1735–1750.

Murphy, A.E., Sageman, B.B., Hollander, D.J., 2000a. Eutrophication by decoupling of the marine biogeochemical cycles of C, N and P: a mechanism for the Late Devonian mass extinction. Geology 28, 427–430.

Murphy, A.E., Sageman, B.B., Hollander, D.J., Lyons, T.L., Brett, C. E., 2000b. Black shale deposition and faunal overturn in the Devonian Appalachian Basin: clastic starvation, seasonal water-column mixing, and efficient biolimiting nutrient recycling. Paleoceanography 15, 280–291.

Murray, R.W., Leinen, M., 1996. Scavenged excess aluminium and its relationship to bulk titanium in biogenic sediment from the Centralm equatorial Pacific Ocean. Geochim. Cosmochim. Acta 60, 3869–3878.

Pedersen, T.F., Calvert, S.E., 1990. Anoxia vs. productivity: what controls the formation of organic-carbon-rich sediments and sedimentary rocks? AAPG Bull. 74, 454–466.

Peterhansel, A., Pratt, B.R., 2001. Nutrient-triggered bioerosion on a giant carbonate platform masking the post-extinction Famennian benthic community. Geology 29, 1079–1082.

Piper, D.Z., Perkins, R.B., 2004. A modern vs. Permian black shale—the hydrography, primary productivity, and water-column chemistry of deposition. Chem. Geol. 206, 177–197.

Pujol, F., Berner, Z., Stüben, D., (in correction). Chemostratigraphy of some European Frasnian–Famennian boundary key section. Palaeogeogr. Palaeoclimatol. Palaeoecol.

Rachold, V., Brumsack, H.J., 2001. Inorganic geochemistry of Albian sediments from the Lower Saxony Basin NW Germany: paleoenvironmental constraints and orbital cycles. Palaeogeogr. Palaeoclimatol. Palaeoecol. 174, 121–143.

Racki, G., 1998. Frasnian–Famennian biotic crisis: undervalued tectonic control? Palaeogeogr. Palaeoclimatol. Palaeoecol. 141, 177–198.

Racki, G., 1999. Silica-secreting biota and mass extinctions: survival patterns and processes. Palaeogeogr. Palaeoclimatol. Palaeoecol. 154, 107–132.

Racki, G., Racka, M., Matyja, H., Devleeschouwer, X., 2002. The Frasnian/Famennian boundary interval in the South Polish-Moravian shelf basins: integrated event-stratigraphical approach. Palaeogeogr. Palaeoclimatol. Palaeoecol. 181, 251–297.

Raiswell, R., Canfield, D.E., 1998. Sources of iron for pyrite formation in marine sediments. Am. J. Sci. 298, 219–245.

Riboulleau, A., Baudin, F., Deconinck, J.-F., Derenne, S., Largeau, C., Tribovillard, N., 2003. Depositional conditions and organic matter preservation pathways in an epicontinental environment: the Upper Jurassic Kashpir Oil Shales (Volga Basin, Russia). Palaeogeogr. Palaeoclimatol. Palaeoecol. 197, 171–197.

Rickard, D.T., 1975. Kinetics and mechanism of pyrite formation at low temperatures. Am. J. Sci. 275, 636–652.

Rimmer, S.M., 2004. Geochemical paleoredox indicators in Devonian–Mississippian black shales, Central Appalachian Basin (USA). Chem. Geol. 206, 373–391.

Rimmer, S.M., Thompson, J.A., Goodnight, S.A., Robl, T.L., 2004. Multiple controls on the preservation of organic matter in Devonian–Mississippian marine black shales: geochemical and petrographic evidence. Palaeogeogr. Palaeoclimatol. Palaeoecol. 215, 125–154.

Riquier, L., Tribovillard, N., Averbuch, O., Joachimski, M.M., Racki, G., Devleeschouwer, X., El Albani, A., Riboulleau, A., 2005. Productivity and bottom water redox conditions at the Frasnian–Famennian boundary on the both sides of the Eovariscan Belt constraints from trace element geochemistry. In: Over, D.J., Morrow, J.R., Wignall, P.B. (Eds.), Understanding Late Devonian and Permian–Triassic Biotic and Climatic Events: Towards an Integrated Approach: Developments in Palaeontology and Stratigraphy, vol. 20, pp. 199–224.

Roemer, F.A., 1850. Beiträge zur Kenntnis des nordwestlichen Harzgebirges. Palaeontographica 3, 1–67.

Sageman, B.B., Murphy, A.E., Werne, J.P., Ver Straeten, C.A., Hollander, D.J., Lyons, T.W., 2003. A tale of shales: the relative roles of production, decomposition, and dilution in the accumulation of organic-rich strata, Middle–Upper Devonian, Appalachian basin. Chem. Geol. 195, 229–273.

Sandberg, C.A., Poole, F., Johnson, J.G., 1988. Upper Devonian of the western United States. In: McMillan, N.J., Embry, A.F., Glass, D.J. (Eds.), Devonian of the World: Volume I. Regional Syntheses, Proceedings of the 2nd International Symposium on the Devonian System, Calgary, Canada. Can. Soc Petrol. Geol., pp. 183–220.

Sandberg, C.A., Morrow, J.R., Ziegler, W., 2002. Late Devonian sea level changes, catastrophic events and mass extinctions. Geol. Soc. Am., Spec. Pap. 356, 473–487.

Schindler, E., 1990. Die Kellwasser Krise (hohe Frasne-Stufe, Ober Devon). Gött. Arb. Geol. Paläontol. 46, 1–125.

Schindler, E., 1993. Event-stratigraphic markers within the Kellwasser Crisis near the Frasnian/Famennian boundary (Upper Devonian) in Germany. Palaeogeogr. Palaeoclimatol. Palaeoecol. 104, 115–125.

Schippers, A., Jørgensen, B.B., 2001. Schippers oxidation of pyrite and iron sulfide by manganese dioxide in marine sediment. Geochim. Cosmochim. Acta 65, 915–922.

Schoonen, M.A.A., Barnes, H.L., 1991a. Reactions forming pyrite and marcasite from solution: I. Nucleation of FeS_2 below 100 °C. Geochim. Cosmochim. Acta 55, 1495–1504.

Schoonen, M.A.A., Barnes, H.L., 1991b. Reactions forming pyrite and marcasite from solution: II. Via FeS precursors below 100 °C. Geochim. Cosmochim. Acta 60, 115–134.

Scotese, C.R., 1997. Paleogeographic Atlas, PALEOMAP Progress report 90-0497. Department of Geology, University of Texas at Airlington. 45 pp.

Sepkoski, J.J., 1986. Phanerozoic overview of mass extinctions. In: Raup, D.M., Jablonski, D. (Eds.), Patterns and Processes in the History of Life. Springer-Verlag, Berlin, pp. 277–295.

Suits, N.S., Arthur, M.A., 2000. Sulfur diagenesis and partitioning in Holocene Peru shelf and upper slope sediments. Chem. Geol. 163, 219–234.

Taylor, K.G., Macquaker, J.H.S., 2000. Early diagenetic pyrite morphology in a mudstone-dominated succession: the Lower Jurassic Cleveland Ironstone Formation, eastern England. Sediment. Geol. 131, 77–86.

Timothy, D.A., Calvert, S.E., 1998. Systematics of variations in excess Al and Al/Ti in sediments from the central equatorial Pacific. Paleoceanography 13 (2), 127–130.

Tribovillard, N., Averbuch, O., Riboulleau, A., 2004a. Influence of marine organic-matter diagenesis on magnetic suceptibility of sedimentary rocks: the sulphide pathway. Ann. Soc. Géol. Nord 11, 57–67.

Tribovillard, N., Averbuch, O., Devleeschouwer, X., Racki, G., Riboulleau, A., 2004b. Deep-water anoxia over the Frasnian–Famennian boundary (La Serre, France): a tectonically induced oceanic anoxic event? Terra Nova 16, 288–295.

Tribovillard, N., Ramdani, A., Trentesaux, A., 2005. Controls on organic accumulation in Late Jurassic shales of Northwestern Europe as inferred from trace-metal geochemistry. In: Harris, N. (Ed.), Deposition of Hydrocarbon Source Rocks. SEPM Spec. Public., vol. 82, pp. 145–164.

Tribovillard, N., Algeo, T., Lyons, T, Riboulleau, A., in press. A practical synthesis about trace metals used as proxies to paleoredox and paleoproductivity conditions. Chem. Geol.

Tyson, R.V., Pearson, T.H., 1991. Modern and ancient continental shelf anoxia. Geol. Soc. Spec. Publ. 58 (470 pp.).

Van der Weijden, C.H., 2002. Pitfalls of normalization of marine geochemical data using a common divisor. Mar. Geol. 184, 167–187.

Walliser, O.H., 1996. Global Events and Event Stratigraphy in the Phanerozoic: Results of International Interdisciplinary Cooperation in the IGCP Project 216 “Global Biological Events in Earth History”. Springer-Verlag, Heidelberg. 333 pp.

Wedepohl, K.H., 1971. Environmental influences on the chemical composition of shales and clays. In: Ahrens, L.H., Press, F., Runcorn, S.K., Urey, H.C. (Eds.), Phys. Chem. Earth. Pergamon, Oxford, pp. 305–333.

Wedepohl, K.H., 1991. The composition of the upper Earth’s crust and the natural cycles of selected metals. In: Merian, E. (Ed.), Metals and their Compounds in the Environment. VCH-Verlagsgesellschaft, Weinheim, pp. 3–17.

Wendt, J., Belka, Z., 1991. Age and depositional environment of Upper Devonian (Early Frasnian to Early Famennian) black shales and limestones (Kellwasser Facies) in the eastern Anti-Atlas, Morocco. Facies 25, 51–90.

Werne, J.P., Sageman, B.B., Lyons, T.W., Hollander, D.J., 2002. An integrated assessment of a “type euxinic” deposit: evidence for multiple controls on black shales deposition in the Middle Devonian Oatka Creek Formation. Am. J. Sci. 303, 110–143.

Wignall, P.B., 1994. Black shales. Geology and Geophysics Monographs, vol. 30. Oxford University Press. 130 pp.

Wignall, P.B., Newton, R., 1998. Pyrite framboid diameter as a measure of oxygen-deficiency in ancient mudrocks. Am. J. Sci. 298, 537–552.

Wignall, P.B., Newton, R., Brookfield, M.E., 2005. Pyrite framboid evidence for oxygen-poor deposition during the Permian–Triassic crisis in Kashmir. Palaeogeogr. Palaeoclimatol. Palaeoecol. 216, 183–188.

Wijsman, J.W.M., Middelburg, J.J., Heip, C.H.R., 2001. Reactive iron in Black Sea sediments: implications for iron cycling. Mar. Geol. 172, 167–180.

Wilkin, R.T., Barnes, H.L., 1996. Pyrite formation by reactions of iron monosulphides with dissolved inorganic and organic sulphur species. Geochim. Cosmochim. Acta 60, 4167–4179.

Wilkin, R.T., Barnes, H.L., Brantley, S.L., 1996. The size distribution of framboidal pyrite in modern sediments: an indicator of redox conditions. Geochim. Cosmochim. Acta 60, 3897–3912.

Wilkin, R.T., Arthur, M.A., Dean, W.E., 1997. History of water column anoxia in the Black Sea indicated by pyrite framboid size distributions. Earth Planet. Sci. Lett. 148, 517–525.

Yarincik, K.M., Murray, R.W., Peterson, L.C., 2000. Clilatically sensitive eolian and hemipelagic deposition in the Cariaco Basin, Venezuela, over the past 578,000 years: results from Al/Ti and K/Al. Paleoceanography 15, 210–228.

Yudina, A.B., Racki, G., Savage, N.S., Racka, M., Malkowski, K., 2002. The Frasnian–Famennian events in deep-shelf succession, Subpolar Urals: biotic, depositional and geochemical records. Acta Palaeontol. Pol. 47, 355–372.

Zheng, Y., Anderson, R.F., van Geen, A., Kuwabara, J., 2000. Authigenic molybdenum formation in marine sediments: a link to pore water sulfide in the Santa Barbara Basin. Geochim. Cosmochim. Acta 64, 4165–4178.

Article 16.

Riquier L., Averbuch O., Tribovillard N., El Albani A., Lazreq N. and Chakiri S. (2007). Environmental changes at the Frasnian-Famennian boundary in Central Morocco (northern Gondwana): integrated rock-magnetic and geochemical studies. In : Devonan Event Stratigraphy and Correlations, T. Becker and B. Kirchgasser eds., Spec. Pub. Geol. Soc. London, 278, 197-217.

Environmental changes at the Frasnian–Famennian boundary in Central Morocco (Northern Gondwana): integrated rock-magnetic and geochemical studies

L. RIQUIER[1], O. AVERBUCH[1], N. TRIBOVILLARD[1], A. EL ALBANI[2], N. LAZREQ[3] & S. CHAKIRI[4]

[1]*UMR 8110, Processus et Bilans en Domaines Sédimentaires, Bâtiment SN5, Université de Lille 1, F-59655 Villeneuve d'Ascq cedex, France (e-mail: Laurent.Riquier@univ-lille1.fr)*

[2]*UMR 6532, Hydrogéologie, Argiles, Sols et Altérations, Bâtiment Sciences Naturelles, Université de Poitiers, 40 Avenue du recteur Pineau, F-86088 Poitiers cedex, France*

[3]*Université Cadi Ayyad de Marrakech, Faculté des Sciences Semlalia, Département de Géologie, Avenue du Prince Moulay Abdellah, BP 2390, 40001 Marrakech, Morocco*

[4]*Université Ibn Tofail, Faculté des Sciences, Laboratoire de Géologie dynamique et appliquée, BP 133, 14000 Kénitra, Morocco*

Abstract: Rock magnetic (magnetic susceptibility and hysteresis parameters) and geochemical analyses (major and trace elements) were carried out on whole rock samples of two Frasnian–Famennian boundary sections, Anajdam and Bou-Ounebdou in the Central Morocco (Western Meseta). During the Frasnian, the decreasing trend of the magnetic susceptibility signal, mainly carried by low-coercivity magnetite grains, indicates a gradual reduction of detrital influx. This decrease in detrital input parallels a Frasnian long-term sea-level rise. In the Late Frasnian Kellwasser Horizons, that are classically considered to represent highstand deposits, the magnetic signal exhibits the lowest intensities in connection with maximum diamagnetic contribution of the carbonate fraction. With respect to geochemical data, the two black carbonate-rich Kellwasser Horizons are characterized by noticeable positive anomalies of bottom-water dysoxic proxies and of marine primary productivity markers. Our data thus suggest that in Central Morocco, the Late Frasnian marine environments were marked by a relatively important biogenic productivity favouring the onset of oxygen-depleted conditions during periods of maximum transgression on the continental platforms.

The Frasnian–Famennian (F–F) boundary (Late Devonian, 374.5 Ma ago; Gradstein *et al.* 2004); was a major period of biodiversity loss and environmental changes. This boundary corresponds to one of the five biggest biological mass extinctions of the Phanerozoic, in which many species of marine organisms died out (e.g. corals, stromatoporoids, trilobites, conodonts, cephalopods) (Sepkoski 1982, 1986; Copper 1986; Sandberg *et al.* 1988; Schindler 1990; Becker & House 1994; McGhee 1996; Walliser 1996; Hallam & Wignall 1999; House 2002; Ma & Bai 2002; Racki *et al.* 2002). This period has been also suggested to be the time of significant climatic variations, attested by the $\delta^{18}O$ signature of marine conodonts apatite (Joachimski & Buggisch 2002; Joachimski *et al.* 2004) and the evolution of the miospore diversity on continents (Streel *et al.* 2000). Such climatic effects are likely to have induced global sea-level fluctuations that, combined with the changes in the erosional processes on land, potentially resulted in varying the intensity of the basinal detrital supply (e.g. Ellwood *et al.* 2000).

On the other hand, the Upper Frasnian interval is generally associated with the deposition of one or two organic-rich units in outer shelf and epicontinental basin settings, i.e. the Kellwasser (KW) Horizons (e.g. Buggisch & Clausen 1972; Sandberg *et al.* 1988; Schindler 1990; Buggisch 1991; Wendt & Belka 1991; Becker & House 1994). These beds have been recognized in many sections, located on the borders of Laurassian (N. America, N. Europe), Gondwanan (S. Europe, Africa), South China and on the southern border of the Siberian continents. Numerous factors controlling the KW organic-rich sediment accumulations have been proposed, such as increased primary productivity or bottom-water oxygen-depleted

From: BECKER, R. T. & KIRCHGASSER, W. T. (eds) *Devonian Events and Correlations*. Geological Society, London, Special Publications, **278**, 197–217. DOI: 10.1144/SP278.9
0305-8719/07/$15

conditions (e.g. Buggisch 1991; Joachimski & Buggisch 1993; Becker & House 1994; Murphy *et al.* 2000*a*, *b*; Bond *et al.* 2004; Tribovillard *et al.* 2004*a*; Riquier *et al.* 2005). These factors have been connected to different driving mechanisms acting in isolation or combined, such as sea-level fluctuations, climatic variations, land plants spreading, volcanism or mountain building (e.g. Becker & House 1994; Algeo & Scheckler 1998; Racki 1998, 1999; Joachimski & Buggisch 2002; Godderis & Joachimski 2004; Averbuch *et al.* 2005).

The aims of this study are to present the sedimentary record of the Late Devonian events from two Moroccan sections, where the KW horizons are particularly well exposed. Rock magnetic data, combined with clay mineralogical studies and geochemical analyses of major compounds, will be discussed with respect to the nature and the intensity of the detrital supply versus carbonate productivity during the F–F boundary events. An additional extensive geochemical data set of inorganic elemental ratios is presented here to document marine oxygen (O_2) levels and productivity conditions during deposition of the KW horizons.

Geological setting

The Central Moroccan Meseta belongs to the Variscan orogenic belt of Northern Africa (Fig. 1a). In Devonian times, it represents a transitional zone between platform domains to the west and southwest (Western Meseta) and a deep turbiditic basin to the east and north (Eastern Meseta, Rif; e.g. El Hassani & Tahiri 2000*a*; Chakiri 2002). This strongly segmented continental margin, which developed at subtropical palaeolatitudes along the northern border of Gondwana, was sequentially dismembered by thrust movements from Late Devonian (the internal metamorphic zones of the Eastern Meseta) to Upper Carboniferous times (the external non-metamorphic Central and Western Meseta; Bouabdelli 1989; Piqué *et al.* 1993; Bouabdelli & Piqué 1996).

In more detail, the two investigated sections, Bou-Ounebdou and Anajdam, were deposited in the Azrou–Kenifra Basin, which forms the easternmost termination of the Moroccan Central Massif. It developed as a transtensional basin in Lower Devonian times and was inverted not earlier than in Upper Viséan times as the thrust front propagated towards the southwest (Bouabdelli 1989). Both Upper Devonian sections, located in the M'rirt area (Fig. 1b), were thus deposited in a relatively tectonically quiet passive margin-type environment.

The sections of Bou-Ounebdou and Anajdam were well-studied Late Devonian sections: during the last decade, detailed investigations on sedimentary sequences and stratigraphy have been done, particularly within the IGCP projects 421 on 'North Gondwanan Mid-Palaeozoic bioevent/biogeography patterns in relation to crustal dynamics' (El Hassani & Tahiri 2000*a*) and by the Subcommission on Devonian Stratigraphy. The Anajdam and Bou-Ounebdou sections were described in detail by Lazreq (1992, 1999), Becker and House (2000), Walliser *et al.* (2000) and Chakiri (2002). The Bou-Ounebdou section has also been studied by Girard and Albarède (1996), Feist (2002) and Joachimski *et al.* (2002).

Bou-Ounebdou

The Bou-Ounebdou section, corresponding to the section M'rirt II in Walliser *et al.* (2000), is located in the M'rirt Nappe, about 5 km southeast of M'rirt (Fig. 1b). The sampled interval records condensed carbonate sedimentation from the Frasnian Lower *hassi* Zone to the Famennian Upper *triangularis* Zone (Fig. 2). The Late Devonian sequence is about 5.5 m thick and exposes a succession of cephalopod limestone beds, mudstones to wackestones in texture, with intercalated calcareous shale levels. The occurrence of pelagic and nektobenthic faunas argues for a moderately deep outer platform setting (Becker 1993; Becker & House 2000; Chakiri 2002). Two black limestone levels, which are globally time-equivalent to the KW horizons of the Rhenohercynian Massif (Germany), have been identified (Lazreq 1992; Becker 1993). The Lower Kellwasser (LKW) horizon is about 25 cm thick and is observed at the base of the Upper *rhenana* Zone. The 20 cm thick Upper Kellwasser Horizon (UKW) consists of lenticular lenses of black limestones, alternating with black shales. The two KW horizons contain abundant nektonic and planktonic fauna, including orthoconic nautiloids and ammonoids, conodonts and tentaculitids. Previously, the base of the UKW horizon was assigned to the uppermost part of the Upper *rhenana* Zone whereas the end of the UKW horizon was regarded as in the *linguiformis* Zone (Lazreq 1992, 1999). New biostratigraphical data from Becker & House (2000) and Girard *et al.* (2005) refined this stratigraphical framework showing that the UKW horizon was only restricted to the *linguiformis* Zone (Fig. 2). On top of the UKW horizon, the F–F boundary is represented by a surface of discontinuity (Lazreq 1999; Becker & House 2000; Chakiri 2002). Based on micro- and biofacies analysis, this discontinuity has been interpreted as the result of a significant sea-level fall (Chakiri 2002). However, the

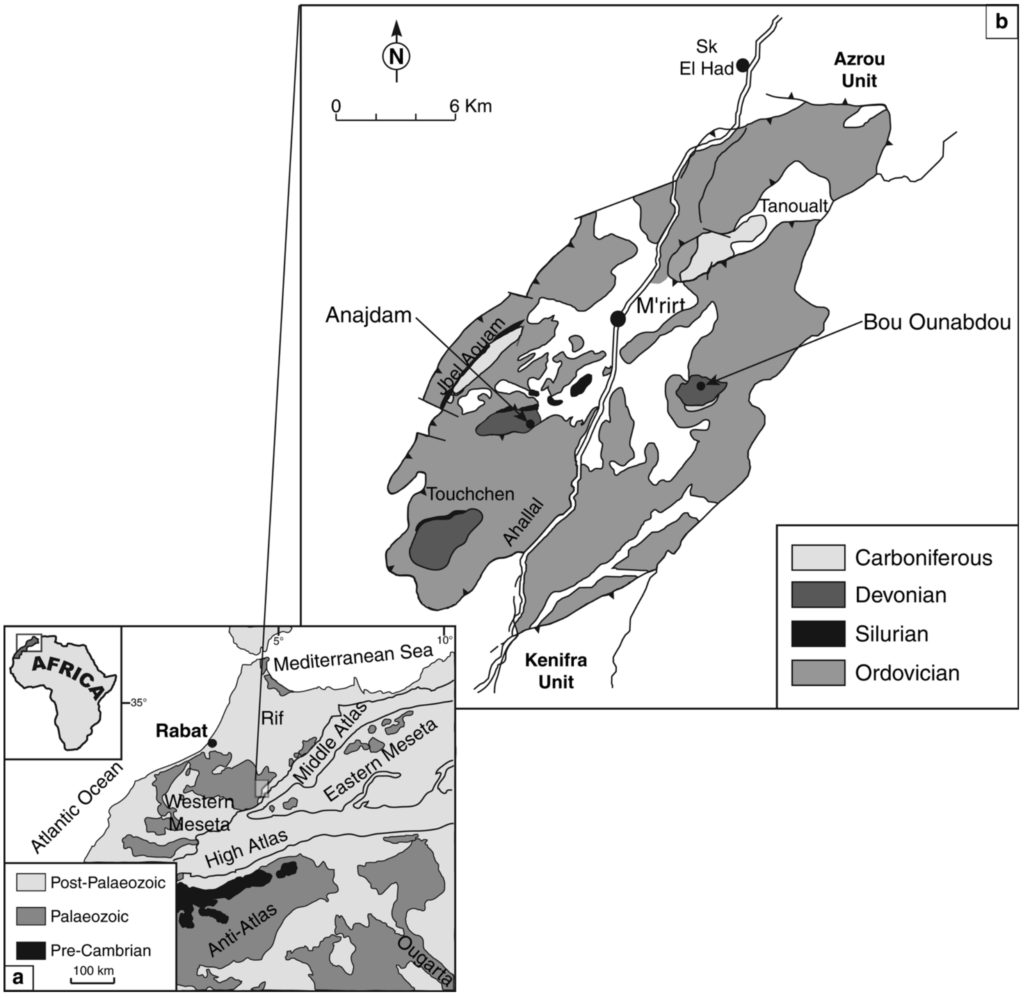

Fig. 1. (**a**) Main structural subdivision of middle and northern Morocco and (**b**) location of the studied sections in the M'rirt unit (modified from Bouabdelli 1989).

regression does not appear to have caused a zonal gap at the base of the Famennian (i.e. *triangularis* Zone), as illustrated by the correlation of the *Phoenixites* limestone (Lower *triangularis* Zone) observed between the M'rirt area and the Mont Peyroux Nappe (Montagne Noire) (Becker & House 2000). The sampled Lower Famennian deposits are characterized by 2 m thick, grey griotte limestones.

Anajdam

This section is located in a thrust-sheet developed in the footwall of the M'rirt nappe (Fig. 1b; Bouabdelli 1989). The exposed Upper Devonian succession is about 4.5 m thick and consists of bioclastic limestones with rare marly beds (Fig. 2). Limestone microfacies are represented mostly by packstones and wackestones. The investigated sequence begins within the *falsiovalis* Zone, at the Givetian–Frasnian boundary, and ranges up to the Lower *triangularis* Zone in basal Famennian times (Lazreq 1999). The faunal associations (conodonts, ammonoids, ostracodes and gastropods) characterize an external platform setting. In the Late Frasnian, two 20–45 cm thick dark-grey and black limestone horizons were biostratigraphically identified as the LKW horizon at the base of the Upper *rhenana* Zone, and the UKW horizon, within the *linguiformis* Zone (Fig. 2).

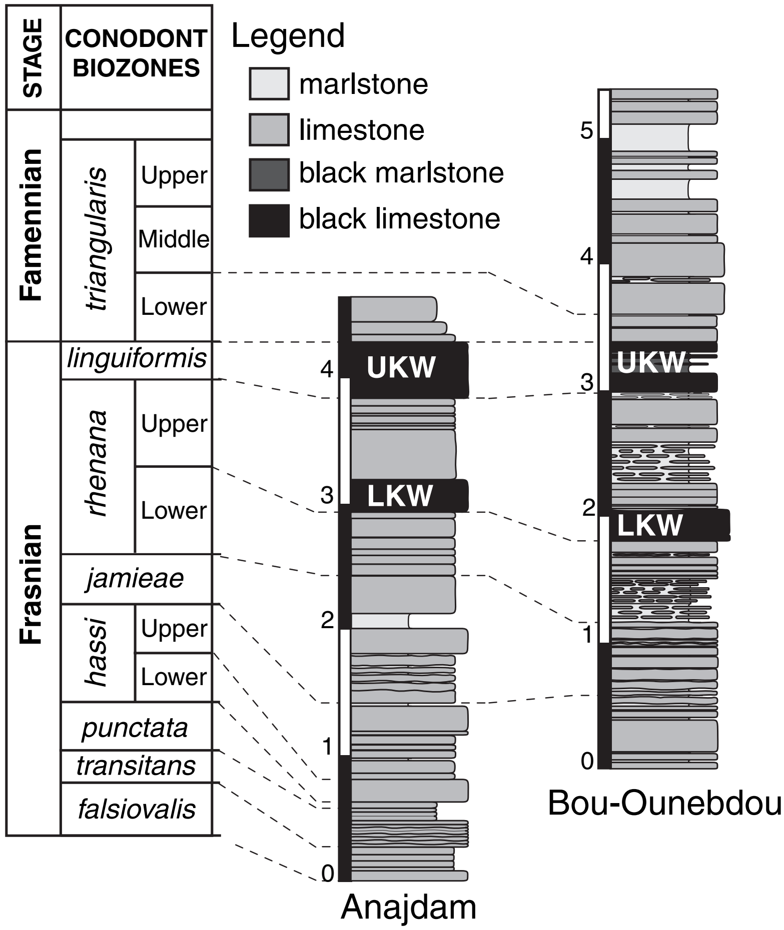

Fig. 2. Stratigraphical columns of the Frasnian–Famennian boundary beds in Anajdam and Bou-Ounebdou (biostratigraphical correlation based on data from Lazreq 1999; Becker & House 2000; Girard *et al.* 2005).

Material and analytical methods

Clay mineralogy

Clay mineral associations have been investigated by X-ray diffraction (XRD) using oriented mounts of the <2 μm size fraction containing non-calcareous particles. Deflocculation of clay aggregates was performed by successive washing with distilled water after decarbonatation of the crushed rock samples. The clay-sized fraction (<2 μm) was separated by settling and centrifugation and placed onto two glass slides and left dry in order to prepare oriented specimens. One of the air-dried, oriented clay-aggregate mounts was saturated in an ethylene glycol atmosphere at 20 °C overnight and another one was heated for two hours at 490 °C (Holtzapffel 1985). So, a series of three X-ray diffractograms was performed for each sample after air-drying, ethylene-glycol solvation and heating. X-ray diffractograms were obtained using a Philips PW 1729 diffractometer, with CuKα radiations and Ni filter, operating at a voltage of 40 KV and a current of 25 mA at a scanning rate of 1°2θ/min.

The identification of clay minerals was made according to the position of the (001) series of basal reflections on the three X-ray diffractograms (Brindley & Brown 1980). Semi-quantitative estimations of major clay minerals, as well as the illite crystallinity index, have been calculated using the Macdiff software (Petschick *et al.* 1996). Measured illite crystallinity index values were converted into the international calibrated scale CIS (Warr & Rice 1994) using a routine correlation process exposed in Robion *et al.* (1999).

The reproducibility of technical works and measurements was tested: the relative error is 5%.

Rock magnetism

The rock magnetic study integrated along-section magnetic susceptibility measurements coupled to representative measurements of magnetic hysteresis loops. The magnetic susceptibility quantifies the ability of the sedimentary rocks under study to be magnetized in a weak magnetic field, according to the respective concentrations of dia- (mainly calcite and quartz), para- (mainly illite, smectite, pyrite) and ferromagnetic *sensu lato* minerals (e.g. magnetite, goethite, haematite, pyrrhotite; see for example Walden *et al.* 1999 or Maher & Thompson 1999 for a more detailed description). In ancient sedimentary rocks, in the absence of intense diagenetic alteration, the magnetic susceptibility has been widely shown to provide a record of the bulk mineralogical changes induced by detrital inputs (magnetite, clays) and biogenic pelagic dilution (diamagnetic calcite; e.g. Crick *et al.* 1997; Devleeschouwer 1999; Ellwood *et al.* 2000; Tribovillard *et al.* 2002). The magnetic susceptibility data set includes 130 samples (70 measurements in Anajdam and 60 in Bou-Ounebdou) collected at 5 to 10 cm intervals, allowing high-resolution study of the magnetic susceptibility fluctuations. Low-field magnetic susceptibility was measured on small rock samples using a Kappabridge KLY-2 susceptibility bridge operating at an alternating-magnetic field of 300 A/m. Each sample was measured three times and a mean of these measurements is reported as the magnetic susceptibility value for that sample. Magnetic susceptibility values are normalized with respect to sample mass. Samples were weighted with a precision of 0.01 g from rock chips. So, results are reported here in mass-normalized magnetic susceptibility, hereafter χ ($m^3\ kg^{-1}$).

Hysteresis parameters were obtained from selected samples (15 measures for each section), using 10–30 mg chips, analysed at room temperature with an Alternating Gradient Force Magnetometer (AGFM 2900) at the Laboratoire des Sciences du Climat et de l'Environnement (Gif-sur-Yvette, France). By definition, hysteresis loops show the evolution of magnetization (M) of magnetic elements as a function of the applied magnetic field (H) (Fig. 3) (e.g. Borradaile *et al.* 1993; Walden *et al.* 1999). The sample is vibrated at room temperature in a magnetic field that is swept from 0 to +1 to −1 T then back to 0 T. From hystereris loop, four parameters are extracted: the saturation (isothermal) magnetization M_s ($\mu A.m^2$), the saturation (isothermal) remanent magnetization M_r ($\mu A.m^2$), the coercive force H_c (mT), and the coercivity of the remanence H_{cr} (mT) (Fig. 3). Values of M_s, M_r and H_c were determined for each hysteresis loop, after corrections for the high-field slope (SC: Slope Correction), which records the combined effects of paramagnetic and diamagnetic contributions. As for χ, magnetic parameters M_s, M_r and SC are normalized with respect to sample mass. H_{cr} was determined by stepwise application of a back-field isothermal remanence to remove the saturation remanence. The hysteresis parameters, described above, will be used here to discuss the origin of the magnetic susceptibility variations by characterizing (1) the relative contributions of the ferromagnetic versus para- or diamagnetic components and (2) the nature and amount of ferromagnetic minerals and especially of magnetite type, which can be generally used as a proxy of the detrital input (e.g. Borradaile *et al.* 1993; Vanderaveroet *et al.* 1999; Walden *et al.* 1999; Ellwood *et al.* 2000).

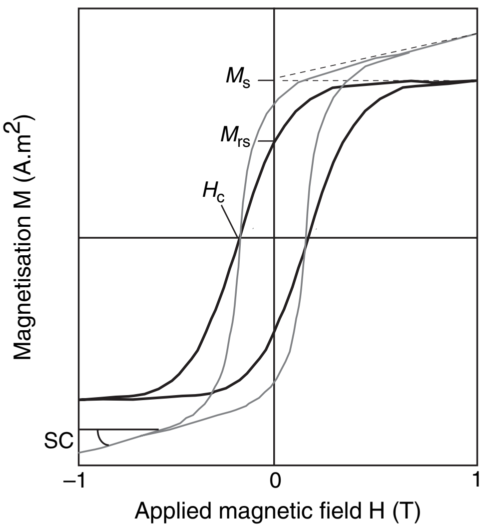

Fig. 3. Schematic hysteresis loop for a magnetite sample. The light grey loop is the original measurement, the black loop represents the same curve after corrections. The parameters saturation magnetization M_s, saturation remanent magnetization M_r, coercive force H_c, coercivity of remanence H_{cr} and slope correction SC are indicated.

Inorganic geochemistry

For each section, about 20 whole-rock geochemical analyses were made allowing the determination of major (Al, K, Si, Ti) and trace (Ba, Co, Cr, Cu, Mo, Ni, Th, U, V) elementary concentrations. Geochemical analyses were performed by ICP-AES (major or minor elements) and ICP-MS (trace elements), at the spectrochemical laboratory of the Service d'Analyse des Roches et des Minéraux of the Centre National de la Recherche Scientifique (Vandœuvre-les-Nancy, France). The samples were prepared by fusion with $LiBO_2$ and HNO_3 dissolution. Precision and accuracy were both found to be better than 1% (mean 0.5%) for major-minor elements, 5% for Co, Cr, Mo, U and V and 10% for Cu, as checked by international standards and analysis of replicate samples, respectively. Carbonate content was determined using a Bernard calcimeter (acid digestion).

The trace-element concentrations were normalized to aluminium to avoid dilution effects by the carbonate fraction and to compare different environmental settings with regard to variations in trace-element contents. Higher element/Al ratios will indicate synsedimentary additions, if a constant composition of the background is assumed. Variations of the Al content in relation to diagenetic formation of clay minerals is unlikely, because in the present study, Al is positively correlated with Ti ($r^2 = 0.99$ for both sections) that is not incorporated during authigenic clay-mineral formation (Calvert & Pedersen 1993).

Results

Clay mineral analysis

X-ray diffraction analyses show that the clay assemblages in both sections are very close and dominantly composed of illite (about 80%) and chlorite (about 10%) (Fig. 4). Diagenesis-sensitive minerals, such as kaolinite or smectite, are either absent or present in traces suggesting a significant diagenetic imprint on the primary detrital clay assemblages. The data of Crystallinity Index Standard (CIS) of illite oscillate globally from 0.25 to 0.50 with an average value of 0.37 for the Bou-Ounebdou section and 0.41 for the Anajdam section (Fig. 4). According to the reference data from Warr & Rice (1994), these analyses indicate that both sections have been affected by a pronounced diagenesis, in the limit of the anchimetamorphic conditions. As a whole, these results are, however, in agreement with recent studies of colour alteration index (CAI) of conodont, suggesting that the maximum temperatures during thrust-related burial in the Central Moroccan Meseta did not exceed about 250 °C (Dopieralska 2003).

Rock-magnetic measurements

Magnetic susceptibility signal. Figure 5 shows the stratigraphical variations of the magnetic susceptibility and the $CaCO_3$ content for the two sedimentary sequences studied. As usually recorded in carbonate formation, the χ signal is broadly low ($<20.0 \times 10^{-8}\ m^3\ kg^{-1}$) but displays significant evolutions along sections, with short- and long-term variations.

Along the Anajdam section, the χ values mostly vary from 2.6 to $15.3 \times 10^{-8}\ m^3\ kg^{-1}$ with the exception of the two KW horizons. In these peculiar horizons, the χ values never exceed $1.5 \times 10^{-8}\ m^3\ kg^{-1}$. During the Frasnian, two successive slight and gradual decreasing trends, separated by a positive shift to values around $8.9 \times 10^{-8}\ m^3\ kg^{-1}$, are observed in the χ signal (Fig. 5). The first decreasing trend occurs from the base of the section (*falsovialis* Zone) up to the early part of the *jamieae* Zone, the second from the middle part of the *jamieae* Zone up to the base of the LKW horizon (Upper *rhenana* Zone). Within the LKW horizon, the χ record shows a sharp decrease to average values around $1.3 \times 10^{-8}\ m^3\ kg^{-1}$. The lowest χ value ($0.4 \times 10^{-8}\ m^3\ kg^{-1}$) is observed just above the LKW horizon. The inter-KW timespan is marked by a well-marked peak (up to the maximum χ value of $15.3 \times 10^{-8}\ m^3\ kg^{-1}$). The base of the UKW horizon displays a strong decrease of χ that remains of low values (around $1.3 \times 10^{-8}\ m^3\ kg^{-1}$) all along the UKW horizon. An increase of χ is recorded at the base of the Famennian times but its amplitude is difficult to resolve as sampling was not extended higher than the Lower *triangularis* Zone in basal Famennian times.

In the Bou-Ounebdou section, the χ values are about twice lower than those observed in the Anajdam section. They vary from 1.5 to $6.7 \times 10^{-8}\ m^3\ kg^{-1}$ with an interval of lowest values of $1.0 \times 10^{-8}\ m^3\ kg^{-1}$, measured in the LKW horizon (Fig. 5). From the base of the section up to the LKW level, the data are noisy and no clear trend is observed in the χ signal. Above the base of the LKW horizon, a comparable trend to Anajdam is observed with, however, a significant decrease in the amplitude of variations. The UKW horizon is marked by a slight decrease of χ values, following by a slight increasing trend toward average χ values of $3.0 \times 10^{-8}\ m^3\ kg^{-1}$ during the early Famennian.

The susceptibility data thus allow evidencing a contrast in the sedimentary record of both Moroccan sections. Unlike the more distal Bou-Ounebdou section, the samples of Anajdam exhibit well-defined variations of χ signal with particularly well-marked KW horizons. The trends point to a general long-term decrease during the Frasnian with minimum values localised within the two KW horizons. It is worth noting that these horizons display some significant increases in the carbonate content (up to 95–98%) but, by contrast, the

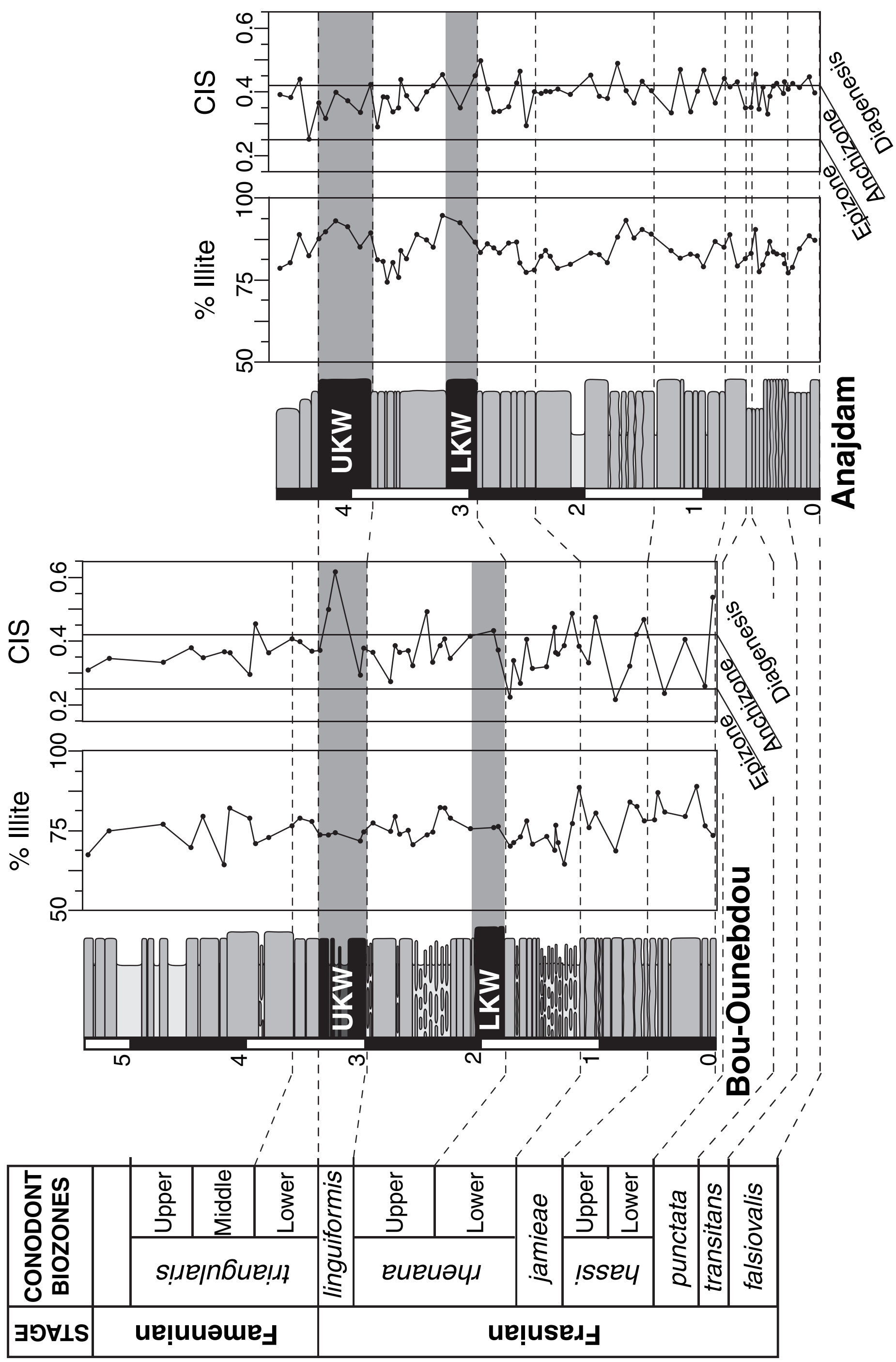

Fig. 4. Stratigraphical variation of percentage of illite and Crystallinity Index Standard of the sedimentary sequence from Bou-Ounebdou and Anajdam. Ranges for CIS are from Warr & Rice (1994).

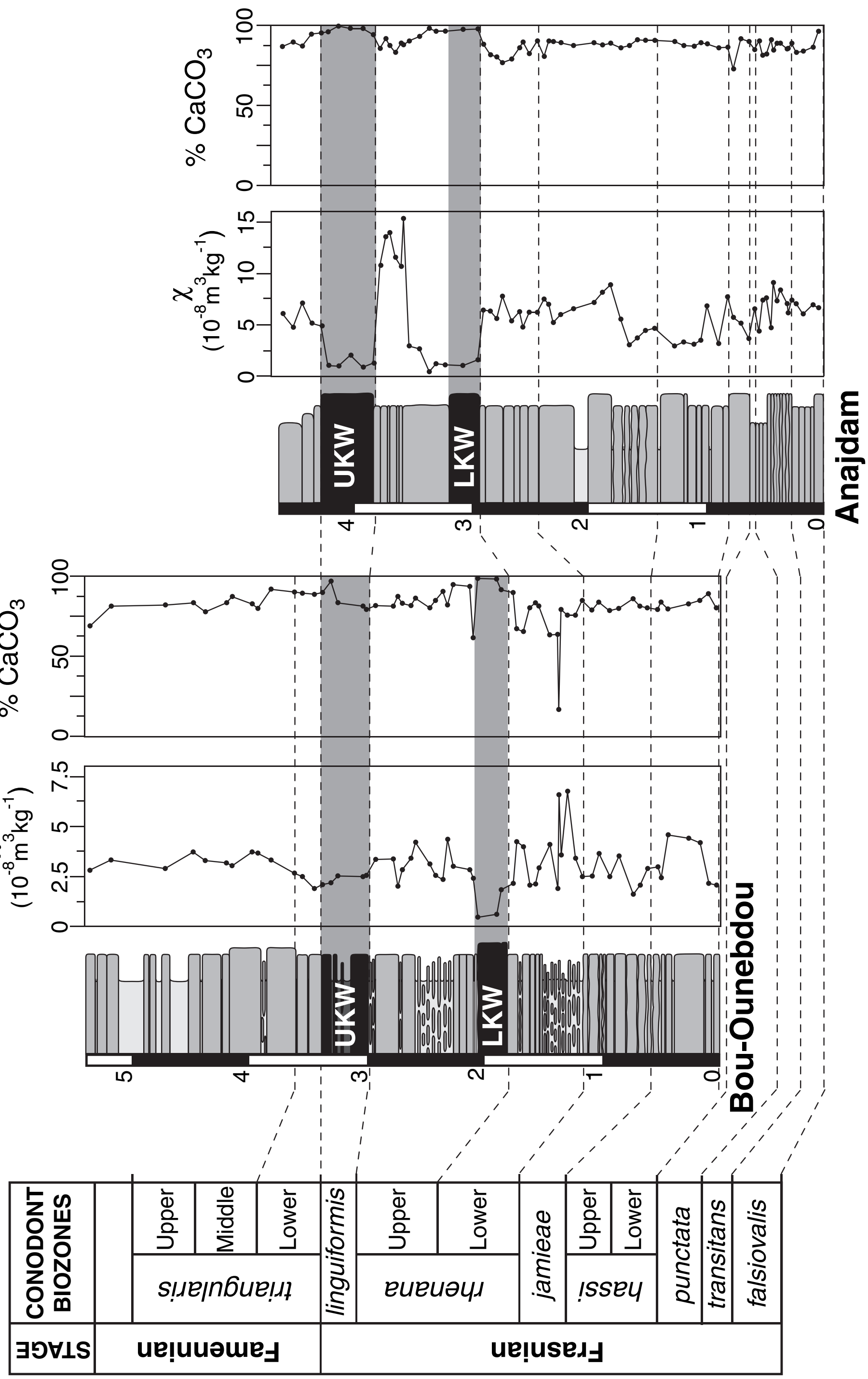

Fig. 5. Stratigraphical variation of mass-normalized magnetic susceptibility and calcium carbonate content of the sedimentary sequence from Bou-Ounebdou and Anajdam.

long-term χ decrease is not accompanied by noticeable variations of the carbonate content (Fig. 5). In both sections, the F-F boundary is marked by an increase in χ values of moderate amplitude.

Magnetic hysteresis properties. Magnetic hysteresis experiments have been carried out for representative samples of both sections (a total of 30 measurements) to provide information about the origin of the χ variations. Measured hysteresis parameters are plotted versus the magnetic susceptibility in Figure 6 to test the possible correlations existing between χ and the different hysteresis parameters.

As expected in carbonate rocks (e.g. Borradaile *et al.* 1993), values of M_s and M_r are globally low. In the Bou-Ounebdou section, as it was observed for χ, the amplitude of variation of M_s is also very low so that any convincing relationship can be drawn between these two parameters. Conversely, in Anajdam, an excellent correlation is observed between χ and M_s (Fig. 6a) thus indicating that the ferromagnetic *sensu lato* contribution controls the χ signal. The H_{cr} values are globally low in Anajdam (around 50 mT) regardless of the χ values (Fig. 6b) but they are significantly higher for much of the samples of Bou-Ounebdou ($60 \leq H_{cr} \leq 250$ mT). These data suggest that, in Anajdam, the χ variations are related to the varying concentration of a low coercivity mineral of magnetite type (Fe_3O_4) whereas, in Bou-Ounebdou, a mixture of magnetite and a higher coercivity phase is put forward. As usually observed in non-red limestone sequences, the latter is probably composed of low susceptibility goethite (FeO(OH); e.g. Heller 1978; Borradaile *et al.* 1993). This suggests an increase of the weathering intensity in the Bou-Ounebdou section compared to that of Anajdam, which is of crucial importance to recognize and understand the difference in the behaviour of iron-bearing minerals in both sections.

Samples with magnetite as the main carrier of the magnetic susceptibility ($H_{cr} < 70$ mT) have been plotted in a classical M_r/M_s versus H_{cr}/H_c graph (Fig. 7) in order to evaluate the bulk grain-size of the ferromagnetic fraction (Day *et al.* 1977). For both sections, the M_r/M_s ratio ranges from 0.1 to 0.25 and the H_{cr}/H_c ratio from 2 to 10. Following boundary values established by Dunlop (1986) and recommended by Borradaile *et al.* (1993), the diagram points to a dominant coarse-grain magnetic fraction with pseudo-single domain (PSD) to multi-domain (MD) behaviours although some points display a slight shift compared to the reference boundaries. Such shift has been observed in other magnetic hysteresis studies of carbonate rocks (e.g. Borradaile *et al.* 1993;

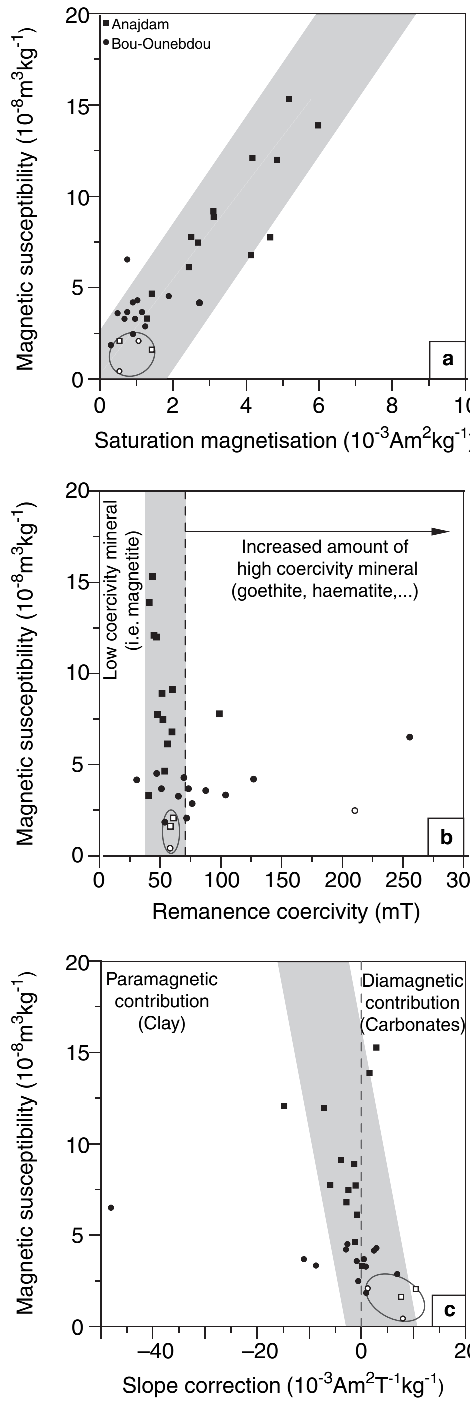

Fig. 6. Hysteresis parameters plotted against low-field mass susceptibility (χ) for representative samples from Anajdam and Bou-Ounebdou. (**a**) Saturation magnetization (M_s) *vs.* χ (**b**), coercivity (H_c) *vs.* χ and (**c**) Slope Correction *vs.* χ.

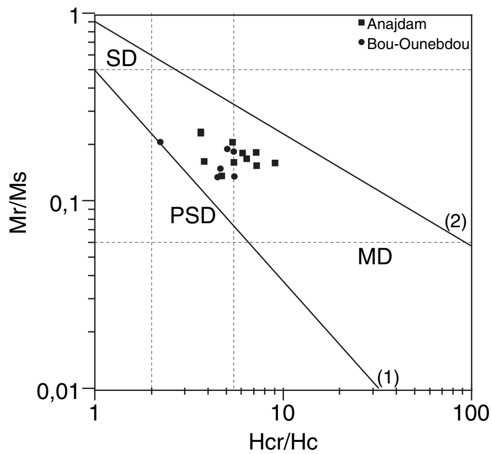

Fig. 7. Hysteresis parameters of samples from Anajdam and Bou-Ounebdou plotted according to Day *et al.* (1977). Ranges for *SD* (single domain), *PSD* (pseudo-single domain) and *MD* (multi-domain) are from Dunlop (1986). Empirical trends are shown for (1) unremagnetized and (2) remagnetized limestones (from Channell & McCabe 1994).

Katz *et al.* 2000) and, to our knowledge, has not yet received any satisfactory explanation. Furthermore, M_r/M_s and H_{cr}/H_c values cluster in between the lines established by Channell and McCabe (1994) for diagenesis-induced remagnetized limestones and non-remagnetized limestones (Fig. 7). This, at least, suggests that the primary depositional ferromagnetic signal has not been completely overprinted by diagenetic processes.

The paramagnetic and diamagnetic contributions, quantified by the high-field slope correction SC (Fig. 6c), display noticeable variations showing the varying respective amounts of iron-bearing clays (illites, chlorites) and carbonates. It clearly appears that the matrix of the limestones is diamagnetic in the KW horizons, whereas it is dominantly paramagnetic for the rest of the sedimentary record in both sections. A general anti-correlation of SC and χ is noticed, illustrating the relative increase of clay concentration in levels with high χ (Fig. 6c). Therefore, almost pure carbonates such as the KW levels display the highest diamagnetic contributions and the lowest χ values.

To summarize, hysteresis data thus demonstrate that the χ signal is controlled by the combined contributions of ferromagnetic *sensu lato* magnetite and paramagnetic clays. As shown in Figure 4, the diamagnetic contribution of calcite only exerts a noticeable control on magnetic susceptibility in the almost pure KW limestones. In Bou-Ounebdou, this pattern is perturbed by weathering processes which reduce the intensity and amplitude of variations of the χ signal by transforming high susceptibility magnetite into low susceptibility goethite. Therefore, the Bou-Ounebdou section cannot be considered as a reference sequence regarding the analysis of detrital input evolution in the F–F times in the M'rirt area. In the following, the discussion of the magnetic data will thus focus on the Anajdam section.

Inorganic geochemistry analysis

Figure 8 shows the stratigraphical evolutions of some Al-normalized elemental ratios, usually considered as reliable geochemical proxies to estimate the fluctuation of clastic fluxes as well as oxygenation and primary productivity levels in marine environments.

Clastic influx proxies. Some elements, including Ti, Si and K are considered to be indicators of detrital influx (Tribovillard *et al.* 1994; Murphy *et al.* 2000*b*). Titanium is usually associated with clay minerals and heavy minerals (ilmenite, rutile). Potassium occurs dominantly in clays, whereas Si occurs in both siliciclastic and biogenic fractions (e.g. quartz *vs.* opal). Normalized to Al, which only occurs in aluminosilicates, the Si, Ti and K ratios provide useful information about change in the contribution of elemental concentrations from detrital non-aluminosilicate sources.

In regard to clastic influx, Al-normalized Si, Ti and K concentrations do not show clear trends at the F–F boundary (Fig. 8). The KW horizons are not marked by noticeable increase or decrease of these elements. For both sections, the Ti/Al profile remains almost constant. The values are nearly around the average shale values of 0.053 (Wedepohl 1991) in the major part of the section whereas most of the samples from the KW horizons have a concentration of Ti below the detection limit. Concerning the evolution of the Si/Al ratio in the Anajdam section, the KW horizons are characterized by relatively lower values compared to the concentrations in the overlying and underlying strata. In Bou-Ounebdou, there is a relative stability of the Si/Al ratio during the Late Frasnian, followed by a gradual decrease in the Early Famennian. To some extent, the Si/Al curves show comparable trends for both studied sections. Finally, K/Al ratio is relatively stable; it records the highest values at the end of the two KW horizons (inputs of K-carrying minerals, such as illite-mica or K-feldspar) and the lowest values during the inter-KW timespan for both sections.

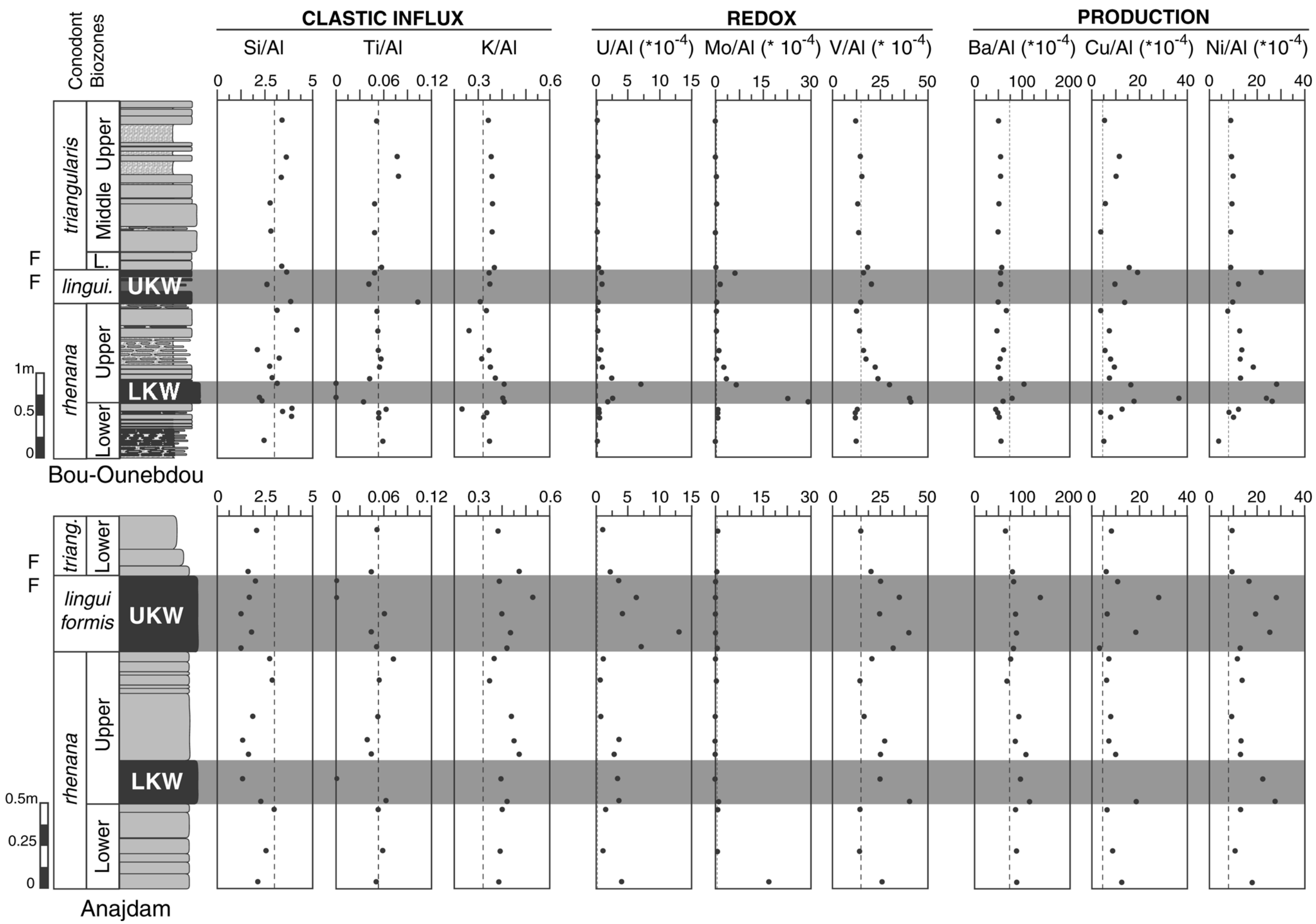

Fig. 8. Stratigraphical plots of elemental concentrations including proxies for clastic input, redox condition and production for the Anajdam and Bou-Ounebdou sections. Dashed lines indicate the metal/aluminium concentration ratios for average shales (Wedepohl 1971, 1991).

Palaeoredox proxies. In each section studied, a significant feature of the F–F boundary sequence is a remarkable enrichment in Mo, U and V in the KW horizons compared to the concentrations in the overlying and underlying strata (Fig. 8). These elements are thought to be redox-sensitive (Calvert & Pedersen 1993; Crusius *et al.* 1996; Dean *et al.* 1997; Algeo & Maynard 2004). The high ratios of these elements in the KW horizons thus suggest that the sediments were probably O_2-deficient. To confirm these observations, V/Cr, V/(V + Ni), U/Th and Ni/Co ratios, which are considered as reliable redox indexes (Hatch & Leventhal 1992; Jones & Manning 1994), were calculated in order to show the contrasted values between the KW horizons and the other parts of the section and to estimate the level of oxygenation (Fig. 9a–d). For each of the indexes used, two clusters of values can be identified, one corresponding to the samples from the KW horizons, the other corresponding to the samples from the overlying and underlying strata. The samples from the KW horizons show the highest values. They are broadly characterized by values of $V/Cr > 1.5$; $U/Th > 1.5$; $Ni/Co > 4.25$ (Fig. 9a, b and d). The values of the $V/(V + Ni)$ ratios are mainly comprised between 0.5 and 0.7 and do not allow clearly distinguishing the KW horizons from the rest of the section (Fig. 9c).

Palaeoproductivity proxies. Vertical concentration profiles of Ba, Cu and Ni to Al ratios indicate slight enrichment in the KW horizons (Fig. 8). In

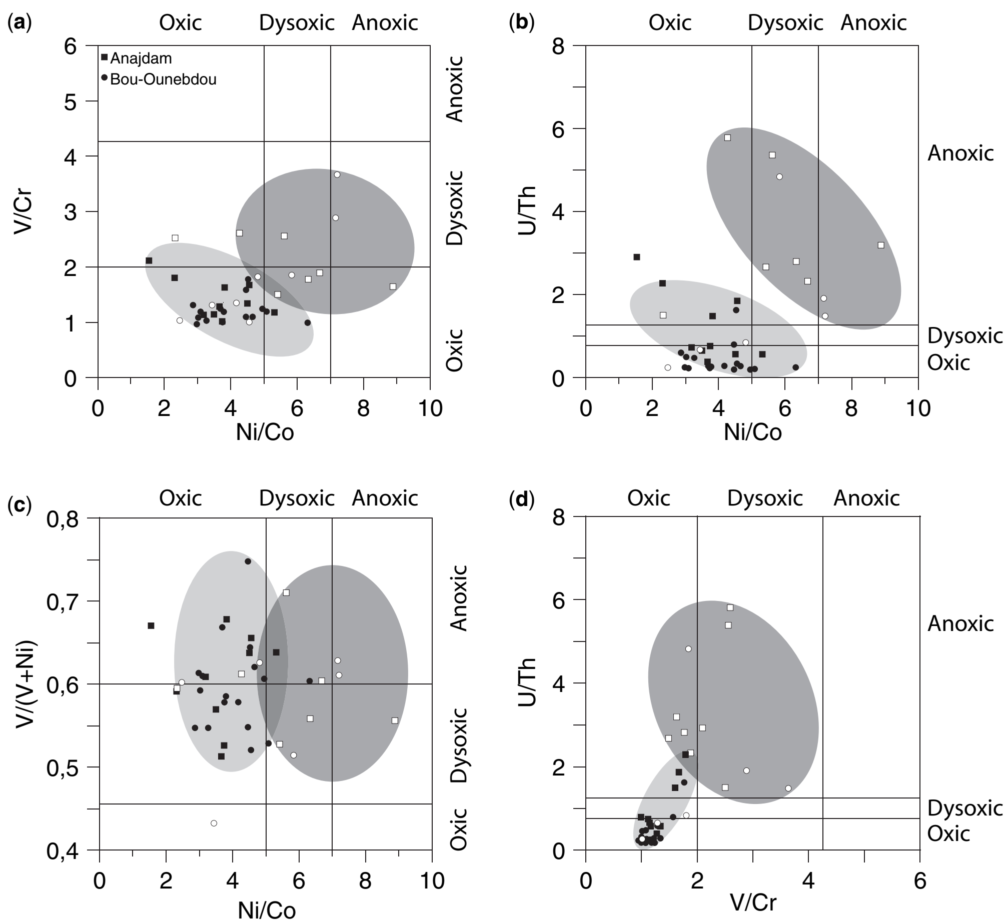

Fig. 9. Crossplots of trace-elements ratios used as palaeoredox proxies. (**a**) V/Cr *vs.* Ni/Co, (**b**) V/(V + Ni) *vs.* Ni/Co, (**c**) U/Th *vs.* Ni/Co and (**d**) U/Th *vs.* V/Cr. Ranges for V/Cr, U/Th and Ni/Co are from Jones & Manning (1994); ranges for V/(V + Ni) are from Hatch & Leventhal (1992). Open symbols: Kellwasser samples.

both sections, most of the KW samples show values of $Cu/Al > 10$ and $Ni/Al > 15$. Ba/Al ratios are higher in Anajdam ($Ba/Al > 90$) than in Bou-Ounebdou ($Ba/Al > 60$) in the KW horizons. Ba abundance is commonly used as a palaeoproductivity marker even if the interpretation is not always straightforward because barite can be dissolved in case of intense sulphate-reduction (McManus *et al.* 1998). In that case, Ba can be released to pore waters, migrate with them, and then reprecipitate when less-reducing conditions are met. Thus barite migration fronts may form (e.g. McManus *et al.* 1998). In the present case, the redox proxies indicate that depositional conditions were probably not very reducing (except for the LKW at Bou-Ounebdou). Consequently, Ba distribution must not have been deeply altered by diagenetical remobilization. The distribution of dissolved Ni and Cu in the ocean appears to be related to settling organic debris, since Ni and Cu behave as micronutrients (Calvert & Pedersen 1993; Algeo & Maynard 2004). These elements are readily adsorbed onto organic particles settling through the water column. So, decaying organic matter (OM) easily forms organometal complexes that can be incorporated into the sediment (Algeo & Maynard 2004; Tribovillard *et al.* 2004*b*). Thus, these elements are usually trapped with organic particles and are incorporated into iron sulphides during diagenesis. Consequently, they are preserved in the sediment even in the case of complete OM remineralization as well as in the case of marked thermal evolution (Mongenot *et al.* 1996). Thus, Ni and Cu may serve as indicators of organic inputs (Tribovillard *et al.* 2000, 2004*b*).

Summary. The distribution of the geochemical data during the Late Devonian suggests that: (1) the KW horizons coincide with two periods of relative decline of detrital influx, marked by a decrease of Ti and Si concentration; (2) the moderate and limited increase of U, Mo and V, as well as Ba, Cu and Ni concentrations are indicators of periods of dysoxic to anoxic conditions and enhanced productivity, that probably caused an increase of OM deposition.

Discussion

Detrital input versus carbonate production in the Frasnian–Famennian times in central Morocco

As previously mentioned, the χ measurements can be used as a good indicator of detrital input in ancient sedimentary rocks if not strongly altered by diagenetic or weathering processes (e.g. Ellwood *et al.* 2000). In the Bou-Ounebdou section, the χ signal is thought to have been modified by weathering processes and goethite formation and, therefore, cannot be considered to decipher detrital supply variations. By contrast, in Anajdam, magnetite and clays are the main minerals controlling the χ signal. This section is thus potentially adequate for relating the detrital input evolution through the F–F times. The possible impact of diagenesis on the magnetic signal still remains to be discussed. As shown by clay mineralogical assemblages, the two sections have been affected by a pronounced diagenesis. In such conditions, the transformation of clays of smectite type into illite has been suggested to induce the formation of authigenic magnetite that can potentially overprint or at least alter the primary detrital magnetic signal (e.g. Katz *et al.* 2000; Zegers *et al.* 2003). As observed in the Day-Fuller plot (Fig. 6c), the distribution of samples from Anajdam cluster below the line established by Channell & McCabe (1994) for diagenesis-induced remagnetized limestones (Fig. 6c).

Therefore, the primary depositional ferromagnetic signal is likely to have not been completely overprinted by diagenetic processes. Furthermore, M_s, that provides a first-order quantitative estimate of the magnetite concentration, does not correlate with either the illite crystallinity index standard or with the illite percentage (Fig. 10a, b). A slight negative correlation can be roughly observed between M_s and the illite percentage, suggesting that the diagenesis-induced illitization is not accompanied by an increase in the magnetite concentration. On the other hand, early diagenetic reductive dissolution of magnetite in the OM-bearing black KW carbonate levels cannot be proposed as an efficient process in the alteration of the primary magnetic signal (e.g. Machel 1995; Robinson *et al.* 2000; Tribovillard *et al.* 2002, 2004*b*), because the high field SC is strongly diamagnetic (Fig. 6c) and thus does not record any effects of authigenic paramagnetic pyrite. Such a poor control of diagenetic processes upon the magnetic signal is corroborated by the correlation of Ti and Th contents ($r^2 = 0.47$ and 0.66, respectively), classically considered as detrital indicators independent of diagenesis-induced remobilization, with the magnetic susceptibility from the Anajdam section (Fig. 11a, b). These whole data thus demonstrate that, although submitted to significant burial, the χ signal can be confidently used as an indicator of the detrital input evolution in the Anajdam section.

The long-term decrease of χ observed during most of the Frasnian times can thus be interpreted

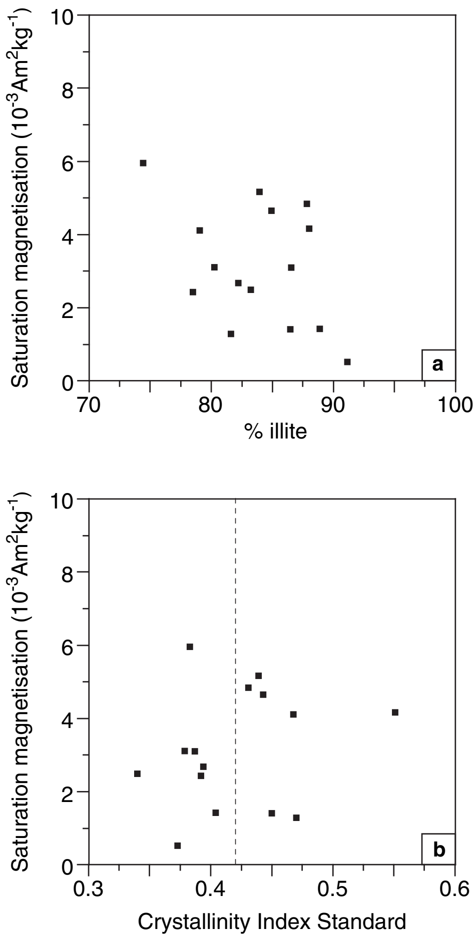

Fig. 10. Hysteresis parameters plotted against clay parameters for representative samples from Anajdam and Bou-Ounebdou. (**a**) Saturation magnetization (M_s) *vs.* CIS. (**b**) Saturation magnetization (M_s) *vs.* % of illite.

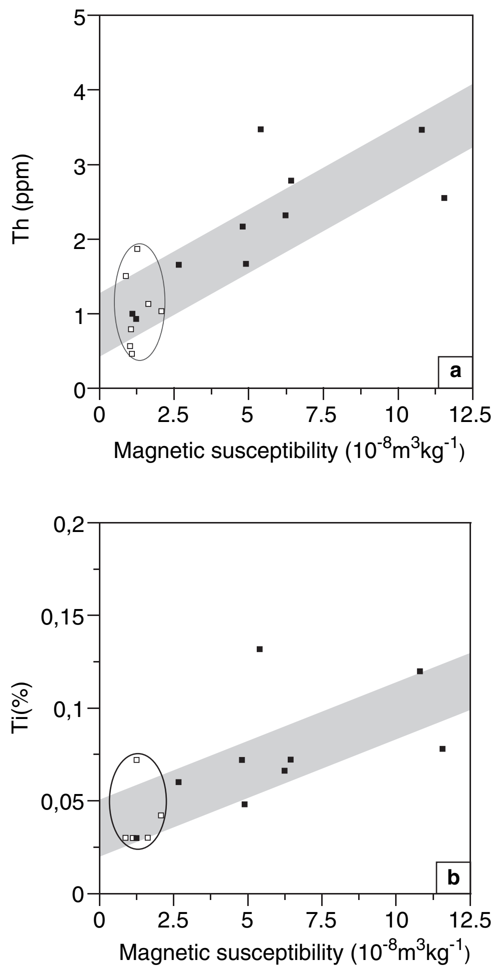

Fig. 11. Detrital-derived element concentrations plotted against low-field magnetic susceptibility (χ) for representative samples from Anajdam. (**a**) Th (ppm) *vs.* χ and (**b**) Ti (%) *vs.* χ.

as a general diminution of the detrital input in the Azrou–Kenifra Basin through Late Frasnian times. This evolution can be traced up to the KW levels that record the lowest χ values, in relation with a minimum detrital input and an enhanced carbonate productivity, as shown by the maximum intensity of the diamagnetic contribution. This is also confirmed by the vertical distribution of Ti/Al and Si/Al ratios related to clastic input (Fig. 8). The F–F boundary represents a significant break in this long-term evolution with a significant increase of the χ, thus suggesting a noticeable increase of the basinal detrital supply. It is worth noting that these variations can be paralleled to the global sea-level fluctuations as synthesized by Sandberg *et al.* (2002) and indicating a general Frasnian sea-level rise, a Late Frasnian highstand, and a F–F boundary sea-level fall (Fig. 12). These sea-level changes have been well documented in several areas, such as Germany (Piecha 2002; Devleeschouwer *et al.* 2002), Poland (Racki *et al.* 2002), NW Australia (Becker & House 1997), China (Chen & Tucker 2003, 2004), and Canada (Mountjoy & Becker 2000).

In a more general perspective, the magnetic susceptibility data from Anajdam are consistent with previous magnetic results obtained from other sections of the northern Gondwana

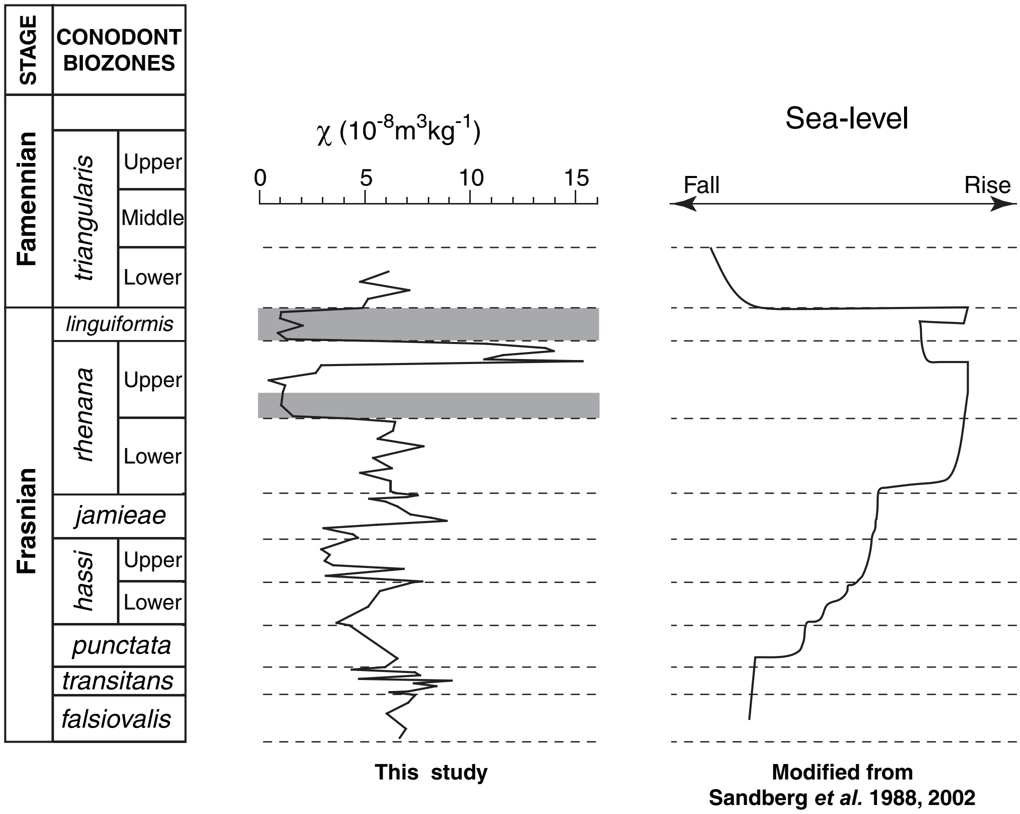

Fig. 12. Synthetic diagram showing the variations of the χ signal obtained from the Anajdam section compared with the Late Devonian sea-level curve (modified from Sandberg *et al.* 1988, 2002).

margin, such as Coumiac (Montagne Noire, S. France), but also from domains of the southern Laurassian margin, such as Steinbruch Schmidt and Beringhausen Tunnel (Rhenish Massif, Germany), Kowala (Holly Cross Mountains, Poland) or Sinsin (Ardennes, Belgium) (Devleeschouwer 1999; Crick *et al.* 2002; Racki *et al.* 2002; Averbuch *et al.* 2005). The mechanisms controlling the first-order observed χ variations have thus to be found in relatively large-scale processes affecting at least the Gondwanan and Laurassian margins. Global climatic warming during Frasnian times with maximum temperatures in the Late Frasnian (Kellwasser events) and global cooling at the F–F boundary are thus the more convincing parameters to account for the observed variations as also suggested by the $\delta^{18}O$ signatures of marine conodont apatite (Joachimski & Buggisch 2002; Joachimski *et al.* 2004) and the miospore diversity evolution on continents (Streel *et al.* 2000).

Marine bottom-water redox-conditions and primary productivity evolution

As mentioned in the ‘Results’ section, the black limestones of the KW horizons show noticeable variations for nearly all trace element ratios compared to the underlying and overlying limestone beds. Broadly, redox-sensitive elements as well as redox indexes show enrichments in the LKW horizon in Bou-Ounebdou and in the UKW horizon in Anajdam (Fig. 8). Molybdenum concentration has been suggested to be enhanced in the presence of sulphides (Helz *et al.* 1996; Adelson *et al.* 2001; Zheng *et al.* 2000; Vorlicek & Helz 2002; Lyons *et al.* 2003; Algeo & Maynard 2004; Rimmer *et al.* 2004; Tribovillard *et al.* 2004*c*). The marked Mo enrichment observed in the LKW of the Bou-Ounebdou section argues for sulphidic conditions, whereas in all the other parts of the two sections studied, dysoxic–anoxic conditions are put forward (no Mo-enrichment but relative enrichment in U and V for the KW horizons).

The depletion in O_2 is confirmed by the stratigraphical variations of reliable palaeo-oxygenation indexes such as V/Cr, V/(V + Ni), U/Th, Ni/Co (Fig. 9a–d). In this study, we adopted thresholds proposed by Jones & Manning (1994) and Hatch & Leventhal (1992). For each of the indices used, values indicate anoxic to dysoxic conditions for the two KW horizons. The observed enrichments in redox-sensitive trace elements confirm that the oxic–anoxic interface was located at a shallower depth in the sediment during the deposition of the KW horizons, perhaps even in the water column for the LKW at Bou-Ounebdou. However, the intensity of O_2 depletion is interpreted differently from one ratio to the other (Fig. 9a–d). According to V/Cr and V/(V + Ni) ratios, Late Frasnian conditions were broadly dysoxic to anoxic in outer platform settings, whereas O_2-depletion would be only limited to the KW horizons according to U/Th and Ni/Co. The consistency of the chemical data thus clearly indicates two pulses of oxygen depletion near the base of the Upper *rhenana* Zone and in the *linguiformis* Zone, i.e. within the two KW horizons.

These geochemical results are in agreement with recent biofacies studies (Lazreq 1999; Feist 2002), which demonstrated that in the M'rirt area, the fauna of KW horizons are characterized by a lack of endobenthos and O_2-sensitive epibenthos, such as trilobites and brachiopods. In a more global pattern, our interpretations are in agreement with recent geochemical studies concerning some F–F sections from Germany, France, Poland, Siberia and China (e.g. Racki *et al.* 2002; Ma & Bai 2002; Yudina *et al.* 2002; Bond *et al.* 2004; Tribovillard *et al.* 2004*a*; Pujol *et al.* in press). In many areas, the F–F boundary records some elemental anomalies related to redox conditions (e.g. U, V and Mo). Thus, both geochemical and palaeontological analyses suggest a noticeable decrease of O_2 concentration in bottom waters during the two KW episodes. Primary productivity tracers such as Ba/Al and OM-related elemental ratios, such as Ni/Al and Cu/Al, display a consistent slight increase through the KW levels. A similar trend is also observed in the carbonate production as shown both by the $CaCO_3$ content and the optimal diamagnetic contribution to the magnetic signal. Trends similar to those observed for the Moroccan sections have been found in the time-equivalent formations of Aeketal (Harz, Germany), along the southern Laurassian outer shelf (Riquier *et al.* 2005). Compared to geochemical results obtained for deeper sections such as La Serre (Montagne Noire, France; Tribovillard *et al.* 2004*a*), the Moroccan sections display a relatively low enrichment in Ba. According to Bishop (1988), precipitation of barite is favoured in microenvironments, where OM decays from surface water to sea floor. Therefore, barite may not be enriched in shallow, highly productive environments, whereas it is enhanced in deeper sites with similar productivity. The relatively poor record of primary productivity in outer shelves can thus be explained by local conditions. In shallow-water settings, even if conditions become eutrophic, favouring the onset of O_2-deprived conditions, generally intense seawater mixing does not allow a good preservation of OM. Organic elements are remineralized before reaching the water/sediment interface. The observed enrichments in productivity indicators are coeval with two positive excursions of the carbon isotopic signal ($\delta^{13}C_{carb} = +3‰$ V-PDB), recorded in Bou-Ounebdou and in many other F–F sections for inorganic carbon (Joachimski *et al.* 2002). These positive shifts in $\delta^{13}C$ are explained by an increase in the global-scale organic carbon burial rate in the Late Frasnian seas (Joachimski *et al.* 2001, 2002; Murphy *et al.* 2000*a*, *b*). In outer shelf settings such as the Moroccan sections, the resultant depletion in marine bottom-water oxygenation and associated OM preservation were probably moderate due to efficient platform ventilation.

Conclusion

In this study, rock magnetic measurements (magnetic susceptibility and hysteresis), combined with clay mineral and geochemical analyses allow to constrain the environmental features of two sections from Central Morocco (Anajdam and Bou-Ounebdou). Although both sections were affected by a pronounced diagenesis (limit of anchizonal conditions), we demonstrate that the magnetic susceptibility represents a semi-quantitative proxy for detrital supply variations. The magnetic signal in the Anajdam section is better defined than that in Bou-Ounebdou, owing to increasing weathering intensity in the latter and transformation of high-susceptibility magnetite into low-susceptibility goethite. The Anajdam section unravels a Frasnian long-term decrease of the basinal detrital input that parallels a general sea-level rise with a major highstand in the Late Frasnian Kellwasser-type levels. The Kellwasser Horizons display the lowest values of magnetic susceptibility and magnetization at saturation, in relation with a minimum detrital input and a maximum carbonate productivity, as shown by the significant diamagnetic contribution to the magnetic signal. The high marine primary productivity in the Late-Frasnian Central Moroccan basin is attested by an increase of the Ba/Al ratio in the Kellwasser levels of both sections. Reliable redox indicators such as V/Cr or U/Th furthermore evidence the general dysoxic conditions prevailing in marine bottom-waters at that time. On top of the Upper Kellwasser Horizon, the Frasnian–Famennian boundary in central Morocco is marked by a break in the sedimentation with possible depositional hiatuses associated with a noticeable sea-level fall (Lazreq 1999; Chakiri 2002). Comparisons with other sections worldwide suggest that the variations in the detrital supply are climatically driven, thus arguing for a long-term Frasnian warming and a significant basal Famennian global cooling event. The latter is subsequent to a Late Frasnian climatic optima leading to a period of particularly increased organic carbon burial (e.g. Joachimski *et al.* 2002). As previously proposed by different authors (e.g. Becker & House 1994; Godderis & Joachimski 2004; Averbuch *et al.* 2005), this mechanism would have produced an important drawdown in the atmospheric CO_2 content, thus resulting in a strong reduction of greenhouse effects in Famennian times. Such rapid variations in seawater oxygenation conditions and temperatures are likely to have had drastic repercussions on marine fauna, potentially leading to the Frasnian–Famennian biological crisis.

This study has been financially supported by the Eclipse program of the C.N.R.S. (project Frasnian–Famennian boundary crisis, O. Averbuch coordinator) and is a contribution of the UMR PBDS 8110. We greatly thank C. Kissel for providing access to the Micromag equipment at the Palaeomagnetic Laboratory in LSCE (Gif sur Yvette), J. Morel for the ICP analyses and M. Frere, P. Recourt and D. Malengros for assistance with X-ray analysis. A. Herbosch, I. Berra and C. Crônier are acknowledged for their participation to the sampling field-trip in Central Morocco. We also thank Michael Joachimski, Grzegorz Racki and Walter Dean for scientific discussions at earlier stages of this study. Finally, we are grateful to Eberhard Schindler and Thomas Becker; the manuscript benefited from their helpful and constructive comments.

References

Adelson, J. M., Helz, G. R. & Miller, C. V. 2001. Reconstructing the rise of recent coastal anoxia; molybdenum in Chesapeake Bay sediments. *Geochimica Cosmochimica Acta*, **65**, 237–252.

Algeo, T. J. & Scheckler, S. E. 1998. Terrestrial–marine teleconnections in the Devonian: links between the evolution of land plants, weathering processes, and marine anoxic events. *Philosophical Transactions of the Royal Society of London*, **B353**, 113–130.

Algeo, T. J. & Maynard, J. B. 2004. Trace element behavior and redox facies analysis of core shales of Upper Pennsylvanian Kansas-type cyclotherms. *Chemical Geology*, **206**, 289–318.

Averbuch, O., Tribovillard, N., Devleeschouwer, X., Riquier, L., Mistiaen, B. & van Vliet-Lanoe, B. 2005. Mountain building—enhanced continental weathering and organic carbon burial as major causes for climatic cooling at the Frasnian–Famennian boundary (ca 376 Ma BP). *Terra Nova*, **17**, 25–34.

Becker, R. T. 1993. Stratigraphische Gliederung und Ammonoideen-Faunen im Nehdenium (Oberdevon II) von Europa und Nord-Afrika. *Courier Forschungsinstitut Senckenberg*, **155**, 1–405.

Becker, R. T. & House, M. R. 1994. Kellwasser Events and goniatite successions in the Devonian of the Montagne Noire with comments on possible causations. *Courier Forschungsinstitut Senckenberg*, **169**, 45–77.

Becker, R. T. & House, M. R. 1997. Sea-level changes in the Upper Devonian of the Canning Basin, Western Australia. *Courier Forschunginstitut Senckenberg*, **199**, 129–146.

Becker, R. T. & House, M. R. 2000. Sedimentary and faunal succession of the allochtonous Upper Devonian at Gara d'Mrirt (Eastern Moroccan Meseta). *Notes et Mémoires, Service Géologique du Maroc*, **399**, 109–114.

Bishop, J. K. 1988. The barite-opal-organic carbon association in oceanic particulate matter. *Nature*, **332**, 341–343.

Bond, D., Wignall, P. B. & Racki, G. 2004. Extent and duration of marine anoxia during the Frasnian- Famennian (Late Devonian) mass extinction in Poland, Germany, Austria and France. *Geological Magazine*, **141**, 173–193.

Borradaile, G. J., Chow, N. & Wernet, T. 1993. Magnetic hysteresis of limestones: facies control? *Physics of the Earth and Planetary Interior*, **76**, 241–252.

Bouabdelli, M. 1989. Tectonique et sédimentation dans un bassin orgénique: le sillon Viséen d'Azrou-Khénifra (Est du Massif Hercynien Central du Maroc). Unpublished Ph.D. thesis, Louis Pasteur University, Strasbourg.

Bouabdelli, M. & Piqué, A. 1996. Du bassin sur décrochement au basin d'avant-pays: dynamique du bassin d'Azrou-Khénifra (Maroc Hercynien central). *Journal of African Earth Science*, **23**, 213–224.

Brindley, G. W. & Brown, G. 1980. Crystal structures of clay minerals and their identification. *Mineralogical Society Monograph No. 5*. Mineralogical Society, London.

Buggisch, W. 1991. The global Frasnian/Famennian "Kellwasser Event". *Geologische Rundschau*, **80**, 49–72.

Buggisch, W. & Clausen, C.-D. 1972. Conodonten- und Goniatiten-Faunen aus dem oberen Frasnium und unteren Famennium Marokkos (Tafilalt, Antiatlas). *Neues Jahrbuch für Geologie und Paläontogie Abhandlungen*, **141**, 137–167.

Calvert, S. E. & Pedersen, T. F. 1993. Geochemistry of Recent oxic and anoxic marine sediments:

Implications for the geological record. *Marine Geology*, **113**, 67–88.

Chakiri, S. 2002. Sédimentologie et géodynamique du Maroc Central Hercynien pendant le Dévonien. Unpublished Ph.D. thesis, Ibn Tofail University, Kenitra.

Channell, J. E. T. & McCabe, C. 1994. Comparison of magnetic hysteresis parameters of unremagnetized and remagnetized limestones. *Journal of Geophysical Research*, **99**, 4613–4623.

Chen, D. & Tucker, M. E. 2003. The Frasnian/Famennian mass extinction: insights from high-resolution sequence stratigraphy and cyclostratigraphy in South China. *Palaeogeography, Palaeoclimatology, Palaeoecology*, **193**, 87–111.

Chen, D. & Tucker, M. E. 2004. Paleokarst and its implication for the extinction event at the Frasnian-Famennian boundary (Guilin, South China). *Journal of the Geological Society of London*, **161**, 895–898.

Copper, P. 1986. Frasnian/Famennian mass extinction and cold-water oceans. *Geology*, **14**, 835–839.

Crick, R. E., Ellwood, B. B., Hassani, A., Fiest, R. & Hladil, J. 1997. Magnetosusceptibility event and cyclostratigraphy (MSEC) of the Eifelian-Givetian GSSP and associated boundary sequences in North Africa and Europe. *Episodes*, **20**, 167–175.

Crick, R. E., Ellwood, B. B., *et al.* 2002. Magnetostratigraphy susceptibility of the Frasnian/Famennian boundary. *Palaeo-geography, Palaeoclimatology, Palaeoecology*, **181**, 67–90.

Crusius, J., Calvert, S., Pedersen, T. & Sage, D. 1996. Rhenium and molybdenum enrichments in sediments as indicator of oxic, suboxic and sulfidic conditions of deposition. *Earth and Planetary Sciences Letters*, **145**, 65–78.

Day, R., Fuller, M. D. & Schmidt, V. A. 1977. Hysteresis properties of titanomagnetites. Grain size and composition dependence. *Physics of the Earth and Planetary Interior*, **13**, 260–267.

Dean, W. E., Gardner, J. V. & Piper, D. Z. 1997. Inorganic geochemical indicators of glacial-interglacial changes in productivity and anoxia on the California continental margin. *Geochimica et Cosmochimica Acta*, **61**, 4507–4518.

Devleeschouwer, X. 1999. La transition Frasnien/Famennien (Dévonien sup.) en Europe: sédimentologie, stratigraphie séquentielle et susceptibilité magnétique. Unpublished Ph.D. thesis, Lille and Brussels Universities.

Devleeschouwer, X., Herbosch, A. & Préat, A. 2002. Microfacies, sequence stratigraphy and clay mineralogy of a condensed deep-water section around the Frasnian–Famennian boundary (Steinbruch Schmidt, Germany). *Palaeoecology, Palaeclimalology, Palaeoecology*, **181**, 171–193.

Dopieralska, J. 2003. Neodymium isotopic composition of conodonts as a palaeoceanographic proxy in the Variscan oceanic system. Unpublished Ph.D. thesis, University of Giessen.

Dunlop, D. J. 1986. Hysteresis properties of magnetite and their dependence on particle size: a test of pseudo-single domain remanence models. *Journal of Geophysical Research*, **91**, 9569–9584.

El Hassani, A. & Tahiri, A. 2000*a*. The eastern part of central Morocco (western Meseta). *Notes & Mémoires du Service Géologique du Maroc*, **399**, 89–92.

El Hassani, A. & Tahiri, A. (eds) 2000*b*. Moroccan Meeting of the Subcommission on Devonian Stratigraphy (SDS) – IGCP 421 (April 24th–May 1st 1999): Excursion guidebook. *Notes & Mémoires du Service Géologique du Maroc*, **399**, 1–150.

Ellwood, B. B., Crick, R. E., El Hassani, A., Benoist, S. L. & Young, R. H. 2000. Magnetosusceptibility event and cyclostratigraphy method applied to marine rocks: detrital input versus carbonate productivity. *Geology*, **28**, 1135–1138.

Feist, R. 2002. Trilobites from the latest Frasnian Kellwasser Crisis in North Africa (Mrirt, central Moroccan Meseta). *Acta Palaeontologica Polonica*, **47**, 203–210.

Girard, C. & Albarède, F. 1996. Trace elements in conodont phosphate from the Frasnian/Famennian boundary. *Palaeogeography, Palaeoclimatology, Palaeoecology*, **126**, 195–209.

Girard, C., Klapper, G. & Feist, R. 2005. Subdivision of the terminal Frasnian *linguiformis* conodont Zone, revision of the correlative interval of Montagne Noire Zone 13, and discussion of stratigraphically significant associated trilobites. *In*: Over, J., Morrow, J. R. & Wignall, P. (eds) *Understanding Late Devonian Triassic Biotic and Climatic Events; Towards an Integrated Approach*, 181–198.

Godderis, Y. & Joachimski, M. M. 2004. Global change in the Late Devonian: Modelling the Frasnian-Famennian short-term carbone isotope excursions. *Palaeogeography*, *Palaeoclimatology Palaeoecology*, **202**, 309–329.

Gradstein, F. M., Ogg, J. G. *et al.* 2004. *A Geologic Time Scale 2004*. Cambridge University Press.

Hallam, A. & Wignall, P. B. 1999. Mass extinctions and sea-level changes. *Earth Science Reviews*, **48**, 217–250.

Hatch, J. R. & Leventhal, J. S. 1992. Relationship between inferred redox potential of the depositional environment and geochemistry of the Upper Pennsylvanian (Missourian) Stark Shale Member of the Dennis Limestone, Wabaunsee County, Kansas, U.S.A. *Chemical Geology*, **99**, 65–82.

Heller, F. 1978. Rock magnetic studies of Upper Jurassic limestones from Southern Germany. *Zeitschrift für Geophysik*, **44**, 525–543.

Helz, G. R., Miller, C. V., Charnock, J. M., Mosselmans, J. L. W., Pattrick, R. A. D., Garner, C. D. & Vaughan, D. J. 1996. Mechanisms of molybdenum removal from the sea and its concentration in black shales: EXAFS evidences. *Geochimica Cosmochimica Acta*, **60**, 3631–3642.

Holtzapffel, T. 1985. Les minéraux argileux. Préparation, analyse diffractométrique et détermination. *Mémoire Société Géologique du Nord*, **12**, 136pp.

House, M. R. 2002. Strength, timing, setting and cause of mid-Palaeozoic extinctions. *Palaeogeography, Palaeoclimatology, Palaeoecology*, **181**, 5–25.

JOACHIMSKI, M. M. & BUGGISCH, W. 1993. Anoxic events in the Late Frasnian—causes of the Frasnian–Famennian faunal crisis? *Geology*, **21**, 675–678.

JOACHIMSKI, M. M. & BUGGISCH, W. 2002. Conodont apatite $\delta^{18}O$ signatures indicate climatic cooling as a trigger of the Late Devonian mass extinction. *Geology*, **30**, 711–714.

JOACHIMSKI, M. M., OSTERTAG-HENNING, C., *ET AL*. 2001. Water column anoxia, enhanced productivity and concomitant changes in $\delta^{13}C$ and $\delta^{34}S$ across the Frasnian–Famennian boundary (Kowala—Holy Cross Mountains/Poland). *Chemical Geology*, **175**, 109–131.

JOACHIMSKI, M. M., PANCOST, R. D., FREEMAN, K. H., OSTERTAG-HENNING, C. & BUGGISCH, W. 2002. Carbon isotope geochemistry of the Frasnian-Famennian transition. *Palaeogeography, Palaeoclimatology, Palaeoecology*, **181**, 91–109.

JOACHIMSKI, M. M., VAN GELDERN, R., BREISIG, S., BUGGISCH, W. & DAY, J. 2004. Oxygen isotope evolution of biogenic calcite and apatite during the Middle and Late Devonian. *International Journal of Earth Science*, **93**, 542–553.

JONES, B. & MANNING, D. A. C. 1994. Comparison of geochemical indices used for the interpretation of palaeoredox conditions in ancient mudstones. *Chemical Geology*, **111**, 111–129.

KATZ, B., ELMORE, D., COGOINI, M., ENGEL, M. H. & FERRY, S. 2000. Association between burial diagenesis of smectite, chemical remagnetization, and magnetite authigenesis in the Vocontian trough, SE France. *Journal of Geophysical Research*, **105**, 851–868.

LAZREQ, N. 1992. The Upper Devonian of M'rirt (Morocco). *Courier Forschungsinstitut Senckenberg*, **154**, 107–123.

LAZREQ, N. 1999. Biostratigraphie des conodontes du Givétien au Famennien du Maroc Central. Biofaciès et événement Kellwasser. *Courier Forschungsinstitut Senckenberg*, **214**, 1–111.

LYONS, T. W., WERNE, J. P., HOLLANDER, D. J. & MURRAY, R. W. 2003. Contrasting sulfur geochemistry and Fe/Al and Mo/Al ratios across the last oxic-to-anoxic transition in the Cariaco Basin, Venezuela. *Chemical Geology*, **195**, 131–157.

MA, X. P. & BAI, S. L. 2002. Biological, depositional, microspherule, and geochemical records of the Frasnian/Famennian boundary beds, South China. *Palaeogeography, Palaeoclimatology, Palaeo-ecology*, **181**, 325–346.

MCGHEE, G. R. 1996. The Late Devonian Mass Extinction. The Frasnian-Famennian Crisis. Columbia University Press, New York.

MCMANUS, J., BERELSON, W. M., *ET AL*. 1998. Geochemistry of barium in marine sediments: Implications for its use as a paleoproxy. *Geochimica Cosmochimica Acta*, **62**, 3453–3473.

MACHEL, H. 1995. Magnetic mineral assemblages and magnetic contrasts in diagenetic environments—with implications for studies of paleomagnetism, hydrocarbon migration and exploration. *In*: TURNER, P. & TURNER, A. (eds) Paleomagnetic application in hydrocarbon exploration and production. *Geological Society Special Publication*, **98**, 9–29.

MAHER, B. A. & THOMPSON, R. 1999. *Quaternary climates, environments and magnetism*. Cambridge University Press, New York.

MONGENOT, T., TRIBOVILLARD, N.-P., DESPRAIRIES, A., LALLIER-VERGÈS, E. & LAGGOUN-DEFARGE, F. 1996. Trace elements as palaeoenvironmental markers in strongly mature hydrocarbon source rocks: the Cretaceous La Luna Formation of Venezuela. *Sedimentary Geology*, **103**, 23–37.

MOUNTJOY, E. W. & BECKER, S. 2000. Frasnian to Famennian sea-level changes and the Sassenach Formation, Jasper Basin, Alberta Rocky Mountains. *In*: HOMEWOOD, P. W. & EBERLI, G.P. (eds). Genetic stratigraphy on exploration and production shales—Case studies from the Pennsylvanian of the Paradox Basin and the Upper Devonian of Alberta. *Bulletin des Centres de Recherches Elf Exploration Production Memoire*, **24**, 181–201.

MURPHY, A. E., SAGEMAN, B. B. & HOLLANDER, D. J. 2000*a*. Eutrophication by decoupling of the marine geochemical cycles of C, N and P: a mechanism for the Late Devonian mass extinction. *Geology*, **28**, 427–430.

MURPHY, A. E., SAGEMAN, B. B., HOLLANDER, D. J., LYONS, T. L. & BRETT, C. E. 2000*b*. Black shale deposition and faunal overturn in the Devonian Appalachian Basin: clastic starvation, seasonal water-column mixing, and efficient biolimiting nutrient recycling. *Paleoceanography*, **15**, 280–291.

PETSCHICK, R., KUHN, G. & GINGELE, F. 1996. Clay mineral distribution in surface sediments of the South Atlantic: sources, transport, and relation to oceanography. *Marine Geology*, **130**, 203–229.

PIECHA, M. 2002. A considerable hiatus at the Frasnian/Famennian boundary in the Rhenish shelf region of northwest Germany. *Palaeogeography, Palaeoclimatology, Palaeoecology*, **181**, 195–211.

PIQUÉ, A., BOSSIÈRE, G., BOUILLIN, J.-P., CHALOUAN, A. & HOEPFFNER, C. 1993. Southern margin of the Variscan belt: the north-western Gondwana mobile zone (eastern Morocco and northern Algeria). *Geologische Rundschau*, **82**, 432–439.

PUJOL, F., BERNER, Z. & STÜBEN, D. Chemostratigraphy of some european Frasnian-Famennian boundary key section. *Palaeogeography, Palaeoclimatology, Palaeoecology*, **240**, 120–145.

RACKI, G. 1998. Frasnian-Famennian biotic crisis: undervalued tectonic control? *Palaeogeography, Palaeoclimatology, Palaeoecology*, **141**, 177–198.

RACKI, G. 1999. The Frasnian-Famennian biotic crisis: how many (if any) bolide impacts? *Geologische Rundschau*, **87**, 617–632.

RACKI, G., RACKA, M., MATYJA, H. & DEVLEESCOUWER, X. 2002. The Frasnian/Famennian boundary interval in the South Polish–Moravian shelf basins: integrated event-stratigraphical approach. *Palaeogeography, Palaeoclimatology, Palaeoecology*, **181**, 251–297.

RIMMER, S. M., THOMPSON, J. A., GOODNIGHT, S. A. & ROBL, T. L. 2004. Multiple controls on the preservation of organic matter in Devonian–Mississippian marine black shales: geochemical and petrographic evidence. *Palaeogeography, Palaeoclimatology, Palaeoecology*, **215**, 125–154.

Riquier, L., Tribovillard, N., Averbuch, O., Joachimski, M. M., Racki, G., Devleeschouwer, X., El Albani, A. & Riboulleau, A. 2005. Bottom water redox conditions at the Frasnian-Famennian boundary on both sides of the Eovariscan Belt constraints from trace element geochemistry. *In*: Over, J., Morrow, J. R. & Wignall, P. (eds) *Understanding Late Devonian and Permian-Triassic Biotic and Climatic Events; Towards an Integrated Approach*, 199–225.

Robinson, S. G., Sahota, J. T. S. & Oldfield, F. 2000. Early diagenesis in North atlantic abyssal plain sediments characterized by rock-magnetic and geochemical indices. *Marine Geology*, **163**, 77–107.

Robion, P., Averbuch, O. & Sintubin, M. 1999. Fabric development and metamorphic evolution of Lower Paleozoic slaty rocks from the Rocroi massif (French-Belgian Ardennes): new constraints from magnetic fabrics, phyllosilicate preferred orientation and illite crystallinity data. *Tectonophysics*, **309**, 257–273.

Sandberg, C. A., Ziegler, W., Dreesen, R. & Butler, J. L. 1988. Late Frasnian mass extinction: conodont event stratigraphy, global changes, and possible causes. *Courier Forschunginstitut Senckenberg*, **102**, 263–307.

Sandberg, C. A., Morrow, J. R. & Ziegler, W. 2002. Late Devonian sea-level changes, catastrophic events, and mass extinctions. *In*: Koeberl, C. & MacLeod, K. G. (eds) Catastrophic Events and Mass Extinctions: Impacts and Beyond: *Geological Society of America Special Paper*, **356**, 473–487.

Schindler, E. 1990. Die Kellwasser Krise (hohe Frasne-Stufe, Ober Devon). *Göttinger Arbeiten zur Geologie und Paläeontologie*, **46**, 1–115.

Sepkoski, Jr, J. J. 1982. Mass extinctions in the Phanerozoic oceans: A review. *Geological Society of America, Special Papers*, **190**, 283–289.

Sepkoski, Jr, J. J. 1986. Phanerozoic overview of mass extinctions. *In*: Raup, D. M. & Jablonski, D. (eds) *Patterns and Processes in the History of Life*. Springer-Verlag, Berlin, 277–295.

Streel, M., Caputo, M. V., Loboziak, S. & Melo, J. H. G. 2000. Late Frasnian-Famennian climates based on palynomorph analyses and the question of the Late Devonian glaciations. *Earth-Science Reviews*, **52**, 121–173.

Tribovillard, N., Dupuis, C. & Robin, E. 2000. Sedimentological and diagenetical conditions of the impact level of the Cretaceous/Tertiary boundary in Tunisia: no anoxia required. *Bulletin de la Société Géologique de France*, **171**, 629–636.

Tribovillard, N. P., Desprairies, A., Lallier-Verges, E., Bertrand, P., Moureau, N., Ramdani, A. & Ramanamposoa, L. 1994. Geochemical study of organic-matter rich cycles from the Kimmeridge clay formation of Yorkshire (UK): productivity versus anoxia. *Palaeogeography, Palaeoclimatology, Palaeoecology*, **108**, 165–181.

Tribovillard, N., Averbuch, O., Bialkowski, A. & Deconinck, J.-F. 2002. The influence of early diagenesis of marine organic matter on the magnetic susceptibility signal of sedimentary rocks. *Bulletin de la Société Géologique de France*, **172**, 295–306.

Tribovillard, N., Averbuch, O., Devleeschouwer, X., Racki, G. & Riboulleau, A. 2004*a*. Deep-water anoxia over the Frasnian-Famennian boundary (La Serre, France): a tectonically induced oceanic anoxic event? *Terra Nova*, **16**, 288–295.

Tribovillard, N., Averbuch, O. & Riboulleau, A. 2004*b*. Influence of marine organic-matter diagenesis on magnetic susceptibility of sedimentary rocks: the sulphide pathway. *Annales de la Société Géologique du Nord*, **11**, 57–67.

Tribovillard, N., Riboulleau, A., Lyons, T. & Baudin, F. 2004*c*. Enhanced trapping of molybdenum by sulfurized marine organic matter of origin in Mesozoic limestones and shales. *Chemical Geology*, **213**, 385–401.

Vanderaveroet, P., Averbuch, O., Deconinck, J.-F. & Chamley, H. 1999. Glacial/interglacial cycles in Pleistocene sediments of New Jersey expressed by clay minerals, grain-size and magnetic susceptibility data. *Marine Geology*, **159**, 79–92.

Vorlicek, T. P. & Helz, G. R. 2002. Catalysis by mineral surfaces: implications for Mo geochemistry in anoxic environments. *Geochimica Cosmochimica Acta*, **66**, 3679–3692.

Walden, J., Oldfield, F. & Smith, J. 1999. Environmental magnetism: a practical guide. *Technical Guide No. 6*, Quaternary Research Association, London, 243pp.

Walliser, O. H. 1996. *Global events and event stratigraphy in the Phanerozoic: Results of international interdisciplinary cooperation in the IGCP Project 216 "Global Biological Events in Earth History"*. Springer-Verlag, Heidelberg.

Walliser, O. H., El Hassani, H. & Tahiri, A. 2000. M'rirt: a key area for the Variscan Meseta of Morocco. *Notes et Mémoires, Service Géologique du Maroc*, **399**, 93–108.

Warr, L. N. & Rice, A. H. 1994. Interlaboratory standardization and calibration of clay mineral crystallinity and crystallite size data. *Journal of Metamorphic Geology*, **12**, 141–152.

Wedepohl, K. H. 1971. Environmental influences on the chemical composition of shales and clays. *In*: Ahrens, L. H., Press, F., Runcorn, S. K. & Urey, H. C. (eds) *Physics and Chemistry of the Earth*, Pergamon, Oxford, pp. 305–333.

Wedepohl, K. H. 1991. The composition of the upper Earth's crust and the natural cycles of selected metals. *In*: Merian, E. (eds) *Metals and their compounds in the Environment*, VCH-Verlagsgesel lschaft, Weinheim, pp. 3–17.

Wendt, J. & Belka, Z. 1991. Age and depositional environment of Upper Devonian (Early Frasnian to Early Famennian) black shales and limestones (Kellwasser Facies) in the Eastern Anti-Atlas, Morocco. *Facies*, **25**, 51–90.

Yudina, A. B., Racki, G., Savage, N. S., Racka, M. & Malkowski, K. 2002. The Frasnian-Famennian events in deep-shelf succession, Subpolar Urals: biotic, depositional and geochemical records. *Acta Palaeontologica Polonica*, **47**, 355–372.

Zegers, T. E., Dekkers, M. J. & Bailly, S. 2003. Late Carboniferous to Permian remagnetization of Devonian limestones in the Ardennes: role of temperature, fluids, and deformation. *Journal of Geophysical Research*, **108**, 2357.

Zheng, Y., Anderson, R. F., van Geen, A. & Kuwabara, J. 2000. Authigenic molybdenum formation in marine sediments: a link to pore water sulfide in the Santa Barbara Basin. *Geochimica Cosmochimica Acta*, **64**, 4165–4178.

Article 17.

Riquier L., Averbuch O., Devleeschouwer X. and Tribovillard N. (2009). Diagenetic versus detrital origin of the magnetic susceptibility variations in some carbonate Frasnian-Famennian boundary sections from Northern Africa and Western Europe: implications for paleoenvironmental reconstructions. International Journal of Earth Sciences 99, 57-73, doi 10.1007/s00531-009-0492-7.

Int J Earth Sci (Geol Rundsch) (2010) 99 (Suppl 1):S57–S73
DOI 10.1007/s00531-009-0492-7

ORIGINAL PAPER

Diagenetic versus detrital origin of the magnetic susceptibility variations in some carbonate Frasnian–Famennian boundary sections from Northern Africa and Western Europe: implications for paleoenvironmental reconstructions

Laurent Riquier · Olivier Averbuch · Xavier Devleeschouwer · Nicolas Tribovillard

Received: 27 September 2007 / Accepted: 26 October 2009 / Published online: 4 December 2009

Abstract To provide a new insight into the diagenetic versus detrital origin of the magnetic susceptibility variations in ancient carbonate sequences, a study was conducted within four Frasnian–Famennian platform carbonate sections from Germany, France and Morocco. The study includes along-section magnetic susceptibility and carbonate content measurements complemented by analyses of magnetic hysteresis parameters, inorganic geochemistry and clay mineralogy. Our results show that the magnetic susceptibility evolution is dominantly controlled by the variations in the concentration of low-coercivity ferromagnetic magnetite grains and, to a lesser extent, of paramagnetic clays. In more detail, hysteresis ratios suggest the coexistence of two magnetite populations with significantly different grain size: (1) a dominantly coarse-grained detrital fraction including a mixture of multi-domain and single-domain particles (2) an authigenic fine-grained fraction composed of a mixture of single-domain and superparamagnetic particles. Despite a diagenetic imprint on the clay assemblages, no relationship is established between magnetic susceptibility and illite crystallinity, therefore discarding a noticeable distortion of primary within-section magnetic susceptibility evolution. The overall inherited character of the magnetic susceptibility fluctuations is corroborated by a significant correlation of magnetic susceptibility with terrigenous proxies (Zr, Th). The poorer correlation of magnetic susceptibility with the Fe content is consistent with the existence of a very fine-grained authigenic magnetite component that possibly induces a global magnetic susceptibility increase at the section scale, but no distortion of the within-section evolution. The magnetic susceptibility curves presented here provide a general record of climate-driven detrital influx and carbonate productivity through Frasnian–Lower Famennian times.

Keywords Rock magnetism · Magnetic susceptibility · Frasnian–Famennian boundary · Paleozoic carbonates

Electronic supplementary material The online version of this article (doi:10.1007/s00531-009-0492-7) contains supplementary material, which is available to authorized users.

L. Riquier · O. Averbuch (✉) · N. Tribovillard
Géosystèmes, UMR CNRS 8157, Université Lille 1,
Bâtiment SN5, 59655 Villeneuve d'Ascq Cedex, France
e-mail: olivier.averbuch@univ-lille1.fr

L. Riquier
e-mail: laurent.riquier@u-bourgogne.fr

X. Devleeschouwer
Department VII: Geological Survey of Belgium,
Royal Belgian Institute of Natural Sciences,
Rue Jenner 13, 1000 Brussels, Belgium

Present Address:
L. Riquier
UMR CNRS 5561 Biogéosciences, Université de Bourgogne,
6, Boulevard Gabriel, 21000 Dijon, France

Introduction

In recent years, a growing number of studies have focused on the use of the magnetic susceptibility (MS) signal as a marker of stratigraphic cycles and paleoenvironmental changes in Paleozoic carbonate rocks (Ellwood et al. 1999; Crick et al. 2002; Averbuch et al. 2005; Hladil et al. 2005; Da Silva and Boulvain 2006; Riquier et al. 2007; Mabille and Boulvain 2007; Whalen and Day 2008). In these studies, variations in MS have been largely shown to relate to sedimentary facies evolution (Ellwood et al. 1999; da Silva and Boulvain 2006; Whalen and Day 2008) and possibly to correlate over long distances within an individual basin or even on the margins of different oceanic realms (Crick et al. 2001; Ellwood et al. 2001). Such recurrent observations have thus underlined the fact that the MS of ancient diagenetic marine limestones could be controlled by a magnetic fraction inherited from the conditions prevailing at the time of deposition, i.e. climate- or tectonic-related detrital input to the basins and in situ carbonate productivity (Ellwood et al. 2000).

Despite such numerous stratigraphic arguments, the preservation of an inherited depositional MS signal in diagenetic carbonates has, however, not been clearly proved by detailed rock magnetic analyses. Conversely, a large number of paleomagnetic studies have highlighted the effects of late diagenesis on the chemical remagnetization of Paleozoic carbonates (Jackson 1990; Elmore et al. 1993; McCabe and Channell 1994; Szaniawski et al. 2003; Zegers et al. 2003; Zwing et al. 2005). More largely, the chemical precipitation (or dissolution) of iron-bearing minerals during early or burial diagenesis has been frequently seen as inducing a substantial alteration in the primary detrital magnetic signal (Machel 1995; Banerjee et al. 1997; Roberts et al. 1999; Katz et al. 2000; Tribovillard et al. 2002).

The preservation of a deposition-related MS in Paleozoic carbonates that were, in most cases, affected by significant burial diagenesis and noticeable deformation thus appears somewhat questionable. This paradoxical situation has to be accounted for by a strong mineralogical and/or grain-size segregation in the magnetic fractions controlling the MS variations on the one hand and the remanent magnetization on the other. This question was generally solved by relating the MS variations to the paramagnetic content of the carbonates (i.e., clays and other iron-bearing silicates; Ellwood et al. 2000) but such interpretation has not been yet corroborated by detailed rock magnetic analyses. However, paramagnetic clays have also been largely proved to be involved in diagenetic and anchimetamorphic reactions (e.g., the smectite–illite transformation; Katz et al. 2000) so that the paramagnetic signal is also likely to be strongly modified during rock burial.

To progress in the understanding of the origin of MS variations in Paleozoic carbonate sequences and as a corollary, to establish the applicability of MS logging as a paleoenvironmental proxy, we conducted rock magnetic experiments in four well-studied Frasnian–Famennian (Upper Devonian) carbonate sections from Western Europe and Northern Africa. Despite the fact that the sections were affected by significant burial diagenesis, along-section variations in the MS were expected to provide a record of large-scale changes in the detrital input versus biogenic carbonate production along the former margins of Gondwana and Laurussia. To test the spatial consistency of magnetic signals, measurements were carried out on sites located on the margins of different oceanic realms. Along-section MS measurements were coupled with hysteresis loop analyses on representative samples from each section to constrain the magnetic phases responsible for the observed MS variations. An additional geochemical and clay mineralogical data set has been used for two reference sections in Morocco and Germany to evaluate the respective parts of the primary detrital versus secondary diagenetic signatures of the measured magnetic record.

Geological setting and sampling

The Frasnian–Famennian (F–F) boundary, during Late Devonian times (374.5 Ma; Gradstein et al. 2004), corresponds to one of the five largest mass extinction events in the Phanerozoic. On a global scale, it has been recognized as a period of drastic environmental changes and biodiversity loss, during which many species of tropical marine fauna became extinct (corals, stromatoporoids, trilobites, conodonts, cephalopods; e.g., Sepkoski 1986). As exemplified by a conspicuous positive δ^{13}C anomaly of marine carbonates (Joachimski et al. 2002), this crisis of the biosphere is associated during Late Frasnian times with an event of extensive burial of organic matter-rich deposits, i.e., the Kellwasser (KW) horizons (Buggisch 1991). These horizons have been described in many sections, located in outer shelf (i.e., 100–200 m depth) and epicontinental basin settings, mainly along the former Prototethysian margins of Laurussia (Northern America, Northern Europe) and Gondwana (Southern Europe, Northern Africa). For all these sites, geochemical proxies for depositional redox conditions and primary productivity show consistent anomalies indicating general oxygen-depleted bottom-water along continental margins and increased marine productivity (Murphy et al. 2000; Tribovillard et al. 2004; Riquier et al. 2005). On top of the KW levels, however, the basal Famennian times are marked by a pronounced depositional break, with frequent hiatuses and breccia developed during a significant worldwide sea-level fall (Isaacson et al. 1999; Casier et al. 2000; Devleeschouwer et al. 2002; Sandberg et al. 2002). Associated climatic cooling has been proposed based on the δ^{18}O signature of marine biogenic apatite (Joachimski and Buggisch 2002) and reduced miospore diversity in continental areas (Streel et al. 2000). Moreover, atmospheric CO_2 concentration estimates and modeling argue for a significant decrease in pCO_2 during that period (Royer 2006), thereby forming a major driving process for climatic changes at the F–F boundary. Such a drop in atmospheric CO_2 content is often thought to be related to enhanced organic-carbon burial in Late Frasnian oceans and increased continental weathering.

Both processes could be linked to the effects of vascular plant development on land (Algeo et al. 1995), the incipient Variscan orogeny (Averbuch et al. 2005) and/or some mantle-plume related volcanic activity (Racki 1998). The combined sea-level, climatic and atmospheric $p\mathrm{CO}_2$ changes, thought to occur at the F–F transition, are expected to produce significant variations in erosional processes on land, resulting in changes in both the detrital input to epicontinental basins and in situ marine biological production (through increases in the nutrient delivery from continents). If not deeply altered by diagenesis, such variations are likely to be recorded by MS evolution which has been shown to be particularly efficient in monitoring the respective changes in the detrital and biogenic carbonate fractions due to their contrasting magnetic behavior (the detrital fraction being generally ferromagnetic sensu lato due to iron oxides or paramagnetic due to iron-bearing silicates, whereas the biogenic carbonate fraction is dominantly diamagnetic, Ellwood et al. 2000).

To test the large-scale spatial consistency of the MS signal, four distant sections were sampled on the margins of two different oceanic realms. They include carbonate platform series deposited on slowly subsiding shelves along the Gondwanian and Laurussian margins. Basinal sequences, with well-developed, organic carbon-rich KW-type levels, were intentionally not included in the sampling set to minimize the effects of early chemical reduction of sediments induced by diagenesis, which is known to alter significantly the depositional signature of the magnetic signal (Machel 1995; Verosub and Roberts 1995; Tribovillard et al. 2002). The four studied sections were selected according to their accurate conodont biozonations and sequence stratigraphy frameworks.

More precisely, the Southern Laurussia margin was studied from two well-known sections, namely Steinbruch Schmidt and Beringhauser Tunnel, located in the Rhenish Massif (Germany, Fig. 1). This Paleozoic Massif forms part of the Rhenohercynian fold Belt, developed at the northern thrust front of the European Variscides. During the Upper Devonian, it was located along the northern passive continental margin of the narrow Lizard-Rhenohercynian marginal sea (e.g., Franke 2000). The Northern Gondwana margin was investigated from two sections situated in Morocco and Southern France (Fig. 1), respectively; the Anajdam section in the Moroccan Western Meseta and the Coumiac section in the Southern France Montagne Noire Massif. During the Upper Devonian, these sites were situated on the southern margin of the previously subducted Massif Central-Moldanubian Ocean and thus formed part of the marine undeformed foreland of the early Variscan mountain belt undergoing incipient uplift (Piqué et al. 1993; Demange 1994). Inversion of these basins and thrust developments did not occur,

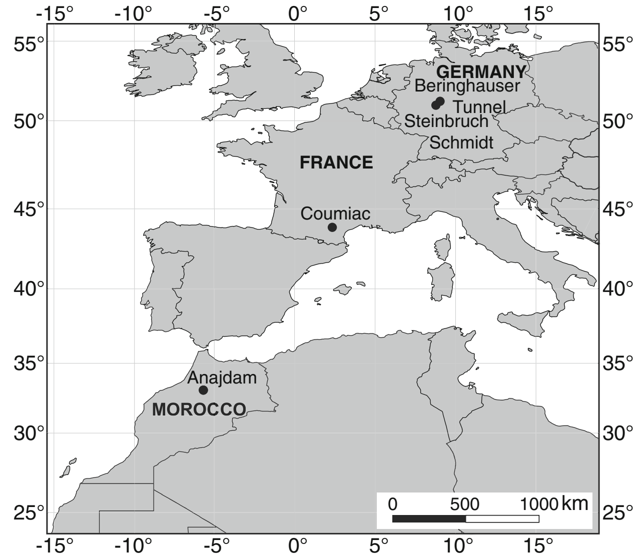

Fig. 1 Map showing the modern locations of the sections studied: Anajdam (Western Meseta, Morocco), Coumiac (Montagne Noire, S France), Beringhauser Tunnel and Steinbruch Schmidt (Rhenish Massif, Germany)

however, before Visean times (Bouabdelli 1989; Demange 1994). During the F–F period, these areas formed the slowly subsiding passive margins of Gondwana and sedimentation was not strongly influenced by early Variscan orogenic processes. The stratigraphic and sedimentological characteristics of the sections under study are presented briefly in Figs. 2 and 3 but can be found in more detail in various publications (Becker 1993; Préat et al. 1998; Lazreq 1999; Devleeschouwer et al. 2002; Schülke and Popp 2005).

Methods

Magnetic susceptibility

Rock magnetism has been extensively used during the last two decades in order to document paleoenvironmental and paleoclimatic changes in recent sedimentary rocks (e.g., Thompson and Oldfield 1986; King and Channell 1991; Maher and Thompson 1999; Walden et al. 1999). MS is surely the most basic of the magnetic parameters that can be measured on rocks, as it quantifies the capacity of a rock specimen of a given volume or mass to be magnetized in a weak magnetic field. MS is dependent on the mineralogical composition of the rock and integrates the contribution of the rock fractions according to their dia-, para- or ferromagnetic sensu lato behavior. Any changes in the nature, composition and grain size of the rock-forming minerals can be recorded in the bulk MS value. This property makes MS a parameter that is very sensitive to mineralogical

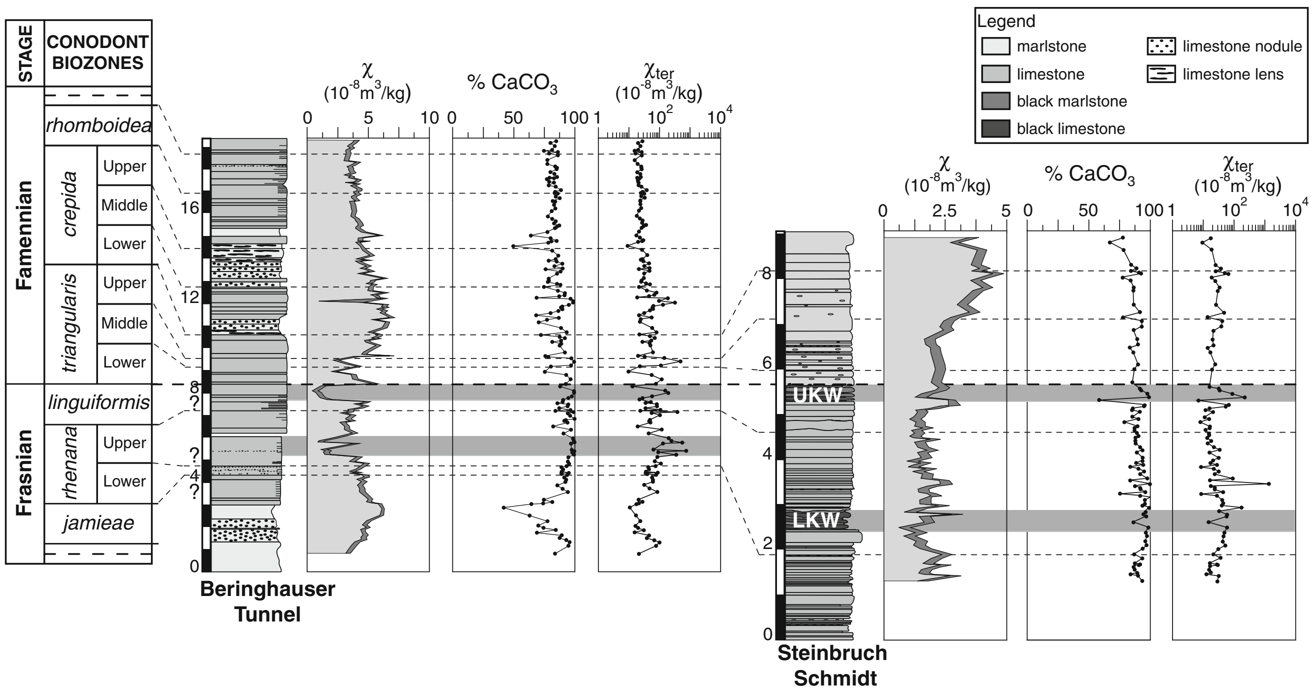

Fig. 2 Sedimentological and biostratigraphic framework of the sections located along the South Laurussia margin, i.e., Beringhauser Tunnel, Steinbruch Schmidt (*LKW* Lower Kellwasser, *UKW* Upper Kellwasser; scale in meters) (after Devleeschouwer et al. 2002; Schülke and Popp 2005) and along-section variations in the measured bulk low-field magnetic susceptibility (χ), the calcium carbonate content and the intrinsic susceptibility of the terrigenous component (χ_{ter}). The carbonate-free susceptibility (χ_{cf}) is reported in dark grey on the (χ) plot. The terrigenous component (χ_{ter}) is obtained by the following formula: $\chi_{ter} = [(\chi)/(1 - \% CaCO_3)] - [(\chi_{calcite} \times \% CaCO_3)/(1 - \% CaCO_3)]$. *Shaded bands* correspond to the KW horizons. Note the absence of organic-matter enrichment in the Late Frasnian part of the Beringhauser Tunnel section

changes. In sedimentary rocks, variations of any of the diamagnetic (mainly quartz, calcite), paramagnetic (mainly clay minerals, pyrite and iron carbonates) or ferromagnetic sensu lato contributions (iron oxides, hydroxides and iron-rich sulphides) are recorded by MS. Therefore, along-section records of MS are potentially related to changes in fluxes and/or sources of detrital inputs (Andrews and Stravers 1993; Robinson 1993; Vanderaveroet et al. 1999; Ellwood et al. 2000) or in the biogenic production or chemical precipitation of a secondary (authigenic/diagenetic) mineralogical phase (Hesse and Stolz 1999; Oldfield 1999).

In this study, the MS data set includes 439 samples collected at 5- to 25-cm intervals. MS was measured on small rock samples using a Kappabridge KLY-2 susceptibility bridge operating at an alternating magnetic field of 300 A/m (frequency 920 Hz). Low-field MS values were normalized with respect to sample mass (hereafter χ in m^3/kg) to allow comparisons between samples of different density. After measurement of the carbonate content ($CaCO_3$) using the Bernard calcimeter method, the carbonate-free MS (χ_{cf}) and the intrinsic MS of the terrigenous content (χ_{ter}) were computed following a standard methodology detailed by Hounslow and Maher (1999).

Magnetic hysteresis parameters

Analyses of magnetic hysteresis loops have been shown to be particularly efficient to discriminate the different causes for MS variations (e.g., Walden et al. 1999; Solheid et al. 2003). In this study, hysteresis loop parameters were obtained from representative samples (about 20 measurements for each section), using 10–30 mg chips, analyzed with an Alternating Gradient Force Magnetometer (AGFM 2900) at the Paleomagnetic laboratory of the Laboratoire des Sciences du Climat et de l'Environnement (LSCE, Gif-sur-Yvette, France). Hysteresis loops show the evolution of magnetization M of magnetic elements, at room temperature, as a function of the applied magnetic field B (up to 1 T). From the hysteresis loops, four basic parameters were extracted: the saturation magnetization M_s, the saturation remanent magnetization M_r, the coercitive force B_c, the high-field slope HF-slope. Values of M_s, M_r and B_c were determined for each hysteresis loop, after correction for the constant HF-slope, which records only the combined effects of paramagnetic and diamagnetic contributions (i.e., the matrix contribution). As for χ, magnetic parameters M_s, M_r and HF-slope were normalized with respect to sample mass. The normalized HF-slope was converted into

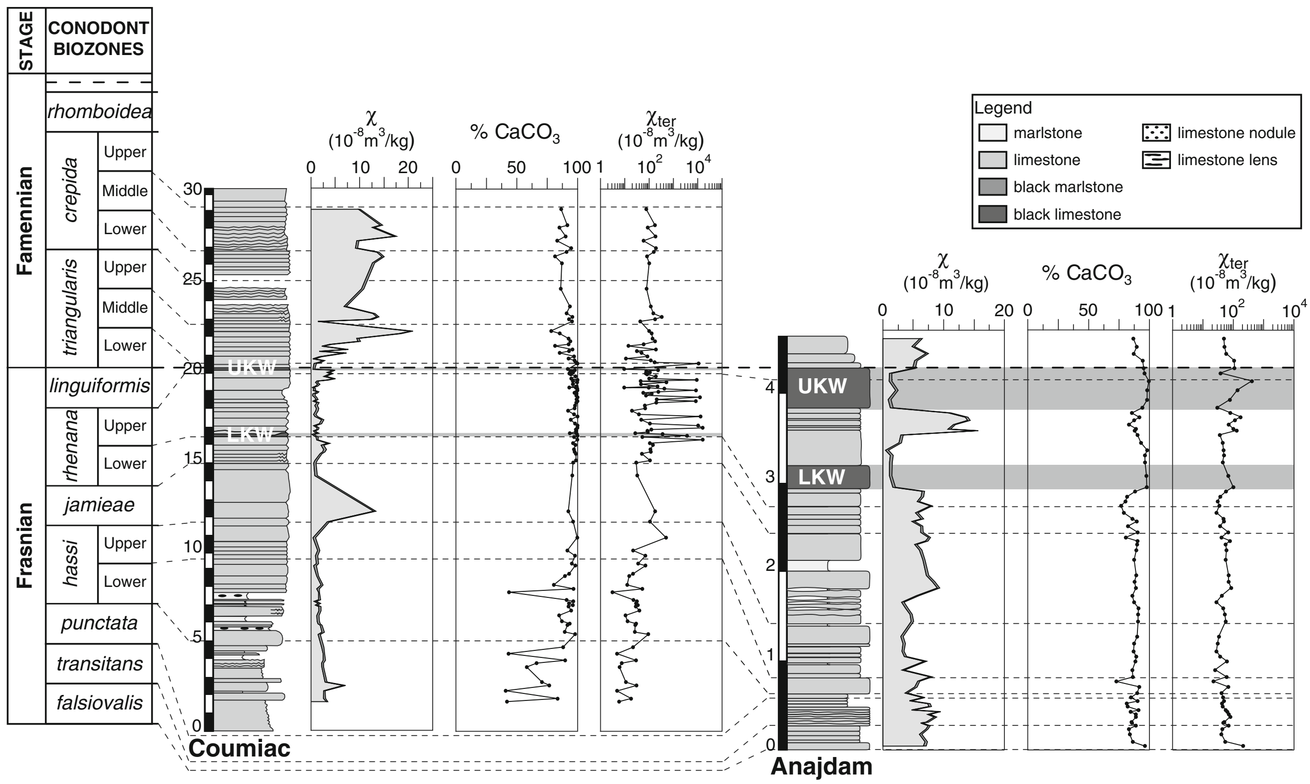

Fig. 3 Sedimentological and biostratigraphic framework of the sections located along the North Gondwana margin, i.e., Coumiac, Anajdam (*LKW* Lower Kellwasser, *UKW* Upper Kellwasser; scale in meters) (after Becker 1993; Préat et al. 1998; Lazreq 1999) and along-section variations in the measured bulk low-field magnetic susceptibility (χ), the calcium carbonate content and the intrinsic susceptibility of the terrigenous component (χ_{ter}). The carbonate-free susceptibility (χ_{cf}) is reported in *dark grey* on the (χ) plot. The terrigenous component (χ_{ter}) is obtained by the following formula: $\chi_{ter} = [(\chi)/(1 - \%\ CaCO_3)] - [(\chi_{calcite} \times \%\ CaCO_3)/(1 - \%\ CaCO_3)]$. *Shaded bands* correspond to the KW horizons

a high-field magnetic susceptibility χ_{HF} (m^3/kg) multiplying it by the magnetostatic constant μ_0 ($\mu_0 = 4\pi \times 10^{-7}$ T/A per m). The ferromagnetic susceptibility χ_{ferro} (m^3/kg), which quantifies the low-field ferromagnetic contribution, was computed by subtracting χ_{HF} from χ (Walden et al. 1999; Solheid et al. 2003). Finally, the coercivity of the remanence B_{cr} was determined by the step-wise application of a backfield isothermal remanence to remove the saturation remanence. The waiting time before taking the reading was kept constant for the entire data set (i.e., 1 s).

Complementary analyses

As previously mentioned, chemical precipitation of diagenetic minerals can significantly distort the primary MS signal. In the Upper Devonian sections studied here, effects of burial diagenesis and deformation have been demonstrated by regional-scale paleomagnetic studies that provide evidence of a pervasive secondary component of natural remanent magnetization, overprinting the primary signal (Coudray et al. 1986; Salmon et al. 1988; Zwing et al. 2002). For two of the studied sections (the Beringhauser Tunnel section in the Rhenish Massif and the Anadjam section in the Moroccan Meseta), we investigated a possible secondary alteration of the magnetic signal, using (1) representative clay mineral assemblages and calibrated illite crystallinity measurements (XRD analyses), (2) major and trace element geochemistry (ICP-AES and ICP-MS analyses) and (3) scanning electron microscopic observations and probe analyses. The detailed measurement protocol of these complementary analyses can be found in Riquier et al. (2006, 2007). The identification of clay minerals was made according to the position of the (001) series of basal reflections on X-ray diffractograms (Brindley and Brown 1980) and following the protocol defined by Bout-Roumazeilles et al. (1999). Semi-quantitative estimations of major clay minerals, as well as the illite crystallinity indexes, were calculated using the Macdiff software (Petschick et al. 1996), to provide information on the diagenetic transformations of clay minerals, i.e. the smectite–illite transformation and illite crystallinity evolution. To estimate the intensity of the burial diagenesis in each section, the measured illite crystallinity index values were converted into the international calibrated scale CIS (Warr and Rice 1994) using a routine correlation procedure described in Robion et al. (1999). The results of the geochemical analyses we present here are for specific chemical elements selected for the purpose of this study, but the whole geochemical data set is available in Riquier (2005). We focused our attention on: (1) elements that can be used as proxies for the terrigenous input; they were selected for their independence regarding the mineralogical components involved in the magnetic signal (iron oxides, clays) and also for the fact that they were not affected by diagenesis. Zirconium (Zr) and thorium (Th) were selected here as the more reliable detrital proxies (Calvert and Pedersen 1993); (2) the total Fe (Fe_{tot}) content that will be used as a proxy of the bulk magnetic mineralogical component. It was separated into an inherited detrital part and a secondary authigenic part. The authigenic Fe-bearing component was estimated by using the Fe/Zr ratio and by the theoretical calculation of the iron in excess (Fe_{exc}). The rationale for calculating the detrital and authigenic fractions of the total iron content is the following. The Fe/Al ratio of the detrital part of the studied rocks is supposed to be the same as that of average shale ($Fe/Al_{average\ shale}$; Wedepohl 1991). Thus, the detrital fraction of iron (Fe_{det}) is calculated as $Fe_{det} = Al_{sample} \times Fe/Al_{average\ shale}$. Consequently, the iron fraction in excess relative to the detrital fraction, namely, $Fe_{exc} = Fe_{tot} - Fe_{det}$, may be considered to be of authigenic/diagenetic origin. The pitfall of this calculation is that it implies that the Fe/Al ratio of the terrigenous fraction of the rocks is close to that of average shale, representing crustal abundance. This assumption is legitimate when the depositional setting collects well-mixed terrigenous particles originating from large-scale drainage systems, which is the case in the margin settings studied here. Analytical precision was estimated to be better than 1% (mean 0.5%) for the Al and Fe content and 10% for the Zr and Th content.

Results

Magnetic susceptibility data

Figures 2 and 3 show the evolution of χ and $CaCO_3$ for the sedimentary sequences under study. The χ_{cf} and χ_{ter}, inferred from these basic measurements are also presented along the same sections. As usually recorded in carbonate rocks, the MS data are generally low and most of the χ values are below 20.0×10^{-8} m^3/kg. Although the diamagnetic carbonate component may represent more than 95% of the total composition of the rocks, it does not, however, significantly affect the total MS as shown by the evolution of the carbonate-free signal. Moreover, it is noteworthy that the intensity of the χ signal significantly fluctuates depending on the areas studied. The sections sampled along the North Gondwana margins record the highest values of χ (Figs. 2, 3). This trend, especially visible for the early Famennian samples of Coumiac, is also recorded by the calculated terrigenous susceptibility signal, as shown by the χ_{ter} values for each section (Figs. 2, 3). Although defined for only four sites, this trend, however, seems to indicate a fundamental variation in the detrital sources between the South Laurussian and North Gondwanian margins. The proximity of the exhumed crystalline massifs of the Early Variscan mountain belt from the Gondwanian sites could be a possible driving factor for such contrasting behavior.

Despite the relatively low amplitude of the χ values, especially in the sections from the Rhenish Massif, the χ signal displays significant short- and long-term variations. The very short-term anomalies defined by one or two data points are generally impossible to correlate from one section to another, due to the within-site sampling density and the condensed character of carbonate series that do not allow such high resolution. Except for these local anomalies, the most significant variations in the MS signal can be correlated between the different sections, but with amplitudes that noticeably differ from one section to one another. Considering first-order variations, some long-term decreasing trends can be observed throughout the Early Frasnian (*transitans* to *hassi* biozones) and Upper Frasnian (Middle *jamieae* to *linguiformis* biozones). These successive decreasing trends lead to section-scale minimum MS values situated in the Latest Frasnian times. Such a long-term MS decrease, which parallels a long-term increase in the carbonate content in all the sections, is strengthened by a shorter-term accentuation of the MS decrease in the KW horizons (Figs. 2, 3). Indeed, whatever the section, the KW horizons correspond to the intervals of lowest χ values (generally below 1.0×10^{-8} m^3/kg). These variations are particularly well defined in the Beringhauser Tunnel and Anajdam sections (Figs. 2, 3). It is noteworthy that the MS lows observed in the KW horizons, do not depend on the presence of organic matter (OM) as demonstrated by the Beringhauser Tunnel section, which does not show the common black facies characterizing the KW time-span.

As also particularly well exemplified in the Anajdam, Coumiac and Beringhauser Tunnel sections, two specific periods of MS increase can be defined within the general low amplitude long-term decreasing trends observed during the Frasnian. The first significant MS increase is situated in the Middle Frasnian, around the transition between the Upper *hassi* and *jamieae* zones. The precise extent of this MS peak is poorly defined in our sections due to the condensed character of the series investigated. However, it is important to note that the observed rise is coeval with a particularly well-defined MS increase, observed in the Upper *hassi*- Middle *jamieae* biozones within thicker platform carbonate series from the Ardennes (S Belgium; da Silva and Boulvain 2006) and Alberta (Canada, Whalen and Day 2008). At sites where the two KW horizons are well defined, the inter-KW time-span (more precisely the upper most Upper *rhenana* zone) is also generally marked by a noticeable increase in the MS.

As previously noted, the F–F boundary, which corresponds to a major erosional surface on top of the Upper KW horizon, appears as a significant discontinuity in the long-term evolution of the MS. Due to the extensive hiatus at the F–F boundary and the associated frequent reworking of sediments (see "Geological setting and sampling"), the basal Famennian does not display a clear MS evolution pattern. From the Middle *triangularis* zone upward, however, the χ signal shows a significant increasing trend, at least up to the Lower *crepida* zone. In Coumiac, for example, a very sharp increase (from 1.0 to 15.0×10^{-8} m^3/kg) is observed in the Middle *triangularis* up to the Lower *crepida* zone. A parallel increase, but with lower amplitude, can be observed in the Steinbruch Schmidt and Beringhauser Tunnel sections. For these sections, however, the most significant increasing trend is situated in the Upper *triangularis*–Lower *crepida* zone. Given the first-order MS evolution in Late Devonian, the F–F transition can thus be regarded as a significant boundary that marks the limit between a long-term Frasnian decreasing trend and a subsequent Lower Famennian increase.

Magnetic hysteresis data

Representative hysteresis loops measured in the F–F carbonates are presented in Fig. 4. Parameters extracted from the total hysteresis loop data set are reported, in more detail, in Figs. 5, 6 and 7 and are listed in Tables 1, 2, 3, 4, available as supplementary files. As usually observed in carbonate rocks (Borradaile et al. 1993), magnetizations at saturation are low (M_s is generally lower than 1.0×10^{-2} Am^2/kg; Fig. 5). However, as observed for the MS, saturation magnetization parameters display significantly higher values for the North Gondwana sections than for the South Laurussia sections. This observation is supported by the broad correlation of the measured M_s with χ (Fig. 5a, b). This correlation is well defined for the North Gondwanian sections but much less pronounced for the Laurussian sites owing to the much lower intensities and amplitudes of variations of both M_s and χ. This general

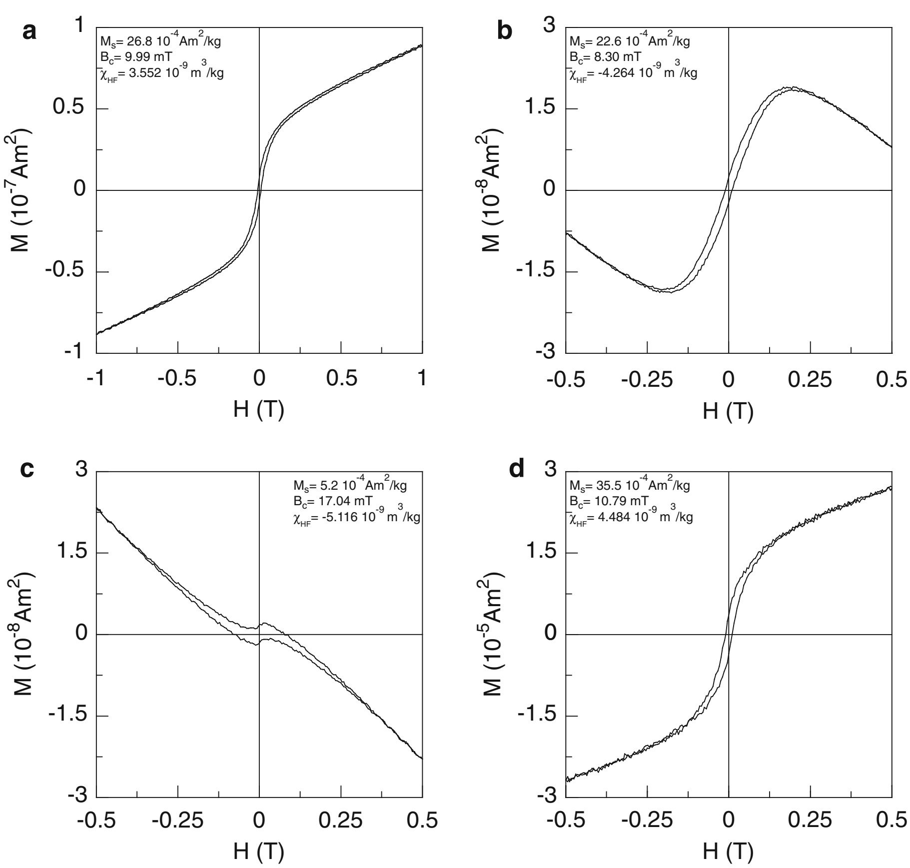

Fig. 4 Characteristic magnetic hysteresis loops measured for samples **a** and **b** from the Anadjam section, and **c** and **d** from the Beringhauser Tunnel section. Hysteresis loops of representative samples from the Late Frasnian Kellwasser horizons are reported in **b** for Anadjam (Lower KW, upper *rhenana* zone) and **c** for Beringhauser Tunnel (Upper KW, *linguiformis* zone). Loop **a** corresponds to a Frasnian sample (lower *rhenana* zone), Loop **d** corresponds to a Famennian sample (lower *crepida* zone). Note the negative high-field slope indicating the diamagnetic behavior of the rock matrix in the Kellwasser levels. The values of B_c are slope-corrected; values of M_s and χ_{HF} are mass-normalized

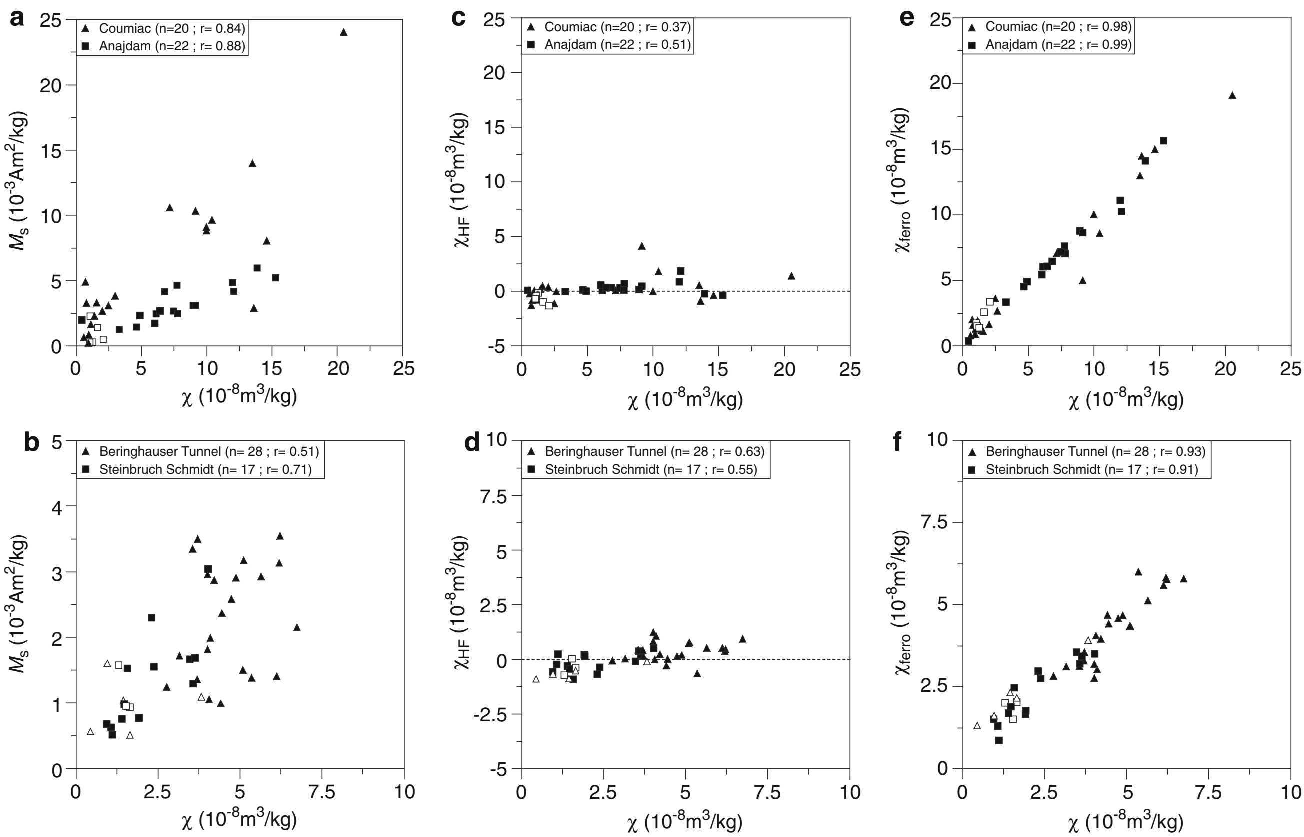

Fig. 5 Crossplots reporting magnetic hysteresis parameters against the bulk low-field magnetic susceptibility (χ) for representative samples from the North Gondwana sections (Anajdam, Coumiac) (**a**, **c**, **e**) and from the South Laurussia sections (Beringhauser Tunnel, Steinbruch Schmidt) (**b**, **d**, **f**). *Open symbols* correspond to the samples collected in the Kellwasser horizons or their time-equivalent (Beringhauser Tunnel). **a**, **b** magnetization at saturation (M_s) versus bulk low-field magnetic susceptibility (χ); **c**, **d** high-field magnetic susceptibility (χ_{HF}) versus (χ); **e**, **f** ferromagnetic susceptibility (χ_{ferro}) versus (χ). The number of samples per section and the correlation coefficient *r* are reported for each diagram

pattern suggests that the variations in the χ signal are related in some way to the changes in the ferromagnetic sensu lato contribution. This preliminary observation can be significantly refined by taking into account the values of χ_{HF} and of χ_{ferro} deduced from the hysteresis loops. The χ_{HF} provides a direct quantification of the combined paramagnetic and diamagnetic components of the rocks. Except very locally, the χ_{HF} values are very low, generally below 1.25×10^{-8} m^3/kg (Fig. 5c, d), indicating a minor contribution of the matrix components to the bulk magnetic signal. In addition, a strongly significant linear correlation (slope close to 0.9 and correlation coefficient $r > 0.9$) can be established between χ_{ferro} and χ (Fig. 5e, f) showing that the concentration in ferromagnetic minerals almost totally controls the variations in the MS. A very subtle correlation can be observed between χ_{HF} and χ, showing that samples displaying high χ values have a dominantly paramagnetic matrix whereas samples with low χ values have a dominantly diamagnetic matrix. This behavior is particularly typical of the samples collected within the KW horizons. As observed in Fig. 5, these levels display very high diamagnetic contributions and very low magnetic susceptibilities. This magnetic behavior is very different from that of most of the F–F samples, which integrate a noticeable paramagnetic component (Fig. 4). As corroborated by the carbonate concentration measurements (Figs. 2, 3), these results show that the KW-type rocks are almost pure limestones. A noticeable amount of organic carbon can be locally present in these levels but they exhibit almost no paramagnetic or ferromagnetic mineralogical components. In other parts of the sections studied, the paramagnetic component is significantly higher due to the relative increase in clay content.

To further constrain the origin of the MS variations, we investigated the nature and grain size of the ferromagnetic sensu lato component, using characteristic parameters of hysteresis loops. As frequently observed in Paleozoic carbonates (e.g., McCabe and Channell 1994), samples from the sections under study frequently displayed “wasp-waisted” hysteresis loops, characteristic of a mixture of both low- and high-coercivity minerals (e.g., Jackson et al. 1990). Depending on the relative amount and/or

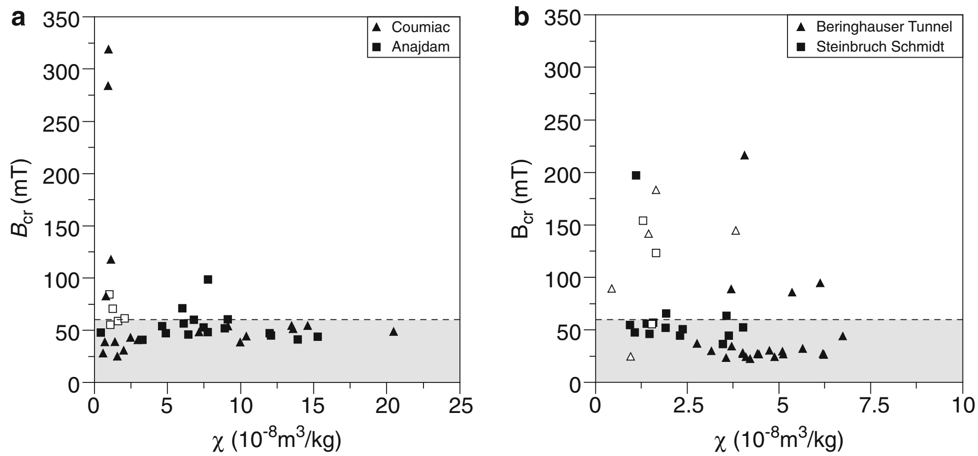

Fig. 6 Crossplots reporting the coercivity of the remanence (B_{cr}) versus the bulk low-field magnetic susceptibility (χ) for representative samples from the North Gondwana sections (Anajdam, Coumiac) (**a**) and from the South Laurussia sections (Beringhauser Tunnel, Steinbruch Schmidt) (**b**). *Open symbols* correspond to the samples collected in the Kellwasser horizons or their time-equivalent (Beringhauser Tunnel). *Shaded bands* correspond to the domain of remanence coercivity values of magnetite

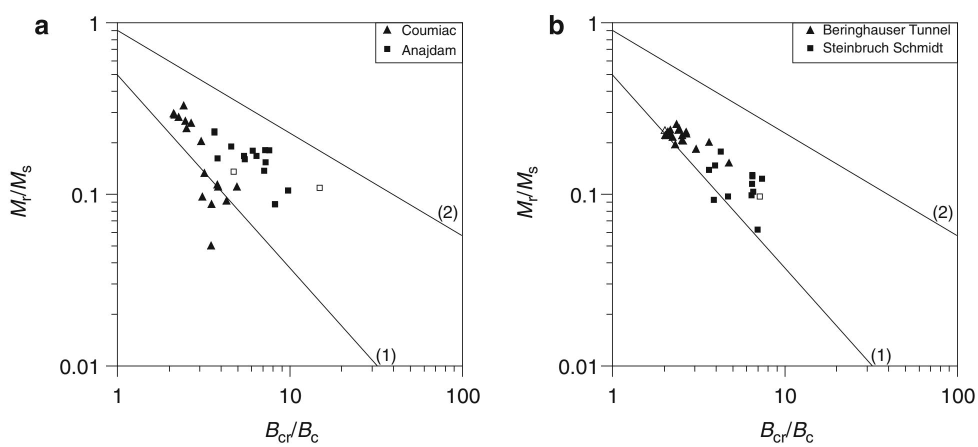

Fig. 7 M_r/M_s versus B_{cr}/B_c plots for the low-coercivity rock samples (B_{cr} < 60 mT) from the Coumiac and Anajdam sections (**a**), and from the Beringhauser Tunnel and Steinbruch Schmidt sections (**b**). Lines *1* and *2*, respectively, show empirical trends for, a mixture of detrital single domain–multi-domain magnetite particles (Parry 1982; trend for unremagnetized limestones after Channell and McCabe 1994) and a mixture of single domain-superparamagnetic authigenic magnetite particles (remagnetized Paleozoic limestones from Jackson 1990)

mineralogy of these two phases, the measured coercivity values appear highly variable within the sampling set (B_{cr} values vary between 25 and 350 mT). As a whole, in the sections, the coercivity values are predominantly low (B_{cr} < 60 mT and B_c < 15 mT) regardless of the χ values (Fig. 6). As usually observed in platform carbonates (e.g. Borradaile et al. 1993; Zwing et al. 2005), these data suggest that the χ variations are mainly related to the varying concentration of a low-coercivity mineral phase of magnetite type (Fe_3O_4). Within the data set, very few samples display higher coercivities. Most of these few samples were collected within the KW horizons, which have been shown to develop under dysoxic to anoxic conditions (e.g., Riquier et al. 2005). As illustrated by rock magnetic analyses in recent sapropel-type levels (Roberts et al. 1999; Passier et al. 2001), such highly reducing depositional conditions suggest that the high-coercivity phase in these levels could be partly composed of ferromagnetic iron sulphides (Fe monosulfides), ultimately transformed into diagenetic pyrrhotite (Fe_7S_8 to $Fe_{11}S_{12}$). However, remanent coercivities greater than 125 mT (the upper limit of remanence coercivity of pyrrhotite according to Peters and Dekkers 2003) indicate that a higher coercivity phase is also present in these samples. The SEM observations carried out on representative samples from the black, KW-type levels reveal the occurrence of hematite as a result of the partial oxidation of early diagenetic pyrite framboids (Riquier et al. 2006). Pyrrhotite was not identified on the thin sections analyzed but it could be present as submicron grains in association with OM. The specific occurrence in the KW-type levels of hematite and pyrrhotite could partly explain the observed MS decrease in these levels as their mass-specific susceptibility is somewhat lower than that of magnetite. However, as shown in Figs. 2 and 3, the KW-type levels display rather high χ_{ter} values compared to other parts of the F–F sections, thereby suggesting that this mechanism alone cannot account for the general low MS values observed in latest Frasnian times.

Samples with magnetite as the main carrier of the MS (B_{cr} considered to be lower than 60 mT) were plotted in a classical M_r/M_s versus B_{cr}/B_c plot in order to evaluate the bulk grain size of the magnetite fraction (Fig. 7; Day et al. 1977). As commonly observed, values of M_r/M_s and B_{cr}/B_c are distributed along a mixing trend characteristic for the combination of various proportions of single-domain and multi-domain magnetite grains (see the recent review in Dunlop 2002). However, the observed trend does not cluster along the mixing line established by Parry (1982) for a classical detrital signature [and correlatively, for diagenetically non-remagnetized limestones (Channell and McCabe 1994)] but is shifted towards higher values of both M_r/M_s and B_{cr}/B_c (i.e., the right part of the plot in Fig 7). The M_r/M_s and B_{cr}/B_c ratios are not high enough, however, to fit the mixing line of single-domain and superparamagnetic particles observed by Jackson (1990) in remagnetized North American Paleozoic limestones. Our data plot along an intermediate trend between these two reference lines very similarly to that observed by McCabe and Channell (1994) and Zwing et al. (2005) in some remagnetized Paleozoic limestones from the Craven basin (Great Britain) and the Rhenish Massif (Germany). Based on a comparison with hysteresis ratios from clastic rocks and biohermal limestones, Zwing et al. (2005) have interpreted such an intermediate distribution as the superimposition of two generations of magnetite grains: (1) a primary detrital fraction including mainly coarse-grained magnetite (predominantly multi-domain) (2) a secondary diagenetic fraction including authigenic fine-grained magnetite (possibly a mixture of single-domain and superparamagnetic magnetite). The recognition of the coexistence of two magnetite populations with significantly different grain size is very important with regard to the decoupling observed between the MS and the natural remanent magnetization of the Paleozoic carbonates (detailed in the "Introduction"), the remanent magnetization being much more sensitive to the single-domain magnetite fraction than the MS. This grain size induced segregation of detrital and diagenetic magnetite fractions could, at least, partly explain the different behaviors of MS on the one hand, and natural remanent magnetization on the other. This point will be further considered in the following section by correlating the MS variations with geochemical and clay mineralogical proxies for both detrital input and diagenetic evolution of the F–F carbonates.

Discussion

Diagenetic versus detrital origin of the magnetic susceptibility variations

The Late Devonian–Early Carboniferous subsidence of the South Laurussian and North Gondwanian margins and the subsequent integration of these margins into the Variscan orogenic wedge during the Upper Carboniferous resulted in the deep burial of the F–F sections studied here. The exhumation of these sections and their recent exposure to weathering processes may also have lead to some oxidation of the iron-bearing mineral phases, which could perhaps have affected the magnetic signal.

In the sections under study, weathering-induced oxidation processes are dominantly associated with the OM-bearing KW horizons. This can be explained by the selective oxidation of early diagenetic pyrite framboids that initially developed in suboxic environments through reductive dissolution of iron oxides (Riquier et al. 2006). Pyrite has been demonstrated to be particularly easy to destabilize and oxidize at low temperature (Bierens de Haan 1991) and the pyrite-bearing KW horizons are thus much more sensitive to weathering processes than the magnetite-bearing carbonates forming the major part of the sections studied.

Early diagenetic reductive dissolution of magnetite and associated pyrite formation in the OM-bearing KW carbonate levels cannot be proposed as a dominant process in the alteration of the primary detrital magnetic signal because the χ_{HF} of the KW samples is strongly controlled by the diamagnetic component (Fig. 4), and consequently, does not show any noticeable record of authigenic paramagnetic pyrite. Pyrite is thus present in small amounts (less than 1 wt%) indicating that initial reactive iron due, at least partly, to the dissolution of detrital iron oxide, was not sufficiently abundant. This is corroborated by the MS lows observed in the KW time-equivalent levels from the Beringhauser Tunnel section (devoid of OM), and suggests that detrital inputs were very limited during the deposition of the Latest Frasnian KW horizons.

These early diagenetic and late oxidation processes are restricted to the KW-type carbonate levels upon which they have only a moderate effect. Yet, the broader question of the burial diagenesis impact on the within-section MS variations requires further consideration. To achieve this, the clay mineral assemblages for each section were analyzed (around 20 XRD measurements per section). These clay assemblages in all the sections under study are dominantly composed of illite and chlorite (minimum 67% of the total clay content; Table 5 in supplementary files). Diagenesis-sensitive minerals, such as smectite or interlayered illite–smectite, are either absent or present in reduced proportions, suggesting a significant diagenetic imprint on the primary clay assemblages. Site-mean calibrated illite crystallinity values (CIS scale of Warr and Rice 1994) oscillate between 0.31 at Beringhauser Tunnel and 0.78 at Coumiac. Although this parameter may be somewhat influenced by the inherited crystallinity of detrital illite, some limits can be broadly defined for the transitions between different diagenetic zones, i.e., 0.25-CIS scale for the base of the anchizone and 0.42-CIS scale for the base of the diagenetic zone (Warr and Rice 1994). Following these boundary values, the clay mineralogical data indicate that the entire sections under study have been submitted to burial within the limits of the highly diagenetic zone down to the anchimetamorphic zone. Despite this diagenetic context, it is worth noting that no direct relationship can be defined between the within-section MS variations and the degree of diagenetic evolution of the carbonate rocks. As shown in Fig. 8 for the representative Anajdam and Beringhauser Tunnel sections, MS evolution correlates neither with the calibrated illite crystallinity nor with the illite percentage of the clay content. This suggests that the burial diagenesis-induced smectite–illite transformation, that has been suggested to have a noticeable affect on the remanent magnetization of carbonate rocks (e.g. Katz et al. 2000), is not accompanied here by a significant change in the MS or if it is, that the change occurs in about the same way throughout the series. In any case, no noticeable distortion of the magnetic signal by ongoing diagenesis is noted here.

To further constrain the diagenetic versus detrital imprints on MS, we compared MS variations and selected geochemical proxies measured for the reference Anadjam and Beringhauser Tunnel sections. As shown in Fig. 9, there is a robust correlation between MS evolution and Zr and Th contents (Beringhauser Tunnel, $r = 0.82$ for Zr and 0.81 for Th; Anajdam, $r = 0.86$ for Zr and 0.81 for Th). These elements are classically considered to be indicators of detrital input that are unaffected by burial diagenesis (Calvert and Pedersen 1993; Mongenot et al. 1996). Such close correlation thus indicates the overall inherited character of the within-section MS evolution. Furthermore, the MS variations correlate significantly better with the Zr and Th contents than with the Fe content ($r = 0.66$ for Beringhauser Tunnel and 0.61 for Anadjam; Fig. 9a–c). As exemplified by the lack of correlation between the Fe/Zr ratio and the MS (Fig. 9d), this strongly suggests that part of the Fe-bearing fraction is not involved in the MS variations. To further test this point, we determined the detrital iron fraction, derived from total iron concentration using the calculation explained in Sect. "Complementary analyses". As shown in Fig. 9 e, f, the calculated Fe_{det} correlates much better with the MS evolution than the measured total Fe ($r = 0.76$ for Fe_{det} and 0.66 for total Fe for Beringhauser Tunnel, $r = 0.67$ for Fe_{det} and 0.61 for Fe total in Anajdam) but the Fe_{exc} shows no significant correlation with the MS variations ($r = 0.28$ for Beringhauser Tunnel and $r = 0.13$ for Anajdam). Although this theoretical calculation gives only a crude estimation of the Fe-bearing fractions, Fe_{det} and Fe_{exc}, it strongly supports the coexistence of a detrital component, controlling the within-section MS evolution, and an authigenic component, that could have induced the widespread remagnetization process observed in these carbonates. Moreover, the authigenic fraction could participate in a general enhancement of the MS at the entire section scale. Yet, our data indicate that it does not significantly distort the inherited depositional-induced variations in the MS, which are related to evolution over time of both detrital inputs and carbonate productivity. As suggested by the hysteresis ratios of the magnetite grains in Fig. 7, the detrital part could mainly include a mixture of multi-domain to single-domain magnetite particles whereas the authigenic part could

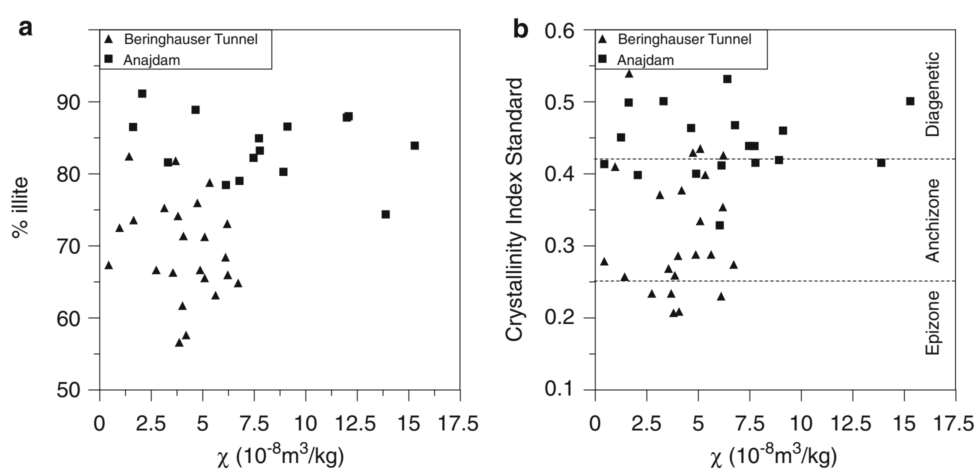

Fig. 8 Crossplots reporting, for samples from the Anajdam and Beringhauser Tunnel sections, the evolution of the bulk low-field magnetic susceptibility (χ) versus **a** the percentage of illite (in the clay fraction); **b** the calibrated values of illite crystallinity (crystallinity index standard). Boundaries between the diagenetic zone, the anchizone and the epizone are taken from Warr and Rice (1994)

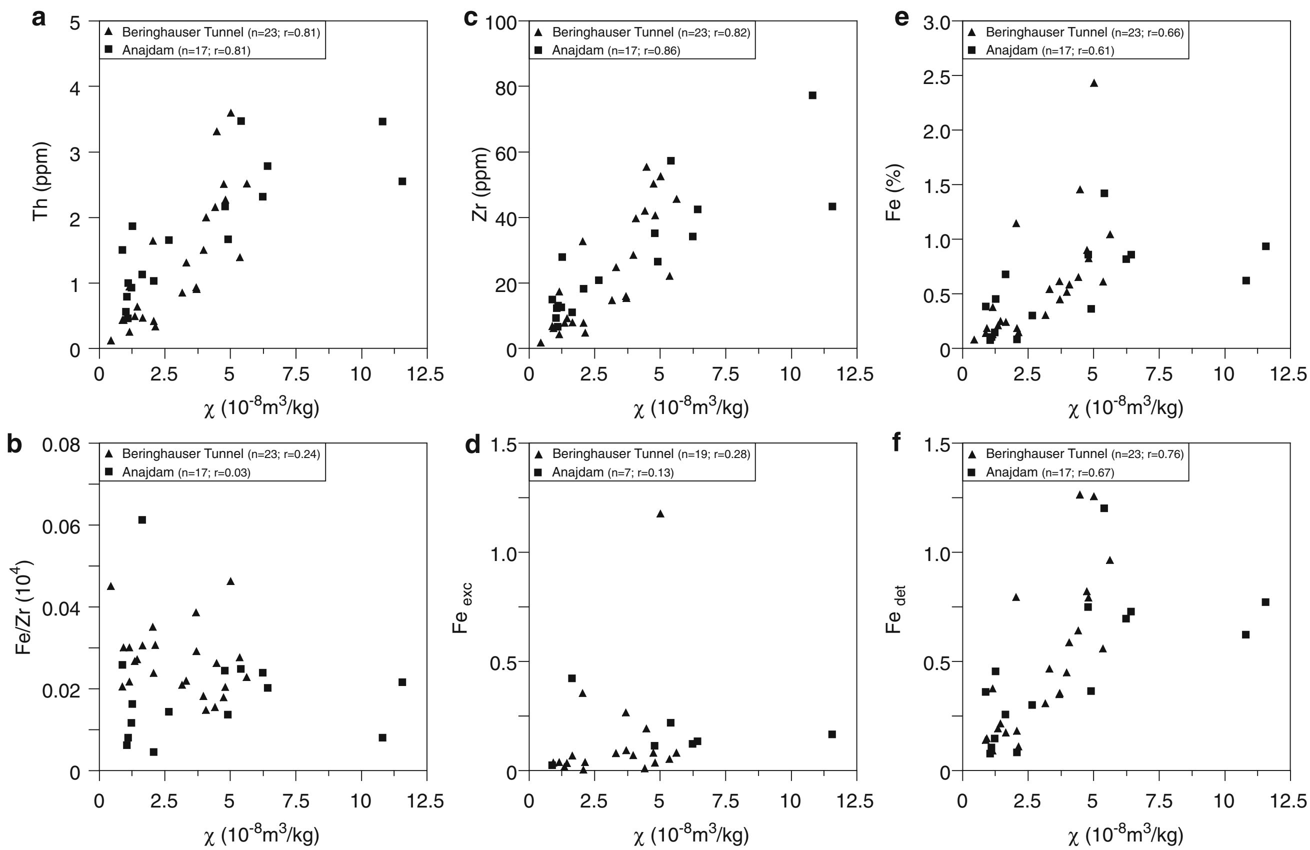

Fig. 9 Crossplots reporting the bulk low-field magnetic susceptibility (χ) versus selected geochemical indexes for samples from the reference Anajdam and Beringhauser Tunnel sections. **a** The thorium (*Th*) concentration; **b** the zirconium (*Zr*) concentration; **c** the iron (*Fe*) concentration; **d** the Fe/Zr ratio; **e** Fe_{exc}, **f** Fe_{det}. Calculation of the Fe_{exc} and Fe_{det} are detailed in Sect. "Complementary analyses". The number of samples per section and the correlation coefficient *r* are reported for each diagram

dominantly involve ultrafine single domain-superparamagnetic magnetite grains. The grain-size segregation of magnetites inherited from the detrital input and formed afterwards by in situ authigenesis during burial or deformation of rocks could be considered as the main driving factor of the observed decoupling between the MS and the remanent magnetization of the Paleozoic carbonates.

Implications for paleoenvironmental changes at the Frasnian–Famennian boundary

The combined rock magnetic, geochemical and clay mineralogical data, presented above, show that, although submitted to significant burial, MS can be used as an indicator of the detrital input evolution in the F–F sections under study. Apart from the basal Famennian *triangularis* zone where the magnetic signal evolution is not well constrained due to widespread depositional hiatuses and frequent reworking (Isaacson et al. 1999), the MS curves display a first-order consistency, thus allowing the reconstruction of the large-scale evolution of the detrital input versus the carbonate productivity through the latest Frasnian and the earliest Famennian times.

The long-term decreasing trend of the MS observed during most of the Frasnian, which parallels a general increase in the carbonate content (Figs. 2, 3), can thus be interpreted as a large-scale decrease in the detrital input along the passive margins of Laurussia and Gondwana throughout the Frasnian period. This trend is particularly accentuated in the Late Frasnian KW levels that consistently display the lowest values of MS, thus characterizing a period of minimum detrital input. An associated enhancement of the carbonate productivity is emphasized by the maximum contribution of the diamagnetic component to the MS. Significant positive anomalies in the barium concentration (Tribovillard et al. 2004; Riquier et al. 2005), as well as the widespread occurrence of algal blooms in the KW-type horizons (Paris et al. 1996; Gong et al. 2002) corroborate this high primary productivity in the Late Frasnian oceans.

The MS curves presented here all record environmental changes affecting marine realms at relatively low latitudes (e.g., Averbuch et al. 2005) but the large-scale geographical extent of the observed variations suggests that they are driven by factors of global significance. This is confirmed by the general correlation of MS evolution and global sea-level fluctuations during the Late Devonian reviewed by Sandberg et al. (2002). The long-term Frasnian decrease in detrital input parallels a general sea-level rise with a maximum flooding period coeval with the deposition of the Late Frasnian KW horizons. Observed fluctuations of detrital input, carbonate productivity and sea-level suggest a strong climatic imprint on the evolution of marine environments with a significant warming trend through the Frasnian period. Rising sea levels during gradual warming associated with an increase in mean temperatures on land likely reduce the basinal supply through the combined effects of the elevation of the erosional base level and the reduction of mechanical erosion on land. In contrast, rock weathering is particularly enhanced in such conditions of elevated temperature and precipitation thereby, stimulating nutrient release from continents and, in turn, primary productivity in marine realms (François et al. 1993; Tribovillard et al. 2004). This process is particularly efficient during periods of increased continental uplift, which is the case during the Late Frasnian due to the incipient development of the Variscan mountain belt (e.g. Averbuch et al. 2005). Such climatic and geodynamic effects could combine to induce the fertilization of Late Frasnian oceans resulting in the extensive burial of carbonate muds and organic carbon during the Lower and Upper KW periods. The data presented here thus corroborate the interpretation whereby the KW levels developed during the two Frasnian climatic optima (tropical sea-surface temperatures above 30°C according to δ^{18}O data from Joachimski and Buggisch 2002).

The F–F boundary represents a significant break in this long-term Frasnian warming. As previously mentioned, the magnetic signal is by far too discontinuous to provide a precise record of detrital input evolution at the base of the Famennian due to the widespread hiatuses and the associated sedimentary reworking, which occurred in the *triangularis* conodont zone as a result of a major sea-level fall. However, an increasing trend in the MS is visible in most of the sections studied at least from the base of the Upper *triangularis* zone onward. This suggests that the Early Famennian sea-level lowstand is associated with a significant increase in the basinal detrital supply, with a maximum situated approximatively around the Upper *triangularis*–Lower *crepida* zones, as shown by the Beringhauser Tunnel, Steinbruch Schmidt and Coumiac sections. Together with the development of extensive siliciclastic depositional systems (Isaacson et al. 1999), these data document a general Early Famennian enhancement of mechanical erosion on land coeval with a significant sea-level fall. The global extent of these mechanisms argues for a significant cooling event extending at least from the base of the *triangularis* zone to the Lower *crepida* zone.

Evolutions in both detrital input and carbonate productivity, extrapolated from the MS curves, thus corroborate the results from the δ^{18}O record of marine conodont apatite (Joachimski and Buggisch 2002) that document a decrease of about 5°C in the mean equatorial sea-surface temperatures at the F–F boundary. They do not, however, support a return in Early Famennian times of the warm conditions that prevailed during the deposition of the KW horizons (Joachimski and Buggisch 2002). In that respect, our results fit better with data on the evolution of miospore diversity on continents, providing evidence for a persistent cooling event during the Early Famennian (Streel et al. 2000). Although no direct evidence for ice caps on Gondwana has so far been documented, the significant worldwide sea-level fall and the related increase in continental mechanical erosion observed at the base of the Famennian could be interpreted as the primary markers of the incipient Late Devonian–Carboniferous ice age.

Conclusions

In this study, we tested the potential of MS logging as a paleoenvironmental proxy in strongly diagenetic F–F carbonates. To evaluate the spatial consistency of magnetic signal and possibly provide a large-scale record of the evolution of detrital inputs to the basins and of marine carbonate productivity, MS and carbonate content measurements were carried out on four F–F boundary sections, deposited in platform settings within two separate oceanic realms situated on either side of the Variscan belt undergoing incipient uplift.

Although submitted to different burial histories and diagenetic conditions, consistent long-term trends are observed in the MS evolution from the sections studied. Specifically, the F–F transition is associated with a significant MS low, resulting from a gradual Late Frasnian decreasing trend and an Early Famennian increase. In more detail, the Late Frasnian Lower and Upper KW events, known to be the time of a major burial of organic carbon (Joachimski et al. 2002), represent the intervals with the lowest MS values. These minima are recorded throughout the sections and are independent of the presence of OM, thus suggesting a large-scale depletion in the (primary detrital) paramagnetic and ferromagnetic mineral phases.

Hysteresis loop measurements for representative samples from each section allowed the nature and grain size of the magnetic minerals at the origin of these MS variations to be characterized. Based on the determinations of both χ_{HF} and χ_{ferro}, the relative parts of the dia- and paramagnetic phases on the one hand, and the ferromagnetic phases on the other hand, were separated in the bulk χ. For all the sections under study, the ferromagnetic sensu lato contribution is strongly predominant in the MS variations (around 90% of MS). Although not predominant in the MS signal, the paramagnetic contribution (due mostly to the clayey component) globally varies in the same manner as the ferromagnetic contribution. Measurements of hysteresis ratios show that the ferromagnetic component is dominantly composed of a low-coercivity mineral phase of magnetite type (B_{cr} dominantly below 60 mT), with an episodic minor contribution of high-coercivity hematite and/or pyrrhotite. The latter is particularly associated with the Late Frasnian OM-bearing KW horizons, due to the successive effects of reductive and oxidative reactions during early diagenesis and late weathering processes.

The within-section MS variations are thus shown to relate predominantly to the varying concentration of magnetite and, to a lesser extent, of clay minerals. These components are primarily associated with the detrital rock fraction but, in the Paleozoic rocks under study, are likely to have been significantly modified by diagenesis. In this respect, as previously observed by Zwing et al. (2005) in the Rhenish Massif, M_r/M_s versus B_{cr}/B_c plots for samples with magnetite as the magnetic carrier, point to the coexistence of two families of magnetite particles with different characteristic grain sizes: (1) a dominantly coarse-grained detrital fraction (a mixture of multi-domain and single-domain magnetite particles) (2) an ultrafine authigenic fraction composed of a mixture of single-domain and superparamagnetic particles.

The uncorrelated MS variations and illite concentration and crystallinity, together with the robust correlation of MS with the Zr and Th contents (detrital proxies independent of diagenetic remobilizations) show that the post-depositional authigenic magnetite fraction does not significantly distort the primary depositional MS signal. Due to its specific ultrafine-grain character and its regional extent, the diagenesis-related authigenic fraction is likely to have induced a secondary component of remanent magnetization in the carbonates under study and possibly, a general enhancement of the MS at the entire section scale but not a significant alteration of the within-section MS evolution.

This study thus emphasizes the potential of MS logging as a paleoenvironmental proxy for Paleozoic carbonates. More specifically, our data demonstrate that the MS evolution of the F–F carbonate sections under study (Beringhauser Tunnel, Steinbruch Schmidt, Coumiac and Anadjam) can be interpreted in terms of paleoenvironmental changes along the former margins of Laurussia and Gondwana. In this respect, the F–F boundary can be regarded as a period of major variations in large-scale detrital input and carbonate productivity in marine realms due to an abrupt climatic transition between a Late Frasnian warm period and an Early Famennian cooler stage.

Acknowledgments This study has been funded by the Eclipse program of the French CNRS (Frasnian–Famennian project, coordinator: O. Averbuch) and is also a contribution to the IGCP 580 "Application of magnetic susceptibility on Paleozoic sedimentary rocks". We are very grateful to C. Kissel and V. Scao for providing access to the Micromag at the Palaeomagnetic Laboratory of the LSCE (Gif-sur-Yvette), and to J. Morel for the geochemical analyses in CRPG (Nancy). We also thank M. Frere-Trentesaux, P. Recourt, L. M. Bernard-Emaille and D. Malengros for assistance with X-ray diffraction and SEM analyses in Lille. We gratefully acknowledge A. Préat, A. Herbosch, I. Berra, A. El Albani, N. Lazreq, S. Chakiri, L. Baidder, C. Crônier and A. Riboulleau for their participations in fieldworks and rock sampling in S. France, Germany and Morocco and C. Chateau for proof-reading the English. Many thanks to B. Ellwood, M. K. Dekkers and an anonymous reviewer for their constructive reviews, which significantly improved previous versions of this article.

References

Algeo TJ, Berner RA, Maynard JB, Scheckler SE (1995) Late Devonian oceanic anoxic events and biotic crises: "rooted" in the evolution of vascular land plants? Geol Soc Am Today 5:64–66

Andrews JT, Stravers JA (1993) Magnetic susceptibility of Late Quaternary marine sediments, Frobisher Bay, NWT: an indicator of changes in provenance and processes. Quat Sci Rev 12:157–167

Averbuch O, Tribovillard N, Devleeschouwer X, Riquier L, Mistiaen B, van Vliet-Lanoe B (2005) Mountain building-enhanced continental weathering and organic carbon burial as major causes for climatic cooling at the Frasnian–Famennian boundary (ca 376 Ma BP) ? Terra Nova 17:25–34

Banerjee S, Elmore RD, Engel MH (1997) Chemical remagnetization and burial diagenesis: testing the hypothesis in the Pennsylvanian Belden Formation, Colorado. J Geophys Res 102:24825–24842

Becker RT (1993) Anoxia, eustatic changes, and Upper Devonian to lowermost Carboniferous. In: House MR (ed) The Ammonoidae: environment, ecology and evolutionary changes. Systematic Assoc Spec, Clarendon Press, Oxford, 47:115–163

Bierens de Haan S (1991) A review of the rate of pyrite oxydation in aqueous systems at low temperature. Earth Sci Rev 31:1–10

Borradaile GJ, Chow N, Werner T (1993) Magnetic hysteresis of limestones: facies control? Phys Earth Planet Inter 76:241–252

Bouabdelli M (1989) Tectonique et sédimentation dans un bassin orogénique: le sillon Viséen d'Azrou-Khénifra (Est du Massif Hercynien Central du Maroc). PhD thesis, Louis Pasteur University, Strasbourg

Bout-Roumazeilles V, Cortijo E, Labeyrie L, Debrabant P (1999) Clay mineral evidence of nepheloid layer contribution to the Heinrich layers in the Northwest Atlantic. Palaeogeogr Palaeoclimatol Palaeocol 146:211–228

Brindley GW, Brown G (1980) Crystal structures of clay minerals and their identification. Mineralogical Society Monograph no. 5. Mineralogical Society, London

Buggisch W (1991) The global Frasnian–Famennian "Kellwasser Event". Geol Rundsch 80:49–72

Calvert SE, Pedersen TF (1993) Geochemistry of recent oxic and anoxic marine sediments: implications for the geological record. Mar Geol 113:67–88

Casier J-G, Devleeschouwer X, Lethiers F, Préat A, Racki G (2000) Ostracods and sedimentology of the Frasnian–Famennian boundary beds in the Kostomloty section (Holy Cross Mountains, Poland). Bull Inst Roy Sci Nat Belg Sci Terre 70:53–74
Channell JET, McCabe C (1994) Comparison of magnetic hysteresis parameters of unremagnetized and remagnetized limestones. J Geophys Res 99:4613–4623
Coudray J, Edinger PF, Michel D, Nairn AEM (1986) Tectonic interpretation of paleomagnetic results from the Upper Devonian Griotte of the Montagne Noire, southern France. Tectonophysics 126:137–151
Crick RE, Ellwood BB, El Hassani A, Hladil J, Hrouda F, Chlupac I (2001) Magnetosusceptibility event and cyclostratigraphy (MSEC) of the Pridoli-Lochkovian GSSP (Klonk, Czech Republic) and coeval sequences in the Anti-Altlas Morocco. Palaeogeogr Palaeoclimatol Palaeoecol 167:73–100
Crick RE, Ellwood BB, Feist R, El Hassani A, Schindler E, Dreesen R, Over DJ, Girard C (2002) Magnetostratigraphy susceptibility of the Frasnian/Famennian boundary. Palaeogeogr Palaeoclimatol Palaeoecol 181:67–90
Da Silva A-C, Boulvain F (2006) Upper Devonian carbonate platform correlations and sea-level variations recorded in magnetic susceptibility. Palaeogeogr Palaeoclimatol Palaeoecol 240: 373–388
Day R, Fuller MD, Schmidt VA (1977) Hysteresis properties of titanomagnetites. Grain size and composition dependence. Phys Earth Planet Inter 13:260–267
Demange M (1994) Antevariscan evolution of the Montagne Noire (France): from a passive margin to a foreland basin. C R Acad Sci Paris 318:921–933
Devleeschouwer X, Herbosch A, Préat A (2002) Microfacies, sequence stratigraphy and clay mineralogy of a condensed deep-water section around the Frasnian–Famennian boundary (Steinbruch Schmidt, Germany). Palaeogeogr Palaeoclimatol Palaeoecol 181:171–193
Dunlop DJ (2002) Theory and application of the Day plot (Mrs/Ms versus Hcr/Hc). 2. Application to data for rocks, sediments and soils. J Geophys Res 107:2057. doi:10.1029/2001JB000487
Ellwood BB, Crick RE, El Hassani A (1999) The magnetosusceptibility event and cyclostratigraphy (MSEC) method used in geological correlation of Devonian rocks from Anti-Atlas, Morocco. AAPG Bull 83:1119–1134
Ellwood BB, Crick RE, El Hassani A, Benoist SL, Young RH (2000) Magnetosusceptibility event and cyclostratigraphy method applied to marine rocks: detrital input versus carbonate productivity. Geology 28:1135–1138
Ellwood BB, Crick RE, Garcia-Alcade Fernandez JL, Soto FM, Truyols-Massoni M, El Hassani A, Kovas EJ (2001) Global correlation using magnetic susceptibility data from Lower Devonian rocks. Geology 29:583–586
Elmore RD, London D, Bagley D, Fruit DJ, Gao G (1993) Remagnetization by basinal fluids; testing the hypothesis in the Viola Limestone, Southern Oklahoma. J Geophys Res 98: 6237–6254
François L, Walker JCG, Opdyke BN (1993) The history of global weathering and the chemical evolution of the ocean-atmosphere system. Geophys Monogr Ser 74:143–159
Franke W (2000) The mid-European segment of the Variscides: tectonostratigraphic units, terrane boundaries and plate tectonic evolution. In: Franke W, Haak V, Oncken O, Tanner D (eds) Orogenic Processes: quantification and modelling in the Variscan Belt. Geological Society, London, Special Publications 179:35–61
Gong Y, Li B, Si Y, Wu Y (2002) Late Devonian red tide and mass extinction. Chin Sci Bull 47:1138–1144
Gradstein FM, Ogg JG, Smith AG et al (2004) A geologic time scale 2004. Cambridge University Press, Cambridge
Hesse P, Stolz JF (1999) Bacterial magnetite and the Quaternary climate record. In: Maher BA, Thompson R (eds) Quaternary climates, environments and magnetism. Cambridge University Press, Cambridge, pp 163–197
Hladil J, Gersl M, Strnad L, Frana J, Langrova A, Spisiak J (2005) Stratigraphic variations of complex impurities in platform limestones and possible significance of atmospheric dust: a study emphasis on gamma-ray spectrometry and magnetic susceptibility outcrop logging (Eifelian–Frasnian, Moravia, Czech Republic). Int J Earth Sci 95:703–723
Hounslow MW, Maher BA (1999) Source of the climate signal recorded by magnetic susceptibility variations in Indian Ocean sediments. J Geophys Res 104:5047–5061
Isaacson PE, Hladil J, Shen J-W, Kalvoda J, Diaz Martinez E, Grader G (1999) Late Devonian glaciation in Gondwana: setting the stage for Carboniferous eustasy. SDS Newslett 16:37–46
Jackson M (1990) Diagenetic source of stable remanence in remagnetized paleozoic cratonic carbonates: a rock magnetic study. J Geophys Res 95:2753–2761
Jackson M, Worm HU, Banerjee SK (1990) Fourier analysis of digital hysteresis data: rock magnetic applications. Phys Earth Planet Inter 65:78–87
Joachimski MM, Buggisch W (2002) Conodont apatite $\delta^{18}O$ signatures indicate climatic cooling as a trigger of the Late Devonian mass extinction. Geology 30:711–714
Joachimski MM, Pancost RD, Freeman KH, Ostertag-Henning C, Buggisch W (2002) Carbon isotope geochemistry of the Frasnian–Famennian transition. Palaeogeogr Palaeoclimatol Palaeoecol 181:91–109
Katz B, Elmore D, Cogoini M, Engel MH, Ferry S (2000) Association between burial diagenesis of smectite, chemical remagnetization, and magnetite authigenesis in the Vocontian trough, SE France. J Geophys Res 105:851–868
King JW, Channell JET (1991) Sedimentary magnetism, environmental magnetism, and magnetostratigraphy. Rev Geophys Suppl:358–370
Lazreq N (1999) Biostratigraphie des conodontes du Givétien au Famennien du Maroc Central. Biofaciès et événement Kellwasser. Cour Forsch Senck 214:1–111
Mabille C, Boulvain F (2007) Sedimentology and magnetic susceptibility of the Upper Eifelian–Lower Givetian (Middle Devonian) in SW Belgium: insights into carbonate platform initiation. In: Alvaro JJ, Aretz M, Boulvain F, Munnecke A, Vachard D, Vennin E (eds) Paleozoic reefs and bioaccumulations: climatic and evolutionary controls. Geological Society, London, Special Publications 275:109–123
Machel H (1995) Magnetic mineral assemblages and magnetic contrasts in diagenetic environments with implications for studies of paleomagnetism, hydrocarbon migration and exploration. In: Turner P, Turner A (eds) Paleomagnetic application in hydrocarbon exploration and production. Geological Society, London, Special Publications 98:9–29
Maher BA, Thompson R (1999) Quaternary climates, environments and magnetism. Cambridge University Press, Cambridge
McCabe C, Channell JET (1994) Late Paleozoic remagnetization in limestones of the Craven Basin (northern England) and the rock magnetic fingerprint of remagnetized sedimentary carbonates. J Geophys Res 99:4603–4612
Mongenot T, Tribovillard N-P, Desprairies A, Lallier-Vergès E, Laggound-Défarge F (1996) Trace elements as paleoenvironmental markers in strongly mature hydrocarbon source rocks : the Cretaceous la Luna Formation of Venezuela. Sediment Geol 103:23–37

Murphy AE, Sageman BB, Hollander DJ (2000) Eutrophication by decoupling of the marine geochemical cycles of C, N and P: a mechanism for the Late Devonian mass extinction. Geology 28:427–430

Oldfield F (1999) The rock magnetic identification of magnetic minerals and grain-size assemblage. In: Walden J, Oldfield F, Smith JP (eds) Environmental magnetism: a practical guide. Technical Guide 6. Quaternary Research Association, London, pp 98–112

Paris F, Girard C, Feist R, Winchester-Seeto T (1996) Chitinozoan bio-event in the Frasnian–Famennian boundary beds at La Serre (Montagne Noire, Southern France). Palaeogeogr Palaeoclimatol Palaeoecol 121:131–145

Parry LG (1982) Magnetization of immobilized particle dispersions with two distinct particle sizes. Phys Earth Planet Inter 28: 230–241

Passier HF, de Lange GJ, Dekkers MJ (2001) Magnetic properties and geochemistry of the active oxidation front and the youngest sapropel in the eastern Mediterranean Sea. Geophys J Int 145:604–614

Peters C, Dekkers MJ (2003) Selected room temperature magnetic parameters as a function of mineralogy, concentration and grain size. Phys Chem Earth 28:659–667

Petschick R, Kuhn G, Gingele F (1996) Clay mineral distribution in surface sediments of the South Atlantic: sources, transport, and relation to oceanography. Mar Geol 130:203–229

Piqué A, Bossière G, Bouillin J-P, Chalouan A, Hoepffner C (1993) Southern margin of the Variscan belt: the north-western Gondwana mobile zone (eastern Morocco and northern Algeria). Geol Rundsch 82:432–439

Préat A, Mamet B, Devleeschouwer X (1998) Microfaciès et séquences dans une série condensée du Dévonien Supérieur, Coumiac, Montagne Noire. Bull Soc Geol Fr 169:331–342

Racki G (1998) Frasnien–Famennian biotic crisis: undervalued tectonic control? Palaeogeogr Palaeoclimatol Palaeoecol 141:177–198

Riquier L (2005) Perturbations des environnements marins à la limite Frasnien–Famennien (Dévonien terminal): apport de la géochimie organique et du magnétisme des roches. Unpublished PhD thesis, Université de Lille 1

Riquier L, Tribovillard N, Averbuch O, Joachimski MM, Racki G, Devleeschouwer X, El Albani A, Riboulleau A (2005) Productivity and bottom water redox conditions at the Frasnian–Famennian boundary on both sides of the Eovariscan Belt: constraints from trace element geochemistry. In: Over DJ, Morrow JR, Wignall PB (eds) Understanding Late Devonian and Permian–Triassic biotic and climatic events: towards an integrated approach. Developments in Palaeontology and Stratigraphy, Elsevier, 20:199–224

Riquier L, Tribovillard N, Averbuch O, Devleeschouwer X, Riboulleau A (2006) The Late Frasnian Kellwasser horizons of the Harz mountains (Germany): two oxygen-deficient periods resulting from different mechanisms. Chem Geol 233:137–155

Riquier L, Averbuch O, Tribovillard N, El Albani A, Lazreq N, Chakiri S (2007) Environmental changes at the Frasnian–Famennian boundary in Central Morocco (Northern Gondwana): integrated rock-magnetic and geochemical studies. In: Becker RT, Kirchgasser WT (eds) Devonian events and correlations. Geological Society, London, Special Publications 278:197–217

Roberts AP, Stoner JS, Richter C (1999) Diagenetic magnetic enhancement of sapropels from the eastern Mediterranean Sea. Mar Geol 153:103–116

Robinson SG (1993) Lithostratigraphic applications for magnetic susceptibility logging of deep sea sediment cores: examples from ODP Leg 115. In: Hailwood EA, Kidd RB (eds) High resolution stratigraphy, Geological Society, London, Special Publication 70:65–98

Robion P, Averbuch O, Sintubin M (1999) Fabric development and metamorphic evolution of Lower Paleozoic slaty rocks from the Rocroi Massif (French–Belgian Ardennes): new constraints from magnetic fabrics, phyllosilicate preferred orientation and illite crystallinity data. Tectonophysics 309:257–273

Royer DL (2006) CO_2-forced climate thresholds during the Phanerozoic. Geochim Cosmochim Acta 70:5665–5675

Salmon E, Edel J-B, Pique A, Westphal M (1988) Possible origins of Permian remagnetizations in Devonian and carboniferous limestones from the Moroccan Anti-Atlas (Tafilalt) and Meseta. Phys Earth Planet Inter 57:339–351

Sandberg CA, Morrow JR, Ziegler W (2002) Late Devonian sea-level changes, catastrophic events, and mass extinctions. In: Koeberl C, MacLeod KG (eds) Catastrophic Events and Mass Extinctions: Impacts and Beyond: Geol Soc Am Spec Pap 356:473–487

Schülke I, Popp A (2005) Microfacies development, sea-level change, and conodont stratigraphy of Famennian mid- to deep platform deposits of the Beringhauser Tunnel section (Rheinisches Schiefergebirge, Germany). Facies 50:647–664

Sepkoski JJ (1986) Phanerozoic overview of mass extinctions. In: Raup DM, Jablonski D (eds) Patterns and processes in the history of life. Springer, Berlin, pp 277–295

Solheid PA, Laj C, Banerjee SK (2003) Data report: mineral magnetic properties of sediments from site 1144, Northern South China Sea. In: Prell WL, Wang P, Blum P, Rea DK, Clemens SC (eds) Proceedings of the ODP scientific results 184:1–8

Streel M, Caputo MV, Loboziak S, Melo JHG (2000) Late Frasnian–Famennian climates based on palynomorph analyses and the question of the Late Devonian glaciations. Earth Sci Rev 52:121–173

Szaniawski R, Lewandowski M, Mansy J-L, Averbuch O, Lacquement F (2003) Syn-folding remagnetization events in the French–Belgium Variscan thrust belt as markers of the fold-and-thrust belt kinematics. Bull Soc Geol Fr 174:511–523

Thompson R, Oldfield F (1986) Environmental magnetism. Allen and Unwin, London

Tribovillard N, Averbuch O, Bialkowski A, Deconinck J-F (2002) The influence of early diagenesis of marine organic matter on the magnetic susceptibility signal of sedimentary rocks. Bull Soc Geol Fr 172:295–306

Tribovillard N, Averbuch O, Devleeschouwer X, Racki G, Riboulleau A (2004) Deep-water anoxia over the Frasnian–Famennian boundary (La Serre, France): a tectonically induced oceanic anoxic event? Terra Nova 16:288–295

Vanderaveroet P, Averbuch O, Deconinck J-F, Chamley H (1999) Glacial/interglacial cycles in Pleistocene sediments of New Jersey expressed by clay minerals, grain-size and magnetic susceptibility data. Mar Geol 159:79–92

Verosub KL, Roberts AP (1995) Environmental magnetism: past, present and future. J Geophys Res 100:2175–2192

Walden J, Oldfield F, Smith J (1999) Environmental magnetism: a practical guide. Technical Guide vol 6. Quaternary Research Association, London

Warr LN, Rice AH (1994) Interlaboratory standardization and calibration of clay mineral crystallinity and crystallite size data. J Metamorph Geol 12:141–152

Wedepohl KH (1991) The composition of the upper Earth's crust and the natural cycles of selected metals. In: Merian E (ed) Metals and their compounds in the environment. VCH, Weinheim, pp 3–17

Whalen MT, Day JE (2008) Magnetic susceptibility, biostratigraphy and sequence stratigraphy: insight into Devonian carbonate platform development and basin infilling, Western Alberta,

Canada. In: Controls on carbonate platform and reef development, SEPM Special Publication 89:291–314
Zegers TE, Dekkers MJ, Bailly S (2003) Late Carboniferous to Permian remagnetization of Devonian limestones in the Ardennes: role of temperature, fluids and deformation. J Geophys Res 108:2357. doi:10.1029/2002JB002213
Zwing A, Bachtadse V, Soffel HC (2002) Late Carboniferous remagnetization of Paleozoic rocks in the NE Rhenish Massif, Germany. Phys Chem Earth 27:1179–1188
Zwing A, Matzka J, Bachtadse V, Soffel HC (2005) Rock magnetic properties of remagnetized Paleozoic clastic and carbonate rocks from the NE Rhenish Massif, Germany. Geophys J Int 160:477–486

Article 18.

Averbuch O., Tribovillard N., Devleeschouwer X., *Riquier L.,* Mistiaen B. and Van Vliet-Lanoe B. (2005). Mountain building-enhanced continental weathering and organic carbon burial as major causes for climatic cooling at the Frasnian-Famennian boundary (ca 376 Ma BP) ? Terra Nova, 17, 33-42.

doi: 10.1111/j.1365-3121.2004.00580.x

Mountain building-enhanced continental weathering and organic carbon burial as major causes for climatic cooling at the Frasnian–Famennian boundary (*c.* 376 Ma)?

O. Averbuch,[1] N. Tribovillard,[1] X. Devleeschouwer,[2] L. Riquier,[1] B. Mistiaen[3] and B. van Vliet-Lanoe[1]

[1]*UMR 8110, Processus et Bilans en Domaines Sédimentaires, Université de Lille 1, 59655 Villeneuve d'Ascq cédex, France;* [2]*Service géologique de Belgique, rue Jenner 13, Bruxelles, Belgium;* [3]*UMR 8014, Paléontologie et Paléogeographie du Paléozoique, FLS et ISA, 13 rue de Toul, 59046 Lille cédex, France*

ABSTRACT

The Late Devonian was a period of drastic environmental changes, as exemplified by a major biotic crisis at the Frasnian–Famennian boundary (FFB) and the onset in Famennian times of glaciations across southern Gondwana. Worldwide evidence for the coeval development of the major Acadian–Eovariscan belt led us to propose a model relating the Late Frasnian–Famennian environmental perturbations to extensive continental uplift through two atmospheric CO_2-depleting mechanisms: (1) the intensification of silicate weathering on the continental areas as attested by a major rise in the $^{87}Sr/^{86}Sr$ composition of sea water at the FFB; and (2) the massive burial of organic carbon (Kellwasser events) in partially confined basins due to the collisional-induced reduction of equatorial oceanic communications between the Palaeotethysian and Panthalassic oceans. This process is also suggested to have been controlled by an important primary productivity connected to an increased nutrient availability triggered by the enhanced continental run-off.

Terra Nova, 17, 25–34, 2005

Introduction

In recent years, much concern has risen about the long-term climatic effects of mountain building (e.g. Ruddiman, 1997). Uplift of continental crust has been suggested to be a significant mechanism for long-term climatic cooling through depletion of atmospheric CO_2 content (and the associated greenhouse effect) by increased silicate weathering (e.g. Raymo, 1991; François *et al.*, 1993; Gaillardet *et al.*, 1999; Kump *et al.*, 1999) and organic carbon burial into marine sediments (France-Lanord and Derry, 1997; François and Goddéris, 1998). Mountain building has also been considered to have a strong effect on oceanic and atmospheric circulations and thereby alter heat transfer on the Earth's surface (e.g. Rind *et al.*, 1997). These problems have so far largely been addressed with regard to Cenozoic global cooling and their relationships with the uplift of the Alpine–Himalayan belt.

Late Palaeozoic times (Late Devonian–Carboniferous–Permian), were, however, probably one of the most intensively orogenic periods of the Phanerozoic due to the multistage accretion of continental blocks, leading to the formation of the Pangea megacontinent during Permian times. Within the Upper Palaeozoic orogenic system, the Acadian–EoVariscan belt resulted in Late Devonian times from the incipient collision of different lithospheric plates, i.e. Laurussia (Old Red Sandstone Continent), Gondwana, Kazakhstan and Siberia due to the closure of intervening oceanic basins. Crustal deformation at the margins of these major blocks induced the uplift of large continental areas extending from Central Asia to South America (including the Urals, Central and Western Europe, Northern Africa and Northern America).

This period is also known to have experienced drastic environmental changes both in terrestrial and oceanic domains with major crises of the biosphere (e.g. the Frasnian-Famennian and the Devonian-Carboniferous mass extinctions) and the onset, in Famennian times, of glaciations upon Southern Gondwana (e.g. Caputo, 1985; Isaacson *et al.*, 1999; Scotese *et al.*, 1999; Streel *et al.*, 2000). Cold-water oceans (e.g. Copper, 1986), sea-level changes (e.g. Hallam and Wignall, 1999), oceanic anoxia (e.g. Joachimski and Buggisch, 1993), oceanic eutrophication (Caplan and Bustin, 1999; Murphy *et al.*, 2000) as well as asteroids impacts (e.g. McGhee, 2001) have been considered as independent driving mechanisms for the Late Devonian mass extinctions. Increased continental weathering has been proposed as a possible source for an atmospheric CO_2 depletion in Late Devonian times but was only restricted to the effects of the development of vascular land plants (e.g. Algeo *et al.*, 1995). Enhanced erosion and weathering due to the major Acadian–EoVariscan orogeny have so far not been considered except at a local scale (Loevezijn, 1989; Peterhansel and Pratt, 2001). In this regard, we review here the environmental changes observed in the stratigraphic record at the Frasnian–Famennian transition and explore their possible relationships with the development of a major orogenic system: the Late Devonian Acadian–EoVariscan mountain belt.

Environmental changes at the Frasnian–Famennian boundary

The Frasnian–Famennian boundary (FFB) in Late Devonian times (*c.* 376 Ma following Tucker *et al.*, 1998) has long been recognized as marking a major environmental crisis (one of the five largest of the Phan-

Correspondence: O. Averbuch, PBDS, Sciences de la Terre, Université de Lille 1, 59 655 Villeneuve d'Ascq cédex, France. Tel.: +33 (0)3 20 33 71 30; fax: +33 (0)3 20 43 41 19; e-mail: olivier.averbuch@univ-lille1.fr

erozoic) with a significant loss of biotic diversity (e.g. Sepkoski, 1986; McGhee, 1989; Hallam and Wignall, 1999; Lethiers and Casier, 1999; House, 2002). One major expression of this crisis is the demise of coral reefs and associated biota assigned to tropical shallow-water environnments that formerly showed a spectacular worldwide development (e.g. Copper, 2002). In comparison, high-latitude and cold-water fauna were less affected (Copper, 1986).

In the stratigraphic record, the FFB is thus characterized by an extensive crisis of reef carbonates, as exemplified by a spectacular drop in the skeletal density of stromatoporoids, some of the most important reef-building fauna during Frasnian times (Mistiaen, 1994)(Fig. 1). This reduction in skeletal density furthermore suggests that the FFB was not only a major mortality period for reef-builders but also that Famennian oceanic environments differed significantly from those of the Frasnian, preventing surviving stromatoporoid species from developing a dense carbonated skeleton (e.g. Stearn, 1987; Mistiaen, 1994). Associated with this scarcity of residual stromatoporoid reefs, crinoidal or microbially mediated limestones form the dominant carbonate deposits on the Famennian platforms (Peterhänsel and Pratt, 2001; Copper, 2002; Whalen *et al.*, 2002; Shen and Webb, 2004).

These changes in platform sedimentation and extinctions in the marine fauna occurred progressively from Late Frasnian times (Upper *Rhenana* Conodont Zone) to basal Famennian times (Early *Triangularis* conodont Zone)(Fig. 2) (e.g. Hallam and Wignall, 1999) over a period of about 2 Myr following recently established Devonian timescales (Tucker *et al.*, 1998). During this period, shelfal oceanic environments suffered a significant ecological shift toward a dominance of siliceous biota (silicisponges, radiolarians) (Racki, 1999). In deep-water basinal environments, this period corresponds also to the deposition of widespread organic carbon-rich deposits (e.g. Joachimski and Buggisch, 1993; Ettensohn, 1995; Lethiers *et al.*, 1998; Streel *et al.*, 2000; Chen *et al.*, 2002; Over, 2002; Tribovillard *et al.*, 2004) with two major levels propagating on outer shelfal environments

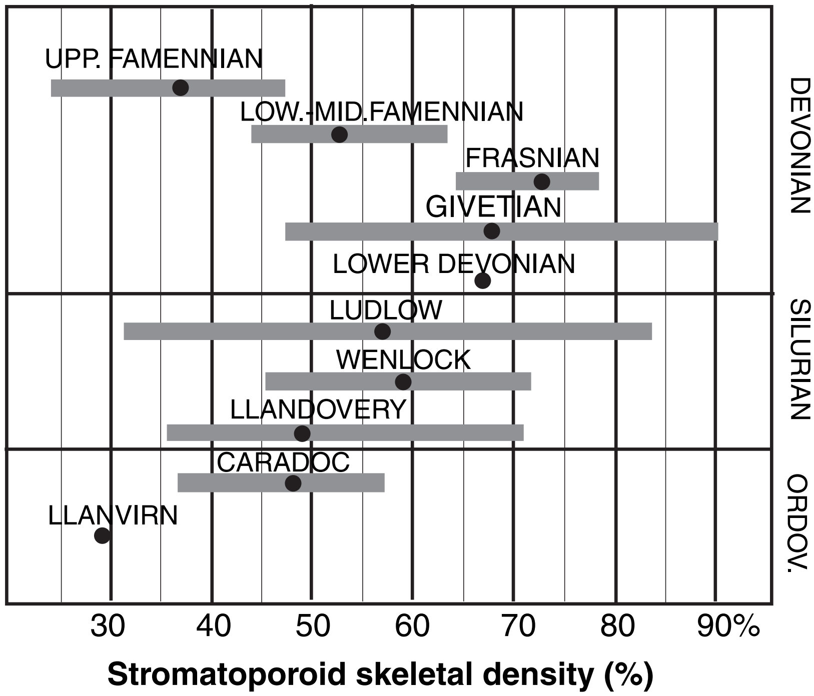

Fig. 1 Diagram representing the evolution of the skeletal density of stromatoporoids through Palaeozoic times (after Mistiaen, 1994). Stromatoporoids are some of the most important reef-building fauna in Frasnian times. Note the significant drop in their skeletal density through the Frasnian–Famennian boundary, indicating that Famennian oceanic environments did not allow stromatoporoids to develop a dense carbonated skeleton. Effects of Famennian sea-water cooling and atmospheric pCO_2 decrease were likely (Stearn, 1987; Mistiaen, 1994).

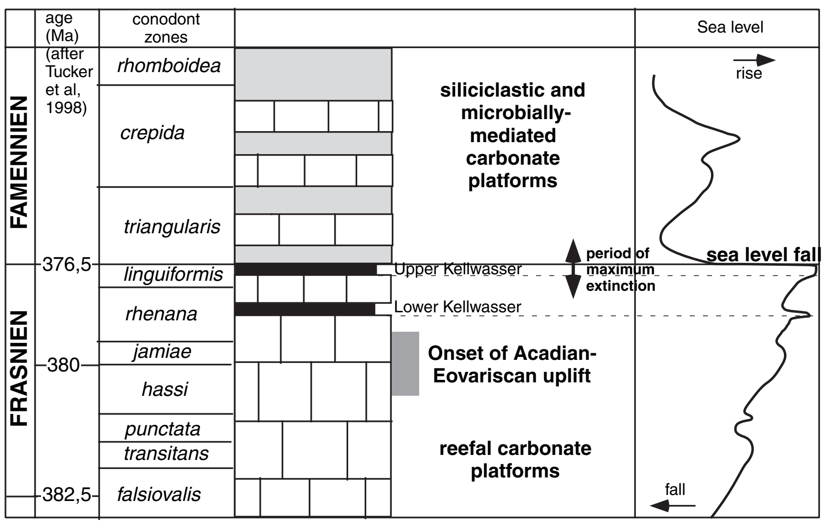

Fig. 2 Synthetic stratigraphic record at the Frasnian–Famennian boundary showing the main environmental changes within oceanic basins. Conodont bio-zonation and absolute ages after Tucker *et al.* (1998). Period of maximum biological extinction after Hallam and Wignall (1999). Sea-level data compiled from Johnson *et al.* (1985), Devleeschouwer (1999) and Sandberg *et al.* (2002). Age of the incipient Eovariscan continental uplift is based on our compilation of tectono-metamorphic data in Fig. 6.

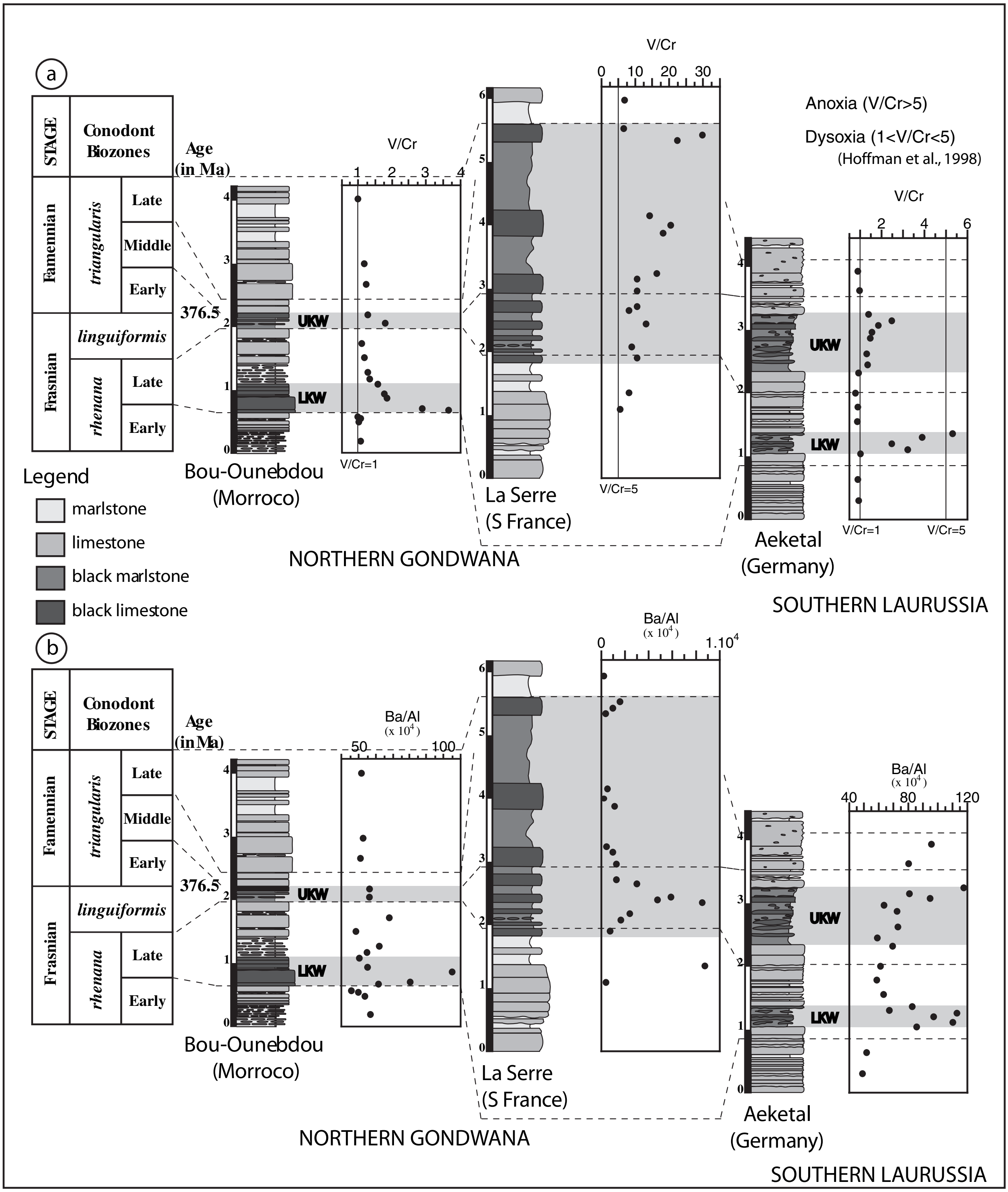

Fig. 3 Whole rock variations in characteristic trace element composition in shelfal and basinal Frasnian–Famennian sections from the Northern Gondwanian and Southern Laurussian margins (after Riquier *et al*., 2003). The general location of study areas is reported in Fig. 5. Conodont biozonation from Feist and Schindler (1994), Feist (2002) and Lazreq (1999). (a) V/Cr ratio (marker of disoxic–anoxic bottom-water environments, e.g. Hoffman *et al*., 1998). (b) Al normalized abundance of Ba (productivity marker, e.g. Schmitz *et al*., 1997). Note the significant increased abundances within the Kellwasser horizons showing enhanced productivity and bottom-water disoxia during Late Frasnian sea-level highstands.

during sea-level highstands, the Kellwasser levels (Fig. 2) (e.g. Schindler, 1990; Buggisch, 1991; Belka and Wendt, 1992; Joachimski and Buggisch, 1993; Becker and House, 1994). These black and highly carbonated mudstone deposits are characterized worldwide by a positive $\delta^{13}C$ anomaly for both carbonated and organic matter fraction that can be interpreted as the massive burial of organic carbon in Late Frasnian oceans (e.g. Joachimski *et al.*, 2002). Significant positive anomalies of normalized levels of characteristic trace elements such as V [exemplified in Fig. 3(a) by the ratio V/Cr (e.g. Hoffman *et al.*, 1998)], U, Mo, Cu, Zn and Ba (Fig. 3b) document disoxic to anoxic bottom water environments and high primary productivities during the Kellwasser depositional events (Bratton *et al.*, 1999; Tribovillard *et al.*, 2004). Such a high productivity along the Late Frasnian continental margins has also been proposed based on the preservation of phosphatic microspherules in limestones from the Great Basin in the United States (Giles *et al.*, 2002).

These oceanic environmental changes occurred within a global Frasnian trend of increased sea level that tops in the Kellwasser horizons (e.g. Johnson *et al.*, 1985; Devleeschouwer, 1999; Sandberg *et al.*, 2002). Together with conodont apatite $\delta^{18}O$ signatures (Joachimski and Buggisch, 2002) and kaolinite occurrence within the clay mineralogical record (Devleeschouwer, 1999), it argues for a warm and humid Late Frasnian climate (tropical sea-surface temperature above 30 °C following Joachimski and Buggisch, 2002) coeval with high CO_2 atmospheric content (15 times greater than the present level following model predictions; Berner and Kothavala, 2001).

On top of the Upper Kellwasser levels, the FFB appears as a pronounced environmental break with an important sea-level fall (e.g. Devleeschouwer, 1999; Sandberg *et al.*, 2002) inducing common depositional hiatuses and breccias (e.g. Isaacson *et al.*, 1999; Piecha, 2002). A coeval increase in the detrital input is attested by the magnetic susceptibility record (Fig. 4) as well as by the development of important siliciclastic depositional

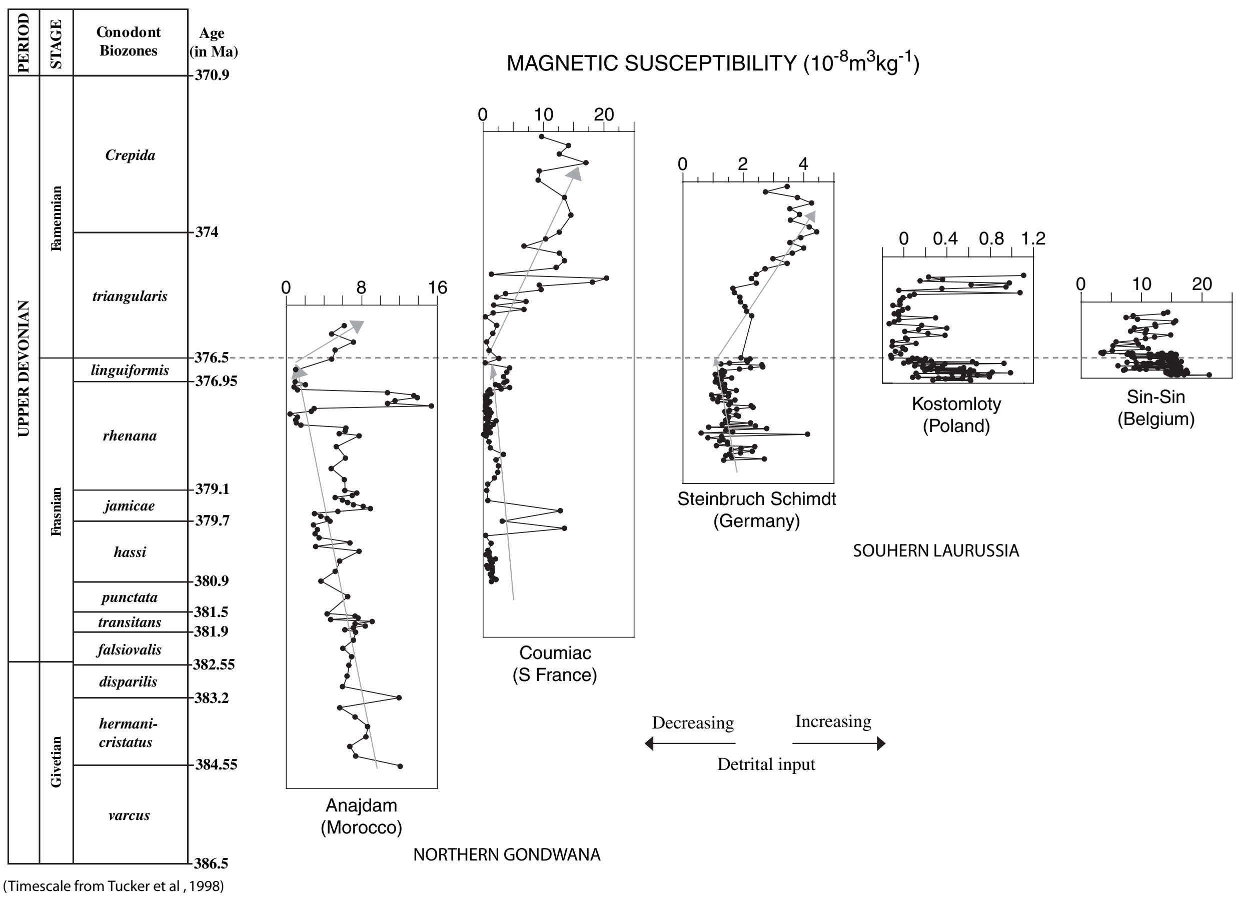

Fig. 4 Magnetic susceptibility record through the Frasnian–Famennian boundary along the northern Gondwanian [(Coumiac, southern France), Anajdam (central Morocco)] and southern Laurussian margins [Sinsin (Ardennes, Belgium), Steinbruch Schmidt (Rhenish massif, Germany), Kostomloty (Holy Cross mountains, Poland)], far from the uplifted continental domains. The general location of study areas is reported in Fig. 5. Data have been reported using a time model based on Tucker *et al.*'s (1998) timescale and conodont bio-zonation. Note (1) the widespread long-term decrease during Frasnian times indicating the lowering of the basinal detrital input during a general sea-level rise and (2) the general drastic increase during the Famennian associated with a major sea-level fall and enhanced mechanical erosion on land.

systems (e.g. Isaacson *et al.*, 1999) such as the Ardennes complex in northern France and southern Belgium (e.g. Thorez and Dreesen, 2002). Feldspar-bearing sandstones as well as dolomitic evaporitic palaeosols interbedded within these alluvial complexes document a significant diminution of chemical weathering on the continents and semi-arid climatic conditions at low latitudes. This argues for a pronounced change in the erosional processes affecting the continents during Famennian times, probably linked to decreasing CO_2 atmospheric content as suggested by modelling experiments and pCO_2 estimates (e.g. Royer *et al.*, 2001). Associated global cooling is suggested by a decrease of about 5 °C in the mean equatorial sea surface temperatures (Joachimski and Buggisch, 2002). Additional cooling evidence has been provided by the reduced miospore diversity on continental areas (Streel *et al.*, 2000). Although there is no direct evidence for ice caps onto Gondwana in basal Famennian times, the significant worldwide sea-level fall observed at the base of the Famennian could be interpreted as the primary signal for the incipient Late Devonian–Carboniferous ice age. The FFB is thus likely to represent a major climatic transition between an Early–Middle Devonian greenhouse and a Late Devonian–Carboniferous icehouse world.

The Acadian-EoVariscan Mountain building event

The Late Devonian was also a period of intense tectonic activity (e.g. Racki, 1998) characterized by the incipient collision of major continental crustal blocks: Laurussia, Gondwana, Kazakhstan and Siberia. This collisional process led to the deformation and uplift of wide continental domains including the Arctic Ellesmerian–Svallbardian belt (e.g. Embry, 1991), the Central Asian belt (e.g. Sengor and Natalín, 1996; Mattern and Schneider, 2000), the southern Uralian belt (e.g. Matte, 1995; Puchkov, 1997), the European Variscides (e.g. Tait *et al.*, 1997; Matte, 2001), the Northern African Variscides (e.g. Piqué *et al.*, 1993; Echarfaoui *et al.*, 2002) and the Appalachian belt (e.g. Ettensohn, 1987; Murphy and Keppie,

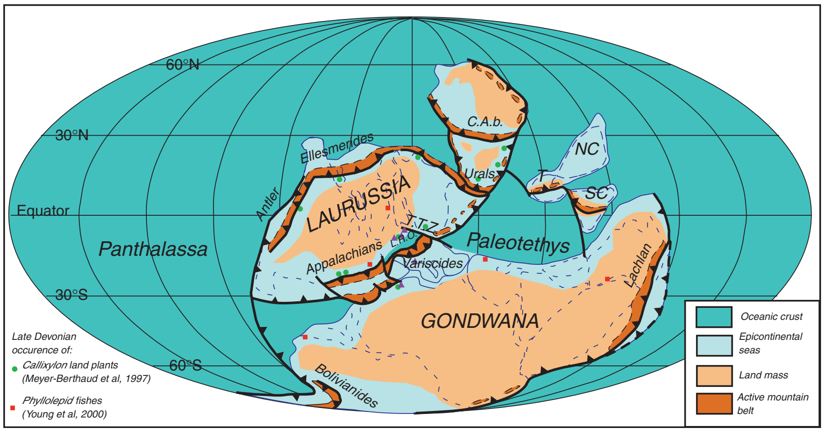

Fig. 5 A palaeogeographical reconstruction (primarily based on a continental reconstruction of Golonka *et al.*, 1994) showing the general geometry of active orogenic systems at the Frasnian–Famennian boundary. Patterns of dispersal for *Phyllolepid* fishes (Young *et al.*, 2000) and *Callixyllon* land plants (Meyer-Berthaud *et al.*, 1997) in Early Famennian times are reported, respectively, by squares and circles. Triangles refer to the location of specific study areas along the northern Gondwanian and southern Laurussian margins presented in Figs 3 and 4. Note the reduction of oceanic circulations between Palaeotethys and Panthalassa due to the collision of Laurussia and Gondwana along the Appalachian–Eovariscan belt. T.T.Z., Teysseire–Tornquist Zone; L.R.O., Lizzard–Rhenohercynian ocean; C.A.b., Central Asian belt; T, Tarim; NC, North China; SC, South China.

1998) (Fig. 5). Although probably not due to collision, but rather to oceanic subduction and restricted terrane accretion (Coney, 1992), Late Devonian continental uplift and deformation is also documented along the western American Antler belt (Johnson and Pendergast, 1981), the South American Bolivianides (e.g. Vicente, 1975) and the eastern Australian Lachlan fold belt (e.g. Fergusson and Coney, 1992; Gray, 1997). Within these mountain ranges, important crustal shortening and thickening toghether with high continental relief are attested by extensive high-pressure metamorphic rocks dated between *c.* 380 and 360 Ma as well as by pervasive deformation distributed along the belts (Fig. 6) (e.g. Piqué *et al.*, 1993; Ballévre *et al.*, 1994; Santallier *et al.*, 1994; Matte, 1995; Maluski and Patocka, 1997). Unconformities of Late Frasnian to Early Carboniferous age (e.g. Echarfaoui *et al.*, 2002) can be observed along these belts depending on the structural position and the local tectonic framework. High rates of exhumation and erosion are recorded by the deposition of thick synorogenic molassic rocks of dominantly Famennian age trapped within the flexural foreland basins (Fig. 6) (e.g. Ettensohn, 1987; Embry, 1991; Tait *et al.*, 1997; Murphy and Keppie, 1998). At a more global scale, high rates of continental chemical weathering and denudation of deep crustal domains are indicated by a major peak in the $^{87}Sr/^{86}Sr$ isotopic composition of the sea water around the FFB (Fig. 7) (Veizer *et al.*, 1999). Rare-earth element spectra measured in conodonts from the Polish and German Rhenohercynian margin further document such a high terrestrial input towards the oceans at the Frasnian–Famennian transition (Girard and Lécuyer, 2002).

Additional evidence for the FFB representing a period of drastic continental reorganization is provided in the palaeontological record. Biotic dispersal between Gondwana and Laurussia has been shown for fishes (*Phyllolepid* placoderms, Young *et al.*, 2000) and land plants (*Callixylon* archaeopterids, Meyer-Berthaud *et al.*, 1997) to occur at the Frasnian–Famennian transition, indicating at best a very narrow residual oceanic domain between these two continents (Fig. 5). As discussed by Copper (1986), the collision-induced closure of such an equatorial oceanic

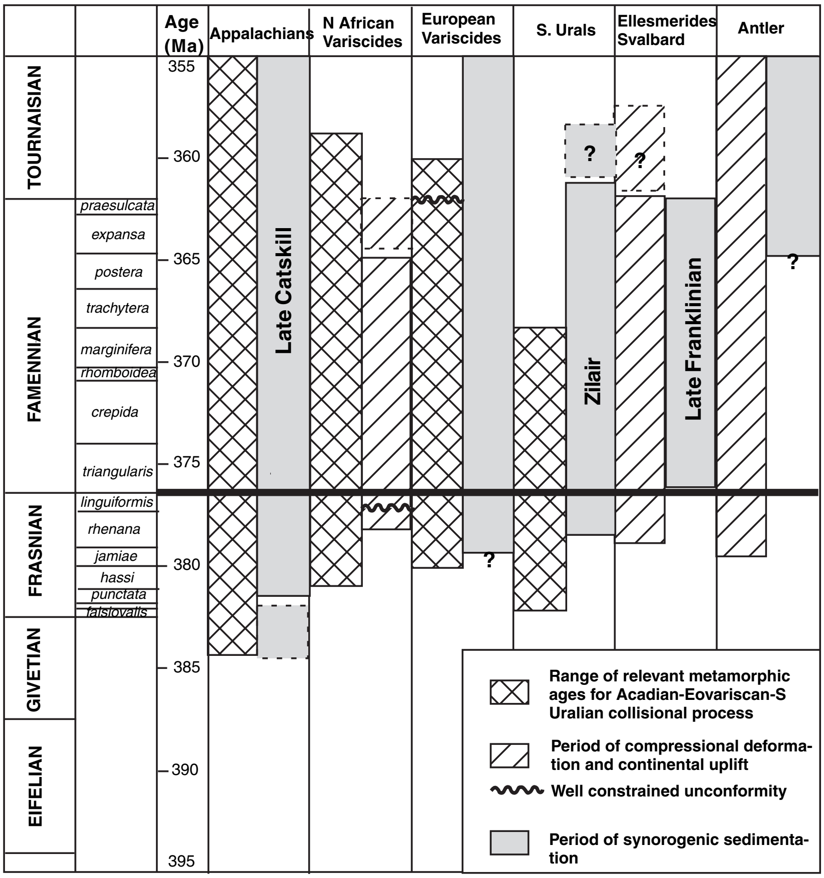

Fig. 6 A synthesis of indicators for continental compressional deformation and mountain building in Late Devonian times for the Appalachians (data from Laird, 1988; Ettensohn, 1995; Murphy and Keppie, 1998), the North African Variscides (data from Piqué *et al.*, 1993; Echarfaoui *et al.*, 2002), the European Variscides (data from Ballévre *et al.*, 1994; Santallier *et al.*, 1994; Matte, 1995; Maluski and Patocka, 1997; Tait *et al.*, 1997), the southern Urals (data from Matte, 1995; Puchkov, 1997), the Ellesmerides–Svalbard belt (data from Roberts, 1988; Embry, 1991) and the Antler belt (data from Johnson and Pendergast, 1981). Note the onset of collision and continental uplift at around 380 Ma.

domain is likely to have induced a complete reorganization of the oceanic currents with a significant reduction of water circulation between the Panthalassa and the Palaeotethys oceans (Fig. 5). This could have had drastic repercussions for heat transfer and furthermore have led to more restricted conditions along the southern Laurussian and the northern Gondwanian continental margins with relatively low oceanic recycling.

A model coupling continental uplift and environmental changes at the FFB

As discussed above, a global-scale increase in chemical and mechanical erosion of continental rocks as well as enhanced terrestrial inputs towards the oceans are evidenced around the FFB. The precise age of the onset of continental uplift is difficult to establish due to the low accuracy of dating, but the oldest radiochronological ages for collisional-induced metamorphism are around 380 Ma (Fig. 6). This corresponds roughly to the base of the Upper Frasnian using latest geological timescales (Tucker *et al.*, 1998; Kauffman *et al.*, in press). Such an age for incipient uplift is corroborated by the occurrence of a well-dated Late Frasnian unconformity within the Moroccan Variscides (Echarfaoui *et al.*, 2002). Although the collisional process is likely to be diachronous along the belt, we speculate the onset of uplift to have occurred around the base of the Upper Frasnian (Fig. 2).

Major mountain belts were located within equatorial domains (Fig. 5) and rock uplift and erosion thus occurred in warm and humid climatic conditions characteristic for the Late Frasnian. In such conditions, chemical weathering of rocks is likely to have been particularly enhanced (e.g. François *et al.*, 1993) and a major increase in the transfer of the dissolved fraction towards the oceans is expected (Fig. 8). The clastic input associated with this orogenically enhanced erosion was trapped in proximal foreland troughs that became incorporated within the final Late Carboniferous belts. Conversely, dissolved material was spread in the oceans and modified the long-term sea water composition. This is exemplified in particular by the increased $^{87}Sr/^{86}Sr$ ratio of sea water during Famennian times, as discussed above. Weathering of continental crust is also expected to release silica and phosphorus in the oceans (e.g. François *et al.*, 1993). Increased transfer of phosphorus could well explain the general increase in the oceanic productivity observed around the continents in Late Frasnian times. Combined with a low oceanic recycling in epicontinental basins due to the reduction of oceanic communications between Panthallassa and Palaeotethys, it is suggested to have driven bottom water anoxia, thus leading to the massive burial of organic carbon (Fig. 8). Models of global biogeochemical cycles suggest that a 40% increase in phosphorus delivery would reproduce the $\delta^{13}C$ anomaly observed in the Kellwasser levels (Goddéris and Joachimski, 2004).

On the continental shelves, this massive transfer of nutrients resulted in more eutrophic conditions and probably turbid sea waters. As proposed by Murphy *et al.* (2000), such a mechanism could have induced the progressive demise of coral–stromatoporoid reefs known to be narrowly adapted to oligotrophic conditions. Increased turbidity of sea water could also account for the development of reduced-eyed or blind trilobites in Late Frasnian seas (e.g. Cronier *et al.*, 2004). By contrast, increased transfer of both nutrients and silica released by

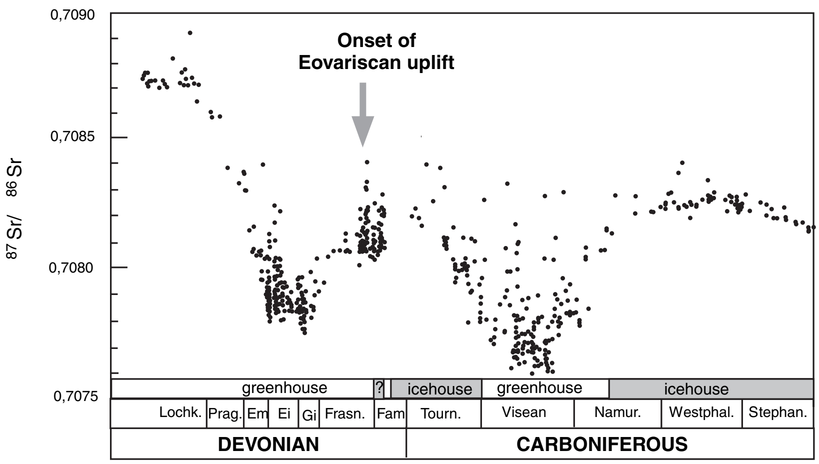

Fig. 7 Variations in sea water $^{87}Sr/^{86}Sr$ composition based on measurements on brachiopod shells (593 data points) and conodont tests (53 data points) (compiled from Veizer *et al*., 1999; Bruckschen *et al*., 1999). Note the peak values at the Frasnian–Famennian transition indicating particularly increased continental weathering and denudation of deep crustal domains.

weathering is suggested to have triggered the bio-siliceous production observed on the Late Frasnian shelves.

An increase in both continental silicate weathering and associated burial of both carbonates and organic carbon during the Kellwasser events would have resulted in a significant drawdown of the atmospheric CO_2 content and associated global cooling during basal Famennian times. Such a mechanism can well explain the sea-level and sea-surface temperature falls observed in the stratigraphic record as well as the changes in the general erosional processes on continents described above. It could also explain why stromatoporoids were unable to develop a dense carbonated skeleton in Famennian oceans (Stearn, 1987; Mistiaen, 1994). Model simulations of Goddéris and Joachimski (2004) have shown that the combined effects of increased continental weathering and deposition of organic matter can reproduce a drop of the $p\mathrm{CO}_2$ of half of its initial value in about four million years (i.e. about the time between incipient collision and the FFB), leading to an average temperature decrease of 2–4 degrees depending on latitude. Following the model of Algeo *et al.* (1995), these authors relate the increased weathering to the development of vascular plants on emergent lands. This process probably also contributed to enhanced chemical weathering of continental soils in Late Palaeozoic times but, in our opinion, it cannot be considered as the primary cause for the Late Palaeozoic CO_2 depletion due to the restoration of high CO_2 levels in Mesozoic times but with a still increased coverage of vascular plants on the land. By contrast, the invasion of land by vascular plants probably did not drastically modify weathering intensity during the Middle–Late Devonian, as terrestrial microbial communities (superficial

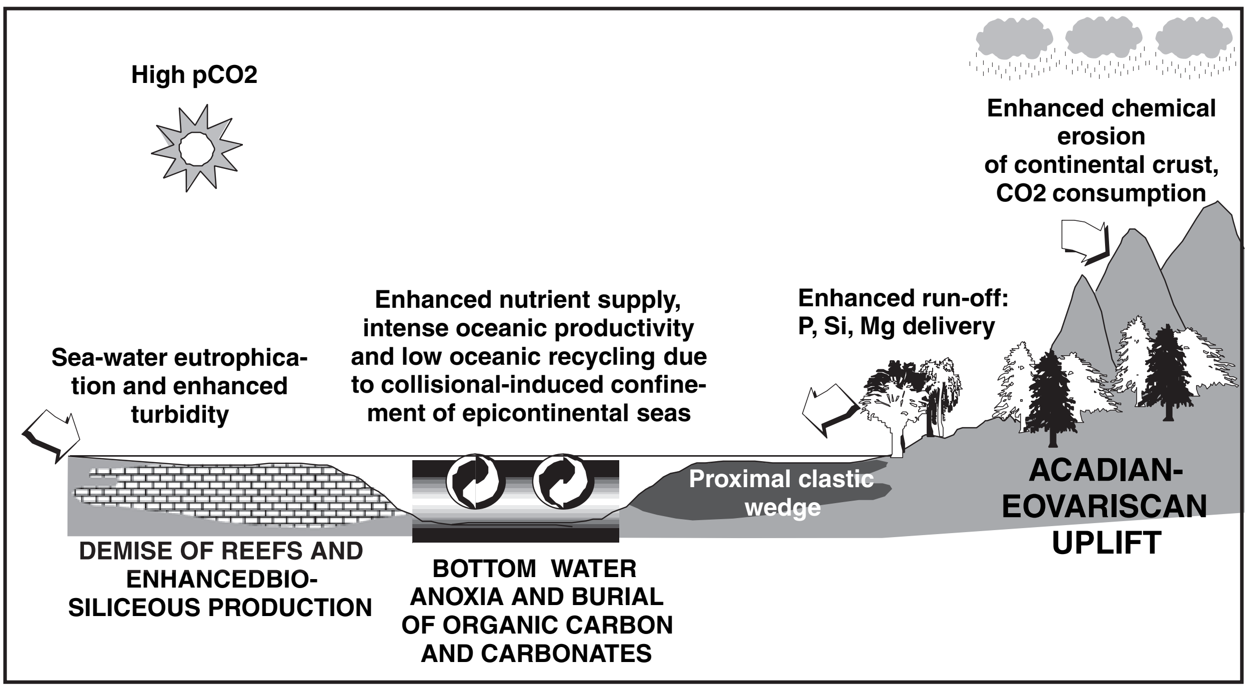

Fig. 8 A model coupling Acadian–Eovariscan continental uplift and environmental changes in Late Frasnian times.

cryptogamic crust) were already very important (Boucot and Gray, 2001), producing enough acidity with the high atmospheric pCO_2 to promote mineral weathering. Moreover, such a mechanism fails to explain the peak of sea water $^{87}Sr/^{86}Sr$ content centred upon the FFB.

To conclude, incipient relief formation along large continental domains due to the collision of Laurussia, Gondwana, Kazakhstan and Siberia during a period with a particularly warm and humid climate is proposed as the primary cause for the drastic environmental changes observed at the FFB. The induced exceptionally high rates of continental weathering combined with the massive burial of organic carbon due to high productivity and low oceanic recycling in restricted epicontinental basins is suggested to have produced a pronounced eutrophication of Late Frasnian platform environments followed by a rapid fall in both sea-level and temperatures in basal Famennian times due to a major drop of atmospheric CO_2 content. These extremely rapid changes in both oxygenation conditions and temperatures are likely to have had drastic repercussions on marine fauna, possibly leading to one of the greatest crises of the biosphere recorded during the Phanerozoic.

Acknowledgements

This study was funded by the French CNRS through the 'ECLIPSE' programme (project Frasnian/Famennian). We wish to thank J-F. Deconinck, L. Francois, J. Gaillardet, Y. Goddéris, A. Herbosch, M. Joachimski, A. Préat and A. Riboulleau for scientific discussions that greatly improved this work. G. Racki, three anonymous reviewers and the journal editor are greatly thanked for valuable comments on the first version of the manuscript.

References

Algeo, T.J., Berner, R.A., Maynard, J.B. and Scheckler, S.E., 1995. Late Devonian oceanic anoxic events and biotic crises: 'rooted' in the evolution of vascular land plants? *GSA Today*, **5**, 64–66.

Ballévre, M., Marchand, J., Godard, G., Goujou, J.-C. and Wins, R., 1994. Eo-Hercynian events in the Armorican Massif. In: *Pre-Mesozoic Geology in France and Related Areas* (J. D. Keppie, ed.), pp. 183–192. Springer-Verlag, Berlin.

Becker, R.T. and House, M.R., 1994. Kellwasser events and goniatite successions in the Devonian of Montagne Noire with comments on possible causations. *Cour. Forsch. Inst. Senckenberg*, **169**, 45–77.

Belka, Z. and Wendt, J., 1992. Conodont biofacies patterns in the Kellwasser facies (Upper Frasnian/Lower Famennian) of the eastern Anti-Atlas, Morocco. *Palaeogeogr. Palaeoclim. Palaeoecol.*, **91**, 143–173.

Berner, R.A. and Kothavala, Z., 2001. Geocarb III: a revised model of atmospheric CO_2 over Phanerozoic times. *Am. J. Sci.*, **301**, 182–204.

Boucot, A.J. and Gray, J., 2001. A critique of Phanerozoic climatic models involving changes in the CO_2 content of the atmosphere. *Earth Sci. Rev.*, **56**, 1–159.

Bratton, J.F., Berry, W.B.N. and Morrow, J.R., 1999. Anoxia pre-dates Frasnian–Famennian boundary mass extinction horizon in the Great Basin, USA *Palaeogeogr. Palaeoclim. Palaeoecol.*, **154**, 275–292.

Bruckschen, P., Oesmann, S. and Veizer, J., 1999. Isotope stratigraphy of the European Carboniferous: proxy signals for ocean chemistry, climate and tectonics. *Chem. Geol.*, **161**, 127–163.

Buggisch, W., 1991. The global Frasnian–Famennian ìKellwasser Eventî. *Geol. Rdsch.*, **80**, 49–72.

Caplan, M.L. and Bustin, R.M., 1999. Devonian–Carboniferous Hangenberg mass extinction event, widespread organic-rich mudrocks and anoxia: causes and consequences. *Palaeogeogr. Palaeoclim. Palaeoecol.*, **149**, 187–207.

Caputo, M.V., 1985. Late Devonian glaciation in South America. *Palaeogeogr. Palaeoclim. Palaeoecol.*, **51**, 291–317.

Chen, D., Tucker, M.E., Shen, Y., Yans, J. and Préat, A., 2002. Carbon isotope excursions and sea-level change: implication for the Frasnian-Famennian biotic crisis. *J. Geol. Soc.*, **159**, 623–626.

Coney, P., 1992. The Lachlan belt of eastern Australia and Circum-Pacific tectonic evolution. *Tectonophysics*, **214**, 1–25.

Copper, P., 1986. Frasnian/Famennian mass extinction and cold-water oceans. *Geology*, **14**, 835–839.

Copper, P., 2002. Reef development at the Frasnian/Famennian mass extinction boundary. *Palaeogeogr. Palaeoclim. Palaeoecol.*, **181**, 27–65.

Cronier, C., Feist, R. and Auffray, J.-C., 2004. Stress related variation in the eye of *Acuticryphops acuticeps* (Phacopina, Trilobite) and its significance: a biometric and morphometric approach. *Paleobiology*, **30**, 217–228.

Devleeschouwer, X., 1999. *La transition Frasnien/Famennien (Dévonien sup.) en Europe*†: sédimentologie, stratigraphie séquentielle & susceptibilité magnétique. PhD Thesis, Université Lille 1 & Université Libre de Bruxelles.

Echarfaoui, H., Hafid, M. and Ôt Salem, A., 2002. Seismic structure of the Doukkala Basin, Paleozoic basement, Western Morocco: a hint for an Eovariscan fold-and-thrust belt. *C.R. Geosci.*, **334**, 13–20.

Embry, A.F., 1991. Middle-Upper Devonian clastic wedge of the Arctic Islands. In: *Geology of the Inuitian Orogen and Arctic Platform of Canada and Greenland* (H. P. Trettin, ed.), pp. 261–279. Geological Society of America.

Ettensohn, F.R., 1987. Rates of relative plate motion during the Acadian orogeny based on the spatial distribution of black shales. *J. Geol.*, **95**, 572–582.

Ettensohn, F.R., 1995. Global and regional controls on the origin and burial of organic matter in Devonian-Mississippian black shales of North America. *Houston Geol. Soc. Bull.*, January, 12–17.

Feist, R., ed., 2002. *Montagne Noire; Guidebook of the Field Excursion for IGCP 421 and ECOS VIII.* Institut des Sciences de l'Evolution, Université de Montpellier II, 85 pp.

Feist, R. and Schindler, E., 1994. Trilobites during the Frasnian Kellwasser Crisis in European Late Devonian cephalopod limestones. *Cour. Forsch. Inst. Senckenberg*, **169**, 195–223.

Fergusson, C.L. and Coney, P.J., 1992. Convergence and intraplate deformation in the Lachlan fold belt of southeastern Australia. *Tectonophysics*, **214**, 417–429.

François, L. and Goddéris, Y., 1998. Isotopic constraints on the Cenozoic evolution of the carbon cycle. *Chem. Geol.*, **145**, 177–212.

François, L., Walker, J.C.G. and Opdyke, B.N., 1993. The history of global weathering and the chemical evolution of the ocean-atmosphere system. *Geophys. Monogr.*, **74**, 143–159.

France-Lanord, C. and Derry, L.A., 1997. Organic carbon burial forcing of the carbon cycle from Himalayan erosion. *Nature*, **390**, 65–67.

Gaillardet, J., Dupré, B., and Allégre, C.J., 1999. Geochemistry of large river suspended sediments: silicate weathering or crustal recycling? *Geochim. Cosmochim. Acta*, **63**, 4037–4051.

Giles, K.A., McMillan, N.J. and McCarson, B.L., 2002. Geochemical analysis and paleoecological implications of phosphatic microspherules (otoliths?) from Frasnian–Famennian boundary strata in the Great Basin, USA *Palaeogeogr. Palaeoclim. Palaeoecol.*, **181**, 111–125.

Girard, C. and Lécuyer, C., 2002. Variations in Ce anomalies of conodonts through the Frasnian/Famennian boundary of Poland (Kowala – Holy Cross Mountains): implications for the redox state of seawater and biodiversity. *Palaeogeogr. Palaeoclim. Palaeoecol.*, **181**, 299–311.

Goddéris, Y. and Joachimski, M., 2004. Global change in the Late Devonian: modelling the Frasnian–Famennian short-term carbon isotope excursions. *Palaeogeogr. Palaeoclim. Palaeoecol.*, **202**, 309–329.

Golonka, J., Ross, M.I. and Scotese, C.R., 1994. Phanerozoic paleogeographic and paleoclimatic modeling maps. In: *Pangea: Global Environments and Resources.* (A. F. Embry, B. Beauchamp and D. J. Glass, eds). *Can. Soc. Petrol. Geol.*, **17**, 1–47.

Gray, D.R., 1997. Tectonics of the southeastern Australian Lachlan Fold belt: structural and thermal aspects. In: *Orogeny Through Time* (J.-P. Burg and M. Ford, eds). *Geol. Soc. Spec. Publ.*, **121**, 149–177.

Hallam, A. and Wignall, P.B., 1999. Mass extinctions and sea-level changes. *Earth. Sci. Rev.*, **48**, 217–250.

Hoffman, D.L., Algeo, T.J., Maynard, B.J., Joachimski, M., Hower, J.C. and Jaminski, J., 1998. Regional and stratigraphic variation in bottom water anoxia in offshore core shales of Upper Pennsylvanian cyclothems from the eastern midcontinent shelf (Kansas), USA. In: *Shales and Mudstones I* (J. Schieber, W. Zimmerle and P. Sethi, eds), pp. 243–269. Schweizerbartísche Verlagsbuchhandlung, Stuttgart.

House, M.R., 2002. Strength, timing, setting and cause of mid-Palaeozoic extinctions. *Palaeogeogr. Palaeoclim. Palaeoecol.*, **181**, 5–25.

Isaacson, P.E., Hladil, J., Shen, J.-W., Kalvoda, J., Diaz, Martinez, E. and Grader, G., 1999. Late Devonian glaciation in Gondwana: setting the stage for Carboniferous eustasy. *Subcommission Devonian Stratigraphy Newsletter*, **16**, 40–49.

Joachimski, M. and Buggisch, W., 1993. Anoxic events in the late Frasnian – Causes of the Frasnian–Famennian faunal crisis? *Geology*, **21**, 675–678.

Joachimski, M. and Buggisch, W., 2002. Conodont apatite $\delta^{18}O$ signatures indicate climatic cooling as a trigger of the Late Devonian mass extinction. *Geology*, **30**, 711–714.

Joachimski, M.M., Pancost, R.D., Freeman, K.H., Ostertag-Henning, C. and Buggisch, W., 2002. Carbon isotope geochemistry of the Frasnian–Famennian transition. *Palaeogeogr. Palaeoclim. Palaeoecol.*, **181**, 91–109.

Johnson, J.G., Klapper, G. and Sandberg, C.A., 1985. Devonian eustatic fluctuations in Euramerica. *Geol. Soc. Am. Bull.*, **96**, 567–587.

Johnson, J.G. and Pendergast, A., 1981. Timing and mode of emplacement of the Roberts Mountain allochthon, Antler orogeny. *Geol. Soc. Am. Bull.*, **92**, 648–658.

Kauffman, B., Trapp, E. and Mezger, K., in press. The numerical age of the Late Frasnian (Late Devonian) Kellwasser horizons – a new U–Pb zircon date from Steinbruch Schmidt (Kellerwald, Germany). *J. Geol.*, in press.

Kump, L.R., Arthur, M.A., Patzkowsky, M.E., Gibbs, M.T., Pinkus, D.S. and Sheehan, P.M., 1999. A weathering hypothesis for glaciation at high atmospheric pCO2 during the Late Ordovician. *Palaeogeogr. Palaeoclim. Palaeoecol.*, **152**, 173–187.

Laird, J., 1988. Arenig to Wenlock age metamorphism in the Appalachians. In: *The Caledonian-Appalachian Orogen* (A. L. Harris and D. J. Fettes, eds). *Geol. Soc. Spec. Publ.*, **38**, 311–345.

Lazreq, N., 1999. Biostratigraphie des conodontes du Givétien au Famennien du Maroc Central. BiofaciËs et événement Kellwasser. *Cour. Forsch. Inst. Senckenberg*, **214**, 1–111.

Lethiers, F., Baudin, F. and Casier, J.-G., 1998. Ostracodes de la limite Frasnien-Famennien en environnement anoxique (La Serre, Montagne Noire, France). *Rev. Micropal.*, **41**, 321–336.

Lethiers, F. and Casier, J.-G., 1999. Autopsy of a biological extinction: the Frasnian–Famennian boundary crisis. *C. R. Geosci.*, **329**, 303–315.

Loevezijn, 1989. Extinction pattern for the Middle–Upper Devonian stromatoporoid coral reefs; a case study from the Cantabrian Mountains. *Proc. Koninklijke Nederlandse Akademie Van Wetenschappen*, **92**, 61–74.

Maluski, H. and Patocka, F., 1997. Geochemistry and $^{40}Ar/^{39}Ar$ geochronology of the mafic metavolcanic rocks from the Richory Mountains complex (West Sudetes, Bohemian massif): paleotectonic significance. *Geol. Mag.*, **134**, 703–716.

Matte, P., 1995. Southern Uralides and Variscides: comparison of their anatomies and evolutions. *Geol. Mijnb.*, **74**, 151–166.

Matte, P., 2001. The Variscan collage and orogeny (480–290 Ma) and the tectonic definition of the Armorica microplate: a review. *Terra Nova*, **13**, 122–128.

Mattern, F. and Schneider, W., 2000. Suturing of the Proto- and Paleotethys oceans in the Western Kunlun (Xinjiang, China). *J. Asian Earth Sci.*, **18**, 637–650.

McGhee, G.R., 1989. The Frasnian–Famennian event. In: *Mass Extinction: Processes and Evidences* (S. K. Donovan), pp. 133–151. Belhaven Press, London.

McGhee, G.R., 2001. The 'multiple impact hypothesis' for mass extinction: a comparison of the Late Devonian and the Late Eocene. *Palaeogeogr. Palaeoclim. Palaeoecol.*, **176**, 47–58.

Meyer-Berthaud, B., Wendt, J. and Galtier, J., 1997. First record of a large *Calllixylon* trunk from the Late Devonian of Gondwana. *Geol. Mag.*, **134**, 847–853.

Mistiaen, B., 1994. Skeletal density: implications for development and extinction of Paleozoic stromatoporoids. *Cour. Forsch. Inst. Senckenberg*, **172**, 319–327.

Murphy, J.B. and Keppie, J.D., 1998. Late Devonian palinspastic reconstruction of the Avalon–Meguma terrane boundary: implication for terrane accretion and basin development in the Appalachian orogen. *Tectonophysics*, **284**, 221–231.

Murphy, A.E., Sageman, B.B. and Hollander, D.J., 2000. Eutrophication by decoupling of the marine biogeochemical cycles of C, N and P: a mechanism for the Late Devonian mass extinction. *Geology*, **28**, 427–430.

Over, D.J., 2002. The Frasnian/Famennian boundary in central and eastern United States. *Palaeogeogr. Palaeoclim. Palaeoecol.*, **181**, 153–169.

Peterhänsel, A. and Pratt, B.R., 2001. Nutrient-triggered bioerosion on a giant carbonate platform masking the post-extinction Famennian benthic community. *Geology*, **29**, 1079–1082.

Piecha, M., 2002. A considerable hiatus at the Frasnian/Famennian boundary in the Rhenish shelf region of northwest Germany. *Palaeogeogr. Palaeoclim. Palaeoecol.*, **181**, 195–211.

Piqué, A., Bossiere, G., Bouillin, J.P., Chalouan, A. and Hoepffner, C., 1993. Southern margin of the Variscan Belt – the north-western Gondwana mobile zone (eastern Morocco and northern Algeria). *Geol. Rdsch.*, **82**, 432–439.

Puchkov, V.N., 1997. Structure and geodynamics of the Uralian orogen. In: *Orogeny Through Time* (J.-P. Burg and M. Ford, eds). *Geol. Soc. Spec. Publ.*, **121**, 149–177.

Racki, G., 1998. Frasnian–Famennian biotic crisis: undervalued tectonic control? *Palaeogeogr. Palaeoclim. Palaeoecology*, **141**, 177–198.

Racki, G., 1999. Silica-secreting biota and mass extinctions: survival patterns and processes. *Palaeogeogr. Palaeoclim. Palaeoecology*, **154**, 107–132.

Raymo, M.E., 1991. Geochemical evidence supporting T.C. Chamberlin's theory of glaciation. *Geology*, **19**, 344–347.

Rind, D., Russell, G. and Ruddiman, W.F., 1997. The effects of uplift on Ocean-Atmosphere circulation. In: *Tectonic Uplift and Climate Change* (W. F. Ruddiman, ed.), pp. 123–147. Plenum Press, New York.

Riquier, L., Tribovillard, N., Averbuch, O., Joachimski, M., El Albani, A., Devleeschouwer, X. and Riboulleau, A., 2003. Etude géochimique des coupes de Bou-ounebdou (Maroc) et de Aeke tal (Allemagne) et comparaisonss avec la coupe de la Serre (France) ‡ la limite Frasnien–Famennien. *Abstract Book Tecto-Clim Congress*, Lille.

Roberts, D., 1988. Timing of Silurian to middle Devonian deformation in the Caledonides of Scandinavia, Svalbard and E Greenland. In: *The Caledonian–Appalachian Orogen* (A. L. Harris and D. J. Fettes, eds). *Geol. Soc. Spec. Publ.*, **38**, 429–435.

Royer, D.L., Berner, R.A. and Beerling, D.J., 2001. Phanerozoic atmospheric CO_2 change: evaluating geochemical and paleobiological approaches. *Earth Sci. Rev.*, **54**, 349–392.

Ruddiman, W.F., ed., 1997. *Tectonic Uplift and Climate Change*. Plenum Press, New York.

Sandberg, C., Morrow, J. and Ziegler, W., 2002. Late Devonian sea level changes, catastrophic events and mass extinctions. In: *Catastrophic Events and Mass Extinctions; Impacts and Beyond* (C. Koeberl and K. G. McLeod, eds). *Geol. Soc. Am. Spec. Pap.*, **356**, 473–487.

Santallier, D.S., Lardeaux, J.-M., Marchand, J. and Marignac, C., 1994. Metamorphism in the French Massif Central. In: *Pre-Mesozoic Geology in France and Related Areas* (J. D. Keppie, ed.), pp. 324–338. Springer-Verlag, Berlin.

Schindler, E., 1990. Die Kellwasser Krise (Hohe Frasne-Stufe, Ober Devon). *Göttinger Arb. Geol. Paläeontol.*, **46**, 115 pp.

Schmitz, B., Charisi, S.D., Thompson, E.I. and Speijer, R.P., 1997. Barium, SiO_2 (excess), and P_2O_5 as proxies of biological productivity in the Middle East during the Palaeocene and the latest Palaeocene benthic extinction event. *Terra Nova*, **9**, 95–99.

Scotese, C.R., Boucot, A.J. and McKerrow, W.S., 1999. Gondwanan palaeogeography and palaeoclimatology. *J. African Earth Sci.*, **28**, 99–114.

Sengor, A.M. and Natalíin, B., 1996. Paleotectonics of Asia: fragments of a synthesis. In: *The Tectonic Evolution of Asia* (A. Yin and T.M. Harrison, eds), pp. 486–640. Cambridge University Press, Cambridge.

Sepkoski, J.J., 1986. Phanerozoic overview of mass extinctions. In: *Patterns and Processes in the History of Life* (D. M. Raup and D. Jablonski, eds), pp. 277–295. Springer-Verlag, Berlin.

Shen, J.W. and Webb, G.E., 2004. Famennian (Upper Devonian) calcimicrobial (Renalcis) reef at Miaomen, Guilin, Guangxi, South China. *Palaeogeogr. Palaeoclim. Palaeoecol.*, **204**, 373–394.

Stearn, C.W., 1987. Effect of the Frasnian–Famennian extinction event on the stromatoporoids. *Geology*, **15**, 677–679.

Streel, M., Caputo, M.V., Loboziak, S. and Melo, J.H.G., 2000. Late Frasnian–Famennian climates based on palynomorph analyses and the question of the Late Devonian glaciations. *Earth-Sci. Rev.*, **52**, 121–173.

Tait, J., Bachtadse, V., Franke, W. and Sofel, H., 1997. Geodynamic evolution of the European Variscan fold belt: paleomagnetic and geological constraints. *Geol. Rdsch.*, **86**, 585–598.

Thorez, J. and Dreesen, R., 2002. The Condroz sandstone group (Upper Famennian) revisited. *Geologica Belgica International Meeting guidebook*. Leuven.

Tribovillard, N., Averbuch, O., Devleeschouwer, X., Racki, G. and Riboulleau, A., 2004. Deep-water anoxia at the Frasnian–Famennian boundary (La Serre, France): a tectonically-induced Late Devonian oceanic anoxic event? *Terra Nova*, **16**, 288–295.

Tucker, R.D., Bradley, D.C., Ver Straeten, C.A., Harris, A.G., Ebert, J.R. and McCutcheon, S.R., 1998. New U–Pb zircon ages and the duration and division of Devonian time. *Earth Planet. Sci. Lett.*, **158**, 175–186.

Veizer, J., Ala, D., Azmy, K., Bruckschen, P., Buhl, D., Bruhn, F., Carden, G.A.F., Diener, A., Ebneth, S., Godderis, Y., Jasper, T., Korte, C., Pawellek, F., Podlaha, O.G. and Strauss, H., 1999. $^{87}Sr/^{86}Sr$, $\delta^{13}C$ and $\delta^{18}O$ evolution of Phanerozoic seawater. *Chem. Geol.*, **161**, 59–88.

Vicente, J.-C., 1975. Essai d'organisation paléogéographique et structurale du Paléozoïque des Andes méridionales. *Geol. Rdsch.*, **64**, 343–394.

Whalen, M.T., Day, J., Eberli, G.P. and Peter, W., 2002. Microbial carbonates as indicators of environmental change and biotic crises in carbonate systems: examples from the Late Devonian, Alberta basin, Canada. *Palaeogeogr. Palaeoclim Palaeoecol.*, **181**, 127–151.

Young, G.C., Moody, J.M. and Casas, J.E., 2000. New discoveries of Devonian vertebrates from South America and implications for Gondwana-Euramerica contact. *C.R. Geosci.*, **331**, 755–761.

Received 24 February 2004; revised version accepted 28 September 2004

Article 19.

Lefebvre V., Averbuch O., François L., Tribovillard N. and Servais T., (en cours). Global carbon cycle and climate modelling at the Frasnian-Famennian boundary crisis (Late Devonian, ca 375 Ma): impact of the incipient Variscan mountain building.

Global carbon cycle and climate modelling at the Frasnian-Famennian boundary crisis (Late Devonian, ca 375 Ma): impact of the incipient Variscan mountain building

Vincent LEFEBVRE[1,2], Olivier AVERBUCH[1], Louis FRANCOIS[2], Nicolas TRIBOVILLARD[1] & Thomas SERVAIS[1]

[1] Laboratoire "Géosystèmes", Université de Lille 1, 59655 Villeneuve d'Ascq Cedex, France E-mail: Vincent.lefebvre@lsce.ipsl.fr

[2] Unité de Modélisation du Climat et des Cycles Biogéochimiques, Université de Liège, 17 allée du Six Août, 4000 Liège, Belgium

Abstract

The Late Devonian is a period of significant climatic and environmental changes exemplified by a severe crisis of the biosphere (the Frasnian-Famennian boundary crisis) and by the onset of an episod of glaciation on Southern Gondwana in the Upper Famennian. The major pulse of the faunal extinction is marked by an extensive perturbation of marine environments expressed by two carbon-organic rich levels (the Kellwasser horizons) deposited under various suboxic conditions. These two levels have been recognized in many places around the Prototethysian realm and are characterized by a positive carbon isotopic shift from 2‰ to 3‰ reflecting a period of enhanced organic carbon burial. The origin of these two events remains strongly debated but we focused here on the « orogenesis » hypothesis (Averbuch et al, 2005) suggesting that organic matter burial was related to a large scale fertilization and stratification of sea waters (especially that from the Prototethysian realm) as the result of the incipient uplift of the large sub-equatorial Appalachian-Eovariscan mountain belt.

To test this hypothesis, we have used a global carbon cycle numerical model coupled with an Energy Balance Climate Model (EBM). The geochemical cycle model allows the computation of phosphorus, carbon and oxygen concentrations as well as the alkalinity, $\delta^{13}C$ and $^{87}Sr/^{86}Sr$ isotopic ratios in each oceanic box and the atmospheric pCO_2 in equilibrium with the modelled oceanic system. The oceanic and continental configurations have been inferred from the Late Devonian palaeogeography (Polar ocean, Panthalassa and Proto-Tethys). Oceanic circulations have been modelled using a present-day type circulation for the Panthalassa

Ocean and the pre-perturbation Prototethys realm, the latter evolving towards isolated conditions during the simulations. The mountain-building effects have been modelled by increasing the mechanical weathering specifically on uplifted continental areas. The respective effects of each process have been tested separately and then coupled to simulate the global environmental impact of mountain-building. Results of these simulations suggest that the transient stage of Eovariscan mountain building is possible to have generated a severe perturbation of the carbon cycle over few My thereby resulting in two peaks of organic matter storage : (1) the first one connected to the direct effects of increased erosion resulting in the enhancement of the marine productivity in nearby oceanic realms (2) the second one connected to delayed anoxia that originated by stratification of the Prototethys sea-water as the equatorial seaway, linking it formerly to Panthalassa, reduced during the collisional process. Our simulations suggest that such two-phase carbon cycle perturbation, coeval with the transient mountain building stage, might result in a severe atmospheric pCO_2 drop (from 3100 to 760 ppmv) resulting, in turn, in an about 6°C cooling of the mean equatorial temperatures at the beginning of the Famennian.

Introduction

In the last twenty years, continental weathering and organic carbon burial have been recognized as the main sinks of atmospheric carbon dioxide at the geological time scale and therefore have been increasingly adressed to account for past long-term climatic and environmental changes (e.g., Berner et al, 1983; Francois et al, 1993; Berner and Kothavala, 2001). Among the different geodynamical processes that have been active in the Earth history, mountain building is surely one of the most efficient for drastically modifying both continental silicate weathering and organic carbon burial as it strongly increases the surface exposure of fresh crustal rocks and the exportation of nutrients and continental organic matter towards oceanic realms (e.g., Raymo, 1994; Gailllardet et al, 1999; Zachos and Kump, 2005; Tribovillard et al, 2004; Galy et al, 2007; Campbell and Allen, 2008). Such mechanisms are likely to be particularly enhanced if rock uplift occurs in sub-equatorial climatic belts because chemical weathering is noticeably dependent on temperature and run-off (e.g., Francois et al, 1993; Godderis et al, 2008). On the other hand, the collision of large continental plates, by closing oceanic gateways, necessarily reduces the water exchanges that formerly existed between oceanic realms thereby favoring the development of suboxic marine bottom waters and the resultant organic carbon burial in sediments (e.g. Tribovillard et al, 2004).

Uplift of the Himalaya-Tibet (and at a larger scale of all tertiary mountain belts) has thus been largely addressed through the last twenty years as the possible driver of the Cenozoic global cooling (e.g., Raymo et al, 1988; Edmond, 1992; France-Lanord and Derry, 1997; Francois and Godderis, 1998; Zachos and Kump, 2005; Galy et al, 2007; Gaillardet and Galy, 2008; Garzione, 2008). In more ancient Phanerozoic times, the Upper Paleozoic period can also be considered as an example of possible coupling between mountain building and climate cooling as the uplift of the large sub-equatorial Appalachian-Variscan-Uralian mountain belt closely matches the development of the Southern Gondwana glaciation (e.g., Raymo, 1991; Eyles, 1993). The first direct evidences of ice cap formation on the southern Gondwana are dated of Late Famennian times (Latest Devonian, ca 365 Ma)(Caputo, 1985; Crowell, 1999; Brezinski et al, 2008) but the onset of the Upper Paleozoic cooling stage is likely to have occurred a few million years earlier, at the Frasnian-Famennian transition (Copper, 1986; Streel et al, 2000; Isaacson et al, 2008), that corresponds to a major eustatic sea-level fall (>75 m following the chart of Haq and Schutter, 2008). This first major cooling pulse of the Late Devonian could result in about 5°C decrease of the temperature of the equatorial oceanic waters as suggested by a significant oxygen isotope shift recorded in conodont apatite (Joachimski and Buggisch, 2002).

The drastic environmental changes, that occurred at the turn between the mid-Devonian Greenhouse and the Late Devonian Icehouse stages, are exemplified by a severe mortality crisis of marine tropical fauna (especially reef-building fauna)(Sepkoski, 1986; Copper, 1986; Mc Ghee, 1989; Kiessling, 2008), with a maximum of biodiversity loss spanning the Frasnian-Famennian transition over ca 2 millions years (from the Late Frasnian to the base of the Famennian)(Hallam and Wignall, 1999). This severe crisis of the biosphere has been shown to be coeval with an extensive perturbation of marine environments expressed by two Late Frasnian carbon-organic rich levels (the Lower and Upper Kellwasser horizons) deposited under various suboxic conditions (e.g. Buggisch, 1991; Joachimski and Buggisch, 1993; Bratton et al, 1999; Bond et al, 2004, 2005; Riquier et al, 2005; 2006; Pujol et al, 2006; Bond and Wignall, 2008). These levels have been recognized in many places around the Protothetysian margins and are coeval with a worldwide positive carbon isotopic shift of 2‰ to 3‰ thereby reflecting a period of significantly enhanced organic carbon burial in oceanic realms (Joachimski et al, 2002).

The origins of these widespread environmental changes remain strongly debated (see for example the review of Racki, 2005) but, recently, Averbuch et al (2005) proposed to link them to the early phase of uplift of the sub-equatorial Appalachian-Variscan mountain belt

(Fig. 1) in response to the incipient collision between Gondwana and Laurussia at ca 380-375 Ma (Mid-Upper Frasnian times)(e.g., Tait et al, 1997; Murphy and Keppie, 1998; Franke, 2000; Matte, 2001; Echarfaoui et al, 2002; Souquet et al, 2003; Keller et al, 2008; Ballèvre et al, 2009).

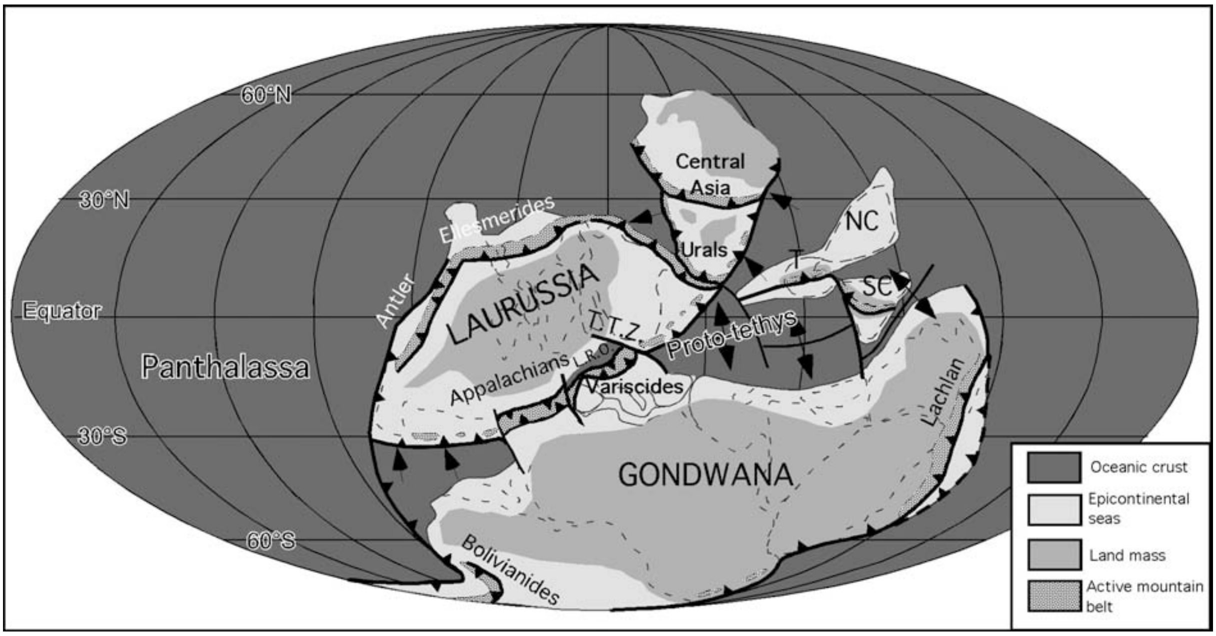

Figure 1. General paleogeographical reconstruction for the Late Devonian times showing the development of large uplifted continental areas along the margin of the Prototethys (after Averbuch et al., 2005). L.R.O. : Lizard-Rhenohercynian oceanic realm ; T.T.Z. : Teysseire-Tornquist Zone ; NC : North China block ; SC : South china block.

Such large-scale collisional process is marked by a significant increase of the $^{87}Sr/^{86}Sr$ ratio of the sea-water (Veizer et al, 1999; Chen et al, 2005), thereby testifying high rates of continental chemical erosion and denudation of deep crustal domains around the Frasnian-Famennian boundary. The increased continental weathering would have enhanced the related nutrient supply from continents and in turn, the marine primary productivity inducing a large-scale fertilization of Late Frasnian sea waters (especially that from the Prototethysian realm). On the other hand, the incipient continental collision is suggested to have driven some increased stratification of the Prototethys sea-water by reducing the oceanic circulations during the progressive closure of the equatorial seaway linking formerly the Prototethysian realm to the Panthalassa. This mountain building-induced carbon cycle perturbation would thus trigger the storage of large amount of organic carbon into the sediments. This chain of coupled mechanisms could have led to a significant drop of the atmospheric carbon dioxide content as suggested by the atmospheric pCO_2 proxies in Famennian times (Royer, 2006) and in turn, could have induced the global cooling pulse initiating the Southern Gondwana glaciation.

This model coupling uplift of continental crust and climate, via the regional enhancement of mechanical and chemical erosion, has been tested here, using a global carbon cycle numerical model coupled with a 1D climatic Energy Balance Model (EBM). In the model, the oceanic and continental configurations have been inferred from the Late Devonian palaeogeography (Polar, Panthalassa and Prototethys oceans) with oceanic circulations initially based on the present-day circulation for the Panthalassa Ocean and the pre-perturbation Prototethysian realm, and evolving towards isolated conditions during the simulations. The mountain-building effects have been modeled by increasing the mechanical erosion (and *de facto* the chemical alteration) specifically on selected latitudinal bands of continental areas submitted to tectonic uplift. The respective effects of each process have been tested separately and then coupled to simulate the global impact of the incipient Variscan continental collision on the Late Devonian climate.

Model characteristics

The model used here is a global geochemical box-model basically designed by Grard et al. (2005) to simulate the environmental impact of trap emplacement. The geochemical model is coupled with a 1D EBM climatic model developped by François and Walker (1992). Basically, the model calculates the concentrations of DIC (Dissolved Inorganic Carbon), Alkalinity and phosphorus in the different oceanic boxes and pCO_2 in the different atmospheric boxes. An upgraded version of the model has been constructed to integrate the possibility to configure easily the number of oceanic and atmospheric boxes and describe more precisely the dependence of the weathering laws on soil CO_2 and physical erosion (Diester-Haas et al., 2008; Lefebvre et al, 2010). The model, presented here, integrates further modifications including: (1) the coupling of the different geochemical cycles with the cycle of oxygen and (2) a latitudinal regionalization of the mechanical erosion. These evolutions have been done, on one hand, to produce the suboxic conditions observed in Late Frasnian basins that strongly influence the organic carbon sequestration in sediments, and, on the other hand, to simulate the orogenesis-related enhancement of crustal erosion.

Description of the cycles

The variation of carbon quantity in atmosphere and oceans is calculated by resolving at each time step the balance between input and output fluxes. For the atmosphere, input sources come from the degassing of the mantle expressed in our model by a global volcanic source (including continental and mid-oceanic volcanism) and from surface ocean degassing, while outputs are formed by the consumption of CO_2 by continental silicate and carbonate weathering and dissolution in surface ocean. For each oceanic box, the inputs comprise the dissolved carbon resulting from continental silicates, kerogen and carbonates weathering fluxes (for surface ocean), the carbon transported by water fluxes, the dissolution of atmospheric CO_2 (for surface ocean), the oxidation of organic matter (OM) and the dissolution of carbonate under the calcite and/or aragonite compensation depth (CCD, ACD). Outputs are carbonate and OM deposition, DIC amount transported towards an adjacent reservoir, surface ocean degassing and *in situ* biological productivity (in surface ocean only).

The alkalinity budget is determined in the same way. Input fluxes are silicates and carbonates weathering (for surface ocean), water fluxes from adjacent reservoir and dissolution of carbonate rain under the CCD and ACD. The output fluxes are carbonate deposition (pelagic and coral reefs) and water fluxes toward an adjacent reservoir.

Concerning the phosphorus cycle, the outputs are formed by the phosphorus buried in carbonates and in OM. The ratio P/C is fixed to 1/1000 in carbonate rocks according to Froelich et al. (1982) and to 1/200 or 1/4000 in OM buried under oxic or anoxic conditions respectively according to Van Cappellen and Ingall (1996). An other output is the phosphorus amount transported via the water fluxes toward the other boxes. The inputs involve the phosphorus brought in oceanic reservoir through oceanic water fluxes and the phosphorus supplied by continental silicate weathering. These sources are calibrated to be in equilibrium with the phosphorus burial flux in the present-day configuration.

The oxygen cycle forms the last major cycle included in the geochemical box-model. Because the residence time of oxygen in surface ocean is very short, atmosphere and surface ocean can be considered as a single reservoir. Based on this hypothesis, the oxygen concentration of the surface ocean is a function of the atmospheric pO_2 and of the oxygen solubility in seawater. Surface ocean productivity is a source of oxygen as a result of photosynthesis. On the other hand, the resultant OM, as far as it is preserved in sediments (i.e. that escaped the oxydation process in the thermocline) represents a long-term source of oxygen and therefore constitutes an indirect input of oxygen into the ocean-atmosphere system. The oxygen is redistributed between the different oceanic reservoirs through the water fluxes. The oxydation of continental kerogen represents the major sink of oxygen in our model.

The silicate weathering laws

Silicate weathering constitutes a major sink of atmospheric pCO_2 and thereby exerts a significant impact on climate. In our model, we consider different kinetics laws for granitic and basaltic lithologies because basalts weather 8 to 10 times faster than granite (Dessert et al., 2001; 2003). These laws have been updated from the version used by Grard et al. (2005) by adding a dependence on soil pCO_2 and on physical erosion for the granite weathering (cf. Equation 1 and 2).

$$f_{gra,i} = A_{gra,i} \times R_i \times \alpha \times \exp(C_{gra} \cdot WT) \times r_{CO_2} \times \sigma_{mech,i} \quad (1)$$

$$f_{bas,i} = A_{bas,i} \times R_i \times \beta \times \exp(C_{bas} \cdot WT) \times r_{CO_2} \quad (2)$$

$f_{gra,i}$ and $f_{bas,i}$ are the silicate weathering fluxes (in mol of silicate per year) in the latitude band i for granitic and basaltic lithologies respectively; $A_{gra,i}$ and $A_{bas,i}$ are the continental areas of exposed granitic or basaltic surfaces in latitude band i; R_i is the continental runoff in latitude band i calculated from the equation proposed by François and Walker (1992) that links continental runoff to latitude, temperature and continental fraction in the latitude band; a and b are constants for granitic or basaltic rocks and are calibrated on the present-day state such as to get the current values for the weathering fluxes estimated by Gaillardet et al. (1999) when the model is forced with modern values; C_{gra} and C_{bas} are constants representing the temperature dependence of the weathering rate for granites and basalts; WT is the average air temperature in °C during the "weathering" season, and is parameterized as a function of the annual mean temperature calculated by the EBM in each latitude band (Grard et al., 2005). r_{CO_2} represents the relative soil CO_2 pressure ($pCO_{2,soil}$) with respect to the present-day value. This ratio can be determined by applying the equation proposed by Volk (1987), which is a function of the primary productivity ratio (P/P_0) and atmospheric pCO_2 (Equations 3, 4 and 5).

$$r_{CO_2} = \left[\frac{pCO_2^{soil}}{pCO_2^{soil,0}} \right]^{0.3} \quad (3)$$

$$\frac{pCO_2^{soil}}{pCO_2^{soil,0}} = \frac{\Pi}{\Pi_0} \times \left(1 - \frac{pCO_2^{atm,0}}{pCO_2^{soil,0}} \right) + \frac{pCO_2^{atm}}{pCO_2^{soil,0}} \quad (4)$$

$$\frac{\Pi}{\Pi_0} = \frac{\Pi_{\max}}{\Pi_0} \times \frac{pCO_2^{atm} - pCO_2^{\min}}{pCO_2^{1/2} + \left(pCO_2^{atm} - pCO_2^{\min} \right)} \quad (5)$$

The value of the soil productivity depends only on the atmospheric CO_2 pressure through a Michaelis-Menten rate law. This CO_2 dependence is adopted for all latitudes, without considering the factors that can affect local soil productivity. Volk's model is used with a maximum soil productivity Π_{max} equal to four times the present-day productivity after 360 Ma. François and Walker (1992) assumed a zero productivity before 440 Ma and let Π_{max} increase linearly between 440 and 360. Considering a reduced soil productivity during Devonian time, we adopted a Π_{max} equal to two times the present-day soil productivity. This assumption is roughly equivalent to the parameterization of Berner and Kothavala (2001) considering the effects of land plant weathering.

$\sigma_{mech,i}$ is a global mechanical weathering factor normalized to 1 at present in latitude band I, and is a function of clastic flux, continental area and runoff (cf. Equation 6)),

$$\sigma_{mech,i} = \left[\frac{\dfrac{F_{clast,i}}{F_{clast0,i}}}{\left(\dfrac{A_{cont}}{A_{cont0}} \times \dfrac{R}{R_0} \right)} \right]^{0.305} \quad (6)$$

where F_{clast}/F_{clast0}, A_{cont}/A_{cont0} and R/R_0 are the clastic flux, the global continental area and the global runoff normalized to their present-day values respectively. This equation is obtained from the relation proposed by Millot et al. (2002) dividing the chemical weathering and physical erosion rates by runoff. This law considers the sedimentary ratio (F_{clast}/F_{clast0}) equal to the total suspended solid multiplied by runoff and continental area normalized to their present-day values.

Organic carbon burial

This flux is calculated in each surface oceanic box using the equation 7, and in each deep reservoir using the equation 8.

$$F_{orgd}^{surf} = \pi_{surf} \times fr \times \alpha \quad (7)$$

$$F_{orgd}^{deep} = C_{rain} \times (1 - R_{oxy}) \times fr \times \alpha \quad (8)$$

In these equations, F_{orgd} represents the flux of organic carbon buried in sediment (in mol/yr) for surface or deep reservoirs, R_{oxy} is a factor dependent of oxygen concentration in the water column and is between 0 (oxic conditions) and 1 (anoxic conditions), *fr* is the fraction of the seafloor area compared to the oceanic box area and a is a constant representing the condition of preservation associated with the sedimentation time (time in water column and time to reach the depth where all oxido-reduction processes do not occur). π_{surf} is the surface exported productivity (in mol C) in surface oceanic boxes calculated as a function of the phosphorus input via water fluxes considering this element as the only biolimiting nutrient converted in mol C with the 106/1 C/P ratio of Redfield (1934). Concerning the deep reservoirs, C_{rain} is defined as the amount of particulate organic matter coming from the reservoir above it.

In these equations, R_{oxy} and π_{surf} are the main parameters that drive organic carbon sequestration in sediments. This assumption is in agreement with the geological concept linking intensification of organic carbon burial to intensification of surface productivity and/or to a decrease in dissolved oxygen concentration in water column. In the numerical model, oceanic reservoirs are global oceans that can't be entirely anoxic. Therefore, R_{oxy} is parameterized to vary linearly from 1 to 0.02 between 0.2 and 0.05 mol O_2/m^3. Thus, if dissolved oxygen concentration in oceanic reservoir is lower than 0.05 mol/m3, R_{oxy} will be equal to 0.02, and if dissolved oxygen concentration is greater than 0.2 mol/m3, it will be equal to 1. For the surface reservoirs, we consider that π_{surf} represent the exported productivity that can't be recycled by oxidation processes. Therefore, R_{oxy} doesn't influence organic carbon burial in these reservoirs. However, π_{surf} is indirectly linked to dissolved oxygen concentration in surface water column because phosphorus uptake in sediments depends on this concentration. Indeed, Van Cappellen and Ingall (1996) have shown that the C/P ratio equals 1/200 in oxidizing and 1/4000 in reducing conditions. In the same way that for R_{oxy}, we have choosen to parameterize this ratio linearly from 1/4000 to 1/200 between 0.05 and 0.2 mol O_2/m^3. Accordingly, the phosphorus uptake in sediment during anoxic events will be lower and thus surface productivity will be increased due to "large-scale upwellings".

Carbon isotope calculation

Carbon isotopic ratio is determined in each boxes of the ocean-atmosphere system at each time step by solving the general differential equation presented below:

$$\frac{d\delta_i}{dt} = \frac{\sum f_{j\to i}(\delta_j - \delta_i) - \sum f_{i\to j}(\delta_i - \delta_j)}{Q_i} \qquad (9)$$

Where $f_{j\to i}$ and $f_{i\to j}$ are input (from a "j" reservoir) and output (toward a "j" reservoir) carbon fluxes respectively, δ_i and δ_j are isotopic values for the "i" and "j" reservoirs and Q_i is the amount of carbon in the reservoir "i". $\delta^{13}C$ of all carbonate species are determined with the relations described below :

$$\delta_{CO_2^{gaz}} = \delta_{H_2CO_3} - \varepsilon_{dg} \tag{10}$$

$$\delta_{H_2CO_3} = \delta_{HCO_3^-} - \varepsilon_{bd} \tag{11}$$

$$\delta_{HCO_3^-} = \delta_{oc} + \frac{[CO_3^{2-}]}{[DIC]} \times \varepsilon_{bc} + \frac{[H_2CO_3]}{[DIC]} \times \varepsilon_{bd} \tag{12}$$

$$\delta_{CO_3^{2-}} = \delta_{HCO_3^{2-}} - \varepsilon_{bc} \tag{13}$$

Where δ* are $\delta^{13}C$ value for gaseous CO_2 (CO_{2gaz}), dissolved CO_2 (H_2CO_3), bicarbonate (HCO_3^-) carbonate (CO_3^{2-}) and ocean considered (oc). ε* represent the fractionation between dissolved and gaseous CO_2 (dg), bicarbonate and carbonate species (bc) bicarbonate and dissolved species (bd). [CO_3^{2-}], [HCO_3^-] and [DIC] are respectively the concentration of carbonate, bicarbonate and total concentration of dissolved carbon. ε_{dg} is determined considering the equation of Mook et al. (1974), ε_{bd} and ε_{bc} are calculated with the equations proposed in the paper of Freeman and Hayes (1992). In the same way, organic carbon $\delta^{13}C$ can be calculated by resolving this equation:

$$\delta_{Corg} = \delta_{H_2CO_3} - \varepsilon_p \tag{14}$$

Where e_p is the biological fractionation calculated with an equation modified from Freeman and Hayes (1992).

Calibration procedure

As a first step, the model has been calibrated using present-day conditions (with 4 oceanic reservoirs) in order to parameterize constants of weathering laws and get the current values proposed by Gaillardet et al. (1999) for global silicate (5.85×10^{12} mol/yr) and carbonate (12.3×10^{12} mol/yr) weathering fluxes. In this procedure, we need to assume that all present-day cycles are in equilibrium (i.e. concentrations of constituents remain constants in each reservoir). In this way, the organic carbon sub-cycle (organic carbon burial and continental kerogen weathering fluxes) is in balance and the atmospheric CO_2 consumed by silicate weathering is compensated by the global CO_2 degassing. Alkalinity and concentrations of DIC, phosphorus and oxygen in surface ocean, thermocline and deep ocean are in agreement with the average present-day gradients.

The Devonian pre-perturbation state has been obtained by changing, primarily, the oceanic configuration, the continental distribution and the solar luminosity. The continental distribution in each latitudinal band (ocean-continent ratio) has been set using the classical paleogeographical charts of Parrish (1985). The solar luminosity has been reduced by 2.4% (Gilliland, 1989) and the oceanic configuration has been set-up to represent the Late Devonian paleogeography with a restricted Prototethys ocean , more or less isolated between the Laurussia and Gondwana continents and an open well oxygenated Panthalassa ocean (Fig. 1). The Prototethys ocean is made of a surface ocean, a thermocline and a deep ocean with a depth down to 3000 m. Panthalassa consists of two surface ocean (polar and equatorial), a thermocline and a deep ocean to a depth of 11 000m (average of 5000m). Oceanic exchanges between both of these reservoirs are fixed in order to have a deep Prototethys reservoir isolated from the deep Panthalassa reservoir. Horizontal water fluxes between surface ocean and thermocline has been fixed to 15 Sv (Sverdrup, $10^6 m^3/s$) for the calibration that represent a good communication between Prototethys and Panthalassa. The oceanic circulation in the Panthalassa ocean is designed to be representative of the present-day average thermohaline circulation. Vertical water fluxes in the Prototethys ocean are defined to have a simple mixing without strong upwelling (Goddéris and Joachimski, 2004). All these considerations are summarized in figure 2.

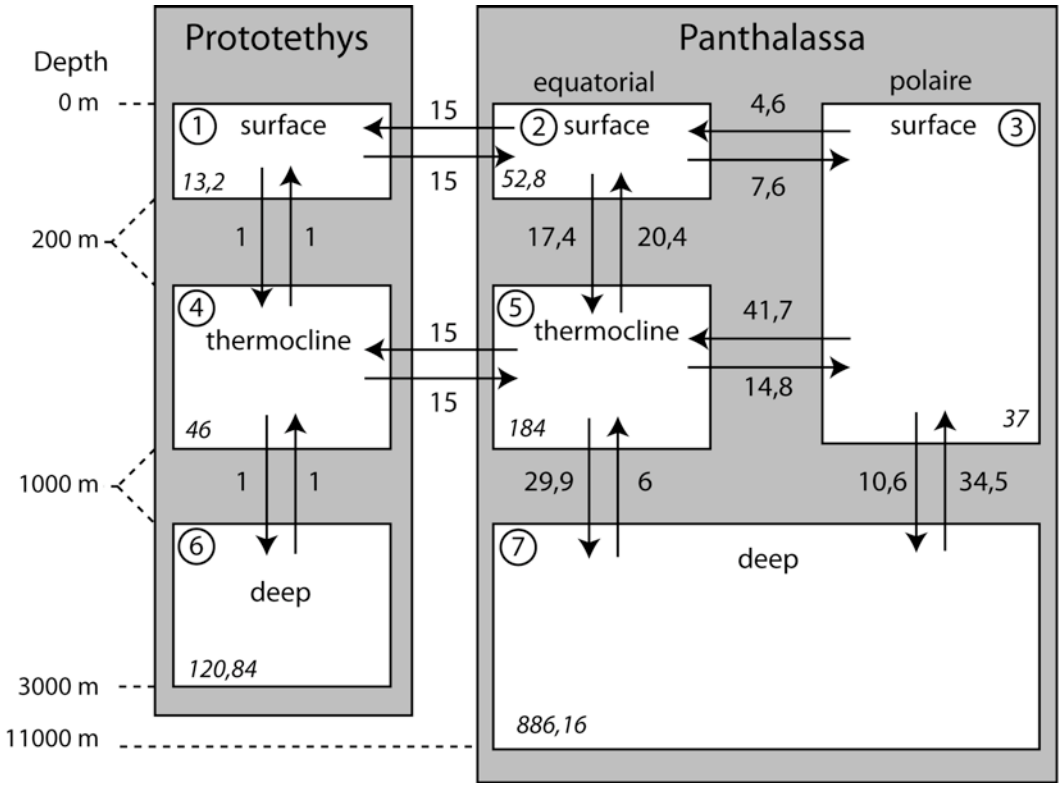

Figure 2. Schematic view of the oceanic configuration considered in the model for the Late Devonian calibration procedure. Water fluxes are in $10^6 m^3/s$ (Sverdrup) and volumes of the reservoirs (italic) are in $10^{15} m^3$

To obtain a pre-perturbation state with concentrations of atmospheric CO_2 and oceanic $d^{13}C$ values in the range of those estimated for the Upper Devonian times (e.g. Goddéris and Joachimski, 2004), the global flux of carbon degassed from mantle (continental and oceanic ridge volcanism) has been decreased to 5.3×10^{12} mol/yr with a carbon isotopic signature of -1‰. Furthermore, carbon isotopic ratio of continental carbonate and continental kerogen have been fixed to 1‰ and -24‰ respectively. Concerning the mechanical erosion on continents, the clastic flux has been decreased to 30% of the present-day flux in each latitudinal band. This consideration is based on the fact that, the present-day clastic flux, which has not yet been determined, is probably one of the highest of the Phanerozoic due to the large mountain ranges covering presently the Earth surface and the relatively cold climatic conditions prevailing during recent times. Based on this estimation, the model reaches an Upper Devonian pre-perturbation steady-state caracterised by atmospheric carbon dioxide and oxygen concentrations of 3104 ppmv and 18.65% respectively resulting in a global average temperature of the earth surface of 293 K.

Model results

We first tested the impacts of mechanical erosion intensification and Prototethys isolation separately in order to observe the response of the system to each perturbation. In a second stage, both perturbations were coupled to evaluate the possible interactions between these mechanisms. Finally, a scenario is proposed to simulate a two-phase organic carbon storage event akin to that represented by the Lower and Upper Kellwasser horizons in Late Frasnian times.

The impact of the mountain-building related erosional increase

In these simulations, the clastic flux ($Fclast_i$) has been increased between the 30°N and 30°S latitudes (representative of the Appalachian-Early Variscan belt localization) from the pre-perturbation equilibrium state (30% of the present-day value) to 60%, 90% and 120% of the present-day clastic flux. In this way, we tested a sub-equatorial orogenic event leading to physical erosion rates lower or slightly higher than the present-day value (which has not yet been determined). The clastic flux remained unchanged in the rest of the Earth surface (i.e., from 30°N to 90°N and from 30°S to 90°S). The time-dependance of the erosional increase was based on the classical view that a mountain belt grows during a transient morphological stage in which the earth surface is progressively uplifted to reach a global steady-state topography (e.g. Burbank and Anderson, 2001). A that point, the erosional rates globally equilibrate uplift rates and afterwards do not increase anymore (but stay at the maximum value until the mountain belt collapse). The duration of such transient period of mountain growth is, of course, difficult to estimate for ancient orogenic events but can be approached using the sedimentary record in the proximal flexural troughs bordering the mountain belts. Actually, it is generally thought to correspond to the recurrent transition, occuring in foreland basins, from underfilled conditions (deep marine) to overfilled conditions (shallow marine or fluvial deposits) and marked by particularly high sedimentation rates (e.g. Covey, 1986). As a first approximation, the time for this transition can be crudely considered as very rapid compared to the life time of a mountain topography as suggested by the dynamics of classical Tertiary mountain belts (Alps, Himalaya) whose reliefs persist since 30-40 Myr. More precise estimates are provided, however, by the Taiwan collisional belt, the most recent collisional zone on Earth (6,5 Myr after Lin et al, 2003). Modelling of the subsidence of the foreland basin actually reveals that the transient filling stage of the basin lasted about 1,5 Myr (Simoes and Avouac, 2006) i.e. that the steady-state mountain belt geometry was achieved in about 1,5 Myr. Following these recent concepts on mountain growth, we considered an average transient stage of clastic flux increase of 2 Myr, erosional fluxes increasing linearly over 2 Myr and then staying constant over 10 Myr. To test, however, the time dependance of the impact of the mechanical erosion, we performed simulations with 1 and 3 Myr linear increases of the clastic flux. During these simulations, oceanic horizontal circulations were kept constants to the value of 15 sv. in surface and in the thermocline reservoirs (deep Prototethys and Panthalassa oceans do not communicate) representing a global well-oxygenated ocean. Phosphorus fluxes issued from continental silicate weathering were injected in the Prototethys reservoir due to the proximity of uplifted areas. This point has not an heavy incidence in the present simulations because phosphorus is rapidly transferred in the Panthalassa reservoir in a well-oxygenated configuration. It is, however, worth to note that this mechanism has a significantly more severe impact on oxygenation conditions in a Prototethys isolated configuration (discussed in the next section).

The Figure 3. presents the results of the reference simulation, including a clastic flux linear increase (from 0.3 to 0.9, normalized to present-day) between 30°N and 30°S during 2Myr.

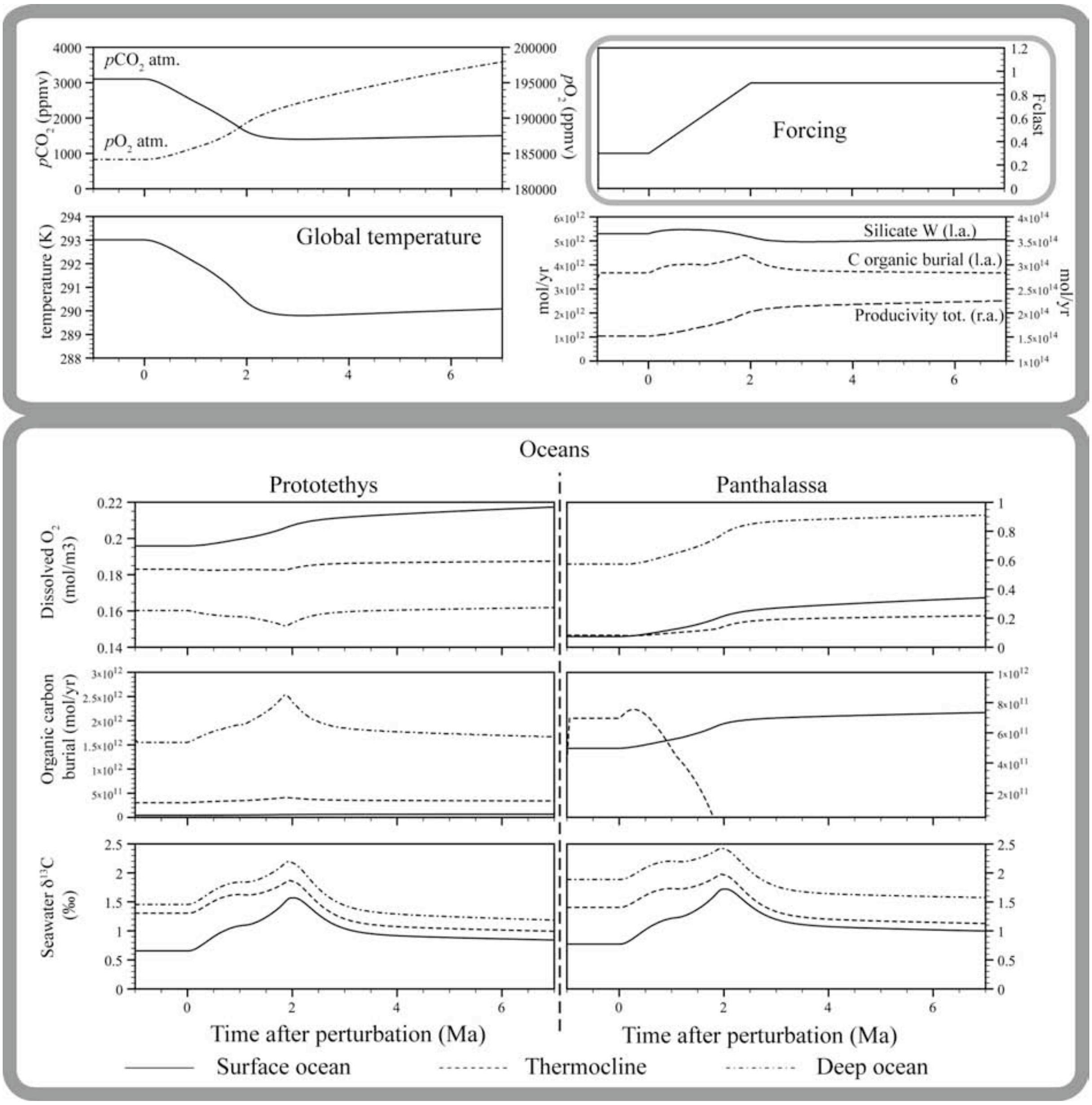

Figure 3. Upper pannel: atmospheric pCO_2 *and* pO_2, *global annual surface temperature, continental silicate weathering, global oceanic surface productivity and global oceanic organic carbon burial in response to an increase in clastic flux from 0.3 to 0.9 (it's present-day value) between 30°N and 30°S during 2Ma (forcing diagram).Lower pannel: Comparative evolutions of the Prototethys and Panthalassa oceanic reservoirs in terms of dissolved oxygen concentration, organic carbon burial and sea-water* $\delta^{13}C$.

A first point to be noticed is that the responses are significantly different in the Prototethys and Panthalassa oceans. Actually, organic carbon burial is dominantly localized in the Prototethys ocean due to a decline of dissolved oxygen concentration in the deep oceanic reservoir. In this run, intensification of the clastic flux leads to increased phosphorus input into the Prototethys resulting, however, in increased oceanic surface productivity in the both oceans (because phosphorus is easily transferred to the Panthalassa ocean). Consequently, a greater amount of organic matter is remineralized in deepest reservoirs of both oceans. This process leads to an increase of organic carbon burial in deepest reservoirs of the stratified Prototethys ocean. However, because organic carbon burial is an oxygen source for the long-term oxygen cycle, the concentration of atmospheric O_2 increases during the intensification of carbon organic burial. Therefore, dissolved oxygen concentrations in each oceanic reservoir of Panthalassa and in the surface Prototethys reservoir increase because surface seawater is in equilibrium with the atmosphere and also because Panthalassa is a well-oxygenated ocean, i.e. with a strong mixing. As a result, organic carbon burial decreases in deepest Panthalassa oceanic reservoirs. Note that the organic carbon burial in surface reservoirs of both oceans depends solely on the surface productivity. Therefore, the organic carbon burial increases in each surface ocean reservoir.

When the clastic flux reaches its maximum value, the perturbation stabilizes and the system reaches a new steady-state characterized by an atmosphere with a lower CO_2 content and a higher O_2 concentration. This coupling is explained by the photosynthesis reaction that can be summarized as follows :

$$CO_2 + H_2O \rightarrow CH_2O + O_2$$

Following this equation, the intensification of the organic carbon (CH_2O) sequestration leads to a decrease in atmospheric CO_2 but also to a decrease in O_2 consumption rates *via the* oxidation of organic matter. As a result, the O_2 concentration in the ocean-atmosphere system increases. The atmospheric CO_2 concentration decline leads, in this simulation, to a 3.2°C lower global temperature and to a decrease of the aragonitic carbonate production on shelves.The carbon isotopic ratio $d^{13}C$ evolves in the same way for both oceans and shows a 0.9‰ positive excursion in the surface reservoirs. Deepest reservoirs record a lower positive excursion. This worldwide positive excursion is the result of the increase of the ^{12}C-rich organic matter burial in the Prototethys Ocean but is also balanced by the continental carbonates and kerogen weathering.

In this simulation, the surface productivity is directly linked to phosphorus input and in turn, to the mountain building-related continental silicate weathering. However, the latter is also strongly influenced by the global climate (T and Runoff). As a result, the phosphorus input in the Prototethys ocean does not evolve similarly than the clastic flux. Figure 4 shows the evolution of surface oceanic productivity and phosphorus input with time. At the beginning of the mechanical erosion rate intensification, the silicate weathering rate increased, together with the phosphorus input. However, following the Urey reaction, the increase in silicate weathering leads to an higher atmospheric CO_2 consumption rate. It results in a negative feedback that balances the effect of the mechanical erosion and leads finally to a decrease of the phosphorus input in the surface oceans when the effect of cooling becomes predominant (Fig. 4). Therefore, the phosphorus input from continental weathering decreases 0.5 to 1 Ma after the initiation of the perturbation.

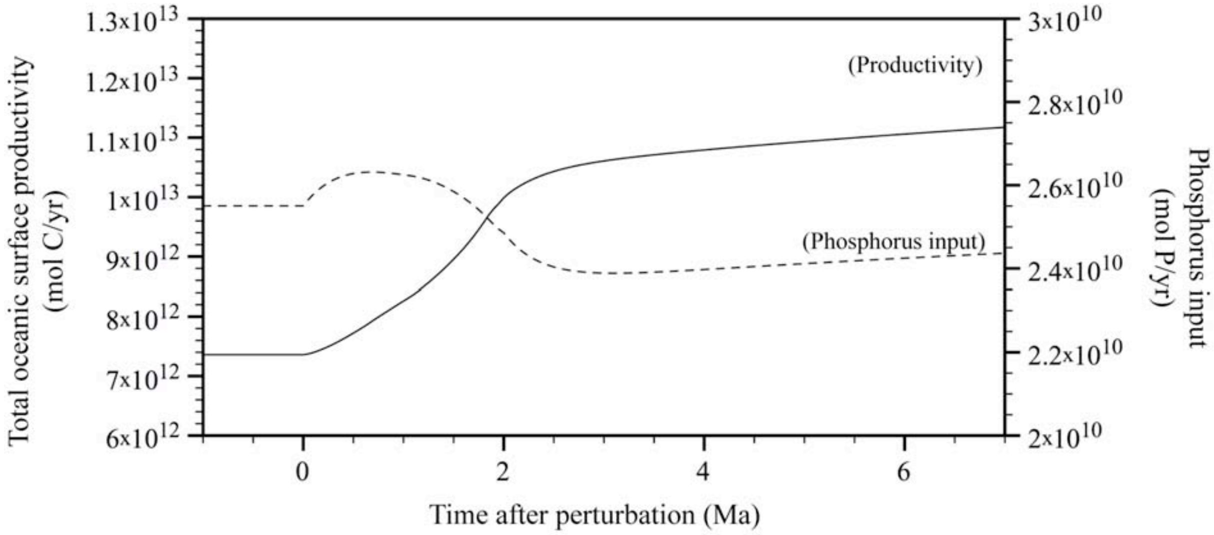

Figure 4. Evolution of surface oceanic Protethys productivity and phosphorus input in response to an increase in clastic flux from 0.3 to 0.9 (it's present-day value) between 30°N and 30°S during 2Ma.

However, phosphorus recycling is intensified in the water column in response to the decrease in O_2 concentration in thermocline and deep Prototethys. Indeed, phosphorus is easily remobilized from the sediment to the water column during episodes of poor oxygenation (Van Capellen, 1996). As this process is involved in the model (cf. model characteristic), the oceanic surface productivity in the Prototethys and in the Panthalassa oceans increases during the perturbation phase (Figure 3). This intensification increases the consumption of O_2 in deepest reservoir *via* remineralisation processes of OM.

This first simulation thus points out that the intensification of the continental erosion induces an increase of the surface ocean productivity by two ways: (1) primarily, the phosphorus input increases at the onset of the uplift but decreases when the climate becomes colder; (2) it is then relayed by an enhanced phosphorus recycling in the thermocline and deep reservoirs of the Prototethys ocean associated with the development of poor-oxygen water conditions. This evolution is balanced by the intensification of O_2 in the atmosphere via the carbon organic preservation in sediments (oxygen feedback).

To further consider the time dependence of such processes, two additional sensitivity tests have been performed considering clastic flux increases of the same amplitude than the reference simulation (from 0.3 to 0.9 of its present-day value) but with varying duration from 1 to 3 Ma. In both cases, we observe an intensification of organic carbon sequestration but more or less spread over time (Fig. 5).

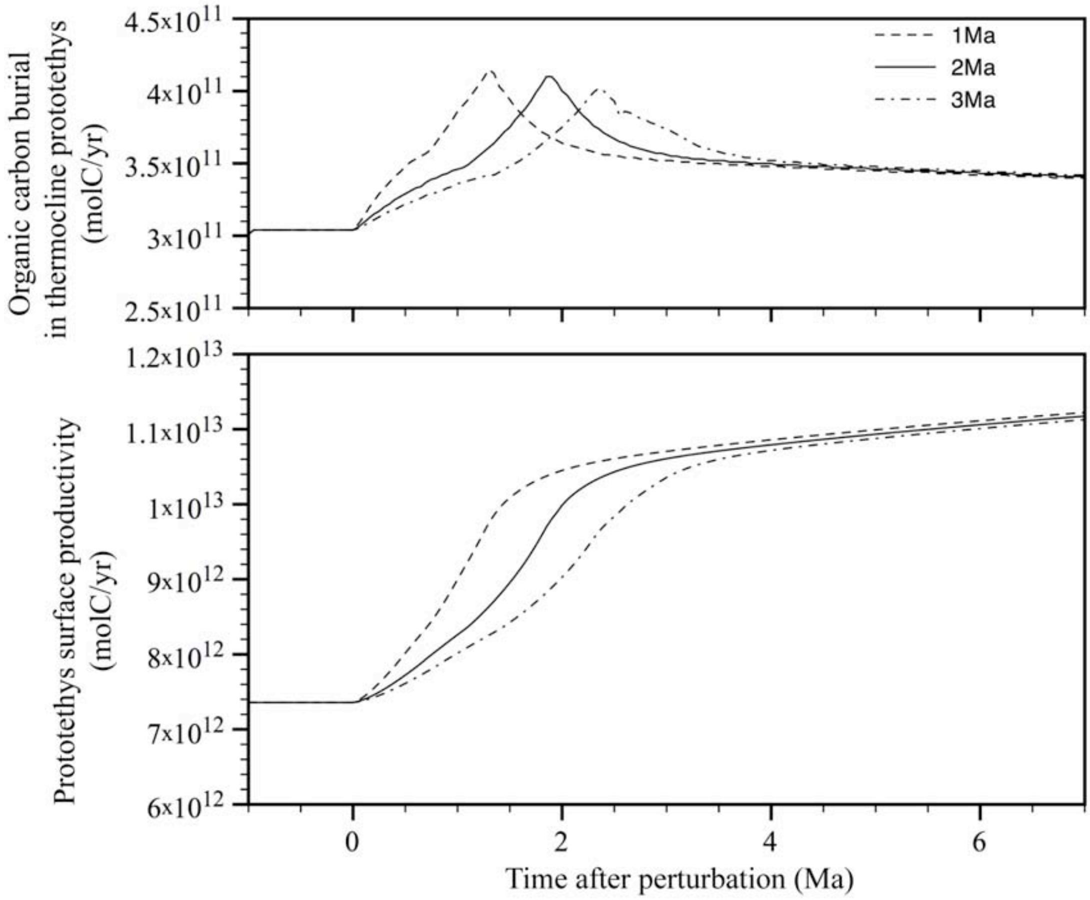

Figure 5. Evolution of oceanic surface productivity and organic carbon burial in the thermocline reservoir of the Prototethys ocean as a function of the duration of clastic flux intensification.

For a 1 Ma linear increase of the clastic flux, the peak of the organic carbon burial event occurs 1.3 Ma after the perturbation. The peak for the 3 Ma and 2 Ma simulations occur after 2.2 Ma and 2 Ma, respectively. These maxima of organic carbon burial correspond with the inflexion point of the surface productivity curve (Fig. 5). At this point, actually, O_2 concentration in the thermocline and in the deep Prototethys reservoirs increases because O_2 consumed by organic carbon remineralization is not maintained. Concerning the amplitude of the organic carbon burial event, it is worth noting that the shorter is the duration of the erosional increase, the higher is the intensification of the organic carbon burial.

Finally, to complete our modelling approach, the amplitude of the clastic flux intensification has been tested. We performed two additional simulations with an increase of clastic flux from 0.3 to 0.6 and from 0.3 to 1.2 relative to its present-day value but with a constant duration (2 Ma). As expected, surface oceanic productivity and organic carbon burial in the thermocline of Prototethys are extremely sensitive to this parameter with peak conditions significantly depending on the amplitude of the clastic flux increase (Fig. 6). However, as clearly expressed in Fig. 6, the latter also strongly affects the duration of the carbon-cycle perturbation through the oxygen and climate negative feedbacks which tend to smooth the instability. As previously shown, the nutrient input towards Prototethys is not directly related to the mechanical erosion due to the progressive cooling of climate. On the other hand, the unconsumed oxygen induced by the OM burial favours OM remineralization thereby counteracting the carbon sequestration. Both these feedback effects operate more rapidly when the amplitude of the mechanical erosion perturbation is more pronounced. Therefore, for a same duration of transient erosional stage, the resultant perturbation of surface oceanic productivity and organic carbon burial is longer for a low clastic flux increase and shorter for a high clastic flux increase.

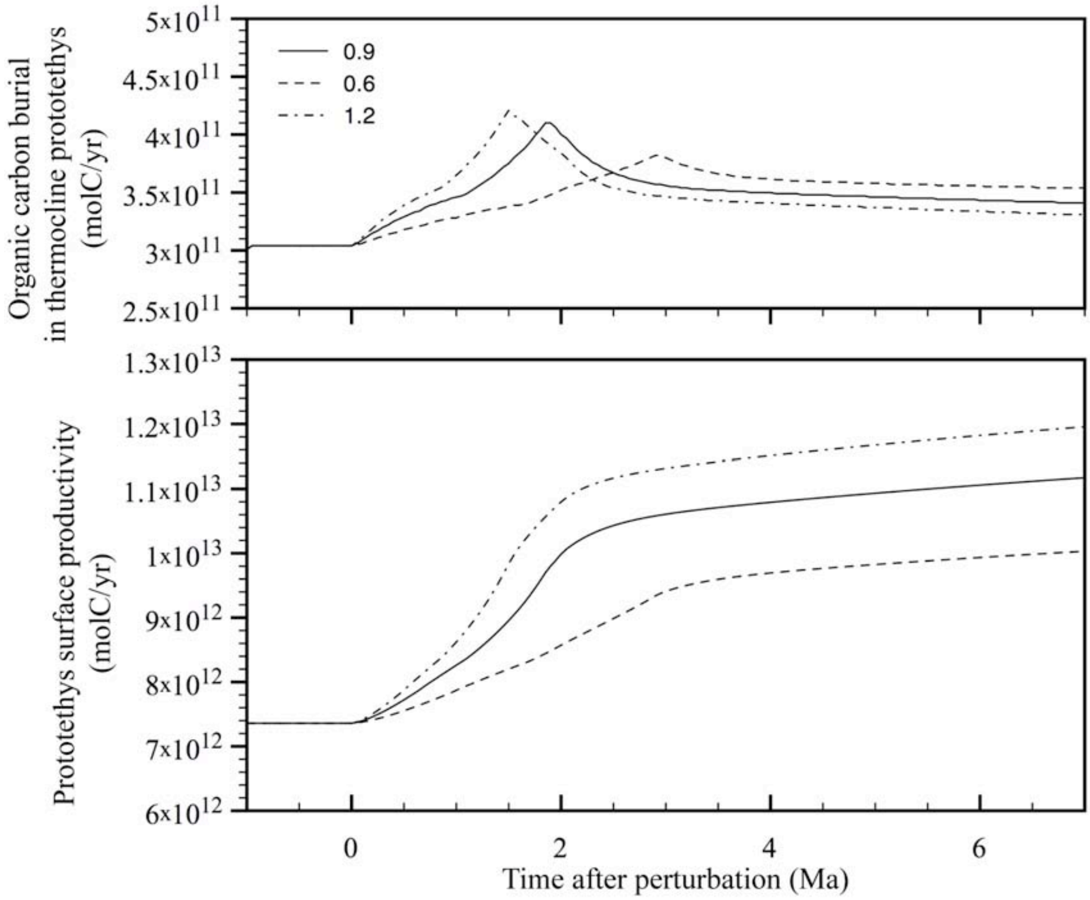

Figure 6. Evolution of oceanic surface Prototethys productivity and organic carbon burial in the thermocline reservoir as a function of the intensification of the clastic flux.

Impact of the Prototethys isolation

Late Devonian early Variscan uplift is associated with the incipient collision of the Gondwana with the Laurussia continent which is likely to have resulted in significantly more confined conditions along the Prototethys oceanic margins (Fig. 1). Based on this geodynamical context, we have tested the impact of the isolation of this ocean by decreasing the water fluxes between surfaces and thermoclines reservoirs of the Prototethys and Panthalassa oceans. In the reference run, we have decreased these fluxes from 15Sv to 1Sv between the thermoclines and 15Sv to 5Sv between surface oceans, representative of a strong isolation and in agreement with the fact that the seaways between Prototethys and Panthalassa were restricted to continental platforms (Scotese and McKerrow, 1990). Note that there is no communication between the deepest reservoirs of both oceans. A similar isolated configuration has already been proposed in the modelling approach of Goddéris and Joachimski (2004).

As expected, the isolation of the Prototethys ocean leads to the development of suboxic to anoxic conditions in its thermocline and deep reservoirs (Fig. 7), and consequently to an increase in organic carbon burial. Such increasing trend is not observed in the Panthalassa ocean that becomes more oxygenated in response to the increase in atmospheric oxygen concentration (increase linked to the intensification of the sequestration of organic carbon). During the decrease in oxygen concentration in the thermocline and deep reservoirs of Prototethys ocean, we observe an oxygenation phase associated to the increase of oxygen content in the atmosphere. This process is a negative feedback caused by the increase of organic carbon burial (Fig 8). This isolation leads to the burial of great amount of organic carbon burial only under the surface reservoir of Prototethys ocean resulting in a decrease in the CO_2 concentration in the atmosphere and a related cooling. As a result, phosphorus input via silicate weathering decreases but surface oceanic productivity in Panthalassa remains constant through 1 Ma after the onset of the perturbation and decreases drastically until 2 Ma (Fig. 9). The surface Prototethys ocean is sensitive to the continental phosphorus input via silicate weathering since the communication with deeper reservoirs is restrained. Consequently, surface productivity into this reservoir decreases as a fonction of continental phosphorus input. However, development of disoxia in deeper reservoirs leads to increasing the phosphorus content of the thermocline and deep Prototethys *via* the solubilisation of phosphorus in sea-water (Van Cappellen and Ingall, 1996) and compensates the decrease of continental phosphorus source.

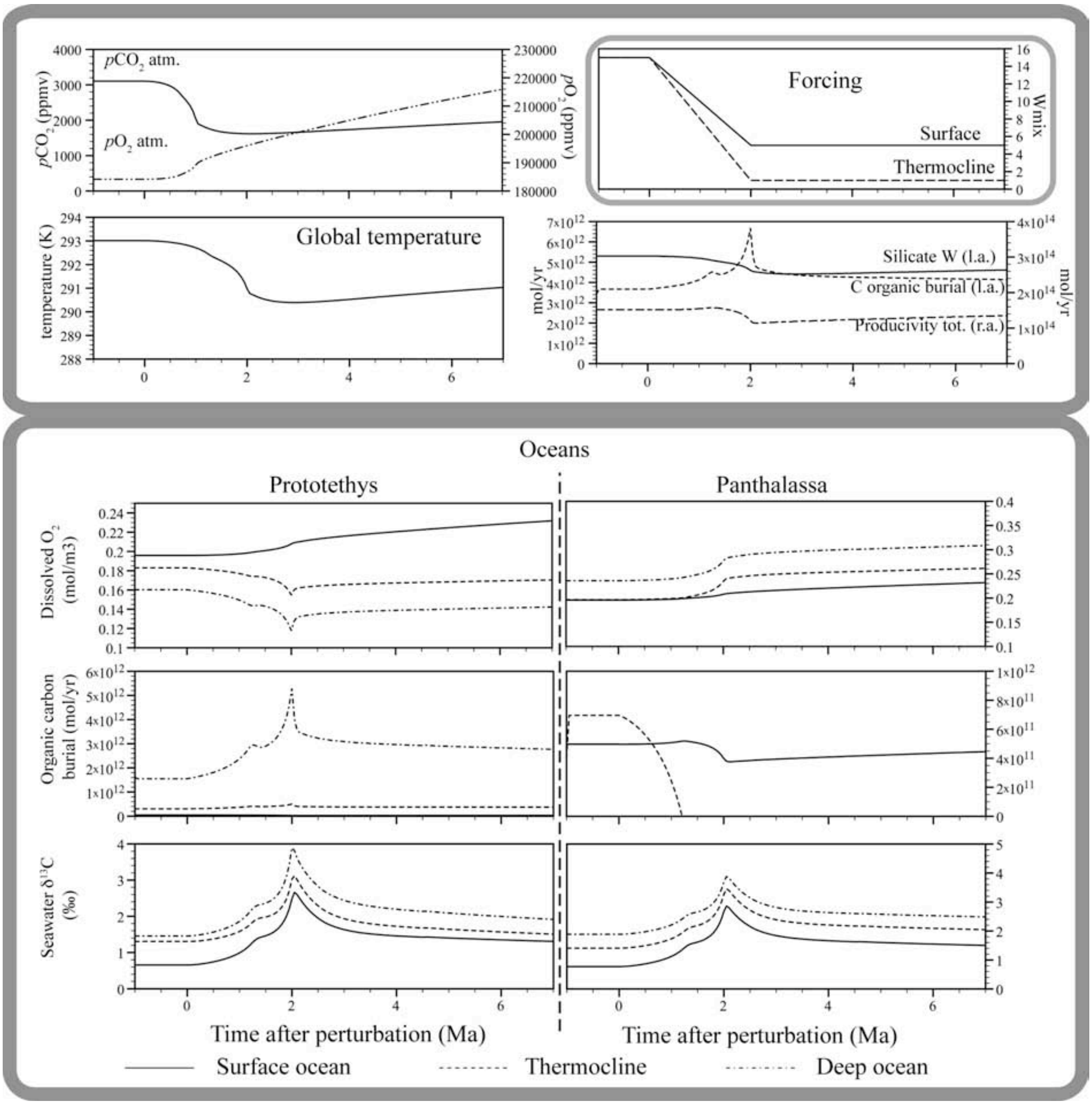

Figure 7. Upper pannel: atmospheric pCO_2 and pO_2, global annual surface temperature, continental silicate weathering, global oceanic surface productivity and global oceanic organic carbon burial in response to a decrease in water fluxes between equatorial surface reservoirs and thermocline reservoirs of Prototethys and Panthalassa ocean from 15 Sv to 5 Sv and 15 Sv to 1 Sv respectively during 2Ma (forcing diagram). Lower pannel: Comparative evolutions of the Prototethys and Panthalassa oceanic reservoirs in terms of dissolved oxygen concentration, organic carbon burial and sea-water $\delta^{13}C$.

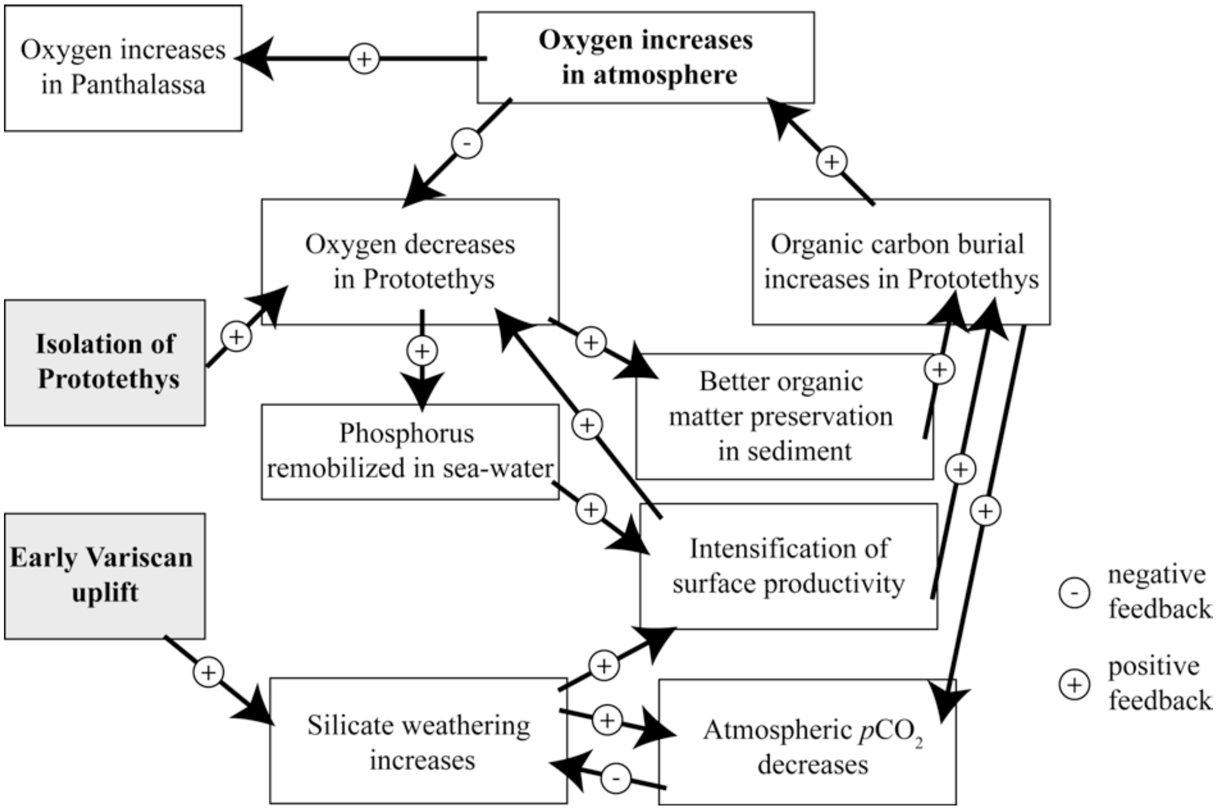

Figure 8. Schematic view of the oxygen feedbacks observed in our model.

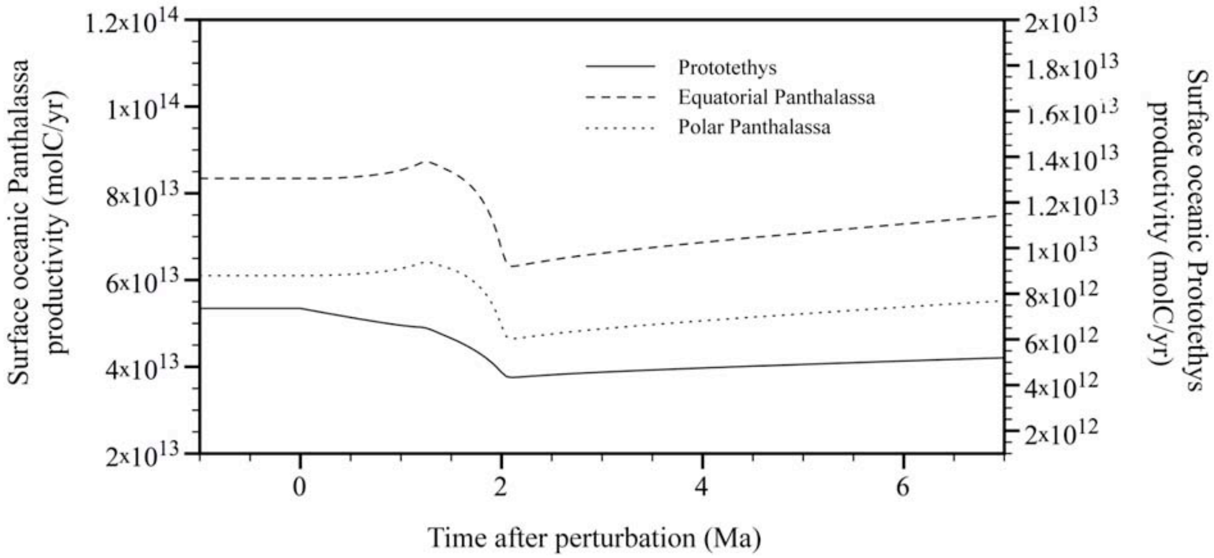

Figure 9. Evolution of surface oceanic productivity in each surface reservoir in response to the isolation of the Prototethys ocean.

For the Panthalassa ocean, surface productivity is more sensitive to the connection between the both oceans. Indeed, in this simulation phosphorus input is drained toward the Prototethys ocean and is distributed into Panthalassa via the water fluxes (i.e. there is no phosphorus input in Panthalassa from continental weathering). As a result, the system reaches a threshold 1 Ma after the onset of the perturbation when the communication between the Prototethys and Panthalassa thermoclines becomes too low to preserve a high surface productivity in Panthalassa.

We have tested the impact of the duration of the reduction of water exchanges on the system. We performed two simulations with the the same parameters for the water fluxes than for the reference run but with a 1 Ma extension for the first and 3 Ma for the second. The figure 10 presents the organic carbon burial in Prototethys thermocline for this two simulation and for the reference simulation for the isolation. Whatever the duration of the process, we observe the same evolution as described earlier, but we can observe that the shorter the duration is, the higher the organic carbon burial is and thus the faster the cooling.

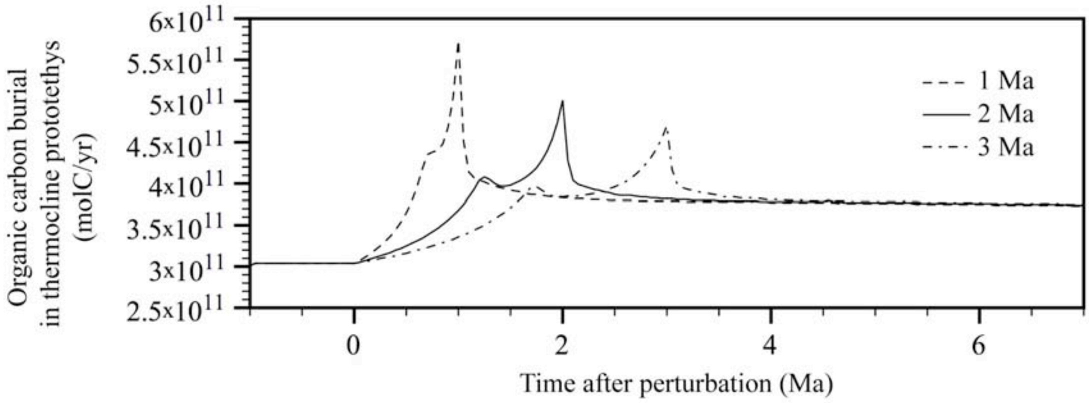

Fig 10. Impact of the duration of the isolation process on the organic carbon burial in the Prototethys thermocline

However, whatever the duration of the perturbation, the organic carbon burial seems to be sensitive to the way both thermoclines of the Prototethys and Panthalassa communicate. To that end, we performed two other sensitivity tests on the degree of isolation of Prototethys (Fig. 11). In the first (the strong isolation simulation), we decreased the Wmix between surface and thermocline reservoirs of both oceans from 15 to 1 Sv. Compared to the reference simulation, organic carbon burial increase is unexpectedly lower. It can be explained by a lower Prototethys surface oceanic productivity linked to a stronger reduction of phosphorus input from surface Panthalassa (Fig. 11). In the second simulation (the soft isolation simulation), the water fluxes between thermoclines and surfaces reservoirs of both oceans is reduced from 15 Sv to 5 Sv. As a result, organic carbon burial is the lowest of the three simulations, whereas productivity keeps higher than the reference and strong isolation simulations. Indeed, in the soft isolation run, the oxygenation of the thermocline reservoir of Prototethys is favoured by an efficient mixing compared to the strong and reference isolation simulations.

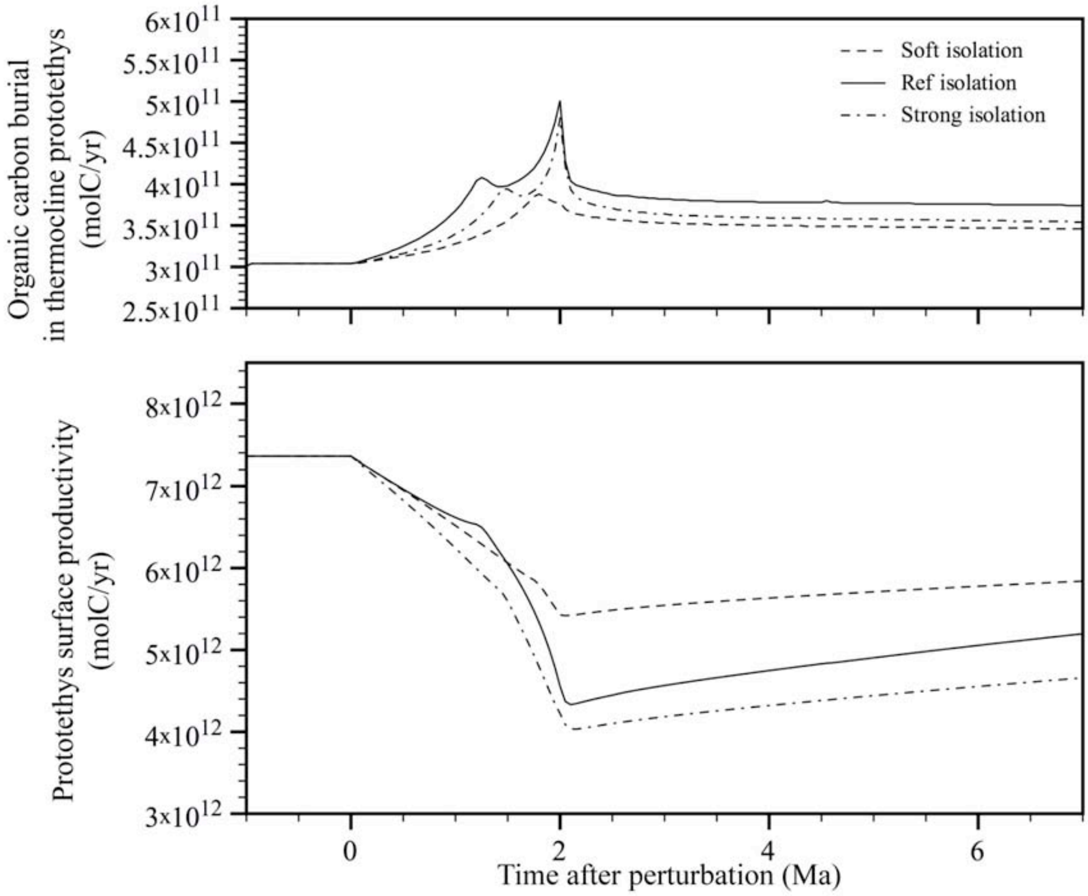

Figure 11. Impact of the intensity of the Prototethys isolation on the surface productivity and organic carbon burial in thermocline.

To summarize, our model thus shows that the isolation of the Prototethys, related to the collisional context, leads to the increase of organic carbon burial only in the thermocline and deep reservoirs (below 200 meters) of Prototethys. It is noteworthy that the perturbation of the system occurs only during the time of reduction of the communication between both oceans. The organic carbon burial is sensitive to the input of phosphorus in Prototethys and to the oxygenation of its deeper reservoirs (thermocline and deep). Indeed, on one hand, if the communication between surface reservoirs is strongly reduced, the Prototethys ocean tends to be phosphorus depleted and thus the exported productivity tends to be lower (strong isolation simulation). On the other hand, organic carbon burial is reduced if thermocline is more oxygenated by the Panthalassa thermocline (soft isolation simulation). This point is really important because modelling shows that a complete isolation of Prototethys is not necessary to obtain a strong carbon cycle perturbation. Indeed, a good communication between surface reservoirs of both oceans is required to maintain a significant productivity in the Prototethys. If such productivity is maintained in surface, it is worth to note that the stronger the thermocline isolation is, the stronger the perturbation should be.

Coupling Early Variscan uplift erosion and Prototethys isolation

As previously mentioned, the Frasnian-Famennian environmental changes (exemplified by the two superposed organic carbon rich Kellwasser horizons) are suggested to result from a major carbon cycle perturbation in response to the onset of the Variscan uplift and the related Prototethys isolation. To test the possible interactions between both processes, we combined the reference runs for the mountain-building related clastic flux increase and the Prototethys isolation (i.e. clastic flux increased from 0.3 to 0.9 between 30°S and 30°N in 2 Ma and reduction of the water fluxes from 15 to 5 Sv and 15 to 1 Sv in 2 Ma between surfaces oceans and thermocline reservoirs of Prototethys and Panthalassa respectively)(Fig. 12). Our numerical simulations pointed out the importance of negative feedbacks (climate and oxygen) thereby emphasizing the time-dependence of the studied processes. The coupling of the mechanical erosion and Prototethys isolation increases is thus very likely to differ depending on the duration of the phenomenons and of their in-phase or out-of-phase character.

In the following simulations, we tested a scenario where these two forcing mechanisms have been set to be in phase, i.e. the perturbation for each process begin at the same time t=0. The results are very close to those presented previously for the Prototethys isolation reference run. However, the amplitude of the response of the system is stronger here, resulting in the additional effects of anoxia in the deep reservoir of Prototethys and the intensification of the phosphorus input during this anoxic event via continental erosion. Therefore, the oceanic surface productivity is stronger than in the Prototethys isolation reference run resulting in globally enhanced organic carbon burial in Prototethys that in turn leads to a more pronounced $\delta^{13}C$ excursion and a more severe drop of the atmospheric pCO_2. As exemplified in Fig. 12, the modelled carbon-cycle perturbation results in a decrease in atmospheric pCO_2 from 3100 ppmv to 760 ppmv in 2 Ma which is very close to the sharp decrease of atmospheric pCO_2 estimated from paleosoil studies for Late Devonian times (Yapp et al., 1996 and Mora et al., 1992 in Royer, 2006)(Fig. 13). Such decrease corresponds to a 5°C to 6°C cooling based on EBM calculations i.e. a temperature drop that could potentially initiate the installation of an ice sheet on Gondwana. This estimation is in the range of that calculated by Joachimski and Buggish (2002) using the oxygen isotope record ($\delta^{18}O$).

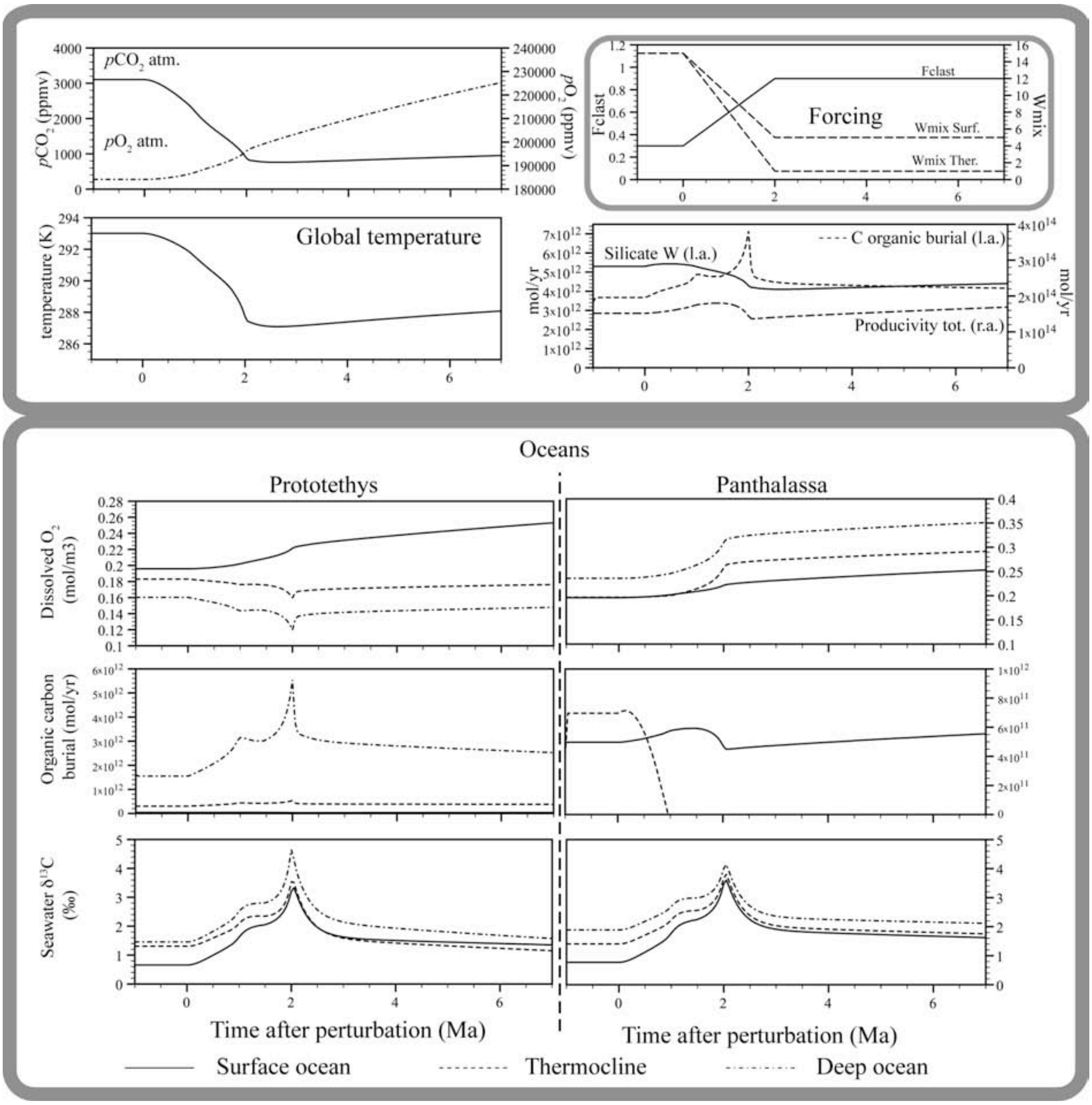

Figure 12. Upper pannel: atmospheric pCO_2 *and p*O_2*, global annual surface temperature, continental silicate weathering, global oceanic surface productivity and global oceanic organic carbon burial in response to a decrease in water fluxes between equatorial surface reservoirs and thermocline reservoirs of Prototethys and Panthalassa ocean from 15 Sv to 5 Sv and 15 Sv to 1 Sv respectively during 2Ma and to a synchronous increase in clastic flux from 0.3 to 0.9 (it's present-day value) between 30°N and 30°S during 2Ma. (forcing diagram). Lower pannel: Comparative evolutions of the Prototethys and Panthalassa oceanic reservoirs in terms of dissolved oxygen concentration, organic carbon burial and sea-water* $\delta^{13}C$.

In more detail, we observe in the Prototethys surface reservoir an intensification of productivity associated with a first postive excursion of $\delta^{13}C$ at t=1Ma (Fig. 14). Then, the

surface productivity decreases thereby reducing the carbon sequestration and $\delta^{13}C$ reaches a plateau. The latter, then, increases a second time to a maximum value (+3.3‰) due to a second phase of organic carbon burial intensification associated to a lower oxygenation of the thermocline and deep reservoirs of the Prototethys (the surface productivity decreases during that phase). The coupling of mountain-building induced mechanical erosion enhancement and Prototethys isolation thus generates a two-phase carbon cycle perturbation resulting in two $\delta^{13}C$ excursions, comparable to that observed in Late Frasnian times (the Lower and Upper Kellwasser events). As exemplified in Fig. 14, the first one is driven by the significant increase of productivity promoted by the mechanical erosion enhancement whereas the second one is developed about 1 Ma later by the development of anoxia in Prototethys.
Such a contrasting origin of the Kellwasser organic carbon burial events have been proposed by Riquier et al. (2006) based on inorganic geochemical markers from these horizons in the Harz region (Germany). These authors proposed that the Lower Kellwasser horizon could be caused by an increase in surface primary productivity leading to the development of dysoxic to anoxic conditions in the deep basins. Conversely, they suggested that the Upper Kellwasser horizon could be caused by anoxia developing from bottom water to shallower environments via strong water stratification during the Late Frasnian maximum flooding. Our modelling results globally corroborates such scenario at the end of the Frasnian.

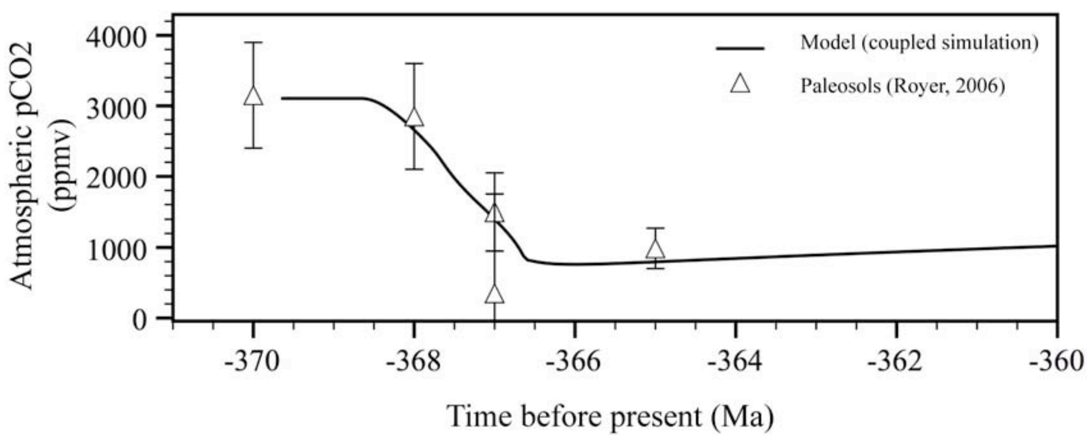

Figure 13. Evolution of atmospheric pCO_2 *for the coupled simulation compared to data from Royer, 2006.*

However, the modelled $\delta^{13}C$ curve does not fit perfectly the $\delta^{13}C$ dataset compiled by Goddéris and Joachimski (2004), particularly for the first excursion (the Lower Kellwasser). The second excursion and the post-perturbation $\delta^{13}C$ value, significantly higher than prior both excursions, are in adequation with the data (Fig. 14).

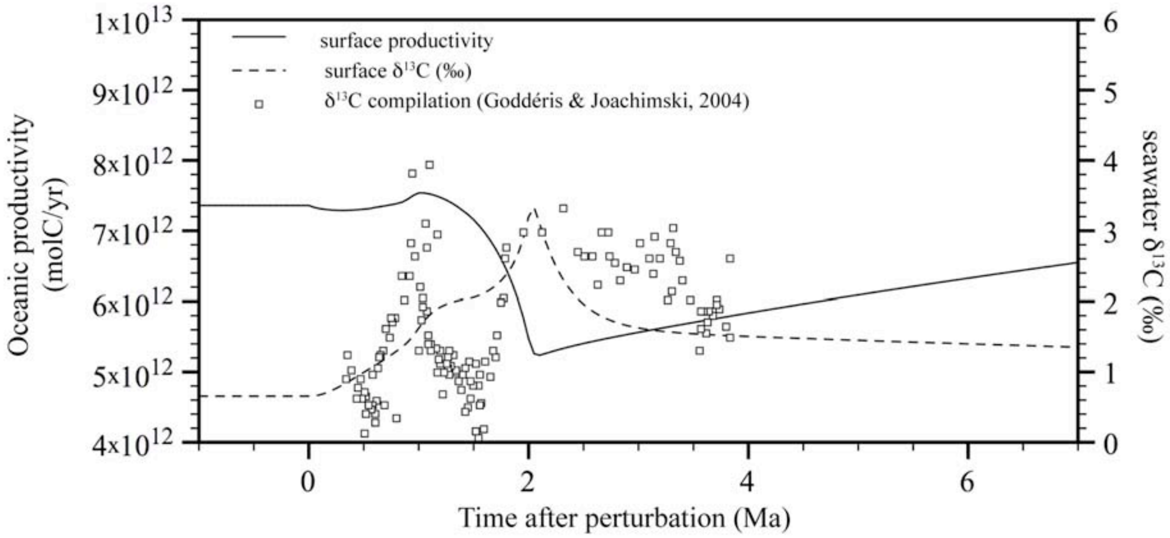

Figure 14. Evolution of Prototethys surface productivity and surface Prototethys seawater $\delta^{13}C$ for the simulation coupling intensification of the clastic flux and Prototethys isolation. $\delta^{13}C$ results are compared to the dataset compiled by Goddéris and Joachimski (2004).

If we consider that the second excursion produced by our model corresponds to the second excursion recorded in the $\delta^{13}C$ dataset compiled by Goddéris and Joachimski (2004), our modelling does not produce a first positive excursion strong enough. Therefore, we made sensitivity tests in order to see the impact of the duration of clastic flux intensification, in the context of the Prototethys isolation, on the first part of the isotopic curve. In these simulations, the model is forced by the isolation of the Prototethys in the same way than for the isolation reference run, and the clastic flux is intensified from t=0 to 1Ma for the first and 3Ma for the second. Surface Prototethys δ^{13}C results for these runs are compared with that from the reference simulation coupling clastic flux and Prototethys isolation (Fig. 15).

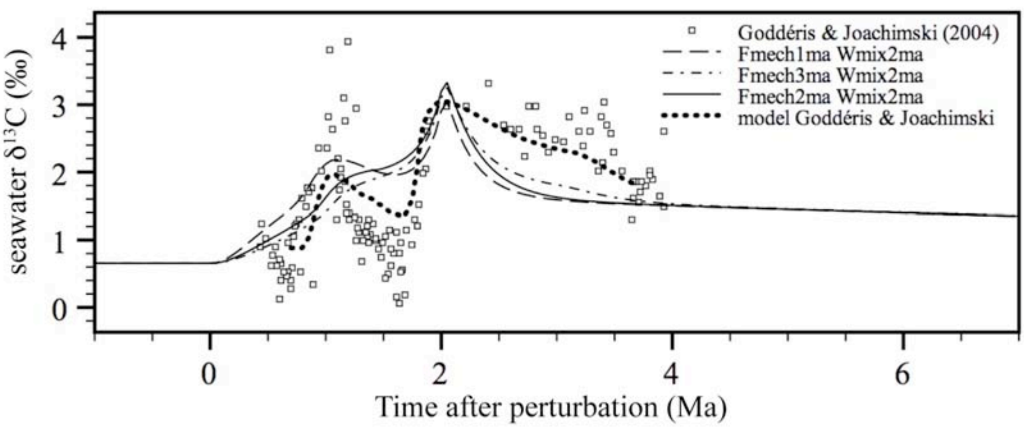

Figure 15. Impact of the duration of the intensification of the clastic flux for a simulation coupling erosion and isolation on surface Prototethys $\delta^{13}C$ signal compared to dataset and modelling by Goddéris and Joachimski (2004).

As expected, we observe that the first $\delta^{13}C$ positive excursion is stronger if the intensification of the classic flux is fast. Indeed, for an intensification of the clastic flux from 0.3 to 0.9 during 1 Ma coupled with an isolation of the Prototethys ocean increasing over 2 Ma, we observe two positive excursions that could be roughly correlated with the $\delta^{13}C$ dataset (Fig. 15, dashed line). This result approaches the modelling results of Godderis and Joachimski (2004) without taking into account the variations of sea-level and the related variations of the carbonate/shale ratio of the continental area that could also influence the amplitude of the $\delta^{13}C$ signal. As emphasized by these authors, the weathering of the carbonate platforms, exposed after the base Famennian sea-level fall, could account for a 1.7‰ $\delta^{13}C$ positive excursion during the Early Famennian. Such processes, that are not considered in our modelling study, could possibly explain the difference observed between our results and the isotope dataset, especially for the end of the $\delta^{13}C$ anomaly.

Conclusion

The global carbon cycle modelling simulations presented here allow better constraining the impact of collisional-induced mountain building on global environments and climate. We more precisely focused on the Early Variscan uplift and its possible effects on the Upper Devonian environmental changes. Using a geochemical box model coupled with an EBM climate model, we tested, as a first step, the impact of the early Variscan uplift and the associated increase of the clastic flux during the transient stage of mountain growth. Numerical simulations show that such process result in an intensification of the nutrient supply to the Prototethys ocean and, in turn, to an intensification of surface oceanic productivity and the development of anoxia in the deep parts of Prototethys. As a result, this process leads to an intensification of the organic carbon burial in the Prototethysian realm at depth. We, furthermore, show that this carbon cycle perturbation is more intense for a short transient time of intensification of mechanical erosion and, of course, for a stronger intensification.

In a second step, we tested the impact of the Prototethys isolation possibly resulting from the Early Varican collisional process. Our simulations show that such process leads to the development of suboxic environments in deep Prototethys (below 200m) and the gradual decline of phosphorus input due to the reduction of continental weathering connected to the climate cooling feedback. These counteracting processes result, however, is an increase of the organic carbon sequestration in Prototethys at depth. We show that the organic carbon sequestration is favoured when the thermocline and deep reservoirs of Prototethys are isolated but is conversely prevented when the surface reservoir is confined. This points out that a strong isolation of Prototethys is not required to promote a major perturbation of the carbon cycle.

As a final step, we coupled both mechanisms to simulate the possible effects of the Early Variscan collision in Upper Devonian times. Our results show that the intensification of the clastic flux in response to the uplift of the sub-equatorial mountain belt, coupled to a restricted Prototethys ocean could lead to a strong global carbon cycle perturbation akin to that observed in Late Frasnian times. This perturbation results in an intensification of organic carbon burial in the Prototethys ocean via a surface oceanic productivity increased and disoxia to anoxia development below 200m. We show that such a scenario leads to two $\delta^{13}C$ positive excursions comparable to the Lower and Upper Kellwasser excursions. The first one is connected to the direct effects of increased erosion resulting in the enhancement of the marine productivity in oceanic realms. The second one is due to delayed anoxia that originated by gradual isolation of the Prototethys as the equatorial seaway, linking it formerly to Panthalassa, reduced during the collisional process. The best fit of our modelled $\delta^{13}C$ curve with the measured $\delta^{13}C$ dataset compiled by Goddéris and Joachimski (2004) corresponds to a duration of 1 Ma of the transient stage of mountain growth (the period of drastic increase of mechanical erosion) superimposed on a 2 Ma-lasting intensification of the Prototethys isolation. However, the variations of sea-level are not taken into account in our simulations which can possibly explain some discrepancies between our results and the measured $\delta^{13}C$. The modelled two-phase carbon cycle perturbation, coeval with the transient mountain building stage, result in a severe atmospheric pCO_2 drop (from 3100 to 760 ppmv) resulting, in turn, in an about 6°C cooling of the mean equatorial temperatures at the beginning of the Famennian. These results are in good agreements with both the pCO_2 drop estimates of Royer (2006) and the cooling estimates of Joachimski and Buggish (2002) for the Frasnian-Famennian times. It is noteworthy that such a cooling could have initiated the installation of an ice sheet on Gondwana as early as the base Famennian times as suggested by the severe sea-level drop (>75 m following Haq and Schutter, 2008) occuring at the Frasnian-Famennian boundary. Based on our modelling approach, the Early Variscan mountain building event and its impact on the oceanic circulations thus appears as a particularly relevant phenomenon to account for the Frasnian-Famennian climatic and environmental changes and the initiation of the Upper Paleozoic Icehouse stage.

References

Averbuch, O., Tribovillard, N., Devleeschouwer, X., Riquier, L., Mistiaen, B., van Vliet-Lanoe, B., 2005. Mountain building-enhanced continental weathering and organic carbon burial as major causes for climatic cooling at the Frasnian-Famennian boundary (c. 376 Ma)? Terra Nova 17, 25-34.

Ballèvre, M., Bosse, V., Ducassou, C., Pitra, P., 2009. Palaeozoic history of the Armorican Massif: Models for the tectonic evolution of the suture zones. Comptes Rendus Geoscience 341, 174-201.

Berner, R.A., Lasaga, A.C., Garrels, R.M., 1983. The carbonate-silicate geochemical cycle and its effect on atmospheric carbon dioxide over the past 100 million years. American Journal of Science 283, 641-683.

Berner, R.A. and Kothavala, Z., 2001. GEOCARB III : A revised model of atmospheric CO_2 over Phanerozoic time. American Journal of Science 301, 182-204.

Bond, D., Wignall, P.B., Racki, G., 2004. Extent and duration of marine anoxia during the Frasnian-Famennian (Late Devonian) mass extinction in Poland, Germany, Austria and France. Geological Magazine 141, 173-193.

Bond, D., Wignall, P. B., 2005. Evidence for Late Devonian (Kellwasser) anoxic events in the Great Basin, western United States, in: Over, D., Morrow, J., Wignall, P. B. (Eds.), Understanding Late Devonian and Permian-Triassic Biotic and Climatic Events: Towards an Integrated Approach. Vol. 20. Elsevier, pp. 225-262.

Bond, D., Wignall, P., 2008. The role of sea-level change and marine anoxia in the Frasnian-Famennian (Late Devonian) mass extinction. Palaeogeography, Palaeoclimatology, Palaeoecology 263, 107-118.

Bratton, J.F., Berry, W.B.N., Morrow, J.R., 1999. Anoxia pre-dates Frasnian-Famennian boundary mass extinction horizon in the Great Basin, USA. Palaeogeography, Palaeoclimatology, Palaeoecology 154, 275-292.

Brezinski, D.K., Cecil, C.B., Skema, V.W., Stamm, R. Late Devonian glacial deposits from the eastern United States signal an end of the mid-Paleozoic warm period. Palaeogeography, Palaeoclimatology, Palaeoecology, 268, 143-151.

Buggish, W., 1991. The global Frasnian-Famennian ”Kellwasser Event”. Geologische Rundschau 80, 49-72.

Burbank, D.W., Anderson, R.S., 2001. Tectonic geomorphology. Blackwell Scientific 274p.

Campbell, I. H., Allen, C. M., 2008. Formation of supercontinents linked to increases in atmospheric oxygen. Nature geosciences 1, 554-558.

Caputo, M. V., Crowell, J. C., 1985. Migration of glacial centers across Gondwana during Paleozoic Era. Geological Society of America Bulletin 96, 1020-1036.

Chen, D., Qing, H., Li, R., 2005. The Late Devonian Frasnian- Famennian (F/F) biotic crisis: Insights from $\delta^{13}C_{carb}$, $\delta^{13}C_{org}$ and $^{87}Sr/^{86}Sr$ isotopic systematics. Earth and Planetary Science Letters 235, 151–166.

Copper, P., 1986. Frasnian/Famennian mass extinction and cold-water oceans. Geology 14, 835–839.

Covey, M., 1986. The evolution of foreland basins to steady state: evidence from the western Taiwan foreland basin, in Allen, P.A., Homewood, P. (eds.), Foreland basins. International Association of Sedimentologists Special Publication 8, 77-90.

Crowell, J.C., 1999. Pre-Mesozoic ice ages; their bearing on understanding the climate system. Geological Society of America Memoirs 192, 106pp.

Dessert, C., Dupré, B., François, L.M., Schott, J., Gaillardet, J., Chakrapani, G., Bajpai, S., 2001. Erosion of Deccan Traps determined by river geochemistry: impact on the global climate and the $^{87}Sr/^{86}Sr$ ratio of seawater. Earth and Planetary Science Letters 188, 459–474.

Dessert, C., Dupré, B., Gaillardet, J., Francois, L.M., Allègre, C.J., 2003. Basalt weathering laws and the impact of basalt weathering on the global carbon cycle. Chemical Geology 202, 257–273.

Diester-Haass, L., Billups, K., Gröcke, R., François, L., Lefebvre, V., Emeis, K.C., 2009. Mid-Miocene paleoproductivity in the Atlantic Ocean and implications for the global carbon cycle. Paleoceanography 24, PA1209, doi:10.1029/2008PA001605.

Echarfaoui, H., Hafid, M., Salem, A.A., 2002. Structure sismique du socle paléozoïque du basin des Doukkala, Môle cotier, Maroc occidental. Indication en faveur de l'existance d'une phase éo-varisque. Comptes-rendus Geosciences 334, 13-20.

Edmond, J.M., 1992. Himalayan tectonics, weathering processes, and the strontium isotope record in marine limestones. Science 258, 1594-1597.

Eyles, N., 1993. Earths glacial record and its tectonic setting. Earth-Science reviews 35, 1-248.

France-Lanord, C., Derry, L.A., 1997. Organic carbon burial forcing of the carbon cycle from Himalayan erosion. Nature 390, 65-67.

François, L.M., Walker, J.C.G., 1992. Modelling the Phanerozoic carbon cycle and climate: constraints from the $^{87}Sr/^{86}Sr$ isotopic ratio of seawater. American Journal of Science 292, 81–135.

François, L.M., Walker, J.C.G., Opdyke, B.N., 1993. The history of global weathering and the chemical evolution of the ocean atmosphere system, in: Takahashi, E., Jeanloz, R., Dubie, D. (eds.), Evolution of the Earth and Planets. American Journal of Science, Internationnal Union of Geodasy and Geophysic, Washington, D.C., Geophysical monograph 74, 14, 143-159.

François, L. M., Goddéris, Y., 1998. Isotopic constraints on the Cenozoic evolution of the carbon cycle. Chemical Geology 145, 177-212.

Franke, W., 2000. The mid-European segment of the Variscides: tectonostratigraphic units, terrane boundaries and plate tectonic evolution, in : Franken W., Haak, V., Oncken, O., Tanner, D. (eds.), Orogenic processes, quantification and modelling the Variscan belt. Geological Society of London, Special Publications, 179, 35-61.

Freeman, K.H., Hayes, J.M., 1992. Fractionation of carbon isotopes by phytoplankton and estimates of ancient CO_2 levels. Global Biogeochemical Cycles 6, 185-198.

Froelich, P.N., Bender, M., Luedtke, N., Heath, G. DeVries, T., 1982. The marine phosphorous cycle. American Journal of Science 282, 474-511.

Gaillardet, J., Dupre, B., Louvat, P., Allegre, C.J., 1999. Global silicate weathering and CO_2

consumption rates deduced from the chemistry of large rivers. Chemical Geology 159, 3-30.

Gaillardet J., Galy A., 2008. Himalaya—Carbon Sink or Source? Science 320, 1727-1728.

Galy, V., France-Lanord, C., Beyssac, O., Faure, P., Kudrass, H., Palhol, F., 2007. Efficient organic carbon burial in the Bengal fan sustained by the Himalayan erosional system. Nature 450, 407-410.

Garzione, C.N., 2008. Surface uplift of Thibet and Cenozoic global cooling. Geology 36, 1003-1004.

Gilliland, 1989. Solar evolution. Palaeogeography, Palaeoclimatology, Palaeoecology (Global and Planetary Change Section) 75, 35-55.

Goddéris, Y., Joachimski, M., 2004. Global change in the Late Devonian: modelling the Frasnian-Famennian short-term carbon isotope excursions. Palaeogeography, Palaeoclimatology, Palaeoecology 202, 309-329.

Goddéris, Y., Donnadieu, Y., Trom-bozafy, M., Dessert, C., 2008. Shield effect on continental weathering: Implication for climatic evolution of the Earth at the geological timescale. Geoderma 145, 439-448.

Grard, A., François, L.M., Dessert, C., Dupré, B., Goddéris, Y., 2005. Basaltic volcanism and mass extinction at the permo-triassic boundary: Environmental impact and modeling of the global carbon cycle. Earth and Planetary Science Letters 234, 207-221.

Hallam, A., Wignall, P. B., 1999. Mass extinctions and sea-level changes. Earth-Science Reviews 48, 217-250.

Haq, B. U., Schutter, R., 2008. A chronology of Paleozoic Sea-Level Changes. Science 322, 64-68.

Isaacson, P. E., Diaz-Martinez, E., Grader, G. W., Kalvoda, J., Babek, O., Devuyst, F. X., 2008. Late Devonian-earliest Mississippian glaciation in Gondwanaland and its biogeographic consequences. Palaeogeography, Palaeoclimatology, Palaeoecology 268, 126-142.

Joachimski, M. M., Buggisch, W., 1993. Anoxic events in the late Frasnian-Causes of the Frasnian-Famennian faunal crisis ? Geology 21, 675-678.

Joachimski, M. M., Buggisch, W., 2002. Conodont apatite $\delta^{18}O$ signatures indicate climatic cooling as a trigger of the Late Devonian mass extinction. Geology 30, 711-714.

Joachimski, M.M., Pancost, R.D., Freeman, K.H., Osterag-Henning, C., Buggish, W., 2002. Carbon isotope geochemistry of the Frasnian-Famennian transition. Palaeogeography, Palaeoclimatology, Palaeoecology 181, 91-109.

Keller, M., Bahlburg, H., Reuther, C.-D., 2008. The transition from passive to active margin sedimentation in the Cantabrian Mountains, Northern Spain: Devonian or Carboniferous? Tectonophysics 461, 414-427.

Kiessling, W., 2008. Sampling-standardized expansion and collapse of reef building in the Phanerozoic. Fossil Record 11, 7-18.

Lefebvre, V., Servais, T., François, L and Averbuch, O., 2010. Did a Katian large igneous province trigger the Late Ordovician glaciation? : A hypothesis tested with a global carbon cycle model. Palaeogeography, Palaeoclimatology, Palaeoecology. In press, DOI; 10.1016/j.palaeo.2010.04.010.

Lin, A.T., Watts, A.B., Hesselbo, S.P., 2003. Cenozoic stratigraphy and subsidence history of the South China Sea margin in the Taiwan region. Basin Research 15, 453-478.

Matte, P., 2001. The Variscan collage and orogeny (480-290 Ma) and the tectonic definition of the armorica microplate: a review. Terra Nova 13, 122-128.

MsGhee, G.R., 1989. The Frasnian-Famennian extinction event. In: Donovan, S.K. (ed.): Mass extinctions: processes and evidence. Columbia University Press, New York 133-151.

Millot, R., Gaillardet, J., Dupré, B., Allègre, C., 2002. The global control of silicate weathering rates and the coupling with physical erosion : new insights from river of the Canadian Shield. Earth and Planetary Science Letters 196, 83-98.

Mook, W. J., Bommerson, J. C., Staberman, W. H., 1974. Carbon isotope fractionation between dissolved bicarbonate and gaseous carbon dioxide. Earth and Planetary Science

Letters 22, 169.

Mora, C.I., Dreise, S.G., Colarusso, L.A., 1996. Middle to Late Paleozoic atmospheric CO_2 levels from soil carbonate and organic matter. Science 271, 1105-1107.

Murphy, J.B., Keppie, J.D., 1998. Late Devonian palinspastic reconstruction of the Avalon-Meguma terrane boundary: implications for terrane accretion and basin development in the Appalachian orogen. Tectonophysics 284, 221-231.

Parrish, J.T., 1985. Latitudinal distribution of land and shelf and absorbed solar radiation during the Phanerozoic. Open-file report (Geological Survey (U.S.)) 85-31.

Pujol, F., Berner, Z., St ben, D., 2006. Palaeoenvironmental changes at the Frasnian/Famennian boundary in key European sections: Chemostratigraphic contrains. Palaeogeography, Palaeoclimatology, Palaeoecology 240, 120-145.

Racki, G., 2005. Toward understanding late devonian global events: few answers, many questions, in: Over, D., Morrow, J., Wignall, P. B. (Eds.), Understanding Late Devonian and Permian-Triassic Biotic and Climatic Events: Towards an Integrated Approach. Elsevier 20, 5-36.

Raymo, M.E., Ruddiman, W.F., Froelich, P.N., 1988. Influence of late Cenozoic mountain building on ocean geochemical cycles. Geology 16, 649-653.

Raymo, M., 1991. Geochemical evidence supporting t.c. chamberlin's theory of glaciation. Geology 19, 344-347.

Raymo, M., 1994. The himalayas, organic carbon burial, and climate in the Miocene. Paleoceanography 9, 399–404.

Redfield, A. C., 1934. On the proportion of organic derivatives in sea water and their relation to the composition of plankton, in: James Johnson Memorial Volume. University Press of Liverpool, 177–192.

Riquier, L., Tribovillard, N., Averbuch, O., Joachimski, M. M., Racki, G., Devleeschouwer, X., El Albani, A., Riboulleau, A., 2005. Productivity and bottom water redox conditions at the Frasnian-Famennian boundary on both sides of the Eovariscan Belt: constraints from trace-element geochemistry, in: Over, D., Morrow, J., Wignall, P. B. (Eds.), Understanding Late Devonian and Permian-Triassic Biotic and Climatic Events: Towards an Integrated Approach. Elsevier 20, 199-224.

Riquier, Tribovillard, Averbuch, Devleeschouwer, and Riboulleau] Riquier, L., Tribovillard, N., Averbuch, O., Devleeschouwer, X., Riboulleau, A., 2006. The Late Frasnian Kellwasser horizons of the Harz Mountains (Germany): Two oxygen-deficient periods resulting from different mechanisms. Chemical Geology 233, 137-155.

Royer, D. L., 2006. CO_2 -forced climate thresholds during the Phanerozoic. Geochimica et Cosmochimica Acta 70, 5665-5675.

Scotese, C.R., McKerrow, W.S., 1990. Revised world map and introduction. In: McKerrow, W.S. and Scotese, C.R. (eds.): Paleozoic paleogeography and biogeography. Geological Society of London Memoirs 51, 1-21.

Sepkoski, J.J., 1986. Phanerozoic overview of mass extinction, in: Raup, D., Jablonski, D. (eds.), Pattern and process in the history of life. Springer-Verlag, Berlin, pp277.

Simoes, M., Avouac, J.-P., 2006. Investigating the kinematics of mountain building in Tawain from the spatiotemporal evolution of the foreland basin and western foothills. Journal of Geophysical Research 111, doi:10.1029/2005JB004209.

Souquet, P., Delvolé, J.-J., Brusset, S., 2003. Identification of an underfilled foreland basin system in the Upper Devonian of the Central Pyrenees: implication for the Hercynian orogeny. International Journal of Earth Science (Geologische Rundschau) 92, 316-337.

Streel, M., Caputo, M. V., Loboziak, S., Melo, J. H. G., 2000. Late Frasnian-Famennian climates based on palynomorph analyses and the question of the Late Devonian glaciation. Earth-Science Reviews 52, 121–173.

Tait, J.A., Bachtadse, V., Franke, W., Soffel, H.C., 1997. Geodynamic evolution of the European Variscan fold belt: palaeomagnetic and geological constraints. Geologische Rundschau 86, 585-598.

Tribovillard, Averbuch, Devleeschouwer, Racki, and Riboulleau] Tribovillard, N., Averbuch, O., Devleeschouwer, X., Racki, G., Riboulleau, A., 2004. Deep-water anoxia over the Frasnian-Famennian boundary (La Serre, France): a tectonically induced oceanic anoxic event ? Terra Nova 16, 288-295.

Van Cappellen, P., Ingall, E.D., 1996. Redox stabilization of the atmosphere and oceans by phosphorus-limited marine productivity. Science 217, 493-496.

Veizer, J., Ala, D., Azmy, K., Bruckschen, P., Buhl, D., Bruhn, F., Carden, G. A. F., Diener, A., Ebneth, S., Goddéris, Y., 1999. $^{87}sr/^{86}sr$, $d^{13}C$ and $d^{18}O$ evolution of Phanerozoic seawater. Chemical Geology 161, 59-88.

Volk, T., 1987. Feedbacks between weathering and atmospheric CO_2 over the last 100 million years. American Journal of Science 287, 763-779.

Yapp, C.J., Poths, H., 1996. Carbon isotopes in continental weathering environments and variation in ancient atmospheric CO_2 pressure. Earth and Planetary Science Letters 137, 71-82.

Zachos, J.C. and Kump, L.R., 2005. Carbon cycle feedbacks and the initiation of Antarctic glaciation in the earliest Oligocene. Global and Planetary Change 47, 51-66.

5. Conclusions et perspectives

Les travaux, présentés dans ce mémoire d'Habilitation à Diriger des Recherches, offrent une vision renouvelée de la géodynamique de la chaîne varisque. Bien que les données la concernant, accumulées depuis la fin du 19ème siècle, en aient fait un objet classique du patrimoine géologique français, du coup peu attractif actuellement pour la communauté scientifique, les travaux, présentés ici, centrés principalement sur son front septentrional, tendent à montrer qu'il reste encore de nombreux points d'interrogation sur les processus majeurs ayant participé à son édification puis à sa destruction. En effet, un certain nombre de nos résultats plutôt que de clôre le débat, tendent au contraire à soulever de nouveaux questionnements et à ouvrir de nouvelles voies de recherche autour du sytème orogénique varisque.

De façon générale, nos travaux appliqués à la chaîne varisque contribuent à une meilleure compréhension des processus orogéniques. A cet égard, un des résultats les plus significatifs concerne l'évolution tardive de l'orogène et le phénomène de délamination lithosphérique, processus par lequel la chaîne va perdre sa racine mantélique afin de retrouver sur le long terme les propriétés thermo-mécaniques standards de la lithosphère. Nous proposons que le détachement du panneau de lithosphére océanique subduit au niveau de la zone de suture nord-varisque (suture de l'océan Lizard-Rhénohercynien) soit un phénomène moteur de l'effondrement de la chaîne, conduisant au final au développement du bassin de Paris en tant que « sag basin » (e.g. Nelson, 1992). De façon plus générale, la subduction de l'océan marginal Lizard-Rhénohercynien sous le bloc continental Armorica-Gondwana, préalablement épaissi, est probablement un processus primordial pour rendre compte de l'érosion thermique et de l'extension de la lithosphère au niveau des zones internes varisques au cours du Carbonifère. Ainsi que le suggèrent Jolivet et al (2009) dans le cas du bassin égéen, l'extension et l'affaissement des reliefs varisques seraient plutôt contrôlés par le dessous (la dynamique mantélique associée à la subduction) plutôt que par des processus de surface (les processus gravitaires). Selon nous, l'impact du retrait de la fosse de subduction nord-varisque est, en particulier, illustré par l'extension différentielle subie par les zones internes varisques du Massif Central de part et d'autre de la zone de faille de transfert majeure qu'est le Sillon Houiller (Burg et al, 1990). En effet, il est proposé que le Sillon Houiller, et son extension vers le nord suivant la faille de la Loire, soit la trace au sein de la plaque lithosphérique supérieure d'une faille de déchirement du panneau plongeant (« slab tear fault ») limitant des segments subduits ayant été affecté par un retrait différentiel de la fosse (les segments « Pays de Bray » à l'ouest et « rhénohercynien » à l'est, ce dernier ayant subi un retrait plus important).

Cette segmentation du panneau plongeant, directement liée à la géométrie initiale de la marge océanique, serait également à l'origine du comportement différent de ces deux segments lors de la collision continentale à la fin du Viséen (aux alentours de 325 Ma BP) et lors de l'évolution orogénique tardive à partir du Stéphanien (environ 300 Ma BP). Au cours de la collision entre le bloc septentrional avalonien et le bloc Armorica-Gondwana, le segment orogénique, orienté WNW-ESE, situé entre la zone de suture du Pays de Bray et le front de chaîne Boulonnais-Artois serait soumis une convergence oblique aux structures (suivant une direction NNW-SSE), résultant en une partition de déformation entre des chevauchements frontaux à vergence vers le NNE et des décrochements dextres d'arrière-pays tels que la faille du Pays de Bray (Matte et al, 1986). Le segment rhénohercynien, globalement perpendiculaire à la direction de convergence, absorberait uniquement la déformation par des structures chevauchantes à vergence vers le NNW, excepté au sein de couloirs transpressifs localisés comme la zone de virgation de la Meuse (dite aussi virgation de Dinant).

Cette configuration aurait induite un sous-charriage, de la marge continentale avalonienne et de la croûte océanique adjacente, notablement plus important au niveau du segment rhénohercynien qu'au niveau du segment « Pays de Bray ». Selon nous, la surface de croûte océanique subduite perpendiculairement à la limite de convergence aurait joué un rôle notable sur la rupture de la racine lithosphérique de la chaîne par simple effet gravitaire (voir par exemple Davies et Van Blankenburg (1995), pour une discussion détaillée du processus de rupture d'un slab plongeant). Ce processus serait à l'origine d'une délamination lithosphérique hétérogène de la chaîne au cours du Stéphano-Permien, le panneau de lithosphère océanique subduit le long de la marge active du segment rhénohercynien (et également du Lizard) étant rompu et enfoui dans le manteau profond alors qu'il serait préservé, au moins partiellement, le long du segment « Pays de Bray ». Ce processus de délamination tardi-orogénique hétérogène aurait induit le développement de remontées asthénosphériques localisées aux zones de suture varisques ayant subi la délamination lithosphérique (i.e. les segments rhénohercyniens et du Lizard). Ces remontées asthénosphériques seraient à l'origine d'une extension et d'une subsidence importantes de la lithosphère, localisées principalement au niveau de fosses majeures intra-montagneuses : les bassins stéphano-permiens de Sarre-Lorraine et de Manche centrale. Le refroidissement long-terme de la lithosphère suite à cet événement thermique initial pourrait être considéré comme

le moteur de base de la subsidence du bassin de Paris ainsi que le suggère la modélisation des courbes de subsidence dans le bassin (Prijac et al, 1999 ; Ziegler et al, 2004). Le caractère hétérogène de ce processus s'accorde, selon nous, avec la migration progressive de la subsidence au cours du temps vers le domaine « Pays de Bray », ainsi que le montre la disposition des séquences transgressives au sein du bassin de Paris (Mégnien, 1980 ; Guillocheau et al, 2000).
Ce nouveau modèle géodynamique de la partie nord de la chaîne varisque fait la synthèse de nombreuses données structurales et géophysiques acquises dans le cadre de ce travail. Pour autant, il s'appuie fondamentalement sur les travaux de tomographie sismique du manteau de Piromallo et Morelli (2003) montrant l'existence d'une anomalie positive de vitesse sismique des ondes P à la base de la lithosphère, moulée sur la zone de suture du Pays de Bray. Ce modèle tomographique d'échelle européenne manque, cependant, de résolution et dans la poursuite des études présentées ici, à la manière des recherches menées sur les points chauds de l'Eiffel (e.g. Ritter et al, 2001) et du Massif Central (e.g. Granet et al, 1995), il serait souhaitable qu'un réseau tomographique à plus petite échelle puisse être mis en place dans le bassin de Paris afin de confirmer et préciser cette anomalie tout à fait surprenante de prime abord. Il s'agit là bien sûr d'un projet d'envergure à établir dans le cadre d'une collaboration large, n'étant, moi-même aucunement compétent dans le domaine en question. Un second volet qui permettrait également de tester ce modèle conceptuel concerne, bien évidemment, la modélisation thermo-mécanique du processus de délamination lithosphérique hétérogène. A la manière de Gögus et Pyskliwec (2008), il serait intéressant de coupler une modélisation numérique thermique et mécanique de la délamination lithosphérique et de la remontée asthénosphérique associée pour essayer de quantifier d'une part l'échelle de temps des processus et de leur migration latérale d'autre part l'amplitude des surrections et subsidences de la surface terrestre. Ces données pourraient, au final, être comparées aux données de subsidence dans le bassin de Paris telles que celles établies par Prijac et al (1999) et Le Solleuz et al (2004). Il est clair, là encore, que ce type de projet ne pourra se faire que dans le cadre d'une collaboration avec un spécialiste de modélisation thermo-mécanique, projet pour lequel je n'ai pas encore prospecté pour l'instant.

Du point de vue des déformations au sein des systèmes plissés faillés de font de chaîne, ce travail sur le front varisque septentrional amène, là encore, un certain nombre de faits nouveaux. Parmi les principaux résultats présentés dans ce mémoire, deux d'entre eux me paraissent présenter un intérêt plus particulier:

(1) le premier concerne la définition d'un nouveau modèle structural de front de chaîne (le modèle de zone triangulaire frontale profonde). Ce modèle implique l'activation de rétro-chevauchements profonds d'avant-pays empêchant la propagation séquentielle classique des chevauchements vers l'avant et induisant au final la dissection « hors-séquence » du front chevauchant ; il est à noter que cette dissection s'opére suivant un chevauchement majeur (la faille du Midi dans le cas du front varisque) sur lequel se localise le déplacement à mesure que les rétrochevauchements profonds sont activés vers l'avant-pays. Ce dernier est soumis à une surrection notable définissant un bombement d'avant-pays qui, de fait, tend à réduire la sédimentation au sein du bassin d'avant-chaîne. Dans le cas du front varisque dans le secteur Boulonnais-Artois, nous proposons que ces rétro-chevauchements soient, en fait, des chevauchements calédoniens à vergence S (d'âge initialement Silurien supérieur), réactivés lors de la propagation du front chevauchant varisque. Il est probable que l'existence de discontinuités profondes à pendage antithétique au front chevauchant soit un préalable au développement de ce type de structure, ce qui la rend dès-lors assez peu commune. Un seul autre exemplaire de ce type a, pour l'heure, été décrit au front de l'Himalaya au Pakistan (Jadoon et Frisch, 1997). Le front chevauchant hors-séquence pyrénéo-languedocien au niveau de l'arc de St Chinian ou des Corbières orientales pourraît, également, en être un exemple, les chevauchements varisques de Montagne Noire pouvant former les rétrochevauchements profonds inhérents au modèle.

(2) le second résultat significatif concerne, à mon avis, le processus d'inversion tectonique négative des chevauchements de front de chaîne. Bien qu'il ait été assez peu étudié (comparativement au processus contraire d'inversion positive), le processus de réactivation en extension des chevauchements est extrêmement fréquent au sein des fronts de chaîne, comme nous l'avions déjà vu lors de ma thèse sur les structures chevauchantes frontales des Corbières orientales (Averbuch et al, 1992 ; 1993) ou des Apennins Centraux (Averbuch et al, 1995). Pour autant, la géométrie de ce type de structures reste peu contrainte du fait de leur enfouissement fréquent sous les dépôts syn-rift et de la faible résolution des images sismiques dans ces structures complexes. L'exploitation des données de sondage et de sismique réflexion au niveau du front chevauchant du Boulonnais et de l'Artois permettent d'apporter de nouvelles contraintes sur la géométrie des structures d'inversion tectonique négative. Elles confirment, en particulier, que les rampes des chevauchements sont le lieu préférentiel de la réactivation en extension alors que les parties moins pentés sont « court-circuitées » par des failles néoformées de pendage fort se raccordant à la rampe. Ce nouvel assemblage forme des

failles normales à caractère listrique ou en escalier définissant des demi-graben en « roll-over » dans lesquels s'accumulent des dépôts en éventail caractéristique.
Pour contraindre plus avant les géométries et cinématiques de développement de ces deux types de structure (zones triangulaires frontales et structures d'inversion tectonique négative), des études de modélisation analogique ont été entreprises en collaboration avec B. Vendeville. Les résultats préliminaires ont été présentés succinctement dans ce mémoire à travers deux courtes publications soumises au congrès GEOMOD de Florence (2008) et de Lisbonne (2010). L'exploitation détaillée et la publication de ces travaux restent cependant à faire ; il s'agit là de priorités à court terme en ce qui concerne les perspectives de ce travail, priorités qui me permettront d'élargir mes travaux vers de nouveaux systèmes orogéniques et de nouveaux horizons géographiques.

Le dernier point majeur des travaux, présentés ici, probablement le plus original, reste le volet concernant les relations possibles entre la surrection initiale de la chaîne varisque au Dévonien supérieur et les changements globaux des environnements terrestres autour de la limite Frasnien-Famennien. En effet, à notre connaissance, cette étude, initiée dans le cadre du programme inter-disciplinaire Eclipse, est l'une des seules à considérer sous ses différentes facettes un tel couplage entre orogenèse et changements environnementaux dans l'ancien. Pour autant, elle n'a pas pour ambition de clore le débat scientifique intense focalisé aussi bien sur les relations entre orogenèses et changements climatiques que sur les origines de la crise environnementale du Frasnien-Famennien. Elle démontre, cependant, que la période transitoire pendant laquelle s'édifie les reliefs (période de quelques Ma tout au plus) va correspondre à une période de déstabilisation rapide du cycle du carbone à travers l'intensification de l'érosion continentale et de l'altération chimique associée.
Cette édification transitoire du relief va avoir un impact d'autant plus important que le relief est d'ampleur conséquente comme dans le cas des grandes phases orogéniques (varisques, alpines, etc...) et qu'il est situé en domaine équatorial (l'altération chimique étant favorisée par l'augmentation de température ambiante et des précipitations). Il est proposé que cette augmentation significative de l'altération continentale, bien que localisée, conduise à un transfert de nutriment accru vers les domaines océaniques en aval de l'orogène (l'océan Protothétys dans le cas étudié), fertilisant ainsi à grande échelle les domaines marins. L'augmentation de la productivité océanique va conduire au stockage soutenu de carbone organique et de carbonates dans les sédiments soutirant ainsi du carbone au réservoir atmosphérique. Ce processus va être favorisé par la diminution des circulations marines suite

à la fermeture des domaines océaniques francs en bordure de la chaîne de collision. La restriction progressive des milieux marins peut conduire à une disoxie étendue des masses d'eau en bordure des reliefs continentaux. Ce phénomène de disoxie, décalé dans le temps par rapport au pic de productivité marine, peut permettre d'accroitre encore l'intensité et la durée de l'événement de stockage de carbone dans les sédiments marins. Ce mécanisme d'enfouissement piégeant aussi des carbonates en grande quantité forme également un puit de carbone associé à l'altération chimique des silicates. Ce double processus de soustraction de carbone à l'atmosphère va induire une chute significative et rapide de la pression de CO_2 atmosphérique avant qu'un équilibre nouveau soit atteint lorsque la chaîne a, elle même, atteint un relief en état permanent (les taux d'érosions et d'altérations équilibrent globalement les taux de surrection au sein de la chaîne). Ce nouvel état d'équilibre correspond à un climat global plus froid (de l'ordre de 6°C de baisse des températures équatoriales moyennes dans le cas des modélisations réalisées ici).

Bien qu'on ait peu d'informations directes sur l'altitude des reliefs au cours de la surrection initiale de la chaîne varisque au Dévonien supérieur, les données paléotectoniques, paléogéographiques, paléoenvironnementales et paléoclimatiques recueillies au cours de cette étude s'accordent significativement bien avec ce modèle. Dans l'état actuel des recherches, le modèle « orogénique » semble le mieux rendre compte de la chute rapide et drastique de la pCO_2 atmosphérique enregistrée autour de la limite Frasnien-Famennien (Royer, 2006) et qui va perdurer sur le long terme au cours du Carbonifère et du Permien (période de persistance du relief varisque et de la glaciation gondwanienne). Ce type d'étude qui considère les couplages entre géodynamique externe et interne, nécessite de mettre en place des projets pluri-disciplinaires intégrant des chercheurs d'horizons variés comme cela a pu être fait dans le cadre du projet Eclipse. Bien qu'il puisse être encore complété par l'acquisition de nouvelles données visant à caractériser toujours plus finement les variations paléoenvironnementales, ce projet a atteint grandement ses objectifs initiaux et a défriché une voie nouvelle, permettant d'intégrer la géodynamique éovarisque à son contexte environnemental global. Dans ce cadre, il reste des thèmes que nous avons peu abordé, par exemple les relations potentielles entre orogenèse et augmentation de la teneur en oxygène atmosphérique ainsi que l'ont suggéré récemment Campbell et Allen (2008). Cet aspect pourrait faire l'objet dans le futur d'études ponctuelles basées sur les expériences de modélisation numériques acquises au cours de la thèse de V. Lefebvre (2009). Hormis des études résiduelles de ce type, grandement ciblées, ce projet est arrivé globalement à son terme et je n'envisage pas de poursuite de grande échelle à ces études dans mes priorités scientifiques pour les années qui viennent.

Au terme de ce mémoire d'habilitation à diriger des recherches, je pense avoir montré combien la chaîne varisque, ce classique du patrimoine géologique français, restait d'actualité pour la compréhension des mécanismes orogéniques et de leur impact sur l'environnement. Ces études ont mis en avant, en particulier, un certain nombre de processus orogénique (la délamination lithosphérique hétérogène, le développement de zones triangulaires frontales, le mécanisme d'inversion tectonique) sur lequel je compte me focaliser dans les années à venir, en particulier avec le support de l'équipe de modélisation analogique de l'université de Lille 1. L'analyse de ces mécanismes sera pour moi l'occasion d'une sorte de retour aux sources, en focalisant de nouveau mon attention sur les aspects thématiques structuraux qui avaient occupé ma thèse, en y intégrant, cependant, de nouveaux outils tels que la modélisation analogique ou les logiciels de modélisation structurale.

Références

Arnold, J., Jacoby, W.R., Schmeling, H., Schott, B., 2001. Continental collision and the dynamic and thermal evolution of the Variscan orogenic crustal root- numerical models. Journal of Geodynamics 31, 273-291.

Artemieva, I.M., Mooney, W.D., 2002. On the relations between cratonic lithosphere thickness, plate motions, and basal drag. Tectonophysics 358, 211-231.

Artemieva, I.M., Thybo, H., Kaban, M.K., 2006. Deep Europe today: geophysical synthesis of the upper mantle structure and lithospheric processes over 3.5 Ga. In: Gee, D.G., Stephenson, R.A. (Eds), European Lithosphere Dynamics. Geological Society, London, Memoirs 32, pp. 11-41.

Autran, A., Lefort, J.P., Debeglia, N., Edel, J.B., Vigneresse, J.L., 1994. Gravity and magnetic expression of terranes in France and their correlation beneath overstep sequences. In: Keppie, J.D. (Ed.), Pre-Mesozoic geology in France and related areas. Springer-Verlag, Berlin, Heidelberg, pp. 49-72.

Averbuch, O., Frizon de Lamotte, D., Kissel, C., 1992. Magnetic fabric as a structural indicator of the deformation path within a fold-thrust structure: a test case from the Corbières (NE Pyrenees, France). J. Struct. Geol. 14-4, 461-474.

Averbuch, O., Frizon de Lamotte, D., Kissel, C., 1993. Strain distribution above a lateral culmination: an analysis using microfaults and magnetic fabric measurements in the Corbières thrust belt (NE Pyrenees, France). Annales Tectonicae 7, 1, 3-21.

Averbuch, O., Mattei, M., Kissel, C., Frizon de Lamotte, D., Speranza, F., 1995. Cinématique des déformations au sein d'un système chevauchant aveugle: l'exemple de la "Montagna dei Fiori" (front des Apennins Centraux, Italie). Bull. Soc. Géol. France 166, 5, 451-461.

Averbuch, O., Mansy, J-L., 1998. The "Basse-Normandie" duplex (Boulonnais, N France): evidence for an out-of-sequence thrusting overprint. J. Struct. Geol. 20, 33-42.

Averbuch, O., Mansy, J-L., Lamarche, J., 2001. Déformations tardi-paléozoïques au front septentrional de la chaîne varisque : l'exemple des massifs paléozoïques du Boulonnais (N France). Ann. Soc. Géol. Nord 9, 13-24.

Averbuch, O., Mansy, J.-L., Lamarche, J., Lacquement, F., Hanot, F., 2004. Geometry and kinematics of the Boulonnais fold-and-thrust belt (N France): implications for the dynamics of the Northern Variscan thrust front. Geodinamica Acta 17/2, 163-178.

Averbuch, O., Tribovillard, N., Devleeschouwer, X., Riquier, L., Mistiaen, B. and Van Vliet-Lanoe, B., 2005. Mountain building-enhanced continental weathering and organic carbon burial as major causes for climatic cooling at the Frasnian-Famennian boundary (ca 376 Ma BP) ? Terra Nova, 17/1, 33-42.

Averbuch, O., Piromallo, C., 2007a. High-velocity seismic anomalies in the lithospheric mantle beneath the Paris basin: remnants of subducted Paleozoic oceanic slabs? Subduction Congress, Montpellier, 5-7 juin 2007.

Averbuch, O. , Piromallo, C., 2007b. Imaging the mantle roots of the Variscan orogen below the Paris basin: Insight from the P-wave velocity model PM0.5. Mechanics of Variscan Orogeny, a modern view on orogenic research, Orléans, 13-15 septembre 2007.

Averbuch, O., 2009. Le Cap Gris-Nez - déformations à la limite septentrionale du bassin jurassique supérieur du Boulonnais. In : Des roches aux paysages dans le Nord-pas de Calais. Richesse de notre patrimoine géologique. Coordination : F. Robaszynski, G. Guyetant. Ed. Société géologique du Nord- Conservatoire des Sites Naturels du Nord et du Pas-de-Calais, pp. 58-59.

Babuska, V., Plomerova, J., Vecsey, L., Granet, M., Achauer, U., 2002. Seismic anistropy of the French Massif Central and predisposition of Cenozoic rifting and volcanism by

Variscan suture hidden in the mantle lithosphere. Tectonics 21, 4,1029, doi: 10.1029/2001TC901035.

Banks, C.J., Warburton, J., 1986. « Passive-roof » duplex geometry in the frontal structures of the Kirthar and Sulaiman mountain belts, Pakistan. J. Struct. Geol. 8, 229-237.

Ballèvre, M., Marchand, J., Godard, G., Goujou, J-C. and Wins, R., 1994. Eo-Hercynian events in the Armorican Massif. In: Keppie, J.D. Pre-Mesozoic geology in France and related areas. Springer-Verlag, Berlin, 183-192.

Ballèvre, M., Capdevila, R., Guerrot, C., Peucat, J.-J., 2002. Discovery of an alkaline orthogneiss in the eclogite-bearing Cellier Unit (Champtoceaux Comlex, Armorican Massif) : a new witness of the Ordocician rifting. C.R. Geoscience 334, 303-311.

Ballèvre, M., Bosse, V., Ducassou, C., Pitra, P., 2009. Palaeozoic history of the Armorican massif: Models for the tectonic evolution of the suture zones. C.R. Geoscience 341, 174-201.

Becq-Giraudon, J.F., 1983. Synthèse structurale et paléogéographique du bassin houiller du Nord. Mémoire B.R.G.M. 123, 72 pp.

Berra, I., 2008. Sédimentologie, stratigraphie isotopique du strontium et chemostratigraphie à la transition Frasnien-Famennien (Dévonien supérieur) en Amérique du Nord : implications orogéniques dans la crise biologique. Thèse de l'Université Libre de Bruxelles, 401 pp.

Bois, C., Cazes, M., Choukroune, P., Gariel, O., Hirn, A., Le Gall, B., Lefort, J.P., Matte, P., Pinet, B., 1994. Seismic reflection images of the pre-Mesozoic crust in France and adjacent areas. In: Keppie, J.D. (Ed.), Pre-Mesozoic geology in France and related areas. Springer-Verlag, Berlin, Heidelberg, pp. 33-48.

Boulvain, F., Coen-Aubert, M., 1997. Le sondage de Focant : lithostratigraphie et implications structurales. Memoirs of the geological survey of Belgium 43, 74 pp.

Bouroz, A., 1950. Sur quelques aspects du mécanisme de la déformation tectonique dans le bassin houiller du Nord de la France. Ann. Soc. Géol. Nord LXX, 2-55.

Bouroz, A., 1956. Contribution à l'étude des failles épicrétacées de l'Artois. Ann. Soc. Géol. Nord LXXVI, 51-62.

Burbank, D.W., Anderson, R.S., 2001. Tectonic geomorphology. Blackwell Science, 274 pp.

Burg, J.-P., Brun, J.-P., Van den Driessche, J., 1990. Le Sillon Houiller du Massif Central français: Faille de transfert pendant l'amincissement crustal de la chaîne varisque? C. R. Acad. Sci. Paris 311, 147-152.

Burg, J.-P., Van den Driessche, J., Brun, J.-P., 1994. Syn- to post-thickening extension: mode and consequences. C. R. Acad. Sci. Paris 319, 1019-1032.

Campbell, I. H., Allen, C. M., 2008. Formation of supercontinents linked to increases in atmospheric oxygen. Nature geosciences 1, 554-558.

Chalard, J, 1960. Contribution à l'étude du Namurien du bassin houiller du Nord de la France. Thèse d'Etat, Un. Lille, 300 pp.

Chen, D., Qing, H., Li, R., 2005. The Late Devonian Frasnian- Famennian (F/F) biotic crisis: Insights from $\delta^{13}C_{carb}$, $\delta^{13}C_{org}$ and $^{87}Sr/^{86}Sr$ isotopic systematics. Earth and Planetary Science Letters 235, 151–166.

Cocks, L.R., Fortey, R.A., 1982. Faunal evidence for oceanic separations in the Paleozoic of Britain. J. Geol. Soc. London 139, 465-478.

Covey, M., 1986. The evolution of foreland basins to steady state: evidence from the western Taiwan foreland basin, in Allen, P.A., Homewood, P. (eds.), Foreland basins. International Association of Sedimentologists Special Publication 8, pp. 77-90.

Davies, J.H., von Blankenburg, F., 1995. Slab breakoff: A model of lithosphere detachment and its test in the magmatism and deformation of collisional orogens. Earth and Planetary Science Letters 129, 85-102.

D'Agostino, N., Chamot-Rooke, N., Funiciello, R., Jolivet, L., Speranza, F., 1998. The role of pre-existing thrust faults and topography on the styles of extension in the Gran Sasso range (central Italy). Tectonophysics 292, 229-254.
Da Silva, A-C., 2004. Sédimentologie de la plate-forme carbonatée frasnienne belge. Thèse de l'Université de Liège, 253 pp.
De Boorder, H., Spakman, W., White, S.H., Wortel, M.J.R., 1998. Late Cenozoic mineralization, orogenic collapse and slab detachment in the European Alpine belt. Earth and Planetary Science Letters 164, 569-575.
Devleeschouwer, X., 1999. La transition Frasnien-Famennien (Dévonien supérieur) en Europe: sédimentologie, stratigraphie séquentielle et susceptibilité magnétique. Thèse de l'Université Libre de Bruxelles, 414 pp.
Diester-Haass, L., Billups, K., Gröcke, R., François, L., Lefebvre, V., Emeis, K.C., 2009. Mid-Miocene paleoproductivity in the Atlantic Ocean and implications for the global carbon cycle. Paleoceanography 24, PA1209, doi:10.1029/2008PA001605.
Echarfaoui, H., Hafid, M. and Aït Salem, A., 2002. Seismic structure of the Doukkala Basin, Paleozoic basement, Western Morocco: a hint for an Eovariscan fold-and-thrust belt. C.R. Geoscience 334, 13-20.
Embry, A.F., 1991. Middle-Upper Devonian clastic wedge of the Arctic Islands. In: Trettin H.P. (Ed.), Geology of the Inuitian Orogen and Arctic platform of Canada and Greenland, Geological Society of America, Geology of North America, pp. 261-279.
Everaerts, M., Mansy, J-L., 2001. Le filtrage des anomalies gravimétriques : une clé pour la compréhension des structures tectoniques du Boulonnais et de l'Artois. Bull. Soc. Géol. France 172, 267-274.
Facenna, C., Nalpas, T ., Brun, J-P., Davy, P., 1995. The influence of pre-existing thrust faults on normal fault geometry in nature and in experiments. J. Struct. Geol. 17, 1139-1149.
Facenna, C., Jolivet, L., Piromallo, C., Morelli, A., 2003. Subduction and the depth of convection in the Mediterranean mantle. J. Geophys. Res. 108 (B2), 2099, doi: 10.1029/2001JB001690.
Facenna, C., Piromallo, C., Crespo-Blanc, A., Jolivet, L., Rossetti, F., 2004. Lateral slab deformation and the origin of the western Mediterranean arcs. Tectonics 23, TC1012, doi:10.1029/2002TC001488.
Facenna, C., Bellier, O., Martinod, J., Piromallo, C., Regard, V., 2006. Slab detachment beneath eastern Anatolia: A possible cause for the formation of the North anatolian fault. Earth and Planetary Science Letters 242, 85-97.
Faure, M., Becq-Giraudon, J.-F., 1993. Sur la succession des épisodes extensifs au cours du désépaississement carbonifère du massif Central français. C. R. Acad. Sci. Paris 316 (II), 967-973.
Faure, M., Bé Mézème, E., Duguet, M., Cartier, C., Talbot, J-Y., 2005. Paleozoic tectonic evolution of Medio-Europa from the example of the french Massif Central and Massif Armoricain. J. Virtual Explorer, 19, 5, doi : 10.3809/jvirtex.2005.00120.
Faure, M., Bé Mézème, E., Cocherie, A., Rossi, P., Chemenda, A., Boutelier, D., 2008. Devonian geodynamic evolution of the Variscan belt, insights from the French Massif Central and Massif Armoricain. Tectonics 27, TC2005, doi: 10.1029/2007TC002115.
France-Lanord, C., Derry, L.A., 1997. Organic carbon burial forcing of the carbon cycle from Himalayan erosion. Nature 390, 65-67.
François, L.M., Walker, J.C.G., 1992. Modelling the Phanerozoic carbon cycle and climate: constraints from the $^{87}Sr/^{86}Sr$ isotopic ratio of seawater. American Journal of Science 292, 81–135.

François, L., Goddéris, Y., 1998. Isotopic constraints on the Cenozoic evolution of the carbon cycle. Chemical Geology 145, 177-212.
Franke, W., 1995. Rhenohercynian foldbelt: autochthon and non metamorphic nappe units-stratigraphy. In: Dallmeyer, R.D., Franke, W., Weber, K. (Eds.), Pre-Permian geology of Central and Eastern Europe. Springer-Verlag, Berlin, Heidelberg, pp. 33-49.
Franke, W., 2000. The mid-European segment of the Variscides: tectonostratigraphic units, terrane boundaries and plate tectonic evolution. In: Franke, W., Haak, V., Oncken, O., Tanner, D. (Eds.), Orogenic Processes: quantification and Modelling in the Variscan Belt. Geological Society, London, Special Publications 179, pp. 35-61.
Franke, W., 2006. The Variscan orogen in Central Europe: construction and collapse. In: Gee, D.G., Stephenson, R.A. (Eds.), European Lithosphere Dynamics Geological Society, London, Memoirs 32, pp. 333-343.
Frizon de Lamotte, D., Guézou, J.C., Averbuch, O., 1995. Distinguishing lateral folds in thrust-systems: examples from the Corbières (SW France) and the Betic Cordilleras (SE Spain). J. Struct. Geol., 17, 233-244.
Gaillardet, J., Dupre, B., Louvat, P., Allegre, C.J., 1999. Global silicate weathering and CO_2 consumption rates deduced from the chemistry of large rivers. Chemical Geology 159, 3-30.
Gaillardet, J., Galy, A., 2008. Himalaya—Carbon Sink or Source? Science 320, 1727-1728.
Garzione, C.N., 2008. Surface uplift of Tibet and Cenozoic global cooling. Geology 36, 1003-1004.
Goddéris, Y., Joachimski, M., 2004. Global change in the Late Devonian: modelling the Frasnian-Famennian short-term carbon isotope excursions. Palaeogeography, Palaeoclimatology, Palaeoecology 202, 309-329.
Gögus, O.H., Pysklywec, R.N., 2008. Mantle lithosphere delamination driving plateau uplift and synconvergent extension in Eastern Anatolia. Geology 36 (9), 723-726. doi: 10.1130/G24982A.1
Goes, S., Sapkman, W., Bijwaard, H., 1999. A lower mantle source for Central European volcanism. Science 286, 1928-1931.
Gosselet, J., 1908. Note sur quelques failles communes aux terrains crétaciques et houiller de l'Artois. Ann. Soc. Géol. Nord XXXVII, 80-109.
Granet, M., Wilson, M., Achauer, U., 1995. Imaging a mantle plume beneath the French Massif Central. Earth and Planetary Science Letters 136, 281-296.
Grard, A., François, L.M., Dessert, C., Dupré, B., Goddéris, Y., 2005. Basaltic volcanism and mass extinction at the permo-triassic boundary: Environmental impact and modeling of the global carbon cycle. Earth and Planetary Science Letters 234, 207-221.
Guillocheau, F., Robin, C., Allemand, P., Bourquin, S., Brault, N., Dromart, G., Friedenberg, R., Garcia, J.P., Gaulier, J.M., Gaumet, F., Grosdoy, B., Hanot, F., Le Strat, P., Mettraux, M., Nalpas, T., Prijac, C., Rigollet, C., Serrano, O., Grandjean, G., 2000. Meso-Cenozoic geodynamic evolution of the Paris Basin: 3D stratigraphic constraints. Geodinamica Acta 2000, 189-246.
Han, G., Preat, A., Chamley, H., Deconinck, J-F., Mansy, J-L., 2000. Palaeozoic clay mineral sedimentation and diagenesis in the Dinant and Avesnes Basins (Belgium, France) : relationships with Variscan tectonism. Sedimentary Geology 136, 217-238.
Han, G., Yans, J., Goudalier, M., Lacquement, F., Corfield, R.M., Mansy, J-L., Boulvain, F., Préat, A., 2003. Recognition and implication of tectonic loading-induced reheating in the northern Variscan front (Belgium and northern France), based on an illite Kübler index and oxygen isotope study. Int. J. Earth Sci. 92, 348-363.
Haq, B. U., Schutter, R., 2008. A chronology of Paleozoic Sea-Level Changes. Science 322, 64-68.

Isaacson, P.E., Hladil, J., Shen, J.-W., Kalvoda, J., Diaz Martinez, E., Grader, G., 1999. Late Devonian glaciation in Gondwana: setting the stage for Carboniferous eustasy. Subcommission on Devonian Stratigraphy Newsletter16, 40-49.
Jadoon, I.A.K., Frisch, W., 1997. Hinterland-vergent tectonic wedge below the Riwat thrust, Himalayan foreland, Pakistan; implications for hydrocarbon exploration. Am. Ass. Petrol. Geol. Bull., 81, 3, 438-448.
Joachimski, M. M., Buggisch, W., 2002. Conodont apatite $\delta^{18}O$ signatures indicate climatic cooling as a trigger of the Late Devonian mass extinction. Geology 30, 711-714.
Johnson, J.G. and Pendergast, A., 1981. Timing and mode of emplacement of the Roberts Mountain allochthon, Antler orogeny. Geological Society of America Bull. 92, 648-658.
Jolivet, L., Faccenna, C., Piromallo, C., 2009. From mantle to crust: Streching the Mediterranean. Earth and Planetary Science Letters 285, 198-209. doi: 10.1016/j.epsl.2009.06.017
Judenherc, S., Granet, M., Brun, J.P., Poupinet, G., Plomerova, J., Moquet, A., Achauer, U., 2002. Images of lithospheric heterogeneities in the Armorican segment of the Hercynian range in France. Tectonophysics 358, 121-134.
Kay, R.W., Kay, S.M., 1993. Delamination and delamination magmatism. Tectonophysics 219, 177-189.
Kissel, C., Averbuch, O., Frizon de Lamotte, D., Monod, O., Allerton, S.,1993. First paleomagnetic evidence for a post-Eocene clockwise rotation of the Western Taurides thrust belt, east of the Isparta reentrant (Southwestern Turkey). Earth. Planet. Sc. Lett. 117, 1-14.
Korsch, R.J., Schäfer, A., 1995. The Permo-Carboniferous Saar-Nahe Basin, south-west Germany and north-east France: basin formation and deformation in a strike-slip regime. Geol. Rundsch. 84, 293-318.
Lacquement, F., Mansy, J-L., Hanot, F., Meilliez, F., 1999. Retraitement et interprétation d'un profil sismique pétrolier méridien au travers du massif paléozoïque ardennais (nord de la France). Compte Rendus Acad. Sciences Paris 329, 471-477.
Lacquement, F., 2001. L'Ardenne Varisque. Déformation progressive d'un prisme sédimentaire pré-structuré, de l'affleurement au modèle de chaîne. Publication de la Société Géologique du Nord 29, 285 pp.
Lacquement, F., Averbuch, O., Mansy, J-L., Szaniawski, R., Lewandowski, M., 2005. Transpressional deformations at lateral boundaries of propagating thrust-sheets : the example of the Meuse Valley Recess within the Ardennes Variscan fold-thrust belt (N France-S Belgium). Journal of Structural Geology, 27, 1788-1802.
Ledru, P., Lardeaux, J.-M., Santallier, D., Autran, A., Quenardel, J.-M., Floc'h, J.-P., Lerouge, G., Maillet, N., Marchand, J., Ploquin, A., 1989. Où sont les nappes dans le Massif central français. Bull. Soc. géol. France 8 (V), 605-618.
Lefebvre, V., 2009. Modélisation numérique du cycle du carbone et des cycles biogéochimiques : application aux perturbations climatiques de l'Ordovicien terminal, du Dévonien terminal et du Miocène moyen. Thèse de l'Université de Lille 1, 214pp.
Lefebvre, V., Servais, T., François, L., Averbuch, O., 2010. Did a Katian Large Igneous Province trigger the Late Ordovician glaciation? A hypothesis tested with a carbon cycle model. Palaeogeography Palaeoclimatology Palaeoecology, doi : 10.1016/j.palaeo.2010.04.010.
Le Gall, B., 1994. Deformation of Nord-Pas de Calais Carboniferous coalfield (France) in the Variscan frontal tectonic pattern. In : Mascle, A. (Ed.), Hydrocarbon and Petroleum Geology of France. Springer Verlag, pp. 379-398.

Le Solleuz, A., Doin, M.-P., Robin, C., Guillocheau, F., 2004. From a mountain belt collapse to a sedimentary basin development: 2-D thermal model based on inversion of stratigraphic data in the Paris Basin. Tectonophysics 286, 1-27.

Lin, A.T., Watts, A.B., Hesselbo, S.P., 2003. Cenozoic stratigraphy and subsidence history of the South China Sea margin in the Taiwan region. Basin Res. 15, 453-478.

Littke, R., Büker, C., Hertle, M., Karg, H., Stroetman-Heinen, V., Oncken, O., 2000. Heat flow evolution, subsidence and erosion in the Rheno-hercynian orogenic wedge of central Europe.. In: Franke, W., Haak, V., Oncken, O., Tanner, D. (Eds.), Orogenic Processes: quantification and Modelling in the Variscan Belt. Geological Society, London, Special Publications 179, pp. 231-255.

Liu Huiqi, McClay, K.R., Powell, D., 1992. Physical models of thrust wedges. In: Mc Clay, K.R. (Ed.), Thrust Tectonics, Chapman and Hall, pp. 71-81.

Malavieille, J., Guihot, P., Costa, S., Lardeaux, J.M., Gardien, V., 1990. Collapse of the thickened Variscan crust in the french Massif Central: Mont Pilat extensional shear zone and St Etienne late Carboniferous basin. Tectonophysics 177, 139-149.

Marshak, S., Wilkerson, M.S., Hsui, A.T., 1992. Generation of curved fold-thrust belts: insight from simple physical and analytical models. In: Mc Clay, K.R. (Ed.), Thrust Tectonics, Chapman and Hall, pp. 83-92.

Marton, E., Mansy, J-L., Averbuch, O., Csontos, L., 2000. The Variscan belt of N France-S Belgium: geodynamic implications of new paleomagnetic data. Tectonophysics, 324, 57-80.

Mascle, A., Cazes, M., 1988. La couverture sédimentaire du bassin parisien. In: Cazes, M., Torreilles, G. (Eds.), Etude de la croûte terrestre par sismique profonde. Profil Nord de la France. Technip, Paris, pp. 157-169.

Matte, P., Respaut, J.-P., Maluski, H., Lancelot, J., Brunel, M., 1986. La faille NW-SE du Pays de Bray, un décrochement ductile dextre hercynien: déformation à 330 Ma d'un granite à 570 Ma dans le sondage Pays de Bray 201. Bull. Soc. géol. France 8 (II), 69-77.

Matte, P., Hirn, A., 1988. Seismic signature and tectonic cross section of the Variscan crust in Western France. Tectonics 7 (2), 141-155.

Matte, P., 1995. Southern Uralides and Variscides: comparison of their anatomies and evolutions. Geologie en Mijnbouw 74, 151-166.

Matte, P., 2001. The Variscan collage and orogeny (480-290 Ma) and the tectonic definition of the Armorica microplate: a review. Terra Nova 13, 122-128

Mansy, J.-L., Manby, G.M., Averbuch, O., Everaerts, M., Bergerat, F., Van Vliet-Lanoe, B., Lamarche, J., Vandycke, S., 2003. Dynamics and inversion of the Mesozoic basin of the Weald-Boulonnais area: role of basement reactivation. Tectonophysics 373, 161-179.

Mégnien, C., 1980. Tectogenèse du Bassin de Paris: étapes de l'évolution du bassin. Bull. Soc.géol. France XXII (4), 669-680.

Ménard, G., Molnar, P., 1988. Collapse of a Hercynian Plateau into a late Palaeozoic European Basin and Range province. Nature 334 (6179), 235-237.

Meilliez, F., André, L., Blieck, A., Fielitz, W., Goffette, O., Hance, L., Khatir, A., Mansy, J.L., Overlau, P., Verniers, J., 1991. Ardenne-Brabant. Sci. Géol. Bull. 44, 3-29.

Meilliez, F., 1989. Importance de l'événement calédonien dans l'allochtone ardennais; essai sur une cinématique paléozoïque de l'Ardenne dans la chaîne varisque. Thèse de Doctorat d'Etat, Un. du Maine, 518 pp.

Mériaux, E., 1961. Observations sur les conglomérats et marbres rouges de l'Artois. Ann. Soc. Géol. Nord LXXXI, 65-71.

Millot, R., Gaillardet, J., Dupré, B., Allègre, C., 2002. The global control of silicate weathering rates and the coupling with physical erosion : new insights from river of the Canadian Shield. Earth and Planetary Science Letters 196, 83-98.
Minguely, B., Mansy, J-L., Everaerts, M., Manby, G.M., Averbuch O., 2005. Apport de la modélisation géophysique à la compréhension de la structuration du Pas-de-Calais. C. R. Geosciences 337, 305-313.
Minguely, B., 2007. Caractérisation géométrique 3-D de la couverture sédimentaire méso-cénozoïque et du substratum varisque dans le nord de la France: apports des données de sondage et des données géophysiques. Thèse de l'Université de Lille 1, 230 pp.
Minguely, B., Folens, L., Averbuch, O., Vendeville B.V., 2008. Formation of deep-seated triangle zones by interaction between two orogenic thrust fronts having opposite vergence : structural evidence from the Caledonian-Variscan system in Northern France and preliminary analogue modelling. Bolletino di Geofisica teorica ed applicata, 49-2, 242-246.
Minguely, B., Averbuch, O., Patin, M., Rolin, D., Hanot, F., Bergerat, F., 2010. Inversion tectonics at the northern margin of the Paris basin (Northern France) : new evidence from seismic profiles and boreholes interpolation in the Artois area. Bulletin de la Société Géologique de France, vol. 5.
Morelli, A., Dziewonski, A., 1993. Body wave traveltimes and a spherically symmetric P- and S-wave velocity model. Geophys. J. Int. 112, 178-194.
Nelson, K.D., 1992. Are crustal thickness variations in old mountain belts like the Appalachians a consequence of lithospheric delamination? Geology 20, 498-502.
Oncken, O., Plesch, A., Weber, J., Ricken, W., Schrader, S., 2000. Passive margin detachment during arc-continent collision (Central European Variscides). In: Franke, W., Haak, V., Oncken, O., Tanner, D. (Eds.), Orogenic Processes: quantification and Modelling in the Variscan Belt. Geological Society, London, Special Publications 179, pp. 199-216.
Ouzgaït, M., Averbuch, O., Vendeville, B.C., Zuo, X., Minguely, B., 2010. The negative tectonic inversion of thrust faults: insights from seismic sections along the Northern France Variscan thrust front and analogue modelling experiments. Geomod 2010, Lisbonne, 27-29 septembre 2010.
Patin, M., 2004. Le front varisque en Artois : une histoire de réactivations. Mémoire de D.E.A., Université de Lille 1, 59 pp.
Pharaoh, T.C., Molyneux, S.G., Merriman, R.J., Lee, M.K., Verniers, J., 1993. The Caledonides of the Anglo-Brabant Massif reviewed. Geol. Mag., 130, 561-562.
Philippe, Y., 1995. Rampes latérales et zones de transfert dans les chaînes plissées: géométrie, conditions de formation et pièges structuraux associés. PhD thesis, Université de Savoie, France.
Piromallo, C., Morelli, A., 2003. P wave tomography of the mantle under the Alpine-Mediterranean area. J. Geophys. Res. 108 (B2), 2065, doi: 10.1029/2002JB001757.
Platt, J.P., England, P.C., 1993. Convective removal of lithosphere beneath mountain belts: thermal and mechanical consequences. American Journal of Science 293, 307-336.
Poupinet, G., Thouvenot, F., Zolotov, E.E., Matte, P., Egorkin, A.V., Rackitov, V.A., 1997. Teleseismic tomography across the middle Urals: lithospheric trace of an ancient continental collision. Tectonophysics 276, 19-33.
Poupinet, G., Avouac, J.P., Jiang, M., Wei, S., Kissling, E., Herquel, G., Guilbert, J., Paul, A., Wittlinger, G., Su, H., Thomas, J.C., 2002. Intracontinental subduction and Paleozoic inheritance of the lithosphere suggested by a teleseismic experiment across the Chinese Tien Shan. Terra Nova 14, 18-24.

Poupinet, G., Arndt, N., Vacher, P., 2003. Seismic tomography beneath stable tectonic regions and the origin and composition of the continental lithosphere. Earth and Planetary Science Letters 212, 89-101.

Prijac, C., Doin, M.P., Gaulier, J.M., Guillocheau F.2000. Subsidence of the Paris basin and its bearing on the late Variscan lithosphere evolution: a comparison between Plate and Chablis models. Tectonophysics 323, 1-38.

Puchkov, V.N., 1997. Structure and geodynamics of the Uralian orogen. In: Burg J-P. and Ford M. (Eds.), Orogeny through time, Geological Society, London, Special Publication 121, pp. 149-177.

Puchkov, V.N., 2009. The evolution of Uralian orogen. In : Murphy, J.B., Keppie, J.D., Hynes, A.J. (Eds), Ancient Orogens and Modern Analogues. Geol. Soc., London, Special Publication 327, pp. 161-195.

Ramos, 1988. The tectonics of the Central Andes ; 30° to 33° S latitude. In : Clark, S.P., Burchfiel, B.C., Suppe, J. (Eds), Processes in continental lithospheric deformation. Geol. Soc. Am. Spec. Paper 218, pp. 31-54.

Raoult, J-F., 1986. Le front varisque du Nord de la France d'après les profils sismiques, la géologie de surface et les sondages. Revue de géologie dynamique et de géographie physique 27, 247-288.

Raoult, J.-F., Meilliez, F., 1987. The Variscan front and the Midi fault between the Channel and the Meuse river. J. Struct. Geol. 9, 473-479.

Raymo, M.E., 1991. Geochemical evidence supporting T.C. Chamberlin's theory of glaciation. Geology 19, 344-347.

Ritter, J.R.R., Jordan, M., Christensen, U.R., Achauer, U., 2001. A mantle plume below the Eifel volcanic fields, Germany. Earth and Planetary Science Letters 186, 7-14.

Riquier, L., 2005. Perturbations des environnements marins à la limite Frasnien-Famennien (Dévonien supérieur) : apport de la géochimie inorganique et du magnétisme des roches, Thèse de l'Université de Lille 1, 408 pp.

Riquier, L., Tribovillard, N., Averbuch, O., Joachimski, M., Racki, G., Devleeschouwer, X., El Albani, A. and Riboulleau, A., 2005. Productivity and bottom water redox conditions at the Frasnian-Famennian boundary on both sides of the Eovariscan belt : constraints from trace-element geochemistry, In Over, D.J., Morrow, J.R., and Wignall, P.B., eds., Understanding Late Devonian and Permian-Triassic Biotic and Climatic Events: Towards an Integrated Approach: Elsevier., Developments in Palaeontology and Stratigraphy, vol. 20, 199-224.

Riquier, L., Tribovillard, N., Averbuch, O., Devleeschouwer, X., Riboulleau, A., 2006. The Late Frasnian Kellwasser horizons of the Harz mountains (Germany) : two oxygen-deficient periods resulting from contrasting mechanism. Chemical Geology 233, 137-155.

Riquier, L., Averbuch, O., Tribovillard, N., El Albani, A., Lazreq, N., Chakiri, S., 2007. Environmental changes at the Frasnian-Famennian boundary in Central Morocco (northern Gondwana): integrated rock-magnetic and geochemical studies. In : Devonan Event Stratigraphy and Correlations, T. Becker and B. Kirchgasser eds., Spec. Pub. Geol. Soc. London, 278, pp. 197-217.

Riquier, L., Averbuch, O., Devleeschouwer, X., Tribovillard, N., 2009. Diagenetic versus detrital origin of the magnetic susceptibility variations in some carbonate Frasnian-Famennian boundary sections from Northern Africa and Western Europe: implications for paleoenvironmental reconstructions. International Journal of Earth Sciences 99, 57-73, doi 10.1007/s00531-009-0492-7.

Robion, P., Averbuch, O., Sintubin M., 1999. Fabric development and metamorphic evolution of the Paleozoic slaty rocks from the Rocroi massif (French-Belgian Ardennes): new constraints from magnetic fabrics, phyllosilicate preferred orientation and illite cristallinity data. Tectonophysics 309, 257-273.

Rolin, D., 2000. Héritage et inversion tectonique en Artois, Mémoire de D.E.A., Université de Lille 1, 58 pp.

Roure, F., Brun, J-P., Colletta, B., Van den Driessche, J., 1992. Geometry and kinematics of extensional structures in the Alpine foreland basin of southeastern France. Journal of Structural Geology 14, 503-519.

Royer, D. L., 2006. CO_2 -forced climate thresholds during the Phanerozoic. Geochimica et Cosmochimica Acta 70, 5665-5675.

Ruddiman, W.F., 1997. Tectonic uplift and climate change. Plenum press, 535 pp.

Ruffell, A., Coward, M.P., Harvey, M., 1995. Geometry and tectonic evolution of the Plymouth Bay Basin, English Channel. . In: Boldy, S.A.R. (Ed.), Permian and Triassic Rifting in Northwest Europe. Geological Society, London, Special Publications 91, pp. 193-214.

Sengor, A.M., Natal'in, B., 1996. Paleotectonics of Asia: fragments of a synthesis. *In*: Yin A., Harrison T.M. (Eds.), The tectonic evolution of Asia. Cambridge University Press, pp. 486-640.

Shail, R.K., Leveridge, B.E., 2009. The Rhenohercynian passive margin of SW England: Development, inversion and extensional reactivation. C.R. Geoscience 341, 140-155.

Simoes, M., Avouac, J.-P., 2006. Investigating the kinematics of mountain building in Taiwan from the spatiotemporal evolution of the foreland basin and western foothills. Journal of Geophysical Research 111, doi:10.1029/2005JB004209.

Sintubin, M., Debacker, T.N., Van Baelen, H., 2009. Early Palaeozoic orogenic events north of the Rheic suture (Brabant, Ardenne) : A review. C. R. Geoscience 341, 156-173.

Sol, S., Thomson, C.J., Kendall, J.M., White, D., VanDecar, J.C., Asudeh, I., 2002. Seismic tomographic images of the cratonic upper mantle beneath the Western Superior Province of the Canadian Shield- a remnant Archean slab? Phys. Earth Planetary Interiors 134, 53-69.

Souquet, P., Delvolé, J.-J., Brusset, S., 2003. Identification of an underfilled foreland basin system in the Upper Devonian of the Central Pyrenees: implication for the Hercynian orogeny. International Journal of Earth Science (Geologische Rundschau) 92, 316-337.

Stein, S., Stein, C.A., 1996. Thermomechanical evolution of oceanic lithosphere: implications for the subduction process and deep earthquakes. Geophys. Monogr. Am. Geophys. Union 96, 1-17.

Streel, M., Caputo, M.V., Loboziak, S., Melo, J.H.G., 2000. Late Frasnian-Famennian climates based on palynomorph analyses and the question of the Late Devonian glaciations. Earth Science Rev. 52, 121-173.

Szaniawski, R., Lewandowski, M., Mansy, J-L., Averbuch, O., Lacquement, F., 2003. Syn-folding remagnetization events in the French-Belgium Variscides as markers of the fold-thrust belt kinematics. Bulletin Société géologique de France, 174, 511-523.

Szaniawski, R., 2004. Paléomagnétisme et tectogenèse des Variscides du nord de la France et du sud de la Belgique. Thèse de l'Université de Lille 1, 151 pp.

Vann, I.R., Graham, R.H., Hayward, A.B., 1986. The structure of mountain fronts. Journal of Structural Geology 8, 215-227.

Van Staal, C.R., Whalen, J.B., Valverde-Vaquero, P., Zagorevski, A., Rogers, N., 2009. Pre-Carboniferous, episodic accretion-related, orogenesis along the Laurentian margin of the northern Appalachians. In : Murphy, J.B., Keppie, J.D., Hynes, A.J. (Eds), Ancient Orogens and Modern Analogues. Geol. Soc., London, Spec. Pub. 327, 271-316.

Vicente, J.-C., 1975. Essai d'organisation paléogéographique et structurale du Paléozoïque des Andes méridionales. Geol. Rundsch. 64, 343-394.

Vignaroli, G., Faccenna, C., Jolivet, L., Piromallo, C., Rossetti, F., 2008. Subduction polarity reversal at the junction between the Western Alps and the Northern Apennines, Italy. Tectonophysics 450, 34-50.

Williams, G.D., Powell, C.M., Cooper, M.A., 1989. Geometry and kinematics of inversion tectonics. In : Cooper, M.A., Williams, G.D. (Eds.), Inversion Tectonics. Geol. Soc. London Spec. Pub. 44, 3-15.

Woodcock, N.H., Fischer, M., 1986. Strike-slip duplexes. Journal of Structural Geology 8, 725-735.

Zachos, J.C. and Kump, L.R., 2005. Carbon cycle feedbacks and the initiation of Antarctic glaciation in the earliest Oligocene. Global and Planetary Change 47, 51-66.

Zielhuis, A., Nolet, G., 1994. Deep seismic expression of an ancient plate boundary in Europe. Science 265, 79-81.

Ziegler, P.A., 1988. Laurussia-the Old Red Continent. In : McMillan, J., Embry, N.J., Glass, D.J. (Eds.), Devonian of the world. Can. Soc. of Petroleum geol., 15-48.

Ziegler, P.A., 1990. Evolution of the North Atlantic-An Overview. In : Tankard, A.J., Balkwill, H.R. (Eds.), Extensional tectonics and stratigraphy of the North Atlantic margins. Am. Ass. Petroleum Geol. Memoir 46, 111-129.

Ziegler, P.A., van Hoorn, B., 1990. Evolution of the North Sea Rift System. In : Tankard, A.J., Balkwill, H.R. (Eds.), Extensional tectonics and stratigraphy of the North Atlantic margins. Am. Ass. Petroleum Geol. Memoir 46, 471-500.

Ziegler, P.A., Schumacher, M.E., Dèzes, P., Van Wees, J.D., Cloethingh, S., 2004. Post-Variscan evolution of the lithosphere in the Rhine Graben area: constraints from subsidence modelling. In: Wilson, M.., Neumann, E.R., Davies, G.R.., Timmerman, M.J., Heeremans, M., Larsen, B.T. (Eds.), Permo-Carboniferous Magmatism and rifting in Europe. Geological Society, London, Special Publications 223, pp. 289-317.

ANNEXE

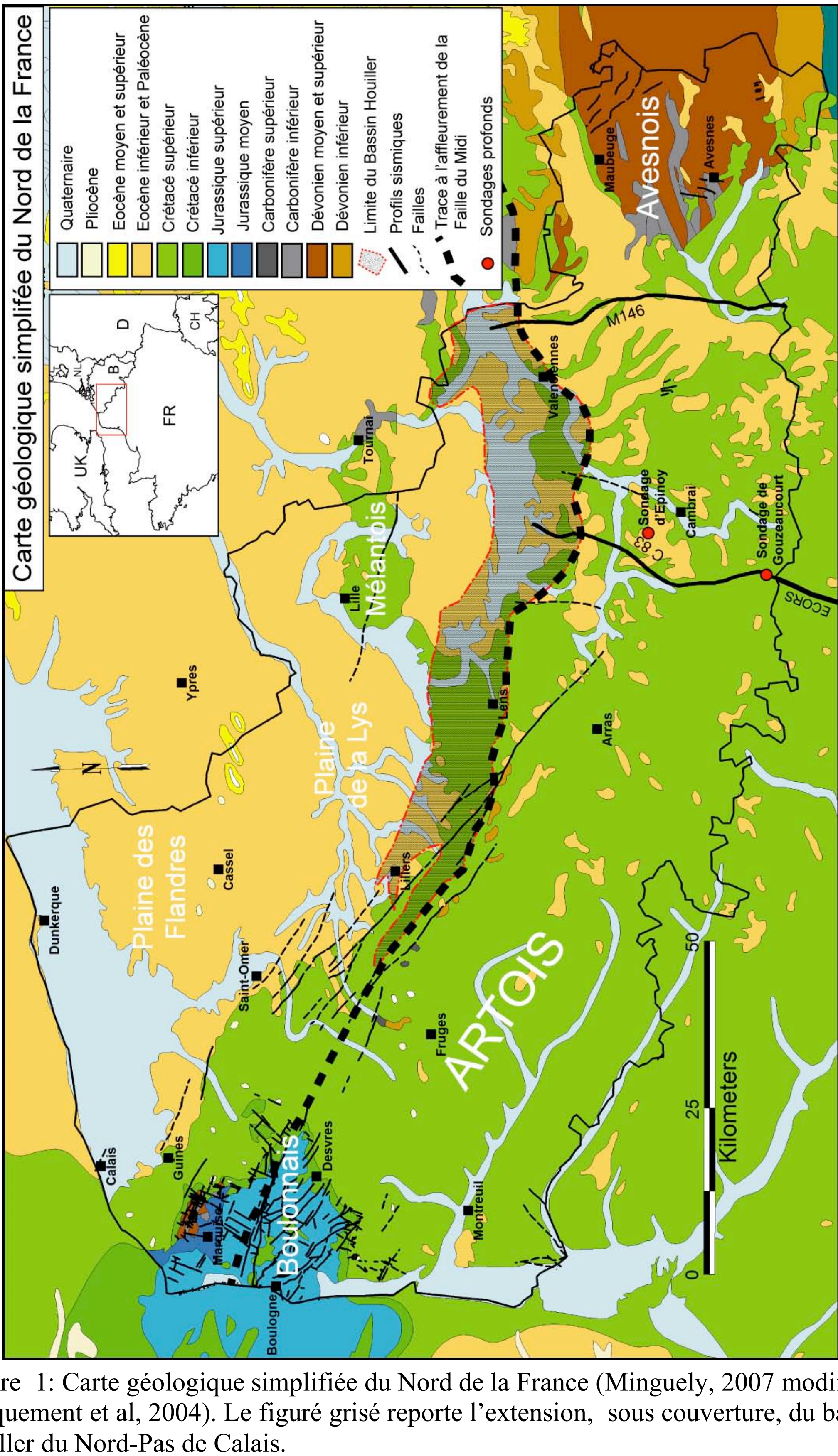

Figure 1: Carte géologique simplifiée du Nord de la France (Minguely, 2007 modifiée de Lacquement et al, 2004). Le figuré grisé reporte l'extension, sous couverture, du bassin houiller du Nord-Pas de Calais.

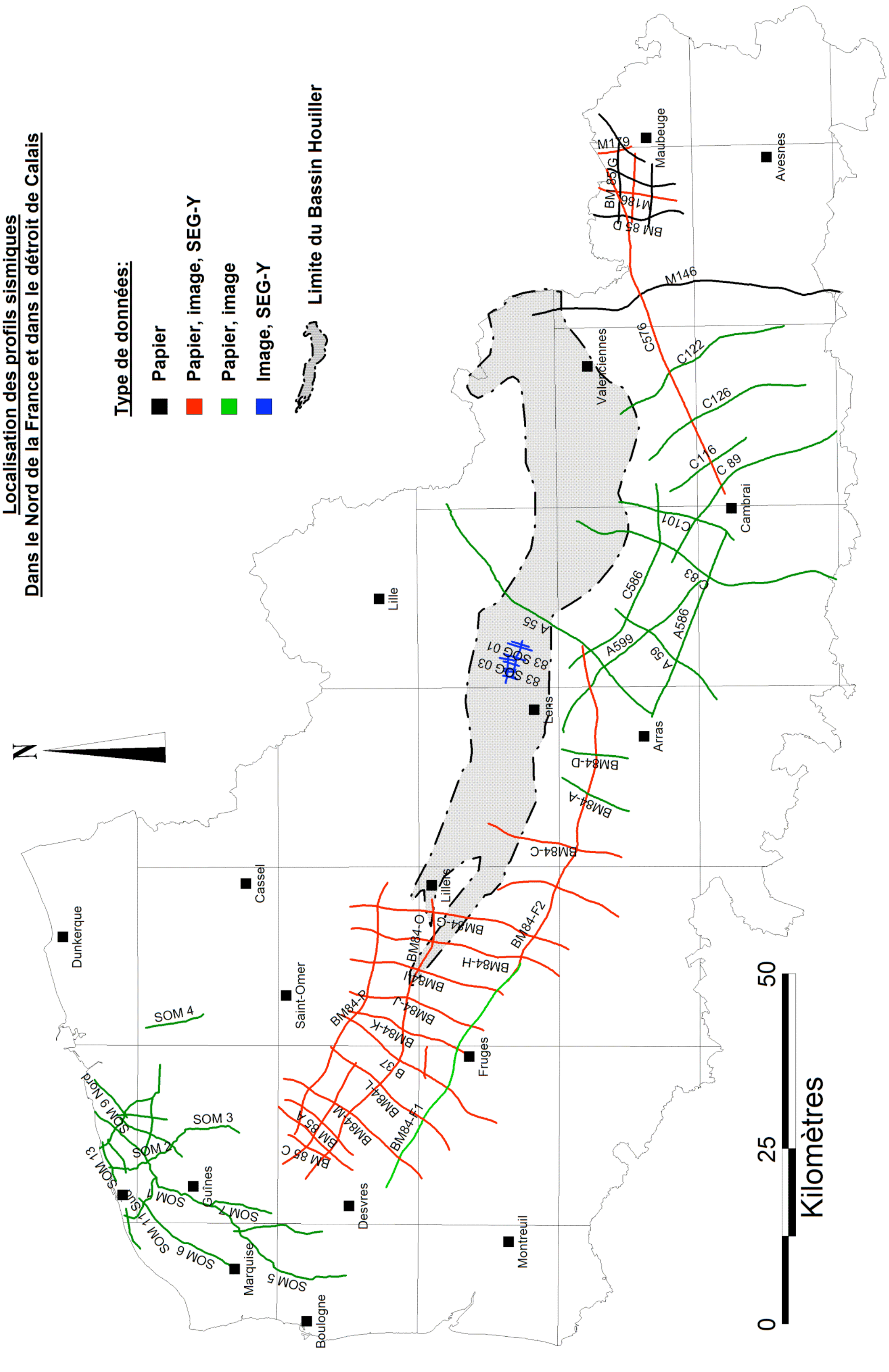

Figure 2: Carte de localisation des différents profils simiques disponibles au sein de la base de données sismique du Nord de la France (Minguely, 2007).

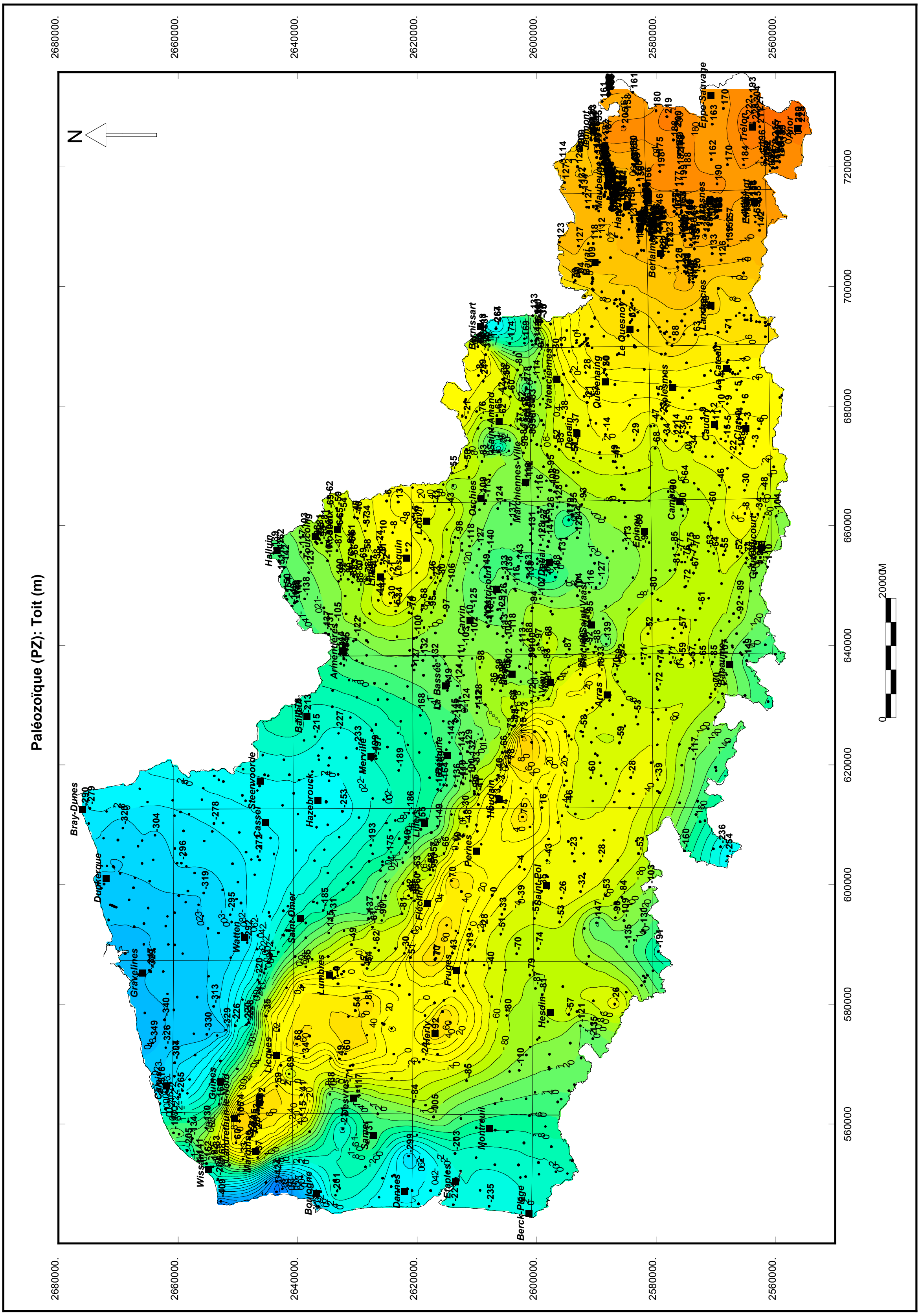

Figure 3 : Carte de profondeur du toit des formations paléozoïques par interpolation des forages profonds touchant le substratum du bassin de Paris dans le nord de la France (Minguely, 2007).

LISTE DES PUBLICATIONS
OLIVIER AVERBUCH

a. Notes dans des périodiques de diffusion internationale (étudiants encadrés, reportés en italique)

a1. **Averbuch O.**, Frizon de Lamotte D. and Kissel C., 1992.- Magnetic fabric as a structural indicator of the deformation path within a fold-thrust structure: a test case from the Corbières (NE Pyrenees, France). J. Struct. Geol. 14-4, 461-474.

a2. Kissel C., **Averbuch O.**, Frizon de Lamotte D., Monod O. and Allerton S.,1993.- First paleomagnetic evidence for a post-Eocene clockwise rotation of the Western Taurides thrust belt, east of the Isparta reentrant (Southwestern Turkey). Earth. Planet. Sc. Lett. 117, 1-14.

a3. Frizon de Lamotte D., Guézou J.C. and **Averbuch O.**, 1995.- Distinguishing lateral folds in thrust-systems: examples from the Corbières (SW France) and the Betic Cordilleras (SE Spain). J. Struct. Geol., 17, 233-244.

a4. **Averbuch O.**, Mattei M., Kissel C., Frizon de Lamotte D. et Speranza F., 1995.-Cinématique des déformations au sein d'un système chevauchant aveugle: l'exemple de la "Montagna dei Fiori" (front des Apennins Centraux, Italie). Bull. Soc. Géol. France., 166, 5, 451-461.

a5. Frizon de Lamotte D., Mercier E., Dupré la Tour A., Robion P. et **Averbuch O.,** 1997.- Cinématique du plissement et déformation interne des roches. L'exemple du pli de Lagrasse (Aude, France). C.R. Acad. Sciences Paris, 324, 591-598.

a6. **Averbuch O.** and Mansy J-L., 1998.- The "Basse-Normandie" duplex (Boulonnais, N France): evidence for an out-of-sequence thrusting overprint. J. Struct. Geol., 20, 33-42.

a7. Robion P., **Averbuch O**. and Sintubin M., 1999.- Fabric development and metamorphic evolution of the Paleozoic slaty rocks from the Rocroi massif (French-Belgian Ardennes): new constraints from magnetic fabrics, phyllosilicate preferred orientation and illite cristallinity data. Tectonophysics, 309, 257-273.

a8. Vanderaveroet P., **Averbuch O.**, Deconinck J-F. and Chamley H, 1999.- Glacial/interglacial cycles in Pleistocene sediments of New Jersey expressed by clay minerals, grain-size and magnetic susceptibility data. Marine Geology, 159, 79-92.

a9. Lamarche J., Mansy J.L., Bergerat F., **Averbuch O.**, Hackenberg M., Lewandowski M., Stupnicka E., Swidrowska Y., Wajsprych B. and Wieczorek J., 1999.- Variscan tectonics in the Holy-Cross Mountains (Poland) and structural inheritance during the Alpine tectonics. Tectonophysics, 313, 171-186.

a10. Lewandowski M., Lamarche J., Mansy J-L., **Averbuch O.** and *Szaniawski R.,* 1999- Paleomagnetic dating of brittle tectonic structures: case studies on the Ferques fault (Boulonnais, France) and two fault zones from the Holy Cross Mountains (Poland). Compte Rendus de l'Académie des Sciences, Paris, 329, 495-502.

a11. Marton E., Mansy J-L., **Averbuch O.** and Csontos L., 2000- The Variscan belt of N France-S Belgium: geodynamic implications of new paleomagnetic data. Tectonophysics, 324, 57-80.

a.12. Tribovillard N., **Averbuch O.,** Bialkowski A. and Deconinck J-F., 2002- Early diagenesis of marine organic-matter and magnetic properties of sedimentary rocks : the role of iron limitation and organic-matter source organisms. Bulletin Société géologique de France, 173, 295-306.

a.13. Deconinck J-F., Hesselbo S., Debuisser N., **Averbuch O.** , Baudin F. and Bessa J. (2003)- Environmental controls on clay mineralogy of an Early Jurassic mudrock (Blue lias formation, southern England). Int. Journal of Earth Sciences, 92, 255-266.

a14. *Szaniawski R.,* Lewandowski M., Mansy J-L., **Averbuch O.** and *Lacquement F.* (2003). Syn-folding remagnetization events in the French-Belgium Variscides as markers of the fold-thrust belt kinematics. Bulletin Société géologique de France, 174, 511-523.

a.15. Mansy J.L., Manby G., **Averbuch O.**, Everaerts M., Bergerat F., Van Vliet-Lanoe B., Lamarche J., Vandycke S. (2003)- Dynamics and inversion of the Mesozoic basin of the Weald-Boulonnais area: role of basement reactivation. Tectonophysics, 373, 161-179.

a.16. **Averbuch O.,** Mansy J-L., Lamarche J., *Lacquement F.* and Hanot F. (2004). Geometry and kinematics of the Boulonnais fold-and-thrust belt (N France) : implications for the dynamics of the NorthernVariscan thrust front. Geodinamica Acta, 17, vol 2, 163-178.

a.17. Tribovillard N., **Averbuch O.,** Devleeschouwer X., Racki G. and Riboulleau A. (2004). Deep-water anoxia over the Frasnian-Famennian boundary (La Serre, S France) : a tectonically induced oceanic anoxic event ? Terra Nova, 16/5, 288-295.

a.18. **Averbuch O.,** Tribovillard N., Devleeschouwer X., *Riquier L.,* Mistiaen B. and Van Vliet-Lanoe B. (2005). Mountain building-enhanced continental weathering and organic carbon burial as major causes for climatic cooling at the Frasnian-Famennian boundary (ca 376 Ma BP) ? Terra Nova, 17/1, 33-42.

a.19. *Minguely B.,* Mansy J-L., Everaerts M., G.M. Manby and **Averbuch O.** (2005). Apport de la modélisation géophysique à la compréhension de la structuration du Pas-de-Calais. C. R. Geosciences 337, 305-313.

a.20. *Riquier L.,* Tribovillard N., **Averbuch O.,** Joachimski M., Racki G., Devleeschouwer X., El Albani A. and Riboulleau A. (2005). Productivity and bottom water redox conditions at the Frasnian-Famennian boundary on both sides of the Eovariscan belt : constraints from trace-element geochemistry, In Over, D.J., Morrow, J.R., and Wignall, P.B., eds., Understanding Late Devonian and Permian-Triassic Biotic and Climatic Events: Towards an Integrated Approach: Elsevier., Developments in Palaeontology and Stratigraphy, vol. 20, 199-224.

a.21. *Lacquement F.,* **Averbuch O.,** Mansy J-L., *Szaniawski R.* and Lewandowski M. (2005). Transpressional deformations at lateral boundaries of propagating thrust-sheets : the example of the Meuse Valley Recess within the Ardennes Variscan fold-thrust belt (N France-S Belgium). Journal of Structural Geology, 27, 1788-1802.

a.22. *Riquier L.,* Tribovillard N., **Averbuch O.,** Devleeschouwer X. and Riboulleau A. (2006). The Late Frasnian Kellwasser horizons of the Harz mountains (Germany) : two oxygen-deficient periods resulting from contrasting mechanism. Chemical Geology, 233, 137-155.

a23.*Riquier L.,* **Averbuch O.,** Tribovillard N., El Albani A., Lazreq N. and Chakiri S. (2007). Environmental changes at the Frasnian-Famennian boundary in Central Morocco (northern Gondwana): integrated rock-magnetic and geochemical studies. In : Devonan Event Stratigraphy and Correlations, T. Becker and B. Kirchgasser eds., Spec. Pub. Geol. Soc. London, 278, 197-217.

a24. *Riquier L.,* **Averbuch O.,** Devleeschouwer X. and Tribovillard N. (2009). Diagenetic versus detrital origin of the magnetic susceptibility variations in some carbonate Frasnian-Famennian boundary sections from Northern Africa and Western Europe : implications for paleoenvironmental reconstructions. International Journal of Earth Sciences. 99, 57-73. doi 10.1007/s00531-009-0492-7

a25. *Lefebvre V.,* Servais T., François L. and **Averbuch O.** (2010). Did a Katian large igneous province trigger the Late Ordovician glaciation ?A hypotheis tested with a carbon cycle model. Paleogeography, Paleoclimatology, Paleoecology 296, 310-319. doi : 10.1016/j.palaeo.2010.04.010

a26. *Minguely B.,* **Averbuch O.,** Patin M., Rolin D., Hanot F. and Bergerat F. (2010). Inversion tectonics at the northern margin of the Paris basin (Northern France) : new evidence from seismic profiles and boreholes interpolation in the Artois area. Bulletin de la Société Géologique de France, volume 5.

b. Autres publications à comité de lecture.

b1. **Averbuch O.**, Frizon de Lamotte D. and Kissel C., 1993.- Strain distribution above a lateral culmination: an analysis using microfaults and magnetic fabric measurements in the Corbières thrust belt (NE Pyrenees, France). Annales Tectonicae, vol 7, 1, 3-21..

b2. Lamarche J., Mansy J.L., Bergerat F., Swidrowska Y., Hackenberg M., Wieczorek J., Lewandowski M., Stupnicka E. and **Averbuch O.**, 1997.- Laramide inversion of a Mesozoic basin and Paleozoic structural inheritance near the Teysseire-Tornquist zone. Example of the Holy-cross Mountains. Geophysical Journal of Ukrainia, 19, 155-156.

b3. Robion P. and **Averbuch O**., 1997.- Fabric development and metamorphic evolution of the Lower Paleozoic rocks of the Rocroi Massif (Belgian-French Ardenne) from rock magnetic and illite cristallinity data. Aardk. Mededel. 8, 157-160.

b4. *Lacquement F.,* Mansy J.L., Mercier E. , **Averbuch O.** et Meilliez F., 1997.- Mécanismes de plissement disharmonique dans le Paléozoïque ardennais. Aardk. Mededel. 8, 119-122.

b5. **Averbuch O.**, Mansy J-L. et Lamarche J., 2001. Déformations tardi-paléozoïques au front septentrional de la chaîne varisque : l'exemple des massifs paléozoïques du Boulonnais (N France). Ann. Soc. Géol. Nord, 9, 13-24.

b6. **Averbuch O.**, *Lacquement F., Szaniawski R.,* Mansy J-L. and Lewandowski M., 2002.- Segmentation of the N France-S Belgium Variscan thrust front : insights into the geometry of the Devonian Rheno-hercynian basin. Contributions to the geology of Belgium and Northwest Europe, P.Degryse and M.Sintubin eds., Aardk. Mededel. 12 , 89-92.

b.7. Tribovillard N., **Averbuch O.** and Riboulleau A., 2004. Influence of marine organic-matter diagenesis on magnetic susceptibility of sedimentary rocks: the sulphide pathway. Ann. Soc. Géol. Nord, 11, 57-67.

b.8. **Averbuch O.,** *Lacquement F.,* Mansy J-L., *Szaniawski R*. et Lewandowski M.,, 2006. Déformations au front septentrional de la chaîne varisque : l'exemple des Ardennes franco-belges dans la région de Givet. Géologie de la France, 1-2, 85-90.

b.9. Guillot F., Lasalle S., Deconinck J-F., Pellenard P., **Averbuch O.,** Paquette J-L., Herbosch A. et Devleeschouwer X.,, 2006. Typologie du zircon des bentonites du Frasnien (carrière du Lion, Belgique) : utilité avant la datation U-Pb. Géologie de la France, 1-2, 59-63.

b.10. *Minguely B.,* Mansy J-L., Hanot F., Everaerts M., Lacquement F. et **Averbuch O.**, 2006. Synthèse des données de sondage et des données gravimétriques depuis l'Avesnois jusqu'au méridien de Lens : résultats préliminaires. Géologie de la France, 1-2, 93-98.

b.11. Lacquement F., Mansy J-L., **Averbuch O.** et Meilliez F., 2006. La carte géologique : un outil au service de la recherche. Géologie de la France, 1-2, 145.

b.12. *Minguely B., Folens L.,* **Averbuch O.** and Vendeville B.V., 2008. Formation of deep-seated triangle zones by interaction between two orogenic thrust fronts having opposite vergence : structural evidence from the Caledonian-Variscan system in Northern France and preliminary analogue modelling. Bolletino di Geofisica teorica ed applicata, 49-2, 242-246.

c. Colloques.

c1. **Averbuch O.**, Kissel C. and Frizon de Lamotte D., 1991.- The use of Anisotropy of Magnetic Susceptibility in characterizing the deformation path within a fold-thrust structure: a test case from the Corbières (NE Pyrenees, France). American Geophysical Union Fall Meeting, San Francisco.

c2. **Averbuch O.**, Kissel C. and Frizon de Lamotte D., 1992.- Aplication of Anisotropy of Magnetic Susceptibility (AMS) to structural studies within fold-thrust structures. American Geophysical Union, Spring Meeting, Montreal.

c3. **Averbuch O.**, Frizon de Lamotte D. et Kissel C.,1992.- Analyse du chemin de la déformation dans la structure de chevauchement-plissement du chaînon de Lagrasse (Corbières). 14e Réunion des Sciences de la Terre, Toulouse, p10.

c4. Frizon de Lamotte D., **Averbuch O.**, Guézou J.C. and Kissel C., 1992.- Modalités du développement de structures accommodant une extension perpendiculaire au transport tectonique dans les chaînes de chevauchement-plissement. 14e Réunion des Sciences de la Terre, Toulouse, p64.

c5. **Averbuch O.**, Frizon de Lamotte D., Kissel C., Robion P. and Aubourg C., 1993.- Magnetic fabric and the evolution of fold-thrust structures. European Union of Geosciences, Strasbourg.

c6. **Averbuch O.**, Speranza F., Kissel C. et Frizon de Lamotte D. 1994.- Géométrie et cinématique des déformations associées au décollement du toit d'une structure de chevauchement-plissement: l'exemple du front des Apennins centraux. 15e Réunion des Sciences de la Terre, Nancy, p91.

c7. Aubourg C., Frizon de Lamotte D., Poisson A., **Averbuch O.** et Kissel C., 1994.- Pli, fabrique magnétique et direction du transport tectonique. Un exemple dans le Taurus Occidental (Turquie). 15e Réunion des Sciences de la Terre, Nancy, p91.

c8. **Averbuch O.**, Mattei M., Kissel C., Frizon de Lamotte D. et Speranza F., 1994.- Passive deformation of the Laga flysch basin at the top of the Central Apennines thrust front (Italy). Les Bassins d'Avant-Chaînes, Séance de la Société géologique de France, Grenoble, p6-7.

c9. Mansy J.L. et **Averbuch O.**, 1996.- Le duplex de "Basse-Normandie" (Boulonnais, N France): une nouvelle interprétation. 16e Réunion des Sciences de la Terre, Orléans, S.G.F. ed., p29.

c10. Lamarche J., Wieczorek J., Bergerat F., Swidrowska Y., Mansy J.L., Hackenberg M., **Averbuch O.**, Stupnicka E., Dumont T. et Wajsprych B., 1996.- Les Monts Sainte Croix (Pologne): formation et déformation d'un bassin mésozoïque de l'Europe Centrale sous l'influence de la ligne Teisseyre-Tornquist. 16e Réunion des Sciences de la Terre, Orléans, S.G.F. ed., p27.

c11. Mercier E., Frizon de Lamotte D., Dupré la Tour A. and **Averbuch O.**, 1996.- Cover fault-propagation fold initiated by the reactivation of basement thrust (a case study from the Corbières area, NE Pyrénées, France). Forced folds, London.

c12. Lamarche J., Bergerat F., Mansy J.L., Swidrowska Y., Hackenberg M., Stupnicka E., Wieczorek J., Dumont T., **Averbuch O.** and Wajsprych B., 1996.- From the origin to the deformation of the Mesozoic basin of the Holy Cross Mountains influenced by the Teysseire-Tornquist line. Amsterdam, Réunion Péritéthys.

c13. Robion P. and **Averbuch O**., 1997.- Fabric development and metamorphic evolution of the Lower Paleozoic rocks of the Rocroi Massif (Belgian-French Ardenne) from rock magnetic and illite cristallinity data. Belgian Symposium on Structural Geology and Tectonics , Aardk. Mededel. 8, 157-160.

c14. Lacquement F., Mansy J.L., Mercier E. , **Averbuch O.** et Meilliez F., 1997.-Mécanismes de plissement disharmonique dans le Paléozoïque ardennais. Belgian Symposium on Structural Geology and Tectonics , Aardk. Mededel. 8, 119-122.

c15. Marton E., Mansy J-L., **Averbuch O.** and Csontos L., 1997. The Variscan belt of Northern France and Belgium: new paleomagnetic results. IAGA 97, Uppsala, 4-15 Aout 1997.

c16. **Averbuch O.**, Deconinck J-F., Proust J.N. et Mammoudia M., 1997.- Enregistrement magnétique et minéralogique à haute résolution des variations tectoniques et eustatiques au sein des formations du Kimméridgien-Tithonien du Boulonnais (Nord de la France). Congrès de l'A.S.F., Montpellier.

c17. Mansy J-L. **et Averbuch O.**, 1997. Les écailles de la carrière de Basse-Normandie (Boulonnais): une réplique hectométrique du front de chevauchement varisque du nord de la France. 1ere Journées Régionales du Patrimoine Géologique, Lille, 20-24 novembre 1997.

c18. **Averbuch O.**, Deconinck J-F., Proust J.N. and Mammoudia M., 1998.- High resolution magnetic and mineralogical record of paleoenvironmental changes within the Kimmeridgian-Tithonian formations of the Boulonnais region (northern France). E.G.S. meeting Nice, Annales Geophysicae, 16C, p 211 .

c19. Lamarche J., Bergerat F., Mansy J.L., Swidrowska Y., Wieczorek J., Lewandowski M., Stupnicka E., Hackenberg M. and **Averbuch O.** , 1998.- Variscan to alpine paleo-stress evolution in the Teysseire-Tornquist zone. E.G.S. meeting, Nice, Annales Geophysicae, 16C, p 107 .

c20. Chapron E., Beck C., **Averbuch O.**, Pourchet M., De Batist M. and Deconinck J-F., 1998. Accoustical and sedimentological signatures of late-glacial and historical lacustrine « homogenites » as seiche deposits in Lake Le Bourget: Seismites related to Northwestern Alps tectonic activity? International Conference on Active Tectonic Continental Basins, Gand, 30 Avril- 2 mai 1998.

c21. Lacquement F., **Averbuch O.** and Mansy J-L., 1999. - Geometry and strain distribution within a major lateral zone of the Variscan Ardennes fold-and-thrust belt (N France-S Belgium). E.G.S. meeting, La Haye, Geophysical Research Abstracts, Vol 1.1, 28.

c22. **Averbuch O.** and Frizon de Lamotte D., 1999.- Strain within foreland fold-thrust structures: an analysis using magnetic fabric measurements and structural data. Thrust Tectonics Conference, London, 128-130.

c23. Devleeschouwer X., Préat A., **Averbuch O.** and Herbosch A., 1999.- Magnetic susceptibility through the Frasnian-Famennian boundary (Steinbruch Schmidt (Germany) and Coumiac (France)). I.A.S. meeting, Copenhagen, 71-72.

c24. Lacquement F., **Averbuch O.**, Mansy J-L. et Meilliez F., 2000.- Géométrie et cinématique des déformations au front septentrional de la chaîne varisque: l'exemple des Ardennes franco-belges. Réunion des Sciences de la Terre, Paris, .

c25. Lacquement F., **Averbuch O.**, Mansy J-L. et Mercier E., 2000.- Plis de décollement au sein de la chaîne varisque ardennaise: géométrie et mécanismes de formation. Réunion des Sciences de la Terre, Paris .

c26.Szaniawski R**.,** Lewandowski M., **Averbuch O.**, Mansy J-L. et Lacquement F., 2000.- New paleomagnetic results along the N France-S Belgium Variscan Ardenne fold-thrust belt. Réunion des Sciences de la Terre, Paris, .

c27. Paturel J., Robert C., Chamley H., Diester-Haas L., Vidal L., Bout-Roumazeilles V., **Averbuch O.**, Recourt P., 2000.- Evolution des flux terrigènes dans le bassin du Cap au Miocène supérieur-Pliocène inférieur (10-4,5 Ma): rôles du système courantologique du Bengula et du climat sud-africain. Résultats préliminaires du site ODP 1085. Journées de Paléocéanographie, Lille.

c28. **Averbuch O.,** Lacquement F., Szaniawski R., Mansy J-L. and Lewandowski M., 2001.- Kinematics of major virgation zone along the Variscan Ardennes fold-and-thrust belt (N France-S Belgium): evidences from strain markers, magnetic fabrics and paleomagnetic data. European Geophysical Society meeting, Nice, Geophysical Research Abstracts.

c29. Szaniawski R., Lewandowski M., **Averbuch O.,** Mansy J-L. and Lacquement F., 2001.- Multicomponent syn-folding magnetizations within the N France- S Belgium Ardennes fold-and-thrust belt: contribution of the fold test analysis. European Geophysical Society meeting, Nice, Geophysical Research Abstracts.

c.30. **Averbuch O.**, Devleeschouwer X. et Tribovillard N., 2002.- lmpact de l'orogenèse acado-ligérienne sur le climat et la biosphère à la limite Frasnien-Famennien. Réunion des Sciences de la Terre 2002, Nantes.

c.31. **Averbuch 0.,** I. Berra, F. Boulvain, C. Cronier, A-C. da Silva, J-F. Deconinck, C. Derycke-Khatir, X. Devleeschouwer, L. François, J. Gaillardet, C. Girard, Y. Godderis, A. Grard, A. Herbosch, B. Mistiaen, A. Préat, A. Riboulleau, L. Riquier, N. Tribovillard, B. Van Vliet-Lanoe, 2002.- Impact d'une orogenèse sur le climat et la biosphère : la chaîne acado-ligérienne (380-360 Ma) et les événements globaux de la limite Frasnien-Famennien. Colloque Eclipse, CNRS Paris, 22-24.

c.32. **Averbuch O.,** Tribovillard N., Devleeschouwer X. and Riquier L., 2003.- Evidences for an orogenic-induced global cooling at the Frasnian-Famennian boundary. EGS, AGU, EUG common meeting, Nice.

c.33. Riquier L., El Albani A., **Averbuch O.,** Tribovillard N., Lazreq N. et Chakiri S., 2003.- Variations paléoenvironnementales à la limite Frasnien-Famennien au Maroc Central. Colloque ASF, Bordeaux.

c.34. Deconinck J-F., Devleeschouwer X. , Guillot F., Herbosch A., Pellenard P., Riboulleau A. et **Averbuch O.**, 2003.- Bentonites du passage Frasnien-Famennien (Belgique, Allemagne) : données préliminaires. Colloque ASF, Bordeaux.

c.35 **Averbuch O.,** Tribovillard N., Riquier L. et Devleeschouwer X., 2003.- Impact d'une orogenèse sur le climat et la biosphère : la chaîne éovarisque (ou acado-ligérienne) (380-360 Ma) et les événements globaux de la limite Frasnien-Famennien (2). Colloque Tectoclim, SGN-SGF-ASF-CNF-INQUA, Lille.

c.36. Riquier L., Tribovillard N., **Averbuch O.,** Joachimski M., El Albani A., Devleeschouwer X. et Riboulleau A., 2003.- Etude géochimique des coupes de Bou Ounebdou (Maroc) et de Aekatal (Allemagne) à la limite Frasnien-Famennien; comparaisons avec la coupe de La Serre (France). Colloque Tectoclim, SGN-SGF-ASF-CNF-INQUA, Lille.

c.37. Riquier L., El Albani A., **Averbuch O.,** Tribovillard N., Lazreq N. et Chakiri S., 2004.- Paleoenvironmental changes at the Frasnian-Famennian boundary in Central Morocco. Meeting Subcommission on Devonian Stratigraphy, Rabat.

c.38. El Albani A., Riquier L., **Averbuch O.,** Tribovillard N., Lazreq N. et Chakiri S., 2004.- Concretion levels and hardgrounds in the Upper Devonian series of Anti-Atlas : their significance for paleoenvironmental analysis. Meeting Subcommission on Devonian Stratigraphy, Rabat.

c.39. Riquier L., Tribovillard N., **Averbuch O.,** 2004.- Late Frasnian mass extinction, anoxia, eutrophication and climate changes, a causal link ? RST 2004, Strasbourg.

c40. Szaniawski R., Lewandowski M., Mansy J-L., **Averbuch O.** and Lacquement F., 2004.- Paleomagnetic study of the fold-and-thrust belt kinematics in the French-Belgium Variscides. Contributions to Geophysics and Geodesy, Geophysical Institute Slovak Academy of Sciences, vol. 34, 151-153.

c41. **Averbuch O.,** Riquier L., Tribovillard N. and Devleeschouwer X., 2004.- Rock magnetic and geochemical records of environmental changes at the Frasnian-Famennian boundary (ca 376 Ma BP). International Workshop on « The evolution of geological environment in paleomagnetic studies : current topics ans problems. », 25-26 novembre 2004, Varsovie.

c42. **Averbuch O.,** Lacquement F., Mansy J-L., Szaniawski R. et Lewandowski M., 2006. Déformations au front septentrional de la chaîne varisque : l'exemple des Ardennes franco-belges dans la région de Givet. Géologie de l'Ardenne occidentale, journées spécialisées, Givet, 4- 6 mai 2006.

c43. Guillot F., Lasalle S., Deconinck J-F., Pellenard P., **Averbuch O.,** Paquette J-L., Herbosch A. et Devleeschouwer X.,, 2006. Typologie du zircon des bentonites du Frasnien (carrière du Lion, Belgique) : utilité avant la datation U-Pb. Géologie de l'Ardenne occidentale, journées spécialisées, Givet, 4- 6 mai 2006.

c44. Minguely B., Mansy J-L., Hanot F., Everaerts M., Lacquement F. et **Averbuch O.**, 2006. Synthèse des données de sondage et des données gravimétriques depuis l'Avesnois jusqu'au méridien de Lens : résultats préliminaires Géologie de l'Ardenne occidentale, journées spécialisées, Givet, 4- 6 mai 2006.

c45. **Averbuch O.** and Piromallo C., 2007. High-velocity seismic anomalies in the lithospheric mantle beneath the Paris basin: remnants of subducted Paleozoic oceanic slabs? Subduction Congress, Montpellier, 5-7 juin 2007.

c46. Lacquement F., **Averbuch O.**, Mansy J-L., Szaniawski R. and Lewandowski M. **T**he Meuse Valley Recess, an example of transpressional deformation within the Ardennes Variscan fold-and-thrust belt (N France). Mechanics of Variscan Orogeny, a modern view on orogenic research, Orléans, 13-15 septembre 2007.

c47. Minguely B., **Averbuch O.**, Everaerts M., Mansy J-L. and Hanot F. The geometry of the northern Variscan thrust front in the Artois area (Northern France): Insight from seismic imaging and 2.5-D gravity modelling. Mechanics of Variscan Orogeny, a modern view on orogenic research, Orléans, 13-15 septembre 2007.

c48. Moulouel H., Lacquement F., **Averbuch O.**, Mansy J-L., Ledru P., Vinchon C. and Meilliez F. The tectonic style of the Western Ardennes-Avesnois Variscan fold-and-thrust belt: evidence for décollement tectonics and widespread back-thrusting. Mechanics of Variscan Orogeny, a modern view on orogenic research, Orléans, 13-15 septembre 2007.

c49. **Averbuch O.** and Piromallo C., 2007. Imaging the mantle roots of the Variscan orogen below the Paris basin: Insight from the P-wave velocity model PM0.5. Mechanics of Variscan Orogeny, a modern view on orogenic research, Orléans, 13-15 septembre 2007.

c50. *Riquier L.,* **Averbuch O.,** *Lefebvre V.* and Tribovillard N., 2008. Environmental changes and climatic perturbations at the Frasnian-Famennian boundary. International Congress on Paleozoic Climates, Lille, Aout 2008.

c.51. *Minguely B., Folens L.,* **Averbuch O.** and Vendeville B.V., 2008. Formation of deep-seated triangle zones by interaction between two orogenic thrust fronts having opposite vergence : structural evidence from the Caledonian-Variscan system in Northern France and preliminary analogue modelling. GEOMOD 2008, Florence.

c52. Devleeschouwer X., *Riquier L.,* Tribovillard N. and **Averbuch O.,** 2009**.** Sedimentology and rock magnetism at the Frasnian-Famennian boundary (Beringhauser Tunnel section, Sauerland, Germany). 27th IAS meeting, Alghero , 20-23 Septembre 2009.

c53. *Riquier L.,* **Averbuch O.,** Devleeschouwer X. and Tribovillard N., 2009. Origin of the magnetic susceptibility variations in some carbonate Frasnian-Famennian boundary sections : implications for paleoenvironmental studies. Scientific meeting of the IGCP 580 (Magnetic susceptibility, correlations and paleoenvironments), Liège, Décembre 2009.

c54. *Lefebvre V.*, **Averbuch O.**, Francois L., Servais T., *Riquier L.* and Tribovillard N., 2010. The Kellwasser Anoxic Events in Upper Devonian times: a global carbon cycle modelling test of the impact of Early Variscan mountain building. EGU meeting, Vienne, 2-7 mai 2010. Geophysical Research Abstracts vol 12.

c55. *Lefebvre V.*, Servais T., Francois L., **Averbuch O.**, 2010. The Late Ordovician crisis: the continental flood basalt hypothesis tested by global carbon cycle modeling. EGU meeting, Vienne, 2-7 mai 2010. Geophysical Research Abstracts vol 12.

c56. *Lefebvre V.*, **Averbuch O.**, Francois L., Servais T., *Riquier L.* and Tribovillard N., 2010. Climate and environmental changes at the Frasnian-Famennian boundary: a global carbon-cycle modelling approach. 3rd International Paleontological Congress, London, 28 juin-3 juillet 2010.

c57. *Ouzgaït M.*, **Averbuch O.**, Vendeville B.C., *Zuo X.* and *Minguely B.,* 2010. The negative tectonic inversion of thrust faults: insights from seismic sections along the Northern France Variscan thrust front and analogue modelling experiments. Geomod 2010, Lisbonne, 27-29 septembre 2010.

d. Ouvrages.

d1. **Averbuch O.**, 1988.- La méthode de polarisation provoquée en prospection: application à une zone test (COGEMA, Auvergne).

d2. **Averbuch O.**, 1990.- Etude paléomagnétique des formations cénozoïques du Taurus occidental à l'est d'Isparta (Turquie). Mémoire de D.E.A., Paris11 Orsay.

d3. **Averbuch O.**, 1992.- Projet “Anisotropie de susceptibilité magnétique”, Rapport interne, ELF-IFP (resp.: C. KISSEL et D. FRIZON DE LAMOTTE).

d4. **Averbuch O.**, 1993.- Caractérisation de la déformation dans les chaînes de chevauchement-plissement. Utilisation couplée du magnétisme des roches et de l’analyse structurale. (Exemples dans les Corbières, l’Apennin Central et le Taurus Occidental). Thèse de l’Université Paris 11 Orsay, 278p.

e. Publications grand public.

O. Averbuch, 2009. Le Cap Gris-Nez - déformations à la limite septentrionale du bassin jurassique supérieur du Boulonnais. In : Des roches aux paysages dans le Nord-pas de Calais. Richesse de notre patrimoine géologique. Coordination : F. Robaszynski, G. Guyetant. Ed. Conservatoire des Sites Naturels du Nord et du Pas-de-Calais, pp. 58-59.

O. Averbuch, 2009. Les écailles chevauchantes de la carrière « Basse-Normandie » à Rinxent - le front de chaîne hercynien dans le nord de la France. In : Des roches aux paysages dans le Nord-pas de Calais. Richesse de notre patrimoine géologique. Coordination : F. Robaszynski, G. Guyetant. Ed. Conservatoire des Sites Naturels du Nord et du Pas-de-Calais, pp. 60-63.

O. Averbuch, 2009. Les calcares carbonifères de la « Petite Brèche » à Limont-Fontaine – niveaux de brèche et plissements. In : Des roches aux paysages dans le Nord-pas de Calais. Richesse de notre patrimoine géologique. Coordination : F. Robaszynski, G. Guyetant. Ed. Conservatoire des Sites Naturels du Nord et du Pas-de-Calais, pp. 116-117.